1st International Conference of the Nigerian Institution of Professional Engineers and Scientists

BOOK OF PROCEEDINGS

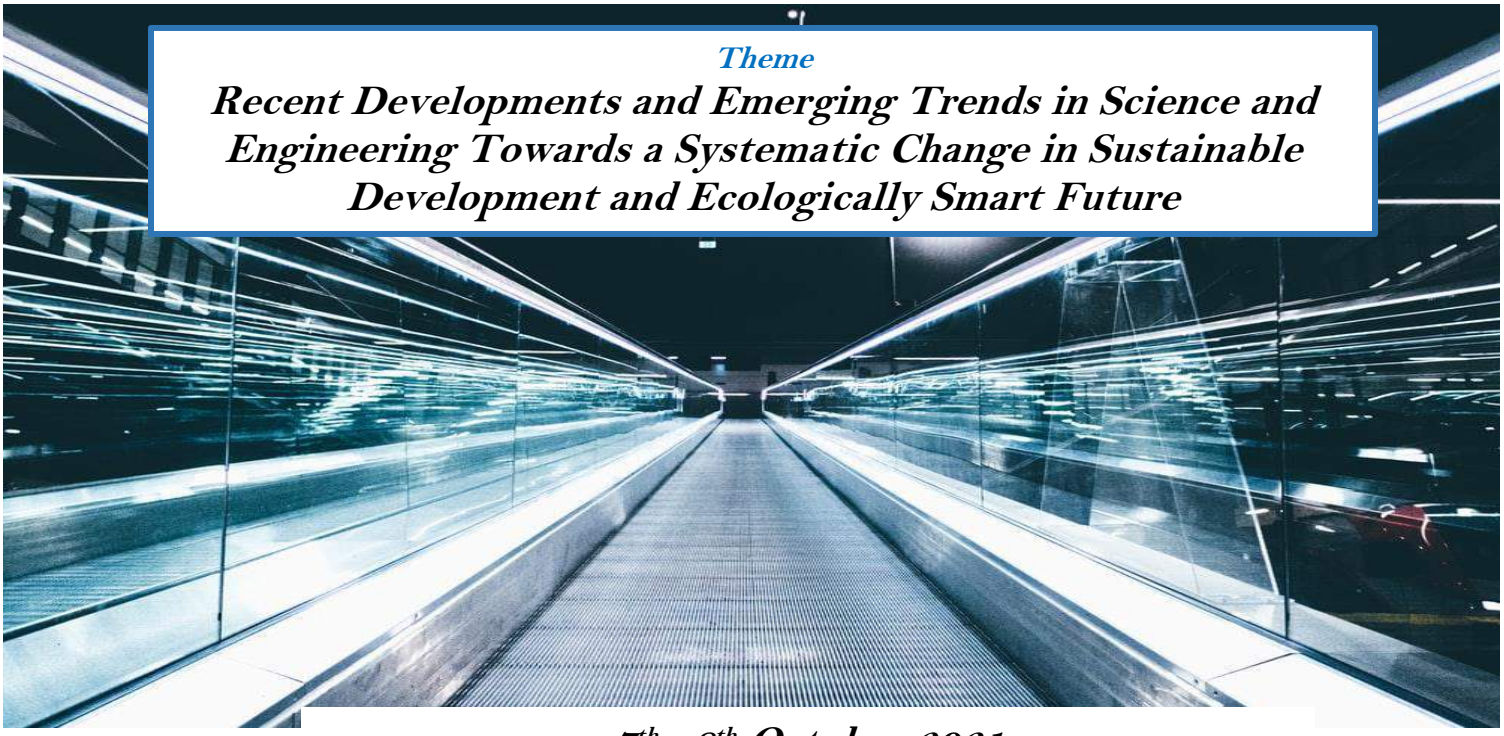

Theme

Recent Developments and Emerging Trends in Science and Engineering Towards a Systematic Change in Sustainable Development and Ecologically Smart Future

7th – 8th October 2021

University of Benin, Benin City Edo State, Nigeria

Prof. (Mrs) Lilian I. Salami (Vice Chancellor, University of Benin, Nigeria)
Chief Host

Engr. Dr. Collins Chike Kwasi-Effah (Chairman, NIPES)
Host

Prof. Jude Iroh, University of Cincinnati, Ohio, USA
International Keynote speaker

Dr. Uche Onochie, Alex-Ekweme Federal University, Nigeria
National Keynote speaker

Background

The Nigerian Institution of Professional Engineers and Scientists under the circumstance of COVID-19 pandemic has decided that her first International Conference be held both physically and virtually on the 7th and 8th of October, 2021. The conference theme is entitled: Recent Developments and Emerging Trends in Science and Engineering Towards a Systematic Change in Sustainable Development and Ecologically Smart Future. The aim of the conference is to promote engineering science interaction on the current trends and research geared towards a systematic change and approach in achieving sustainable development and ecologically smart future within the shortest possible time. The thematic sessions are grouped under the following category:

- ***Bioresources (BR)***
- ***Chemical Process & Petroleum Engineering (CP)***
- ***Energy and Power (EP)***
- ***Environmental Sustainability (ES)***
- ***Ecotoxicology (EC)***
- ***Information Technology (IT)***
- ***Materials and Industrial Process (MI)***
- ***Mathematics-Industrial Physics (MP)***
- ***Modelling, Simulations and Designs (MSD)***

Engineers and Scientists of all disciplines belonging to educational, research, industry, governmental or non-governmental organizations are welcome to participate in the conference.

Venue: *Faculty of Engineering Board Room, University of Benin, Edo State Nigeria*

Steering Committee

Dr. C.C. Kwasi-Effah
Dr. O.O. Ighodaro
Mr. J. Madu
Dr. H. O. Egware
Dr. M.O. Oisakede
Dr. Efe Orumwense
Miss T. Amanokhai
Mr. O. Omoyele
Mr. O. O. Omenu
Mr. O. Osaro

Chairmanship:

Oral Presentation (Virtual & Physical) Faculty of Engineering Board Room

Environmental Sustainability, Mathematics and Bioresources, Information Technology, Ecotoxicology
Chair- Prof. J.O. Osarenmwinda
Co-Chair – Dr. Efe Orumwense

Oral Presentation LT-2

Energy and Power, Materials and Ind. Process
Chair- Prof. A.I Obanor
Co-Chair- Dr. S. A Aliu
Co-Chair -Dr. Godwin Sadjere

Oral Presentation Chemical Engineering Board Room

Chemical Process and Petroleum Engineering
Chair- Prof. Kessington Obahiagbon
Co-Chair. Dr. O.O. Ighodaro
Co-Chair Dr. David Onaiwo

Oral Presentation Met and Mat Building

Designs

Chair- Prof. P.O.B Ebunilo
Co- Chair – Dr. N. Enoma

Modelling and Simulations

Chair- Prof. Godfrey O. Ariavie
Co-Chair- P.O Olagbegi

Correspondence:
C/o Department of Mechanical Engineering, University of Benin, Benin City, Nigeria
Email: nipesjournals@gmail.com Website: www.nipesjournals.org.ng

Editorial Office: *Department of Mechanical Engineering, Faculty of Engineering, University of Benin, PMB 1154 Ugbowo, Edo State Nigeria*

The Nigerian Institution of Professional Engineers and Scientists

Contents

NIPES Conference Proceedings
The 1st International Conference of the Nigerian Institution of Professional Engineers and Scientists 7th-8th Oct. 2021: 1-9
www.nipesjournals.org.ng

Modelling and Optimization of Material Removal Rate and Tool Wear Rate in a Straight Turning Operation

A.A. Erameh[a], D.D. Olodu[b], E.K. Orhorhoro[a*]

[a]Department of Mechanical Engineering, Igbinedion University, Okada, Nigeria
[b]Department of Mechanical Engineering, Benson Idahosa University, Benin City, Nigeria

Abstract
This research work used Response Surface Methodology approach to addressed a multi-objective optimization problem in a straight turning operation of EN 8 mild steel bar, using HSS cutting tool. The study aimed at evaluating the best turning parameters setting which could simultaneously satisfy the requirements of both quality and productivity. The predicted optimal setting ensured maximization of material removal rate and minimization of tool wear rate, through a developed Central Composite Design using version 7.0 of Design Expert software. An Electronic Numeric Control lathe machine was used to carry out the turning operation, with work pieces, measuring 100 mm diameter and length 60 mm. A total of 20 experimental runs were done. The experimental results (data) were recorded and Response Surface Methodology was used to analyze the data. R^2 values of 0.9958 and 0.9887 for Material Removal Rate and Tool Wear Rate respectively. From the analysis, it was found that all three input parameters of spindle speed, feed rate and depth of cut have significant influence on Material Removal Rate. Only spindle speed and depth of cut were found to have significant influence on Tool Wear Rate. From the numerical optimization solution, it was observed that a spindle speed of 113.99 rpm, feed rate of 0.18 mm/rev and a depth of cut of 1.5 mm resulted in a turning process, with the following properties: Material Removal Rate of 9641.87 mm^3/min. and Tool Wear Rate of 0.35293 mm^3/min, with a composite desirability value of 96.4%.

***Keywords*:**
Response Surface Methodology, Material Removal Rate, Tool Wear Rate, Central Composite Design, Electronic Numeric Control

1. Introduction

Machining operations are accomplished using cutting tools. The Material Removal Rate (MRR), and Tool Wear Rate (TWR) are very important factors in the machining operations and have effect on the machining and tooling costs during turning operation [1-4]. The high forces and temperatures during machining create a very harsh environment for the tool. If cutting force becomes too high, the tool fractures. If cutting temperature becomes too high, the tool material softens and fails. If neither of these conditions causes the tool to fail, continual wear of the cutting edge ultimately leads to failure. Fracture and temperature failures result in premature loss of the cutting tool. These two modes of failure are therefore undesirable. Of the three possible tool failures, gradual wear is preferred because it leads to the longest possible use of the tool, with the associated economic advantage of that longer use. Product quality must also be considered when attempting to control the mode of tool failure. When the tool point fails suddenly during a cut, it often causes damage to the work surface. This damage requires either rework of the surface or possible scrapping of the part. The damage can be avoided by selecting cutting conditions that favor gradual wearing of the tool rather than fracture or temperature failure, and by changing the tool before the final catastrophic loss of the cutting edge occurs.

Furthermore, to increase productivity and reduce machining and tooling costs, the engineer needs to select optimum process parameters during turning. Optimization is usually applied to enhance the performance of a system, part or component while satisfying the desired constraints and is achieved by optimizing the process parameter, thus obtaining the desired finish. There are many studies on optimization of process parameters to achieve desired surface finish at reduced

machining costs. A method of coupling artificial neural network and use of improved harmony search algorithm to determine the optimum cutting parameter settings necessary for minimizing surface roughness when turning polyamide materials was reported [5-6]. Response Surface Methods (RSM) were employed to evaluate the effect of material removal rate, electrode wear rate and surface roughness in die sinking EDM with hollow tool [2]. A parametric study and optimization of the wire electric discharge machining (WEDM) parameters for CK 45 steel using the response surface methodology was conducted and reported [7]. The Taguchi technique have been employed in optimization during machining process using different parameters and quality characteristics as reported in [7-9]. This work present research used Response Surface Methodology (RSM) approach to addressed a multi- objective optimization problem in a straight turning operation of EN 8 mild steel bar, using HSS cutting tool.

2. Materials and Methods

2.1 Materials

EN8 mild steel of size 100 mm diameters and length 60 mm was selected for this research work. M42 HSS single point cutting tool is used for turning operation. ENC lathe machine, with a spindle speed range from 100 to 2500 rpm was employed for the experiment. The machining centre was driven by 10kW electric motor. The experiment was carried out under dry machining environment.

2.2 Methods

The ranges for the machining parameter were chosen, as presented in Table 1. Twenty different machining settings were generated by Design expert, each setting was used to turn the EN8 mild steel to the required form and size and the values of the respective responses were measure and recorded, as shown in Table 2.

2.2.1 Identification of Important Process Parameters

Cutting parameters of spindle speed, feed rate and depth of cut, each at two levels were considered for the turning process. Table 1 shows the process variables and their level**.**

Table 1: Process Variables and their Level

Factor	**Range**	
	Low	**High**
Spindle speed, A, (rpm)	105 rpm (32.99m/mim)	220 rpm (61.12m/min)
Feed rate, B, (mm/mim)	0.12mm/mim	0.18mm/min
Depth of cut, C, (mm)	0.50mm	1.50mm

2.2.2 Responses

A. Material Removal Rate (MRR)

The material-removal rate (MRR) in turning is the volume of material removed per unit time, with the units of mm^3/min. It was derived for each experimental run by the expression presented by Kalpakjian and Schmid, (2009):

$$MMR = \pi * D_{av} * \ doc * f * N \quad (1)$$

D_{av} is average diameter of work piece, mm

Doc is depth of cut, mm,

F is feed rate, mm per rev N is spindle speed, rev per min

Empirical formula for tool wear rate, developed by El-Hossainy *et al*. in 2010, was adopted for this study. This formula is presented as in equation 2.

B. Tool Wear Rate (TWR)

$$TWR = KV^{\alpha} f^{\beta} d^{\gamma} t^{\sigma} \quad (2)$$

Where k, $\propto$, β, γ and σ are constants, whose values were determined empirically, using regression analysis as 8.2961X10^{-5}, 2.747, 1.473, 1.261 and 0.43 respectively. The variable t represents the length of time in minutes spent in cutting under the cutting conditions specified by the cutting speed (V) in m/min, the feed rate (f) in mm/rev, and the initially adjusted depth of cut (d), in mm.

3. Results and Discussion

Table 2 shows the result of experimental design matrix and output response

Table 2: Experimental Design Matrix and Output Response

Std.	Run	Factor				Response	
		Block	Spindle Speed (rpm)	Feed rate (mm/rev)	Dept of cut (mm)	Material Removal Rate, MRR (mm^3/min.)	Tool Wear Rate, TWR (mm^3/min.)
13	1	Block 1	162.5	0.15	0.16	1024.69	0.029
18	2	Block 1	162.5	0.15	1	7091.04	0.368
10	3	Block 1	259.2	0.15	1	12228.9	1.113
3	4	Block 1	105	0.18	0.5	2954.34	0.067
20	5	Block 1	162.5	0.15	1	7502.04	0.402
17	6	Block 1	162.5	0.15	1	7502.04	0.348
5	7	Block 1	105	0.12	1.5	5849.3	0.177
19	8	Block 1	162.5	0.15	1	7680.4	0.273
9	9	Block 1	65.8	0.15	1	2935.16	0.041
12	10	Block 1	162.5	0.2	1	10208.5	0.501
11	11	Block 1	162.5	0.1	1	4955.54	0.236
7	12	Block 1	105	0.18	1.5	8773.96	0.27
15	13	Block 1	162.5	0.15	1	7182.65	0.307
8	14	Block 1	220	0.18	1.5	18383.5	1.496
1	15	Block 1	105	0.12	0.5	1969.56	0.044
4	16	Block 1	220	0.18	0.5	6190.05	0.374
16	17	Block 1	162.5	0.15	1	7382.04	0.393
14	18	Block 1	162.5	0.15	1.84	14024.5	0.807
6	19	Block 1	220	0.12	1.5	12255.7	0.98
2	20	Block 1	220	0.12	0.5	4126.7	0.245

The experimental results were analysed with ANOVA, to identify the factor(s) that significantly influence the responses, as shown in Tables 3 and 4. Quadratic model was suggested from the sequential model sum of squares [Type II] for the two responses.

Table 3: ANOVA prediction for Material Removal Rate

Source	**Sum of Square**	**df**	**Mean Square**	**F Value**	**p-value Prob > F**	
Model	9885.61	9	1098.4	264.05	< 0.0001	Significant
A-Spindle Speed	2788.68	1	2788.68	670.39	< 0.0001	
B-Feed Rate	849.11	1	849.11	204.12	< 0.0001	
C-Depth of cut	5951.81	1	5951.81	1430.79	< 0.0001	
AB	20.8	1	20.8	5	0.0493	
AC	144.82	1	144.82	34.81		
BC	44.09	1	44.09	10.6	0.0086	
A^2	7.48	1	7.48	1.8	0.2096	
B^2	0.33	1	0.33	0.079	0.7847	
C^2	80.15	1	80.15	19.27	0.0014	
Residual	41.6	10	4.16			
Lack of Fit	34.67	5	6.93	5	0.0051	Not significant
Pure Error	6.93	5	1.39			
Cor Total	9927.21	19				

Table 4: ANOVA prediction for Tool Wear Rate

Source	**Sum of Square**	**df**	**Mean Square**	**F Value**	**p-value Prob > F**	
Model	2.83	9	0.31	97.53	< 0.0001	Significant
A-Spindle Speed	1.38	1	1.38	427.82	< 0.0001	
B-Feed Rate	0.11	1	0.11	33.07	< 0.0002	
C-Depth of cut	0.9	1	0.9	278.48	< 0.0001	
AB	0.035	1	0.035	10.85	0.0081	
AC	0.29	1	0.29	89.71	< 0.0001	
BC	0.026	1	0.026	8.1	0.0174	
A^2	0.092	1	0.092	28.52	0.0003	
B^2	5.47E-04	1	5.47E-04	0.17	0.689	
C^2	8.07E-03	1	8.07E-03	2.5	0.1447	
Residual	0.32	10	3.22E-03			
Lack of Fit	0.02	5	3.92E-03	1.55	0.3213	Not significant
Pure Error	0.013	5	2.53E-03			
Cor Total	2.86	19				

Table 3 presents the ANOVA for the cutting parameters against Material removal rate. it can be seen that factors A, B and C have significant influence for the maximization of material removal

rate, since they possessing values of "Prob > F" less than 0.0500. Also, the probability value associated with the lack of fit is 0.0522, which is not significant. It is desirable to have an insignificant lack of fit. Table 4 depicts the ANOVA generated at 95% confidence level for the input factors and the response (TWR). In this model, it is observed that A, B and C are the significant model terms for the minimization of Tool Wear Rate.

3.1 Goodness of Fit

To validate the adequacy of the quadratic model based on its ability to and maximize Material Removal Rate (MRR) and minimize Tool wear rate (TWR), the goodness of fit statistics presented in Tables 5 and 6 were employed;

Table 5: GOF statistics for validating model significance towards maximizing MRR

GOF statistics for validating model significance towards maximizing MRR	
R-Squared	0.9958
Adj R-Squared	0.992
Pred R-Squared	0.9347
Adeq Precision	35.114

The Adjusted R-Squared and Predicted R-Squared should be within approximately 0.20 of each other to be in "reasonable agreement.

Table 6: GOF statistics for validating model significance towards minimizing TWR

GOF statistics for validating model significance towards minimizing TWR	
R-Squared	0.9887
Adj R-Squared	0.9786
Pred R-Squared	0.9347
Adeq Precision	36.114

Tables 6 reports an R^2 value of 0.9958 for MRR, which implies that the model can explain 99% of the variability in MRR. Tables 6 shows that the R^2 value of 0.9887 for TWR implies that the model can explain 98.87% of the variability in TWR. The respective adjusted R-squared and predicted R-squared in both Tables 5 and 6 are in good agreement. Adequate precision is greater than the desired value is 4. Implying, it can be used to navigate the design space.

3.2 Surface Plots and Inferences

A. Material Removal Rate (MRR)

The 3D response surface, showing the expected Material Removal Rate (MRR) as a function of spindle speed (A) and feed rate (B) is presented in Figure 1.

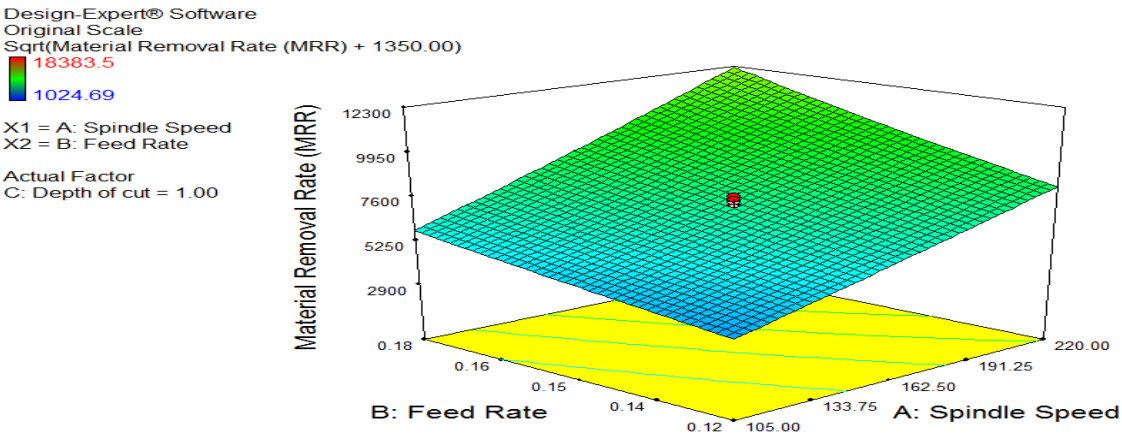

Figure 1: 3D response surface plot, showing the expected MRR as a function of A and B

The 3D response surface, showing the expected Material Removal Rate (MRR) as a function of spindle speed (A) and Depth of cut (C) is presented in Figure 2.

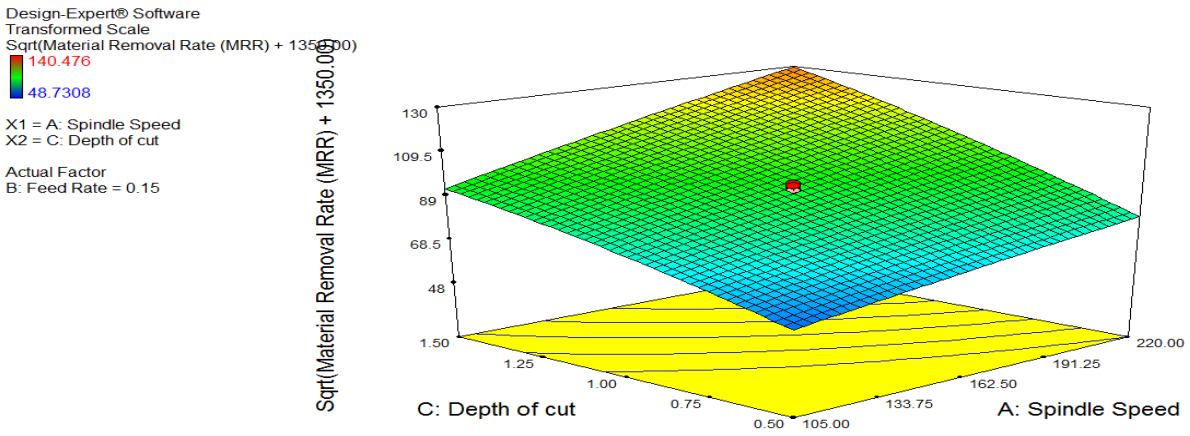

Figure 2: 3D response surface plot, showing the expected MRR as a function of A and C

The 3D response surface, showing the expected Material Removal Rate (MRR) as a function of feed rate (B) and depth of cut (C) is presented in Figure 3.

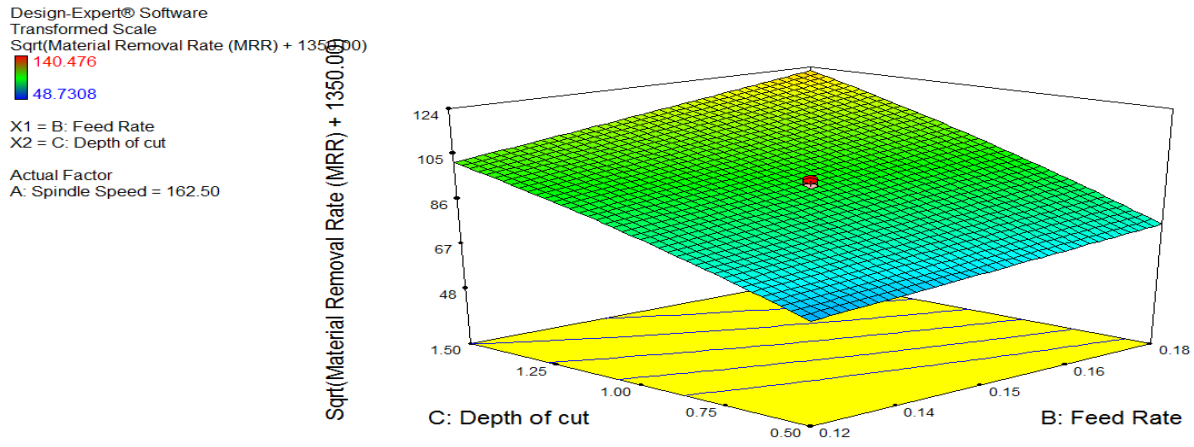

Figure 3: 3D response surface plot, showing the expected MRR as a function of B and C

The 3D response surface, showing the expected Tool Wear Rate (TWR) as a function of spindle speed (A) and feed rate (B) is presented in Figure 4.

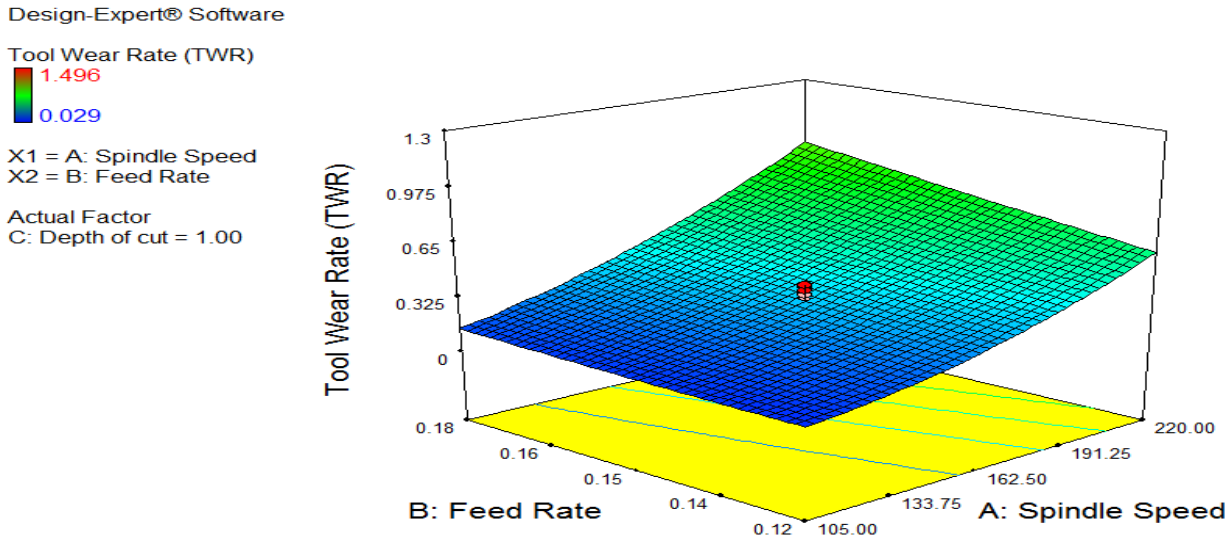

Figure 4: 3D response surface plot, showing the expected TWR as a function of A and B

The 3D response surface, showing the expected Tool Wear Rate (TWR) as a function of spindle speed (A) and Depth of cut (C) is presented in Figure 5.

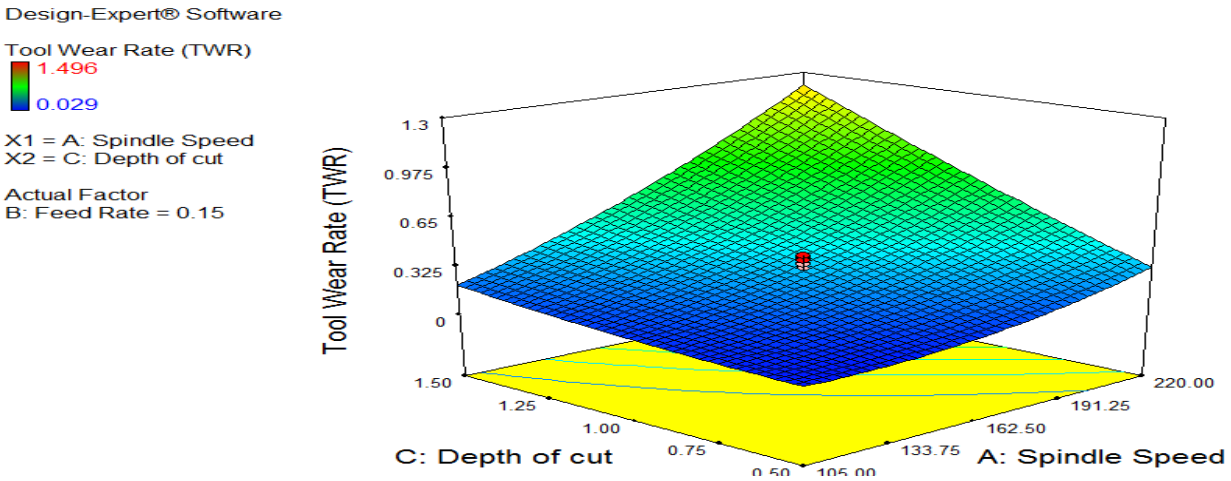

Figure 5: 3D response surface plot, showing the expected TWR as a function of A and C

The 3D response surface, showing the expected Tool Wear Rate (TWR) as a function of feed rate (B) and depth of cut (C) is presented in Figure 6.

3.3 Mathematical Modeling

The values of the responses were evaluated using mathematical models, for various combinations of input parameters. This method of data evaluation helps in theoretical decision making for finding optimal cutting conditions. The mathematical models of Material removal rate and Tool wear rate generated from this study are shown in Equations 3 and 4. Final Equation in terms of coded factors:

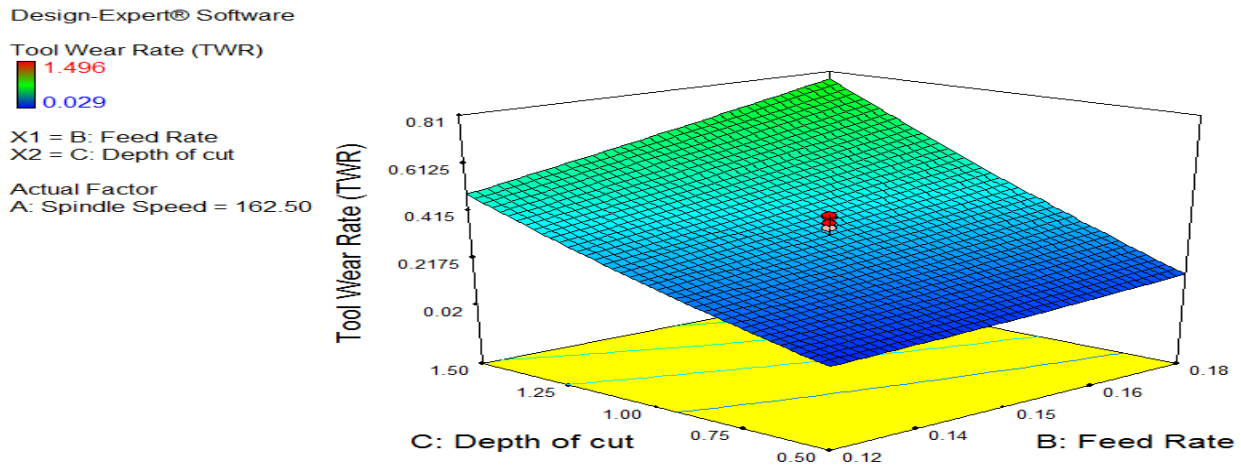

Figure 6: 3D response surface plot, showing the expected TWR as a function of B and C

$$MRR + 1350.00 = +93.46 + 14.29 * A + 7.89 * B + 20.88 * C + 1.61 * A * B + 4.25 * A * C + 2.35 * B * C + -0.72 * A^2 + 0.15 * B^2 - 2.36 * C^2 \quad (3)$$

Where: MRR= Material removal rate, A= Spindle speed, B= Feed rate and C= Depth of cut.

Final equation in terms of coded factors

$$TWR = +0.35 + 0.32 * A + 0.088 * B + 0.26 * C + 0.06 * A * B + 0.19 * A * C + 0.057 * B * C + 0.080 * A^2 + 6.163E - 003 * B^2 + 0.024 * C^2 \quad (4)$$

Where:

TWR= Tool wear rate, A= spindle speed, B= feed rate, C= depth of cut, A*B= spindle speed*feed rate, A*C= spindle speed*depth of cut, B*C= feed rate*depth of cut, A^2= spindle speed^2, B^2= feed rate^2, C^2= depth of cut^2

3.4 Optimization

To acertain how desirable the developed models are, Numerical optimization was carried out. During this numerical optimization stage, design expert was set to maximize material removal rate (MRR) and minimize Tool wear rate (TWR) and determine the optimum input parameters settings. The results are presented in Table 7. Design Expert found twelve (12) solutions but selected one. All solutions are optimal, depending on response of priority.

Table 7: Results for Numerical optimization

Number	A	B	C	MRR	TWR	Desirability
1	113.99	0.18	1.5		0.35293	0.964
2	113.17	0.18	1.5	9641.87	0.34659	0.964
3	112.72	0.18	1.5	9576.61	0.34319	0.964
4	115.23	0.18	1.5	9736.94	0.36232	0.964
5	110.6	0.18	1.5	9377.59	0.32723	0.964
6	113.99	0.18	1.5	9623.11	0.35192	0.964
7	116.88	0.18	1.5	9865.69	0.37506	0.964
8	114.43	0.18	1.49	9637.12	0.35379	0.964
9	116.22	0.18	1.47	9642.18	0.35885	0.963

10	119.18	0.17	1.5	9698.44	0.3742	0.963
11	124.54	0.18	1.44	10039.9	0.40693	0.963
12	132	0.18	1.5	10788.1	0.48201	0.962

4. Conclusion

In this study, we investigated how different machining parameters settings affect material removal rate and Tool wear rate, using response surface methodology. The results obtained from the ANOVA Table 3 revealed that the spindle speed, feed rate and depth of cut have significant influence on material removal rate. Also, from Table 4, spindle speed, feed rate and depth of cut have significant influence on Tool wear rate. It was also observed, from Table 7, that optimum machining setting of spindle speed of 113.99 rpm, feed rate of 0.18 mm/rev and a depth of cut of 1.5 mm will result in a turning process with an optimum (maximized) material removal rate of 9641.87 mm^3/min and Tool wear rate (minimized) of 0.35293 mm^3/min, with a composite desirability value of 96.4%.

References

[1] C. Mgbemena, C. Mgbemena, G. G. Etebenumeh, F. Ashiedu. (2016). Effect of Turning parameters on metal removal and tool wear rates of AISI 1018 low carbon steel. Nigerian Journal of Technology (NIJOTECH) Vol. 35, No. 4, pp. 847 – 854

[2] M. Adinarayana, G. Prasanthi, G. Krishnaiah (2014). Paraelectric analysis and ulti-objective optimization of cutting parameters in turning operation of AISI 434 Alloy Steel with CVD Cutting Tool" International Journal of Research in Engineering and Technology, Vol. 3, Number 2, pp 449-456

[3] A.A. Erameh, E.K. orhorhoro (2020). Prediction and optimization of en8 mild steel material removal rate and surface roughness using response surface methodology. Journal of Engineering and Technology (JET), Vol.11, No. 1, pp. 1-6

[4] T.Z. Quazi, P. More, V. Sonawane (2013). A case study of Taguchi method in the optimization of turning parameters. International journal of Emerging Technology and Advanced Engineering, Vol. 3, Number2, pp. 616-626

[5] M. Madic, D. Markoic, M. Radovanovic (2012). Application of surface roughness when turning polyamide using ANN-IHSA approach. International Journal of Engineering and Technology, Vol. 1 Number 4, pp. 432-443

[6] M. Ajay, G. Anshul (2012). Application of Taguchi method in optimization of tool flank wear width in turning operation of AISI 045 steel. Industrial Engineering Letters, Vol. 2, Number 8, pp. 11-18

[7] H. Dave, L. Patel, H. Raval (2012). Effect of machining conditions on MRR and surface roughness during CNC turning of different materials using TiN coated cutting tools: A Taguchi approach. International Journal of Industrial Engineering Computations Vol. 3, pp. 925–930

[8] T. Kanase, D.B. Jadhav (2013). Enhancement of surface finish for CNC turning cutting parameters by using Taguchi method" Indian Journal of Research, Vol. 3, Number 5, (2013), pp. 88-91

[9] M. Kaladhar, K. Subbaiah, C. Rao (2012). Parametric optimization during machining of AISI 304 Austenitic Stainless Steel using CVD coated DURATOMIC cutting insert. International Journal of Industrial Engineering Computations, Vol 3, Number 4, pp 577-586

NIPES Conference Proceedings
The 1st International Conference of the Nigerian Institution of Professional Engineers and Scientists 7th-8th Oct. 2021: 10-19
www.nipesjournals.org.ng

Development of Calibration Combined Ratio Estimators of Finite Population Mean in Stratified Random Sampling

J. O. Muili[a]*, R. V. K. Singh[b], G. I. Onwuka[c] and A. Audu[d]
[a, b, c]Department of Mathematics, Kebbi State University of Science and Technology Aliero, Nigeria
[d]Department of Mathematics, Usmanu Danfodiyo University, Sokoto, Nigeria

Abstract
This study deals with modification of combined ratio estimator in stratified random sampling using calibration estimation approaches. Calibration distance measures with their associate constraints were used to modify combined ratio estimator. New sets of optimum calibration weights are derived and used to obtained new calibration estimators of population mean in stratified random sampling. Empirical study through simulation was conducted to investigate the efficiency of the new estimators obtained. The results revealed that the proposed calibration estimators are more efficient than other existing estimators considered in the study.

***Keywords*:**
Calibration weights, Combined Ratio, Estimators, Mean Squared Error, Stratified Sampling.

1. Introduction

Calibration estimation adjust the original design weights by incorporate the known population parameters of auxiliary variables. Calibration approach is used in stratified random sampling to obtain optimum strata weights for improving the precision of survey estimates of population parameters. The technique of estimation by calibration in survey sampling was introduced by [1]. The idea is to use auxiliary information to obtain a better estimate of parameters for population of interest. Following [1], many researchers have studied calibration estimation using different calibration constraints of auxiliary variables in survey sampling design. [2] was the first researcher that extended calibration approach to stratified sampling design. [3], [4], [5], [6] and [7] applied calibration estimation to ratio-type estimators in stratified sampling. [8] developed a multivariate calibration estimator for the population mean with using different distance measures with two auxiliary variables in stratified sampling. [9] have suggested calibration estimators for estimating the population mean in stratified sampling based on different calibration constraints of auxiliary information.
The existing calibration estimators such as [2], [4], [5], [8], [10], [6], [9], [11], [12], [7], and [14] have modified the stratum weight of the unbiased estimators using auxiliary variables in stratified sampling to improve its efficiency whereby strata with large sizes are favoured and more represented in the estimation. To overcome this challenge, strata sample means are computed based on the information and sizes of each of the stratum using calibration techniques to produce more efficient estimators.
Consider a finite population ψ of N elements, $\psi = \{\psi_1, \psi_2, \psi_3, ..., \psi_N\}$ consists of L strata with N_h units in the hth stratum from which a simple random of size n_h is taken from the population using SRSWOR. Total Population size $N = \sum_{h=1}^{L} N_h$, sample size $n = \sum_{h=1}^{L} n_h$ where $y_{hi}, i = 1, 2, ..., N_{hi}$ and $x_{hi}, i = 1, 2, ..., N_{hi}$ of study variable y and x auxiliary variable. Let $W_h = N_h / N$ be the strata weights, $\bar{y}_h = n^{-1} \sum_{i=1}^{n_h} y_{hi}$ and $\bar{Y}_h = N^{-1} \sum_{i=1}^{n_h} y_{hi}$ are the sample and population means respectively for the study variables.

1.2 Related Literature Review

According to [15], the traditional estimator of population mean in stratified sampling given as:

$$\bar{y}_{st} = \sum_{h=1}^{L} W_h \bar{y}_h \tag{1}$$

$$V\left(\bar{y}_{st}\right) = \sum_{h=1}^{L} W_h^2 \left(\frac{1-f_h}{n_h}\right) s_{hy}^2 \tag{2}$$

where $s_{hy}^2 = \left(n_h - 1\right)^{-1} \sum_{h=1}^{n_h} \left(y_{hi} - \bar{y}_h\right)^2,\ f_h = n_h / N_h$

[16] suggested a combined ratio estimator as

$$\bar{y}_{st}^{RC} = \frac{\bar{y}_{st}}{\bar{x}_{st}} \bar{X} \tag{3}$$

where $\bar{y}_{st} = \sum_{i=1}^{n_h} W_h \bar{y}_h$, *and* $\bar{x}_{st} = \sum_{i=1}^{n_h} W_h \bar{x}_h$

The mean square error of the combined ratio estimator is

$$MSE\left(\bar{y}_{st}^{RC}\right) = \sum_{h=1}^{L} W_h^2 \gamma_h \left(S_{yh}^2 + R^2 S_{xh}^2 - 2RS_{yxh}^2\right) \tag{4}$$

where $R = \frac{\bar{Y}}{\bar{X}}$

[2] introduced the calibration approach for the combined general regression estimator for the population mean in the stratified sampling design given by:

$$\bar{y}_{st(SH)} = \sum_{h=1}^{L} \Omega_h^{SH} \bar{y}_h \tag{5}$$

[2] obtained new calibration weights by minimizing of the Chi-Square distance measure in (6) subject a calibration constraint:

$$\left.\begin{aligned} &\min Z_1 = \sum_{h=1}^{L} \left(\Omega_h^{SH} - W_h\right)^2 \Big/ Q_h W_h \\ &s.t. \quad \sum_{h=1}^{L} \Omega_h^{SH} \bar{x}_{1h} = \bar{X} \end{aligned}\right\} \tag{6}$$

The calibrated weights and the estimator of (5) are obtained as show in (7) and (8) respectively.

$$\Omega_h^{SH} = W_h + \left(\sum_{h=1}^{L} W_h Q_h \bar{x}_h \Big/ \sum_{h=1}^{L} W_h Q_h \bar{x}_h^2\right)\left(\bar{X} - \sum_{h=1}^{L} W_h \bar{x}_h\right) \tag{7}$$

And thus, [2] proposed calibrated estimator is given by:

$$\bar{y}_{st(SH)} = \sum_{h=1}^{L} W_h \bar{y}_h + \left(\sum_{h=1}^{L} W_h Q_h \bar{x}_h \bar{y}_h \Big/ \sum_{h=1}^{L} W_h Q_h \bar{x}_h^2\right)\left(\bar{X} - \sum_{h=1}^{L} W_h \bar{x}_h\right) \tag{8}$$

The variance of the calibrated estimator is given by

$$V\left(\bar{y}_{st(SH)}\right) = \sum_{h=1}^{L} \Omega_h^{SH^2} \frac{\left(1-f_h\right)}{n_h} s_{eh}^2 \tag{9}$$

where $s_{eh}^2 = \left(n_h - 1\right)^{-1} \sum_{i=1}^{nh} e_{hi}^2$ is the h^{th} strata sample mean square and $e_{hi} = \left(y_{hi} - \bar{y}_h\right) - b\left(x_{hi} - \bar{x}_h\right)$

with $b = \sum_{h=1}^{L} W_h Q_h \bar{x}_h \bar{y}_h \Big/ \sum_{h=1}^{L} W_h Q_h \bar{x}_h^2$ and $f_h = n^{-1} - N^{-1}$ is the h th strata sample.

[4] proposed two constraints: first and second order moments of auxiliary variable to obtain calibration weights for estimating the population mean in stratified sampling and the calibration estimator of the population mean under stratified sampling given by:

$$\bar{y}_{st(Tr)} = \sum_{h=1}^{L} \Omega_h^{Tr} \bar{y}_h \tag{9}$$

[4] derived new calibration weights by minimizing of the Chi-Square distance measure in (11) subject to the following calibration constraints:

$$\left.\begin{aligned} &\min Z_3 = \sum_{h=1}^{L} \left(\Omega_h^{Tr} - W_h\right)^2 \Big/ Q_h W_h \\ &s.t. \quad \sum_{h=1}^{L} \Omega_h^{Tr} \bar{x}_h = \bar{X} \\ &\qquad \sum_{h=1}^{L} \Omega_h^{Tr} s_{xh}^2 = \sum_{h=1}^{L} W_h S_{xh}^2 \end{aligned}\right\} \tag{11}$$

where $s_{xh}^2 = \sum_{i=1}^{nh} \left(x_{hi} - \bar{x}_h\right)^2 \Big/ \left(n_h - 1\right)$ and $S_{xh}^2 = \sum_{i=1}^{nh} \left(x_{hi} - \bar{x}_h\right)^2 \Big/ \left(N_h - 1\right)$ are the sample and population mean squares of the auxiliary variable respectively.

The calibrated weights and the estimator of (9) are obtained as show in (12) and (13) respectively

$$\begin{aligned} \Omega_h^{Tr} = W_h &+ \left(W_h Q_h \bar{x}_h\right) \frac{\left(\sum_{h=1}^{L} W_h \left(\bar{X}_h - \bar{x}_h\right)\right)\left(\sum_{h=1}^{L} W_h Q_h s_{xh}^4\right) - \sum_{h=1}^{L} W_h \left(S_{xh}^2 - s_{xh}\right)\left(\sum_{h=1}^{L} W_h Q_h \bar{x}_h s_{xh}^2\right)}{\left(\sum_{h=1}^{L} W_h Q_h s_{xh}^4\right)\left(\sum_{h=1}^{L} W_h Q_h \bar{x}_h^2\right) - \left(\sum_{h=1}^{L} W_h Q_h \bar{x}_h s_{xh}^2\right)^2} \\ &- \left(W_h Q_h s_{xh}^2\right) \frac{\left(\sum_{h=1}^{L} W_h \left(\bar{X}_h - \bar{x}_h\right)\right)\left(\sum_{h=1}^{L} W_h Q_h \bar{x}_h s_{xh}^2\right) - \sum_{h=1}^{L} W_h \left(S_{xh}^2 - s_{xh}\right)\left(\sum_{h=1}^{L} W_h Q_h \bar{x}_h^2\right)}{\left(\sum_{h=1}^{L} W_h Q_h s_{xh}^4\right)\left(\sum_{h=1}^{L} W_h Q_h \bar{x}_h^2\right) - \left(\sum_{h=1}^{L} W_h Q_h \bar{x}_h s_{xh}^2\right)^2} \end{aligned} \tag{12}$$

$$\bar{y}_{st(Tr)} = \sum_{h=1}^{L} W_h \bar{y}_h + \hat{\beta}_{1(T)} \left(\bar{X} - \sum_{h=1}^{L} W_h \bar{x}_h\right) + \hat{\beta}_{2(T)} \sum_{h=1}^{L} W_h \left(S_{xh}^2 - s_{xh}^2\right) \tag{13}$$

where $\hat{\beta}_{1(T)} = \dfrac{\left(\sum_{h=1}^{L} W_h Q_h \bar{x}_h \bar{y}_h\right)\left(\sum_{h=1}^{L} W_h Q_h s_{xh}^4\right) - \left(\sum_{h=1}^{L} W_h Q_h \bar{y}_h s_{xh}^2\right)\left(\sum_{h=1}^{L} W_h Q_h \bar{x}_h s_{xh}^2\right)}{\left(\sum_{h=1}^{L} W_h Q_h s_{xh}^4\right)\left(\sum_{h=1}^{L} W_h Q_h \bar{x}_h^2\right) - \left(\sum_{h=1}^{L} W_h Q_h \bar{x}_h s_{xh}^2\right)^2}$

$$\hat{\beta}_{2(T)} = \frac{\left(\sum_{h=1}^{L} W_h Q_h \bar{y}_h s_{xh}^2\right)\left(\sum_{h=1}^{L} W_h Q_h \bar{x}_h^2\right) - \left(\sum_{h=1}^{L} W_h Q_h \bar{x}_h \bar{y}_h\right)\left(\sum_{h=1}^{L} W_h Q_h \bar{x}_h s_{xh}^2\right)}{\left(\sum_{h=1}^{L} W_h Q_h s_{xh}^4\right)\left(\sum_{h=1}^{L} W_h Q_h \bar{x}_h^2\right) - \left(\sum_{h=1}^{L} W_h Q_h \bar{x}_h s_{xh}^2\right)^2}$$

The variance of [4] calibrated estimator is given by

$$V\left(\bar{y}_{st(Tr)}\right) = \sum_{h=1}^{L} \Omega_h^{Tr^2} \frac{\left(1 - f_h\right)}{n_h} s_{eh}^2 \tag{14}$$

where $s_{eh}^2 = (n_h - 3)^{-1} \sum_{i=1}^{nh} e_{hi}^2$ is the hth strata sample mean square and $e_{hi} = (y_{hi} - \bar{y}_h) - \hat{\beta}_{1(T)} \left\{ (x_{hi} - \bar{x}_h)^2 - s_{xh}^{*2} \right\}$ with $s_{xh}^{*2} = n_h^{-1} \sum_{i=1}^{nh} (x_{hi} - \bar{x}_h)^2$ is the maximum likelihood.

[17] developed a calibration estimator for estimating population mean under stratified random sampling using a distance function of the sum of weighted squared deviation of calibrated and stratum weights as follows:

$$\bar{y}_{st}^{LA} = \sum_{h=1}^{L} \Omega_h^{LA} \bar{y}_h \tag{15}$$

$$Z = \sum_{h=1}^{L} S_{hx}^2 (Q_h)^{-1} \left(\Omega_h^{LA} - W_h \right)^2 \tag{16}$$

where Ω_h^{LA} are the calibrated weights and S_{hx}^2 is the mean square of auxiliary variable in hth stratum subject to the calibration constraint

$$\sum_{h=1}^{L} \Omega_h^{LA} \bar{x}_{1h} = \bar{X} \tag{17}$$

The calibrated weights and the estimator of (15) are obtained as show in (18) and (19) respectively.

$$\Omega_h^{LA} = W_h + \frac{\bar{x}_h Q_h \left(S_{hx}^2 \right)^{-1}}{\sum_{h=1}^{L} \bar{x}_h^2 Q_h \left(S_{hx}^2 \right)^{-1}} \left(\bar{X} - \sum_{h=1}^{L} W_h \bar{x}_h \right) \tag{18}$$

$$\bar{y}_{st}^{LA} = \sum_{h=1}^{L} W_h \bar{y}_h + \hat{\beta} \left(\bar{X} - \sum_{h=1}^{L} W_h \bar{x}_h \right) \tag{19}$$

where $\hat{\beta} = \dfrac{\sum_{h=1}^{L} \bar{x}_h \bar{y}_h Q_h \left(S_{hx}^2 \right)^{-1}}{\sum_{h=1}^{L} \bar{x}_h^2 Q_h \left(S_{hx}^2 \right)^{-1}}$

The variance of the calibrated estimator is given by

$$V\left(\bar{y}_{st}^{LA} \right) = \sum_{h=1}^{L} \Omega_h^{LA^2} \frac{(1 - f_h)}{n_h} s_{eh}^2 \tag{20}$$

where $s_{eh}^2 = (n_h - 1)^{-1} \sum_{i=1}^{nh} e_{hi}^2$ is the h^{th} strata sample mean square and $e_{hi} = (y_{hi} - \bar{y}_h) - \hat{\beta}(x_{hi} - \bar{x}_h)$.

[12] proposed a calibration estimator of the population mean in stratified sampling by introducing new calibration equations. [12] calibration estimator of the population mean $\bar{Y}$ under stratified sampling given by

$$\bar{y}_{st}(c) = \sum_{h=1}^{L} \Omega_h^C \bar{y}_h \tag{21}$$

where Ω_h^C is calibrated weight which is chosen such that the sum of the Chi-Square distance mean

$$\left.\begin{aligned} &\min Z = \sum_{h=1}^{L} \left(\Omega_h^C - W_h \right)^2 \Big/ Q_h W_h \\ &s.t. \quad \sum_{h=1}^{L} \Omega_h^S \bar{x}_h = \sum_{h=1}^{L} W_h \bar{X}_h \\ &\qquad \sum_{h=1}^{L} \Omega_h^C = 1 \end{aligned}\right\} \tag{22}$$

The calibrated weight and the estimator of (21) are obtained as show in (23) and (24) respectively

$$\Omega_h^C = W_h + \frac{\left(W_h Q_h \bar{x}_h\right)\left(\sum_{h=1}^{L} W_h Q_h\right) - \left(W_h Q_h\right)\left(\sum_{h=1}^{L} W_h Q_h \bar{x}_h\right)}{\left(\sum_{h=1}^{L} W_h Q_h\right)\left(\sum_{h=1}^{L} W_h Q_h \bar{x}_h^2\right) - \left(\sum_{h=1}^{L} W_h Q_h \bar{x}_h\right)^2}\left(\bar{X} - \sum_{h=1}^{L} W_h \bar{x}_h\right) \quad (23)$$

$$\bar{y}_{st}(c) = \sum_{h=1}^{L} W_h \bar{y}_h + \hat{\beta}_{st}\left(\bar{X} - \sum_{h=1}^{L} W_h \bar{x}_h\right) \quad (24)$$

where $\hat{\beta}_{st} = \dfrac{\left(\sum_{h=1}^{L} W_h Q_h \bar{x}_h \bar{y}_h\right)\left(\sum_{h=1}^{L} W_h Q_h\right) - \left(\sum_{h=1}^{L} W_h Q_h \bar{y}_h\right)\left(\sum_{h=1}^{L} W_h Q_h \bar{x}_h\right)}{\left(\sum_{h=1}^{L} W_h Q_h \bar{x}_h^2\right)\left(\sum_{h=1}^{L} W_h Q_h\right) - \left(\sum_{h=1}^{L} W_h Q_h \bar{x}_h\right)^2}$

The variance of [12] calibrated estimator is given by

$$V\left(\bar{y}_{st}(c)\right) = \sum_{h=1}^{L} \Omega_h^{C^2} \frac{\left(1 - f_h\right)}{n_h} s_{eh}^2 \quad (25)$$

where $s_{eh}^2 = \left(n_h - 1\right)^{-1} \sum_{i=1}^{nh} e_{hi}^2$ is the hth strata sample mean square and $e_{hi} = \left(y_{hi} - \bar{y}_h\right) - \hat{\beta}_{(ols)}\left(x_{hi} - \bar{x}_h\right)$

2. Methodology

2.1 Proposed Estimator

Having studied [12] calibration estimator, and motivated by his work. A new set of calibration estimators are proposed as:

$$\bar{y}_{st}(m) = \sum_{h=1}^{L} \Omega_h^M \bar{y}_h \quad (26)$$

$$\left.\begin{aligned} &\min Z^* = \sum_{h=1}^{L}\left(\Omega_h^M - W_h^*\right)^2 \Big/ Q_h W_h^* \\ &s.t. \quad \sum_{h=1}^{L} \Omega_h^M \bar{x}_h = \sum_{h=1}^{L} W_h^* \bar{X}_h \\ &\qquad \sum_{h=1}^{L} \Omega_h^M = \sum_{h=1}^{L} W_h^* \end{aligned}\right\} \quad (27)$$

where $W_h^* = W_h \bar{X} / \sum_{h=1}^{L} W_h \bar{x}_h$, Ω_h^M are the new calibrated weights and Q_h is a chosen weight that determine the form of the proposed estimators.

To derive new calibrated weights $\left(\Omega_h^M\right)$ of the proposed estimator $\left(\bar{y}_{st}(m)\right)$, the Lagrange Multiplier function L of $\bar{y}_{st}(m)$ is defined as:

$$L = \sum_{h=1}^{L}\left(\Omega_h^M - W_h^*\right)^2 \Big/ W_h^* Q_h - 2\lambda_1\left(\sum_{h=1}^{L} \Omega_h^M \bar{x}_h - \sum_{h=1}^{L} W_h^* \bar{X}\right) - 2\lambda_2\left(\sum_{h=1}^{L} \Omega_h^M - \sum_{h=1}^{L} W_h^*\right) \quad (28)$$

where λ_1 and λ_2 are Lagrange's multipliers, differentiate (28) with respect to Ω_{h2}, λ_1 and λ_2, then equate to zero to obtained (29), (30), and (31) as follows:

$$\Omega_h^M = W_h^* + \lambda_1 W_h^* Q_h \bar{x}_h + \lambda_2 W_h^* Q_h \bar{x}_h \quad (29)$$

$$\sum_{h=1}^{L}\Omega_h^M\bar{x}_h-\sum_{h=1}^{L}W_h^*\bar{X}_h=0 \tag{30}$$

$$\sum_{h=1}^{L}\Omega_h^M-\sum_{h=1}^{L}W_h^*=0 \tag{31}$$

Substituting (29) in (30), and (31), the results are obtaining as:

$$\lambda_1\sum_{h=1}^{L}W_h^*\Omega_h^M\bar{x}_h^2+\lambda_2\sum_{h=1}^{L}W_h^*\Omega_h^M\bar{x}_h=\sum_{h=1}^{L}W_h^*\bar{X}_h-\sum_{h=1}^{L}W_h^*\bar{x}_h \tag{32}$$

$$\lambda_1\sum_{h=1}^{L}W_h^*\Omega_h^M\bar{x}_h+\lambda_2\sum_{h=1}^{L}W_h^*\Omega_h^M=0 \tag{33}$$

Solve equations (32) and (33) simultaneously, the results are obtaining as:

$$\lambda_1=\frac{\left(\sum_{h=1}^{L}W_h^*\bar{X}_h-\sum_{h=1}^{L}W_h^*\bar{x}_h\right)\left(\sum_{h=1}^{L}W_h^*Q_h\right)}{\left(\sum_{h=1}^{L}W_h^*Q_h\bar{x}_h^2\right)\left(\sum_{h=1}^{L}W_h^*Q_h\right)-\left(\sum_{h=1}^{L}W_h^*Q_h\bar{x}_h\right)^2} \tag{34}$$

$$\lambda_2=\frac{-\left[\left(\sum_{h=1}^{L}W_h^*\bar{X}_h-\sum_{h=1}^{L}W_h^*\bar{x}_h\right)\left(\sum_{h=1}^{L}W_h^*Q_h\bar{x}_h\right)\right]}{\left(\sum_{h=1}^{L}W_h^*Q_h\bar{x}_h^2\right)\left(\sum_{h=1}^{L}W_h^*Q_h\right)-\left(\sum_{h=1}^{L}W_h^*Q_h\bar{x}_h\right)^2} \tag{35}$$

On substituting (34) and (35) in (29) the new calibrated weights can be written as:

$$\begin{aligned}\Omega_h^M=W_h^*+\left(W_h^*Q_h\bar{x}_h\right)&\frac{\left(\sum_{h=1}^{L}W_h^*\bar{X}_h-\sum_{h=1}^{L}W_h^*\bar{x}_h\right)\left(\sum_{h=1}^{L}W_h^*Q_h\right)}{\left(\sum_{h=1}^{L}W_h^*Q_h\bar{x}_h^2\right)\left(\sum_{h=1}^{L}W_h^*Q_h\right)-\left(\sum_{h=1}^{L}W_h^*Q_h\bar{x}_h\right)^2}\\-\left(W_h^*Q_h\bar{x}_h\right)&\frac{\left(\sum_{h=1}^{L}W_h^*\bar{X}_h-\sum_{h=1}^{L}W_h^*\bar{x}_h\right)\left(\sum_{h=1}^{L}W_h^*Q_h\bar{x}_h\right)}{\left(\sum_{h=1}^{L}W_h^*Q_h\bar{x}_h^2\right)\left(\sum_{h=1}^{L}W_h^*Q_h\right)-\left(\sum_{h=1}^{L}W_h^*Q_h\bar{x}_h\right)^2}\end{aligned} \tag{36}$$

Substituting (36) in (26) obtain the new combined calibration estimator $\left(\bar{y}_{st}(m)\right)$ as:

$$\bar{y}_{st}(m)=\sum_{h=1}^{L}W_h^*\bar{y}_h+\hat{\beta}_m\sum_{h=1}^{L}W_h^*\left(\bar{X}_h-\bar{x}_h\right) \tag{37}$$

Substituting $W_h^*=W_h\bar{X}\Big/\sum_{h=1}^{L}W_h\bar{x}_h$ in (37), gives

$$\bar{y}_{st}(m)=\bar{X}\left(\sum_{h=1}^{L}W_h\bar{y}\right)\left(\sum_{h=1}^{L}W_h\bar{x}_h\right)^{-1}+\hat{\beta}_m\bar{X}\left(\sum_{h=1}^{L}W_h\right)\left(\sum_{h=1}^{L}W_h\bar{x}_h\right)^{-1}\left(\bar{X}_h-\bar{x}_h\right) \tag{38}$$

where $\hat{\beta}_m=\dfrac{\left(\sum_{h=1}^{L}W_hQ_h\right)\left(\sum_{h=1}^{L}W_hQ_h\bar{x}_h\bar{y}_h\right)-\left(\sum_{h=1}^{L}W_hQ_h\bar{y}_h\right)\left(\sum_{h=1}^{L}W_hQ_h\bar{x}_h\right)}{\left(\sum_{h=1}^{L}W_hQ_h\bar{x}_h^2\right)\left(\sum_{h=1}^{L}W_hQ_h\right)-\left(\sum_{h=1}^{L}W_hQ_h\bar{x}_h\right)^2}$

By setting $Q_h=1$, and $Q_h=1/\bar{x}_h$, set of new estimators were obtained respectively as:

$$\bar{y}_{st}(m)_1 = \bar{X}\left(\sum_{h=1}^{L} W_h \bar{y}\right)\left(\sum_{h=1}^{L} W_h \bar{x}_h\right)^{-1} + \hat{\beta}_{m1}\bar{X}\left(\sum_{h=1}^{L} W_h\right)\left(\sum_{h=1}^{L} W_h \bar{x}_h\right)^{-1}\left(\bar{X}_h - \bar{x}_h\right) \quad (39)$$

$$\bar{y}_{st}(m)_2 = \bar{X}\left(\sum_{h=1}^{L} W_h \bar{y}\right)\left(\sum_{h=1}^{L} W_h \bar{x}_h\right)^{-1} + \hat{\beta}_{m2}\bar{X}\left(\sum_{h=1}^{L} W_h\right)\left(\sum_{h=1}^{L} W_h \bar{x}_h\right)^{-1}\left(\bar{X}_h - \bar{x}_h\right) \quad (40)$$

where $\hat{\beta}_{m1} = \dfrac{\left(\sum_{h=1}^{L} W_h \bar{x}_h \bar{y}_h\right) - \left(\sum_{h=1}^{L} W_h \bar{y}_h\right)\left(\sum_{h=1}^{L} W_h \bar{x}_h\right)}{\left(\sum_{h=1}^{L} W_h \bar{x}_h^2\right) - \left(\sum_{h=1}^{L} W_h \bar{x}_h\right)^2}$ and

$$\hat{\beta}_{m2} = \frac{\left(\sum_{h=1}^{L} W_h \bar{x}_h^{-1}\right)\left(\sum_{h=1}^{L} W_h \bar{y}_h\right) - \left(\sum_{h=1}^{L} W_h \bar{x}_h^{-1}\bar{y}_h\right)\left(\sum_{h=1}^{L} W_h\right)}{\left(\sum_{h=1}^{L} W_h \bar{x}_h\right)\left(\sum_{h=1}^{L} W_h \bar{x}_h^{-1}\right) - \left(\sum_{h=1}^{L} W_h\right)^2}$$

Hence, the variance of the proposed estimator is:

$$Variance\left(\bar{y}_{st}(m)\right) = \sum_{h=1}^{L} \Omega_h^{M^2}\left(\frac{1-f_h}{n_h}\right)s_{eh}^2 \quad (41)$$

where $s_{eh}^2 = \dfrac{1}{n_h - 1}\sum_{i=1}^{n_h} e_{ih}^2$ is the hth strata sample mean square and $e_{ih} = \left(y_{hi} - \bar{y}_h\right) - \left(\hat{R} + \hat{\beta}_m\right)\left(x_{hi} - \bar{x}_h\right)$

3.1 Simulation Study

Simulation study is carried out to assess the performance and the efficiency of the proposed combined calibration estimators with other existing calibration estimators. Data of size 1000 units were generated for study Populations stratified into 3 non-overlapping heterogeneous groups as 200, 300 and 500 using function defined in Table 1. Samples of sizes 20, 30 and 50 were selected 10,000 times by method SRSWOR from each stratum respectively. Mean square error (MSE) of the considered estimators were computed as:

$$MSE\left(\bar{y}_{sti}\right) = \frac{1}{10000}\sum_{j=1}^{10000}\left(\bar{y}_{sti} - \bar{Y}\right)^2,\ \bar{y}_{sti} = \bar{y}_{st}(m)_i, and\ \bar{y}_{st}(c)_i,\ i = 1, 2. \quad (42)$$

3. Results and Discussion

Table 1: Populations Used for Empirical Study

Population	**Auxiliary variable** x	**Study variable** y
I	$x_h \approx \text{chisq}\left(\theta_h\right), \theta_1 = 5, \theta_2 = 6,$ $\theta_3 = 4, h = 1, 2, 3$	$y_{hi} = \alpha_h x_{hi}^j + \xi_{hi},\ \alpha_{1h} = E\left(x_h\right),\ j = 2, 3, 4$ $\alpha = 0.5,\ \xi_h \approx N\left(0, 1\right), h = 1, 2, 3$
II	$x_h \approx gamma\left(\theta_h, \eta_h\right), \theta_1 = 3, \eta_1 = 2,$ $\theta_2 = 3, \eta_2 = 1, \theta_3 = 3, \eta_3 = 3,$	

Different distributions with their parameters of the auxiliary and study variables

Table 2: MSE of Some Existing and Proposed Estimator Using Population I

Model I: $y_{hi} = \alpha_h x_{hi}^2 + \xi_{hi}$	
Estimator	**MSE**
Stratified Mean $\bar{y}_{st}$	0.75583

Combined Ratio $\bar{y}_{st}^{RC}$	0.2657842
[12] $\bar{y}_{st}(c)_1$	0.1734461
[12] $\bar{y}_{st}(c)_2$	0.1769351
Proposed Estimator $\bar{y}_{st}(m)_1$	0.1769035
Proposed Estimator $\bar{y}_{st}(m)_2$	0.1724445
Model II: $y_{hi} = \alpha_h x_{hi}^3 + \xi_{hi}$	
Estimator	**MSE**
Stratified Mean $\bar{y}_{st}$	76.43739
Combined Ratio $\bar{y}_{st}^{RC}$	47.38096
[12] $\bar{y}_{st}(c)_1$	37.46485
[12] $\bar{y}_{st}(c)_2$	37.93442
Proposed Estimator $\bar{y}_{st}(m)_1$	31.56949
Proposed Estimator $\bar{y}_{st}(m)_2$	31.41492
Model III: $y_{hi} = \alpha_h x_{hi}^4 + \xi_{hi}$	
Estimator	**MSE**
Stratified Mean $\bar{y}_{st}$	10101.63
Combined Ratio $\bar{y}_{st}^{RC}$	7747.475
[12] $\bar{y}_{st}(c)_1$	6653.738
[12] $\bar{y}_{st}(c)_2$	6713.285
Proposed Estimator $\bar{y}_{st}(m)_1$	6087.004
Proposed Estimator $\bar{y}_{st}(m)_2$	6073.968

Table 2 shows Mean Square Errors (MSE) of the proposed and some existing estimators using Population I. The result revealed that the proposed estimators have least MSE compared to the existing estimators under stratified random sampling. This implies that the proposed estimators are proficient and more efficient than stratified sample mean, combined ratio estimator.

Table 3: MSE of Some Existing and Proposed Estimators Using Population II

Model I: $y_{hi} = \alpha_h x_{hi}^2 + \xi_{hi}$	
Estimator	**MSE**
Stratified Mean $\bar{y}_{st}$	0.1533715
Combined Ratio $\bar{y}_{st}^{RC}$	0.07184717
[12] $\bar{y}_{st}(c)_1$	0.0367516
[12] $\bar{y}_{st}(c)_2$	0.03768872
Proposed Estimator $\bar{y}_{st}(m)_1$	0.03864333
Proposed Estimator $\bar{y}_{st}(m)_2$	0.0376159
Model II: $y_{hi} = \alpha_h x_{hi}^3 + \xi_{hi}$	
Estimator	**MSE**
Stratified Mean $\bar{y}_{st}$	8.590126

Combined Ratio $\bar{y}_{st}^{RC}$	6.034635
[12] (2017) $\bar{y}_{st}(c)_1$	3.907282
[12] $\bar{y}_{st}(c)_2$	3.987594
Proposed Estimator $\bar{y}_{st}(m)_1$	3.385937
Proposed Estimator $\bar{y}_{st}(m)_2$	3.400304
Model III: $y_{hi} = \alpha_h x_{hi}^4 + \xi_{hi}$	
Estimator	**MSE**
Stratified Mean $\bar{y}_{st}$	589.8373
Combined Ratio $\bar{y}_{st}^{RC}$	478.693
[12] $\bar{y}_{st}(c)_1$	361.0893
[12] $\bar{y}_{st}(c)_2$	366.8283
Proposed Estimator $\bar{y}_{st}(m)_1$	329.5701
Proposed Estimator $\bar{y}_{st}(m)_2$	332.2734

Table 3 shows Mean Square Errors (MSE) of the proposed and some existing estimators using Population II. The result revealed that the proposed estimators have least MSE compared to the existing estimators under stratified random sampling. This implies that the proposed estimators are proficient and more efficient than stratified sample mean, combined ratio estimator and [12].
Tables 2 and 3 show the Mean Square Error (MSE) of the proposed combined calibration estimators and other estimators using simulated data. The results revealed that the proposed combined calibration estimators have minimum MSE compared to the traditional estimators and other estimators considered under stratified random sampling.

4. Conclusion

The In this paper, dimensional analysis was applied to develop an empirical model for the energy density of lithium ion battery. Result showed that the energy density of the lithium battery is significantly dependent on the elastic property of the material i.e the specific modulus. Hence improving the actual energy density is possible with materials having very low energy density, high compressibility and high young modulus. Result also showed that increasing the specific modulus will not only significantly improve the energy density but also increase the mechanical durability of the lithium ion battery. Hence in order to create a significant breakthrough, it is suggested that research should focus more on the elastic property of the electrode material.

In this paper, new calibration combined stratified ratio estimators for estimating population mean proposed with two set of constraints which minimized a given chi-squared distance measure and new calibration weights are developed. The simulation study showed that the proposed calibration combined ratio estimators performed (having least MSE) better than other estimators considered in the study. In conclusion, the proposed calibration combined ratio estimators give better estimate for the population mean of the study variable and more efficient that usual traditional estimator, combined ratio estimator and [12] estimators.

Nomenclature

N	Total Population size,
n	Sample size where
y_h	Study variable
x_h	Auxiliary variable
W_h	Strata weights

References

[1] J.C Deville and C.E Särndal (1992). Calibration Estimators in Survey Sampling. J. Amer. Statist. Assoc. Vol. 87, pp.376–382
[2] S. Singh, S. Horn and F. Yu (1998). Estimation Variance of General Regression Estimator: Higher Level Calibration Approach. Survey Methodology. Vol. 48, pp.41-50.
[3] S. Singh (2003). Advanced Sampling Theory with Applications. Dordrecht: Kluwer Academic Publishers.
[4] D.S Tracy, S. Singh and R. Arnab (2003). Note on Calibration in Stratified and Double Sampling, Survey Methodology. Vol.29, pp.99–104.
[5] J.M Kim, E.A Sungur and T.Y Heo (2007). Calibration Approach Estimators in Stratified Sampling. Statistics and Probability Letters. Vol.77(1), pp.99 – 103.
[6] E.P Clement and E.I Enang (2015). Calibration Approach Alternative Ratio Estimator for Population Mean in Stratified Sampling. International Journal of Statistics and Economics, Vol.16(1), pp.83-93.
[7] N. Ozgul (2018a). New Calibration Estimator in Stratified Sampling. Journal of Statistical and Simulation, Vol. 88(13), pp.2561-2572.
[8] D. Rao, M.G.M Khan and S. Khan (2012). Mathematical Programming on Multivariate Calibration Estimation in Stratified Sampling. World Academy of Science, Engineering and Technology International Journal of Mathematical, Computational, Physical, Electrical and Computer Engineering. Vol.6(12), pp.1623-1627.
[9] N. Koyuncu and C. Kadilar (2016). Calibration Weighting in Stratified Random Sampling. Communications in Statistics- Simulation and Computation. Vol.45, pp.2267-2275.
[10] N. Koyuncu and C. Kadilar (2013). Calibration Estimators Using Different Distance Measures in Stratified Random Sampling. International Journal of Modern Engineering Research. Vol.3(1), pp.415-419.
[11] E.P Clement (2015). Calibration Approach Separate Ratio Estimator for Population Mean in Stratified Sampling. International Journal of Modern Mathematical Sciences. Vol.13(4), pp.377-384
[12] B.V.S Nidhi, S.S Singh and S.K Singh (2017). Calibration Approach Estimation of the Mean in Stratified Sampling and Stratified Double Sampling, Communications in Statistics - Theory and Methods. Vol.46(10), pp.4932-4942.
[13] N. Ozgul (2018b). New Calibration Estimator Based On Two Auxiliary Variables in Stratified Sampling. Communications in Statistics—Theory and Methods. Vol.0, pp.1-12.
[14] N. Garg and M. Pachori (2019). Use of Coefficient of Variation in Calibration Estimation of Population Mean in Stratified Sampling, Communications in Statistics - Theory and Methods. Vol.0, pp.1 – 11.
[15] W.G Cochran (1977). Sampling Techniques. Third Edition. John Wiley and Sons Limited.
[16] M.H Hansen, W.N Hurwitz and M. Gurney (1946). The Problems and Methods of the Sample survey of business, Journal of the American Statistical Association. Vol.41, pp.173-189.
[17] A.S Lata, D.K Rao and M.G.M Khan (2017). Calibration Estimation Using Proposed Distance Function. 4th Asia-Pacific World Congress on Computer Science and Engineering, pp.162-166.

NIPES Conference Proceedings
The 1st International Conference of the Nigerian Institution of Professional Engineers and Scientists 7th-8th Oct. 2021: 20-28
www.nipesjournals.org.ng

Application of Machine Learning to Facies Classification from Well Logs

Tahiru I.T[b], Otobo S.A[b], Maju-Oyovwikowke G.E[c]

[a]Physics Department, University of Benin, Benin City, Nigeria.
[b]Department of Geology, Niger-Delta University, Ammasoma, Bayelsa.
[c]Department of Geology, University of Benin, Benin City, Nigeria.

Abstract

Facies otherwise known as lithofacies are mappable subdivision of a stratigraphic unit that can be distinguished by its lithology (texture, mineralogy, grain size and depositional environment that produced it). The classification of lithofacies is crucial in seismic interpretation because different rocks have different permeability and fluid saturation for a given porosity. The usual sources for lithofacies classification are core samples of rocks extracted from wells. However, due to cost implications, it is usually difficult to obtain core samples at every location of the well. Thus, it is imperative to develop a method of classifying facies from indirect measurements such as from well logs. This will allow facies classification to be carried out by assigning a rock type or class to a specific sample on the basis of measured features. In this work, machine learning, a branch of artificial intelligence was employed to carry out this classification. Several machine learning algorithms were tested on well logs in order to determine how best to employ machine learning to classify lithofacies based on the measurement of wireline logs. Each algorithm was assessed based on the performance metrics and it was observed that the random forest algorithm performed best. Consequently, this algorithm was used to build the final model and tested on a blind well. The results obtained was very satisfactory. Hence, machine learning can be a veritable tool that can replace the costly core sample retrieval and measurement for mapping stratigraphic unit.

***Keywords*:**
Machine Learning, Lithofacies,Well logs.

1. Introduction

Facies are mappable subdivision of a stratigraphic unit that can be distinguished by its lithology (texture, mineralogy, grain size and depositional environment that produced it) [1]. The physical and organic characteristics found in rock units usually provide some insight into the different process and systems which may have occurred in the region. When several facies are combined with physical models and other geologic data, this can help provide informative low-dimensional models of the geologic region. Facies can be of different types including sedimentary facies, lithofacies, seismic facies, etc.

The classification of lithofacies is crucial in seismic interpretation because different rocks have different permeability and fluid saturation for a given porosity [2]. The main sources of data for subsurface study usually comes from variety of sources most especially those involving drilling. The ideal source of data for facies classification is the core samples obtained from drilled wells which gives us direct assessment of the sedimentary structure. The problem with this is that it is usually very costly to obtain cores from every level of the well and thus, this is not usually a feasible option to many cases.

Machine Learning is very good at helping large amounts of data simultaneously. It can help in determining relationships between several types of data at once. It can also help discover nonlinearities in the law of the solutions that we have in interpretation processes [5]. We often make the assumption that some elements of the Earth are linear, while in its real sense, they are non-linear. Ultimately, machine learning can help to improve efficiency and accuracy over time and we will be able to automate interpretive processes. This will help geoscientists to be more effective and efficient. Machine Learning helps to reveal trends, geological features or properties in our data. Ordinarily, most of these are difficult to be seen with conventional approaches [6]. This will ultimately reduce risks in drilling for oil and gas.

This study is aimed at providing an alternative means to achieve facies classification with the use of wireline logs which involves the process of lowering instruments into a borehole and recording measurements that detail the physical characteristics of the surrounding rock and fluid depth.

Figure 1: Photographed slabbed core layout in the core shed at SPDC [3]

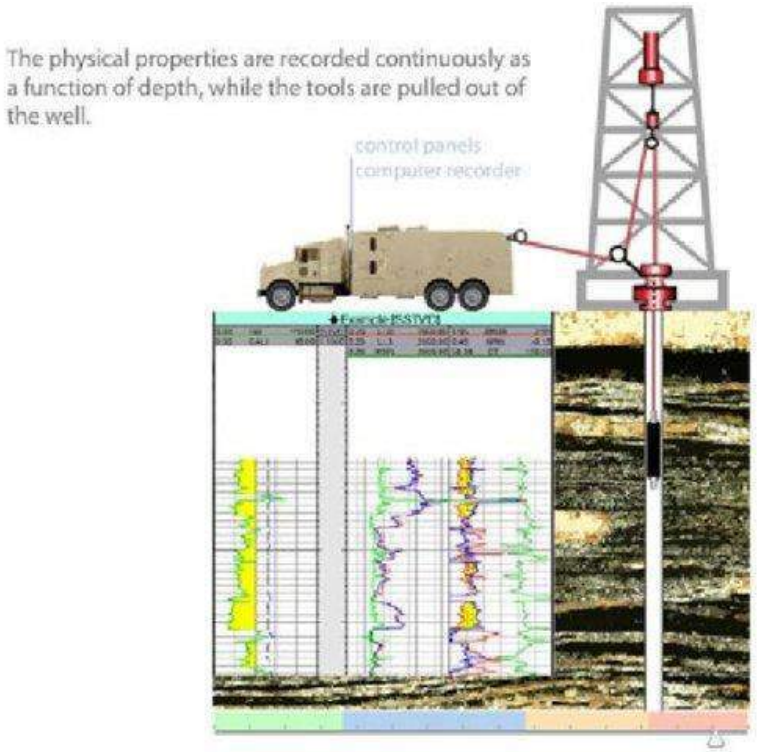

Figure 2: Well logging [4]

2. Materials and Methods

Available for this work are datasets from six (6) wells drilled in the X-field in the North Sea. The well logging datasets include gamma ray log (GR*) which* measures natural formation radioactivity, resistivity log (RT) *which* measures the subsurface ability to impede the flow of electric current, density log (RHOB), Neutron-density porosity difference *and* average neutron-density porosity which are measurements correlated to facies density, Photoelectric effect measures electrons emission of a facies illuminated by light rays, Nonmarine/marine indicator *which* is a binary flag

attributed by experts to distinguish between marine and on marine facies upon data inspection, and Relative position which is the integer index of each layer depth starting from 1 for the top layer, and increasing with depth. All six (6) except two (2) of the wells missing the facies logs have full suites of well logs. Figure 1 shows the variation of logs in well SHRIMPLIN. The statistical properties of the dataset also are shown in Table1.

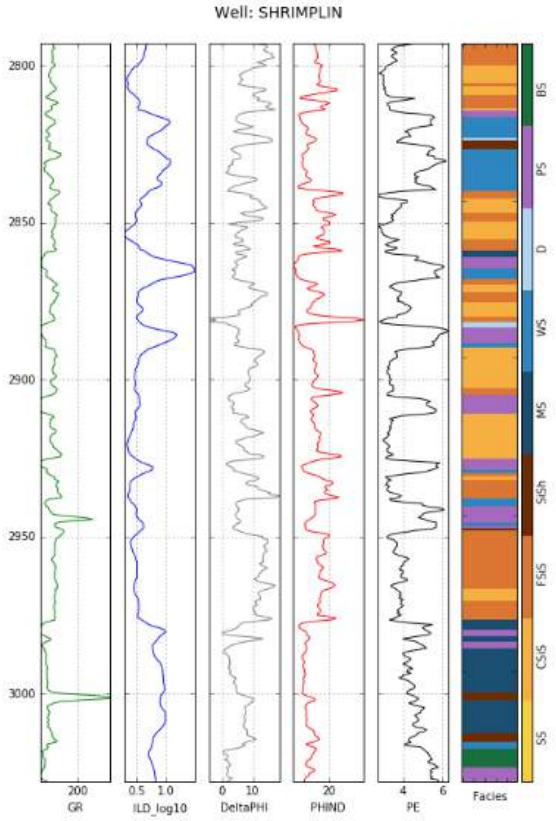

Figure 3: Visualization of well logs showing facies in different colors

The nine discrete facies (classes of rocks) identified for the field of study are:

1. Nonmarine sandstone
2. Nonmarine coarse siltstone
3. Nonmarine fine siltstone
4. Marine siltstone and shale
5. Mudstone (limestone)
6. Wackestone (limestone)
7. Dolomite
8. Packstone-grainstone (limestone)
9. Phylloid-algal bafflestone (limestone)

Table1: Descriptive Statistics of Training Data

	Facies	**Depth**	**GR**	**ILD_Log**	**DeltaPhi**	**PHIN**	**PE**	**NM_M**	**RELPOS**
Count	3232	3232	3232	3232	3232	3232	3232	3232	3232

Mean	4.42	2875.82	66.14	0.64	3.56	13.48	3.73	1.50	0.52
Std	2.50	131.01	30.85	0.24	5.23	7.70	0.90	0.50	0.29
Min	1.00	2573.50	13.25	-0.03	-21.83	0.55	0.20	1.00	0.010
Max	9.00	3122.50	381.15	1.48	18.60	84.40	8.09	2.00	1.00

The distribution of these facies to be used to train the predictive model is given in table 2 below.

Table 2: Distribution of Training Data

S/N	Facies	Distribution
1	Nonmarine sandstone	170
2	Nonmarine coarse siltstone	649
3	Nonmarine fine siltstone	498
4	Marine siltstone and shale	177
5	Mudstone (limestone)	198
6	Wackestone (limestone)	391
7	Dolomite	81
8	Packstone-grainstone (limestone)	458
9	Phylloid-algal bafflestone (limestone)	161

It can be seen that some facies (facies 7: Dolomite) has very low examples. This is usually a problem for classifiers to correctly predict classes with fewer representation [7].

The first step for the predictive model building involves preprocessing of the data. This process involves missing data and outlier detection. In cases where there are missing data or outliers, it is usual practice in machine learning to remove the entire sample comprising the missing data and outliers or the missing values are filled by average values [8]. One way to effectively determine such error prone data is by looking at the descriptive statistics of the dataset as shown in table 1 above.

The table shows that no missing data are found in the dataset with the counts of all the feature being the same (3232). Also, by examining other statistical values such as mean and standard deviations, this is indicative that the data are in good conditions. The well logs have been environmentally corrected.

The next important step is to analyze the features that will be useful for the building of the predictive model. It is important to filter out features that are not useful for the creation of the model. This can be achieved by assessing the correlation coefficient of the features against each other (Figure 4). Those that are highly correlated will have to be filtered out by selecting either of the two variables. This will allow a less complex model to be achieved.

It can be seen in figure 4 above that all features weakly correlated with each other, thus all available features will be useful as input parameters for the model.

The machine learning algorithms used in this work were implemented in PYTHON's scikit-learn library. The model algorithms include Linear Regression, Decision Tree, Support Vector Machine, Random Forest, Gradient Boosting and Multilayer Perceptron. Several parameters are needed to be correctly selected to achieve better generalizability of each of the models.

To assess which of the model gave better result, a model validation was carried out for each of the algorithms using a 10-fold cross validation (CV) frequently used approach in model validation [9]. This involves partitioning the datasets into 10 equally size folds. Nine of the fold is used as training

set for the model building while the remaining one-fold was used as testing dataset to evaluate the prediction.

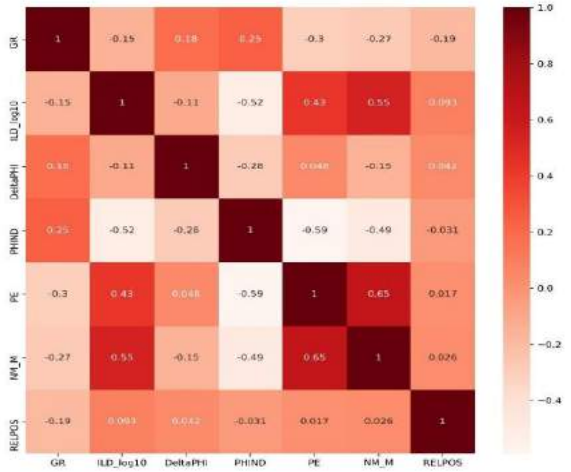

Figure 4: Correlation coefficient of features

A way used to ascertain which of the models gave best result is by measuring the performance of each of the models using the metric performance, the confusion matrix as in Table 3. The confusion matrix is a summary of prediction results on a classification problem. This gives insight not only into the errors being made by the classifier but the types of error that are being made. From these the classification accuracy can be measure as True Positive + True Negative.

Table 3: Confusion Matrix

	PREDICTED CLASS A	**PREDICTED CLASS B**
ACTUAL CLASS A	TRUE POSITIVE	FALSE NEGATIVE
ACTUAL CLASS B	FALSE NEGATIVE	TRUE NEGATIVE

3. Results and Discussion

Tables 4 to 10 shows the confusion matrix used to assess the performance of the six machine learning algorithms tested for the facies classification task.

Table 4: Linear Regression Confusion Matrix

Predicted/ Actual	**SS**	**SCiS**	**FSiS**	**SiSh**	**MS**	**WS**	**D**	**PS**	**BS**	**TOTAL**
SS	23	11	0	0	0	0	0	0	0	34
SCiS	6	38	22	0	0	0	1	1	0	68
FSiS	5	16	25	0	0	1	0	0	0	47
SiSh	0	0	0	8	0	7	0	0	1	16
MS	0	0	0	3	1	15	1	1	0	21

WS	0	0	0	3	0	25	1	2	1	32
D	0	0	0	0	0	1	7	2	0	10
PS	0	0	0	0	1	13	0	19	5	38
BS	0	0	0	0	0	1	0	3	12	16
F1 - Score	0.68	0.57	0.53	0.53	0.09	0.53	0.70	0.58	0.69	282

Table 5: Decision Tree Confusion Matrix

Predicted/ Actual	**SS**	**SCiS**	**FSiS**	**SiSh**	**MS**	**WS**	**D**	**PS**	**BS**	**TOTAL**
SS	23	10	1	0	0	0	0	0	0	34
SCiS	3	48	15	0	1	0	0	1	0	68
FSiS	1	14	30	0	0	1	0	1	0	47
SiSh	0	0	0	14	0	2	0	0	1	16
MS	0	0	0	3	10	5	0	3	0	21
WS	0	0	0	2	2	22	1	4	1	32
D	0	0	0	1	0	0	6	3	0	10
PS	0	0	0	2	6	4	0	23	3	38
BS	0	0	0	0	0	1	0	1	14	16
F1-Score	0.75	0.61	0.65	0.74	0.50	0.66	0.71	0.62	0.82	282

Table 6: Support Vector Machine Confusion Matrix

Predicted/ Actual	**SS**	**SCiS**	**FSiS**	**SiSh**	**MS**	**WS**	**D**	**PS**	**BS**	**TOTAL**
SS	21	12	1	0	0	0	0	0	0	34
SCiS	2	45	20	0	0	0	0	1	0	68
FSiS	3	11	32	0	0	1	0	0	0	47
SiSh	0	0	0	8	0	7	0	1	0	16
MS	0	0	0	1	0	15	1	4	0	21
WS	0	0	0	0	0	26	0	5	1	32
D	0	0	0	0	0	1	7	2	0	10
PS	0	0	0	1	0	7	0	28	3	38
BS	0	0	0	0	0	0	0	4	14	16
F1-Score	0.70	0.66	0.64	0.62	0.00	0.58	0.78	0.67	0.77	282

Table 7: Random Forest Confusion Matrix

Predicted/ Actual	**SS**	**SCiS**	**FSiS**	**SiSh**	**MS**	**WS**	**D**	**PS**	**BS**	**TOTAL**
SS	27	7	1	0	0	0	0	0	0	34
SCiS	2	46	19	0	0	0	0	1	0	68
FSiS	0	8	38	0	0	1	0	0	0	47
SiSh	0	0	0	10	0	4	0	1	0	16
MS	0	0	0	3	11	5	0	2	0	21
WS	0	0	0	1	1	27	1	0	2	32

D	0	0	0	0	0	0	6	4	0	10
PS	0	0	0	1	1	1	0	34	1	38
BS	0	0	0	0	0	0	0	1	15	16
F1-Score	0.86	0.71	0.73	0.65	0.61	0.77	0.71	0.84	0.91	282

Table 8: Gradient Boosting Confusion Matrix

Predicted/ Actual	**SS**	**SCiS**	**FSiS**	**SiSh**	**MS**	**WS**	**D**	**PS**	**BS**	**TOTAL**
SS	22	12	1	0	0	0	0	0	0	34
SCiS	1	45	21	0	0	0	0	1	0	68
FSiS	1	10	35	0	0	0	0	1	0	47
SiSh	0	0	0	10	0	5	0	1	0	16
MS	0	0	0	1	9	6	1	4	0	21
WS	0	0	0	2	0	27	0	2	1	32
D	0	0	0	0	0	1	6	3	0	10
PS	0	0	0	2	0	4	0	30	2	38
BS	0	0	0	0	0	0	0	0	16	16
F1-Score	0.76	0.67	0.68	0.65	0.60	0.72	0.71	0.75	0.91	282

Table 9: MultiLayer Perceptron Confusion Matrix

Predicted/ Actual	**SS**	**SCiS**	**FSiS**	**SiSh**	**MS**	**WS**	**D**	**PS**	**BS**	**TOTAL**
SS	23	10	1	0	0	0	0	0	0	34
SCiS	3	43	21	0	0	0	0	1	0	68
FSiS	4	5	36	0	0	0	0	2	0	47
SiSh	0	0	0	11	1	3	0	1	0	16
MS	0	0	0	4	6	6	1	4	0	21
WS	0	0	0	2	0	26	0	3	1	32
D	0	0	0	0	0	2	7	1	0	10
PS	0	0	0	1	0	9	0	25	3	38
BS	0	0	0	0	0	0	0	3	13	16
F1-Score	0.72	0.68	0.69	0.69	0.40	0.67	0.78	0.64	0.79	282

The classification accuracy is presented in table 10 below.

Table 10: Classification accuracy of the different machine learning algorithm

Algorithm	Accuracy
Linear Regression Classifier	0.56
Decision Tree	0.67
Support Vector Machine	0.64
Random Forest	**0.75**
Gradient Boosting	0.71
Multilayer Perceptron	0.67

From the results presented by the confusion matrix, it can be seen that it is possible to notice that some facies are actually easier to classify than others. This is because some facies are represented many more times than others, thus making the classification problem strongly unbalanced [7].

By comparing the results of all the algorithms that were tested, the random forest algorithm performed best, thus adopted for the creation of our predictive model. The performance in terms of the F1-score and classification accuracy gave values 0.75 and 0.75 respectively higher than the other five results.

After building the facies classification model adopting the random forest algorithm, the model was tested on a blind well to assess it performance qualitatively. The result is shown in figure below and it is very satisfactory.

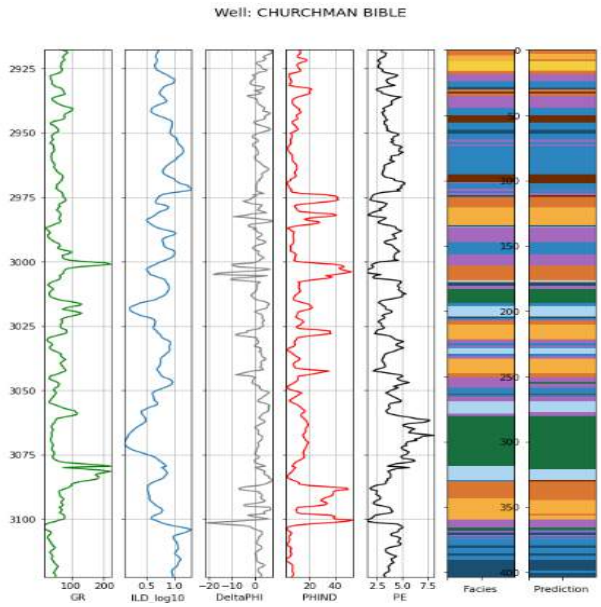

Figure 5: Comparison of Actual facies and Predicted facies for Test well data

Satisfied with the performance of the model, it was deployed to predictive the missing facies for two other wells. Figure show the result of this prediction.

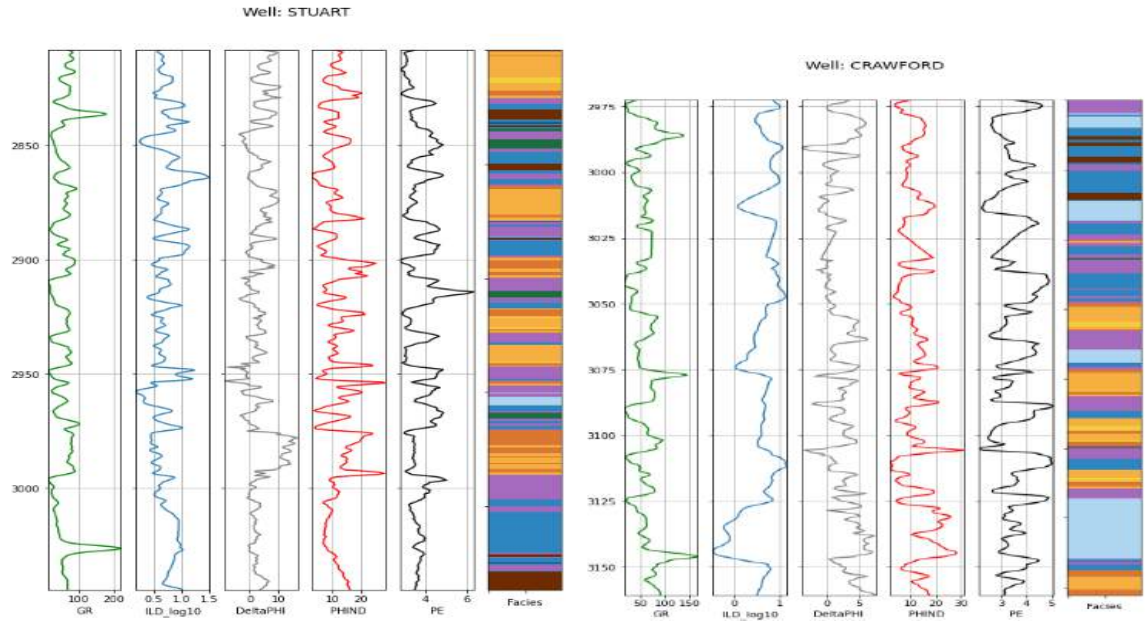

Figure 7: Prediction of facies for well data without values. a: Well Stuart, b: Well Crawford

4. Conclusion

We have been able to demonstrate in this work that it is possible to utilize machine learning algorithms in classifying facies so as to aid geological and geophysical data interpretation. We proposed that the Random Forest classifier be employed to build the predictive model for facies classification as it shows better results as compared with others. Moreover, there with the advent of deep neural network, there is prospect of having much better result when these networks are employed.

References

[1] Cross T.A., Homewood, P.W. (1997). Amanz Gressly's role in founding modern stratigraphy. Geological Society of America Bulletin. Geological Society of America. 109 (12): 1617-1630.

[2] Hall, B., 2016, Facies classification using machine learning: The Leading Edge, **35**, 906–909, https://doi.org/10.1190/tle35100906.1.

[3] Maju-Oyovwikowhe,.G. E 2019. PhD Thesis, Department of Geology, University of Benin.

[4] Reem S. M, 2018. Well logging Analyzing in Misan Province South of Iraq with Estimation of Logging Expenses, Jour of Adv Research in Dynamical & Control Systems, Vol. 10, No. 11 pp 361-370

[5] Bishop, C. M., 2006, Pattern recognition and machine learning (information science and statistics): Springer-Verlag New York, Inc.

[6] Kobrunov, A., and I. Priezzhev, 2016, Hybrid combination genetic algorithm and controlled gradient method to train a neural network: Geophysics, *81*, no. 4, IM35–IM43, https://doi.org/10.1190/geo2015-0297.1.

[7] Cao, J., Shi, Y., Wang, D. and Zhang, X., 2017, Acoustic Log Prediction on the Basis of Kernel Extreme Learning Machine for Wells in GJH Survey, Erdos Basin: Journal of Electrical and Computer Engineering, 2017.

[8] Menold, P.H., Pearson, R.K. and Allgower, F., 1999, Online outlier detection and removal: Presented at MED conference, MED99.

[9] Cruz, J.A. and Wishart, D.S., 2006, Application of Machine Learning in Cancer Prediction and Prognosis: Cancer Informatics, **2** 59 - 78.

NIPES Conference Proceedings
The 1st International Conference of the Nigerian Institution of Professional Engineers and Scientists 7th-8th Oct. 2021: 29-35
www.nipesjournals.org.ng

Prospects of Green Fuel to the Management of Wastes in Nigeria

Toyese Oyegoke* and John E. Oguche

Ahmadu Bello University, Faculty of Engineering. Chemical Engineering Dept., Samaru Campus, Zaria 234, Nigeria.
**Corresponding Email:* OyegeokeToyese@gmail.com

Abstract

With the rising rate of greenhouse gas emissions observed due to the use of fossil fuels and the global demand of the world to reduce the level of dependency on the use of crude oil-based products, science and industries across the globe are not significantly giving greater attention to the use of bio-based materials. Many advanced countries are already investing a lot in this aspect of science; many developing nations, including Nigeria, are yet to follow suit. In addition, waste management in Nigeria has long received poor attention from the government and its residents. Potentials that the wastes, including municipal, domestic, and industrial wastes, would continue to rise. The need to consider the engagement of the waste-to-wealth approach where the wastes, in this case, could be transformed into green fuels like bioethanol, biodiesel, biogas, and a lot more. As a way of unfolding details on the potentials that it has to offer for the development of the rising nations like ours, this report tends to provide highlights on the concept of green sciences, benefits it tends to offer, recent advances reported so far on the subject and possible recommendations on areas that required the attention of our academia. Efforts should be put in place to promote the development and commercialization of local technologies which are eco-friendly, sustainable, and renewable.

Keywords
Wastes Management, Biomass, Biofuels, Biorefinery, Greenhouse Gas, Renewable Fuel

1. Introduction

The waste deposit around our communities is significantly rising annually, and persistent poor government attention to waste management in developing nations like Nigeria. These waste deposits are composed of domestic wastes from our various homes in the form of waste food and many other disposed materials. Other classes of these wastes are municipal wastes, industrial wastes, and agricultural wastes, which entails substances like sugarcane bagasse, sorghum bagasse, rice husk, maize cob, cassava peels, plant stalks, leaves, and a lot more [1]–[4]. Most of which is managed mainly via the burning of substances, which contributes to the generation of greenhouse gases (GHG) which contributes to global warming. A picture of some selected cities' waste dumpsites is presented in Figure 1, showing the unfriendly situation of the dumpsites widely spread across our communities.

The current dependence of our nation on fossil fuels as the primary source of fueling our power generating sets and automobiles has also become a serious subject of concern even as the world is promoting the campaign for the adoption of green fuels over fossil fuels. It is crucial to consider the use of green fuels like bioethanol, biodiesel, biomethane, biohydrogen, and a lot more as complementary or substitute fuel to the current use of fossil fuels like petrol, petro-diesel, kerosine, and many others[5]–[8].

With the understanding of the potentials of transforming our vast wastes, which in the present state are not adequately managed, the promotion of green fuels usage in developing nations like Nigeria can go a long way to promote effective management of waste via the use of waste-to-wealth approach where the wastes aforementioned could be subjected to transformation processes to them converted into different classes of green fuels especially in the Northern Nigeria where vast land and green environment is mainly available for the establishment of the biorefineries.

(a) Ijagun dumpsite in Ogun state[2]

(b) Port Harcourt City [1]

(c) Lagos Dumpsite [4]

(d) Nyanya-Karu-Jikwoyi Road Dumpsite in Abuja [3]

Figure 1. View (a-d) of different dumpsites in some Nigerian cities.

This report seeks to unfold the prospect of the fuels to effectively manage our waste in Nigeria by promoting and adopting green fuels and establishing biorefineries in Nigeria.

2 Overview of Waste, Green Fuels and their Relationship

In presenting this concept of green fuels as a way to better manage our waste via the consideration of transforming them into valuable materials like green fuels and summarized for the survey, a framework is presented in Figures 2 to 4.

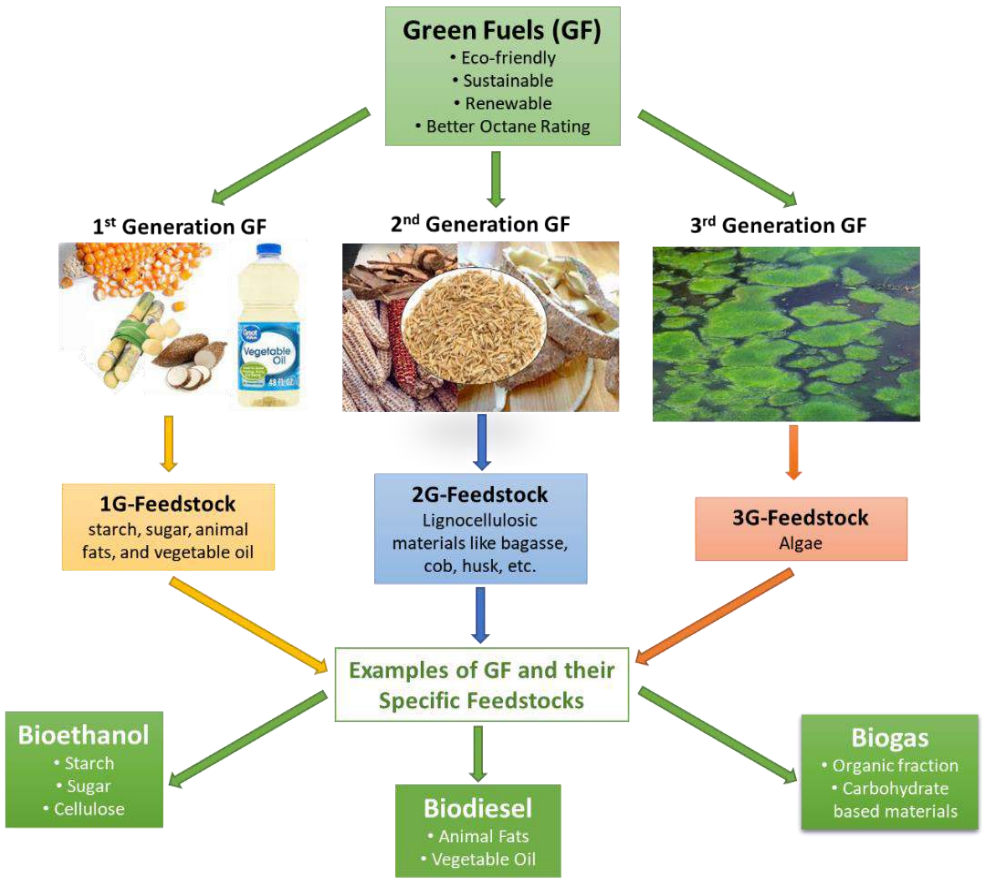

Figure 2. Framework showing the survey of green fuel (GF): Generations, Feedstock and Examples of GFs.

Literature was surveyed to properly present the green fuel concept, classes, and potential feedstocks for their production. Alongside, the wastes often collected in Nigeria were surveyed were equally presented, showing their classes. A different way into how each class of wastes [9], [10] could be transformed into a particular class of green fuel was presented, as shown diagrammatically in Figure 2.

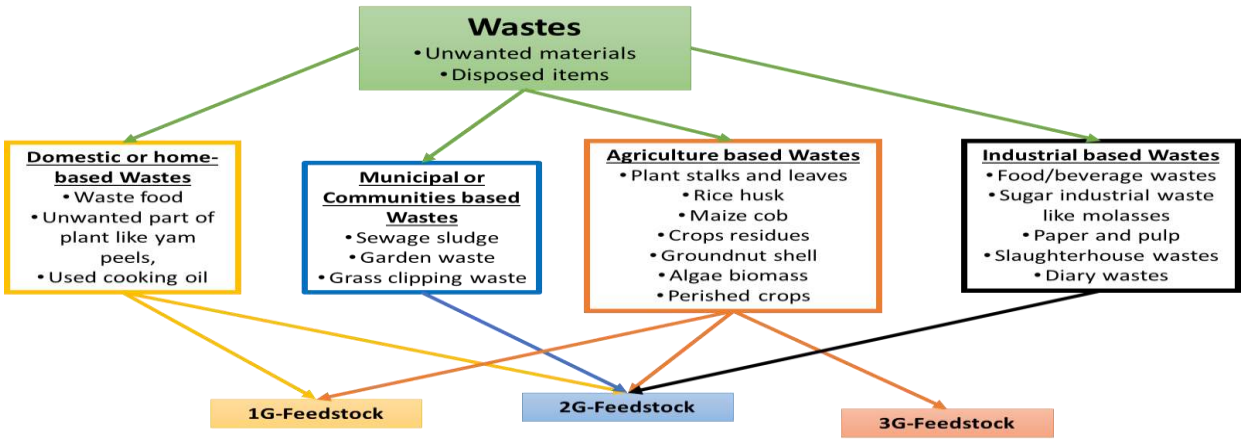

Figure 3. Wastes (biomass) classification and the green fuels feedstock class are associated with each waste category

Figure 2 presents the large concept and structures of green fuels. Figure 3 presents the classes of wastes collected daily across our cities and the generation of fuels where they can find good application as a potential feedstock for such generation of fuels.

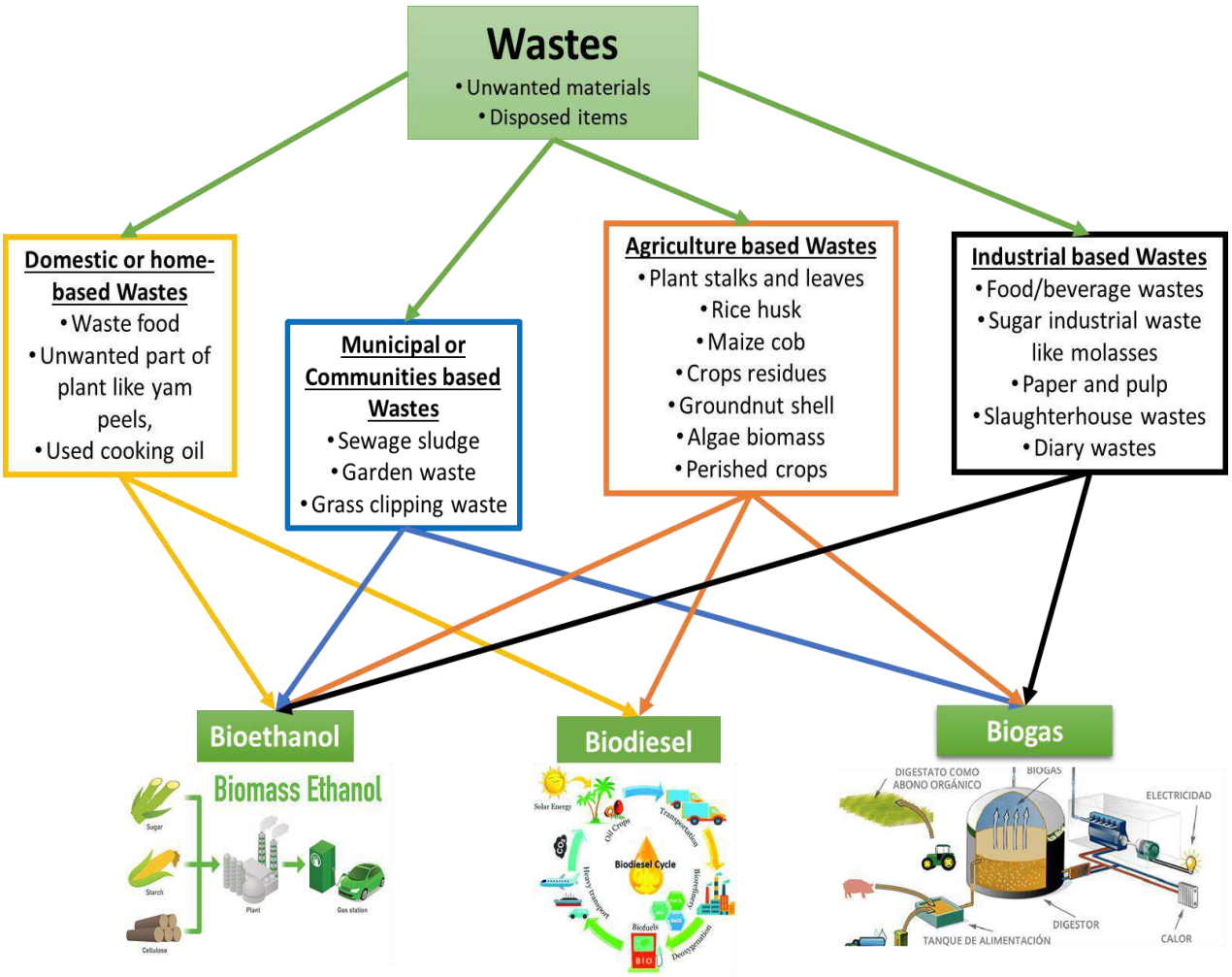

Figure 4. The relationship of the waste classes to the needed feedstock across various green fuels examples like bioethanol, biogas, and biodiesel.

In contrast, Figure 4 presented the relationship of the various classes of waste to bioethanol, biodiesel, biogas, showcasing the possible type of green fuels that can be obtainable from each class of wastes in line with the report of literature [8], [11]–[23].

3. Prospect of the Green Fuel to Management of Wastes in Nigeria

The consideration of the approach of waste-to-wealth via the conversion of wastes in our communities into valuable materials like green fuels would go a long way to proffering solutions to some of our present challenges and offer the government and residents further advantages, which are presented here.

3.1 Reduction of stockpiles in the dumpsite

A lot of the sites where these wastes are dumped would begin to record lower stock pills on the site due to the continuous collection and transportation of the wastes to the biorefineries, where they

would be transformed into green fuels and possible biochemicals which would be eco-friendly [22], [24].

3.2 Lesser generation of the poisonous gases on the dumpsite

With the less volume of wastes present on the dumpsites, the number of poisonous gases like ammonia, hydrogen suphide, and many other dangerous gases generation on the sites would be significantly reduced [25], [26] via the continuous waste transformations into green fuels.

3.3 Promotion of a cleaner environment:

With less waste deposited around peoples' residences, our communities would look cleaner. The community health would be generally improved with a conducive environment that would be obtained with lesser or negligible land pollution with these solid wastes [24], [27], [28].

3.4 Safer fuels to use:

Adopting this process would go a long way to promoting clean air with the potential use of green fuel. Lesser usage of fossil fuels would lessen the volume of greenhouse gases (GHG) often released during the incomplete combustion of the fossil fuels, which are not consumed, unlike that of the green fuels, which have the potential of capturing carbon monoxide and carbon dioxide via the methanation process is presented. The concept is presented in Figure 5 of how this was done in their lifecycles.

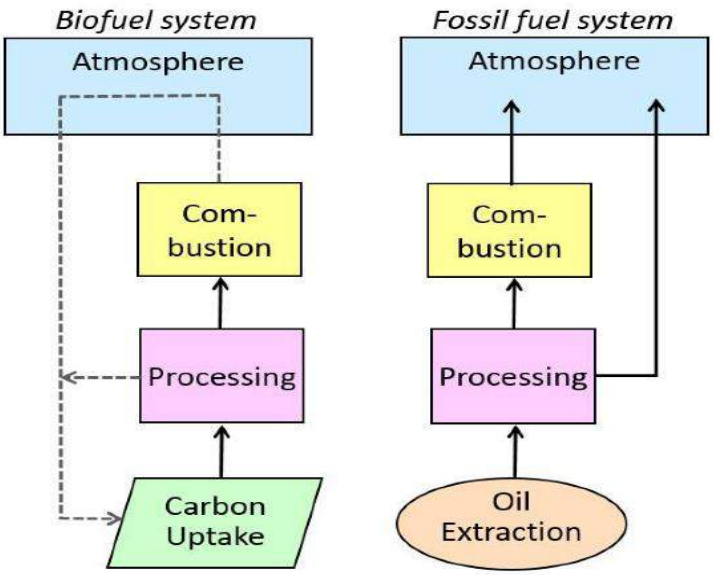

Figure 5. A comparing of fossil fuels and green fuels potential in the management of carbon dioxide using their lifecycle report [29].

In Figure 5, it can be justified that green fuels, otherwise known as biofuels, shows better management of carbon throughout the process its lifecycle compared to fossil fuel, which only produces carbon without the stage where the carbon is consumed or taken back in the report of the literature [29]. Instead, the fossil fuel system's carbon pollutes our environment and further promotes global warming.

3.5 Complementary or substitution potential for the current fossil fuels:

Our economy has long been largely dependent on fossil fuels as the primary source of revenue. The consideration of the approach would be a long to promote diversification of our economy and energy mix, where green fuels are currently missed. As the world is promoting green fuel, adopting the said approach would also attract both local and foreign investors to come into the sector to invest. Existing reports have to unfold the economic benefits of investing in green fuels like bioethanol [13], [14], [30], [31] in Nigeria. Although, there is no existing report accounting for the economic viability of investing in biodiesel and biogas in Nigeria.

4. Conclusion

This report successfully presented the current waste management situation in our communities, green fuel, and its relation to waste management, and the potential benefits of adopting this process or approach to our nation. These benefits include promoting a clean environment, cleaner air, complement or substitute to the current use of fossil fuels, and better waste management.

Further studies are therefore recommended to give preferential attention to the development and commercialization of local technologies which are eco-friendly, sustainable, and renewable for the establishment of the biorefineries in Nigeria, especially the case of biodiesel and biogas, whose economic viability is yet to be reported.

References

[1] T. R. Binafeigha and A. Enwin, "The State of Solid Waste Management in Port Harcourt City, Nigeria," *American Journal of Civil Engineering and Architecture*, vol. 5, no. 4, pp. 160–166, Oct. 2017, doi: 10.12691/AJCEA-5-4-4.

[2] D. A. Omoboyowa, C. O. Akinnubi, and T. C. Ajueyisi, "Level of Heavy Metals in Selected Vegetables Collected from Ijagun Dumpsite in Ogun State, Nigeria," *Asian Food Science Journal*, vol. 10, no. 1, pp. 1–8, Jun. 2019, doi: 10.9734/AFSJ/2019/V10I130027.

[3] Leadership Newspaper, "Nyanya-Karu-Jikwoyi Road Dumpsite: Evolving Infection-Breeding Place." https://leadership.ng/nyanya-karu-jikwoyi-road-dumpsite-evolving-infection-breeding-place/ (accessed Oct. 17, 2021).

[4] "The Cleaner Lagos Initiative Threatens Wastepicker Livelihoods, Nigeria | EJAtlas." https://ejatlas.org/conflict/the-cleaner-lagos-initiative-threatens-wastepicker-livelihoods-nigeria (accessed Oct. 17, 2021).

[5] NNPC, "History of the Nigerian Petroleum Industry," *NNPC Publication*, Sep. 25, 2021. https://nnpcgroup.com/NNPC-Business/Business-Information/Pages/Industry-History.aspx (accessed Sep. 25, 2021).

[6] A. Galadima, Z. N. Garba, B. M. Ibrahim, M. N. Almustapha, L. Leke, and I. K. Adam, "Biofuels Production in Nigeria: The Policy and Public Opinions," *Journal of Sustainable Development*, vol. 4, no. 4, p. p22, Aug. 2011, doi: 10.5539/JSD.V4N4P22.

[7] A. M. O. Agba, M. E. Ushie, F. I. Abam, Michael S. Agba, and James Okoro, "Developing the Biofuel Industry for Effective Rural Transformation in Nigeria," *European Journal of Scientific Research*, vol. 40, no. 3, pp. 441–449, 2010, [Online]. Available: https://www.researchgate.net/publication/278329081

[8] T. Oyegoke and K. A. Ibraheem, "Kinetic modeling of the biodiesel production process using neem seed oil: An alternative to petroleum-diesel," *European Journal of Chemistry*, vol. 12, no. 3, pp. 242–247, 2021, doi: 10.5155/eurjchem.12.3.242-247.2085.

[9] S. John, "The five types of biomass used in biofuel production - London Business News | Londonlovesbusiness.com," *LondonLoveBusiness*, Jun. 20, 2020. https://londonlovesbusiness.com/the-five-types-of-biomass-used-in-biofuel-production/ (accessed Nov. 11, 2021).

[10] G. Matthew, J. Andrew, C. Mo, and C. Jean, "Biomass - Using Anaerobic Digestion," *Biomass*, 2020. http://www.esru.strath.ac.uk/EandE/Web_sites/03-04/biomass/background%20info4.html (accessed Nov. 11, 2021).

[11] T. Oyegoke and F. Dabai, "Techno-economic feasibility study of bioethanol production from a combined cellulose and sugar feedstock in Nigeria: 1-modeling, simulation and cost evaluation," *Nigerian Journal of Technology*, vol. 37, no. 4, pp. 913–920, Nov. 2018, doi: 10.4314/njt.v37i4.8.

[12] T. Oyegoke, F. Dabai, J. Abubakar Muhammed, and B. El-Yakubu Jibiril, "Process Modelling and Economic Analysis for Cellulosic Bioethanol Production in Nigeria," in *1st National Conference On Chemical Technology (NCCT 2017)*, 2017, pp. 125–128. Available: http://www.narict.gov.ng/ncct/

[13] A. Abemi, T. Oyegoke, F. N. Dabai, and B. Y. Jibril, "Technical and Economic Feasibility of Transforming Molasses Into Bioethanol In Nigeria," in *National Engineering Conference*, 2018, pp. 531–537.

[14] O. O. Ajayi, K. Rasheed, A. Onadeji, and T. Oyegoke, "Techno-economic Assessment of Transforming Sorghum Bagasse into Bioethanol Fuel in Nigeria: 1-Process Modeling, Simulation, and Cost Estimation," *Journal of Engineering Studies and Research*, vol. 26, no. 3, pp. 154–164, 2020, Accessed: Mar. 18, 2021. [Online]. Available: http://jesr.ub.ro/1/article/view/219

[15] S. B. Oyeleke, B. E. N. Dauda, Oyewole, I. N. Okoliegbe, and T. Ojebode, "Production of Bioethanol From Cassava and Sweet Potato Peels 1 Production of Bioethanol From Cassava and Sweet Potato Peels," *Advances in Environmental Biology*, vol. 6, no. 1, pp. 241–245, 2012.

[16] O. E. Juwon and O. F. Oluwatoyin, "Production of Bioethanol from Selected Lignocellulosic Agrowastes," *Journal of Advances in Biology & Biotechnology*, vol. 21, no. 2, pp. 1–17, Apr. 2019, doi: 10.9734/jabb/2019/v21i230089.

[17] M. Aiyejagbara *et al.*, "Production of Bioethanol from Elephant Grass (Pennisetum purpureum) Stem," *International Journal of Innovative Mathematics, Statistics & Energy Policies*, vol. 4, no. 1, pp. 1–9, 2016, [Online]. Available: www.seahipaj.org

[18] M. I. Misau, B. I. Muhammad, M. I. Ali, and M. Jibril, "Design and Construction of A Bioethanol Pilot Plant in Nigeria," *Journal of Applied Phytotechnology in Environmental Sanitation*, vol. 3, no. 1, pp. 11–16, 2014, Accessed: Mar. 26, 2021. [Online].

[19] H. Danjuma Banu, T. B. Shallangwa, T. O. Magu, L. Hitler, and S. Ahmed, "Biodiesel Production from Neem Seed (Azadirachta indica) Oil Using Calcium Oxide as Heterogeneous Catalyst," *J Phys Chem Biophys*, vol. 8, pp. 1–3, 2018, doi: 10.4172/2161-0398.1000266.

[20] A. G. Taiwo, Ijaola, S. O. Lawal, Y. A. Lanreiyanda, and //Nipesjournals Org Ng, "Characterization of Neem Seed Oil and its Biodiesel (B100)," *NIPES Journal of Science and Technology Research*, vol. 2, no. 2, pp. 2020–178, 2020, doi: 10.37933/nipes/2.2.2020.18.

[21] E. T. Akhihiero, B. V. Ayodele, M. A. Alsaffar, T. O. K. Audu, and E. O. Aluyor, "Kinetic Studies of Biodiesel Production from Jatropha curcas Oil," *Journal of Engineering*, vol. 27, no. 4, pp. 33–45, Mar. 2021, doi: 10.31026/J.ENG.2021.04.03.

[22] O. G. Igbum, A. C. Eloka-Eboka, and S. Adoga, "Feasibility study of biogas energy generation from refuse dump in a community-based distribution in Nigeria," *International Journal of Low-Carbon Technologies*, vol. 14, no. 2, pp. 227–233, Jun. 2019, doi: 10.1093/IJLCT/CTZ011.

[23] S. O. Dahunsi and U. S. Oranusi, "Co-digestion of Food Waste and Human Excreta for Biogas Production," *Research Article British Biotechnology Journal*, vol. 3, no. 4, pp. 485–499, 2013, Accessed: Sep. 25, 2021. [Online]. Available: www.sciencedomain.org

[24] O. O. Ojuri, T. O. Ajijola, and I. I. Akinwumi, "Design of an engineered landfill as possible replacement for an existing dump at Akure, Nigeria," *African Journal of Science, Technology, Innovation and Development*, vol. 10, no. 7, pp. 835–843, Nov. 2018, doi: 10.1080/20421338.2018.1523827.

[25] S. Kumar, S. A. Gaikwad, A. v. Shekdar, P. S. Kshirsagar, and R. N. Singh, "Estimation method for national methane emission from solid waste landfills," *Atmospheric Environment*, vol. 38, no. 21, pp. 3481–3487, Jul. 2004, doi: 10.1016/J.ATMOSENV.2004.02.057.

[26] M. Palmiotto, E. Fattore, V. Paiano, G. Celeste, A. Colombo, and E. Davoli, "Influence of a municipal solid waste landfill in the surrounding environment: Toxicological risk and odor nuisance effects," *Environment International*, vol. 68, pp. 16–24, 2014, doi: 10.1016/J.ENVINT.2014.03.004.

[27] D. A. Okpara, M. Kharlamova, and V. Grachev, "Proliferation of household waste irregular dumpsites in Niger Delta region (Nigeria): unsustainable public health monitoring and future restitution," *Sustainable Environment Research 2021 31:1*, vol. 31, no. 1, pp. 1–10, Jan. 2021, doi: 10.1186/S42834-020-00077-1.

[28] A. Nwosu and S. Olofa, "Effect of Waste Dumpsites on Proximate Residential Property Values in Ibadan, Oyo State, Niger," *Ethiopian Journal of Environmental Studies and Management*, vol. 8, no. 2, pp. 976–982, Jun. 2016, doi: 10.4314/ejesm.v8i2.11S.

[29] J. M. DeCicco, "Methodological Issues Regarding Biofuels and Carbon Uptake," *Sustainability 2018, Vol. 10, Page 1581*, vol. 10, no. 5, p. 1581, May 2018, doi: 10.3390/SU10051581.

[30] C. N. Ogbonna and E. C. Okoli, "Economic feasibility of on-farm fuel ethanol production from cassava tubers in rural communities," *African Journal of Biotechnology*, vol. 12, no. 37, pp. 5618–5626, 2013, doi: 10.5897/AJB2013.12855.

[31] T. Oyegoke and F. Dabai, "Techno-economic feasibility study of bioethanol production from a combined cellulose and sugar feedstock in Nigeria: 2-economic analysis," *Nigerian Journal of Technology*, vol. 37, no. 4, pp. 921–926, Nov. 2018, doi: 10.4314/njt.v37i4.9.

NIPES Conference Proceedings
The 1st International Conference of the Nigerian Institution of Professional Engineers and Scientists 7th-8th Oct. 2021: 36-49
www.nipesjournals.org.ng

Location, Distance, and Utilization of Primary Health Care Facilities in Isiala-Mbano, Imo, Nigeria

Chinyere Lawrencia Charles-Akalonu; Ikpong Sunday Umo *; John C. Amadi
Department of Geography and Environmental Studies, Alvan Ikoku Federal College of Education, Owerri, P.M.B. 1033, Imo State, Nigeria.
* Corresponding Author: E-mail Address: umohikpong@yahoo.com Phone Number: +2348037565958

Abstract
Although primary health care remained the first point of contact for most rural communities in Nigeria with respect to health issue, the level of clients' access and utilization are mostly plagued with distinct problems across geographic spaces, thereby impeding sustainable development of rural communities. The aim of this study is to evaluate the intriguing relationships existing between spatial distance and the utilization of government-owned primary health care facilities (PHCF) by residents in Isiala-Mbano, Imo State. A stratified random sampling method was used to select a sample population of 475. Questionnaire and interviews were used to elicit information from the respondents, while geospatial tools were used for mapping the spatial distributions of three Health Posts and fourteen Health Centers. Analyses of data using descriptive statistics, geographic information system, nearest neighbour analysis, Pearson product moment correlation coefficient, and student's t-test revealed that: (i) PHCF's are randomly distributed within the study area as indicated by the Nearest Neighbour Index of R = 1.164. (ii) Estimated Euclidean distances from users' houses to nearest PHCFs showed that 66.5 percent of the users live within 1 km and 33.5 percent live between 1 km to 2.3 km from the nearest PHCFs. (iii) Average Nearest Neighbour Distance gave 1.3708 km with good topography. (iv) The ratio of population to health center gave 11,972:1, implying that Isiala-Mbano is adequately served by primary health care centers, but the levels of utilizations were generally very low due to lack of doctors and valid drugs for patients. A test of Hypothesis showed that there is no significant relationship between the distance of primary health care facilities and the level of utilization in the study area. Hence, this study recommended timely health care facility reform through the supply of essential drugs and employment of specialized manpower sustainably to attend to patients in the study area

***Keywords*:**
Geographic space, distance, utilization, health care facilities, sustainability

1. Introduction

One of the most focal agendas of sustainable development that have attracted the attention of the Nigerian government and international communities is the health sector. Yet, many reforms, funding, and supplies of facilities are concentrated at the Federal and State levels in recent times. Hence, most rural poor may lack access to adequate utilization of those specialized health care facilities at the centers due to factors such as distance, road network, insecurity, and/ or cost. The utilization not only reflects need but service-related factors such as availability, affordability, income, and practice patterns [1, 2].

In Nigeria and Imo State in particular, primary health care services (PHCS) are established for services such as prevention and control of locally endemic and epidemic diseases, provision of essential drugs and supplies, maternal and child care services, family planning and immunization against infectious diseases, educating the people about prevailing health issues and prevention or control measures, promotion of food supply and adequate nutrition (National Primary Health Care Development Agency [3,4]. Yet, people access and utilization of the services in most rural communities is not clearly known.

Discounting the splendid responsibilities of PHCS highlighted, there is an increase in speculations that the available health care facilities in many rural communities are underutilized, abandoned, or neglected patients. The utilization of health care facilities can be constrained or accelerated by certain geographic variables such as distance, location, and time. Therefore, utilization denotes an individual's ability to use health services when and where they are needed.

In a perspective, Alegana, Wright, Petrina, Noor, Snow, and Atkinson [5] established that utilization of health care is affected by several factors such as geographical accessibility, bad roads, lack of electricity, lack of pipe-borne water, poverty level, and life-supporting amenities. The factors tend to pose serious challenges to sustainable development of the health sector in the 21st century.

In sub-Sahara Africa, [6] adopted grey literature approach in analyzing on human resources for health in Mali, Sudan, Uganda, Botswana and South Africa. The results revealed that a minority of the doctors, nurses and midwives were working in primary health care and shortages of qualified staff were key issues in rural areas. They further opined those shortages of personnel was the greatest issue in primary health care settings than at higher levels, leading to an upsurge in clients' patronages of traditional healers.

In exploration of the factors affecting access to PHC in rural areas of mostly low and middle-income Countries [2] used five data-based (CINAHL, EMBASE, Global Health, Medline and Web of Science). Analyses using deductive and inductive approaches revealed that people were unable to access PHC due to obstacles including the interplay of availability, acceptability, affordability, and geography factors. In particular, limited availability of health care facilities and services and perceived low quality of care meant that those in need of health care services frequently had to travel for care.

World Health Organization and UNICEF [7] have emphasized that sustainable investments in PHC will not only improve equity and access, but health care performance, accountability of health systems, and health outcomes. However, there are indications that variables such as awareness/ education, quality of food system, socio-economic security, local geography, and environment manifested as critical factors in determining health services and well-being of rural residents in this era of COVID-19 challenges.

Recent developments in the COVID-19 pandemic and the corresponding effects on humans necessitate the placement of primary health care services at the center for optimum access and utilization by the vulnerable poor in rural communities. Amidst the expectations, there are issues associated with meeting the recommended standard of about 1,140 doctors and 3,620 nurses/midwives in primary and secondary health care System of Imo State [8]. The figures were below World Health Organisation (WHO) recommended global threshold of 22.8 skilled health professionals per 10,000 populations for less economically developed countries [9, 10].

The Local Governments are responsible for the Primary Health Care Facilities under the support of the State Ministries of Health and within the overall national health policy under the supervision of the National Primary Health Care Development Agency. There are also private medical practitioners and organizations that provide health care facilities both in the urban and rural areas. International agencies such as United Nations International Children's Emergency Fund (UNICEF), United States Agency for International Development (USAID) and World Health Organization (WHO) have been supporting the provision of Primary Health Care Services in various ways in the past.

The upsurge in population and the demand for better quality of life among residents especially in the rural area has created disequilibrium in resource utilization and sustainable development. The aim of this study is to assess the effect of location, distant, and utilization of primary health care facilities in Isiala-Mbano, Imo State.

To accomplish the aim, the following specific objectives were formulated to guide this study:

(i) To determine the relationship between primary health care facilities and the level of utilization.
(ii) To evaluate the condition of the road network, services, users' preferences, facilities on the utilization of primary health care facilities.
(iii) To examine the implication of findings on the sustainable health sector reform and development in Isiala-Mbano, Imo State.

Sequel to the stated objectives, it is therefore hypothesized that there is no significant relationship between distance and utilization of primary health care facilities in the study area.

1.1. The Central Place versus Neighbourhood: Contexts and Applications

The location and distribution of geographic events in space over time scale often vary with distance away from the center. The affinity of number, size, types, locations, access, planning, and utilization of health care facilities can be explained using central place model as advocated by a German geographer, Walter Christaller [11,12]. Amidst of that, the Nearest Neighbour model also offers an intuitive analytical toolbox for elucidation of location-distance relations especially when backed by geospatial tools of this postmodern era.

Contextually, the central place represents a health center (business) for the exchange of goods (e.g. drugs, injections) and services (e.g. diagnosis, education, dispensary, advising) by people attracted from the surrounding communities. It is assumed to be centrally located to maximize access and utilization from the nearby patients. Central places compete against each other to serve as markets for medical and pharmaceutical goods and services.

According to Briney [12], Christaller postulated that a center is characterized by an unbound isotropic homogenous surface, with evenly distributed population and equidistant settlement/ transport cost, evenly distributed resources, distance decay mechanism, consumers having similar purchasing power and demand for goods, minimize distance travelled. Each supplier has a monopoly over a hinterland, there is only one type of transport equally easy in all directions and transport cost is equal to the distance travelled. This theory applies most clearly in regions that are neither heavily industrialized nor interrupted by major physical features such as rivers or mountain ranges.

The application of Nearest Neighbour Analysis (NNA) is traced to Clark and Evans [13]. The nearest neighbour statistic represents the degree to which an observation departs from a predicted random distribution [13,14]. The idea was used to analyze and describe plant patterns and distribution of plant species over the surface and later gained wide applications geography as emphasized in [15].

Within the discipline of geography and geographical researches, the application of Nearest Neighbour Analysis (NNA) had gained wide popularity in land use, industrial location, and analysis of landform/ physical features as demonstrated in [16]. Mayhew [17] noted that NNA is the study of settlements in order to discern any irregularity in spacing by comparing the actual pattern of settlement with a theoretical random pattern. The linearized (straight line)

distance from each settlement to its nearest neighbour is measured and this is divided by the total number of settlements to give the observed mean distance between nearest neighbours

According to Abdulraheem et al. [18] most rural health care facilities in various States in Nigeria are in disrepair, with equipment and infrastructure being either absent or obsolete and the referral system, almost non-existent. In Imo State, the challenges of poor working conditions, low salaries and the corresponding effect of (mass exodus) of health professionals have been reported [8]. Many health workers posted to the rural areas prefer to work in the urban (core) health facilities due to better infrastructure leading to improved life quality among residents.

Within the Tshwane, Gauteng Province of South Africa, [19] The result indicated that availability of transport, the physical distance of facility, and time taken to reach the facility has influences on health care utilization. The study however, found out that in terms of distance, the clinics were accessible as most of the participants lived within 5km of such facility in conformity with the norms and standards of South African PHCS.

Similarly, [20] studied intriguing relationships between the conditions of infrastructure and the level of socio-economic development of 44 rural communities in Imo State. The results of the qualitative and quantitative assessments of data generated through questionnaires and interviews revealed that the conditions of infrastructure (health centers, roads, and schools) were mostly poor across the three zones in Imo State. Also, significant relationships exist between the conditions of infrastructure and the level of development in rural communities in Imo State.

In Kogi State of Nigeria, [21] examined the effects of distance on the utilization of health care services in rural areas. The quantitative analyses using distinct accessibility indices revealed unequal access to modern health care facilities in the study area. They concluded that household size, distance, and cost of accessing health care services were dominant constraints to adequate utilization by clients.

Agaja [22] studied the distribution of primary health care centers in Ughelli and Warri areas of Delta State using cluster and nearest neighbour analyses. The results indicated that health centers in Ughelli South were mostly randomly distributed, with traces of fairly clustered pattern in the northern axis. On the contrary, the distributive pattern in Warri South showed a clustered pattern. He attributed the distributive pattern to poor topography (swampy terrain) of Warri South, inadequate funding by the local government authorities and misuse of allocated funds by administrative and political leaders in the study area.

2.0 Materials and Method

2.1 Location of the Study Area

Isiala-Mbano is one of the twenty-seven (27) Local Government Areas in Imo State. It is located between Longitudes 07º 00' and 07º 22' East of Greenwich Meridian and Latitudes 05º 37' and 05º 45' North of the Equator (Figure 1). Relatively, it is bounded by Isu and Nwangele Local Government Areas on the West, Ehime-Mbano Local Government Area on the East, Onuimo Local Government Area on the North, and Ikeduru and Ehime-Mbano Local Government Areas on the South. Isiala-Mbano has a land area of about 165.63 km^2 and is made up of thirty-eight (38) autonomous communities with twenty-five (25) Primary Health Care facilities. It has a projected population of 299,308 by 2019 at 3.2 percent annual growth rate by National Population Commission and sixteen (16) political wards (2006 Census data indicated in Government Gazette) cited in [23].

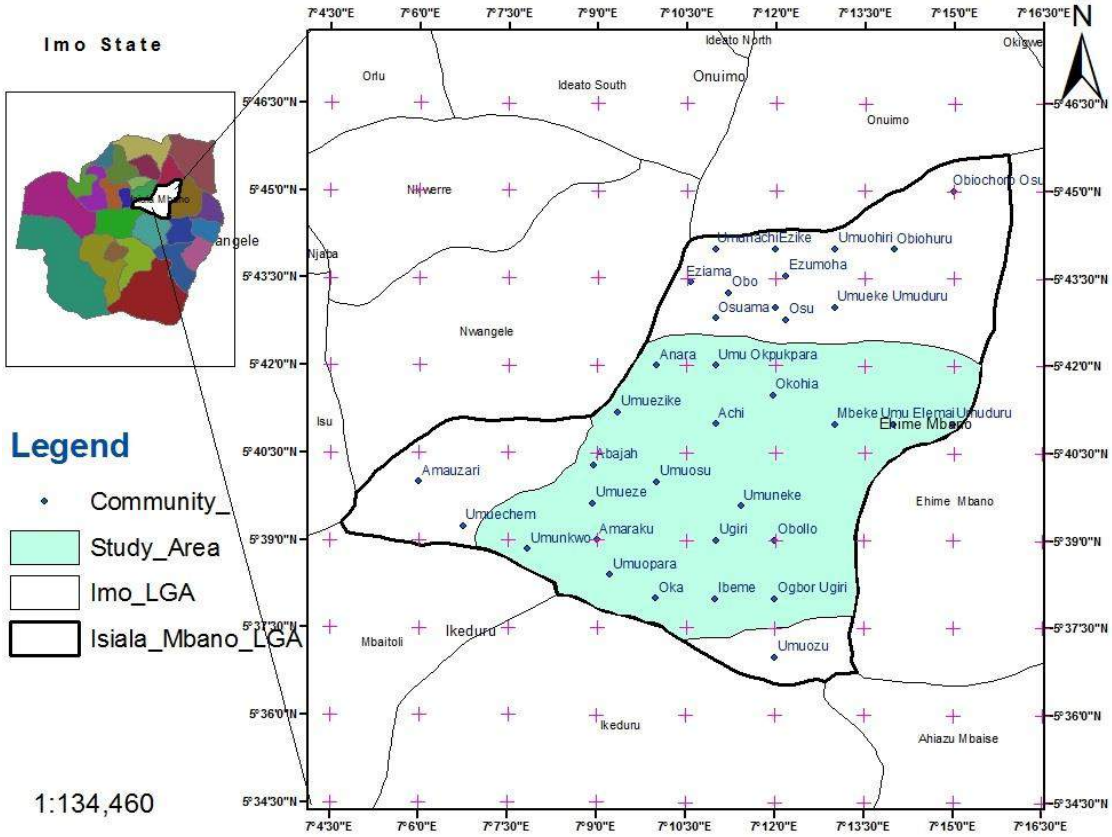

Figure 1: Locations and Sampled Communities with Health Care Centers in Isiala-Mbano
Source: Authors' Field Work (2021).

2.2 Climate, Geology, and Pedo-geomorphology

The climate of the Isiala-Mbano lies within the humid tropical (Am) climatic classification. It has a mean annual temperature that ranges between 27º C and 30º C. The rainfall varies based on season due to alternating wet and dry seasons. The vegetation of the area can be described as disturbed secondary or immature forest that represents a spontaneous regeneration of the original tropical rain forest cover [24].

The geology and local geomorphology vary across geographic spaces. The study area is in the transitional zone between the Alluvium that extended to Imo Shale dominating places such as Okohia, Anara, Achi and Umuezike in the North and the Coastal Plain Sand Deposits of Tertiary Times dominating Oka, Ebeme, Amauzo, Ugiri, and Umuokpara in the South. The transitional nature of geologic formations gives the soil a red Ferralitic sandy-loam class. The top soil of 60 cm to 80 cm is characterized by brownish colour with a friable, weak structure and a rapid percolation rate. The topography of the study area ranged between 80 and 166 meters above average mean sea level. The geomorphology shows an undulating coastal plain dissected by gullies, ravines, river valleys. It is drained by Mbaa River and Otamiri River.

2.3 Land Use and Vegetation

In terms of land use, the people of Isiala-Mbano engaged in subsistence farming. Crops cultivated are cassava (*Manihotspp*), maize (*Zea Mays*), yam (*Dischoreaspp*), cocoyam *(Colocasie esculenta)*, plantain (*Musa x paradisiacal*), banana (*Musa spp*), oil palm (*Elias guineens*), breadfruit (*Trechulia Africana*), oil bean (*Pentraclethramacrophylla*), pear (*Dacroydesedulis*) among others. Palm Oil extraction is also practiced at the commercial level. Other secondary and tertiary economic activities found in the study area are banks, block moulding, weekly markets, retail trading, pharmacies, hairdressing salons, food vendors, furniture, public/ civil service, sand/ gravel mining.

3.1 Sample and Sampling Techniques

The population of the study comprises all adult males and females in the study area. Stratified random sampling was carried out in two stages. The first stage was the random selection of nineteen (19) communities out of thirty-eight (38) communities that make up the area. Random selection of communities was done by writing the community names on pieces of paper and blind picking them without replacement.

A total of nineteen communities were served by seventeen (17) primary health care facilities. The second stage was the selection of twenty-five (25) adults from each of the nineteen communities, making a total of four hundred and seventy-five (475) respondents. Only a total of four hundred and sixty-six (466) questionnaires were returned and used as valid for this study. Random selection of respondents was used in selecting the family head and a member from each household in the nineteen communities.

3.2 Data Collection

Data for this study were collected through two distinct (primary and secondary) sources. The primary data were obtained through structured questionnaires and interviews of health care facilities users, and direct personal observations of utilization for a 6-month period. Also, geospatial tools (Global Positioning System, remote sensing, and geographic information system) were used for the recording of coordinates and capturing images regarding the locations and conditions of health care facilities. Secondary data were generated from published and unpublished documents as recommended in [24].

Locational attributes of primary health care were obtained by acquiring geometric data (Co-ordinate points) of the PHCFs using a Garmin 12 handheld Global Positioning System (GPS) Receiver at their respective communities in Isiala-Mbano in Geodetic format and Nearest Neighbour Distances were generated with Arc GIS 9.3 software to estimate straight-line distances from their houses to the nearest primary health care facility.

The geographical coordinates of the seventeen PHCCs obtained were converted to Universal Transverse Mercator (UTM) using the Geo-scale software. An area map of the communities in Isiala-Mbano was delineated from Nigerian Local Government Area Shapefile (Nigerian LGA Data Base Copy Collected from RECTAS) in Geodetic format, reified in Arc GIS 9.3 software, and converted to UTM zone 32 N (Figures 1 & 2).

3.3 Method of Data Analysis

The descriptive statistics (percentages, simple bar graph, and scatter plot) were used to determine the proportion of utilization, condition of the access road, and distributive patterns of primary health care facilities. The Pearson Product-Moment Correlation Coefficient (r) and student's t-test were employed as the surrogate for the determination of the significant relationship between distance of primary health care facilities and respondents' utilization at 0.05 confident level.

Also, the Estimated Euclidean distance from the locations of respondents' homes to the nearest primary health facilities were generated using ArcGIS version 9.3 and the analytical toolbox queried to determine the linearized distance of each primary health center/ health post to its nearest neighbour in Isiala-Mbano.

4. Results and Discussion

4.1 Relationship of Distance and Utilization of Primary Health Care Facilities

In other to establish the relation between distance and client utilization of primary health care facilities in Isiala-Mbano, Pearson Product-Moment Correlation Coefficient was used. The result gave is very low positive correlation coefficient of 0.042 and statistically insignificant at 0.05 confident level.

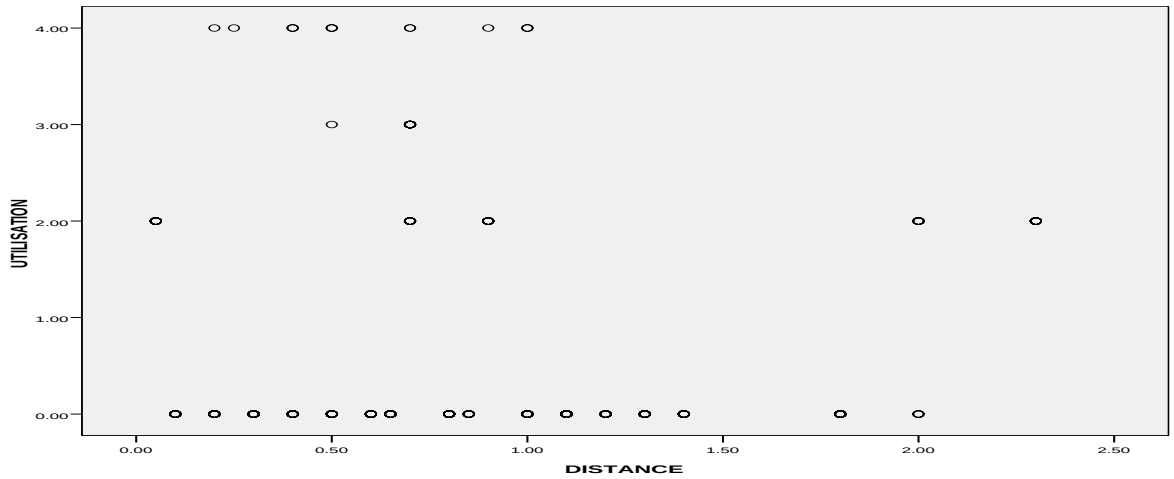

Figure 2: Scatter Plot of Correlation between Utilization and Distances (in Km).
Source: Authors' Analysis.

The result was further validated using a student t-test. The computed t-test value gave 0.905 while the tabulated value gave 1.960. Since the calculated t-test value is lower than the tabulated value, null hypothesis one was accepted. It is thus, affirmed that there is no significant relationship between the distance of primary health care facilities and the level of utilization in the study area. The result contradicted [19] observation in South Africa that availability of transport, the physical distance of facility, and time taken to reach the health facilities had significant influences on health care utilization. The pattern of the relationship between distance and utilization is depicted in a linearized scatter plot presented in Figure 2.

4.2 Types of Primary Health care Facilities

Using [8,9] recommended standards of the number of wards and population as criteria, this study established that Isiala-Mbano has a total of twenty-five (25) Primary Health Care Facilities (PHCFs) serving the entire study area. However, the sampled area has three (3) health posts, and fourteen (14) health centers were identified. The analysis using graphs and percentages revealed that health centers represented by 82.4 percent were more dominant in Isiala-Mbano than health posts represented by 17.6 percent, as depicted in Figure 3.

Similarly, the analysis of ratio of population to health center gave 11,972:1, which is a clear indication that the population is adequately served by the primary health care facilities in the study area. The decision is based on the standard stipulated by the Nigeria National Primary Health Care Development Agency [3, 4] which recommended one health facility to a population that range between 10,000 to 20,000 people. The Health Posts are usually indicated for lower threshold population, the pattern in distribution is graphically depicted in Fig. 3.

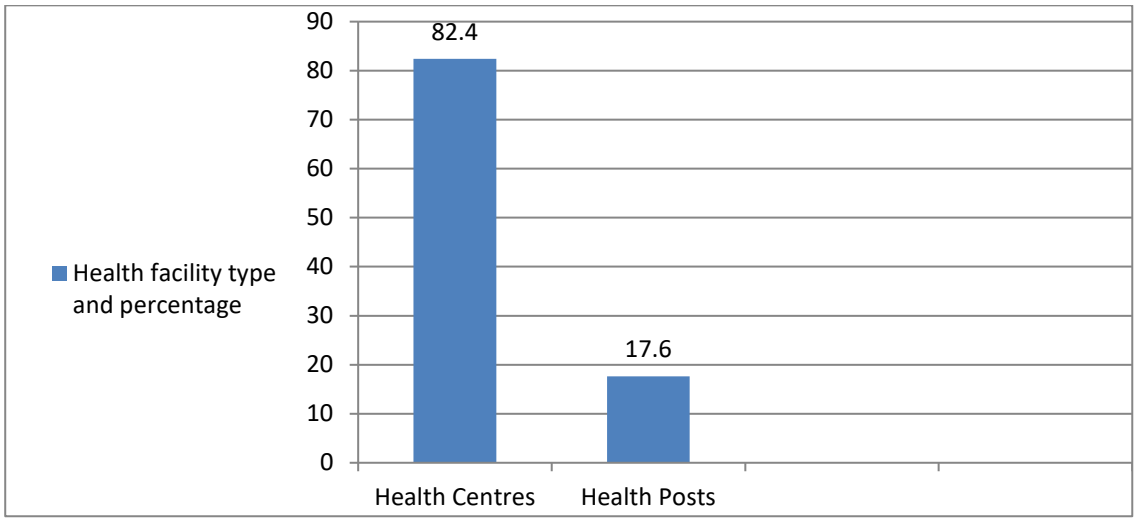

Figure 3: Health facility type and their relative dominance.

4.3 Spatial Distribution and Nearest Neighbour Assessment of Distance

The converted coordinate points were reproduced to describe the spatial distribution of the PHCFs using the Nearest Neighbour Index (R) is defined by a linearized model. The total nearest neighbour distance yielded 23.3036 km, average nearest neighbour distance gave 1.3708 km, the number of points (n) generated was 17, the density of points was 0.181, observed mean gave 1.370, and expected mean gave 1.176. Subsequently, the result obtained was 1.164 which depicted a random distribution of the PHCCs in the study area (Figure 4).

The distance decay has been observed in the way patronage diminishes with distance across the product's gravitational field. PHCFs users' experience of distance summarized in Figure 4 indicated that 66.5 percent of respondents live within 1km from the nearest PHCF while 33.5 percent live within the range of 1 to 2.3 km from the nearby primary health care facility. The distance is distinct from South African stipulated norms and standards whose participants live within 5 km to the primary health center (clinic) as reported in [19].

The result of shorter distance suggested that PHCFs could be accessed by trekking or any other means of transport used in the locality. Hence, the health care facilities, therefore, generally comply with National Primary Health Care Development Agency minimum standards of distribution according to Ward Health System as regards distance.

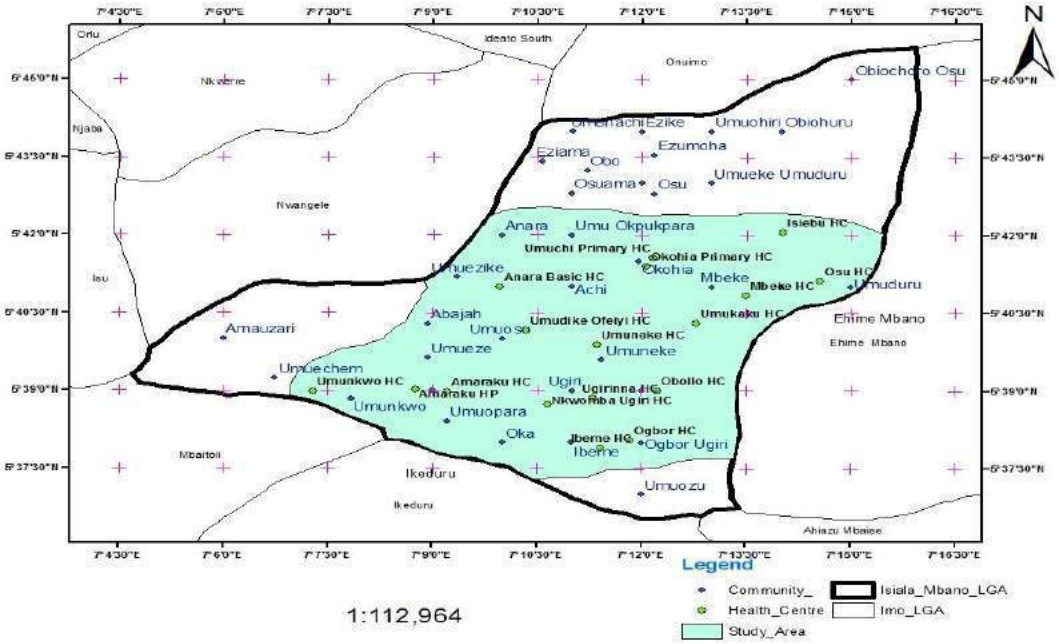

Figure 4: Spatial Distribution of Primary Health Care Centres in Relations with Communities.
Source: Authors' Analysis.

4.4 The Perception of Road Conditions to the Primary Health Facilities

The states of the roads often played critical role in clients' utilization of the facility. Where distance is short enough to encourage the use of a facility, transferability might still be hampered by a bad road network. The result presented in Table 1 showed that the highest proportion of 72 percent, representing 337 respondents, have good access road to the health centers in their domains. This is followed by 19 percent representing 88 respondents that reportedly have very good access road to their primary health centers in their communities. Furthermore, only 3 percent (representing 15 respondents) have bad access roads to their health centers, while 6 percent (26 respondents) reportedly have very bad access road to their health center. The above results are clear indications that physical accessibility to HCFs defined by road network in Isiala-Mbano is generally good. The results contradicted [20] report of the poor state of rural infrastructure (such as road) in Imo State. Hence, the differences could be attributed to the area of coverage.

Table1: The Assessment of Access Road to Health Centres.

Assessment of Access Road to HCF	Frequency	Percentage (%)
Very good	88	19
Good	337	72
Bad	15	3
Very bad	26	6
Total	**466**	**100**

Source: Authors' Analysis.

4.4 The Utilizations of Primary Health Care Facilities

The utilization of facilities or healthcare delivery in any health service location can be enabling or disabling over a period time due to antecedent encounters, experiences, and histories. Health authorities do not just provide facilities; they also grapple with issues of patronage, while creation of more awareness to encourage utilization of facilities among rural clients had been envisaged [7]. The analysis of peoples' utilization of primary health care facilities presented in Table 2 showed that 13 percent (representing 58 of respondents) had attended HCFs two times in the past six months, 27 percent representing 127 respondents attended once, 4 percent attended three times, 3 percent utilized the facility four times. The highest proportion of 53 percent (representing 288 respondents) had not utilised HCFs in the past six months. This result showed a very low level of utilization, thereby collaborating [5,25] attribution of poor utilization to the amalgams of multiple geographic and human factors. Hence, the high level of morbidity and poverty in most rural areas of Nigeria and Isiala-Mbano amidst insecurity is quite a worrying situation.

Table 2: Frequency of Primary Health Care Facility Utilizations in Isiala-Mbano

Utilisation of Facility in the Last 6 months.	**Frequency**	**Percentage (%)**
4 times	15	3
3 times	18	4
2 times	58	13
Once	127	27
None	248	53
Total	**466**	**100**

Source: Authors' Analysis.

4.5 Clients Behaviours and Responses during Health Emergencies

The initial behaviours and responses of the clients tend to vary across places with respect to utilization of health care facilities in distinct communities. The variations in behaviours towards utilization of health care services affects patients healing process and whether a case will ever get to HCFs. There is a mix of responses to sicknesses as shown in Table 3. The result revealed that 54 percent, representing 263 of the respondents engaged in self-medication when they are sick, followed by 39 percent, representing 183 respondents first visit the clinic when they are sick, 4 percent representing 18 respondents preferred traditional herbs first when they are sick and 1 percent visited faith clinic first, when they are sick. The large followership of self-medication is worrisome and calls to question, the present arrangement of HCFs that breed apathy. This shows that people visit HCFs as a last resort.

Table 3: Spectrum of Preference Initial Actions taken by People When Sick.

Action Taken When Sick	**Frequency**	**Percentage (%)**
Take traditional herbs	18	4
Visit the clinic	183	39
Attend faith clinic	2	1
Self-medication	263	56
Total	**466**	**100**

Source: Authors' Analysis.

4.6 Patterns of Utilization of Health Care Services in Isiala-Mbano

The level of people utilization of primary health care facilities in Isiala-Mbano from 2011 to 2015 is summarized in Table 4. Results indicated that the Osu health center attracted the highest patronage by 912 patients, followed by Okohia with 609 patients, and Umuneke with 556 patients, while were classified Umunkwo registered a total of 541 patients respectively. Hence, the identified four health centers as highly utilized.

In another perspective, 3 health centers comprising Ogbor, Obollo, and Mbeke health centers had registered 536, 503, and 466 patients respectively within the six-month period and is classified moderate level of patronage as evidence in Table 4. The remaining 10 health care facilities such as Nkomba (with 288 patients), Anara (with 395 patients), Iheme (with 331 patients), and Umunchi (with 397 patients) recorded level of patronages due to the limited number of patients in their health care centers. The health posts comprising Isiebu, Ugirinna, and Amaraku with a total number 210, 213, and 235 accordingly, tend to registered low patients in their various communities.

Table 4: The Levels of Utilization of Primary Health Care

S/N	Health Care Facility	Average number of Patients from 2011 – 2015	utilization/10,000 Population
	HIGHLY UTILIZED		
1	Osu HC	912	35
2	Okohia HC	619	23
3	Umunkwo HC	556	21
4	Umuneke HC	541	21
	MODERATELY UTILIZED		
1	Mbeke HC	466	18
2	Obollo HC	503	19
3	Ogbor HC	536	20
	LOWLY UTILIZED		
1	Amaraku HC	401	15
2	Anara HC	395	15
3	Ibeme HC	331	15
4	Nkomba HC	288	11
5	Umudikeofeiyi HC	406	15
6	Umukaku HC	289	11
7	Umunchi HC	397	15
8	Amaraku HP	235	9
9	Isiebu HP	210	8
10	Ugirinna HP	213	8

Source: Author's Analysis.

4.7 Conditions of Services and Issues of Utilizations

The peculiar problems to clients' optimum utilization of primary health care facilities during past consultations in Isiala-Mbano were identified and descriptively analyzed for easy perusal and comparison in Table 5. The results showed that the two dominant problems associated with utilization of primary health care facilities were lack of essential drugs for patients supported by

23 percent (representing 106 respondents) and protracted non-availability of doctor in the health centers as supported by 23 percent (representing 105 respondents).

Furthermore, a total of 17 percent represented by 78 respondents indicated finance as their problem to sustainable utilization, 12 percent (54 respondents) identified poor state of the facility and 7 percent (33 respondents) reported absent of delivery equipment, while 4 percent (20 respondents) identified poor workers attitudes to clients as a hindrance to optimum utilization of primary health care facilities in the study area.

The problems of utilization tend to vary based on the community's health facility, type of health challenges involve, and individual perception of each facility over a period of time. User-friendliness is always a factor in the patronage of facilities. The public sector is unfortunate, yet, to imbibe salutation consumer service character seen in the competitive environment of private business. The attitude and work ethic can be poor enough to repel potential users. Ultimately, the absence of doctors and viable drugs remained the focal factors that triggered initial users' apathy coupled with the high level of poverty among the rural residents in the study area.

Table 5: Problems Encountered in Utilizing Health Care Facilities.

Problems encountered when utilizing the health care facilities.	**Frequency**	**Percentage (%)**
Transportation difficulties	33	7
Poor workers attitude	20	4
Delay in services	22	5
Protracted absent of doctor	105	23
Absent of delivery equipment	44	9
Lack of essential drugs	106	23
Poor state of facility	54	12
Financial problem	78	17
Total	**466**	**100**

Source: Authors' Analysis.

5. Implication of Findings on Sustainable Health Sector Reform and Development

The results of the Nearest Neighbour Index (R) of 1.164 implied random distribution of PHCFs while the estimated Euclidean distances of 66.5 percent of users living 1km and 33.5 percent living between 1km to 2.3km from nearest PHCFs and with good topography fall within the acceptable standard of the World Health Organization. Similarly, the population ratio to the health center of 11,972:1 clearly implied that Isiala-Mbano is adequately served by the primary health care centers. Hence, distance of primary health care facilities is not a major to resident's utilization in the study area.

The discourses and findings tend to present a scenario of well-plan and adequately distributed primary health care facilities in rural communities of Isiala-Mbano. Yet, optimum utilizations by rural residents for sustainable health, enhanced quality of life, and users' satisfaction during this post-modern era, rock by the COVID-19 pandemic are hampered by amalgams of human-induced factors such as the nature of personnel, facilities, and finance.

There is a need for concerted efforts by the Government (Federal, State, and Local), individuals, and donor agencies to increase funding, supply modern facilities/ equipment, and employ more

specialized personnel in the already strategically located primary health care facilities in Isiala-Mbano and beyond. Such actions will boost users' confidence, timely responses during health emergencies, boost capacities and redirect the interest of rural residents from unnecessary consultations and belief on the traditional healers to government facilities which is more scientific and reliable in terms of diagnosis and treatment of sicknesses, thereby averting avoidable death caused by ignorance. The observed reform options will facilitate both sustainable utilization and development of primary health care facilities in Isiala-Mbano and Imo State in general.

6. Conclusion and Recommendations

The study established that location, and distance, and physical accessibility are not hindrances to the sustainable utilization of primary health care facilities in the study area. Also, the spatial dynamic in population distribution to the ratio of health care facilities within geographic space depicts normal pattern but the level of utilization (patronage) among patients in the study area were low. The low utilizations were partly relating to factors such as the physical conditions, personnel and facilities available for users.

In consideration of the findings reached at the course of this study, the following recommendations are envisaged:

(i) Timely supplies of vital drugs, laboratory equipment, and employment of well-trained medical personnel (human resources), and enhanced service delivery to promote access, utilization, sustainability of health care facilities in Isiala-Mbano.

(ii) There is a need for the creation of more awareness on the need to avoid self-medication and over reliance on traditional healers in case of health challenges in the study area.

(iii) There is need boost the socio-economic conditions in the rural communities in Isiala-Mbano through partnership among donor agencies, stakeholders, and the local government authority to invest and empower health and allied sectors in the rural communities.

It is hope that if the preceding recommendations are strictly adhered to, the issue under-utilization of facilities will be averted or mitigated, and sustainability in primary health sector development promoted in consonance with the sustainable development agenda. The recommended actions are very urgent, given the divergence and complex health challenges posed by the novel COVID-19 pandemic, monkey, Ebola and other deadly diseases ravaging the world population in the 21st century.

References

1. S. McLafferty (2003). GIS and health care. *Annual Review of Public Health,* 24, 25 – 42.
2. E. Dassah, H. Aldersey, M.A. McColl,. *et al.* (2018). Factors affecting access to primary health care services for persons with disabilities in rural areas: a "best-fit" framework synthesis. Global Health Resources Policy, vol. 3, pp. 36 -56.. https://doi.org/10.1186/s41256-018-0091-x
3. National Primary Health Care Development Agency (NPHCDA, 2012). National guidelines for development of primary health care system in Nigeria (4th Edition).
4. Nigeria National Primary Health Care Development Agency (NPHCDA, 2012). Minimum standards for primary health care in Nigeria. The Production of Planning Research and Statistics, Abuja. Retrieved from http://www.nphcda.gov.ng/

5. V. Alegana, U. Petrina, A. Noor, S. Robert., and P. Atkinson (2012). Spatial modelling of health care utilisation for treatment of fever in Namibia. International Jour. of Health Geogr. Vol. 11(6), 1 - 21.
6. M. L., Willcox, W. Peersman, P. Daou, et al. (2015). Human resources for primary health care in sub-Saharan Africa: Progress or stagnation? Hum. Res and Health. Vol. 13, 76. https://doi.org/10.1186/s12960-015-0073-8
7. WHO and UNICEF (2021). A vision for primary health care in the 21st century. News Letter, 1st April 2021. Retrieved from https://www.who.int/news-room/factshhets-details
8. Imo State Government. (2009). Imo State strategic health development plan (2010-2015). A Working Document on Strategic Health Development.
9. World Health Organization (2014). Health for the world's adolescents. A second chance in the second decade. Geneva, World Health Organization. Retrieved from http://apps.who.int/adolescent/second-decade/
10. World Health Organization (2015). Global standards for quality health-care services for adolescents: A guide to implement a standards-driven approach to improve the quality of health-care services for adolescents. WHO Library Cataloguing-in-Publication Data.
11. W. Christaller (1933). Die zentralen Orte in Süddeutschland. Eine ökonomisch-geographische Untersuchung über die Gesetzmäßigkeit der Verbreitung und Entwicklung der Siedlungen mit städtischen Funktionen. Darmstadt, 1980 (1ère édition: Jena, 1933).
12. A. Briney (2012). Central place theory. Retrieved on 17/9/2018 from http://Geography.about.com./od/urbaneconomicgeography/a/centralplace.htm
13. P. J Clark and F.C. Evans. (1954). Distance to nearest neighbour as a measure of spatial relationships in populations. Ecology, Vol. 35, pp. 445 – 453.
14. L. A. Rossbacher (1986). Nearest neighbour analysis: A technique for quantitative evaluation of polygonal ground patterns. Geografiska Annaler, Vol. 68(1-2), pp. 101 – 105.
15. B. Ayeni (2000). Quantitative methods for geography students. Ibadan, Research Support Services.
16. O. Omotosho (2010). Location distribution of rural medical services for effective development: A case of Ekiti State, Nigeria. Jour of Innov. Research in Mgt and Humanities, vol. 1(1), pp. 62 – 65.
17. S. Mayhew (2004). Oxford dictionary of geography. Oxford University Press.
18. I. S. Abdulraheem, A.R. Olapipo, and M.O. Amodu (2012). Primary healthcare services in Nigeria: Critical issues and strategies for enhancing the use by rural communities. Jour. of Publ. Health and Epidem.. vol. 4(1), pp. 5 – 13.
19. P. Thembi, M. Mokgatte-Nthabu, and O.O. Oguntibeju (2010). Utilisation of the primary health care services in the Tshwane region of Gauteng Province, South Africa. PLoS ONE vol. 5(11), pp. 55 - 59.
20. A. I. Enwereuzor, I. S. Umo and C. L. Charles-Akalonu (2021). The conditions of infrastructure and the development of rural communities in Imo State, Nigeria. Jour of Social Sciences, vol. 10(3), pp. 46 – 65. doi: 10.11648/jss.20211003.18
21. Awoyemi, T. T., Obayelu, O. A., and Opaluwah, I. (2011). Effect of distance on utilization of health care services in rural Kogi, Nigeria. J Hum. Ecol, Vol. 35 (1), pp. 1–9.
22. S. A. Agaja (2012). Spatial distribution of primary health care centres in Ughelli South and Warri South Local Government Areas of Delta State, Nigeria. International Journal of Scientific & Technology Research Vo;. 1(9), pp. 38 – 41.
23. C. L. Charles-Akalonu, (2017). The utilization of primary health facilities in Isiala Mbano LGA, Imo State. Unpublished thesis, Abia State University.
24. Government of Imo State of Nigeria (1984). Atlas of Imo State of Nigeria. State Ministry of Land, Survey, and Urban Planning.
25. 1. S. Umo and M. C. Ike (2021). A dimension of geographic regions and landforms. Owerri, Ekenegrace Publisher.

NIPES Conference Proceedings
The 1st International Conference of the Nigerian Institution of Professional Engineers and Scientists 7th-8th Oct. 2021: 50-61
www.nipesjournals.org.ng

Mathematical Models of Seasonal Dynamics of Bedload Sediments in Eco-Geomorphologic Units of the Tropical Rivers, Southeastern Nigeria

[a] Ikpong Sunday Umo; [b] Mary N. Ezemonye; [a] Angela Iweka Enwereuzor

[a] Department of Geography and Environmental Studies, Alvan Ikoku Federal College of Education, Owerri, P.M.B. 1033, Imo State, Nigeria. E-mail Address: umohikpong@yahoo.com Phone Number: +2348037565958
[b] Department of Geography and Regional Planning, University of Benin, Benin City, Nigeria

Abstract

The paucity in application of multivariate analysis of variance (MANOVA) as a model for testing and clarifying complex associations and variances among the sets of dependent and independent variables for sound ecosystem and engineering policy/ decision-making toward the protection of fragile and endangered hydrological and geomorphological units in the future. This study adopted the direct field survey and laboratory techniques. Using stratified and systematic sampling methods, eight eco-geomorphological sub-units comprising one first-order stream, six fourth-order tributaries, and the estuary were selected. A total of 32 bedload samples were systematically collected during the four climatic seasons, digest properly to ensure standard compliance, and analyzed in the laboratory. The MANOVA tests of variations, overlapping variances, and homogeneities among the groups of parameters gave Pillai's Trace (2.027), Wilks' Lambda (24.745), Hotelling's Trace (6139.576), and Roy's Largest Root (40035.113) each significant at 0.00 confidence level. The results implied that variations in eco-geomorphologic units and climatic seasons have a significant effect on the dispersal of bedload sediments within the study area. Also, the prevalence of flood and erosion hazards in the area has strong affinity with natural forces and anthropocentric parasitism, with serious threats to the future of the regional ecosystem. This study recommended: (i) sustainable and deliberate promotions of community-driven afforestation programmes with strong supports from the governments and donor agencies to facilitate ecosystem services and mitigate the impacts of climate that induced geomorphic hazards in the area and, (ii) periodic dredging of silted small rivers and construction of drainages/ roads to regulate surface runoff/ discharge from cities to Rivers.

***Keywords*:**
MANOVA models, climatic seasons, eco-geomorphologic units, bedload sediments, humid tropic, river ecosystem.

1.0 Introduction

The cardinal icons of earth sciences is the nexus of the atmosphere (climatology), lithosphere (geomorphology), hydrosphere (hydrology) and biosphere (bio-geography) which is collectively defined as physical geography. Hence, modern physical geographers usually draw their philosophies and methodologies from earth science tradition with geomorphology at the center. The flexible and complex nature of geographic and earth science phenomena necessitates the adoption of modern methods such as field, laboratory and geo-spatial technologies for enhanced understanding of the linkages especially at the basin scale.

The dynamisms in climatic and fluvial processes in the humid Tropics are among the focal geographical and earth science phenomena that instigate variations in the circulations of bedload sediments across distinct geographic spaces from tributaries of a river to the ultimate base level at time scales. The quantity and quality of land denudated and sediments discharge across given eco-geomorphological units is believed to vary based on climatic season, nature of vegetation, geology, soil, land use, and specific geomorphometry [1 - 4].

The concept "eco-geomorphology" is an interdisciplinary approach to the study of a river system that integrates geomorphology, hydrology, and ecology [5, 6]. It represents the functional fluvio-geomorphological units with viable interfaces existing among the biotic (e.g. plants, animals, and humans) and abiotic (e.g. rainfall, temperature, sediment, river, and landform) components. The capability of a river to distribute bedload sediments from the eco-geomorphological units (sub-

basins) to the estuary is controlled by river discharge, which in turn is a function of climate, vegetation, topography, rock properties, soil, geology, basin area, and human [7].

The hydrologic cycle controls the timing and volume of their delivery from various eco-geomorphologic units of a River basin to the Ocean. The concept "eco-geomorphology" is an interdisciplinary approach to the study of a river system that integrates geomorphology, hydrology, and ecology [5, 6]. It also represents the functional interactive unit among biotic (e.g. plants, animals, and humans) and abiotic (notably climate, sediment/ soil, and landform) components. The complex nature of interactions often varies across ecosystem units and time, which necessitates the choice of viable mathematical models that can aid the elucidation of such relationships among distinct phenomena in disciplines.

Contextually, mathematical models are formal equations that can be used to represent the relationships among geomorphic parameters, their components, and rates of changes within the river ecosystem. Such relationships can range from simple equations to complex software codes or by applying many interlinks to determine the explicit outcomes over discrete time scales such as a hydrological year or climatic seasons [8]. It can take two broad approaches comprising empirical-statistical and deductive-deterministic model [9].

Although there are many operational procedures involved in quantitative evaluation of fluvial landform properties in earth science and geomorphological literature within the past three decades, differences tend to exist based on content, context, and researchers' interest as exhibited in [3, 10, 11, 12]. Amidst the apparent differences, Richards [13] statements offered intriguing viewpoints, thus:

> *"A conceptual image of the landform must be translated into measurable attributes that represent the concept satisfactorily, and can be quantified with accuracy, precision, and reproducibility. Thus, a rigorous operational definition is essential, and this must consider: (a) delimitation of the landform boundary; (b) the quantitative index itself; (c) the sampling scheme required to define a representative subset of the relevant population; (d) the appropriate and available data sources and methods of measurement and; (e) the measurement procedures and practices"* [13].

The choice of procedures is individual's (researcher's) dependent, usually driven by quantitative tools that may range from simple (e.g. mean or percentage) to complex model (e.g. factor analysis or multivariate analysis of variance). However, it is the viability of underlying philosophy that will facilitate the achievement of a given aim and/ or a set of objectives. Hence, the indomitable fact is that Richard's principles offer very instructive methodological guides in the perspective of dynamism in bedload sediments dispersal across eco-geomorphological units of the humid Tropical Rivers in Southern Nigeria.

The spatial characteristics of landforms such as river basin geomorphometry, climate, and land use often have influences on the bedload particle accumulations and discharge. Surian [14] found that the downstream changes in flow resistance and sediment transportation were closely related to the rate of change in sediment size. Also, Di Stefano and Ferro [15] established that fully dispersed size was important in certain sediment chemical/ physical properties as well as the processes of erosion and sediment transported by overland flow were dependent on the sediment aggregation.

In Baraolt depression of Olt River, Csiszer and Petrea [16] assessed the connections between the tectonics and the geologic structures and how they reflected on landscapes. Cartographic analyses revealed the division of the area into depression in hollows, bays, and other basins compartments.

Accordingly, understanding of the geographic coverage (basin area demarcation) remained the starting point in exploring fluvio-morphology dynamics, while the presence of coal is believed to instigated anthropogenic parasitism as depicted on land complexities in the Olt catchment [16].

Much of the identified studies tend to rely on accurate DEM for the calculation of geomorphic metrics (with emphasis on slope and curvature) or extraction of geomorphic features such as channels, hill slopes, hilltops [17]. In spite of the efficacies, Fisher and Tate [18] have reported sources of errors in DEM, which suggests the need to shift emphasis to laboratory and quantitative tools in studying geomorphologic and hydrologic parameters of interest.

The fluvial systems often play a vital role in land sculpturing and responses of drainage networks, adjustment of river, shape, relief, and flow of sediments still form the basis for discussions as exemplified in Whipple, DiBiase, and Crosby, [19]. Besides, an understanding of dynamics in river processes requires in-depth knowledge of bedload sediment generation and discharge because they usually influence channel hydraulics and stability, river quality, and aquatic habitats as well as the rivers' age and utilization.

Although mathematical model (multivariate analyses of variances (MANOVA)) have attracted the attention of researchers in various fields such as mathematics, statistics, economics, business, psychology, and education [20, 21, 22], its applications in physical geography and earth science explorations are rather eclipsed or scarce [3, 12]. The perceived lacuna constitutes a major source of concern, especially when considering the multitude and complex nature of phenomena modern physical geographers and allied earth scientists work with to clearly comprehend and elucidate their interactions for informed river ecosystem service.

The cardinal questions agitating the psyches of the scholars in this study are: (i) Do variations in eco-geomorphologic units and climatic seasons have a significant influence on the dispersals of bedload sediments (sand, silt, clay, organic carbon, and organic matter) in the humid tropical Rivers of Southeastern Nigeria? (ii) What are the implications of results on the fluvial and ecosystem services in the humid tropical rivers of Southeastern Nigeria? It is against the perceived issues that this study is instituted to use MANOVA tests as surrogates for assessing the intriguing associations and variations in climatic seasons and eco-geomorphic units on bedload sediments dispersals in the humid tropical rivers of Southeastern Nigeria, using the Kwa Iboe River as a case study.

The paucity in the application of viable models in the robust testing of dynamics, associations and variances among diverse hydrological and geomorphological parameters in the 21st century have necessitated the adoption of mathematical equations as surrogates in evaluating seasonal dynamics of bedload sediments dispersal across eco-geomorphologic units and climatic seasons in the humid tropical rivers of Southeastern Nigeria. In consideration of the stated aim, the following specific objectives were investigated.

(i). To determine the influence of variations in eco-geomorphologic units and climatic seasons on the dispersals of bedload sediments in the humid tropical Rivers of Nigeria.

(ii). To develop the viable policy frameworks for the sustainability of River and ecosystem resources in the humid tropical Rivers of the Southeastern Nigeria.

2.0 The Study Area

2.1 Geographical Settings

The Kwa Iboe River eco-geomorphologic unit is located approximately between Latitude 4^0 20' and $5^0$40' North of the Equator and Longitude 7^0 10^1 and 8^0 25^1 East of the Greenwich Meridian [3]. It covers parts of the humid Tropical rainforest belt covering part of Abia and Akwa Ibom States of Southeastern Nigeria, ramified by the mangrove swamp forest occupying parts of the continental shelf of the Atlantic Ocean. The populations of the study area are dominated by agrarian communities (fishermen, hunters, and farmers) and miners.

2.2 Climate and Vegetation

The rainfall and temperature patterns across the study area vary based on climatic seasons. The total annual rainfall decreases persistently from the coastal belt of the Atlantic Ocean especially Ibeno, Ikot Abasi, Eket, and old Nsit clan toward the interior. The core coastal border of the Atlantic Ocean received convectional rainfall annually with no month of dry season with Tropical wet climate. It has a mean annual rainfall of 2443.3 mm from 1977 to 2013 while the mean annual temperature is 27 ^{0}C [3, 23, 24].

The middle and the upper catchments of the study area recorded 2 to 4 months of dry season annually with Köppen's Am climate [25, 26]. The hydromorphic soils occur over the impervious shale and the seasonal waterlogging is frequent especially during the rainy periods, thereby providing enable ground for the cultivation of rice, cocoa yam, yam, and allied crops in wetlands eco-geomorphology. The study area often recorded four climatic seasons annually (comprising two dry and two rainy seasons). The short dry season is associated with the month of August (August break) while the long dry season is recorded between the months of December and March, while the coldest month recorded during the month of July.

2.3 Pedo-geomorphological Setting

The soils within the upper part of the study area vary from deeply buried pebbles underlain by finer sands to clay sub-surface soils of distinct grains. Around the Umuohia-Ikwano axis of the Abia State, some traces of Imo clay-shale of the early Eocene formation with deep porous red soils (Ferralsols) tend to dominate the area (Imo State Survey and Urban Planning, 1984). At the middle fringe of Ikwano, Isiala, and Obot Akara, the deep porous brown (Ferrallitic) soils are dominant (Figure 1). The traces of shale are basically at the divide of Imo and Kwa Iboe Rivers offer the soil its shelly grey colour and studded with brown cylindrical to conical structures [3, 26]. Within the Akwa Ibom axis, over 80 percent of the soils composed of deep porous brown soils, collectively called Ferrallitic soils. It is not well mature, hence highly susceptible to varying types of upstream erosion and downstream flood [3]. These soils according to Bassey cited in Usoro and Akpan [25] are widely distributed across Ikot Ekpene, Ukanafun, Essien Udim, Uyo, Abak, Etinan, Nist Ibom, and Nsit Ubium with the exceptions of the floodplain and river channels where hydromorphic soils prevail. The lower part of the study area is under the strong influence of marine activities such as coastal flood and marine erosion due to the proximity to and influence of the Atlantic Ocean as depicted in Figure 1.

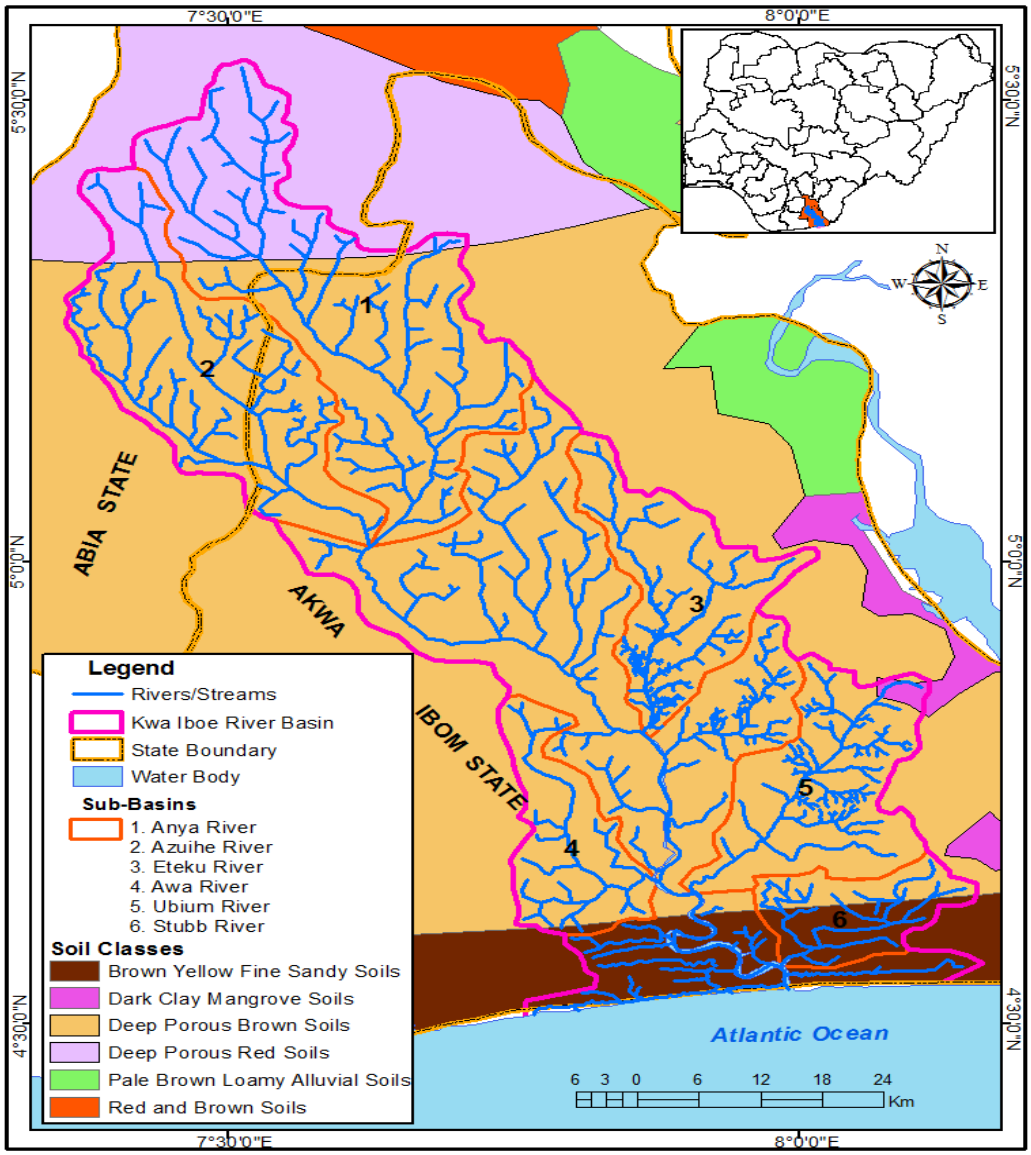

Figure 1: The Study Area showing Soil formations across Eco-geomorphic Units.
Source: Adapted from Umo [3].

3.0 Materials and Methods

The upsurge in demands for the application of innovative methods especially laboratory and computer-aided quantitative tools in physical geography and geomorphology in particular, during this 21st century justifies the choice techniques to conform with the globally recommended researches and practices discussed in what follow.

3.1 Sampling and Sediments Collection Techniques

The study area was stratified into eight sub-units using stratified sampling method and each unit represents eco-geomorphologic units for the bedload sediments. The units are composed of one first-order tributary where the basin originated from, six fourth-order eco-geomorphologic units (Anya River, Azuihe River, Awa River, Eteku River, Ubium River, and Stubbs River), and estuary where the river enters the Atlantic Ocean (Figure 2).

In each eco-geomorphological unit, three core samples were collected along each transect (at the left, center, and right side) in an undisturbed manner [3]. The collection was carried out using a specially constructed galvanized 8.5 cm by 10 cm diameter sediment corer at a depth of 0 to 15 cm. The rationale was for easy access and collections of bedload sediment deposits that interact with water discharge, as recommended in Umo [3]. The collections were carried out during the months of November for early dry season; second set during February for the peak dry season; a third set during the month of April for the early rainy season and; fourth set during the month of July for the peak rainy season to examine the effects of dynamics in climatic seasons. Each set of bedload sediments collected across eco-geomorphologic units (Figure 2) were stored in a clean plastic polythene bag, labelled orderly, and packaged in a cooler before being transported to the National Laboratory at Umudike for further treatments and analyses.

3.2 Sediments Preparation, Analyses, and Classification

At the laboratory, sedimentation by pipette method was employed as a basis for the eight sediment sample analyses. The details of procedures, experiments, methods and standard compliances as passionately described in [27, 28], and reiterated in Whalley [29], Gouldie *et al.* [30] and Umo [3] were adopted and strictly followed in the laboratory. The sediment classification followed García-Gaines and Frankenstein [31] scheme, with the diameter limits (mm): very fine sand (0.05 – 0.10); fine sand (0.10 – 0.25); medium sand (0.25 – 0.50); coarse sand (0.50 – 1.00); very coarse sand (1.00 – 2.00). The rationales were to facilitate clear physical description of bedload sediment characteristics, comparisons of sample size dispersals at distinct eco-geomorphologic units and relate the samples to the sedimentological history, and enhance statistical modellings.

3.3 Demarcation of Eco-geomorphological Units and Geomorphometry

The study is delimited to river tributaries that made up the Kwa Iboe River. It was carried out using Shuttle Radar Topography Mission (SRTM) with 30 m resolution. The image (Raster) was used for eco-geomorphologic (fluvial) units' delineation and in the derivation of sub-catchment area geomorphometry. The SRTM was complemented with the topographic maps (Afikpo 313 SW; Ikot Ekpene 322 NE; 322 SW) each produced by Federal Survey Department, Lagos on a scale of 1:50,000 to avert the limitation posed by dense vegetation along the wetlands that eclipse the river channel in the satellite imagery (Raster).

The delineation of the study area was carried out using the geospatial methods described in Umo [3], while eco-geomorphological units were demarcated using the standard envisaged by Strahler [32] and recommended in Umo et al. [2]. The fourth-order sub-basins were selected because geomorphologists and allied earth scientists accept medium-sized river basins as well matured for catchment studies [11, 33]. The recorded GPS locations/ ground truth information and maps were rectified and geo-referenced in a GIS environment with Arc-GIS 10.2 model assigning Universal Transverse Mercator (UTM), World Geodetic System (WGS) dating from 1984 as revised in 2004). A 32 N Zone Projection System with ERDAS Imagine 8.5 and Terrain Analysis System were employed as emphasized in Hajam et al [34] and Umo et al [35].

3.4 Data Analyses

Data generated from distinct sources across the eight (8) eco-geomorphologic units and four climatic seasons (Figure 2) were analyzed using MANOVA model (Pillai's Trace, Wilks' Lambda, Hotelling's Trace and Roy's Largest Root) tests to explore research question one. A

regression model was used to ascertain the proportion of variance explained by the independent variables on the linear combination of the dependent variables. One way analysis of variance was employed as a surrogate to test for the variances in the mean dispersal among the studied parameters in the humid tropical Rivers of Southeastern Nigeria.

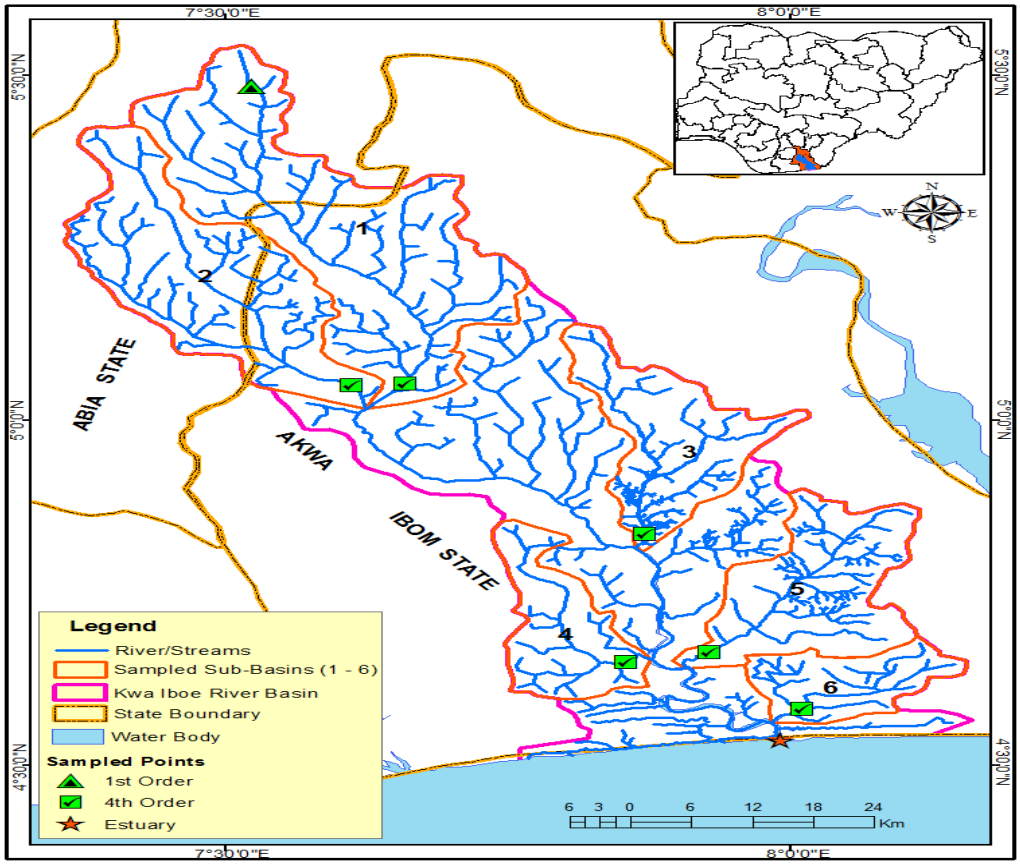

Figure 2: Geospatial Delineation of Study Area showing the Sampling Points.
Source: Adapted from Umo [3]

4. Discussion

4.1 Eco-geomorphologic Units, Climatic Seasons and Bedload Sediments' Dispersals

In an attempt to address the research question one that states thus: "do variations in eco-geomorphologic units and climatic seasons have significant influence on the dispersal of bedload sediments (sand, silt, clay, organic carbon, and organic matter) in the humid tropical Rivers of Southeastern Nigeria? Data generated on bedload sediments across eco-geomorphologic units and climatic seasons were analyzed using mathematical models (comprising MANOVA and Regression models) as summarized in Tables 1 and 2.

MANOVA is used to determine the influence of variations in eco-geomorphologic units (sampled location) and climatic seasons on the linear combination of bedload sediments (sand, silt, clay, organic carbon, and organic matter) dispersal, and the results summarized in Table 1. The four statistical tests presented in Table 1 are answering the same question, but with different testing powers as evidenced in the degrees of freedom. Also, the results are reported both as intercept to aid the scaling of the result and sampled location to form the basis for tests of significance as recommended in Umo [3]; Olson [20]; Warne [21].

The assessment of the influence of the size (homogeneity) among the groups of variables across the eco-geomorphologic units and climatic seasons using Pillai's Trace model yields a value of 2.016 which is a good representative result because of its proximity to zero. The result of the Pillai's value means that the sum of size effects within the groups' variance are contributing more to the model, but taking decision must be backed-up by testable level of significance [21, 23]. Hence, the calculated F value associated with Pillai's model gave 2.027. The test of significant at $(0.05)_{40/120}$ confidence level gave a Table value of 1.4290. It is therefore inferred from the results that variations in eco-geomorphologic units and climatic seasons have significant influence on the dispersals of bedload sediments in the humid tropical Rivers of the Southeastern Nigeria.

Similarly, Wilks' Lambda as a tool in MANOVA is used as a surrogate for determining the proportion of variance influenced by ego-geomorphologic unit and climatic seasons on the combination of the groups of dependent variables in study area. The model result presented in Table 1 gives a unique statistical value of 0.000 that shows perfect corroboration of Umo [3] and Nath and Pavur [36] observations that a value of zero means that there is no any variance that is not explained by the independent variables. The result implies that both groups of variables contribute to the model's stability. Consequently, the test of variances using Wilk's Lambda model yields the calculated F value of 24.745. A test of significant at $(0.05)_{40/89}$ confidence level yields a Table value of 1.4290. The high calculated F value suggested that variations in eco-geomorphologic units and climatic seasons do have significant influence on the dispersals of bedload sediments in the area.

Furthermore, the Hotelling's Trace that operates with the highest matrix yields a model value of 13,346.90 and a corresponding F value of 6,139.58. A test of significant at $(0.05)_{40/92}$ confidence level yields a Table value of 1.4290. It is infers from the result of Hotelling model that variations in the locations of eco-geomorphologic units and climatic seasons do have significant influence on the dispersal of the bedload sediments in the humid Tropical Rivers. The result showed strong collaboration with the decision level reached base on the Pillai's Trace and Wilk's Lambda tests.

In order to measure the association strength (influence) among the groups of variables, Roy's Largest Root is used. This is because of its focus on the proportion of overlapping variance (influence) among the independent factors and the first linear combination of the dependent variables. The model result gives a very high value of 13,345.038. The calculated F value yields 40,035.113. A test of significant at $(0.05)_{8/24}$ confidence level reveals a Table value of 2.3551. The result of the Roy's largest Root reveals that variations in the locations of eco-geomorphologic units and climatic seasons have significant influence on the dispersal of bedload sediments in humid Tropical Rivers.

The results supported Akpan [10] observation that multivariate statistical methods often showed a valid explanatory power to complex array of data in watershed research. Hence, the statistical tests associated with the MANOVA model showed deviation from that of the single response model (ANOVA and t-test) results used in Umo and Enwereuzor [23] due to differences in tested parameters and statistical methods.

Table 1: The Multivariate Tests[a] of Variations among Eco-geomorphologic Units and Climatic Seasons and Bedload Sediment Dispersals

Effect	Model	Value	F	df_h	df_e	Sig.	Decision
Eco-gemorphologic Unit	Pillai's Trace	2.016	2.027	40	120	.002	Rejected
	Wilks' Lambda	.000	24.745	40	89	.000	Rejected
	Hotelling's Trace	13346.905	6139.576	40	92	.000	Rejected
	Roy's Largest Root	13345.038	40035.113	8	24	.000	Rejected

a. Design: Intercept + eco-geomorphologic units. b. Exact statistic. c. The statistic is an upper bound on F that yields a lower bound on the significance level. Decision Level is 0.05 Confidence.

4.2 The Proportion of Variations between Parameters in the Humid Tropical Rivers

In order to establish the proportion of variance attributed to the influence of eco-geomorphologic units and climatic seasons on bedload sediment dispersals in the humid tropical Rivers of Southeastern Nigeria, MANOVA is used. The results summarized in Table 2 revealed widespread disparities. The sums of squares associated with each model indicated that sand is 283,607.500, silt is 188.318, clay is 491.010, organic matter shows 11.398, and organic carbon yields 4.219 accordingly. Also, the mean squares associated with the model vary with a value of 35,450.937 for sand, 23.450 for silt, 61.376 for clay, 1.425 for organic matter, and 0.527 for organic carbon. The calculated F values for the proportion of variation between eco-geomorphologic units and each parameter revealed that sand possessed a value of 3898.921. The silt exhibited a value of 6.403, clay gave a value of 12.075, organic matter yielded a value of 3.481, and organic carbon yields 19.283. The test of significant variations between parameters at $(0.05)_{8/24}$ confidence level reveals a Table value of 2.3551 that is less than the calculated F values presented in Table 2. The results indicate that variations in eco-geomorphologic units have a significant influence on bedload sediments dispersed within the humid tropical Rivers of Southeastern Nigeria. The results showed a strong affinity with the initial report by Umo and Enwereuzor [12] of southeastern Nigeria, though differences existed in terms of content, geology geographic coverage, and pedo-geomorphology. Discounting the MANOVA results, a linear regression model was used as a surrogate to determine the proportion of influence accounted for by variation in eco-geomorphologic units on a linear combination of each bedload sediment dispersal in eco-geomorphologic units. The result of the adjusted R square presented in Table 1 showed that sand attracted a very high positive regression coefficient of 0.999 that explained 99.9 percent of the proportion of variance. The organic carbon has a coefficient of 0.865 that explained 86.5 percent of the effect of variance. Clay particle possessed 0.801 representing 80.1 percent of the variance, silt yields a coefficient of 0.681 that accounted for 68.1 percent of the variance, and organic matter gives 0.537 that explains 53.7 percent of the variance in the series. The revealed patterns in the results using MANOVA are rather contradictory to Umo and Enwereuzor [12] whose emphasis was placed on ANOVA and t-test models as surrogate for quantifying the pedo-geomorphologic attributes of Rivers in Southeastern Nigeria. The contradiction could probably be attributed to the differences in methods and sampled attributes. Also, the high regression coefficients and the corresponding high proportion of variances explained in this context strongly corroborated the pattern of interrelation and variations exhibited in Table 1.

Table 2: The tests of Effects of Variations Between-Bedload Sediments and. Eco-geomorphologic Units

Source	Variable	Type III Sum of Squares	df	Mean Square	F	Sig.	R Squared	Adjusted R Squared
Model	Sand	283607.500[a]	8	35450.937	3898.921	.000	.999	.998
	Silt	188.318[b]	8	23.540	6.403	.000	.681	.575
	Clay	491.010[c]	8	61.376	12.075	.000	.801	.735
	O_M	11.398[d]	8	1.425	3.481	.008	.537	.383
	TOC	4.219[e]	8	.527	19.283	.000	.865	.820
Error	Sand	218.220	24	9.093				
	Silt	88.233	24	3.676				
	Clay	121.990	24	5.083				
	O_M	9.823	24	.409				
	TOC	.656	24	.027				

Source: Author's Fieldwork (2017 -2018).

The error term in the multivariate presented in Table 2 represents the residual of unexplained variance "noise". The errors associated with the sum of squares vary from one bedload sediments to the other across the eco-geomorphologic units. For instance, sand constitutes the highest value of 218.220, followed by clay with 121.990. Silt attracts 88.233 and organic matter is associated with an error margin of 9.823 while the lowest error margin of 0.656 is associated with total organic carbon. The variations in each error margin exhibit a very strong and direct link with the computed values for the sums of squares. However, a similar trend of error in dispersal is recorded for the mean squares summarized in Table 2.

5. Policy Implications on River and Ecosystem Sustainability

The ecosystem restoration and sustainability has been largely the purview of biologists and engineers in the 19th and early 20th centuries. However, physical geographers (geomorphologist, climatologist, hydrologist, and bio-geographer) are now assuming the central position for any effort to successfully restore river and allied ecosystem to more natural arrangements, especially, when the focus is on the non-structural domain [37]. The highlights partly justifies why physical geographical researches, ideologies, and expertise applications in this post-modern century emphasize more on the eco-geomorphological system services for the sustainability of the Earth's environment.

The dynamics in the dispersal, quantities, and qualities of bedload sediments, landforms and allied fluvial resources within the humid tropical belt of the Southeastern Nigeria had persistently been subjected to despoliation in different eco-geomorphologic units [3, 4, 25, 38], due to exploitative excesses emanating from population growth, urbanization, and climate change impacts. The exploitative excesses from anthropogenic agents have further triggered threats to exotic, yet endangered ecosystem species (in rivers, land, and forests) that humans are supposed to protect, rehabilitate, conserve, and own for posterity.

The tests of variations, overlapping variances, and homogeneities of the groups of parameters using mathematical models sustain that variations in eco-geomorphologic units and climatic seasons have a significant influence on the dispersals of bedload sediments in the humid tropical Rivers. A test of the linear combination of each group of dependent variables using weighted models revealed that variations in eco-geomorphologic units have significant influence on the mean dispersal of bedload sediments in the humid tropical Rivers of Southeastern Nigeria.

The implication is that persistent increase in the dispersal rate of bedload sediments especially during the early and peak rainy seasons suggest the possibilities of siltation, sedimentation, and drying up of small (1st, 2nd and 3rd) order river ecologies. The increase was accelerated by the impact of climate variability and the poor or absence of appropriate ecosystem services by resource users in the area. Further losses in fluvio-hydrological and biospheric resources imply the risk of continuous rise in global temperature. It will also result in the rising incidences of geomorphological and geo-physical hazards such as storms, floods, erosion, mass wasting, and sediment yield which Southeastern Nigeria had protracted histories.

6. Concluding Remarks and Recommendations

There is a sustained dynamics (variabilities) between and among climatic seasons and bedload sediment dispersals across eco-geomorphologic units in the humid tropical Rivers of Nigeria. The

patterns of dynamics in the characteristics of bedload sediment dispersals constitute more risk to sustainability of ecosystem (hydrospheric, biospheric, lithospheric and atmospheric resources) in the study area, if urgent steps are not taken through partnership between governments, donor agencies and the affected communities to enforce the existing Laws for the protection of landscape and ecosystem species in this 21st century.

It is clear from the preceding discourses that a sustain and deliberate promotions of community-driven afforestation programmes with adequate funding from the government and donor agencies will facilitate ecosystem services and mitigate geomorphic hazards such as erosion, flood, sediment yield, and mass wasting that are prevalence in most eco-geomorphologic units at the upper and middle streams of the study area.

The poor states of infrastructure especially roads and drainages necessitate proactive actions. For instances, timely dredging of the already silted small (e.g. 1st, 2nd, and 3rd order) river channels and beds will be very helpful in averting siltation and drying up of endangered sub-catchments. Also, construction of standard drainages will be very helpful in reducing sediment yields and regulating surface runoff and discharge from the cities and town into Rivers will boost the sustainability of the river resources for posterity.

7. References

[1] I. Zavoianu (1985). *Morphometry of drainage basin*. Amsterdam, Elsevier.
[2] I.S. Umo, C.C. Ojinma, and M.C. Ike (2019). Issues and Application of Linearized Models of Geomorphic Properties in the Ikpa Watershed, Nigeria. Asian Jour. Geog. Research, Vol. 10(3), pp. 1 – 12. Retrieved on 27/6/2020 from http://dx.doi.org/10.9734/ajee/2019/430123
[3] I.S. Umo (2019). The dynamics of sediment, heavy metals and nutrients in the Kwa Iboe River Basin. Ph.D thesis, Department of Geography and Regional Planning, University of Benin, Nigeria.
[4] M.N. Ezemonye, I.S. Umo, C.C. Ojinma, M.C. Ike, A.I. Enwereuzor (2017). Geomorphometric parameters of Ikpa River and its implications for the planning of fluvial hazards in the Northeast of Akwa Ibom State. Jour. of Geogr. Earth Sci. & Environ., Vol. 11(1), pp. 1 – 12. http://dx.doi.org/10.9734/JGEESI/2017/34674
[5] M.C. Thoms and M. Parsons (2002). Eco-geomorphology: An interdisciplinary approach to River science. Symposium on the Structure and Implication of Fluvial Sedimentary System, 272. Retrieved from https://www.researchgate.net/publication/267378184
[6] P. Mondal (2014). A review study of eco-geomorphology an interdisciplinary approach to River science. *Gideon Research Thoughts*. Vol. 3(8), pp. 1 – 7.
[7] G. Sofia, J.K. Hillier, and S.J. Conway (2016). Frontiers in geomorphometry and earth surface dynamics: possibilities, limitations and perspectives. Earth Surf. Dynamics, Vol. 4, pp. 721–725. Retrieved from http://dx.doi.org/10.5194/esurf-4-721-2016.
[8] I.S. Umo, O. A. Ibanga and M.C. Ike (2018). Application of Geospatial Technologies in Assessing Gully Erosion in the Humid Tropics of Eniong Offot, Uyo, Akwa Ibom State. *Jour. of Envir. & Eco. Vol.* 6(3), pp. 1 – 13. Available online on http://dx.doi.org/10.9734/AJEE/2018/40224
[9] C.C. Ojinma and I.S. Umo (2019). A dimension geography philosophy and development. Owerri, Kristel Publishers.
[10] I.I. Akpan (2013). Assessment of water quality in Imo River estuary using multivariate statistical method. *IOSR Journal of Applied Chemistry*, Vol. *4*(5), pp. 35 - 40.
[11] I.S. Umo (2014). *Drainage basin morphometry and discharge in Ikpa River, Akwa Ibom State, Nigeria.* M. Sc. Thesis, Department of Geography and Regional Planning, University of Benin, Nigeria, 30th June
[12] I.S. Umo and Enwereuzor, A.I. (2021). The implications of spatial variations in geographic location, geology and pedology on food security in the Southeast Nigeria. Jour. Of Earth Sciences, Vol. 10(3), pp. 83 – 89. Available online on http://dx.doi.org/10.11648/j.earth.20211003.12
[13] K.S. Richards (1990). General problems in morphometry. In A.S. Gouldie et al. (Editors) Geomorphological techniques. Second edition, edited for the British society for Geomorphological Research Group. Routledge.
[14] N. Surian (2002). Downstream variation in grain size along an Alpine River: Analysis of controls and process. Geomorphology, vol. 43, pp. 137 – 149.
[15] C. Di Stefano and V. Ferro. (2002). Linking clay enrichment and sediment delivery processes. Bio-system Engineering, Vol. 81(4), pp. 465 – 477.

[16] L. Csiszer and D. Petrea (2012). The reflection of the geological factors within the morphology of the Baraolt depression. Revista de Geomorfologie, Vol. 14, pp. 57 – 66.
[17] G. Sofia, J.K. Hillier and S.J. Conway (2016). Frontiers in geomorphometry and earth surface dynamics: possibilities, limitations and perspectives. Earth Surface Dynamics, vol. 4, pp. 721–725. Retrieved from http://dx.doi.org/10.5194/esurf-4-721-2016.
[18] Fisher, P.F. and Tate, N.J. (2006). Causes and Consequences of Error in Digital Elevation Models. *Progress in Physical Geography*, 30, 467 – 489
[19] K.X. Whipple, R.A. DiBiase and B.T. Crosby (2013). Bedrock Rivers. In A. Switzer and D. M. Kennedy (eds), *Treatise in Geomorphology*, *Methods in Geomorphology*, pp. 550 – 573. Elsevier, Amsterdam.
[20] C.L. Olson (1976). On choosing a test statistic in multivariate analysis of variance. Psychological Bulletin, Vol. 83, pp. 579 – 586.
[21] T.R. Warne (2014). A primer on multivariate analysis of variance for behavioural scientists. Practical Assessment, and Evaluation, Vol, 19(17), pp. 1 – 10.
[22] J.W. Grice and M. Iwasak (2007). A truly multivariate approach to MANOVA. Applied Multivariate Research, Vol. 12(3), pp. 199 – 226.
[23] I.S. Umo and A.I. Enwereuzor (2021). The implications of area morphology and particulate matters' distributions on the Kwa Iboe River Basin restoration, Southeastern Nigeria. Jour. of Water Resour. and Ocean Science, Vol. 10(3), pp. 53 – 60. Available online on http://dx.doi.10.11648/j.wros.20211003.13
[24] C.E. Udosen (2008). *Gully erosion in Ikpa river basin: a threshold phenomenon*. Lagos, Time Communication.
[25] E.J. Usoro and P.A. Akpan (editors) (2010). *Akwa Ibom State: Its geographical perspective*. A special publication of the Department of Geography and Environmental Resources Management University of Uyo, Nigeria. Immaculate Publication Limited.
[26] Ofomata, G.E.K. (1985). *Nigeria in maps: Eastern States*. Benin, Ethiope Publishing House.
[27] T.N.W. Akroyd (1969). *Laboratory testing in soil engineering.* London, Soil Mechanics.
[28] J.S. Galehouse (1971). Sedimentation analysis. In *Procedures in sedimentary petrology*, R.E. Carver (ed.), PP. 69–94. New York: Wiley.
[29] W.B. Whalley (1990). Material properties. In A.S. Goudie *et al.* (ed.) Geomorphological techniques. 2nd Edition, edited for the British Geomorphological Research Group. Pp. 126 – 195. New York, Routledge.
[30] A. Gouldie, M. Anderson, T. Burt, J. Lewin, K. Richards, B. Whalley and P. Worstley (Editors) (1990). (Second Edition). *Geomorphological techniques*. Edited for the British Geomorphological Research Group. Chapter three. London and New York, Routledge.
[31] R.A. García-Gaines and S. Frankenstein. (2015). USCS and the USDA Soil Classification System Development of a Mapping Scheme. Cold Regions Research and Engineering Laboratory Retrieved on 22/5/2020 from http://acwc.sdp.sirsi.net/client/default.
[32] A.N. Strahler (1952). Hypsometric analysis of erosional topography, *Bulletin of the Geological Society of America*, vol. 63, pp. 1117 – 1142.
[33] B. Sumeghy and T. Kiss (2012): Morphological and Hydrological Characteristics of Paleo-channels on the Alluvial Fan of Maros River, Hungary. Jour. of Envir. Geogr. Vol. 5(1&2), pp. 11 – 19.
[34] R.A. Hajam, A. Hamid, and S. Bhat (2013). Application of morphometric analysis for geo-hydrological studies using geo-spatial technology –A case study of Vishav drainage basin. Hydrological Current Research, Vol. 4. http://dx.doi.org/10.4172/2157-7587.1000157
[35] I.S. Umo, M.N. Ezemonye, M.C. Ike and A.I. Enwereuzor. (2018). Dimensional basin morphometry and discharge in the Coastal Plains Sands of the Ikpa River, Akwa Ibom State, Nigeria. Jour. of Geogr. Envir. & Earth Science International, Vol. 13(3), pp. 1-13. http://dx.doi.org/10.9734/jgeesi/2017/38699
[36] R. Nath. and RPavur, R. (1985). A new statistic in the one way multivariate analysis of variance (MANOVA). Computational Statistics and Data Analysis, Vol. 2, pp. 297–315.
[37] B.L. Rhoads and C.E. Thorn (Editors) (1996). The scientific nature of geomorphology. Proceedings of the 27th Binghamton Symposium in Geomorphology held 27-29 September, pp. 392 – 492. John Wiley & Sons.
[38] U.J. Ituen and I. U. Johnson. (2015). Kwa Iboe River: Its physical characteristics and economic potentials to host communities in Abia and Akwa Ibom States, Nigeria. The International Journal of Social Sciences and Humanities Invention, vol. 2(1), pp. 922 – 934.

NIPES Conference Proceedings
The 1st International Conference of the Nigerian Institution of Professional Engineers and Scientists 7th-8th Oct. 2021: 62-71
www.nipesjournals.org.ng

Effect of Seawater Corrosion on 0.32%C and 0.17%C low alloy Steels with Strain Induced Cavities

Unueroh Ufuoma Georgina[a] , Igbinomwahia Noel[b]

[a,b]Department of Mechanical Engineering, University of Benin. Benin City. PMB1154. Nigeria

Abstract

The specimens from both steels were machined into tensile specimens but not notched while others were notched. Some of the notched tensile specimens were then fractured to obtain three different strain levels. Based on these strain levels obtained, the notched specimens were prestrained. Some of the specimens were immersed in liquid nitrogen at -196°C and then fractured by impact. The fracture surfaces were examined using scanning electron microscope. Some of the specimens were stress relieved to remove virtually all the residual stress present, leaving just cavities. The remaining specimens were not stress relieved, leaving both the residual stress and cavities. The specimens, were then immersed in seawater for 90 days and corrosion effect were measured using weight loss method. At the end of 90 days exposure, specimens with only cavity, had a corrosion rate of 17.69, 46.38 and 50.72 mg/cm^2/yr for the low alloy steel, at three different prestrained levels respectively. For the 0.32%C steel, it was 15.66, 41.09 and 44.42 mg/cm^2/yr. Though the specimens with cavities and residual stress were found to have higher corrosion rate, with a corrosion rate of 21.25, 48.05, 57.51mg/cm^2/yr and 16.43, 42.86, 50.75 mg/cm^2/yr for the 0.17%C low alloy and 0.32%C steel respectively, the cavities were found to contribute more to the high corrosion rate.

***Keywords*:**
Prestrained, Stress Relieve, Cavities, Residual Stress.

1. Introduction

Generally, corrosion in seawater involves two reactions:

$$Fe \rightarrow Fe^{2+} + 2e^- \quad \text{(Anodic Reaction)} \quad (1)$$
$$O_2 + 2H_2O + 4e^- \longrightarrow 4OH^- \text{ (Cathodic Reaction)} \quad (2)$$

The surface of iron develops oxide layers that strongly limits the rate of the anodic reaction and prevents further attack by the chloride ions [1-4]. [1] reported that about nine different oxide phases develop on the surfaces of iron and steel. Passivity breakdown however can occur when the concentration of the chloride ions from seawater exceeds the threshold value [5,2,6]. In this case, the steel is said to undergo active dissolution which result in a large increase in the rate of oxidation of iron.

It is widely known that carbon steel undergoes uniform corrosion. If carbon steel experiences uniform corrosion, which is a surface phenomenon, how then can cavities created within these steels cause increased corrosion in seawater? If indeed cavities cause increased uniform corrosion in seawater, what could possibly be the mechanism behind this? Very little has been done on this area. Walsh and Sagues, [7] who studied steel corrosion in Submerged Concrete Structures in marine environments, provide an interesting line of reasoning into a possible explanation of how this could happen. They examined a small part of the steel surface in a submerged zone and discovered that the portion of the steel examined had experienced severe corrosion. They proposed two reasons for this. First the part of the steel that had low corrosion rate must have been in the active condition, but

corroding slowly or secondly, the steel part was in a passive condition, though having a high chloride content on its surface.

To accept the first proposition, that the submerged steel was corroding differently, where no protective film is present, despite being in the active condition, they proposed a scenario where the corroding portions are probably with local concrete deficiencies, such as cracks and these cracks somehow allows quick removal of iron ions from the corroding area, thus enhancing the anodic reaction rate when compared to that of the rest of the steel. They argued that in order to balance the removal of positive metal ions at the anodic region and stabilize the local corrosion pattern, there will be more chloride ion accumulation in these regions, resulting in local Ph depression by associated hydrolysis. This process was believed to have strongly increased the anodic reaction rate over the other active regions.

To accept the second preposition that the steel which did not show high corrosion rate was in a passive state, the concept of chlorine threshold dependence on local potential was used to provide a possible explanation. It was explained that the anodic reaction occurred at a very slow rate which is usually associated with anodic passive dissolution, until significant chloride builds up at the steel to cause damage. As time goes on, chloride buildup at one spot on the steel, resulting in the chloride threshold to be exceeded there. The localized corrosion was found to be as a result of local concrete deficiency, a slightly faster transportation of local chloride, a greater surface chloride at the surface of the concrete near a given spot, and a lower local threshold as a result of variability in the steel-concrete interface. The corrosion rate at the spot dramatically increases over the normal passive dissolution rate and the chloride penetration from the outside and its consequent buildup at the surface of the steel increases.

This line of reasoning by Walsh and Sagues, (2016), (7) agrees with the basic fact that the deposition of salt particles on the surface of a metal accelerates corrosion [7]. Researches also show that a high Cl^- concentration in the aqueous adlayer on the metal and high moisture retention in determined areas of the rust usually give rise to the formation of ferrous chloride ($FeCl_2$), which is said to hydrolyze water.

$$FeCl_2 + H_2O \longrightarrow FeO + 2HCl \qquad (3)$$

When this happens, the acidity of the electrolyte increases and the cathode reaction of hydrogen evolution becomes important and accelerates the corrosion process. The anolyte on the surface of the steel and in the pits formed becomes saturated with $FeCl_2$ solution, which is highly acidic. The metallic cations and hydrogen ions are neutralized by the entry of Cl^- ions, leading to an increase in the Cl^- concentration, thus intensifying the dissolution of the metal. This results in further entry of more Cl^- ions. This attack mechanism is enhanced by the corrosion products produced and is sometimes referred to as an autocatalytic process [9].

Studies have shown that plastic deformation forms heterogenous dislocation structures such as pile ups, patches, walls and cells. These dislocations are said to affect the dissolution process. [10-12]

Several factors have been said to influence the corrosion rate of plastically deformed steels [13]. One factor is that plastic deformation is said to produce active sites of low activation energy which enhances anodic dissolution [11,14,12]. These active sites are produced by slip steps, where dislocations slip out to the surface of the specimens or the stress concentration which are induced by dislocation, pile-ups beneath the specimen surface [15] Another factor is that the active sites may be related to areas with high dislocation densities. The number of active sites normally increases with increased deformation as a result of higher dislocation density [11,13,12]

The effect of varied plastic straining of different materials on corrosion has been extensively studied. [16-19,20] To the best of my knowledge very little has been done on the effect, plastic strain induced cavities (devoid of the effect of work hardening and residual stress) would have on medium carbon steel (0.32%C) and low alloy steel (0.17%C) in seawater

Most of these researchers observed that plastic deformation resulted in increased corrosion rate. The corrosion rate was found to increase with increasing deformation or work hardening. They attributed this to the fact that plastic deformation causes increased activity of dislocations at the steel

surface. This acts as sites for anodic dissolution as a result of the lower bending energies of atoms at these points. Most of the authors however worked on different steel materials in varied environment. Only a few worked on carbon steel and in seawater. This work is therefore focused on the effect of cavities on carbon steel

El Alami et al. [19] studied how hydrogen influences plastic strain in nickel electrodes immersed in 1M H_2SO_4. They established a direct relationship between defects associated with dislocations at the surface of the nickel electrodes in terms of the distribution of the defects and density, to the adsorption of hydrogen. Xu and Cheng. [20] worked on the effect of plastic strain on corrosion of X100 pipeline steel. They discovered that applied strain accelerated the corrosion rate of the steel. They also observed that while both cathodic and anodic reactions increased with prestrain, the anodic reaction was found to be more influenced by the prestrain levels. Harwood [16] discovered that there was an increase in the rate of attack of dilute sulfuric acid on iron with increased strain, although he found no appreciable difference in the rate of corrosion in seawater between strained and unstrained. He explained that corrosion rate in aerated salt solution is largely controlled by the rate of oxygen supply and therefore there should be no reason why strained iron should have a better supply of oxygen. The author did not explain the reason for this in detail, it could however be as a result of the corrosion products generated on the metal surface. It has been explained that the corrosion products generated slows down supply of the cathode polarizer (oxygen soluble in seawater) to the metal surface, which eventually leads to slower rate of metal dissolution [1,21] The author (Harwood, 1950), however probably failed to take into account, the actual mechanism of corrosion in seawater, as explained earlier. Greene and Saltzman,[17] studied the effect of plastic deformation on carbon steel in 1M sulphuric acid and 0.1M hydrochloric acid. Mazza et al., [18] also studied the corrosion behaviour and the structure of metallic materials that are subjected to cold plastic deformation in 1M solution of sulphuric acid. They worked on carbon steel and austenitic stainless steel and nickel and concluded that the degree of work hardening in the carbon steel studied resulted in an enhanced anodic behavior of the material in the active region as against, the other materials considered. No explanation was however given for this. It could however be as a result of the low corrosion resistant property of carbon steel.

2. Materials and Method

2.1 Materials

A 20mm diameter rod was used for this research. The 0.32%C steel and 0.17%C low alloy steel were gotten from Universal Steel Company, Lagos. The chemical composition was done by using spark spectrometer metal analyser (NCS labspark 750B) at the quality control laboratory of universal steel company. The data obtained from the medium carbon steel and low alloy steel are shown in Table 1. The natural seawater was obtained from Escravos, Delta State, Nigeria. The source of the seawater was from the Gulf of Guinea, Coast of the Atlantic Ocean. The analysis of the composition of the seawater was done in Chemistry Department, University of Benin. The result of the analysis is shown in Table 2.

Table 1: Chemical Composition of the Investigated Steel

Elements	C	Si	Mn	P	S	Cr	Mo	Ni
Low Alloy Steel (Wt %)	0.1728	0.3016	1.2089	0.0352	0.0334	0.2559	<0.0100	0.1218
Medium Carbon Steel (Wt %)	0.322	0.2720	0.9490	0.0500	0.0640	0.112	0.0001	0.131

Elements	Al	Cu	Ti	V	Nb	W	Co	B
Low Alloy Steel (Wt. %)	<0.0100	0.2560	<0.0100	<0.0100	<0.0150	<0.0500	<0.0200	0.0047
Medium Carbon Steel (Wt %)	0.0010	0.340	0.0001	0.0001	0.0001	0.0001		
Elements	Sn	As	Pb	Fe				
Low Alloy Steel (Wt %)	<0.0100	<0.0100	<0.0200	97.5604				

Table 2: Seawater Composition

S/NO	**PARAMETERS**	**RESULT**
1	pH at 27.7°C	7.38
2	Dissolved Oxygen (mg/l) at 27.5°C	8.00
3	Salinity in Chloride form (mg/l)	7102.5
4	Sulphate (mg/l)	2524.0
5	Sodium (mg/l)	6.91

2.2. Tensile Test Specimens

The tensile test is a standard test, which was done at room temperature at a constant speed. An average value of four readings was taken for more accuracy.
The specimens were machined into tensile test specimens in accordance with the American society for Testing and Materials Specifications. (ASTM A370, 2014) The tensile specimen's geometry and dimensions are shown in Figure 1.

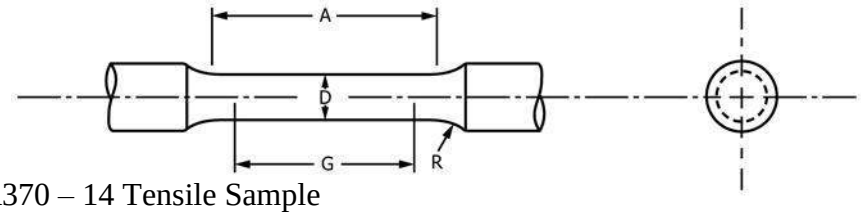

Figure 1: ASTM A370 – 14 Tensile Sample

Where A = Length of reduced section. (100mm)
D = Diameter of guage length. (12.5mm)
G = Guage length. (50mm)
R = Radius of fillet. (2mm)

2.3. Notched Tensile Specimens.

To localize damage, circumferential v-notched round bar tensile specimens were tested. In notched tensile specimens, the load is concentrated in the core of the notch. When load is applied, the unstressed mass of the material tends to resist the deformation of the central core. This produces radial and tranverse stresses and a triaxial state of stress in the notch region, leading to stable cavity formation at the particle-matrix interface [22]. Notched bars are able to reach high deformation levels, such that the hardening behaviour can be obtained over a wide range of plastic strain. The

ability to achieve this serve as an advantage over the use of smooth tensile bars which need to be analyzed beyond necking in order to achieve high level of deformation [23].
A circumferential V- notch of angle 60^o was machined to a depth of 1.5mm at the centre of some of the specimens. The notch radius was as small as possible (0.075mm). The machining of the V- notch on the specimens were achieved by using a programmable lathe machine.

Figure 2: A picture of the notched specimen used for this research

2.4. Smooth Tensile Specimens

To fully observe the effect of discontinuities like notching on the specimens, circumferential V-notch was not machined on some of the samples.

2.5. Prestraining

To observe the effect of prior plastic strain on the specimens, the notched specimens were prestrained to three different prestrain levels. To achieve this prestrain values, some notched specimens were fractured to failure. Strain guages were attached to the surface of tested specimens and connected to a strain meter to check the actual strain levels before fracture.

2.6. Fracturing with Liquid Nitrogen

In order to fully characterize the damage done on the prestrained specimens, some specimens prestrained at the various strain levels, were immersed in liquid nitrogen at -196^{o}C and thereafter fractured in a bench vice.

2.7. Re-Machining the Tensile Specimens

After prestraining, the essence of introducing the circumferential V-notch have been achieved. At this stage of the experiment the reduced section of the notched tensile specimens was re-machined to remove the notch to about 1.5mm. For uniformity and better comparison, the reduced section of the smooth tensile specimens was also re-machined to a depth of 1.5mm

2.8. Stress-Relieving

Some of the specimens were stress relieved in the furnace at 550^{o}C and held for about 1 hour 30 minutes before cooling in air. During the process of inducing strain in the material to cause cavities, a lot of stresses build up in the specimens. The essence of stress relieving some of the specimens is to compare the effect of plastic strain on some specimens to those whose residual stress has been significantly reduced. Researches shows that stress relieving carbon steels and alloy steel between 550^o- 650^o for about 1 to 2 hours provides virtually complete stress relief. The process removes more than 90% of the internal stresses [24-25].

2.9. Determination of Corrosion Penetration Rate

Corrosion penetration rate is the rate at which a material is removed as a result of chemical action. The corrosion penetration rate was done by using the weight loss method. This method is widely used because of its simplicity and reliability. It is said to be the most preferred method of all the corrosion measurment procedures. [26,27]

The specimens were weighed using a digital chemical weighing balance before they were exposed to the seawater medium. Some specimens were fractured before exposing them to seawater environment to determine the yield strength, ultimate tensile strength and fracture strength. On each monitoring day, some specimens were retrieved, washed thoroughly with distilled water, rinsed in acetone and dried. Some were then weighed and fractured to obtain their yield point, tensile strength, fracture strength, percentage elongation and percentage reduction in area. The corrosion rate was evaluated by using Equation 4 (28,29) The total duration for exposure was 90 days, while the specimens were removed and examined at every 15 days interval.

$$CPR = \frac{W}{At} \quad (4)$$

Where $W = W_i - W_f$

W = Weight Loss

W_I =Initial Weight

W_f = Final Weight on each monitoring day

t = Exposure time in days converted to year

A = Total surface area of sample (cm^2)

$A = 2\pi r(r+L)$ because the samples are cylindrical in shape

Where

r = Radius of sample (cm) L = Length of samples (cm)

3. Results and Discussion

Figures 4 and 5 show that the corrosion rate of specimens with cavities and residual stress is greater than the ones with just cavities. This is possible because, plastic strain produces many active sites by slip steps, where the dislocation slips at the surface of the specimens or stresses induced by the dislocation pile up beneath the specimen surface [15, 11, 14, 12] These active sites present at the surface and beneath the surface of the specimens are possible sites for anodic dissolution. After the first initial increase in the corrosion rate, the rate of increase decreases and as the chloride threshold is exceeded, more chloride ion is penetrated through the dislocation slips at the surface and into the cavities present. This led to more corrosion rate as against the specimens with just cavities, since all the effect of residual stress have been removed by stress relieving.

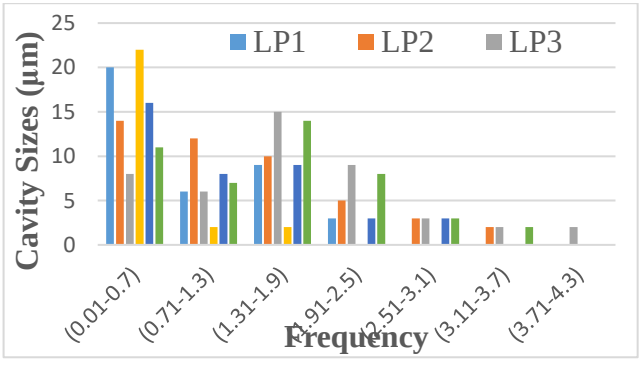

Figure 3: Frequency of Cavity Size Distribution of the Investigated Steels

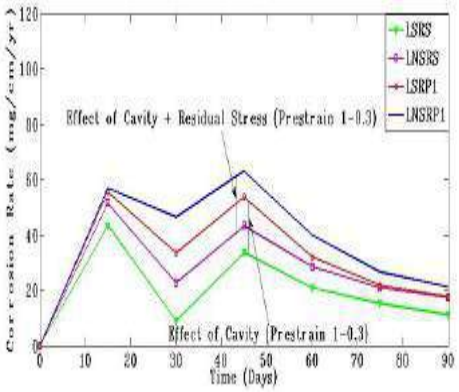

[a].

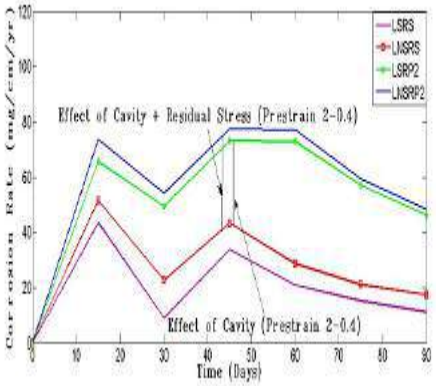

[b].

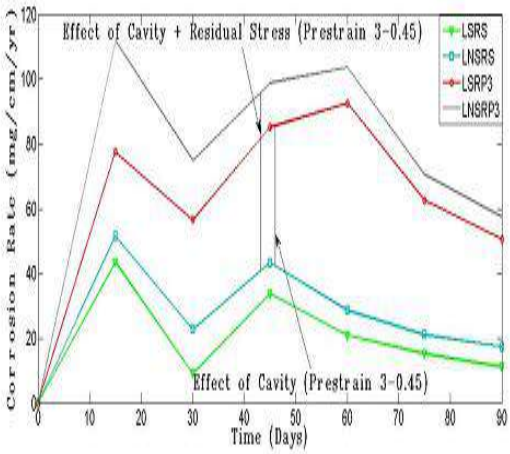

[c]

Figure 4: Comparative corrosion rates of 0.17% low alloy steel. [a]. Stress and Non-Stress relieved Unprestrained Specimens, Specimens with Cavities and Specimens with Cavities and Residual Stress. Prestrain 1-0.3. [b]. Stress and Non-Stress Relieved Unprestrained Specimens, Specimens with Cavities and Specimens with Cavities and Residual Stress. Prestrain 2-0.4. [c]. Stress and Non-Stress Relieved Unprestrained Specimens, Specimens with Cavities and Specimens with Cavities and Residual Stress. Prestrain 3-0.45

The result also shows that corrosion rate in the specimens induced with cavities is greater than the smooth specimens. Two possible explanations can be given as to why the rate of corrosion is possibly greater for prestrained steels. First, the high Cl^- concentration in the aqueous adlayer on the metal and high retention of moisture in deteriorated areas of the rust gave rise to the formation of ferrous chloride which hydrolysis the water, thus raising the acidity (Ph depression) of the electrolyte, (Seawater). Some of the hydrogen evolved during this process are possibly adsorbed by the metal, concentrating at the cavity spot that are spread all over the steel, leading to more corrosion loss. Secondly, since metallic cations and hydrogen ions require neutralization, this task is achieved by the entry of Cl^- ions, which then leads to an increase in the Cl^- concentration, thus intensifying metal dissolution, which gives rise to further entry of more Cl^- ions. It is possible that a lower localised chloride threshold is achieved as a result of the variability of spots with cavities and spots without cavities within the steel. There could be more injection of positive metal ions at the anodic spots with cavities, which in turn results in more chloride ion accumulating at these spots, penetrating from the outside, thus reducing the chloride threshold. As this phenomenon is repeated from one cavity spot to another, it leads to an overall uniform corrosion. These observations align with Walsh et al, [7], though they investigated on the reason why some regions in steel in submerged concrete structures in seawater corrode faster than some. These findings, however disagrees with Harwood, [16] who reported that corrosion in seawater between strained and unstrained samples is

largely controlled by oxygen supply and therefore there could be no possible reason why strained specimens should have better supply of oxygen, since corrosion products generated slows down the supply of oxygen soluble in seawater.

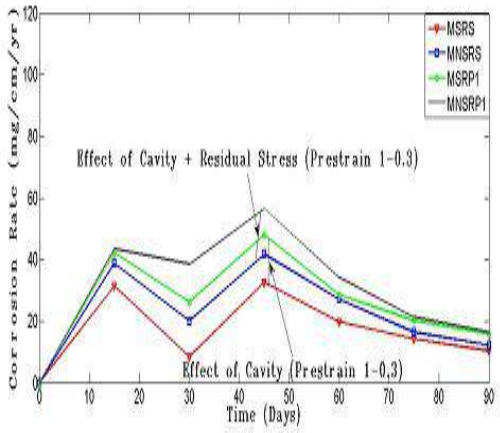

[a].

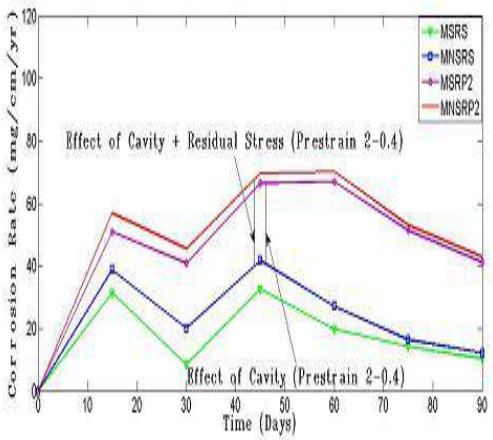

[b].

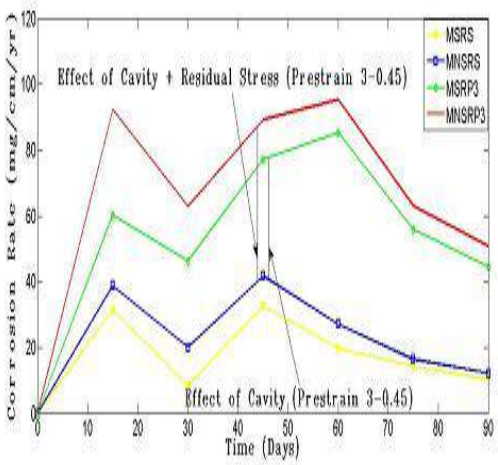

[c]

Figure 5: Comparative corrosion rates of 0.32% low alloy steel. [a]. Stress and Non-Stress Relieved Unprestrained Specimens, Specimens with Cavities and Specimens with Cavities and Residual Stress. Prestrain 1-0.3. [b]. Stress and Non-Stress Relieved Unpresrained Specimens, Specimens with Cavities and Specimens with Cavities and Residual Stress. Prestrain 2-0.4. [c]. Stress and Non-Stress Relieved Unprestrained Specimens, Specimens with Cavities and Specimens with Cavities and Residual Stress. Prestrain 3-0.45

The shape of the curves for both steel shows that corrosion increases at first and then decreases. The reason for this could be as a result of the iron oxide layer deposited on the surface layer of the specimens, until the chloride threshold value at a point in time on the surface is exceeded, leading to breakdown of the plastic film at that point [5,2,1].

4. Conclusion

In this paper, the effect of cavities on 0.32%C and 0.17%C was examined. Cavities was found to have a detrimental effect on the corrosion of the investigated steels in seawater. It resulted in an overall increase in corrosion rate. Though the specimens with cavities and residual stress were

found to have a higher corrosion rate, the cavities contributed more to the higher corrosion rate than the residual stress. Corrosion rate was found to be higher in low alloy steel than in the medium carbon steel

Nomenclature

LP1	Low alloy steel samples prestrained at 0.3
LP2	Low alloy steel samples prestrained at 0.4
LP3	Low alloy steel samples prestrained at 0.45
MP1	Medium carbon steel samples prestrained at 0.3
MP2	Medium carbon steel samples prestrained at 0.4
MP3	Medium carbon steel samples prestrained at 0.45
LSRS	Stress relieved low alloy steel samples not notched and prestrained
LSRP1	Stress relieved low alloy steel samples prestrained at 0.3
LSRP2	Stress relieved low alloy steel samples prestrained at 0.4
LSRP3	Stress relieved low alloy steel samples prestrained at 0.5
LNSR	Non-Stress relieved low alloy steel samples not prestrained
LNSRP1	Non-Stress relieved low alloy steel samples prestrained at 0.3
LNSRP2	Non-Stress relieved low alloy steel samples prestrained at 0.4
LNSRP3	Non-Stress relieved low alloy steel samples prestrained at 0.45
MSRS	Stress relieved medium carbon steel samples not notched and prestrained
MSRP1	Stress relieved medium carbon steel samples prestrained at 0.3
MSRP2	Stress relieved medium carbon steel samples prestrained at 0.4
MSRP3	Stress relieved medium carbon steel samples prestrained at 0.45
MNSR	Non-Stress relieved medium carbon steel samples not notched and prestrained
MNSRP1	Non-Stress relieved medium carbon steel samples prestrained at 0.3
MNSRP2	Non-Stress relieved medium carbon steel samples prestrained at 0.4
MNSRP3	Non-Stress relieved medium carbon steel samples prestrained at 0.45

References

[1] Sherif, E.S.M., Erasmus, R.M. and Comins, J.D. (2010): In situ Raman spectroscopy and electrochemical tec hniques for studying corrosion and corrosion inhibition of iron in sodium chloride solutions. Electrochim. Ac ta, 55, pp3657–3663.

[2] Sherif, E.S.M. (2013): Comparative Study on the Inhibition of Iron Corrosion in Aerated Stagnant 3.5 wt % S odium Chloride Solutions by 5-Phenyl-1H-Tetrazole and 3-Amino-1,2,4-Triazole. *Ind. Eng. Chem. Res. 52*, p p14507–14513.

[3] Bertolini, L., Elsener, P., Pedeferri, P. and Polder, R. (2004): Corrosion of Steel in Concrete Prevention, Diagnosis, Repair, Weinheim, Germany: Wiley-VCH, pp 356

[4] Broomfield, J.P. (2007): Corrosion of Steel in Concrete: Understanding, Investigation, and Repair, 2ed, New York, NY: Taylor and Francis, pp 9

[5] Ann, K.Y. and Song, H.W. (2007): Chloride Threshold level for Corrosion of Steel in Concrete, *Corrosion Science*, 49(11), pp 4113

[6] Sherif, E.-S.M. and Almajid, A.A. (2014): Anodic Dissolution of API X70 Pipeline Steel in Arabian Gulf

Seawater after Different Exposure Intervals. *J. Chem.*, pp1–7.
[7] Walsh M.T and Sagues A.A. (2016) Steel Corrosion in Submerged Concrete Structures- Part 1: Field Observ ations and Corrosion Distribution Modelling, *Corrosion*, 72:4, pp518-533
[8] Nishimura T., Katayama, H., Noda, K. and Kodama, T. (2000): Electrochemical Behavior of Rust Formed on Carbon Steel in a Wet/Dry Environment Containing Chloride Ions, *Corrosion*, 56(9), pp935-941
[9] Alcantara J., Chico, B., Diaz I., De la Fuente, D. and Morcillo, M. (2015): Airborne Chloride Deposit and its Effect on Marine Atmospheric Corrosion of Mild Steel, *Corrosion Science*, 97, pp74-88
[10] Drazic, D.M., Gojkoovic, S., Zecavic S. K and Radmilovic, V. (1992): Cathodic Processes on Corroding Low -Carbon Steel: The Effect of the Degree of Deformation, *Corrosion Science*, 33, pp791-797
[11] Despic, A.R., Raicheff, R.G and Bockris, J.O.M. (1967): Dependence of the Velocity of the Anodic Dissoluti on of Iron on its Yield Rate under Tension, *Journal of Chemical Physics B.*, 49, pp2198-2199
[12] Sahal, M., Creus, J., Sabot, R and Feaugas X. (2006): The Effects of Dislocation Patterns on the Dissolution P rocess of Polycrystalline Nickel. *Acta Materialia*, 54(8), pp2157-2167
[13] Lu, B.T., Luo J.L and Norton P.R (2010): Environmentally Assisted Cracking Mechanism of Pipeline Steel in Anaerobic Groundwater of Near-Neutral Ph, *Corrosion Science*, 52, pp1787-1795pp1878-1895
[14] Benzerga, A.A., Brechet, Y., Needleman, A and Van der Giessen, E. (2005): The Stored Energy of Cold Wor k: Predictions from Discrete Dislocation Plasticity, *Acta Materialia*, 53, pp4765-4779
[15] Gutman, G.M. (1998): Mechanochemistry of Materials, Cambride International Science Publishing, London.
[16] Harwood J.J. (1950): The Influence of Stress on Corrosion, *National Association of Corrosion Engineers.* Vo l 6. pp249-259
[17] Greene, N.D and Saltzman, G.A. (1964): Effect of Plastic Deformation on the Corrosion of Iron and Steel, *Co rrosion- National Association of Corrosion Engineers.* 20:293-298
[18] Mazza P., Pedeferri, P., Sinigagliu, D., Sala, U.D and Lazzaru, L. (1974): Contribution to the knowlegede of t he relationship between the electrochemical and corrosion behavior and the Structure of Metallic Materials S ubjected to Cold Work Plastic Deformation, *Materials and Corrosion*, 25(4), pp239-253
[19] El Alami, H., Creus J. and Feaugas, X. (2007): Thermodynamic Parameters Evolution versus Plastic Strain d uring HER on Nickel in Sulphuric Acid. Electrochimica Acta , 52 (12), pp4004-4014.
[20] Xu L.Y and Cheng Y.F (2012): Corrosion of X100 Pipeline Steel under Plastic Strain in a Neutral pH Bicarb onate Solution. *Corrosion Science*, 64, pp145-152
[21] Sherif, E.-S.M. (2011): Effects of 5-(3-aminophenyl)-tetrazole on the inhibition of unalloyed iron corrosion i n aerated 3.5% sodium chloride solutions as a corrosion inhibitor. *Mater. Chem. Phys. 129*, pp961–967.
[22] Onyekpe, B.O. and Wright, J.O (1983): The Influence of Hydrogen on Plain Carbon and Low Alloy Steel Co ntaining Strain Induced Cavities, International Journal of Fracture, 22, pp231-239
[23] Mirone, G. (2004): A new model for the elastoplastic characterization and the stress–strain determination on the necking section of a tensile specimen. *International Journal of Solids and Structures*, *41*(13), pp.3545-3564.
[24] Chandler, H. ed., (1994): Heat Treater's Guide: Practices and Procedures for Irons and Steels. ASM International
[25] Vohringer, O., 1987. Relaxation of residual stresses by annealing or mechanical treatment. *Pergamon Press, Advances in Surface Treatments. Technology--Applications--Effects. 4*, pp.367-396.
[26] Adebiyi K. A., Hammed K.A. and Ajayi E.O. (2003): Predictive Model for Evaluating Corrosion Rate of Mil d Steel in Six Environments. LAUTEECH *Journal of Engineering and Technology. In Jekayyinfa* S.O. (Ed): Effect of Cassava Fluid on Corrosion Performance of mild Steel. 52(5), pp286-292
[27] Sodile, J.L. (2002): The Effect of Surface Finnish on the Corrosion Rate of Steel. *Nigerian Journal of Engine ering Research and Development*, 1(2), p1
[28] Ogunleye, I.o., Adeyemi, G.J., Onyegoke, .O.V. (2011): Effect of Grape Fruit Juice on the Corrosion Behavio ur of Mild Steel in Acidic Medium, *American Journal of Scientific and Industrial Research,* 2(4), pp611-615
[29] Oloruntoba, D.T., Ogunniyi I.O. and Fabuyide A.A. (2013): Nickel Plating and Cathodic Protection of Low C arbon Steel in Chloride Environment, *NSE Technical Transactions*, 47(2), pp29-38

NIPES Conference Proceedings
The 1st International Conference of the Nigerian Institution of Professional Engineers and Scientists 7th-8th Oct. 2021: 72-85
www.nipesjournals.org.ng

A Review of Studies on Castor Seed (*Ricinus Communis L.*) Shrub and Potential Utilization of its Oil

Samuel Ayodeji Omotehinse[1,*] Lucksyn. A Omidih[2]
[1,*]Department of Mechanical Engineering, Benson Idahosa University, Benin City, Edo State.
[2]Department of Mechanical Engineering, Delta State Polytechnic, Oghara. Delta State.

Abstract
Castor bean plant (*Ricinus Communis L.*) is one of the oldest cultivated crops, but at present the oil produced from the seed represents only 0.15% of the vegetable oil produced in the world. Castor seed is an industrial oilseed crop belonging to the Euphorbiaceae family, widespread in the tropical region as a spontaneous plant, having its main cultivated area in India, China, and Brazil. As a crop, the main advantage of castor is its tolerance to drought stress and adaptation to several growing conditions. As an industrial product, castor oil composition is different in many respects from any other oil because it consists largely (up to 90%) of the unusual ricinoleic fatty acid. This review was conducted to provide a collation of the most relevant historic research information published by global community of researchers and define the remarkable future potential of castor seed oil. This article was also prepared to give a general overview of the industrial and domestic importance of castor seed oil to the world at large. The topics discussed in this review include: (i) Applications of castor seed oil in various field of study; (ii) phytochemical studies on Castor bean; (iii) Pharmacological studies on Castor bean; (iv) Evaluation of previous research; (v) Nature of existing research; (vi) Merit of previous studies; (vii) Potential and challenges of castor seed oil production. It is the belief of the author that this review will serve as a baseline for researchers who intend to venture into castor seed oil production.

***Keywords*:**
Ricinus communis, Phytochemical, Pharmacological, Industrial application

1. Introduction

Varied opinions are held regarding the exact land of origin of the castor plant. Some pundits view that though castor is cultivated throughout India, yet it is indigenous to Africa. Castor is native to India by some persons. They hold this view mainly on the basis of knowledge of the medicinal uses of this plant as found in Sanskrit literature. Some toured to India and found some evidence only at the foot of Himalayas to show that castor is a native of India. They therefore believe that it may have originated in India as well as in Africa and widely grown elsewhere as an ornamental plant. The castor bean plant (Ricinus Communis L.) has been cultivated for centuries for the oil produced by its seeds. The Egyptians burned castor oil in their lamps more than 4,000 years ago. The plant is a member of the spurge family, Euphorbiaceae. The seeds with hulls removed contain 35 to 55% oil. The seeds, leaves, and stems of the plant contain ricin and ricinine, which are poisonous to humans and animals. Eating a castor bean causes nausea and eating several may cause death. These toxic compounds are not present in the oil. Castor may be large perennials often developing into small trees, others behave as short-lived dwarf annuals and every gradation between these extremes can be found. The tree and short-internodes types are commonly referred to as giant and dwarf castor types respectively. However, castor grows at an amazingly fast rate, if they are situated in full sun and provided with ample fertilizer and water. Seedlings emerge 7 to 21 days after planting. Castor seed is the source of castor oil, which has a wide variety of uses. The oil has been used by the military in aircraft lubricants, hydraulic fluids, and in the manufacture of explosives. It has also been used in the synthesis of soaps, linoleum, printer's ink, nylon, varnishes, enamels paint, and electrical insulations [1, 2, 3, and 4]. Textile scientists have used sulphonated castor oil in the dyeing and finishing of fabrics and leather. The most infamous application of castor oil may have been as a purgative popular for the treatment or prevention of many ailments in the first half of the twentieth century. Castor oil is fast becoming one of the most sought after plant oils, owing to its rich properties and variety of end-uses. With

biopolymer and bio-fuels industries picking up a lot of steam in the last couple of years, the potential for castor oil to play a much larger role in the world economy had increased dramatically in the international market. While the importance of castor oil has this increased recently, there appears to be dearth comprehensive report that addresses all important aspects of castor oil applications. *Ricinus communis* L. (Castor bean) is an important multipurpose crop viz., Agricultural, Energy, Environmental and Industrial crop [5]. The current status of knowledge about castor oil plant is abundant but scattered which need to be exploited for sustainable development. This review however collates and evaluates all the strewed information and provides a critical view on the possible options for exploiting its potential in industrial and domestic applications.

2. Applications of Castor Seed Oil

2.1 Application of Castor oil in Biodiesel

Castor bean (Ricinus communis) is a good candidate for biodiesel production and also an industrial crop [6] and the cultivation has encouraged for biodiesel and bioethanol production [7, 8]. Some of the research work done on the use of castor seed oil for biodiesel production includes: Bello and Makanju [9] who investigated the use of castor oil methyl ester as possible alternative fuel for diesel engines. The results obtained by the researchers gave properties, torque outputs and specific fuel consumption that are close to those of diesel fuel thus confirming that it can be used as alternative fuel for diesel engines. Asmare and Gabbiye [10] produced biodiesel by transesterification of Ricinus Communis (RC) oil with methanol in the presence of KOH as a catalyst. The study analyzes the fuel properties of Ricinus Communis biodiesel and diesel fuel blend to use castor oil methyl ester as a possible alternative fuel for diesel engines. Various properties of the RC biodiesel and their blends such as density, kinematics viscosity, iodine value, saponification number, cetane number, heating value, flash point and acid value were determined. Zuleta et al [11] evaluated the oxidative stability and cold-filter plugging points (CFPP) of blends of biodiesel from palm, Sacha - inchi, jatropha and castor oils. Blends were made as a strategy to obtain a biodiesel with a better performance. The best biodiesel blend that was produced during the experimental runs was made of 75% jatropha and 25% castor. Among the pure biodiesels, only castor oil biodiesel achieved this quality because its induction time and CFPP were 31h and -7^{o}C respectively. Babu and Mamilla [12] produced biodiesel from castor oil (treated with mineral turpentine oil) by trans-esterification of the crude oil with methanol in the presence of NaOH as catalyst. Important fuel properties of methyl esters of biodiesel produced from castor oil like viscosity, flash point, fire point, calorific value e.t.c was found out and compared to the properties of Indian standard biodiesel. Santana et al [13] designed a continuous biodiesel plant that was simulated in HYSYS simulator using castor oil as feedstock. The developed process was capable of producing biodiesel at high purity using an alkali catalyst. Material and energy flows, as well as sized unit operations were used to conduct an economic assessment of the process. Attia et al [14] carried out biodiesel production from castor oil with methanol in presence of potassium hydroxide as catalyst at room temperature using ultrasonic bath. A factorial design of experiments and a central composite design were used to evaluate the influence of operating conditions on biodiesel synthesis from inedible castor oil. In Dairo et al [15] optimization of in- situ biodiesel production from raw castor oil-bean seed was carried out from raw castor bean oil seed (37.9% oil content) by alkaline catalyzed in situ trans-esterification with sodium hydroxide as catalyst and ethanol as the solvent in a laboratory batch processor. In a study by Berman et al [16] it was found that methyl esters of castor oil can be used as a biodiesel alternative feedstock when blended with diesel fuel. However, the maximum blending level was limited to 10% due to the high levels of ricinoleic acid (RA) present in the oil, which directly affects biodiesel's kinematic viscosity and distillation temperature. Another study by Shojaeefard et al. [17] examined the effects of castor oil biodiesel blends on diesel engine performance and emissions. They found that a 15% blend of castor oil–

biodiesel was an optimized blend of biodiesel–diesel proportions. The results indicated that lower blends of biodiesel provide acceptable engine performance and even improve it.

2.2 Application of Castor oil in food industry

In food industry, castor oil is used in food additives, flavouring, candy and as mold inhibitor [18]. The white, large seeds of castor are important sources of food condiment called Ogiri in the South-Eastern part of Nigeria. Ogiri is a food condiment obtained by traditional fermentation of Ricinus communis seeds. The condiment is believed to improve eye vision. Past research efforts on the use of castor seed in food preparation are: Ojinnaka and Ojimelukwe [19], they studied the effect of addition of 2% salt and 3% lime on some biochemical changes occurring in the fermentation of castor oil bean into ogiri using B.Subtilis as starter culture. Three different fermented castor oil bean samples were produced viz: B_1 (0% Nacl/Lime), B_2 (2% Nacl), B_3 (3% Lime). However, it was observed that the ammonia content of the three samples increase as the fermentation period progressed, while the ricin content of the fermented castor oil bean samples decreases as fermentation period increased. According to Kolapo et al. [20] the use of fermented food condiments and flavouring agents are becoming popular in the diets of many nations. Apart from the fact that condiments improve sensory properties of foods, the authors noted that they add to the nutritional values providing dietary fibre, energy, minerals and vitamins. Some of them contain antioxidants and nutracenticals that provide health benefits. The traditional fermentation of castor oil bean seed into ogiri has been reported to be accomplished by mainly bacteria especially Bacillus species notably B. Subtilis, B. Pumillus and B. licheniformis [21, 22]. Odunfa [23] discussed the traditional fermentation of castor oil bean to produce ogiri-igbo via alkaline fermentation. He also reported that predominant fermenting organisms were of Bacillus species, B. Subtillis being the predominant species.

Several other researchers have also reported B. Subtilis in the alkaline fermentation of protein rich plant materials [24, 25]. It was reported that proteolysis is the most principal and complex biochemical event occurring during the preparation of some legume based fermented condiments. The degradation products, amino-acids, not only have a considerable influence on the nutritional values, but also contribute directly to the taste characteristics, in some cases serving indirectly as precursors of aromatic products [26]. Fermented products continue to remain of interest since they do not require refrigeration during distribution and storage. The traditional condiments have not attained worldwide commercial status however, due to the short shelf – life, objectionable packaging materials, stickiness and the characteristic putrid odour [27]. Fermented condiments often have a stigma attached to them as they are considered as food for the poor.

2.3 Application of Castor oil in surface coating

There are numerous applications of castor oil in surface coatings. Example of such includes [28] who studied the role of castor oil in epoxy and polyamide systems for coating and adhesive application. Valero and Ortegon [29] synthesized Polyurethanes (Pus) from castor oil and modified through transesterification by pentaerythritol, poly(ε-caprolactone)diol (PCL), and isophorone diisocyanate to form PU coatings. The PU coatings were characterized using Fourier transform infrared spectroscopic analysis, and the physicochemical properties, such as tensile strength, elongation at the break, shore A hardness, and the results of a lap shear test, were reported. Campos et al [30] evaluated the performance of medium density fibre board produced with the wood species pinus caribaea var hondurensis and the performance of the castor oil based polyurethane adhesive, comparing the results with the properties of MDF reported in the European standard requirement. The test results showed higher values than those recommended by the European standard, indicating that the castor oil-based polyurethane resin is promising adhesive for the manufacture of MDF.

To expand the application of this product, [31] and [32] studied the behavior of castor oil based polyurethane adhesive for use in glued laminated timber (GLT) with reforested species of the genera Pinus and Eucalyptus. The adhesive's efficiency was evaluated based on mechanical tests of shearing strength parallel to the grain, tensile strength perpendicular and tensile strength parallel to the grain. The results reported by these authors demonstrated that castor oil based polyurethane adhesive is a good alternative for the technological use for GLT. Campos and Lahr [33] studied the strength properties of MDF panels with pinus and Eucalyptus fibres with 8, 10 and 12% urea formaldehyde, polyurethane bi-component derived from castor oil and inorganic resin, found that the best internal adhesion (0.91 and 0.89Mpa) and bending strength (29.4 Mpa and 28) were obtained in the panels made with Pinus and Eucalyptus fibres with 12% polyurethane adhesive. In a study conducted by de martins et al. [34] the sealing ability of castor oil polymer (COP), mineral trioxide aggregate (MTA), and glass ionomer cement (GIC) as root-end filling materials were evaluated. MTA is primarily composed of tricalcic silicate, tricalcic alluminate, and bismuth oxide and is a particular endodontic cement [35]. GICs, on the other hand, are mainstream restorative materials that are bioactive and have a wide range of uses such as lining, bonding, sealing, luting, or restoring a tooth [36]. Results of their study show that the COP had a greater sealing ability when used as a root-end filling material than MTA and GIC. Trevino and Trumbo [37] studied the utilization of castor oil as a coating application by converting the hydroxyl functionalities of castor oil to β-ketoesters using *t*-butyl acetoacetate.

2.4 Application of Castor oil in Medicine and Cosmetics

Castor has an array of chemical diversity of which reflects in the pharmaceutical activity and it is a good alternative source of bioactive compounds aims to develop plant-based new drug discovery [38]. According to Welch et al. [39] Castor oil is one of natural products that fight several ailments. It contains active ingredients that make it take central position in production of several medicinal and cosmetic products. Castor oil is very effective when it comes to treatment of skin problems like, sunburn, ringworm, stretch marks, wrinkles and acne. It also prevents infections like boils, athlete's foot, warts and chronic itching. The oil is a good skin moisturizer and disinfectant of wound. Castor oil when mixed with coconut or almond oil helps to initiate hair growth, thicken of eyebrows and eyelashes. The oil boosts blood circulation to the follicles, leading to faster hair growth. The oil also has omega-6 essential fatty acids, responsible for healthy hair. The oil is also used or correction of bald patches and hair darkening.

Castor oil is a good additive and powerful laxative that serves as remedy for ailments like menstrual disorders, migraines, skin abrasions, rheumatism and inflammation. The leaves have been used for treatment of rheumatic pains and as antibacterial and anti-inflammatory [40, 41, 42, 43]. Infusion of the leaves was used as a remedy for rash, itch and eye inflammation. The decoction of leaves also used for skin diseases, diarrhea, kidney, urinary bladder infections [44]. Lamadah et al [45] carried out a study to assess the safety and effectiveness of castor oil on labour induction and Neonatal outcome. In this study a quasi-experimental design was used. It was concluded that, the probability of labour initiation increases during the first 24 hours after using castor oil.

Mein et al [46] evaluated the potential for transdermal absorption of castor oil, a treatment modality recommended by Edgar Cayce and used as an alternative medical treatment. Specific epoxydicarboxylic acids are known to be excreted via the urine when castor oil is administered orally. The result showed that oral administration of castor resulted in high levels of excretion of epoxydicarboxylic acids in all subjects. In contrast, the level of urinary epoxydicarboxylic acids with the external application (abdominal pack) sessions did not vary from the relatively low endogenous levels of these molecules that are normally present.

McGarey [47] and McGarey [48] documented the historical applications of castor oil and noted the more recent trend for it to be applied as an external pack in its use as an alternative medicine therapy. McGarey's work relies heavily on the legacy of Edgar Cayce, an important

figure in the development of holistic medicine in the modern era. The work of Cayce discussed by [49] and [50] places great significance on the healing properties of castor oil when applied externally as a pack. The typical application recommended by Cayce is that of a hot abdominal pack placed over the right side of the abdomen covering the liver, upper small intestines, cecum and ascending colon. A study by Arslan and Eser [51] highlighted how castor oil packs helped to effectively reduce constipation among the elderly. The U.S. Food and Drug Administration (FDA) actually deem this oil "generally regarded as safe and effective" for use as a stimulant laxative. A 2009 study published in Phytotherapy Research supports this, and reveals that castor oil helps relieve pain among patients with knee osteoarthritis [52]. Because of its antimicrobial and anti-inflammatory properties, it may have some beneficial effects on skin tags, acne and warts. One study by FDA [53] published in the Journal of International Toxicology also found that castor oil may have positive effects against occupational dermatitis. The study conducted by Garry et al [54] found that pregnant women who receive castor oil have an increased likelihood of initiation of labour within 24 hours compared to women who receive no treatment. Another study by Kelly et al [55] also warned that the castor oil-induced contractions may lead to the passage of meconium (a baby's first stool) while still inside the womb - putting him at risk of meconium aspiration that may result in neonatal respiratory distress while [56] evaluate the benefits and harms of a policy of labour induction at term or post-term compared with awaiting spontaneous labour or later induction of labour.

2.5 Application of castor in Agriculture

In recent years, castor oil is largely used in the specialty chemical industry worldwide, and the growth of its consumption is limited by insufficient and unreliable feedstock supply rather than by the industry demand [57]. Therefore, castor bean crop can become a cash crop in modern agriculture, in particular, for non-food uses including bioenergy purposes [58, 59]. Although increased castor production in the world can be obtained with the use of varieties and hybrids with higher genetic potential and an improved crop management. The transition from a low input/low-yield to a high yielding crop will require a deeper understanding of castor plant growth and development. This knowledge is the key for the breeding of high yielding varieties adapted to each growing environment and for the optimization of crop management in order to express the maximum yielding potential of the crop [60]. According to Salihu et al. [61] Castor oil plant (*Ricinus communis* L.) is an important oil crop that has been widely accepted as an agricultural solution for tropical and subtropical regions, addressing the need for commercial crops with low input costs and viable returns. The authors noted that Castor plant is very easy to establish on the field, resistant to drought, tolerate different types of soil even marginal soil and yield 350 – 900 kg oil per hectare. They went ahead to evaluate castor production practices, checked various industrial opportunities in castor business and current challenges of castor production in Africa. Castor provides opportunities in all aspects of agribusiness ranging from crop production, seed supply, agrichemicals, breeding, farm machinery, distribution, processing, marketing and retail sales [62]. Apart from the various benefit derived from the castor oil, the cake obtained after extraction of the oil can also be used as organic fertilizer. The use of castor cake/meal as organic fertilizer is very advantageous because of high Nitrogen content, fast mineralization, and anti-nematode effects.

2.5.1 Agronomic practices

Castor plant from all the research reviewed grows in all kinds of soils but prefers a well-drained moisture retentive soil like clayey and sandy loam. The most important factor in fertility level identified is the supply of Nitrogen to the soil. The amount requires depends on the soil organic matter contents. Insufficient nitrogen results in reduced seed yields. Excessive nitrogen results in extensive and heavy vegetative growth with non-significant increase in yields. The amount of nitrogen requirement depends on the soil organic matter content. Basically, castor

requires the same amount of nutrients as other low-demand field crops [63]. For a typical slit loam soils testing in the optimum range (6 to 10ppm P; 81 to 100 ppm K), approximately 20 Ib P_2O_5 and 40 Ib K_2O should be applied per acre. If soil tests are below optimum, approximately 5 Ibs P_2O_5 and 20 to 30 Ib K_2O should be applied in addition to previous amounts [64].

In most of the regions of castor production, seed yield can be rapidly increased with the used of improved agronomic practices. The main technologies include selection of the appropriate cultivars combined with use of good quality seeds, appropriate planting date, weed management and optimizing population [65]. In Southern Nigeria where soil fertility is high, castor is grown productively without application of fertilizer [66]. Castor is often planted in early May, about the same time as corn. However, where there are high incidences of pest and diseases, the planting can be delayed to July – August without significant decrease in yield.

2.5.2 Castor Meal as an organic fertilizer and Husk for Animal Feed

Meal and husks are the two major by-products in the production of castor oil. The capsule husks are produced at the farm level during harvest while the meal is produced during oil extraction. If it is assumed that 38% of the fruit's weight is husks and the seed contains 470 g kg–1 of extractable oil, then production of only 1 kg of castor oil would generate 1.31 kg of husks and 1.13 kg of meal [67]. According to Lima et al. [68, 67] castor husks can be used as organic material to provide a better nutrient balance for plant growth. Castor meal has been reported to promote the growth in wheat and castor plant [69]. ICOA [70] noted that detoxified by boiling could be added up to $100gkg^{-1}$ in broiler finishing diets without deleterious effects [71]. Castor meal is not being widely used as an animal feed because of the toxic levels of ricin in the meal. The husks often contain ricin residue in the form of seed fragments. If the ricin toxicity were eliminated or highly reduced, castor meal would become an excellent source of protein in animal rations. The husks could also be used in high fiber but low N animal feed products. There are reports of castor meal being used for animal feed in large scale. A detoxified castor meal named *Lex Proteico* was sold commercially in Brazil during the 1960s [72, 70]. The safety of *Lex Proteico* for dairy cows was confirmed by Miranda et al. [73]. Castor meal is more toxic to monogastrics than to ruminants. This was demonstrated in the death of 13 dogs after accidental ingestion of a soil conditioner containing castor meal [74]. Castor meal detoxified by autoclaving can replace up to 67% of the soybean meal in sheep rations [75].

2.6 Review of phytochemical studies on Castor bean (Ricinus communis)

Phytochemicals are the compounds that are isolated from plant kingdom. The composition of these chemicals is dependent on their geographical locations and harvesting conditions. Hence, their quantitative and qualitative investigations are necessary to understand their applications. Some of the researches carried out in this area are described as follows: Kumar [76] carried out a preliminary phytochemical study of *Ricinus communis.* The study revealed the presence of steroids, saponins, alkaloids, flavonoids, and glycosides in the plant. He noted that the constituents present in this plant are beneficial for the purpose of contraception, leaving no detrimental effects on the body. Rathod and Pandhure [77] presented phytochemical analysis and antibacterial activity in Ricinus Communis L.using various solvents. It was observed that the leaves and stem of Ricinus communis indicated the presence of alkaloids, flavonoids, steroid, terpenoids, cardiac Glycosides, saponins. As well as chloroform, methanol extract showed presence of flavonoids, steroid, terpenoids, saponins, glycosides and tannins. Many phytochemicals found in the plant tissue and seeds of castor have potential medicinal uses as reported by [78]. Pradeep et al. [79] carried out an activity-guided isolation and purification process to identify the DPPH (1, 1-diphenyl-2-picrylhydrazyl) free radical scavenging components of the castor seed plant *Ricinus communis*. Marta et al. [80] studied the localization of invertase activities in *Ricinus communis* leaves. Leaf tissue from *Ricinus communis* possesses cell wall and soluble invertases. These activities may be distinguished on the basis of their optimum pH and Michaelis constant (Km) and

the action of various inhibitors Ca 84% of the soluble invertase was found in vacuolar preparations. Cornelia et al. [81] identified homologous very long-chain 1, 3-alkanediols and 3-hydroxyaldehydes in leaf cuticular waxes of *Ricinus communis*. Surface extracts from primary leaves of castor bean were found to contain 1.8*ug* $cm^{-2}$of cuticular waxes. The mixture comprised alkanes, primary alcohols, aldehydes, fatty acids and triterpenoids. Aziz et al. [82] investigated the phyto-constituents present within the seed oil of *Ricinus communis* and estimated its antibacterial, antifungal and antioxidant activities. The Phytochemical studies carried out confirmed the presence of alkaloids, terpenoids, cardiac glycosides, tannins, steroids and saponins whereas flavonoids, anthraquinone and reducing sugars were found absent. Eight phyto-components were identified from the seed oil of *R. communis* by using GC-MS. The *R. communis* seed oil showed moderate antibacterial and antifungal activity. Singh and Geetanjali [83] carried out phytochemical and pharmacological Investigations of *Ricinus communis* Linn. It was reported that in modern pharmacology, castor seed plant possess antioxidant, anti-inflammatory, anti-diabetic, central analgesic, antitumor, anti-nociceptive, antiasthmatic activity and other medicinal properties. These activities of the plant are due to the presence of important phytochemical constituents like flavonoids, glycosides, alkaloids, steroids, terpenoids etc.

2.7 Review of Pharmacological studies on Castor bean (Ricinus Communis)

Pamela et al [84] studied the effects of ingestion of castor bean in a puppy. Ingestion of masticated seeds resulted in high morbidity, with vomiting and watery to hemorrhagic diarrhea. The prognosis varied with the number of seeds ingested, the degree of mastication, individual susceptibility and the delay in treatment. Despite supportive therapy, the puppy died several hours after presentation for acute vomiting, diarrhea and lethargy. Vera et al [85] studied the suicidal death after injection of a castor bean extract (*Ricinus communis*). A case report was presented of a 49-year old man who committed suicide by intravenous and subcutaneous injection of a castor bean extract. The patient was admitted in the emergency department after 24 hours with a history of nausea, vomiting, diarrhea, dyspnoea, vertigo and muscular pain. Despite symptomatic and supportive intensive care, the man died 9 hours after admission due to multi organ failure. Exposure to the castor bean extract was confirmed by identification of the biomarker ricinine in blood, urine and vitreous humor using solid phase extraction and liquid chromatography tandem mass spectrometry. It is the first time that ricine had been identified in vitreous humor in a case of castor bean poisoning. Based on the clinical symptoms and the results of the toxicological analysis, it was concluded that death was caused by intoxication with plant toxins originated from *Ricinus communis.* Jose et al [86] investigated the effects of demineralized bone matrix and a *Ricinus communis* polymer on bone regeneration histologically in rabbits. Two surgical bone defects were created in rabbit calvaria, one on the right and the other on the left side of the parietal suture. The experimental defects were treated with bovine demineralized bone matrix, human demineralized bone matrix and polyurethane resin derived from *Ricinus communis* oil in three groups of rabbits respectively. Histological analysis revealed that in all groups bone regeneration increased with time. Polyurethane resorbed more slowly and demonstrated considerably better results than the demineralized bone matrices. Makonnen et al [87] studied the anti-fertility activity of castor (*Ricinus communis)* seeds in female guinea pigs. The seed extract was found to possess anti implantation and abortificient effects. It was also observed that the seed extract prolonged the oestrus cycle of guinea pigs. The dioestrus phase was significantly prolonged as well. After stopping the administration of the extract, the normal dioestrus phase and oestrus cycle started to resume. The seed extract also reduced the weight of the uterus without affecting that of the ovaries significantly. The antifertility effect of castor bean (*Ricinus communis)* in female guinea pigs might be extrapolated to human beings. Anete et al [88] studied the pharmacological evaluation of ricinine, a central nervous system stimulant isolated from castor bean (*Ricinus communis)* in mice. The extract of the pericarp of castor bean when administered to mice, the animals became exophthalmic, presented tremors and clonic seizures and died a few minutes after receiving larger

doses of the extract. At lower doses, the extract improved memory consolidation and showed some neuroleptic-like properties, such as a decrease in exploratory behavior and catalepsy. The memory-improving effect and the seizure-eliciting properties were also observed with the administration of ricinine, a neutral alkaloid isolated from the extract. However, the neuroleptics like properties of the extract were not observed with ricinine. Some pharmacological applications were studied by [83]. These includes: Traditional Pharmacological Uses and Modern Pharmacological Uses. Under the Modern Pharmacological uses, the following were considered: Antioxidant activity, Antidiabetic activity, Antimicrobial activity, Anti-Inflammatory activity, Antinociceptive activity, Anti-fertility activity, Anti-hepatotoxicity, Cytotoxic Activity, Toxicological Analysis.

Jena and Gupta [89] also carried out phyto-pharmacological properties of *Ricinus communis*. These are Antiulcer activity, Molluscicidal, Insecticidal and Larvicidal activity, Lipolytic activity, wound healing activity, In vitro immunemodulatory activity, Antihistaminic Activity among others. Sarfaraz et al [90] reviewed the phytochemistry, biological and pharmacological activities, and ethnomedicinal uses of *Ricinus cmmunis* L. (Castor oil plant). The reported chemical constituents showed the presence of flavonoids, phenolic compounds, fatty acids, amino acids, terpenoids, phytosterol etc. The compounds have been reported to exhibit anticonceptive, antidiabetic, antifertility, anti-inflammatory, antimicrobial, antioxidant, hepatoprotective, insecticidal and wound-healing activities. They also showed free radical scavenging and Hg scavenging activities, and repellent properties.

3. Evaluation of Previous Research

While the proximate analysis to estimate the oil content and other food values of the seed preceded the main work of parameter effects on the oil yield, the physico-chemical analysis of the extracted oil was carried out later as a guide to the uses and applications of the oil. Many researchers in the past have worked in this area of the effects of process conditions on the yield of oil from local seeds [91]. Kutama et al [92] reviews some important aspects of plants which include their origin, classification, morphology, as well as economic uses especially in the Nigerian context. Mbah et al [93] evaluated the physicochemical properties of castor seed oil using standard analytical technique. Nahar and Pan [94] conducted an indoor pot culture experiment in the growth chamber during the period of vegetative growth to evaluate the influence of inorganic nitrogen fertilizer in the form of urea on nutrient uptake, growth and root development of castor bean plant. Abolfazl et al. [95] investigated the impact of 10 different climatic conditions in Iran on the castor oil production by castor bean (*Ricinus communis* L.) from the standpoints of the quality, oil content and physicochemical properties of castor oil.

4. Nature of Existing Research

From the literature, the nature of existing research on castor seed plant is largely centered on the use of its oil in various industrial and domestic applications as well as study about the morphological and physiochemical properties of the seed oil. Existing research however, pursued objectives away from backward integration but the need to ensure steady and sustainable supply of the seed has become more intensive. Therefore, research focus is now on how to promote the growing of the plant in order to meet the ever increasing demand of the seed for the supply of oil. For example, Omotehinse, Igboanugo and Bello [96] applied Split-Split plot theoretic approach to modelling castor shrub development. The study analyzed optimum conditions for the growth and development of castor shrub so that it can meet the yearning of the society to complement fossil fuel that is non-renewable.

5. Merits of Previous Studies

Past research efforts were very rich on the use of castor seed oil for both domestic and industrial purposes as earlier outlined. However, there appears to be a dearth of research work on

furnishing information on the growth capacity of castor shrub that will sustain the backward integration of its seed for subsequent production of its oil suitable for several industrial purposes.

6. Potential and challenges of castor seed oil production

Extensive future research effort will play a critical role in the increased production of castor seed and subsequent production of its oil for both domestic and industrial applications. There is an urgent need for community of researchers working on castor to cultivate increased international cooperation in the development of solutions to the critical constraints affecting castor seed oil production, processing and marketing. The most challenging and time-consuming operation in castor production among peasant farmers are harvesting and capsule shelling. The shelling of capsules is done manually by the farmers. The prevalent lingering problems are uneven ripening and variation in thickness of capsule wall. In Nigeria however, the production constraints includes poor and inadequate agronomic practices among farmers, lack of improved varieties of castor seed, lack of functional processing facilities like capsule shellers and oil expellers, lack of awareness among Nigerians, lack of government commitment, and lack of stable, reliable and organized castor markets. The current castor production is not increasing at a sufficient rate to meet even the anticipated increases in demand. However, mechanized castor seed oil production is rapidly becoming very crucial to sustain or increase castor production globally. The use of castor seed oil for biodiesel production has been difficult due to its cost and its high viscosity. Castor also has tremendous future potential as a bioenergy and industrial feedstock because of its high oil content, potential modification in fatty acid composition, very high oil yield, wide range of adaptation, and ability to be grown on marginal sites subject to drought and saline conditions.

7. Conclusion

This review has been able to identify several areas of castor seed oil applications and research exertions carried out by various researchers in different fields. Castor seed oil taken through this review has proven to have excellent performance for production of high value products in industrial world. The high potential yield and unique fatty acid composition inherent in castor seed allow castor oil to produce economically competitive feedstock needed for production of premium quality biodiesel, short chain aviation fuels, derived fuel lubrication additives and very high value biopolymers. Besides, research priority should be placed on holistic castor seed collection and characterizations, generation of improved varieties, development of technology for improved agronomic practices and completely mechanized castor production, and sensitization of Nigerians on castor production and its position in world economy. Considering the high percentage yield of the castor seed oil (48%), farming castor plant should be encouraged to boost the commercialization of castor seed to enhance the economic growth of individual and the country at large particularly in this era of biotechnology and industrialization to feed these industries. The presence of phytochemical constituents and pharmacological activities reported in the present review proved that the plant has a leading capacity for the development of new good efficacy drugs in future.

References

[1] H.J. Caupin, “Products from castor oil: past, present and future”. In: Gunstone, F.D., Padley, F.B. (Eds.), Lipid Technologies and Application. Marcel Dekker, New York, NY, pp. 787–795, 1997.

[2] H. Mutlu, M.A.R. Meier, “Castor oil as a renewable resource for the chemical industry”. Eur. J. Lipid Sci. Technol. 112, 10–30, 2010.

[3] V. Sharma, P.P Kundu, “Addition polymers from natural oils—a review”. Prog.Polym. Sci. 31, 983–1008, 2006.

[4] Jr. W. Johnson, “Final report on the safety assessment of ricinus communis(castor) seed oil, hydrogenated castor oil, glyceryl ricinoleate, glycerylricinoleate SE, ricinoleic acid, potassium ricinoleate, sodium ricinoleate, zincricinoleate, cetyl ricinoleate, ethyl ricinoleate, glycol ricinoleate, isopropylricinoleate, methyl ricinoleate, and octyldodecyl ricinoleate”. Int. J. Toxicol. 26,31–77, 2007.

[5] B.R Kiran and M.N.V Prasad (2017) "Ricinus communis L. (Castor bean), a potential multi-purpose environmental crop for improved and integrated phytoremediation". The EuroBiotech Journal, Vol.1 issue 2, pp. 101-116.

[6] B.S. Baldwin, R.D Cossar. "Castor yield in response to planting date at four locations in the south-central United States", Ind. Crops Prod., 2009, 29: 443–448.

[7] L.B. Oliveira, M.S.M Araujo, L.P. Rosa, M. Barata, E.L.L. Rovere. "Analysis of the sustainability of using wastes in the Brazilian power industry, Renew. Sustain. Energy Rev. 2008, 12: 883–890.

[8] C.A de Abreu, M. Cantoni., A.R. Coscione, J. Paz-Ferreiro. "Organic matter and barium absorption by plant species grown in an area polluted with scrap metal residue". Applied Environ. Soil Science, 2012, Article ID 476821, 7 pages http://dx.doi. org/10.1155/2012/476821.

[9] E.I Bello, and A. Makanju, "Production, Characterization and Evaluation of Castor oil biodiesel as an alternative fuel for diesel engines". Journal of Emerging Trends in Engineering and Applied Sciences, 2(3), 2011: 525-530.

[10] M. Asmare, N. Gabbiye "Synthesis and characterization of biodiesel from castor bean as alternative fuel for diesel engine'. *American Journal of Energy Engineering; 2(1), 2014: 1-15*

[11] E.C Zuleta, L.A Rios, and P.N Benjumea, "Oxidative Stability and Cold flow behavior of palm, Sacha-inchi, Jatropha and Castor oil biodiesel blends". Fuel Processing Technology, 102: 96-101, 2012.

[12] P.U Babu, and V.R Mamilla, "Methanolysis of castor oil for production of biodiesel". International Journal of Advanced Engineering Technology, 3(1): 146-148, 2012.

[13] G.C.S Santana, P.F Martins, N Lima da Silva, C.B Batistella, R. Maciel Filho, M.R WolfMaciel, "Simulation and cost and estimate for biodiesel production using castor oil". Chemical Engineering Research and Design, 86: 626-632, 2010.

[14] N.K Attia, A.G. Gadalla, N.N Ibiari, R. El-Araby, G.I El-Diwani. "Studying the ultrasonic assisted transesterification of castor oil by using factorial design for optimization of biodiesel production". *AFINIDAD LXXI, 566, Abril - Junio 2014*

[15] O U Dairo, T.M.A Olayanju, E.S.A Ajisegiri, O.J Alamu, A.E Adeleke "Optimization of in-Situ Biodiesel Production from Raw Castor Oil-Bean Seed". Journal of Energy Technologies and Policy, Vol. 3, No.13. ISSN 2224-3232, 2013.

[16] P Berman, S. Nizri, & Z. Wiesman, "Castor oil biodiesel and its blends as alternative fuel". *Biomass Bioenergy*, *35*(7), 2861–2866, 2011

[17] M.H Shojaeefard, M.M, F Etgahni Meisami, A Barari "Experimental investigation on performance and exhaust emissions of castor oil biodiesel from a diesel engine". Environ Technol. 34(13–16):2019–2026, 2013.

[18] R. Wilson, B.J Van Schie, D. Howes, "Overvew of the preparation, use and biological studies on polyglycerol polyrecinoleate (PGPR)". Food Chem. Toxicol., 36(9-10): 711-8, 1998.

[19] M.C Ojinnaka, P.C Ojimelukwe "Effect of Salt and lime on Bacillus Fermented Castor oil Bean Condiment". Global Research Journal of Agricultural and Biological Sciences, 3(5): 381-389, 2012.

[20] A.L Kolapo, T.O.S Popoola, M.O Sanni, R.O Afolabi, "Preservation of soybean Daddawa Condiment with Dichloromethane Extract of Ginger". Res. J. Microbiol. 2, 254-259, 2007.

[21] B.O Omafuvbe, O.O Shonukan, S.H Abiose, "Microbiological and biochemical changes in the fermentations of soybean for soy-daddawa-Nigeria food condiments". Food Microbiol. 17: 469 – 474, 2000.

[22] S. Dakwa, E. Sakyi-Dawson, C. Diako, N.T Annan, and W.K Amoa-Awua, "Effects of boiling and roasting on the fermentation of soybeans into dawadawa (Soy-dawadawa)". Int. J. Food. Microbiol. 104: 69-82, 2005.

[23] S.A Odunfa "Microbiological and toxicological aspects of fermentation of castor oil seeds for Ogiri Production". Journal of Food Sciences, 50(6): 1758-1759, 1985.

[24] P.O Uaboi-Egbenni, P.N Okolie, A.O Sobande, O. Alao, O Teniola, P.O Bessong "Identification of Subdominant lactic acid bacteria in dawadawa (a soup condiment) and their evolution during laboratory scale fermentation of parkia biglobosa (African locust beans)". Afri. J. Biotechnol. 8(25): 7241-7248, 2009.

[25] L.I.I Ouoba, M.D Cantor, B. Diawara, A.S Traore, M. Jakobsen, "Degradation of African Locust bean oil by Bacillus Subtilis and Bacillus Pumillus Isolated from Soumbala, a fermented African locust bean contiment". J. Appl. Microbiol. 95(4): 868-874, 2003.

[26] B.Z Han, F.M Rombouts, M.J.R Nout, "Amino acid profiles of sufu, a Chinese fermented soybean food". Journal of Food Composition and Analysis, 17: 689 – 698, 2004.

[27] S.S Arogba, A Ademola, M Elum, "The effect of solvent treatment on the chemical composition and organoleptic acceptability of traditional condiments from Nigeria". Plant Foods for Human Nutrition 48(1):31-8, 1995.

[28] V.Shukla, M. Singh, D.K Singh, R.I Shukla, "The role of castor oil in epoxy and polyamide systems for coating and adhesive application". Surface Coatings International Part B: Coatings Transactions, Volume 88, Issue 3, pp 217–220, 2005.

[29] M.F Valero and Y Ortegon "Polyurethane elastomers-based modified castor oil and poly(ε-caprolactone) for surface-coating applications". Journal of Elastomers & Plastics, 2013.

[30] C.I De campos,F.A.R Lahr, A.L Christoforo, M.F Do Nascimento, "Castor oil Based Polyurethane Resin used in the Production of Medium Density Fiberboard". International Journal of Composite Materials, 4(4): 185-189, 2014.

[31] J.M.H Jesus, "Estudo do adesivo Poliutetano a base de mamona em madeira laminada colada. Tese (Doutorado), Escola de Engenharia de Sao Carlos, Universidade de sao Paulo, P. 106, 2000.

[32] M.A Azambuja, "Avaliacao do adesivo poliuretano a base de mamona na fabricacao de MLC, Dissertacao (Mestrado), Escola de Engenharia de Sao Carlos, universidade de Sao Paulo, sao carlos, 2003.

[33] C.I Campos, F.A.R Lahr "Propriedades fisico-mecanicas de MDF a partir de fibras de madeira de reflorestamento e adesivos alternativos". Tese de doutorado a presentada no curso de pos-graduacao ciencia e Engenharia de materials, *Programa Interunidades, EESC/IFSC/IQSC-USP; p.113; Sao Carlos –SP, 2005.*

[34] G.R de Martins, C.A.T Carvalho, M.C Valera, L.D de Oliveira, L. BUSO, A.S Carvalho "Sealing Ability of Castor Oil Polymer as a Root end Filling Material". J Appl Oral Sci. *17(3):220-3, 2009.*

[35] G. Casella and S. ferlito "The use of mineral trioxide aggregate in endodontics". *Minerva stomatologica, 55 3,123-43, 2006.*

[36] M. Almuhaiza "Glass-ionomer Cements in Restorative Dentistry: A Critical Appraisal". J Contemp Dent Pract; 17(4): 331-336, 2016.

[37] A.S Trevino, & D.L Trumbo "Acetoacetylated castor oil in coatings applications". *Prog Org Coat., 44*(1), 49 – 54, 2002.

[38] P.R Ribeiro, R.D de Castro, and L.G Fernandez, "Chemical constituents of the oilseed crop *Ricinus communis* and their pharmacological activities: a review". *Industrial Crops and Products* 2016, 91, 358-376.

[39] Welch, Holme & Clark Co., Inc. (2013). Castor Oil /Home Remedies Using Castor oil http://www.medindia.net/homeremedies/castoroil. asp#ixzz2tEAefaYX**.**

[40] A. Bonjean "Castor". 2002. Available:http://www.ienica.net/crops/castor.htm.

[41] D. Luseba, E.E Elgorashi, D.T Ntloedibe, J Van Staden. "Antibacterial, anti-inflammatory and mutagenic effects of some medicinal plants used in South Africa for treatment of wounds and retained placenta in livestock". South African Journal of Botany. 2007;73:378– 383.

[42] K.G Kumari, M Ganesan, N Jayabalan. "Somatic organogenesis and plant regeneration in *Ricinus communis".* Biol. Plantarum. 2008:52:17-25.

[43] T. O Akande, A.A Odunsi, O.S Adedeji. "Toxicity and nutritive assessment of castor (*Ricinus communis)* and processed cake in rat diet". Asian J. Anim. Sci. 2011;5:330-339.

[44] L. Boulos. "Medicinal plants of North Africa.Algonoc", Michigan Reference Publications, Inc USA; 1983.

[45] S.M Lamadah, H.A.E Mohamed, S.M El-Khedr, "Castor oil Safety and Effectiveness on Labour Induction and Neonatal Outcome". Journal of Biology, Agriculture and Healthcare, 4(4): 1-10, 2014.

[46] E.A Mein, D.G Richards, D.L McMillin, C.D Nelson, "Transdermal Absorption of Castor oil". Evid Based Integrative Med, 2(4): 239-244, 2005.

[47] W.A McGarey, Edgar Cayce and the Palma Christi Virginia Beach (VA): Edgar Cayce Foundation, 1970.

[48] W.A McGarey "The oil that heals". Virginia Beach (VA): A.R.E Press, 1993.

[49] J.P Callan, "Holistic health or holistic hoax? JAMA 241: 1156, 1979.

[50] E.A Mein, D.G Richards, D.L McMillin, C.D Nelson, "Transdermal Absorption of Castor Oil". Evidence-Based Integrative Medicine 2(4):239-244, 2005.

[51] G.G Arslan, & I Eşer, "An examination of the effect of castor oil packs on constipation in the elderly". *Complimentary Therapies in Clinical Practice, 17*(1), 58–62, 2011.

[52] B Medhi, K Kishore, U Singh, & S.D Seth, "Comparative clinical trial of castor oil and diclofenac sodium in patients with osteoarthritis". *Phytotherapy Research*, *23*(10), 1469-73, 2009.

[53] FDA (2007) Final report on the safety assessment of Ricinus Communis (Castor) Seed Oil, Hydrogenated Castor Oil, Glyceryl Ricinoleate, Glyceryl Ricinoleate SE, Ricinoleic Acid, Potassium Ricinoleate, Sodium Ricinoleate, Zinc Ricinoleate, Cetyl Ricinoleate, Ethyl Ricinoleate, Glycol Ricinoleate, Isopropyl Ricinoleate, Methyl Ricinoleate, and Octyldodecyl Ricinoleate. Int J Toxicol. 2007;26 Suppl 3:31-77.

[54] D Garry, R Figueroa, J Guillaume, & V Cucco, "Use of castor oil in pregnancies at term. *Altern Ther Health Med*. Jan; *6*(1), 77-79, 2000.

[55] S.L Kelly, D.C Lamb, M Cannieux, D Greetham, C.J Jackson, T Marczylo, C Ugochukwu, D.E Kelly "An old activity in the cytochrome P450 superfamily (CYP51) and a new story of drugs and resistance". *Biochem Soc Trans* 29(Pt 2):122-8, 2011.

[56] A.M Gülmezoglu, C.A Crowther, P Middleton. and E Heatley "Induction of labour for improving birth outcomes for women at or beyond term". Cochrane Database Syst Rev. 2012; 6: CD004945.

[57] L.S Severino, D.L Auld, M. Baldanzi, M.J.D Cândido, G Chen, W Crosby, "A review on the challenges for increased production of castor. Agron. J., 104:853–880, 2012a.
[58] R. Vignolo, F Naughton. "Castor: A new sense of direction". Int. News Fats Oils Relat. Mater. 1991;2:692-699.

[59] D.J Murphy "Structure, function and biogenesis of storage lipid bodies and oleosins in plants". Prog. Lipid Res.1993;32:247–280.
[60] L.S Severino, D.L Auld. "A framework for the study of the growth and development of castor Plant". Industrial Crops and Products. 2013;46:25-38.

[61] B.Z Salihu, A.K Gana, T Gbadeyan, and M.B Alabi, "Castor Oil Plant (*Ricinus communis* L.): A Potential Oil Crop for Agribusiness in Africa". *International Journal of Applied Research and Technology.* 3(8): 29 – 35, 2014.
[62] A.K Gana, A.F Yusuf, and B. Apuyor, "Castor Oil Plant and its Potential in Transformation and Industrialization of Under Developing Nations in the World". *Advanced Journal of Agricultural Research.* 1(005): 072-079, 2013.
[63] B.Z Salihu, A.K Gana, T Gbadeyan, and M.B Alabi, "Castor Oil Plant (*Ricinus communis* L.): A Potential Oil Crop for Agribusiness in Africa". *International Journal of Applied Research and Technology.* 3(8): 29 – 35, 2014.

[64] A.K Gana, A.F Yusuf, and B Apuyor, "Castor Oil Plant and its Potential in Transformation and Industrialization of Under Developing Nations in the World". *Advanced Journal of Agricultural Research.* 1(005): 072-079, 2013.

[65] S.S Liv, L.A Dick, B. Marco, J.B Magno, G.C Candido, C. William, D Tan, H. Xiaohua, P. Lakshmamma, C. Lavanya, C.; Olga, L. T. M.; Thomas, M.; Maira, M.; Travis, D. M.; Morris, J.; Stephen, B.; Morse, A.; Alejandro, A. N.; Dartanha J. S.; Valdinei, S.; Ming, L. W.; Mauricio, D. Z. and Helege, Z. "A Review on the Challenges for Increased Production of Castor". *Agronomy Journal.* Vol. 104. Pp. 853 – 880, 2012.

[66] NCRI, (2014). "Castor Breeding, National Cereal Research Institute, Nigeria". Report of castor germplasm collections and stakeholder identification.

[67] R.I .S Lima, S. Severino, I.R Sampaio, V Sofiatti, J.A Gomes, and N.E.M Beltrao, "Blends of castor meal and husks for optimized use as organic fertilizer. Ind. Crops Prod. 33:364-368, 2011.

[68] R.I.S Lima, S Severino, M.I.L Silva, I.S Vale, and N.E.M Beltrao, "Recipients volume and substrate composition for castor seedlings production". Ciencia Agrotecnol. 30:480-486, 2006b.

[69] A.P Gupta, R.S Antil, and R.P Narwal, "Utilization of deoiled castor cake for crop production. Arch. Agron. Sci. 50:389-395, 2010.

[70] ICOA. (1989). The processing of castor meal for detoxification and deallergenation. International Castor Oil Assoc., Cinnaminson, NJ.

[71] A.O Ani, and A.U Okorie, "Response of broiler finishers to diets containing graded levels of processed castor oil bean (*Ricinus communis* L.) meal. J. Anim. Physio. Anim. Nutr. 93:157 – 164, 2009.

[72] J.C Perone, A. Iachan, G.B. Domont, L.V. Disitzer, V.R.O. Castro, R. Roitman, and S.M. Gomes. 1966. Contribuicao ao estudo da torta de mamona. Dep. de Imprensa Nacional, Rio de Janeiro. (In Portuguese.)

[73] R.M Miranda, H.A. Bareira, E.V. Faria, and D.D. Machado. 1961. O farelo de mamona destoxicado na alimentacao de novilhas leiteiras. Instituto de Zootecnia, Rio de Janeiro. (In Portuguese.)

[74] I.H Hong, T.E. Kwonb, S.K. Lee, J.K. Park, M.R. Ki, S.I. Park, and K.S. Jeong. 2011. Fetal death of dogs aft er the ingestion of a soil conditioner. Exp. Toxicol. Pathol. 63:113–117. doi:10.1016/j.etp.2009.10.004

[75] R.C.F.F Pompeu, "Substituicao do farelo de soja pela torta de mamona destoxifi cada em dietas para ovinos: Valor nutritivo e desempenho bioeconomico. Ph.D. diss. Univ. Federal do Ceara, Fortaleza. (In Portuguese, with English abstract.), 2009.

[76] M Kumar "A Review on Phytochemical Constituents and Pharmacological Activities of *Ricinus communis* L. Plant". International Journal of Pharmacognosy and Phytochemical Research 2017; 9(4); 466-472, 2017.

[77] G Rathod, and R Pandhure, "phytochemical analysis and antibacterial activity in Ricinus Communis L". RNI No. UPBIL/2012/55438 VOL.-III, ISSUE-I, 49-51, 2014.

[78] J.B Morris, "Phytochemical traits in the genetic resources of castor bean". Current Topics Plant Biol. 5:63-67, 2004.

[79] Pradeep Pratap Singh, Ambika and S.M.S. Chauhan "Activity guided isolation of antioxidants from the leaves of *Ricinus communis* L" - *Food Chemistry*, 114: 1069-1072, 2009.

[80] Marta Amelia Vattuone, Olga Lilia Fleischmacher, Fernando Eduardo Prado, Alberto Lopez Vinals and Antonio Rodolfo Sampietro. "Localisation of invertase activites in *Ricinus communis* leaves "- *Phytochemistry*, 22(6):1361-1365, 1983.

[81] C P.Vermeer, P Nastold and R Jetter. "Homologous very long-chain 1,3-alkanediols in leaf cuticular waxes of *Ricinus communis" -Phytochemistry*, 62(3): 433-438, 2003.

[82] S Aziz, A Rabniwaz, K.h Habib-ur-Rehman, Shakil Ghani "Phytochemical and Biological Screening of *Riccinus communis* Seed Oil Grown. Wild in Jammu & Kashmir" Journal of Pharmacognosy and Phytochemistry; 5(3): 89-92, 2016.

[83] R Singh and Geetanjali "Phytochemical and Pharmacological Investigations of *Ricinus communis* Linn". Algerian Journal of Natural Products 3:1,2015, 120-129.

[84] Pamela Mouser, Michael, S, Filigenzi, Birgit Puschner, Johnson, V, Margaret A, Miller and Stephen, B. "Fatal ricin toxicosis in a puppy confirmed by liquid Chromatography /mass spectrometry when using ricinine as a marker" - *Science direct*, **51**: 451-456, 2009.

[85] V Copman, M De Leeuw, J Codonnier and W Jacobs. "Suicidal death after injection of a castor bean extract (*Ricinus communis* L)"- *Forensic Science International*, 189, e3-e20, 2009.

[86] Jose R Laureano Filho, Emanuel S.S Andrade, Jose R Albergaria-Barbosa, Igor B Camargo and Robson R Garcia. "Effects of demineralized bone matrix and a "*Ricinus communis*" polymer on bone regeneration: a histological study in rabbit calvaria" – *Exp. Lung Res*, 33:459-481, 2007.

[87] E Makonnen, L Zerihun, G Assefa and A.A Rostom "Antifertility activity of *Ricinus communis* seed in female guinea pigs" - *East African Medical Journal*, 76:335-337, 1999.

[88] Anete C Ferraz, Miriam Elizabeth M Angelucci, Mariana L Da costa, Liza R Batista, Bras H De Oliveira and Claudio Da Cunha. "Pharmacological evaluation of Ricinine, a central nervous system stimulant isolated from *Ricinus communis" - Pharmacol Biochem Behav*, 63(3): 367-375, 1999.

[89] J Jena, A.K Gupta "Ricinus Communis Linn: A phytopharmacological review". International Journal of Pharmacy and Pharmaceutical Sciences. *Vol 4, Issue 4, 25-29,* 2012.

[90] K.M Sarfaraz, Fazal-ur-Rehman, A.K Ejaz, S.B Mohammad, S Muhammad, U Imdad, J Sadaf and S Salma "*Ricinus cmmunis*: Ethnomedicinal uses and pharmacological activities", Pak. J. Pharm. Sci., Vol.30, No.5, pp.1815-1827, 2017.

[91] J Igwe, and G. O Mbah, "Effect of Some Process Parameters on the Optimum Yield of Oil from Soya Bean", Journal of Science and Technology. (JST), Vol. 17(1) pp 82-92, 2011.

[92] A.S Kutama, I.I Dangora, W Aisha, M.I Auyo, U Sharif, M Umma and K.Y Hassan **"**An overview of plant resources and their economic uses in Nigeria". Global Advanced Research Journal of Agricultural Science, Vol. 4(2) pp. 042-067, 2015.

[93] G.O Mbah, N.F Amulu, M.I Onyiah, "Effects of Process Parameters on the Yield of oil from Castor Seed". American Journal of Engineering Research (AJER), Volume-03, Issue-05, pp-179-186, 2014.

[94] K. Nahar and W.L Pan "Urea Fertilization: Effects on Growth, Nutrient Uptake and Root Development of the Biodiesel Plant, Castor Bean (*Ricinus communis* L.)" *American Journal of Experimental Agriculture, 5(4): 320-335,* 2015.

[95] A Abolfazl, F Nasrin, S Habib, H Saeid "The Effect of Climatic Factors on the Production and Quality of Castor Oil". *Nature and Science; 9(4):15-19,* 2011.

[96] S.A Omotehinse, A.C Igboanugo, K.A Bello "Split- split Plot theoretic approach to modeling optimum conditions for the growth and development of Castor Shrub". Confluence Journal of Environmental Studies, 12 (1): 12-24, 2018.

NIPES Conference Proceedings
The 1st International Conference of the Nigerian Institution of Professional Engineers and Scientists 7th-8th Oct. 2021: 86-94
www.nipesjournals.org.ng

Computation of Heat Transfer in a Flat Plate Solar Collector System Using Energy Balance Method

Eghosa Omo-Oghogho*, Ikpe Aniekan Essienubong and Aliu Sufianu Adeiza
Department of Mechanical Engineering, University of Benin, P.M.B 1154, Benin City, Nigeria

Abstract
Input parameters measured from a prototype designed flat plate solar collector system in Benin Metropolis was employed in this study. A model was developed using energy balance method, the developed model was then computed using Explicit Finite Difference Method in MATLAB environment to predict the thermal behavior of the system. The principles and laws of thermodynamics were used in the modelling process. From the model developed, 330K, 370K and 320K were obtained as outlet water temperature, absorber plate temperature and glass temperature respectively. An optimal insulation thickness of 0.05m, 0.06m and 0.07m were achieved. 0.020m, 0.024m and 0.026m were obtained as optimal design condition for thickness of housing and this is with respect to the input parameters considered.

Keywords: Solar energy, Heat transfer, Flat plate, Solar collector, Glass cover, Absorber plate.

1. Introduction

Solar is a renewable energy resource that has contributed positively to the energy sector and the world at large [1]. Solar energy is a combination of photon and thermal energy captured and applied over a range of ever-evolving technologies such as solar collector plate, solar thermal energy, molten salt power plants, artificial photosynthesis etc [2].

The amount of solar energy depends basically on the astronomical geometric parameter such as the actual distance from sun to earth. Since the earth moves around the sun on an elliptical orbit, the sun-earth distance is a function of the day. With regard to the mean value of the earth-sun distance, the sum of the energy per unit area obtained from the sun exterior of the earth's atmosphere, known as the solar constant, is approximately 1367W/m^2. Furthermore, the earth's cross-sectional area is estimated to be 127400000km^2 and the total power released to the earth by the sun is estimated to be 1.75 × 1014 kW [3].

While passing through the atmosphere a major part of the incident energy from the sun is suppressed by reflection, scattering or absorption by air molecules, clouds and particulate matter also called aerosols. Due to this, only 60% (approximately 1.05×10^{14} kW) of sunlight from the sun to the earth's atmosphere reaches the earth's surface [4].

In recent times, solar energy collectors have been used in transforming solar radiation energy from the sun to the internal energy of the transport medium and working fluid. One of the major components of any solar thermal system is the solar collector. This is a device which uses the incoming solar radiation energy, converts it into heat and transfers this heat (form of energy) to a fluid (usually water, air or oil) passing through the tubes of the collector. The solar thermal energy that is collected comes from circulating fluid either directly to the hot water or space conditioning system or to a thermal energy storage tank from which can be drawn for use at night or cloudy days [5].

[6] carried out an investigation on a polymer collector in which the solar energy was directly absorbed by the black colored working fluid. The model was validated both experimentally

and through computational fluid dynamics (CFD) under steady-state conditions. From the CFD model validation, parameters obtained for temperature and velocity distribution across the solar collector surface area were found to be in agreement with the experimental results. The performance was obtained by CFD under steady-state conditions.

[7] developed a 3-dimensional numerical model for solar collector considering the multidimensional and transient character of the problem. Effect of non-uniform flow on the solar collector performance was quantified and the degree of deterioration of collector performance was analyzed. The analysis showed that deterioration increased with increase in non-uniformity of the flow. The results indicated that collector efficiency does not change reasonably even when the flow at the outer risers is 1.5 times the flow of the central one but the outlet temperatures for each tube differs.

Angular solar relations analysis of a flat plate solar collector was experimentally conducted by [8] using a prototype designed flat plate solar collector system. Average declination angle of 14.6675, average zenith Angles of the sun of 22.1850, average incidence angle of 21.7650, average solar Azimuth angle of 77.0625 and average ratio of beam radiation of 1.0875 were obtained respectively. The average radiation on a tilted surface was obtained as 1025.3258w/m^2 for enhanced flat plate solar collector design.

The tilt angle for several cities in Saudi Arabia was optimized by [9] using MATLAB model. Adjustment of tilt angle of the solar collector was suggested as six times annually. For optimum tilt angle, frequent adjustments was suggested in the months near equinox, due to rapid change in the direction of the sun compared to solstices.

In this study, MATLAB was employed in the computation of heat transfer in a flat plate solar collector system using energy balance method. Equations considered were energy balance of glass cover, energy balance of absorber plate and energy balance of the water stream.

2. Methodology

The model was developed using energy balance method and then computed using explicit finite difference method in MATLAB solver. MATLAB codes were written to provide access to matrix and data structures provided by the LINPACK (Linear system package) and EISPACK (Eigen system package) projects. MATLAB is a high-performance language which is capable of performing technical computing. It combines visualization, computation and programming environment. The MATLAB software provides a modern programming language environment as well as complex data structures containing in-built editing and debugging tools. The constant parameters and variable parameters were also considered in the process. For effective modelling, energy balance in the glass, energy balance in the absorber plate and energy balance of the water stream were considered as follows:

2.1 Energy Balance of the Glass Cover

The small thickness of the glass covering the solar flat plate collector makes it reasonable to consider a uniform glass temperature distribution through the whole part of the glass cover. Considering the constant properties of the glass material, the governing equation can be derived from an energy balance in a differential volume of thickness (δ), area (A_c) and time variation over period of the day. The heat energy received by the collector is given by Equation 1, solar energy emitted through the glass is given by Equation 2, heat transfer between absorber and

glass is given by Equation 3, heat transfer between the glass and atmosphere is given by Equation 4 and heat energy emitted from the absorber to the glass is given by Equation 5.

$$\mathrm{H_g} = (\mathrm{m_g\, C_g})\frac{\mathrm{dT_g}}{\mathrm{dt}} \quad (1)$$

$$\mathrm{H_S} = \mathrm{A_C} I_T \alpha_\mathrm{g} \quad (2)$$

$$\mathrm{H_{pg}} = \mathrm{A_C h_{pg-cp}(T_p - T_g)} \quad (3)$$

$$\mathrm{H_{ga}} = \mathrm{A_C h_{ga-wv}(T_g - T_a)} \quad (4)$$

$$\mathrm{Hr_{pg}} = \sigma \mathrm{A_p}(T_p^4 - T_g^4)(\mathrm{m_g\, C_g})\frac{\mathrm{dT_g}}{\mathrm{dt}} = \mathrm{A_C} I_T \alpha_\mathrm{g} + \mathrm{A_C h_{pg-cp}}\big(\mathrm{T_p - T_g}\big) - \mathrm{A_C h_{ga-w}}\big(\mathrm{T_g - T_{am}}\big) + \sigma \mathrm{A_p}\big(T_p^4 - T_g^4\big) \quad (5)$$

The radiative heat transfer coefficient between the plate and the cover is given by Equation 6, the radiative heat transfer coefficient between the cover and the sky is given by Equation 7, the convective heat transfer coefficient between the plate and the cover is given by Equation 8, the top loss coefficient for a single glass cover is given by Equation 9.

$$h_{pg} = \frac{\sigma\left(T_p^2 + T_g^2\right)(T_p + T_g)}{\frac{1}{\epsilon_p} + \frac{1}{\epsilon_g} - 1} \quad (6)$$

$$h_{ga} = \epsilon_g \sigma (T_g^2 + T_s^2)(T_g + T_s) \quad (7)$$

$$h_{cp} = \frac{N_u K_a}{L_a} \quad (8)$$

$$U_T = \left(\frac{1}{h_{cp} + h_{pg}} + \frac{1}{h_{wv} + h_{ga}}\right)^{-1} \quad (9)$$

2.2 Energy balance of absorber plate

A small thickness of the absorber plate was considered for a uniform plate temperature distribution through the whole part of the absorber plate. Applying the energy balance for the absorber plate zone, using the thermo-physical properties of the absorber material and considering the solar irradiance on the absorber plate in the solar flat plate collector, the radiation and convection heat transfer between the absorber and the glass cover, the conduction and convection heat transfer between the absorber and the insulation zone and the heat transfers by convection with the fluid flow were considered. The heat energy gained by the plate is given by Equation 10, solar energy absorbed by the plate is given by Equation 11, the heat transfer between the plate and glass is given by Equation 12, heat transfer between plate and water is given by equation 13, heat transfer between the absorber and insulation is given by Equation 14, heat transfer between the insulation and housing is given by Equation 15, heat energy emitted from the absorber to the glass is given by Equation 16.

$$\mathrm{H_p} = \mathrm{m_p c_p}\frac{\mathrm{dT_p}}{\mathrm{dt}} \quad (10)$$

$$H_S = A_p I_T \alpha_g \tau \quad (11)$$

$$H_{pg} = A_p h_{pg-cp}(T_p - T_g) \quad (12)$$

$$H_{pw} = A_f h_f(T_p - T_f) \quad (13)$$

$$H_i = K_i \frac{A_i}{\delta_i}(T_p - T_i) \quad (14)$$

$$H_h = K_h \frac{A_h}{\delta_h}(T_i - T_h) \quad (15)$$

$$Hr_{pg} = \sigma A_p(T_p^4 - T_g^4) m_p c_p \frac{dT_p}{dt} = A_p I_T \alpha_g \tau + A_p h_{pg-cp}(T_p - T_g) - A_f h_f(T_p - T_f) - K_i \frac{A_i}{\delta_i}(T_p - T_i) - K_h \frac{A_h}{\delta_h}(T_i - T_h) - \sigma A_p(T_p^4 - T_g^4) \quad (16)$$

2.3 Energy balance of the water stream

Applying the heat energy balance to the system helps to show and demonstrate the effect of heat gained and losses within the system. The energy balance describing the heat transfer between the water, pipe, absorber plate and the glass cover is expressed in the following Equation. Net heat gained by the water is given by Equation 17, heat energy transfer to the water is given by Equation 18, output heat energy is given by Equation 19

$$H_w = m_w c_w \frac{dT_w}{dt} \quad (17)$$

$$H_{pw} = A_f h_f(T_p - T_f) \quad (18)$$

$$H_O = m_f c_w (T_{wo} - T_{wi}) \quad (19)$$

The initial input parameters used for the modelling and simulation of the system is presented in Table 1.

Table: 1 Initial input parameters for the model

Parameters	Value
Emmitance of plate	0.84
Emissivity of glass	0.04
Heat capacity of glass (KJ/kg.K)	0.80
Heat capacity of absorber plate (kJ/kg.K)	0.90
Heat capacity of water (KJ/kg.k)	4.18
Area of collector (m^2)	0.84
Area of fluid pipe (m^2)	0.047
Insulation thickness (m)	0.05
Housing thickness (m)	0.02
Mass of glass (kg)	18.8
Mass of absorber plate (kg)	8.93
Mass flow rate (kg/s^2)	0.03
Wind velocity (m/s)	1.648
Initial glass temperature (K)	315
Initial water inlet temperature (K)	305
Initial housing temperature (K)	315
Initial insulation temperature (K)	325

Thermal conductivity of insulation (glass wool) (W/mk)	0.034
Thermal conductivity of housing (W/mk)	0.12
Thermal conductivity of air (W/mk)	0.024
Thermal conductivity of copper (W/mk)	386
Thermal conductivity of aluminium (W/mk)	239
Transmittance of glass	0.94
Radiation on a tilted surface (W/m^2)	937.18

3. Results and Discussion

Figure 1, 2, 3, 4, 5, 6, 7, 8, 9 and 10 shows the temperature of plate, temperature of glass, and the temperature of water from initial to final conditions with respect to time.

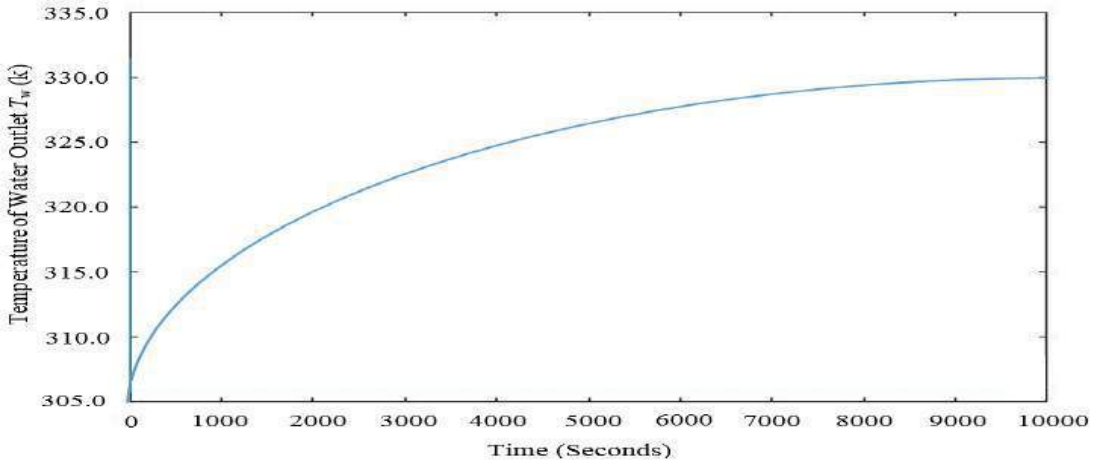

Figure 1: A graph of outlet temperature against time

Figure 1 shows the thermal behavior of the collector system, the model was able to simulate the behavior of the collector for 10000seconds and the temperature of water achieved was about 330K.

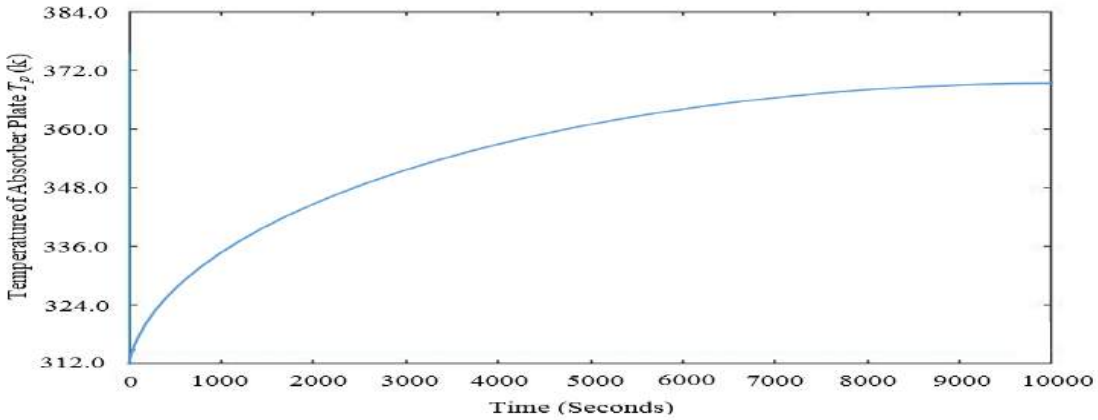

Figure 2: A graph of absorber plate temperature against time

As shown in Figure 2, the graph of absorber plate temperature against time indicates the temperature distribution on the absorber plate within a time frame of 10000 seconds. A temperature of about 370K was achieved.

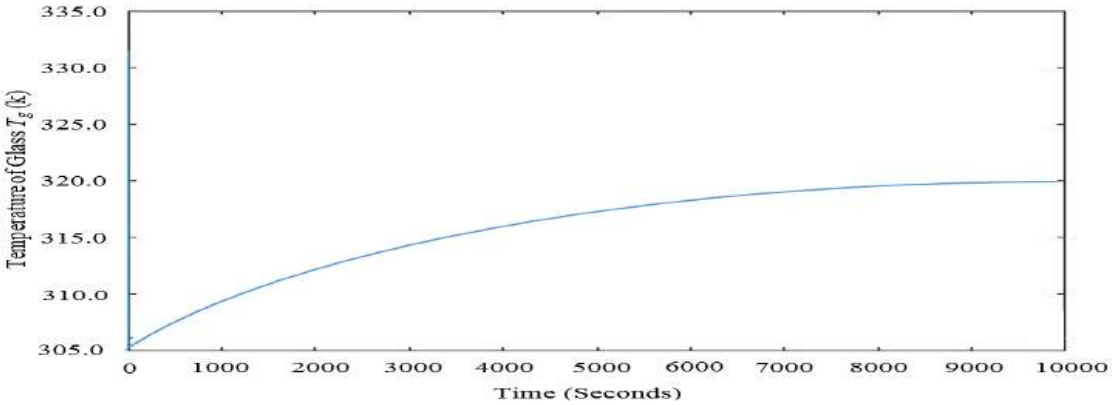

Figure 3: A graph of glass temperature against time

Figure 3 shows the effect of temperature on the glass of the collector system and its distribution over its surface area. The glass temperature got up to 320K.

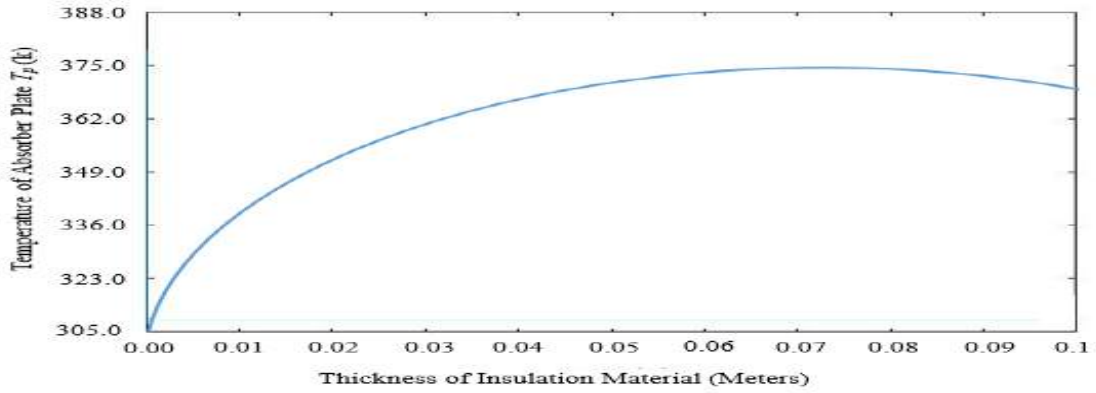

Figure 4: A graph of absorber plate temperature against insulation thickness

Figure 4 shows the thermal behavior of the absorber plate when the insulation thickness is varied with respect to time, from the graph it shows that a temperature of 375K was achieved considering insulation thickness of 0.05m, 0.06m, 0.07m. The insulation thickness within this range of values are parameters that can yield maximum output for optimum conditions.

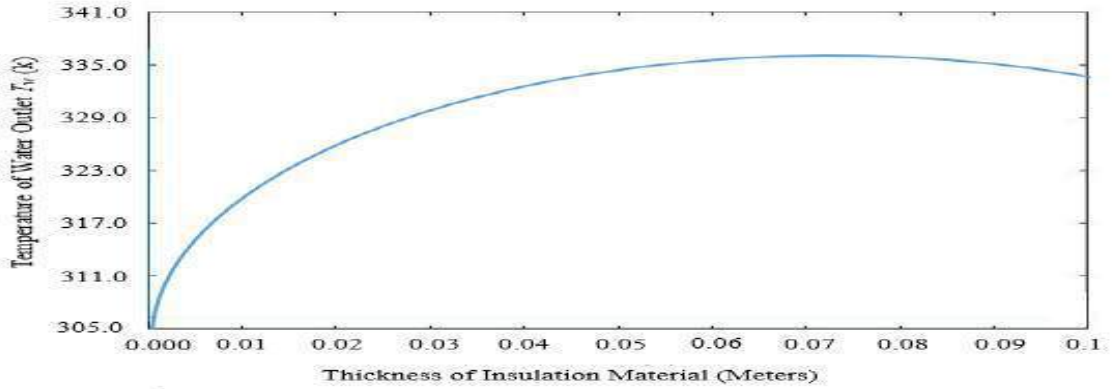

Figure 5: A graph of outlet water temperature against insulation thickness

The graph in Figure 5 describes the effect of insulation thickness on outlet water temperature, from the graph it shows that at a range of insulation thickness (0.05m, 0.06m and 0.07m), an outlet temperature of 335K was achieved.

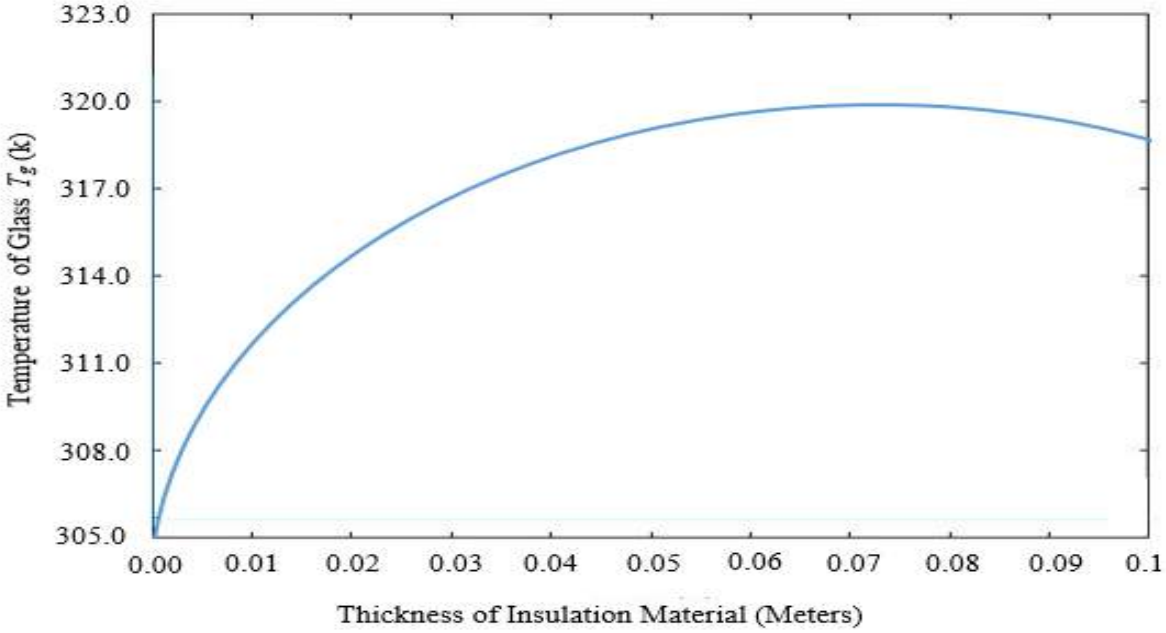

Figure 6: A graph of glass temperature against insulation thickness

Figure 6 shows that a temperature of 320K was achieved as the glass temperature at an insulation thickness range of 0.07m. 0.05m and 0.06m can also be considered, the temperature starts dropping at 0.08m. Hence 0.07m, 0.05m and 0.06m are optimum design parameters that can improve the overall efficiency of the solar collector.

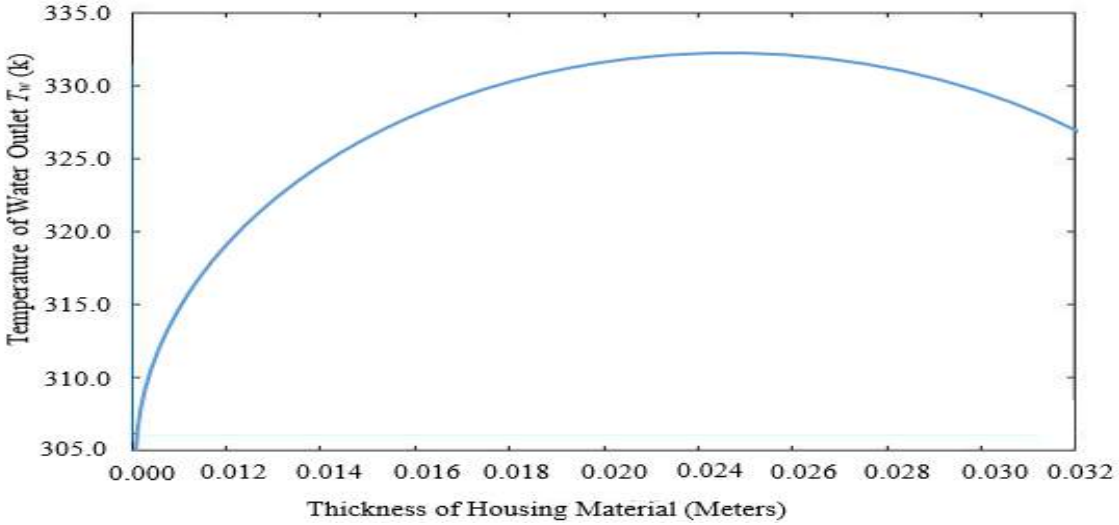

Figure 7: A graph of outlet water temperature against housing thickness

Figure 7 indicates that housing thickness of range (0.020m, 0.024m and 0.026m) achieved an outlet temperature of 333K. This indicates that at the range of the above housing thickness considered, the system performance can improve if they are used as design parameters for optimum conditions.

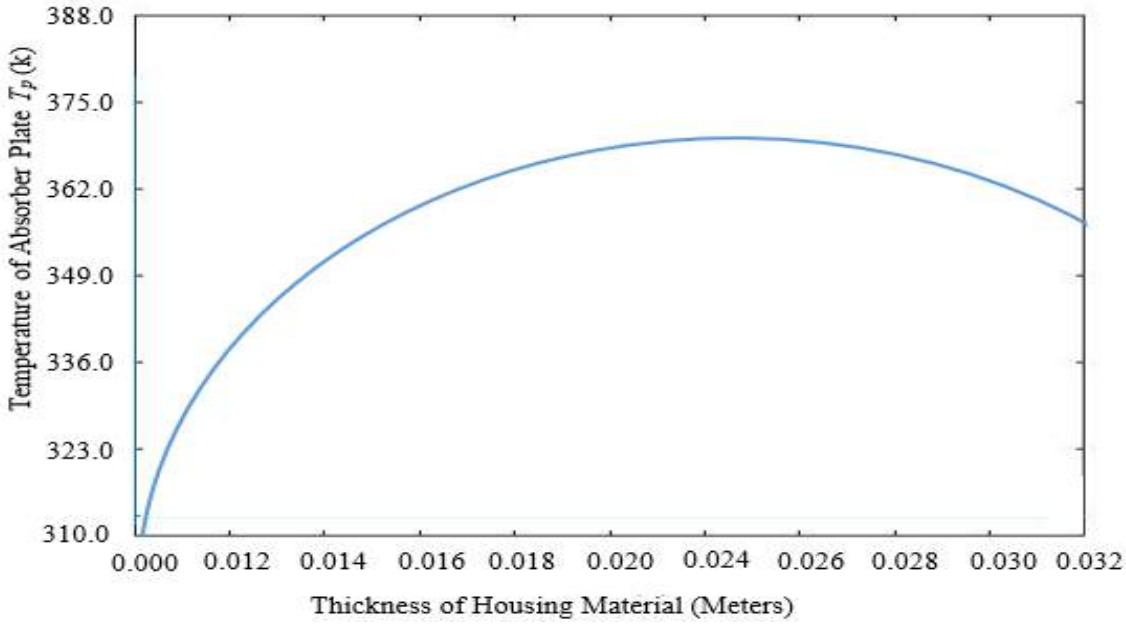

Figure 8: A graph of absorber plate temperature against housing thickness

Figure 8 indicates that a temperature of 370K was achieved at a range of 0.020m, 0.024m and 0.026m respectively. The range of housing thickness shown to yield a high absorber plate temperature are best considered as optimum conditions for design.

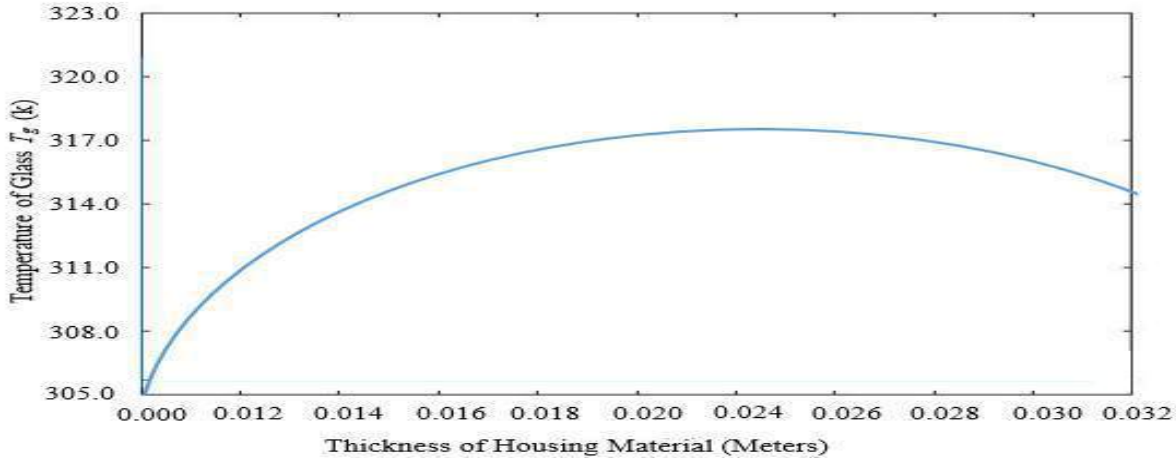

Figure 9: A graph of glass temperature against housing thickness

Figure 9 shows that the glass attained a temperature of about 318k within a housing thickness range of 0.020m, 0.024m and 0.026m. The graphs present a thermal description of the glass, and the housing thickness within this range is valuable for optimum conditions for better performance of the overall system.

4. Conclusion

A thermodynamic model has been successfully developed using energy balance method and solved with MATLAB to predict the output temperature of water, glass and absorber temperature of a flat plate solar collector. Outlet water temperature, absorber plate temperature

and glass temperature of 330K, 370K and 320K as well as optimal insulation thickness of 0.05m, 0.06m and 0.07m were obtained from the model developed. The model considered the heat transfer between the absorber plate, insulation and housing which provided a more realistic assumptions and simplified approach to studying the thermal behavior of a flat plate collector system.

References

[1] Goswami, D. Yogi, Frank, K. and Jan F. Kreider. (1999) Principles of solar engineering. 2nd. Philadelphia: Taylor & Francis.
[2] Oselen, I. J., Oseiga, O. V. and Ikpe A. E. (2019) Design and Performance Testing of a Solar Water Heater. International Journal of Advances in Scientific Research and Engineering, 5(11), 15-22.
[3] Duffie, J.A. and Beckman, W.A. (2013) Solar Engineering of Thermal Processes. John Wiley and Sons, Inc., New York.
[4] Kalogirou, S.A. (2009) Solar Energy Engineering: Processes and Systems. Elsevier, USA.
[5] Duffie J. and Beckman W., (2006): Solar engineering of thermal processes, 3rd edition (Wiley Interscience, New York).
[6] Martinopoulos G., (2010) CFD modeling of a polymer solar collector, Renewable Energy, 35, 1499-1508.
[7] Molero Villar N., Cejudo Lopez J., and Dominguez Munoz F., (2009): Numerical 3-D heat flux simulations on flat plate solar collectors, 83, 1086-1092.
[8] Omo-Oghogh, E. and Ikpe, A. E. (2020) Angular Solar Relations Analysis of a Flat Plate Solar Collector in Benin City Metropolis. International Journal of Engineering and Innovative Research, 2(2), 67-77.
[9] Kaddoura, T. O., Ramli, M. A. M. and Al-Turki, Y. A. (2016) on the estimation of the optimum tilt angle of PV panel in Saudi Arabia. Renew. Sustain. Energy Rev., 65, 626–634.

NIPES Conference Proceedings
The 1st International Conference of the Nigerian Institution of Professional Engineers and Scientists 7th-8th Oct. 2021: 95-100
www.nipesjournals.org.ng

Development and Performance Indices of a Palm Kernel Cracking Machine

I. T. Okafor[1], C. C. Nwigwe[2]
Nigerian Naval Engineering College, Ogorode, Sapele, Delta State[1]. University of Benin, Benin City Edo State[2].
izunnaokafor@gmail.com[1], cynthianwigwe@gmail.com[2]

Abstract

Palm kernel oil has been utilized in very many facet of life, and the abundant of this palm fruit bunches in the southern part of Nigeria, if well maximized will nudge the economy of this country into a decent future. This study has been able to develop a palm kernel cracking machine with higher efficiency above what was obtainable in literature reviewed so far. The component for the development of the machine for cracking the palm fruit were sourced locally and Solid Works served as the design expert for the development of the machine as relating to the design working diagram. To boot the design process of the machine will eliminate loss of man hour time and reduce cost. The cracking machine was tested to determine its performance characteristics and it has shown an efficiency level of 96.6% with processing rate at 96 nuts per second with 2.5hp electric motor that is an improvement over existing palm kernel cracking machine that have 87.6% efficiency to cracking with processing rate of 89 nuts per second without re-cracking.

Keywords: Cracking Machine, Palm Kernel, Palm Kernel Oil, Performance efficiency

I. Introduction

The palm kernel oil (P.K.O) (Elaeis guineesis) belongs to the Palmae family, among the oil producing plants, it is the richest vegetable oil plant [1]. Palmae family is made up of about 225 family members with over 3620 species. Palm kernel oil (P.K.O) is a rich source of fatty acid as well as fat and oil, and the importance of this product cannot be overemphasized, but the wastage of this product in the southern part of Nigeria has been come a major concern because lack of production units in large quantity has been a source hindrance.

. Fig. 1.Palm Nut

The three most common types of palm kernel fruit bunches present in the southern part of Nigeria is the Dura, Tenera and Pisifera. [2]. from literature reviewed it has shown that the most common type in commercial quantity in the southern Nigeria is Tenera species [3]. the oils from palm kernel fruit bunches are utilized in various ways such as for the production of margarine, soap, cream, polish, glycerine as well as medical purposes etc. [5]., some authors have also tried to utilize the palm kernel oil (P.K.O) as biofuels. To boot the shells or husk from the palm fruit are used for the production of brake pads and as source of energy for cooking, blacksmithing and industrial purposes [6]. In Illorin Nigeria, [8]. developed a palm kernel cracking machine in National Centre for Agricultural Mechanization (NCAM), and they obtained cracking efficiency of about 94.50 and 87.50 with 14.70 and 6.0% kernel damage respectively [9].and [1]. applied the use of locally source materials in production of palm kernel cracking machine and they were able to save some considerable amount of money while prioritizing the technological aspects. The prime mover i.e electric motor for this study is rated 2.5hp and a speed of 7500rpm and the optimal efficiency was achieved at 96% and 4% of cracking damage on the kernel.

2.0. Materials and Method

A. The in-feed unit

The feeding unit consists of the feed hopper and the in-feed elbow. The feed hopper design was largely influenced by the throughput capacity required to make the performance of the machine atisfactory. The feed hopper is made in the shape of a frustum (290 × 80 ×240mm), and is inclined horizontally at an angle of 60°. This is to ensure free fall of the kernels through the hopper, to prevent jamming of kernels at the throat, and to make the feed hopper self-cleaning. However, the feed hopper itself is made of mild steel.

B. The cracking unit

The cracking chamber, takes the shape of a hollow cylindrical tube with rectangular (channel-shaped) impeller blades at its core. The cylinder measures 385 × 410mm in its minor and major diameters respectively, and 165mm in its length. The cracking chamber is bored at a diameter of 90mm at the back surface to enable the passage of the driving shaft to the core of the chamber through the ball bearing. However, the core of the cracking chamber is characterized with the impeller tube and blades; the tube being the carriage for the rotation of the blades.

C. The driven unit

The driven unit consists of the prime mover; the electric motor, the 2 two-way pulleys and the belt drive. The electric motor is rated 2.5hp, with the pulleys ranging in diameter sizes of 130mm to 90mm. The belt drive is a V-belt (A60) spanning through a length of 680mm.

D. The Cleaning Unit

The cleaning unit is made up of a rectangular metallic mesh with uniform rectangular grooves of diameter 15mm. This unit is directly attached to the nut outlet discharge of the cracking chamber, and it spans a total length of 420mm, width of 200mm, and height of 120mm. This unit operates in the form of an agitated basket, and is stimulated by the vibration effect from the electric motor; an action which operate as a gyroscopic motion.

2.1. Design Consideration

In order to design a robust system that will crack palm kernel nut without damaging the kernel, we have to put a lot of measures in the designing process to forestall the man – hour time lost, cost of production as well as energy conservation

1. the physical and mechanical configuration of the palm kernel nut

2. the machine durability

3. energy conservation

4. the ease of machine usage and repair.

2.2. Design Analysis

A. The cracking unit

Kinetic energy of kernels = Impact energy of kernels on the cracking wall

$$\frac{1}{2}mv^2 = \text{Impact Energy} \quad (1)$$

But, Impact energy on the cracking wall = Work required to deform a kernel

$$\text{Work } \frac{F}{2} \times x \quad (2)$$

Where F is the force or load applied, and x is the distance travelled; in this regard, the deformation on the kernels (e).

$$\text{Work required to deformation kernel } (w) = \frac{F}{2} \times e$$

$$r = \frac{\sigma}{\sigma} \times x \quad (3)$$

$$\sigma = \frac{2p}{A} \text{ and } \sigma = \frac{p}{A} \quad (4)$$

Therefore, r =2, and F = 2P

$$\text{Substituting this into W } = \frac{2p}{2} \times e$$

$$w = p_e$$

$$\text{Therefore, } \frac{1}{2}mv^2 = p_e \quad (5)$$

The product (P_e), defined as the energy of deformation, is given from experimental results as: 0015Nm for Tenera nuts respectively.

B. The design of impeller

Tenera Variety:

By substituting the value of mass and energy of deformation of Tenerant, the velocity required for cracking is obtained as:

$$\frac{0.00766kg}{2}v^2 = 0.9012 \quad (6)$$

$v = 15.33m/s$

But v = r ω; for a cracking impeller of radius, r = 100mm, angular velocity, ω is determined as:

$$\omega = \frac{v}{r} \quad (7)$$

$$N = \frac{60\omega}{2\pi} \quad (8)$$

Average linear speed required for the machine $= 205.52m/s$

Average linear speed required for the machine $205.15rad/s$

C. The shafting design

Shafts are designed on the basis of strength, rigidity and stiffness. Radius of gyration (k), taking the cracking impeller and tube as a rectangular cross-section, just as shown in Figure 1:

K = 0.289h (9)

K =0.289 x0.35=0.1012m

But moment of inertial about the x- axis (1_{xx}):

$1_{xx} = mk^2$

Also $1_{xx} = \frac{bh^3}{12}$ (10)

The tangential force (f) to the axis of rotation given by the relation:

F = $m\alpha$

Where α is the angular acceleration; whose maximum value is given as

$\alpha = \omega^2 r$

$f = m\omega^2 r$ (11)

(12)

Torque (T) = Fr

D. Mechanical power requirement

The minimum power requirement (p) = $T\omega$ (13)

ED. The design for stiffness and rigidity (Torsional deflection)

The design for stiffness and rigidity of a shaft is determined from its torsional deflection during usage. The torsional deflection per unit length of a working shaft should not be greater than 0.25°/m. Torsional deflection of shafts:

$$\theta = \frac{TL}{GJ} \quad (14)$$

Torsional deflection per unit length:

$$\frac{\theta}{L} = \frac{T}{GJ}$$

Where T is the torsional stress on the shaft

L = Length of shaft

G = Modulus of rigidity of shaft (mild steel)

J = Polar moment of inertia of shaft.

But polar moment of inertial of shaft, $J = \frac{\pi d^4}{32}$

The basic calculations for the sorting unit are embedded in the vibration effect required for motion along the sorting route.

2.3. Machine Testing and Performance Analysis

The developed the machine as shown in Fig 2. Tests were carried out to determine the efficiency of the machine. Three different test were conducted in order to determine the efficiency of the palm kernel cracking machine, each of the sample contained 300, 400 and 500 palm kernels. The palm kernels for each of the sample value were fed through the hopper and flows through to the cracking chamber at a steady speed. The results were then recorded for the machine efficiency, cracking efficiency and mechanical damage kernel efficiency were also calculated using the equations below (15 - 17).

$$E_m = \frac{W_U}{W_T} \times 100 \quad (15)$$

$$E_C = \frac{W_C}{W_T} \times 100 \quad (16)$$

$$M_d = \frac{W_C - W_U}{W_T} \times 100 \quad (17)$$

Where E_m is the machine performance efficiency, E_c is the percentage cracked kernel efficiency, M_d is the mechanical damaged efficiency, W_U is the undamaged cracked kernel, W_C is the total cracked kernel (damaged and undamaged) and W_T the total number of kernel fed into the system.

3.0. Results and Discussion

The result of the experiment carried out on the performance testing is shown below in Table 1. From the analysis it is observed that the performance of the palm kernel cracking machine is meritorious or a surefire.

Table 1: Experimental result

Input	Cracked	Uncracked	Damaged	Undamaged	Percentage cracked (%)	Machine efficiency (%)	Machine damaged (%)
300	289	11	3	286	95.3	96.3	1
400	384	16	2	382	95.5	96	0.5
500	488	12	4	484	96.8	97.6	0.8

4.0. Conclusion

From the result supra it is obvious that the cracking machine developed locally have been able to eliminate drudgery in manufacturing of palm kernel oil (P.K.O). the mean efficiency for the palm kernel cracking is at 96.6% machine efficiency suggesting that the system is meritorious.

Furthermore, the production of the palm kernel cracking machine is cost effective as the total cost of production did not exceed one hundred and forty thousand naira only (#140,000), the cost of

production can further be subsidized if the machine is produced in large quantity, the machine can be operated in small, medium and large scale. It is our prayer that the government should make finances available to our local farmers in order to bolster the production of palm kernel oil (P.K.O). This will reduce the lame production of the palm kernel oil (P.K.O). whilst reengineering our economy into a decent one.

References

[1] F.O. Ologunagba,"Design and evaluation of a horizontal-shaft palm nut cracking machine,"Journal of Engineering and Applied Science,vol. 4, pp.80-86, 2012.
[2] G.A. Badmus,"NIFOR Automated Small Scale Oil Palm Processing Equipment,"Proceeding of PORIM INTERNATIONAL Palm Oil Conference, Nigeria 9-14 September 1990.
[3] Idowu D. I, Tamba J., Rotimi E. S., Olive S., Onyema J. O., Williams K.K. (2016) 3rd International Conference on African Development Issues (CU – ICAD 2016).
[4] M.S.A Kheiri,"Present and Prospective Development in the Palm Oil Processing Industry,"Journal of American Oil Chemists Society,vol. 2, pp. 210-219, 1985.
[5] O.I. Mba, M.-J. Dumont, M. Ngadi, "Palm oil Processing, characterization and utilization in the food industry – A review," Food Bioscience, vol. 10, pp. 26-41, 2015.
[6] M. Asadullah, A.M. Adi, N. Suhada, N.H. Malek, M.I. Saringat and A. Azdarpour. "Optimization of palm kernel shell torrefaction to produce nenergydensified bio-coal," Energy Conversion and Management, vol. 88 pp. 1086-1093, 2014.
[7] M.H. Mosarof, M.A. Kalam, H.H. Masjuki, A.M. Ashraful, M.M. Rashed, H.K. Imdadul, I.M. Monirul. "Implementation of palm biodiesel based on economic aspects, performance, emission, and wear characteristics, Energy," Conversion and Management, vol. 105 pp. 617–629, 2015.
[8] O.O. Babatunde, and J.O. Okoli,"Investigation into the effect of nut size on the speed needed for cracking palm nut in centrifugal nut cracker,"Nigerian Journal of Palm and Oil Seeds, vol.9, pp. 84-88, 1988
[9] S.I. Manuwa,"Design, Fabrication and Testing of a Low Cost Palm Nut Cracker,"Proceeding of the 19th Annual Conference of Agricultural Engineers held at the Federal University of Technology, Owerri, Nigeria. 2-6 September 1997.

Appendix

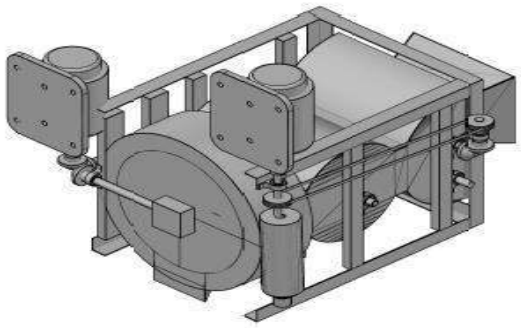

Pictorial View of Machine

NIPES Conference Proceedings
The 1st International Conference of the Nigerian Institution of Professional Engineers and Scientists 7th-8th Oct. 2021: 101-113
www.nipesjournals.org.ng

Gamma Radiation Shielding and Liquid Permeability Properties of Granite - Kaolin Composites Bricks for Liquid Radioactive Waste Management

E.O. Echeweozo [a]*, E.L. Efurumibe[b], K.H. Idu[c]
[a] Department of Physics with Electronics, Evangel University Akaeze, Ebonyi State, Nigeria.
[b] *Department of Physics Michael Okpara University of Agriculture Umudike, Abia State, Nigeria*
[c] Department of Physics, Taraba State University, Jalingo, Taraba State, Nigeria.

Abstract
Gamma radiation shielding of baked and unbaked granite bricks produced with 0%,10%, 20%, 30%, 40%, 50% of kaolin powder were investigated. A 3x3 inches NaI(Ti) detector and WinXCOM program were used to measure the linear attenuation coefficients at different energies levels respectively. Element composition of samples were analyzed using particle induced X-ray emission (PIXE) spectroscopy. Experimental and theoretical results were in good agreement based on low values of relative deviations (RD). Results show that adding kaolin to granite positively reduced the liquid permeability coefficients of the bricks but negatively reduced the shielding properties of the bricks. Optimum results were obtained from unbaked sample of granite brick produced with 50% of micro scale kaolin powder (GK50) with linear attenuation coefficient (LAC) 0.1698 cm^{-1}, 0.1464 cm^{-1} and 0.1412 cm^{-1}, mass attenuation coefficient of 0.0663 cm^2/g, 0.0572 cm^2/g and 0.0552 cm^2/g ,radiation protection efficiency (RPE) of 38.36%, 34.11% and 33.13% for radiation energies levels of 661.6 keV, 1,173.2 keV, and 1,332.5 keV respectively and liquid permeability coefficient of $6.53x10^{-11}$ m/s. The study concludes that all brick samples were thermally stable, good in radiation shielding and efficient in liquid radioactive waste immobilization

***Keywords*:**
Granite; Kaolin; Gamma shielding; Radioactive waste management; Liquid Permeability

1. Introduction
After the Chernobyl and Fukushima nuclear disasters, the safe storage and disposal of liquid radioactive wastes as well as environmental protection around hazardous materials have become a burning issue for some researchers in Environmental management and Engineering. The growing applications of nuclear technology in agriculture, medicine, power generation and research has generated global concern for environmental safety around radioactive wastes. Liquid radioactive wastes which are by-products of nuclear activities are major sources of hazardous radiations. The negative health and environmental impact of these radioactive wastes and their radiations are so enormous. Among all the radiations produced by radioactive wastes, gamma radiations have proved to be the most difficult to manage [1]. This is due to the higher penetrating power of gamma radiations. Therefore, the application of solid-state engineered barrier is important to immobilized these liquid radioactive wastes and shield all nuclear radiations especially gamma radiations emitting from these nuclear wastes [2]. In any cases where the radioactive waste is in liquid form, the liquid permeability, radiation shielding properties and the thermochemical stability of the shielding material are important factors for choosing high performance materials for the management and immobilization of liquid radioactive waste.
Recently, several authors have investigated the radiation shielding capability of different materials like; kaolin, granite [3-6] without consideration to liquid permeabilities coefficients and thermochemical stabilities of these materials and their composites which are important factor to consider in choosing the right material for liquid radioactive waste immobilization and management. The lack of liquid permeability and thermochemical stability evaluation of any radiation shielding material may result to radioactive waste leakage which has the potential to contaminate the environment and underground water bodies [7,8].
Some traditional radiation shielding materials such lead (Pb) and red mud (bauxite residue) have become less attractive because of their inherent disadvantages such as toxicity in the case of lead; corrosion and high liquid permeability in the case of red mud [9]. Among alternative materials

which include concrete, granite-kaolin, clay- steel slag, clay- fly ash, bentonite – red mud composites etc are under consideration for effective radiation shielding [10,11,1,12,3,4,13,5,6] Several researchers have shown granite and clay materials as a naturally, inexpensive materials with high density, thermo-chemical stable, eco-friendly, corrosion resistant, and readily available with excellent performance in radiation shielding [5,14,13,6]. In this study, radiation shielding, liquid permeability properties as well as thermochemical stability of granite bricks produced with different percentage of kaolin powder were investigated. Obtained results were compared with results of other emerging alternatives for possible deployment in liquid radioactive waste storage and management.

2. Theoretical Background

Gamma radiation passing through any sample of thickness x (cm) under narrow collimated -beam geometry is transmitted according to Beer-Lambert's law,

$$I = I_0 e^{-\mu x} \quad (1)$$

$$\mu = \frac{In\frac{I_0}{I}}{X} \quad (2)$$

I is attenuated radiation intensity, I_o is initial radiation intensity, μ is linear attenuation coefficient (LAC), x is thickness of absorber. The mass attenuation coefficient, μ/ρ is the ratio of the linear attenuation coefficient to the density of the absorber [15].

$$\text{Mass attenuation coefficient (MAC)} = \frac{\mu}{\rho} \quad (3)$$

The Half-Value Layer (HVL) and the Tenth Value Layer (TVL) are the thickness of the absorber that will reduce the intensity of radiations by a factor of two and ten, respectively. The HVL and TVL values which depend on the linear attenuation coefficient are given by Equations 4 & 5;

$$HVL = \frac{\ln 2}{\mu} = \frac{0.693}{\mu} \quad (4)$$

$$TVL = \frac{\ln 10}{\mu} = \frac{2.303}{\mu} \quad (5)$$

Another parameter which depends on the linear attenuation coefficient is the Mean Free Path (MFP). It is the thickness of absorber that attenuates the original intensity of radiation to 36.8 %, and it is determined by:

$$MFP = \frac{1}{\mu} \quad (6)$$

Where, μ is the linear attenuation coefficient for a monoenergetic photons/ radiations.

The Radiation Protection Efficiency (RPE) is a parameter that gives the effectiveness of any absorber of specific thickness to shield radiations. The RPE values for the samples under investigation was estimated by the Equation 7 [15].

$$RPE = (1 - \frac{I_x}{I_0}) \text{ x } 100. \quad (7)$$

Relative Deviations (RD) between experimental and theoretical results for MAC were deduced from the relations shown in Equation 8 [16].

$$RD = \left[\frac{\frac{\mu(\text{exp})}{\rho} - \frac{\mu(winxcom)}{\rho}}{\frac{\mu(\text{exp})}{\rho}} \right] \text{ x } 100. \quad (8)$$

Where $\frac{\mu(\text{exp})}{\rho}$ and $\frac{\mu(winxcom)}{\rho}$ denote the experimental and theoretical values of mass attenuation of the samples respectively.

Liquid permeability coefficient (K) is a measure of the ease at which a sample will permit the passage of radioactive liquids through it. To determine the liquid permeability coefficients of samples, Darcy's formula was applied [2]. Darcy's formula is expressed as

$$K = \frac{QL\Omega}{A\Delta ht} \quad (9)$$

Where, Q = volume of liquid collected after passing through the absorber (cm^3), t = time of fluid flow (sec). Δh = change in water pressure height (cm), A = the area of the absorber (cm^2)
Ω = the dynamic viscosity of the fluid (poise or Pa.s) for distill water is 1
L = the vertical Thickness of the absorber (cm), K = the permeability of the absorber (darcy or m/s)
Few experimental and theoretical studies have been carried out to determine radiation shielding properties and liquid permeability of different materials and composites. Isfahani *et al.*,[2] determined the liquid permeability and gamma shielding efficiency of clay modified by barite powder using both experimental and simulation methods. In that study, bentonite clay with 10%, 20%, 30%, 40%, 60% and 80% of barite powder was prepared to find the optimum percent of barite powder with highest linear attenuation coefficient and lowest liquid permeability coefficient A (high pure germanium (HPGe) detector was used at gamma energies of 661.6, 1173.2 and 1332.5 keV. They concluded that bentonite clay with 40% of barite is the optimum composition with a permeability factor of 8.87 9 x 10^{-11} m/s and linear attenuation coefficient of 16.46 m^{-1}, 12.2 m^{-1} and 11.99 m^{-1} at gamma energies of 661.6, 1173.2 and 1332.5 keV respectively.
Agar *et al.*,[16] considered shielding properties of Pb/Ag-based alloys in the attenuation of gamma rays. The mass attenuation coefficients (μ/ρ) of these alloys were measured at various gamma energies between 81 keV – 1333 keV using HPGe detector. They reported that μ/ρ, RPE and HVL for four alloy samples composed of different percentage of Pb and Ag were determined experimentally, theoretically (WinXCom software) and computationally (MCNPX simulation code). The relative deviations between both experimental data - WinXCom and experimental data-MCNPX values are less than 6% which confirmed that the μ/ρ values were obtained with high accuracy.75% Pb and 25% Ag alloy sample has the maximum radiation protection efficiency (about 53% at 81 keV). Jawad *et* al., [17] studied the Radiation shielding properties of some ceramic samples. Eight types of ceramic materials were tested against gamma ray, each type of ceramic modified as glazed and unglazed. The results of the study showed that glazed ceramics are better than unglazed in the attenuation of gamma radiation. Isfahani *et al.*, [12] experimentally studied the effect of adding steel slag (industrial wastes,) at 10, 20, 30 and 40% mixture to bentonite clay using HPGe detector in order to improve gamma radiation shielding performance at different gamma energies. The results showed that adding steel slag improved the radiation shielding performance of bentonite clay, whereas the mixtures were more permeable to liquid. They noted that 40% steel slag gives the highest gamma radiation shielding coefficient.
Mann *et al.*,[4] experimentally investigated clay fly ash bricks for gamma-ray shielding using NaI(Tl) detector at 661.6 keV, 1,173.2 keV, and 1,332.5 keV. The clay fly ash bricks showed good shielding properties for moderate energy gamma rays.
Olukotun *et al.*,[3] studied gamma radiation shielding strength of two clay-materials (Ball clay and Kaolin). They employed theoretical and experimental procedures to determine the mass attenuation coefficient, μ/ρ (cm^2g^{-1}) of clay at gamma energies between 609.31 and 1764.49 keV. A (HPGe) detector was used for the experiment.

3. Materials and Method

3.1 Samples

The granite sample used in this research was obtained from Ezillo, quarry site Ebonyi state, Nigeria (5.4155°N, 7.8586°E) while kaolin sample was obtained from Umuahia kaolin mining site Abia state, Nigeria (5.5166^0N, 7.4539^0E). The granite specimen was gray, with an average density of 2.68 g/cm^3.

3.2 Samples Preparation

The samples preparation procedures were carried out as follows;

i. Test samples were collected as mined in lump forms, crushed to suitable sizes and sun-dried for five days. Samples were pulverized, sieved (with sieve of mesh sizes 2μm).

Natural granite (GK00) and granite modified with 10% (GK10), 20% (GK20), 30% (GK30), 40% (GK40) and 50% (GK50), of micro scale Kaolin powder were also prepared into two parts.

ii. Samples were weighed accurately using an electronic weighing balance with an accuracy of 0.01g and mixed thoroughly by adding appropriate amount of distilled water. Mixtures prepared were molded and pelletized into bricks of thickness 3cm, labeled and sun-dried for 3 days for curing and to remove natural moisture in accordance with American Society for Testing and Material ASTM D6913 [18],[19]. This means twelve samples for gamma attenuation tests. The first part of the test samples GK00 GK10, GK20, GK30, GK40, GK50, was labeled and left to maintain normal lab temperature of 27^0C and was referred to as 'UNBAKED SAMPLES'. The second part GK00 GK10, GK20, GK30, GK40, GK50, were baked to temperature of 1000^0 C for 100 min at a heating rate of 10 °C/min using a carbolite muffle furnace. After which the baked samples were relabeled to GK00B GK10B, GK20B, GK30B, GK40B, GK50B, and referred to as 'BAKED SAMPLES'. At the end of the experiments, the melting points of all brick samples were determined

3.3 Measurement

3.3.1 Radiation Shielding test

Twelve (12) of these samples (6 baked and 6 unbaked samples) were subjected to gamma radiations test at commonly used gamma radiation energies 661.6 keV and 1173.2keV and 1332.5 keV. The gamma spectrometry system employed consist of a 3 x 3 inches NaI(Ti) detector, at Centre for Energy Research and Development (CERD), Obafemi Awolowo University, Ile-Ife. The detector was coupled to Gamma Spectacular (model GS-2000 Pro) multichannel analyzer and further linked to a computer for display. During the determination of counts, source materials ^{137}Cs and ^{60}Co was enclosed in a lead enclosure with a single face aperture of 6mm, placed at the back of the source collimator. Samples were irradiated under narrow beam transmission geometry by photons emitted from 137Cs (661.6 keV) and 60Co (1173.2 keV and 1332.5 keV) procured from National Institute of Radiation Protection and Research Ibadan (Nigerian Nuclear Regulatory Authority). Counting was accomplished by measuring the spectra of point sources emitting gamma rays. The transmitted spectra were then allowed to record for sufficient time (900 seconds) to collect adequate number of counts under the photopeak so as to limit the statistical error to the lowest level. The background counts were recorded (I_o). When a new sample was inserted, a new spectrum was recorded and the count rate of interest area in the photopeak was measured for each sample(I). The experimental setup for radiation shielding test is shown in Figure 1.

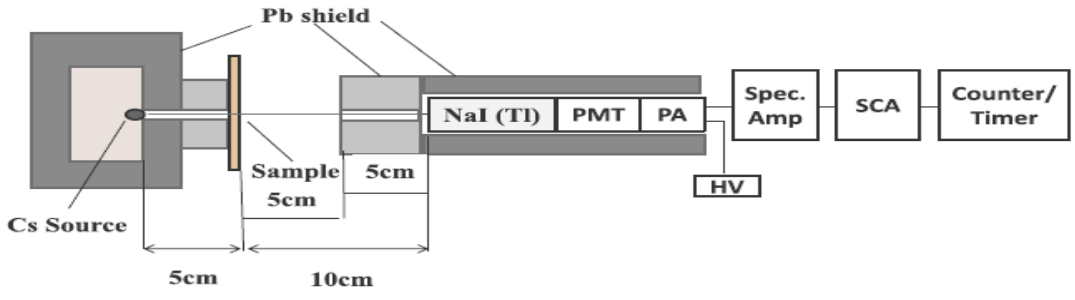

Figure 1: The experimental setup for radiation shielding test.

Data acquisition and analysis of gamma-ray spectra for I and I_o were achieved using Theremino software. This measuring method, similar to other experimental tests, includes little uncertainty.

Therefore, the maximum experimental uncertainty of the measured linear attenuation coefficients (LAC) was calculated by using the Equation 10 derived from the error propagation formula[20].

$$\Delta(\mu) = \frac{1}{X}\sqrt{(\frac{\Delta I_0}{I_0})^2 + (\frac{\Delta I}{I})^2 + (In\frac{I_0}{I})^2(\frac{\Delta x}{x})^2} \quad (10)$$

Where: Δt, ΔI_0 and ΔI are errors in the value of x, I_0 and I, respectively.
The estimated error in the measurement of linear attenuation coefficient was computed. These errors / uncertainties were mainly due to counting procedures, thickness measurements, the evaluation of peak areas, and slight deviations from narrow beam geometry in source detector arrangements. Furthermore, results of element analysis of these samples carried out using PIXE spectrometry shown in Table 6 was also imputed to determine the radiation shielding performance using WinXCOM database program. This is to enable a comparative analysis of experimental and theoretical results and also to validate the experimental radiation shielding results.

3.3.2 Liquid permeability test

To measure the liquid permeability coefficient of each of the brick samples, a rigid wall permeameter was used. The constant head permeability test procedure was adopted for simplicity. Cylindrical tube / mould with 3.8cm diameter and 40cm height were used to measure the liquid permeability coefficient of each of the brick samples. The powdered samples were fried for 15 minutes to eliminate moisture and put in the cylindrical mold and each layer compacted into bricks by 25 drops of the standard hammer in accordance with ASTM D 5856-95 [18]. Initially, the specimen was allowed to be saturated with distil water at very low hydraulic gradient (so as to avoid any compression of air into the voids). After the saturation was completed, the measurement for liquid permeability tests was carried out. The water output rate becomes relatively permanent and the system reaches the steady state condition. Thus, by recording the time 60sec, volume of out coming water flow (Q), change in water pressure height (Δh) and geometry properties of sample such as area (A) and thickness/ Length of the sample (L), liquid permeability coefficient of the samples (K) by Darcy's law were calculated

Table 1: Mass attenuation coefficient & relative deviation for unbaked granite – kaolin composite bricks

SAMPLE	**DENSITY (g/cm^3)**	**MAC for 661.6 KeV in** (cm^2/g)		**MAC for 1173.2 KeV in** (cm^2/g)		**MAC for 1332.5 KeV in** (cm^2/g)		RELATIVE DEVIATION BETWEEN EXP. AND WINXCOM RESULTS FOR VARIOUS ENERGY LEVELS (%)		
		Experimental **± 5%**	Theoretical	Experimental **± 5%**	Theoretical	Experimental **± 5%**	Theoretical	661.6keV	1173.2keV	1332.5keV
GK00	2.68	0.0703	0.0697	0.0625	0.0617	0.0595	0.0595	0.74	1.34	0.00
GK10	2.65	0.0694	0.0682	0.0615	0.0610	0.0584	0.0584	1.66	0.78	0.00
GK20	2.63	0.0685	0.0679	0.0605	0.0570	0.0576	0.0565	0.75	4.37	1.96
GK30	2.60	0.0681	0.0656	0.0585	0.0574	0.0567	0.0543	3.64	1.83	4.18
GK40	2.58	0.0674	0.0641	0.0579	0.0569	0.0559	0.0537	4.89	1.63	4.00
GK50	2.56	0.0663	0.0631	0.0572	0.0572	0.0552	0.0547	4.79	0.00	0.80

Table 2: Mass attenuation coefficient & relative deviation for baked granite – kaolin composite bricks

SAMPLE	**DENSITY (g/cm^3)**	**MAC for 661.6 KeV in** (cm^2/g)		**MAC for 1173.2 KeV in** (cm^2/g)		**MAC for 1332.5 KeV in** (cm^2/g)		RELATIVE DEVIATION BETWEEN EXP. AND WINXCOM RESULTS FOR VARIOUS ENERGY LEVELS (%)		
		Experimental **± 5%**	Theoretical	Experimental **± 5%**	Theoretical	Experimental **± 5%**	Theoretical	661.6keV	1173.2keV	1332.5keV
GK00B	2.68	0.0703	0.0696	0.0616	0.0616	0.0594	0.0583	0.91	0.00	1.83
GK10B	2.65	0.0690	0.0688	0.0616	0.0615	0.0581	0.0564	0.30	0.17	3.00
GK20B	2.63	0.0689	0.0680	0.0603	0.0595	0.0575	0.0562	1.26	0.18	1.89
GK30B	2.60	0.0679	0.0663	0.0581	0.0573	0.0564	0.0545	2.31	1.39	3.41
GK40B	2.58	0.0673	0.0669	0.0577	0.5664	0.0557	0.0544	0.52	1.83	2.21
GK50B	2.56	0.0672	0.0649	0.0584	0.0581	0.0562	0.0545	3.45	0.46	3.02

Table 3: Radiation protection efficiency of samples

RADIATION PROTECTION EFFICENCY (%) FOR UNBAKED SAMPLES				RADIATION PROTECTION EFFICENCY (%) FOR BAKED SAMPLES			
SAMPLE CODE	661.6 (KeV)	1173.2 (KeV)	1332.5 (KeV)	SAMPLE CODE	661.6 (KeV)	1173.2 (KeV)	1332.5 (KeV)
GK00	43.30	39.58	38.15	GK00B	42.60	38.51	37.46
GK10	41.98	38.27	36.76	GK10B	41.37	37.89	36.17
GK20	41.01	37.24	35.87	GK20B	41.00	36.73	35.37
GK30	39.72	34.99	34.14	GK30B	39.20	34.69	33.83
GK40	39.38	34.96	33.98	GK40B	38.79	34.36	33.39
GK50	38.36	34.11	33.13	GK50B	37.82	33.83	32.83

Table 4: Liquid permeability measuring constants/parameters

TIME (sec)	60
DIAMETER OF SAMPLE BED (L) (cm)	3.8
LENGTH OF SAMPLE BED (L) (cm)	31.5
AREA OF SAMPLE BED (cm^2)	11.34
TEMPRATURE ^{0}C	28.5

Table 5: Liquid permeability test result for granite – kaolin composite bricks

SAMPLE	% of Kaolin in Granite	DENSITY (g/cm^3)	WATER DISCHARGED (Q) (cm^3)	FLOW RATE (cm^3/s)	h_1 (mmH_2O)	h_2 (mmH_2O)	CHANGE IN WATER HEIGHT (Δh) (mmH_2O)	LIQUID PERMEABILITY (Darcy)	LIQUID PERMEABILITY (ms^{-1})
GK00	**00**	**2.68**	60.89	1.01	236.00	239.98	3.98	40.72	$4.03x10^{-11}$
GK10	**10**	**2.65**	56.15	0.94	232.00	235.84	3.84	43.74	$4.32x10^{-11}$
GK20	**20**	**2.63**	51.30	0.86	242.00	245.69	3.69	49.13	$4.85x10^{-11}$
GK30	**30**	**2.60**	48.89	0.81	224.00	227.48	3.48	55.70	$5.50x10^{-11}$
GK40	**40**	**2.58**	45.13	0.75	232.00	235.21	3.21	61.85	$6.10x10^{-11}$
GK50	**50**	**2.56**	44.01	0.78	234.00	237.07	3.07	66.21	$6.53x10^{-11}$

Liquid permeability is measure in Darcy (D) or m/s, where 1 D = 0.9869×10^{-12} m/s. One Darcy is the permeability of a sample 1 cm long with a cross-sectional area of 1 cm^2, when a pressure difference of 1 dyne/cm^2 between the ends of the sample causes a fluid with a dynamic viscosity of 1 poise to flow at a rate of 1 cm^3/s [21,11,22].

Table 6: Element analysis result for unbaked granite– kaolin composite bricks

SAMPLE CODE	**GK00**	**GK10**	**GK20**	**GK30**	**GK40**	**GK50**
MELTING POINT	**1334**°C	**1796**°C	**1812**°C	**1827**°C	**1844**°C	1856°C
DENSITY (g/cm^3)	**2.68**	**2.65**	**2.63**	**2.60**	**2.58**	**2.56**
Element	**Element concentration by weight per 1millgram**					
Mg	0.0134	0.0144	0.0168	0.0182	0.0218	0.0230
Al	0.1861	0.2201	0.2421	0.2694	0.2882	0.3014
Si	0.6482	0.5281	0.5101	0.4816	0.3965	0.3241
P	0.0481	0.0366	0.0231	0.0120	0.0084	0.0031
K	0.0245	0.0623	0.0859	0.0994	0.1002	0.1021
Ca	0.0181	0.0198	0.0200	0.0894	0.1038	0.2041
Ti	0.0101	0.0102	0.0096	0.0088	0.0072	0.0041
V	0.00014	0.00004	-	-	-	-
Cr	-	-	-	-	0.0002	0.0002
Mn	0.00024	0.00024	0.00020	0.00018	0.00018	0.00018
Fe	0.0285	0.0224	0.0101	0.0064	0.0046	0.00019
Cu	0.00081	0.0010	0.0014	0.0019	0.0022	0.0024
Zn	0.0052	0.0031	0.0018	-	0.0008	0.00013
Others	0.0166	0.0816	0.0794	0.0127	0.0656	0.03319
TOTAL	**1.0000**	**1.0000**	**1.0000**	**1.0000**	**1.0000**	**1.0000**

Table 7: Comparison of some materials / composites for gamma attenuation and Liquid waste immobilization

Samples with maximum Mass attenuation coefficient	Density (g/cm^3)	Linear attenuation coefficient (cm^{-1})			Liquid permeability (m/s)	References
		661.6 keV	1173.2 keV	1332.5 keV		
Clay& 40% barite powder composite	2.55	0.1646	0.1220	0.1199	$8.87x\ 10^{-11}$	[2]
Clay- 40% steel slag composite	2.00	0.1587	0.1191	0.1098	$3.31x10^{-10}$	[12]
Baked kaolin (B2)	1.96	-	0.1180	0.1105	-	[3]
Concrete	2.30	-	0.1366	0.1279	-	[10]
Lead (Pb)	11.34	1.0331	0.7258	0.6940	-	[6]
Bauxite residue (Red Mud)	2.65	0.2165	0.1590	0.1495		[37]
Unbaked kaolin	2.25	0.1656	0.1262	0.1186	$2.33\ x\ 10^{-12}$	[11]
Clay-10% fly ash bricks	2.47	0.1364	0.1076	0.1023	-	[4]
Granite100% (GK00)	2.68	0.1885	0.1674	0.1596	$4.03x10^{-11}$	Present study
Granite-50% Kaolin (GK50)	2.56	0.1698	0.1464	0.1412	$6.53x10^{-11}$	Present study

- Not reported

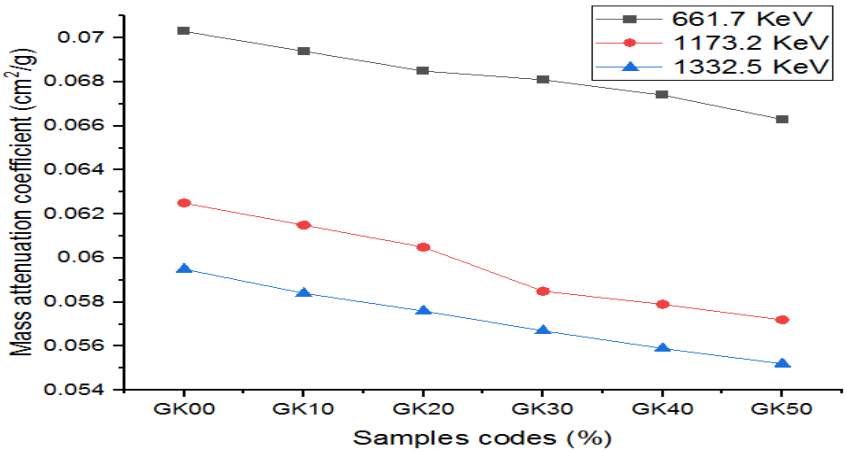

Figure 2: Variation of % mixture against Mass attenuation coefficients for unbaked granite – kaolin composite bricks

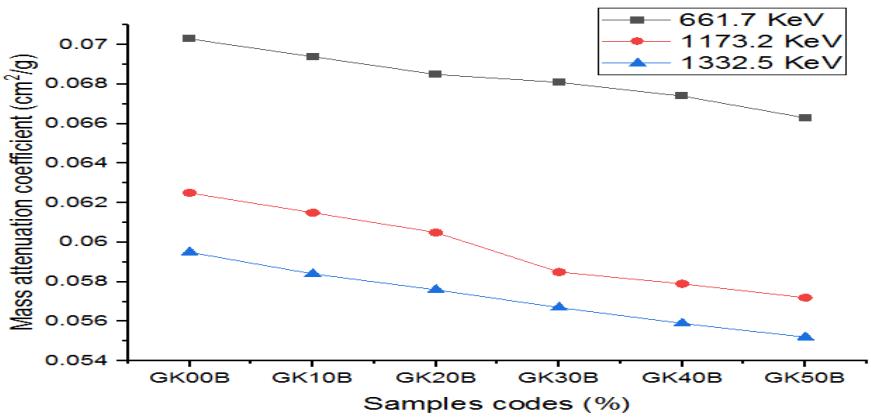

Figure 3: Variation of % mixture against Mass attenuation coefficients for baked granite – kaolin composite bricks

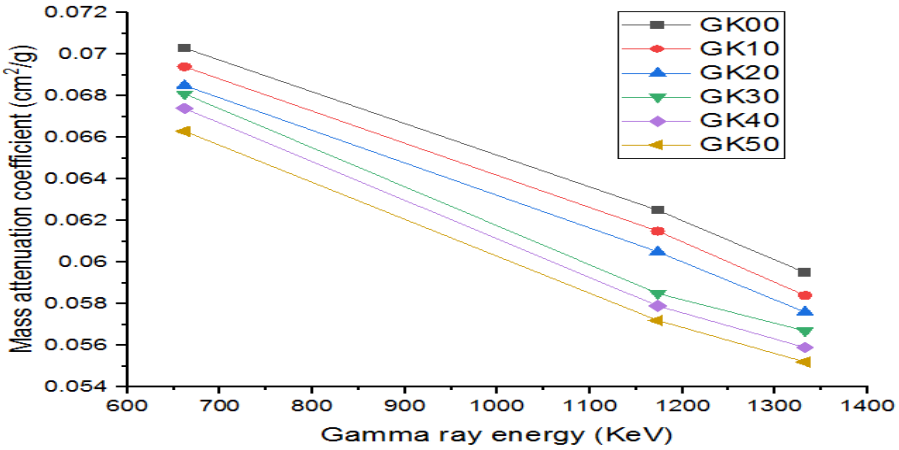

Figure 4: Variation of mass attenuation coefficient with incident energy for different samples of unbaked granite – kaolin composite bricks

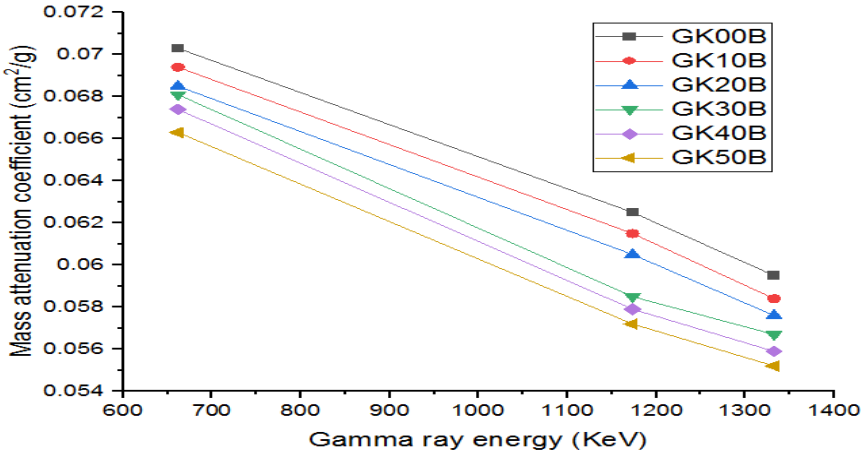

Figure 5: Variation of mass attenuation coefficient with incident energy for different samples of baked granite– kaolin composite bricks

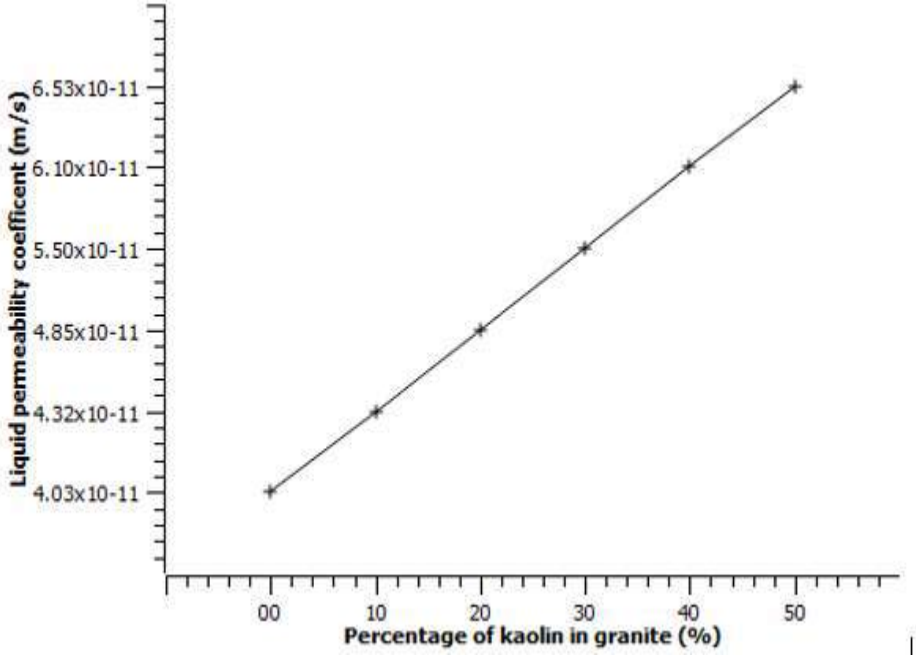

Figure 6: variation of liquid permeability coefficient against bricks % mixture.

4. Results and Discussion

Gamma radiation shielding properties (LAC, MAC & RPE) and liquid permeability coefficients of baked (1000^{o}C) and unbaked (27^{o}C) Natural granite (GK00) and granite bricks produced with 10% (GK10), 20% (GK20), 30% (GK30), 40% (GK40) and 50% (GK50), of micro scale kaolin powder were investigated to determine the optimum composition mixture of granite and kaolin composite brick with maximum linear attenuation coefficient and allowable liquid permeability coefficient. The experimental and theoretical mass attenuation coefficient for all the samples at gamma-ray energies of 661.6, 1173.2 and 1332.5 keV for both baked and unbaked composites are shown in Tables 1 and 2, and graphically presented in Figure 1and 2. The mean values of relative deviations (RD) between experimental and theoretical mass attenuation coefficient were computed as 2.75%, 1.66%, 1.82% for gamma energies 661.6, 1173.2 and 1332.5 keV respectively. Considering the low relative deviation values, which is within an acceptable limit of less than 5% [16], we can comfortably assert that the experimental results were in good agreement with the theoretical results. The discrepancy between theoretical values and experimental values were due to deviations from narrow-beam geometry in the source-detector geometry, error in density measurements, mixture rule that ignores the interactions between atoms and other unforeseeable errors as reported by [23]. Such effects and discrepancies have been observed by earlier investigators on different materials [24,25]. Therefore, any of these techniques (experimental or theoretical) could be applied independently with reasonable accuracy for the measurement of linear attenuation coefficient and investigation of radiation shielding of materials. Radiation protection efficiency (RPE) as clearly displayed on the result in Tables 3 which signifies the shielding abilities of these materials in percentage.

The result showed that unbaked samples were slightly more efficient than baked samples for gamma radiation shielding in term of their linear attenuation coefficients. This implies that the energy expanded in the baking process did not yield the expected result due to slight decrease in densities of baked bricks. From the study, it was observed that linear attenuation coefficient is dependent on density, atomic mass, thickness of the sample and the energy of the radiation which is in line with assertion made by other researchers. It was also observed that the mass attenuation coefficient (MAC) decreases as the gamma-ray energy increases for both baked and unbaked samples, indicating the strong dependence of MAC on gamma-ray energy. Mass attenuation coefficient is higher for lower energies. Baked brick samples have different mass attenuation coefficient, this is as a result of effect of density on the shielding of materials. The decrease in density observed was mainly caused by a breakdown of interlayer structures (200 °C), loss of zeolite (200–300 °C), loss of crystalline (400 °C), and loss of structural water (above 600 °C) in granite and kaolin [26,27] and dehydroxylation (loss of hydrogen bonds) and reorientation (resultant phase shift) or the shrinking of kaolin crystal structure which is usually around 20% [28] at temperature above 950^{0}C. Although slight cubic expansion was expected during temperature treatment this occurred between 60^{o}C - 300^{o}C before slight volume contractions were observed due water loss, dehydroxylation and intra space occupation which is common for granite and kaolin materials [27,1,19]. In this study, melting temperatures of these brick samples were observed between 1334°C - 1856 °C, at ambient pressure as shown in Table 6. It is important to note that the highest melting point was observed in 50% granite – 50% kaolin composite brick with samples code of GK50 which signify high level of thermochemical stability. It could be observed that introduction of kaolin to granite significantly elevated the melting points of brick samples based on percentage/quantity of kaolin added. This is also in line with recent studies carried out by Diaz,[30] and Xu Xiao-li *et al*, [31]. Considering the melting points of these bricks, granite – kaolin composite bricks have shown to be thermochemically stable to withstand temperature fluctuations which may occur during radioactive waste storage and management. The observed Similarities in results obtained from gamma radiation test of baked and unbaked brick samples shown in Figures 2 & 3, and 4 & 5, signify the thermochemically stability of these bricks

and by extension their firm mechanical properties enough to withstand environmental fluctuations during radiation shielding and radioactive waste storage procedures.

The liquid permeability and radiation shielding tests indicate that increasing the percentage of kaolin powder in granite will not satisfy both maximum linear attenuation coefficient and minimum liquid permeability at the same time. These were clearly shown in Table 4. It was further observed that adding kaolin to granite powder negatively reduces the gamma radiation shielding ability of granite but positively reduces the liquid permeability coefficient of samples. This is similar to early observation made by Isfahani *et al*., [2] for clay and barite composites. Literature has shown that the liquid permeability coefficient of every material is determined by many factors like; particle size, nature of absorbed liquid, impurities in the liquid, void ratio of material, pressure, temperature and Atterberg limit [32]. However, this study has displayed a clear dependence of liquid permeability on the percentage of kaolin used for each brick. From Table 5 which is graphically represented in Figure 6, liquid permeability decreases with an increase in density. The radiation shielding properties and liquid permeability of granite - kaolin gave good result when compared with other radiation shielding alternatives as clearly in Table 7.

Elemental composition analysis performed on all the brick samples showed that the major components of these bricks were Silicon, Aluminum, Magnesium, Potassium and Calcium oxides, as also reported by [33,34]. The deeper coloration of samples after temperature treatment were due to Fe^{2+} ions oxidized to Fe^{3+} ions by expelled oxygen molecules.

5. Conclusion

The study concludes that, granite – kaolin composite bricks as naturally inexpensive materials with relative high density, high thermo-chemical stability, eco-friendly, corrosion resistance, and readily available have shown good performance in radiation shielding and liquid permeability coefficient. All results obtained from all samples were good in radiation shielding with permeability coefficient factors under allowable limit of 1 x 10^{-6}m/s to 1 x 10^{-14}m/s [35,36]. This makes all unbaked samples under consideration emerging alternatives for liquid radioactive waste immobilization and management.

However, due special consideration to liquid permeability coefficient and thermochemical stability, optimum results were obtained from unbaked sample of granite brick produced with 50% of micro scale kaolin powder (GK50) with linear attenuation coefficient (LAC) 0.1698 cm^{-1}, 0.1464 cm^{-1} and 0.1412 cm^{-1}, mass attenuation coefficient of 0.0663 cm^2/g, 0.0572 cm^2/g and 0.0552 cm^2/g, radiation protection efficiency (RPE) of 38.36%, 34.11% and 33.13% for radiation energies levels of 661.6 keV, 1,173.2 keV, and 1,332.5 keV respectively and liquid permeability coefficient of 6.53x10^{-11} m/s. Therefore, a multilayered exterior wall made of compacted unbaked granite bricks produced with 50% kaolin powder should be deployed in liquid radioactive waste management due its excellent radiation shielding for low energy gamma radiations, its thermochemical stability and good result in liquid radioactive waste immobilization.

References

[1]. Yilmaz, G, (2011)The effects of temperature on the characteristics of kaolinite and bentonite Scientific Research and Essays 6(9) 1928-1939, http://dx.doi.org/10..5897/SRE10.727

[2]. Isfahani, H.S.; Abtahi, S.M.; Roshanzamir, M.A.; Shirani, A.; Hejazi, S.M (2018a) Permeability and Gamma-Ray Shielding Efficiency of Clay Modified by Barite Powder .*Geotech Geol Engineering 37(2) 845-855* https://doi.org/10.1007/s10706-018-0654-0

[3] Olukotun,S.F.; Gbenu, S.T.; Ibitoye, F.I.; Oladejo, O.F; Shittu, H.O.; Fasasi, M.K.; Balogun, F. A (2018) Investigation of Gamma Radiation Shielding Capability Of Two Clay Materials; *Nuclear Engineering and Technology 14, 1-13.* http://dx.doi.org/10.1016/j.net.2018.05.003.

[4] Mann, H.S.; Brar, G.S.; Mann, K.S.; Mudahar, GS (2016a) Experimental investigation of clay fly ash bricks for gamma-ray shielding. *Nucl Eng Technol 48(5) 1230–1236*

[5] Kacal, M.R, Akman, F. and Sayyed, M. I (2018). Investigation of radiation shielding properties for some ceramics. *De Gruyter*. 43; 1-5.

[6] Najam, L.A.; Hashim, A.K.; Ahmed, H.A.; Hassan, I.M. (2016) Study the Attenuation Coefficient of Granite to Use It as Shields against Gamma Ray Detection, Scientific Research Publishing Inc.4, 33-39. http://dx.doi.org/10.4236/detection.2016.42005.

[7] Kozlowski, T.; Ludynia, A. (2019) Permeability Coefficient of Low Permeable Soils as a Single-Variable Function of Soil Parameter.mdpi- Water , (11) 2500; https://doi.org/10.3390/w11122500.

[8] Le, T.D.; Moyne, C.; Marcio, A.; Murad, M.A. (2015) A three-scale model for ionic solute transport in swelling clays incorporating ion–ion correlation effects. Adv. Water Resour. 75, 31–52. https://doi.org/10.1016/j.advwatres.2014.10.005.

[9] Obaid, S.S; Sayyed, M.I.; Gaikwad, D.K.; Pawar, P.P (2018) Attenuation coefficients and exposure buildup factor of some rocks for gamma ray shielding applications. *Radiation Physics & Chemistry journal.*(8) 44-50. http://dx.doi/10.1016/j.radphyschem.2018.02.026.

[10] Oto, B., Gur, A., (2013). Gamma-ray shielding of concretes including magnetite in different rate. Int. J. Phys. Sci. 8, 310–314.

[11] Echeweozo, E.O. and Igwesi, D.I. (2021) Investigation of gamma shielding and liquid permeability properties of kaolin for liquid radioactive waste management Applied Radiation and Isotopes 176, 109908. https://doi.org/10.1016/j.apradiso.2021.109908

[12] Isfahani, H.S.; Abtahi, S.M.; Roshanzamir, M.A.; Shirani, A.; Hejazi, S.M (2018b) Investigation on gamma-ray shielding and permeability of clay-steel slag mixture. *Bulletin of Engineering Geology and the Environment.60, 51-59.* https://doi.org/10.1007/s10064-018-1391-6

[13] Mann, K.S, Heer, M.S, Rani, A (2016c) Investigation of clay bricks for storage facilities of radioactive-wastage. *Appl Clay Sci*. 119, 249–256

[14] Galán, E.; Aparicio, P. (2014) Experimental study on the role of clays as sealing materials in the geological storage of carbon dioxide. Appl. Clay Sci. 87, 22–27. https://doi.org/10.1016/j.clay.2013.11.013

[15] Singh, K.; Singh, S.; Dhaliwal, A.S.; Singh, G. (2014). Gamma radiation shielding analysis of lead-fly ash concretes. *Applied radiation and isotopes*.89, 15-21 http://dx.doi.org/10.1016/j.apradiso.2014.10.022.

[16] Agar,O; Sayyed, M.I; Akman, F.; Tekin, H.O.; Kaçal, M.R.; (2018) An extensive investigation on gamma ray shielding features of Pd/Ag-based alloys, *Nuclear Engineering and Technology,45*, 23-29 https://doi.org/10.1016/j.net.2018.12.014.

[17] Jawad, A.A.; Demirkol, N; Gunoğlu, K; Akkurt, I. (2019) Radiation shielding properties of some ceramic wasted samples. *International Journal of Environmental Science and Technology. 5, 16-20*

[18] ASTM D 5856-95 (2007) Standard test method for measurement of hydraulic conductivity of porous material using a rigid-wall compaction-mold permeameter ASTM International, West Conshohocken, PA, pp20

[19] Akande J.M., Agbalajobi, S.A. (2013). Analysis on some physical and chemical properties of Oreke dolomite deposit. *Journal of Minerals and Materials Characterization and Engineering.* 4, 33-38. http://dx.doi.org/10.4236/jmmce.2013.12007.

[20] Mann, H.S.; Brar, G.S.; Mudahar, G.S. (2016b) Gamma-ray shielding effectiveness of novel light-weight clay-flyash bricks. *Radiat Phys Chem* 127, 97–101.

[21] Rashid, F.; Glover, P.W.J.; Lorinczi, P.; Hussein, D.; Collier, R.; Lawrence, J, (2015) Permeability Prediction in Tight Carbonate Rocks using Capillary Pressure Measurements.

[22] Glover, P.W.J.; Zadjali, I.I.; Frew, K.A. (2006) Permeability prediction from MICP and NMR using an electro-kinetic approach. Geophysics, 71(4), F49-F60.

[23] Medhat, M.;Wang,Y.,(2013) GEANT4 code for simulation attenuation of gamma rays through scintillation detectors.Ann.Nucl.Energy(62) ,316–320.

[24] Kerur, B.R; Thontadarya, S.R.; Hanumaiah, B (1992) A study on the range of non-validity of the Bragg's additivity law for compounds at photon energies below 10 keV, *Applied Radiation and Isotopes*, vol. 43, no. 7, 893–898.

[25] Akça, B.; Erzeneolu, S.Z (2014) .The Mass Attenuation Coefficients, Electronic, Atomic, and Molecular Cross Sections, Effective Atomic Numbers, and Electron Densities for Compounds of Some Biomedically Important Elements at 59.5 keV Hindawi Publishing Corporation, *Science and Technology of Nuclear Installations Volume 2014, Article ID 901465,8-13* http://dx.doi.org/10.1155/2014/901465.

[26] Zhang W, Sun Q, Hao S, Geng J, Ly C. (2016) Experimental study on the variation of physical and mechanical properties of rock after high temperature treatment. Appl Therm Eng 98:1297–1304

[27] Qin Y, Tian H, Neng-Xiong Xu, Yu Chen (2019) Physical and Mechanical Properties of Granite After High-Temperature. Treatment Rock Mechanics and Rock Engineering https://doi.org/10.1007/s00603-019-01919-0

[28] Varga, G. (2007) The Structure of Kaolinite and Metakaolinite. *Epitoanyag*, 59, 4-8. http://dx.doi.org/10.14382/epitoanyag-jsbcm.2007.2

[29] Jaradat, K.A.; Darbari Z; Elbakhshwan ,M; Abdelaziz, S.L.; Gill, S.K.; Dooryhee ,E.; Ecker, L.E (2017)Heating-freezing effects on the orientation of kaolin clay particles *Applied Clay Science 150, 163–174* http://dx.doi.org/10.1016/j.clay.2017.09.028

[30] Diaz, P.M (2017.*)* Rock Mechanical Properties of Granite/ Clay/ Basalts/ Argillite / Glass and its Alterations at Different Temperatures-A Review *Journal of Advances in Civil Engineering, Vol. 3(1) 9-20* https://dx.doi.org/10.18831/djcivil.org/2017011002.

[31] Xu Xiao-li, Feng Gao, X.Shen and H.Xie, (2008). Mechanical Characteristics and Microcosmic Mechanisms of Granite under Temperature Loads, *Journal of China University of Mining and Technology*, 18 (3). 413-417, http://dx.doi.org/10.1016/S1006-1266(08)60086-3.

[32] Andavan S. and Varun V. (2017) Infiltration, Permeability, Liquid Limit and Plastic Limit of Soil, International Journal for Innovative Research in Science & Technology 4 (6) 2349-601

[33] Tekin, H.O.; Erguzel, T.T.; Sayyed. M.I.; Singh V.P.; Manici, T; Altunsoy, E.;Agar, O.(2018)An Investigation on Shielding Properties of Different Granite Samples using MCNPX code. *Digest Journal of Nanomaterials and Biostructures vol. 13(2) 381 – 3*

[34] Chukwu, G.U and Ajumiwe, C.F (2013) Investigation of mechanical/physico-chemical properties of kaolinite ore (clay) from Umuariaga-Umudike, Abia State of Nigeria, *International Research Journal of Geology and Mining (IRJGM)* (2276-6618) Vol. 3(5). 195-205

[35] Ebrahimi-B, N., Gitirana Jr.G.F.N., Fredlund, D.G., Fredlund, M.D.,Samarasekera, L., (2004) A Lower Limit for the Water Permeability Coefficient. 57TH CANADIAN GEOTECHNICAL CONFERENCE PAPER. Uploaded 4 April 2020 and accessed 25 November 2020 https://www.researchgate.net/publication/271515363

[36] Fredlund, D. G., Xing, A., and Huang, S. (1994) Predicting the permeability function for unsaturated soils using the soil-water characteristic curve. Can. Geotech. J., 31. 533-546.

[36] Reddy, P.S; Reddy, N.G; Serjun, V.Z; Mohanty, B; Das, S.K; Reddy, K.R ; Rao, B.H. (2021) Properties and Assessment of Applications of Red Mud (Bauxite Residue): Current Status and Research Needs. *Waste and Biomass Valorization* 12.1185–1217. https://doi.org/10.1007/s12649-020-01089-z.

NIPES Conference Proceedings
The 1st International Conference of the Nigerian Institution of Professional Engineers and Scientists 7th-8th Oct. 2021: 114-124

www.nipesjournals.org.ng

Comparing the Analytical and Matlab Solution to the Cauchy–Riemann Equations

Abdel Radi Abdel Rahman Abdel Gadir[1] and Neama Yahia Mohammed[2]
[1]Department of Mathematics, Faculty of Education, Omdurman Islamic University, Omdurman, Sudan
[2]Department of Mathematics, College of Science,Tabuk University,Saudi Arabia

Abstract

Cauchy – Riemann equations is considered as one of the simplest equations in complex analysis. The Cauchy – Riemann equation was solved analytically and using Matlab which is one of the most famous mathematical programs in solving mathematical problems. This paper compares the individual solutions using the Matlab algorithm and the analytical method

Keywords: *Comparative, Analytical Solution, Matlab Solution, Cauchy – Riemann Equations, Harmonic.*

1. Introduction:

Consider the Cauchy – Riemann equations are important equations in the complex analysis through which it is possible to know the function of the ear to which he was able to derive or not. We found through the equations of Cauchy – Riemann as the function accepts the derivation it is analysis either did not accept derivation is non – analysis.

The meaning is due to French Mathematician Argstine Louis Cauchy and German mathematician Bernard Riemann.

The Cauchy – Riemann equations on a pair of real – valued functions of two real variables $u(x, y)$ and $v(x, y)$ are the two equations:

$$\frac{\partial u}{\partial x} = \frac{\partial v}{\partial y} \quad , \quad \frac{\partial u}{\partial y} = -\frac{\partial v}{\partial x}$$

Matlab is one of the high – performance languages that is generally used for purpose of technical computing. Matlab creates an easy – to use environment where understandable mathematical notations are used express the problems and solutions.

2.Some Definitions

Definition (2.1): Let F be a function whose domain contains a neighborhoods of a point $z_\circ$. The derivative of F at $z_\circ$ written $\acute{F}(z_\circ)$is defined by the equation

$$\acute{F}(z_\circ) = \lim_{z \to z_\circ} \frac{F(z) - F(z_\circ)}{-z_\circ} \qquad (1)$$

Provided this limit exists the function F is said to be differentiable at $z_\circ$ when its derivative at $z_\circ$ exists by expressing the variable z in definition (1) in terms of the new complex variable $\Delta z = z - z_\circ$

We can write that definition as

$$\acute{F}(z_\circ) = \lim_{\Delta z \to 0} \frac{F(z_\circ + \Delta z) - F(z_\circ)}{\Delta z} \quad \textbf{[7]}$$

Definition (2.2): If the derivative $\acute{F}(z)$ exists at all point z of a region R then $F(z)$ is said to be analytic in R and is referred to as an analytic function in R. A function $F(z)$ is said to be analytic at a point $z_\circ$ if there exists a neighborhood $z - z_\circ < \delta$ at all point of with $\acute{F}(z)$ exists.**[12]**

Example (2.3): Determine if the function $\bar{z}$ is analytic or not.

Solution: Let $F(z) = \bar{z} = z - iy$

$$u(x, y) = x, \qquad v(x, y) = -y$$

Differentiating partially, we get

$$\frac{\partial u}{\partial x} = 1, \quad \frac{\partial u}{\partial y} = 0, \quad \frac{\partial v}{\partial x} = 0, \quad \frac{\partial v}{\partial y} = -1$$

Which shows that Cauchy – Riemann equations are not satisfied there fore $F(z) = \bar{z}$ is not analytic.**[1]**

Definition (2.4): A real valued function u of two real variables x, y defined a domain D is said to be harmonic in D if it has continuous partial derivatives of second order that satisfy in D Laplac's equation:

$$\Delta u = u_{xx} + u_{yy} = 0 \textbf{ [8]}$$

Theorem (2.5): If $F(z) = u(x, y) + iv(x, y)$ is analytic and the functions $u(x, y)$ and $v(x, y)$ have continuous second order partial derivatives then $u(x, y)$ and $v(x, y)$ are harmonic.

Proof: The second hypothesis is redundant because it can be shown that an analytic function has continuous partial derivatives of all order.

The harmonically of u and v is a simple consequence of the following Cauchy – Riemann equations: $\frac{\partial u}{\partial x} = \frac{\partial v}{\partial y}$, $\frac{\partial u}{\partial y} = -\frac{\partial v}{\partial x}$ (2)

Using these equations we obtain :

$$\frac{\partial^2 u}{\partial y^2} = \frac{\partial}{\partial x}\left[\frac{\partial v}{\partial y}\right], \frac{\partial}{\partial y}\left[\frac{\partial v}{\partial x}\right] = -\frac{\partial^2 u}{\partial y^2}$$

From which $\frac{\partial^2 u}{\partial x^2} = -\frac{\partial^2 u}{\partial y^2}$ Or $\frac{\partial^2 u}{\partial x^2} + \frac{\partial^2 u}{\partial y^2} = 0$

So u is harmonic .Similarly by differentiating both sides of (2) we found

$\frac{\partial^2 v}{\partial x^2} + \frac{\partial^2 v}{\partial y^2} = 0$. So v is harmonic

$\therefore F(x) = u(x,y) + iv(x,y)$ is harmonic function.**[12]**

Definition (2.6): If a function in not analytic at $z_\circ$ but is analytic for are least one point in every neighborhood of $z_\circ$ then $z_\circ$ is called a singularity of that function.**[2]**

3.Cauchy – Riemann Equation:

Theorem (3.1): If γ is a simple closed anticlockwise curve in the complex plane and $F(z)$ analytic or some open set that includes all of the curve γ and all points inside γ then :

$$\int_{\gamma} F(z)\ dz = 0$$

Proof: We write $dz = dx + i\ dy$ and use Green's theorem on:

$$\int_{\gamma} F(z)\ dz = \int F(z)\ dx + \big(iF(x)\big)\, dy$$

$$= \iint_{R} \left[\frac{\partial\big(iF(z)\big)}{\partial x} - \frac{\partial F(z)}{\partial y}\right] dx\, dy$$

(with R demoting the inter of γ)

If you recall the proof of CR equation you will remember that:

$$F(z) = \lim_{h\to 0} \frac{F(z+h) - F(z)}{h}$$

Can be taken in any direction at once

$$\overline{F}(z) = \frac{\partial F(z)}{\partial x} = \frac{1}{i}\frac{\partial F(z)}{\partial y}$$

It follows that the integrand of the double integral we get from Green's theorem

$$\frac{\partial\big(iF(z)\big)}{\partial x} - \frac{\partial F(z)}{\partial y} = i\left[\frac{\partial(z)}{\partial y} - \frac{1}{i}\frac{\partial F(z)}{\partial y}\right] = 0$$

So we get

$\int_\gamma F(z)\ dz = 0$ **[14]**

Definition (3.2):A necessary conditions that $w = F(z) = u(x,y) + iv(x,y)$ be analytic in a region R are u and v satisfy the Cauchy – Riemann equations

$$\frac{\partial u}{\partial x} = \frac{\partial v}{\partial y}, \quad \frac{\partial u}{\partial y} = -\frac{\partial v}{\partial x} \qquad (3).\ \textbf{[12]}$$

Proposition (3.3):Let $F = u + iv$ be holomorphic on an open set U then both the partials of both u and v exist or U and for any $z = x + iy \in U$.

$$\frac{\partial u}{\partial x} = \frac{\partial v}{\partial y} \text{and } \frac{\partial u}{\partial y} = -\frac{\partial v}{\partial x}$$

Proof: Since F is holomorphic at $z = x + iy$

$$\overline{F}(z) = \lim_{w\to o} \frac{F(z+w) - F(z)}{w}$$

$$= \lim_{w\to 0} \frac{u(z+w) - u(z)}{w} + i \lim_{w\to 0} \frac{v(z+w) - v(z)}{w}$$

Exist let $w = h + ik$ so we get

$$\overline{F}(z) = \lim_{h+ik} \frac{u(x+h, y+k) - u(x,y)}{h+ik} + i \lim_{h+ik} \frac{v(x+h, y+k) - v(x,y)}{h+ik}$$

In particular if we let $k = 0$ and $h \to 0$ and let $h = 0$ and $k \to 0$ we get the same limit so that

$$\overline{F}(z) = \lim_{\substack{h\to 0 \\ k\to 0}} \frac{u(x+h, y+k) - u(x,y)}{h+ik} + i \lim_{\substack{h\to 0 \\ k\to 0}} \frac{v(x+h, y+k) - v(x,y)}{h+ik}$$

$$= \lim_{h\to 0} \frac{u(x+h, y) - u(x,y)}{h} + i \lim_{k\to 0} \frac{v(x+h, y) - v(x,y)}{h}$$

$$= \frac{\partial u}{\partial x} + i \frac{\partial v}{\partial x}.$$

And also

$$\overline{F}(z) = \lim_{\substack{h\to 0 \\ k\to 0}} \frac{u(x+h, y+k) - u(x,y)}{h+ik} + i \lim_{\substack{h\to 0 \\ k\to 0}} \frac{v(x+h, y+k) - v(x,y)}{h+ik}$$

$$\overline{F}(z) = \lim_{k\to 0} \frac{u(x, y+k) - u(x,y)}{ik} + i \lim_{k\to 0} \frac{v(x, y+k) - v(x,y)}{ik}$$

$$= i\frac{\partial u}{\partial y} + \frac{\partial v}{\partial y}$$

Thus the four partials exist and we get

$$\frac{\partial u}{\partial x} + i\frac{\partial v}{\partial x} = \frac{\partial v}{\partial y} - i\frac{\partial u}{\partial y}$$

Equating the real and imaginary part we get

$$\frac{\partial u}{\partial x} = \frac{\partial v}{\partial y} \text{ and } \frac{\partial v}{\partial x} = -\frac{\partial u}{\partial y}$$

The conditions $\frac{\partial u}{\partial x} = \frac{\partial v}{\partial y}$ and $\frac{\partial v}{\partial x} = -\frac{\partial u}{\partial y}$ are know as Cauchy – Riemann equations.**[9]**

Definition (3.4): The function of z in the form $F(z) = u(x, y) + iv(x, y)$ it is convenient to change to the polar system r, θ so that:

$x = r\cos\theta$, $y = r\sin\theta$ where $r = \sqrt{x^2 + y^2}$ and $\theta = \tan^{-1} y/x$ thus $F(z) = u(r, \theta) + iv(r, \theta)$ then:

Cauchy – Riemann equation in polar give by:

$$\frac{\partial u}{\partial r} = \frac{1}{r}\frac{\partial v}{\partial \theta}, \qquad \frac{\partial v}{\partial r} = -\frac{1}{r}\frac{\partial u}{\partial \theta}, \qquad \textbf{[2]}$$

4.Matlab Program: Matlab can be used for math computations modeling and simulation data analysis and processing visualization and graphic and algorithm development. Matlab is widely used in universities and colleges in introduction and advanced courses in mathematics science and especially engineering. Matlab program has tools that can be used to solve common problems.**[3]**

Definition of Matlab (4.1): Matlab a high – performance language for technical computing it integrates computation visualization and programming in an easy – to use environment where problems and solution are expressed in familiar mathematical notation.

Typical use include: Math and computation, Algorithm development, Data analysis exploration and visualization and application development.**[10]**

Complex Numbers (4.2): We can also enter complex numbers in Matlab to remind method of our audience who are aggie graduates the root of -1 is defined as $i = \sqrt{-1}$ a complex number is one that can be written in the form $z = x + iy$ where x is the real part of z and y is the imaginary part of z.It is easy complex numbers in Matlab by default it recognizes i as the square root of minus on.**[4]**

5. Solve Partial Differential Equations by Matlab:

The Matlab partial differential equation solver pdepe initial – boundary value problems for systems of parabolic and elliptic part differential equation in the one space variable x and time t.
There must be at lead on parabolic equation in the system. The pdepe solver converts the PDF to ODE using a second order accurate spatial discrtization based on a set of nodes specified by the use.**[11]**

i.Part Differential Equation Solver Basic Syntax:

The basic syntax of the solver is:
soL= pdepe (m, pde fun, ic fun, bc fun, xmesh, tspan)
m is specifies the symmetry of the problem.
$pde\ fun$ is a function handle that computes $m, f\ and\ s[m\,u, F, s]$: pde fun (m, t, u, ux)
$ic\ fun$ is a function handle that computes $\emptyset$

$$phi: ic\ fun\ (x)$$

$bc\ fun$: is a function handle that computes the $BC[pa\ , qq\ , pb, qb]: bc\ fun(a, uq, b, ub, t)$
$x\ mesh$: is a vector of points in $[a, b]$
$tspan$: is a vector of time values.**[6]**

6.Solve Cauchy – Riemann Equations using Matlab

Here we used MATLAB function diff to solve Cauchy - Riemann equation problems in one spatial dimension :

1. applied know the function F with F(z)= z^2 is complex different able there for Cauchy equation m of hold.

Solution :

```
function f=cauchy1(z)
syms xyz
f = x^2 - y^2 + 2*i*x*y;
U=x^2 - y^2
V=2*x*y
Ux=diff(U,x)
Ux=diff(U,y)
Vx=diff(V,x)
Vx=diff(V,y)
```

Result:

```
>> cuchy
    Ux = 2*x
    Ux =-2*y
    Vx =2*y
    Vx = 2*x
```

note: Ux(f,x)= Vy(f,y) and Uy(f,x)= -Vx(f,y) therefore the Cauchy – Riemann equations are satisfied.

2. Verify that the Cauchy – Riemann equations is

$$f(z)=|z|^2$$

Solution :

```
function U=cauchy1(z)
syms xyzi
U = x^2 + y^2;
V=0;
Ux=diff(U,x)
Uy=diff(U,y)
Vx=diff(V,x)
Vy=diff(V,y)
```

Result

```
Ux = 2*x
Uy =2*y
Vx = 0
Vy=    0
```

note: Ux(f,x)≠ Vy(f,y) and Uy(f,x)≠ -Vx(f,y)

3. Let $f(x,y)= x^2 +y^2 +ixy$ find Cauchy – Riemann equations condition.
   Solution :

```
function f=cauchy3
syms xyi
f = x^2 + y^2 + i*x*y;
U=x^2 + y^2;
V=x*y;
Ux=diff(U,x)
Uy=diff(U,y)
Vx=diff(V,x)
Vy=diff(V,y).
```

Result

```
>> cauchy3
Ux = 2*x
Uy = 2*y
Vx = y
Vy =x
```

note: Ux(U,x)≠ Vy(V,y) and Uy(V,x)≠ -Vx(V,y)

therefore the Cauchy – Riemann equations is not satisfied conditions.

4. Verify that the Cauchy – Riemann equations is

$$f(z)=e^z=e^x(\cos y + i*\sin x)$$

```
function f=cauchy4
syms xyei
f = e^x*(cos(y) + i*sin(x));
U= (e^x)*(cos(y));
V=(e^x)*(sin(y));
Ux=diff(U,x)
Uy=diff(U,y)
Vx=diff(V,x)
Vy=diff(V,y)
```

Result

```
>> cauchy4

Ux = e^x*log(e)*cos(y)

Uy =-e^x*sin(y)

Vx = e^x*log(e)*sin(y)
Vy = e^x*cos(y)
```

note: Ux(U,x)=Vy(V,y) and Uy(V,x)= -Vx(V,y). Therefore the Cauchy – Riemann equations is satisfied conditions.

7. Polar coordinate form Cauchy – Riemann equations:

1. Consider the function:

$$f(z)=\frac{1}{z}=\frac{1}{re^{ik}}=re^{-ik}\frac{1}{r}(cosk-isink)$$

verify that the Cauchy – Riemann equations polar are if satisfied or not

$$f(z)=\frac{1}{r}(cosk-isink)$$

Solution :

```
function f=cauchy5(z)
syms kri
f = 1/r*(cos(k) + i*sin(k));
U=1/r*(cos(k));
V=1/r*(sin(k));
Uk=diff(U,k)
Ur=diff(U,r)
Vk=diff(V,k)
Vr=diff(V,r)
```

Result

```
>> cauchy5
Uk = -sin(k)/r
Ur =-cos(k)/r^2
Vk = cos(k)/r
Vr = -sin(k)/r^2
```

∴ the Cauchy – Riemann equations polar is satisfied conditions

2. Verify that the Cauchy – Riemann equations polar are is satisfied or not

Solution :

```
function f=cauchy6(z)
syms  reik
f = r^(1/3)*e^(i*k/3);
U=r^(1/3)*(cos(k/3));
V=r^(1/3)*(sin(k/3));
Uk=diff(U,k)
Ur=diff(U,r)
Vk=diff(V,k)
Vr=diff(V,r)
```

Result

```
>> cauchy6

Uk =
-(r^(1/3)*sin(k/3))/3
Ur =
cos(k/3)/(3*r^(2/3))
Vk =
(r^(1/3)*cos(k/3))/3
Vr =
sin(k/3)/(3*r^(2/3))
```

∴ the Cauchy – Riemann equations polar is satisfied conditions

8.Compare between analytical Solution and Matlab Solution:

Table 1 explain the comparison between the analytical and Matlab calculation where we found that manual calculation is identical to the Matlab calculation but the Matlab has been shown to be more correct in the problems (3) and (6) because the functions used are relative function.

```
clear all
clc
x=[1;2;3;4;5;6];
y=[1 1;1 1;1 2;1 1;1 1;1 2];
bar(x,y);
legend('Manuals Solutions','Matlab Solutions')
xlabel('problems');
ylabel('Result');
title('Compare between analytical Solutions & Matlab Solutions')
grid
shg
```

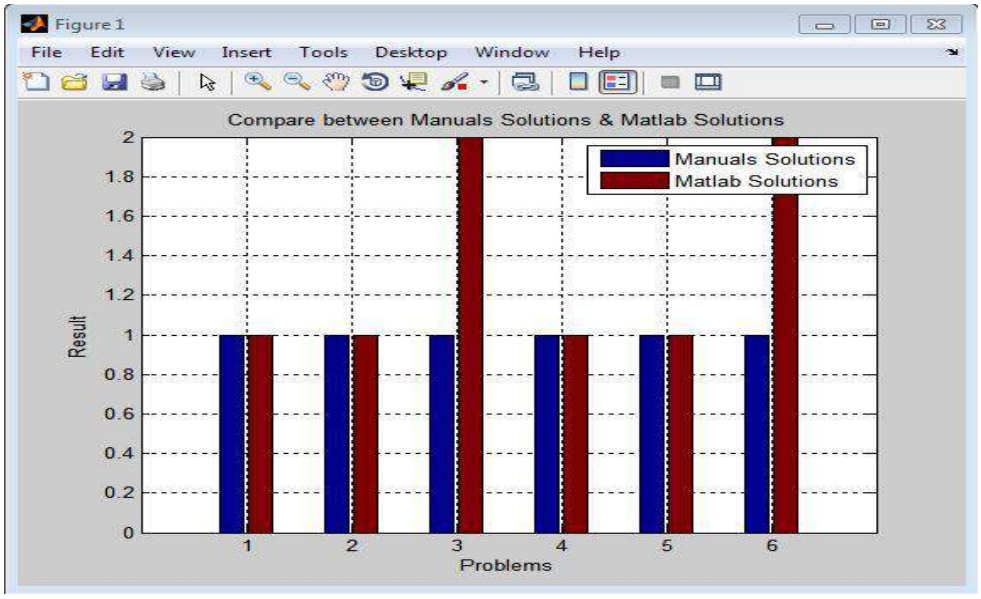

Figure 1: Manual and Matlab Solutions

Table 1: Comparison

Problems	analytical **Calculation**	**Matlab Calculation**	**result**
Problem 1	Ux = 2x , Ux = -2y Vx =2y, Vx = 2x	Ux = 2*x , Ux = -2*y Vx =2*y, Vx = 2*x	Equal and accurate
Problem 2	Ux =2x , Uy = 2y Vx = y , Vy =x	Ux =2*x , Uy = 2*y Vx = y , Vy =x	Equal and accurate
Problem 3	Uk =-sin(k)/r rUr =cos(k)/r^ Vk =-cos(k)/r rVr =-sin(k)/r^	Uk =-sin(k)/r Ur =cos(k)/r^2 Vk =cos(k)/r Vr =-sin(k)/r^2	Different solutions
Problem 4	Uk =(r^(1/3)*sin(k/3))/3 Ur =cos(k/3)/(3*r^(2/3)) Vk =(r^(1/3)*cos(k/3))/3 Vr =sin(k/3)/(3*r^(2/3))	Uk=(r^(1/3)*sin(k/3))/3 Ur=cos(k/3)/(3*r^(2/3)) Vk=(r^(1/3)*cos(k/3))/3 Vr=sin(k/3)/(3*r^(2/3))	Equal and accurate
Problem 5	tan(z)	tan(z)	Equal and accurate
Problem 6	f(z)=(1-2i)(sinz+(z^2)	f(z) =sin(z)*(1 -2*sqrt(-1)) + z^2*(1 - 2*sqrt(-1))	Different solutions

From Figure (1) note that the difference results of calculation between analytical calculation and Matlab calculation shown that the Matlab has more accurate in problem (3) and (6).

9.Results

The study explained that Cauchy – Riemann equations were the test for the analysis of the function or not, also explained that all analysis functions are harmonic but the inverse is not true, the possibility of calculating Cauchy – Riemann equations using Matlab and the Matlab calculation is more speed and accurate than the manual calculation.

10.Conclusion

Different concepts of Cauchy – Riemann Equation was analyzed. Results were discussed and compared for both analytical and Matlab calculations.

References:

[1] A.C sravastava and P.K srivastave – Engineering Mathematics – PHI Loarning – Eastern Economy Edition- 2013.
[2] A. David Munsch – Complex variables with Appications – Third Edition – Pearson Education – 2005.
[3] Amos Gilat – Matlab an Introduction with Application – fourth Education – John wiley sonsLnc – 2011.
[4] David Mcmahon – Matlab Demystified – Mc Graw Hill companies – New York – 2017.
[5] Ebrahard Freitag and Rolf Busam – Complex Analysis – second edition – springer verlag Berlin Heidelberg – August – 2008.
[6] Ela pekalsk and Marjolem vander Glas – Introduction to Matlab – January 2002.
[7] Jams Word Brown and Ruelvv Chrchill – complex variavles and Applications – seventh edition – Mc Grow Hill – New York – 2004.
[8] Jank Krzyz – Problems in complex Variable Theory Number 36 – New York – 1971.
[9] Jv Despande – Complex analysis – first edition – Mc Graw Hill publishing Company – New Delhi – 1986.
[10] Math Work – Getting stated with Matlab – second printing – may 1997.
[11] Math Work – using Matlab – versin6 – 2001.
[12] Murray and Other – complex variable – second edition – Mc Graw Hill companies – New York – 2009.
[13] Naisank Halag Mosah and Shankar –some application of R. equation of complex analysis - IJMETMR – volume 2 -10/October 2015.
[14] Rakesh kumar pandey – theory of complex variable – first edition – DPH – New Delhi – 2007.

NIPES Conference Proceedings
The 1st International Conference of the Nigerian Institution of Professional Engineers and Scientists 7th-8th Oct. 2021: 125-136
www.nipesjournals.org.ng

Climate Variability and the Issues in Flood Disaster Risk Awareness in Nigerian Communities

Ikpong Sunday Umo *; Patience E. N. Okoroafor; Ifeanyi Gerry Ukwe

Department of Geography and Environmental Studies, School of Social Sciences, Alvan Ikoku Federal College of Education, P.M.B. 1033, Owerri, Imo State, Nigeria.
Corresponding Author: umohikpong@yahoo.com; Phone Number: +2348037565958

Abstract

Prior to human civilization, floods have been identified as one of the most lethal environmental and geophysical disasters with destructive consequences. Yet, individual/ group risk awareness levels and impact mitigations vary across distinct geographic locations and times. This study explores issues in climate-induced flood disaster risk awareness in Nigeria. The discourse analyses using qualitative and quantitative tools revealed that the causative factors and levels of flood disaster awareness in Nigerian communities varied across geographic locations and timescale. Also, the flood disaster profiles in Nigeria reflect dominant control by variations in the climatic (rainy) seasons. Hence, most of the historic flood disasters in Northern Nigeria have strong affinities with river discharge and dam failure while those in Southern Nigeria were mostly influenced by the high frequency, density, intensity of rainfall, and poor land-use planning. Also, the government, donor agencies, and the vulnerable people were basically passive in their management approaches, with emphasis on post-disaster rehabilitation, which hampered sustainable development and exacerbate the negative impacts on the realization of an ecologically smart future. The perceived flaws led to very high risk, defined by limited capacity and locational effect. The paper, therefore, recommended adequate promotion of pre-flood disaster risk mitigation options through environmental education programs to boost community awareness, increase the sense of responsibility and safety of vulnerable people.

Keywords: *Climate variability, flood disaster, risk awareness, reaction, impact mitigation.*

1. Introduction

Flood disaster has long been recognized as one of the earliest and most destructive climate-induced geomorphic events in the history of an Anthropocene (Age of Humans). Yet, the levels of individual and group awareness of the risk and choice reactions for enhanced management of human-environment toward sustainability varied across geographical areas and time [1]. Hence, Nwafor [2] identifies flood as one of the most lethal to humans among the geophysical agents. It is instigated by natural factors such as rainfall, soil, topography, and accelerated by anthropogenic factors especially the nature of city planning, roads/ drainage system, urbanization, and land use.

From the regional dimension, [3] observe that Asia is the flood most affected, accounting for over 50 percent of climate and water-related global disaster in the last quarter of the 20th century. Nigeria is not left out in the scene following the potential and actual effects of climate variability and change, accelerated by the increase in human population and the corresponding scramble for land for diverse uses. Such uses encompass settlements, agriculture, industries, and infrastructure/ social amenities in flood vulnerable areas such as coasts, shoreland, and floodplains.

Amidst the flood disaster occurrences, countries, regions, groups, households, and even individuals' reactions to mitigate or control the risks associated with them seem to vary. The variations are partly influenced by their level of awareness, exposure to the flood event, demographic attributes of the people at risk, and their socio-economic status. Climate variability and change issues are very critical within the Tropics [2]. In Southern Nigeria (e.g., Lagos, Rivers, Akwa Ibom), where weather activities have become quite erratic, and the existing water bodies tend to worsen the situation for coastal and shoreland communities with their ever-growing population; thereby increasing flood and related losses.

Although irregular climate variability and change example global rainfall patterns have some positive impacts especially desert regions that were initially faced with water scarcity, with a tendency to wet the land for agriculture production. Similarly, where the extreme temperature becomes a case, the negative impacts on the production of major traditional food crops and loss of biodiversity may become eminent. Additionally, farmers remain concerned about an increasing intensity of extreme weather events that will and has continued to occur as a result of climate variability and change. Weather-induced flood and storm disasters have negative impacts on wetland agriculture, housing, rising sea level, and increased salinization.

Recent researches have indicated the past efforts to mitigate or avert the impacts of flood disaster accelerated by climate variability for the actualization of sustainable development and ecologically smart future are plagued by factors such as limited capacities and awareness across geographic locations [4, 5]. In spite of the observed issues, flood disaster risk awareness, reaction, and communication patterns in Nigeria are not given the expected attention [5]. Yet, historic flood disaster has remained a recurrent decimal with devastating consequences on governments, groups, and individuals. The preceding notions justifies the need to review some striking flood events and their possible causes with a view to identifying key options in boosting risk awareness, potential/ actual impacts communication, and mitigation options.

The aim of this study is to explore the thrust in climate variability and issues in flood disaster risk awareness in Southeast Nigeria with a view to providing a direction toward building ecologically smart future. To accomplish the aim, the following specific objectives were investigated.

1. To review the major flood disaster profiles and their causative factors in Nigerian communities.

2. To examine the influence of climate-induced flood disaster awareness and timing of impacts communication on losses in the Nigerian environment.

3. To assess the dominant factors governing flood disaster risk losses in Nigerian communities.

4. To evaluate flood mitigation options for the development of a sustainable environment and ecological smart future for Nigerians.

1.2 Description of the Study Area

1.3 Location

The study area is located within the humid tropical region of West Africa. It has diverse climate, soils, vegetation, landmass, population, and allied resources. The vastness of the Nigeria necessitates the scoping of the study area to focus on the Southeast region. The Southeast Nigeria is commonly called the Igbo land. It comprises of five (Abia, Anambra, Ebonyi, Enugu, and Imo) States. From the Geographical perspective, the region lies within Latitude 5^0 14^1 to 7^0 28^1 North of Equator and between Longitudes $6^0 11^1$ to $8^0 33^1$ East of Greenwich Meridian.

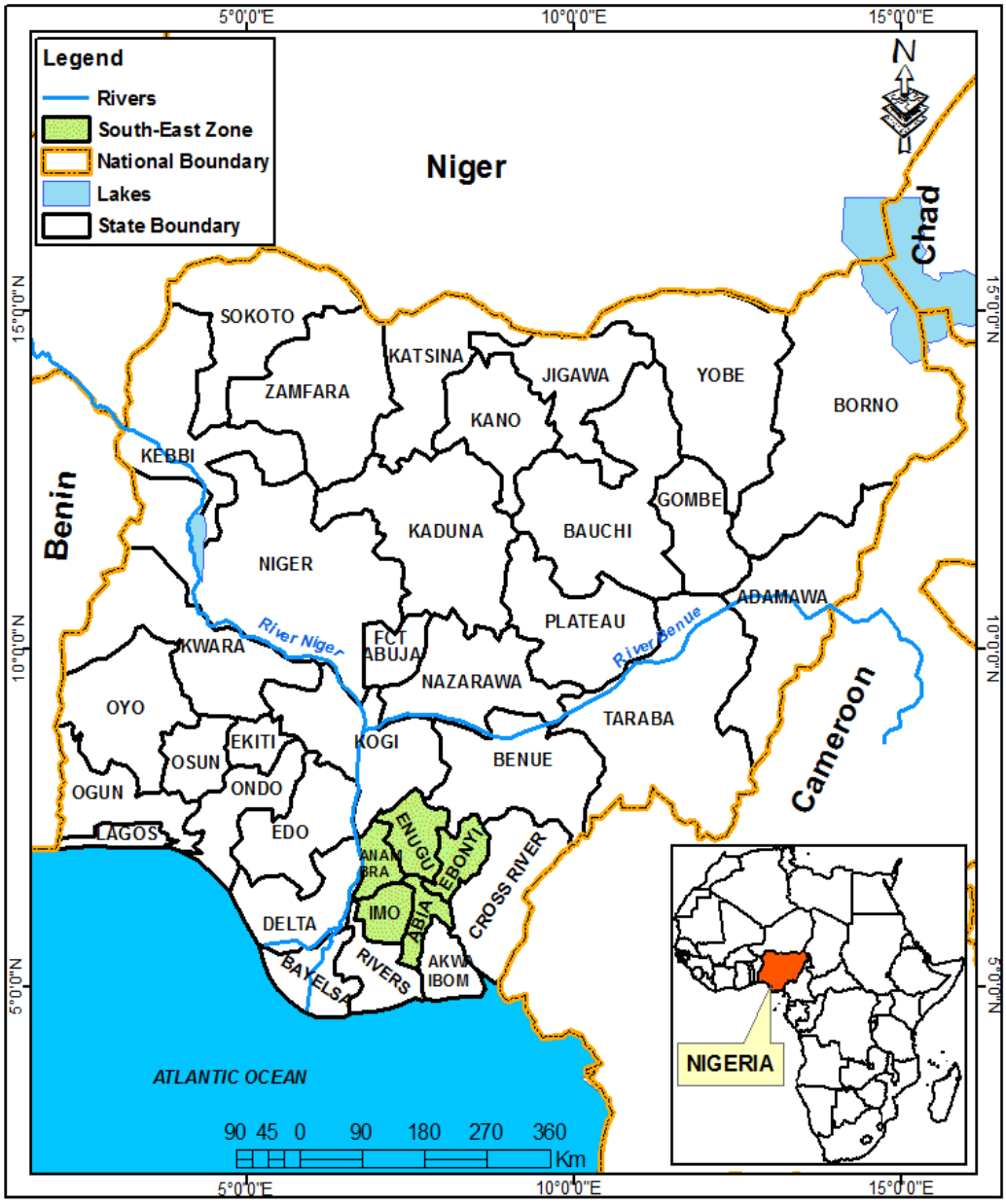

Figure I: Nigeria showing Southeast Nigeria.

1.4 Climate and Geology

The climate of Southeast Nigeria is humid tropical environment based on Köppen's classification scheme. The Af-climate is occasion found in some pocket locations of Ohafia and Abriba in Abia State due to the influence of adjoining rivers. The Am-climate is most dominant in the five States, while the Aw-climate is common in the northern part of Enugu and Ebonyi States due to the influence of Northeast wind.

The climate of the area grouped as Af (Humid Tropical) climate in the Southern part (comprising Abia, Imo, Anambra States) and Am (wet and dry climates) around Enugu and Ebonyi States based on Köppen's climatic classification scheme. Similarly, the rainfall distributions vary across geographic space and seasons. The area usually received double rainfall maxima (April to July and August to November) with a mean annual total that ranges between 1,770 mm and over 2,710

mm. The magnitude, frequency, intensity, and amount often diminish from the North to the south [6].

The geologic formations of the study area also vary across geographic space along with the pedology as presented with respect to Southeast Nigeria (Figure 2). For instances, the distributive patterns of the hydromorphic soils in the Aba and Ikwo, Nwewi, and Obolo areas of the southeast Nigeria is influenced by the Tertiary and recent Quaternary Alluvium deposits. Similarly, Ferrallitic soils in Aba area is accelerated by the Coastal Plains Sands of Tertiary Time (Holocene) deposits while the dominant of gravelly ironstone concretions in Abakaliki is associated with Cenozoic era which Orajaka cited in Umo and Enwereuzor [6] opines that the Anticlinorium had undergoes some elements of rejuvenation following the prevalence of protracted weathering, denudation, and allied geomorphological processes.

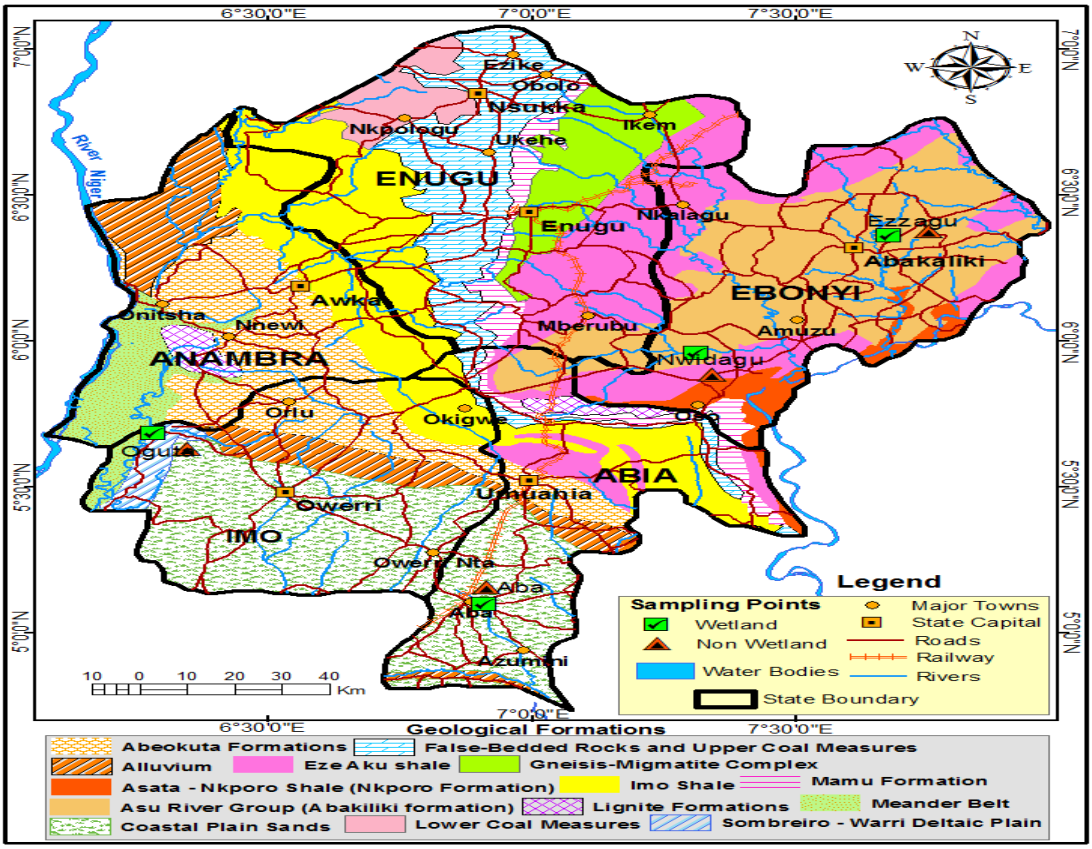

Figure II: Southeast Nigeria showing Geologic Formations.

3. Methodology

This study is preliminary in nature with a strict emphasis on discourse and quantification as analytical tools. The researchers employed both qualitative and secondary methodologies in data generation to evaluate climate variability and issues in flood disaster risk awareness in the Nigerian environment. Data were generated through historical traditions. Other vital data were generated from the existing published and unpublished literature such as journals, textbooks, government documents, eyewitness accounts/ historical experiences by individuals.

4.0 Results and Discussion

4.1 Flood Disaster Profiles and Major Causative Factors in Nigeria

Flood is a geophysical concept that depicts a situation where a large volume of water submerges a wide landscape (area) that was initially a dry land for a reasonable period of time. The severity and intensity of its occurrence vary from one location to another based on the type propel by prevailing natural and anthropogenic factors in an area. In most cases, the variability in flood events is classed based on their types. For instance, Akpofure [7] Emeriiole [8], Umo and Enwereuzor [9], identified four distinct flood types (flash; urban; coastal; and river) that are prevalent in Nigerian environment and Southeast in particular.

A flood disaster is a situation where the flood event causes widespread destruction of life and property to such a magnitude that is beyond the coping capacity of the affected people using their available resources. That means once the capacity of the flood-affected people are overwhelmed, and they resorted to external (national or international) assistance, then disaster has occurred. Capacity is, therefore, measure in terms of the physical, economic, social, environmental, and other resources within the affected region which enable people to cope effectively with the flood disaster. The identified resources are what enable the vulnerable people to prepare for, prevent, mitigate, or quickly recovered from the effect of the disaster over a period of time.

Table 1: Trends in major Flood Events and Causative Variables

S/N	Some Historic Flood Events	Major Possible Causes
1	Ogunpa flood in Ibadan, 1981, 1984	Blocking of river channels with solid wastes and illogical activities along the river channel.
2	Bagauda flood in Kano, 1988.	Excessive storage leading to Dam failure due to protracted and heavy rainfall.
3	Bauchi flood in 1991.	Overflowing of Yuli River due to excess rainfall.
4	Benin City flood, 1984, 2008	Heavy rainfall & blocking of drainage channels.
5	Angwan Rogo (1992) and Lamingo flood (2012) in Jos.	Heavy rainfall, unregulated urbanization along floodplain and drainage lines.
6	Ikot Ekpene flood in Akwa Ibom, 1998.	Deforestation and urbanization.
7	Port Harcourt City flood, 1984, 2006.	Heavy rainfall and building structures along natural water ways.
8	Benue River/ Niger Delta flood 2008, 2012, 2020	Excessive and unprecedented rainfall coupled with the release water storage from Dam.
9	Oguta Flood in Imo State, 2012, 2014	Excessive and unprecedented rainfall coupled with flooding of Niger River

Source: Modified from Akpofure [7] and Emeribeole [8]

Assessing from Table I, there are clear indicators that flood disaster is majorly a natural occurrence but its severity and impacts over geographic location and time vary due to the level of anthropogenic interferences (activities). Outstanding among the natural forces that cause flood events in the humid Tropics and Nigeria in particular, are weather and climate (heavy and prolong rainfall), underlying soil structure and texture, nature of the underlying topography, proximity to water bodies (such as River, Ocean, dam, or waterlogged, and nature of vegetation cover as observed in Umo and Enwereuzor [6].

Similarly, major anthropogenic variables that instigate flood disaster in a settlement/ industries/ farms and others, in the flood-prone areas, are: poor monitoring and gauging of water projects/ bodies, blockages of river channels, and drainages with solid wastes, poor sanitation, urbanization, and poor town planning, poor legal framework that guide human occupation in government reserve areas (such as parks, green land, open space, bye pass, gulf, and game resort).

4. Categorization of Flood Disaster Risks and Determinants of Losses

Flood risk depicts the qualitative and/ or quantitative measures of the probability and severity of losses in events of flood disaster. Very often, flood risks are rated based on one's exposure and vulnerability to the impact of the hazard in an area over a period of time. Therefore, since each flood event has a frequency (magnitude) and the corresponding consequences, the risk can be defined based on whether the potential risk (impact) is very high, high, moderate, low, or very low as depicted in Table 2.

Flood disaster risk signifies the possibility of adverse effects of flood in the future. It derives from the interactions of social and environmental processes, as well as the combinations of physical hazards and the vulnerabilities of elements. A flood event is not the sole driver of risk. There is increasing confidence that the levels of adverse effects are in part determined by the vulnerability and exposure of societies and socio-ecological systems [10, 11, 12, 13].

Table 2: Flood Risk Rating and Possible Effect Definition.

Exposure Rating	Flood Disaster Impact Definition
A = Very Low	Exposures to the flood risks are often negligible with almost zero loss.
B = Low	Risks are controlled and may likely remain same in accordance with the assessment criteria used by the assessors.
C = Moderate	Risks are currently under control to meet assessment, but such control is often difficult to measure.
D = High	Risks are not adequately controlled to meet assessor's criteria.
E = Very High	Exposures to flood disaster risks are enormously high and will certainly lead to huge losses of life and property.

Source: Modified from Iwuchukwu [14].

Deducing from Table 2, it is clear that flood disaster risk is not fixed over time and place, but a continuum in constant evolution, yet individual and/ or group level of awareness, responses, and management can influence how severe or minute the impact is felt. This is more evident because what one may perceive as potential often comes into manifestation, if adequate measures are not introduced to avert or mitigate its occurrence.

Disaster risk is associated with differing levels and types of adverse effects on the elements. The effects may assume catastrophic level or levels commensurate with small disasters. Some have limited financial costs, but very high human costs in terms of loss of life and numbers of people affected as the case of Rivers Niger and Benue flood (of October 6) instigated by the forceful release of water from a dam in Cameroun; others have very high financial costs but relatively limited human costs as the case of Oguta Lake flood.

Modern space observers such as geographers, engineers, environmentalists, and allied scientists believe that the cumulative effects of what may be considered as small disaster can affect the capacities of communities, societies, or social-ecological systems to deal with future events at sub-

national or local levels [15, 16]. To promote sustainable development and create ecological smart future with limited or zero flood disaster risk demands developing, working, and sustaining pre-disaster plans blueprint, whose principles, methods, and applications in Nigerian environment need be people-society friendly.

5. Flood Disaster Losses, Risk Awareness, and Communication

It is commonly recognized that once a disaster occurs and no life and/ or property is affected, or the affected peoples' capacities are not overwhelmed the hazard; then it is not classed as a disaster. Similarly, the intensity or magnitude of flood events are usually determined partly by environmental degradation, level of human preparedness and intervention, the severity of natural and anthropogenic elements, local geomorphology and geology in a given geographical location.

Contextually, individuals' losses to flood disaster over time may depend squarely on one or more of the following factors: the magnitude of the flood disaster, population density in the flood risk zone, structure, and composition of the vulnerable people in the flood risk zones, the socio-economic structure of the elements in the risk zones, level of awareness, timing of information/ responses, geologic foundation of the flood risk zone, and the institutional framework of the area.

Viewing from Cardonna et al. [16] perspective, individual, or group exposure to flood events involves taking inventory (such as pictorial, mapping, and recording) of elements in an area in which hazard events may occur. Such documentaries often serve as guides for future responses and evacuations. However, if the population and economic resources of the vulnerable groups are not located in or exposed to potentially dangerous settings, the problem of flood disaster risk may be either not exist or negligible.

Exposure is necessary, but not sufficient determinant of risk. It is possible to be exposed but not vulnerable, for example by living in a floodplain but having sufficient capacities to manipulate (building structures, proper timing of information and response and behaviour to mitigate) potential loss. However, to be vulnerable to the extreme flood event, it is necessary to also be exposed, but ones' knowledge of the event and ability to control the situation is very vital in this post-modern age of climate change and variability to boost sustainable development and ecologically smart future in Nigeria.

Risk awareness and communication are vital tools that influence people's perception and response to flood disasters in any region. Risk communication represents complex multidisciplinary actions that involve reaching different audiences to make risk comprehensible, understanding and respecting audience values, predicting the audience's response to the communication, and improving awareness, collective and individual decision-making as emphasized in [16]. Failures in flood risk awareness and communication have been revealed in past disasters, such as Hurricane Katrina in 2005 or Pakistan floods in 2010 [17]. Particularly, the loss of trust in official institutions responsible for early warning and disaster management were the key factors that contributed to the increasing disaster risk.

Effective and people-oriented flood risk communication is, therefore, a key to improving vulnerability and risk reduction in the context of extreme events like floods, particularly in the context of people-centered early warning [17]. Weak and insufficient risk communication as well as the loss of trust in government institutions in the context of early warning or mitigation can be seen as a core component of institutional and individual vulnerability.

The effectiveness or failure of people-centered flood risk communication can contribute to increasing people vulnerability and disaster losses. Peoples' awareness (knowledge) of factors that determine how people perceive and respond to a specific flood risk often enhances the management and mitigation of losses [12].

Effective risk awareness and communication can be built on risk assessment and tailored to a specific audience. The channels may range from decision-makers at various levels of government, to the private sector and the public at large, including local communities and specific social groups [16]. Impediments to information flows and limited awareness are risk amplifiers. Beliefs, values, and norms influence risk perceptions, risk awareness, and choice of action.

In most cases, poor people often suffer worse during flood disasters due to low level of awareness, cultural ties, poor information sources, and low income which together limits their capacity. To some extent, most of the blame should be shifted to the Government and allied authorities because they owe their people the duties of organizing periodic seminars, workshops, orientation, and awareness programs regarding the causes and effects of flood disaster in their domains and how to respond timely for their safety. Indeed, the flood disasters that occur around September to October 2012 along the Lower Niger River and Coastal belt of southern Nigeria attests to this.

Recent efforts by the Federal and State Governments through their agencies especially Federal Emergency Management Agency and State Emergency Management Agency are highly recommendable but seem to be grossly inadequate because of information gaps between the Federal, State, and Local level of the agencies and above all funding of research and advocacy programs on flood and allied weather/climate-related disaster in the 21st century. Appropriate and timely risk communication is critical for effective flood disaster risk awareness and impact mitigation.

6. Flood Disaster Risk Management and Impact Mitigation

Flood disaster risk management include all the activities, programs, measures which can be taken before, during and after a given flood event for the purpose of averting its occurrence, reducing its impacts and/or recovering from the losses over time and scale. It is obvious that the levels of individuals, groups, and government awareness and response to flood disaster risk is a key determinant of how effective the given management strategies are appropriately adopted. Timing of each flood disaster scenario is crucial in each management perspective (Figure 3).

There are ranges of vital action plans involved at each stage of management and/or mitigation as shown in Srinivas Hari [18]; Warfield [19]; United Nations Development Programme [20]; NEMA [21]. For instance, pre-flood disaster risk management encompasses all appropriate actions are taken to reduce or avert losses before a given flood event. The actions include the creation of awareness through public education and enlightenment programs, early warning signal, proper monitoring, and enhanced information sources regarding a flood event, timely evacuation/ relocation plans, strengthening existing structures (buildings, infrastructures, amenities, and drainages), building capacity and mobilization of manpower at government/volunteer group/household levels.

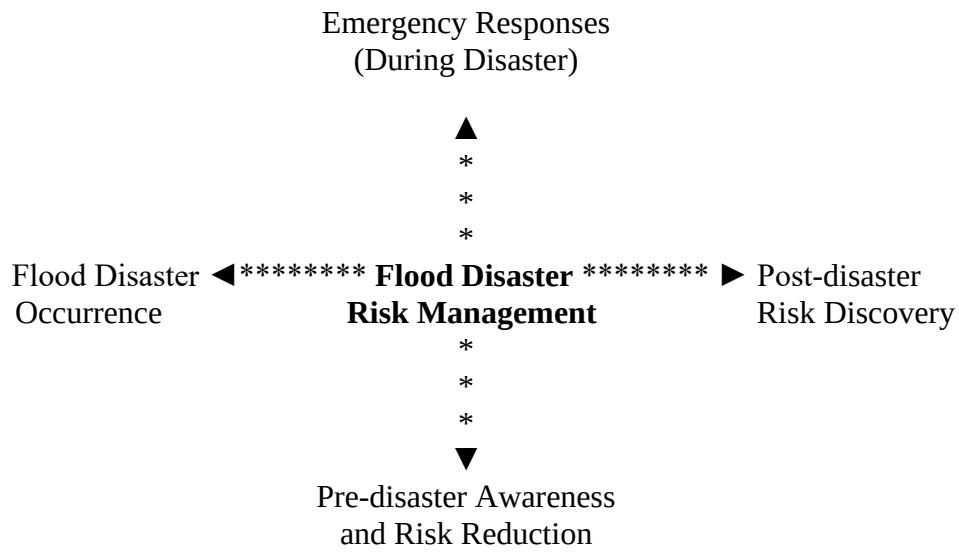

Figure 3: The diverse Perspectives for Flood Disaster Risk Management.

On the other hand, emergency response actions are those actions taken during a flood disaster to mitigate or avert the impacts on people over a period of time. Such actions embrace emergency aid/supplies (food, drugs, clothes, water, money, and etcetera), search and rescue mission for the weaker people, evacuation and rehabilitation, hospitalization and others. Hence, most of the services at this stage are very essential, risky, and highly specialized.

The third phase is post-disaster actions. It encompasses all the actions taken for the purpose of reassuring the flood victims of their early recovery from the psychological, health, socio-economic and physical effects imposed on them as a result of the event. Some major plans at this stage include reconstruction, rehabilitation, medication, counselling, reintegration, quarantine/ immunization, training, and retraining programs which usually take a longer period of time and heavy capacities investments.

7. Mitigation Options for Environmental Sustainability and Ecologically Smart Future

Contemporary researchers have suggested that flood disaster risk cannot be completely control, but its impacts on people and property can be mitigated through coordinated plans and actions as envisaged in Umo [1], Ojinma et al. [5], Adedeji et al. [13], Pollner et al. [22], Ologunorisa [23],. Since the past efforts have failed to yield the expected results at present, we are confident that promoting sustainable development and working towards ecologically smart future necessitate the adoption of proactive, sensitive, and vital options that are people-oriented, as identified and chronologically elucidate in the discussions that follow.

I. Promotion and Implementation of existing Legal and Institutional Frameworks.

Although there are diverse viable legislative and institutional frameworks put in place to guiding and regulate human activities at both urban and rural areas of Nigeria, some exploitative actions such as building on green/ shelter belts, drainage lines, power lines, right of way, colonization of waterways/ parks/ reserve area, and indiscriminate wastes dumping have serious adverse influence on flood disaster.

The outlined actions and structures are considered illegal, yet the regulatory bodies like Town Planning Authorities, City Development Authorities, environmental Protection Agencies, and allied institutions' levels or efforts against such unwarranted activities are abysmally low, thereby de-accelerating the promotion of environmental sustainability and impairing actions towards creating an ecologically smart future.

This is necessary because previous laws that were supposed to regulate unplanned and illegal activities in the floodplain region are either neglected or not carefully implemented as exemplified in areas close to the lower Niger Bridge. Generally, the regulatory and institutional framework re-establishes national responsibilities for risk mitigation by providing authority to respective government agencies and individuals to discharge certain responsibilities relating to agreed government measures.

II. Introduction and Promotion of Flood Disaster Risk Assessment.

The development of natural hazard risk assessments for selected areas and hazards, based on the analysis of historical events at these locations, can feed into probability distributions and predictions of likely future occurrences. To undertake a risk assessment, data on climate and land use change should be collected and analyzed on the assets and populations exposed in a given location. Probable damage scenarios, vulnerability models, and loss scenarios analyses are useful tools, which constitute key foundations for the development of preparedness actions and investments, as well as for risk financing options.

III. Curriculum Reviews and Promotion of Environmental Education.

There is an urgent need for the review and inclusion of disaster risk mitigation in the curriculum as aspect of environmental education at the primary and secondary schools' levels. Such inclusion will serve as catalyst to the public for enhanced people's level of awareness and response for safety. Also, the use of mass media (e.g., television, radio, schools), social media (e.g., Facebook, Twitter, WhatsApp, and e-mails), and community outreach programs can disseminate information on flood and allied disasters in various domains. Public awareness of various flood-risks also helps monitor developments on the ground and keeps authorities accountable for their actions in hazard risk management/ mitigation.

IV. Control, Approval, and Implementation of Building Plans.

Land use planning, flood-resistant designs and construction, building regulations and permitting systems, and enforcement of urban plans and building codes address the safety of future structures. These measures are particularly important in fast-growing and often unregulated developmental areas (urbanization). Spatial development plans and regulations for natural hazards, as well as enforcement of the existing or newly formulated building codes and regulations, are of key importance for mitigation against all hazards.

V. Reinforcement of Catchment Management Plans and Existing Dam Projects.

The sustainability of any flood management plan depends of the feasibility, utility, and adaptability of people to the standard engineering structures and rules. Investments toward enhancing flood prevention projects such as erecting seawalls, building safe houses, and constructing levees along the river bank especially in the South; improvement of reservoirs and dykes; retrofitting of existing dams for safety with larger spillways and gates especially in the

North; enlarging flood ways; building levees, flood walls, seawalls/ bulkheads; dam monitoring, reviews and revisions of operating rules for dams in Nigeria.

Contextually, frantic efforts can be focus on periodic reinforcement of existing engineering, infrastructure, and environmental structure to protect and mitigate the impacts of flood and allied disasters associated with a specific catchment. Proper feasibility and follow-up studies that incorporate economic, environmental, and social assessments should precede decisions on flood protection investments, accounting not only for historical frequency and loss data projections, but require a modified technical approach.

VI. Building Capacities for Flood Specific-Hazard Risks.

There is a need to build valid guidelines for flood disaster risks based on their distinct types and causative variables. The enhancement of capacities through flood hazard-specific capital investment can strengthen tools and equipment procurements for flood-risk communities. For example, the level of risk associated with a flash flood in the urbanized areas of World Bank/ Amakohia/ Akwakuma/ Uratta in Owerri axes of Imo State or Nnewi/ Awka/ Ekworobia/ Ihiala axes in Anambra State are not the same as the historic Ogunpa River or Oguta Lake flood. More so, promotion of insurance policies for flood risks and educating people on flood preparedness and response actions are effective and relatively low-cost measures, which Federal, State, and Local governments can pursue.

8. Conclusion and Recommendations

The preceding discourses on climate-induced flood disaster risk awareness in Nigeria indicated that the causative variables have a strong affinity with the changing patterns of weather and climate. Yet, the contemporary increase in negative impacts on the vulnerable elements is accelerated by the anthropocentric parasitism on the human environment. There is an urgent need for human activities in ecosystem to focus more on caring, protecting, loving, harmonizing, sustaining, and symbiotic for posterity; instead of the destructive and parasitic.

The perceived past neglect and/ or poor enforcement of valid environmental Laws and Regulations in Nigeria tend to promote human insensitivity to environmental protection thereby hampering the sustainability of sound future ecological systems. To eradicate the lapses, functional legislations need to be carefully enforced in distinct geographic regions and States in Nigeria. The areas of urgent attention, are those pertaining to land use ordinances, building codes, and colonization of prohibited spaces such as green belt, drainage channels, and grass verge for illegal structures. The flood disaster vulnerability mapping is not given the expected attention that is commensurate with the prevailing issues of climate variability and change. Such exercises can be sponsored by the government through its ministries, agencies, and donor organizations to facilitate the assessment of risks and identify actual/ potential mitigation measures, and viable action plans to guide future actions. Also, investments need to be prioritized, implement, administer, and sustain to promote appropriate ecological smart future and sustainable development.

References

[1] I.S. Umo. (2016). Flood disaster risk inventory in Southern Nigeria. A paper presented at a 3-day Seminar on Building Capacity for Disasters Emergency Management at Asaba, Delta State from 27th – 29th April, 2016.

[2] J.C. Nwafor (2006). *Environmental impact assessment for sustainable developments: The Nigerian perspective.* Enugu, El'Demark Publication.
[3] S. Doocy, A. Daniels, S. Murray, and T.D. Kirsh (2013). Human impacts of floods: A historical review of events 1980 – 2009 and a systematic literature review. *National Science Foundation's Human and Social Dynamic Program Grant Number 0624106.* Retrieved from http://www.current.plos.org/flooddisaster/article
[4] I.S. Umo, C.C. Ojinma and I.I. Orie (2015). Residents' perception of flash floods and its management challenges in ancient city of Aba, Abia State. *International Journal of Geography and Earth Science, 1*(6), 81 – 88.
[5] C.C. Ojinma, I.S. Umo, M.N. Obasi, and E. P. Ukaegbu. (2017). *Flash floods and household reactions toward safety among urban residents in the Southeast Nigeria.* A Completed Project for the 2014/2015 TETFund Institution Based Group Research.
[6] I.S. Umo and A.I. Enwereuzor (2021). The implications of area morphology and particulate matters' distributions on the Kwa Iboe River Basin restoration, Southeast Nigeria. *Journal Water Resources and Ocean Science, 10*(3), 53–60. http://dx.doi.org//10.11648/j.wros.20211003.13
[7] R. Akpofure. (2009). *Environmental science. An introduction*. Ibadan, Kraft Books.
[8] A. C. Emeribeole (2015). Managing flood disaster in Nigerian Cities: Issues and strategies toward meeting the challenges in the modern world– a case study of Owerri Metropolis Imo State, Nigeria. *FIG Working Week 2015: from the Wisdom of the Ages to the Challenges of the Modern World. Sofia, Bulgaria, 17th – 21st May 2015*
[9] A.L. Enwereuzor and I.S. Umo (2020). Environment: Issues, management, and sustainability. Owerri, Ekenegrace Publishers.
[10] I. Davis. and M. Wall (editors) (1992). *Christian perspectives on disaster management: A training manual*. Middlesex, International Relief and Development Association.
[11] J. Birkmann (2006). Measuring vulnerability to promote disaster-resilient societies: conceptual frameworks and definitions. In J. Birkmann (editor), *Measuring Vulnerability to Natural Hazards: Towards Disaster Resilient Societies*. United Nations University Press, Tokyo, Japan, pp. 9-54.
[12] M.K. Van Aalst, T. Cannon, and I. Burton. (2008). Community level adaptation to climate change: The potential role of participatory community risk assessment. *Global Envir. Change*, Vol. 18, PP. 165-179.
[13] O.H. Adedeji, B.O. Odufuwa, and O.H. Adebayo (2012). Building capabilities for flood disaster and hazard preparedness and risk reduction in Nigeria: Need for spatial planning and land management Journal of Sustainable Development in Africa, Vol. 14(1), pp. 45 – 58.
[14] J.J.I. Iwuchukwu. (2006). Environmental hazards management: Principles and procedures. Owerri, Cel-Bez Didactic Books.
[15] M.C. Marulanda, O.D. Cardona, and A.H. Barbat (2011). Revealing the impact of small disasters to the economic and social development. In: Coping with Global Environmental Change, Disasters and Security - Threats, Challenges, Vulnerabilities and Risks [Brauch, H.G., U. Oswald Spring, C. Mesjasz, J. Grin, P. Kameri-Mbote, B. Chourou, P. Dunay, and J. Birkmann (eds.)]. Springer-Verlag, Berlin, Germany.
[16] O.D. Cardona, M.K. van Aalst, J. Birkmann, M. Fordham, G. McGregor, R. Perez, R.S. Pulwarty, E.I.F. Schipper, E.L.F., and Sinh, B.T. (2012). Determinants of risk: Exposure and vulnerability. In Field, C.B. *et al*., (eds.), "*Managing the Risks of Extreme Events and Disasters to Advance Climate Change Adaptation*" A Special Report of the Working Groups I and II of the Intergovernmental Panel on Climate Change. Cambridge, Cambridge University Press, United Kingdom, pages 65-108.
[17] DKKV (2011). Adaptive disaster risk reduction – enhancing methods and tools of disaster risk reduction in the light of climate change. DKKV Publication Series no. 43, German Committee for Disaster Reduction, Bonn, Germany. www.dkkv.org/de/publications/schriftenreihe.asp?h=5
[18] Srinivas, Hari, (2020). Pre- and post-disaster management: environmental management tools to reduce disaster risks. GDRC Research Output - Management Tools Series E-118. Kobe, Japan: Global Development Research Center. Accessed from http://www.gdrc.org/uem/disasters/disenvi/tools/pre-post
[19] Warfield, C. (2008). The disaster management cycle.
[20] United Nations Development Programme (2008). Disaster management-preparedness methodology in Assam. http://data.undp.org.in/dmweb/Article-DRM%20Assam.pdf.
[21] National Emergency Management Agency (NEMA, 2012). Unpublished national disaster management framework. Pp. 1 – 19.
[22] J. Pollner, J. Kryspin-Watson, and S. Nieuwejaar (2010). Disaster risk management and climate change adaptation in Europe and Central Asia. Global Facility for Disaster Reduction and Recovery, World Bank. Pp. 1 – 66.
[23] T.E. Ologunorisa (2009). Strategies for mitigation of flood risk in the Niger Delta, Nigeria. Jour. of Applied Sciences and Envir. Mgt,, vol. 13(2), pp. 17 – 22.

NIPES Conference Proceedings
The 1st International Conference of the Nigerian Institution of Professional Engineers and Scientists 7th-8th Oct. 2021: 137-143
www.nipesjournals.org.ng

Suitability of Laterite Soil Reinforced with Periwinkle Shell and Palm Kernel Shell as Sub Base Materials in Road Construction in Edo State

Kayode-Ojo, N.[a] and Edeoghon, E. E.[b]
[a,b]Department of Civil Engineering, Faculty of Engineering, University of Benin, Benin city, Edo State, Nigeria.

Abstract

Pollution is a very predominant problem in Nigeria. As a developing nation, we face challenges of constant economic recession and this can have effect on so many facets of life including construction. In order to combat pollution and bad roads, waste can be used with other construction materials to construct better roads. The study was to investigate the suitability of laterite soil reinforced with a mixture of palm kernel and periwinkle shells as material for subbase course in road construction. The soil samples were obtained from a burrow pit at Iguosa Housing Estate, Benin City, Edo state. The geotechnical properties of natural soil were determined, which included specific gravity, mechanical sieve analysis, consistency limit, compaction, and California Bearing Ratio (CBR) tests. The strength properties of the soil reinforced with periwinkle shell (PS) and palm kernel shell (PKS) were carried out. These were done in proportions of 6%, 9%, 12% and 15% by volume. For the control sample, the average result of the specific gravity obtained was 2.47 which was below the standard of 2.50 to 3.0 for lateritic soils. The plasticity index was 19.49% which indicated that the soil is of medium plasticity. The sieve analysis indicated that the soil is classified as an A-2-6 soil. The Maximum Dry Density and the Optimum Moisture Content were 1.78 g/cm^3 and 10.3% respectively. The average value for the soaked CBR was 15.11%. When the soil was reinforced with equal proportion of PS and PKS, the OMC ranged from 11.30% to 11.70%, the MDD ranged from 1.73g/cm^3 to 1.75g/cm^3 and from the CBR tests, the value for the soaked CBR ranged from 1.26% to 23.21%. The optimum mix proportion was obtained to be 12%. This did not meet the requirement of 30% for subbase stated by the Federal Ministry of Works and Housing. Therefore, these soil reinforcement techniques with PS and PKS can only be used for Trunk D roads or as subgrade materials which require a minimum soaked CBR of 5%. For Trunk A, B and C roads, the mixture would require a binder like cement before being considered as subbase materials.

***Keywords*:** *Laterite soil, Palm Kernel Shell, Periwinkle Shell, Sub base, reinforcement*

1. Introduction

Soil is any natural loose mineral particle that may or may not be organic, lying over the bedrock that is formed by the weathering of rocks. The soil type that is predominant in Edo State is laterite [1]. Lateritic soils located in Nigeria have been used extensively in the construction industry as subgrade and sub-base materials for road construction and are usually found in different drainage and sub-climate environments. Lateritic soils found everywhere shows unique physical, chemical and engineering properties. Therefore, a comprehensive evaluation must be carried out on any lateritic soil to determine if it meets the requirements of lateritic soils, before its utilization for any engineering purpose [2]. How then can we employ laterite soil as main materials in sub-bases and base courses? By Soil reinforcement or stabilization. Almost all road construction projects would require soil stabilization of some sort. It has even been recommended for developing countries. The release of waste into the environment from agriculture, industries and homes is increasing at an exponential rate all around the world. In developing countries, there are no functional waste management and monitoring systems and consequently, environmental pollution has become a threat to the sustainability of the human race. At the same time, the economic recession has greatly affected construction in Nigeria and other developing countries. The cost of cement, coarse aggregates and other conventional building materials have caused contractors to use substandard materials for road construction. The growing concern of resource depletion and global pollution has challenged many researchers and engineers to seek and to develop new materials relying on renewable resources. These include the use of by-products and waste materials in building

construction [3]. Laterite soil is widely available in Edo State and is a potential material for road construction but it has some drawbacks. It consists of high plasticity that results in cracks and damage on building foundations, pavements and highway construction. For a material to be used as either a base course or sub-base course depends on its strength in transmitting the axle-load to the sub-soil and or sub-grade (the mechanical interlock) [4],[5]. So, there is a need to reinforce it with some aggregates. Palm kernel shells are abundant in palm oil-producing states in southern Nigeria. They are underutilized and are usually discarded or used on a small scale as fuel in furnaces and materials for filling potholes [6]. On the other hand, periwinkle shells are discarded after the edible parts are consumed by people in the coastal regions of Nigeria. These cause environmental pollution in that area [7]. The study was to investigate the suitability of laterite soil reinforced with a mixture of palm kernel and periwinkle shells as material for subgrade and subbase courses in road construction. If palm kernel shells and periwinkle shells are found suitable for construction, their large supply could be harnessed to reduce construction cost without undermining the strength/integrity of roads. This study has the potential for making sustainable roads from laterite reinforced with palm kernel shell and/or periwinkle shell which in turn would help to promote a cleaner environment. Periwinkle shells and palm kernel shells have been used by researchers in Nigeria for over 30 years as a conglomerate in concrete reinforcement, green concrete and asphaltic concrete [8],[9],[10],[11],[12]. However, in this study, palm kernel shells and periwinkle shells were used as a partial replacement for expensive coarse aggregates in sub-base and base course of flexible pavements in an area where laterite soil is abundant.

2. Methodology

2.1 Materials and Sample Preparation

The laterite soil was obtained from a burrow pit in the Iguosa Housing Estate Benin City Edo State Nigeria at 6°26’55’’N 5°36’16’’E. (Figure 1.0)

Commercially available periwinkle shells was air dried and broken into smaller bits (average of 6mm diameter) with pestle to reduce voids as shown in Figure 2.0 and the palm kernel shell (Figure 3.0)was obtained from a small palm oil producing corporation.

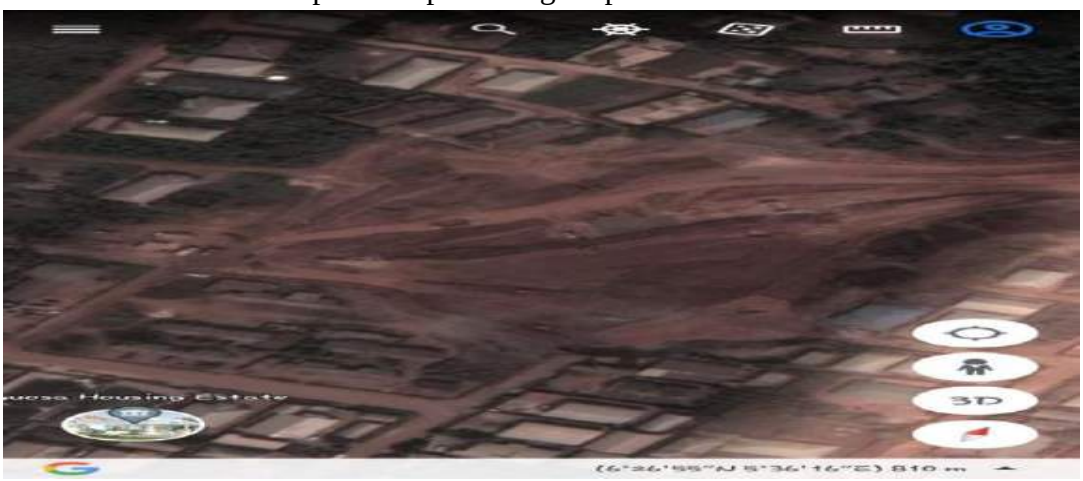

Figure 1.0: Location of the sample collection area (Google Earth)

Figure 2.0: Crushed Periwinkle Shell Sample

Figure 3.0: Crushed Palm Kernel Shell Sample

2.2 Laboratory Tests

The following tests were carried out on the laterite soil which is the control sample (CS) in accordance with the American Society for Testing and Materials (ASTM) standards and British Standards [13], [14].

1. Sieve analysis
2. Specific gravity test
3. Moisture Content test
4. Atterberg Limits test

When the soil was reinforced with a mixture of PKS and PS, these engineering tests were done:

1. Compaction test (Proctor test)
2. California Bearing Ratio (CBR) test

3. Results and Discussion

3.1 Control Sample

The summary of the mean results of the geotechnical engineering tests carried out on the control sample CS (soil only) are presented in Table 1.0.

Table 1.0: Summary of the geotechnical engineering test results (Control sample)

S/No	Laboratory Test		Result
1	Natural Moisture Content (%)		11.30
2	Specific Gravity		2.47
3	Atterberg Limit	Liquid limit (%)	39.12
		Plastic limit (%)	19.63
		Plasticity index (%)	19.49
4	Sieve analysis	Sieve size (mm)	Percentage passing (%)
		3.35	100
		2.36	96.5
		2.00	94.7
		1.18	86.1
		0.6	64.5
		0.425	54.9
		0.3	41.9
		0.212	30.2
		0.15	26.8
		0.075	23.1
5	Compaction	OMC (%)	10.3
		MDD (g/cm^3)	1.78
6	CBR	Top (%)	3.96

		Bottom (%)	15.11

From the sieve analysis, the percentage passing the 0.075mm sieve is 23.1%, the percentage passing the 0.425mm sieve is 54.9% and the percentage passing the 2.00mm sieve is 94.7%. From Atterberg limit test, liquid limit is 39.12%, the plastic limit is 19.63% and the plastic index is 19.49%. Since, the percentage passing 0.075mm sieve is less than 35% therefore it is a granular soil. The plasticity index is 19.49% and this shows the soil is of clayey type and has medium plasticity. Considering all other parameters, the soil is classified as an A-2-6 soil. Based on AASTHO specifications, soils in the A-2-6 class are good as subgrade materials [15].
The CBR for the bottom unsoaked was obtained to be 15.11% showing that it is suitable only to be used as subgrade material [16]. If it is to be used for subbase or base course, it would have to be stabilized or reinforced with other materials.

3. 2 Control Sample and PKS only

The summary of the results of the geotechnical tests carried out on the control sample reinforced with PKS only is presented in Table 2.0

Table 2.0: Summary of the geotechnical test results (Sample with Palm Kernel Shell - PKS)

S/No	Percentage Replacement (%)	Test		Result
1	6	Compaction	OMC (%)	9.80
			MDD (g/cm^3)	1.74
		CBR	Top (%)	7.43
			Bottom (%)	1.57
2	9	Compaction	OMC (%)	10.50
			MDD (g/cm^3)	1.68
		CBR	Top (%)	25.19
			Bottom (%)	13.38
3	12	Compaction	OMC (%)	12.0
			MDD (g/cm^3)	1.63
		CBR	Top (%)	16.60
			Bottom (%)	15.18
4	15	Compaction	OMC (%)	11.20
			MDD (g/cm^3)	1.68
		CBR	Top (%)	4.76
			Bottom (%)	6.11

From Table 2.0, no linear relationship was observed between increase in CBR and increase in the quantity of stabilizer added. The OMC reduced in each sample except in the sample with addition of 12% PKS to the natural soil as compared to the control sample with OMC of 11.30%. No sample reinforced with PKS has a higher MDD than the control of 1.78. The maximum CBR was obtained in the sample with 9% PKS with a value of 25.19% at the top. According to the Federal Ministry of Works and Housing, this value is below the minimum requirement of subbase material. Hence, it cannot be used as subbase on Trunk A roads and can be used as subbase in Trunk D (rural) roads.

3. 3 Control Sample and PS only

Table 3.0 shows the summary result of the geotechnical engineering tests carried out on the control test reinforced with PS only.

Table 4.3: Summary of the geotechnical test results (Sample with Periwinkle Shell - PS)

S/No	Percentage Replacement (%)	Test		Result
1	6	Compaction	OMC (%)	10.70
			MDD (g/cm^3)	1.79
		CBR	Top (%)	6.30
			Bottom (%)	6.35
2	9	Compaction	OMC (%)	10.90
			MDD (g/cm^3)	1.83
		CBR	Top (%)	8.42
			Bottom (%)	3.63
3	12	Compaction	OMC (%)	11.10
			MDD (g/cm^3)	1.80
		CBR	Top (%)	7.35
			Bottom (%)	3.06
4	15	Compaction	OMC (%)	10.80
			MDD (g/cm^3)	1.83
		CBR	Top (%)	9.08
			Bottom (%)	4.95

From Table 3.0, it can be seen that there is no linear relationship was observed between increase in CBR and increase in the quantity of stabilizer added. No Sample has OMC greater than the OMC of the control sample of 11.30% but there was an increase in the MDD of each Sample stabilized with PS. The maximum CBR was obtained in the sample with 15% PS with a value of 9.08% at the top. According to the Federal Ministry of Works and Housing, this value is below the minimum requirement of subbase material. Hence, it cannot be used as subbase on Trunk A roads and can be used as subbase in Trunk D (rural) roads.

3. 3 Control Sample with PKS and PS

Presented in Table 4.0 are the summary of the results of the geotechnical tests carried out on the control sample reinforced with a mixture of PKS and PS in equal proportions

Table 4.0: Summary of the geotechnical test results (Sample with Periwinkle Shell and Palm Kernel Shell added in equal proportions)

S/No	Percentage Replacement (%)	Test		Result
1	6	Compaction	OMC (%)	11.70
			MDD (g/cm^3)	1.74
		CBR	Top (%)	7.43
			Bottom (%)	1.26
2	9	Compaction	OMC (%)	11.40
			MDD (g/cm^3)	1.75
		CBR	Top (%)	15.93
			Bottom (%)	4.77
3	12	Compaction	OMC (%)	11.30
			MDD (g/cm^3)	1.73
		CBR	Top (%)	23.21
			Bottom (%)	9.32
	15	Compaction	OMC (%)	11.30
			MDD (g/cm^3)	1.73
		CBR	Top (%)	8.51
			Bottom (%)	2.81

From Table 4.0, no sample had OMC less than the OMC of the control sample of 11.30% but the minimum MDD was obtained as 1.73 g/cm^3.The maximum CBR was obtained in the sample with 6% PS and 6% PKS (Mix) with a value of 23.21% at the top. According to the Federal Ministry of Works and Housing General Specification for Roads and Bridges, Volume II, this value is below the minimum requirement of subbase material. Hence, it cannot be used as subbase on Trunk A roads and can be used as subbase in Trunk D (rural) roads.

4. Conclusion

From the critical examinations and analyses, it can be concluded that the appropriate mix ratio for the natural soil and the mixture of PS and PKS, is 6%. The use of soil reinforced with PKS and PS for subbase should be restricted to Trunk D roads. PS and PKS increase CBR of the soil but not in substantial amounts so a binder e.g. cement can be added to make it suitable for its use in the subbase and basecourse of the road.

Nomenclature

AASHTO	American Association of State Highway and Transportation Officials
ASTM	American Society for Testing and Materials
PKS	Palm Kernel Shell
PS	Periwinkle Shell
LL	Liquid limit
PL	Plastic limit
PI	Plastic index
CBR	California Bearing Ratio
MDD	Maximum Dry Density
OMC	Optimum Moisture Content

References

[1] Imhangulaya, C. (2016). Geomorphology and Hydrology of the Benin Region, Edo State, Nigeria. International Journal of Geosciences. 07. pp144-157.
[2] Enaworu E., Ugbe F. C. Rotimi O. J., Ameloko A. A. (2017). Geochemistry and Geotechnical Analysis of Lateritic Soils in the Anambra Basin. Electronic Journal of Geotechnical Engineering, pp 4395- 4413.
[3] Adewuyi P., and Adegoke T. (2008). Exploratory study of periwinkle shells as coarse aggregates in concrete works. ARPN Journal of Engineering and Applied Sciences Vol (6) pp 1-6
[4] Oke, S. A., Amadi, A. N., Abalaka, A. E., Nwosu, J. E. and Ajibade, S. A., (2009). Index and Compaction Properties of Laterite Deposits for Road Construction in Minna Area, Nigeria. Nigerian Journal of Construction Technology and Management, 10 (1&2), pp28-35.
[5] Nwankwoala, H.O., Amadi, A.N., Ushie, F.A. and Warmate, T., (2014). Determination of Subsurface Geotechnical Properties for Foundation Design and Construction in Akenfa Community, Bayelsa State, Nigeria. American Journal of Civil Engineering and Architecture, 2 (4), pp130-135.
[6] Owolabi, A.O. and Dada, M.O. (2012). Cocoa pod and palm kernel shell ashes as partial replacement of Portland cement in stabilizing laterites for road construction, Journal of applied science and technology, vol. 17, no. 1 &2, pp. 53-57.
[7] Joseph O.A., Kehinde O., Ogundipe K.E. (2018). Geotechnical Properties of Lateritic Soil Stabilized with Periwinkle Shell Powder, International Journal of Civil Engineering and Technology Vol 10 (1) pp 2014-2025
[8] Olufemi I.A. and Joel M. (2009). Suitability of Periwinkle Shell as Partial Replacement for River Gravel in Concrete. Leonardo Electronic Journal of Practices and Technologies, Issue 15, pp 59-66.
[9] Salmabanu L., Ta-Wui C., Ismail L.(2019). Incorporation of natural waste from agricultural and aquacultural farming as supplementary materials with green concrete: A review. Elsevier Composites Part B: Engineering, Vol 175

[10] Santhanam N., Ramesh B., Joshua S., Joshua R.P.(2019). Experimental study on use of E-waste plastics as coarse aggregate in concrete with manufactured sand. Materials today Proceedings. Vol 22, Part 3. pp 715-721.
[11] Ndoke, P.N. (2006). Performance of Palm Kernel Shells as a Partial Replacement for Coarse Aggregate in Asphalt Concrete. Leonardo Electronic Journal of Practices and Technologies Issue 9 pp 145-152.
[12] Okpala D.C. (1990). Palm Kernel Shells as a lightweight aggregate in concrete. Building and Environment. Vol 25, Issue 4. pp 291-296.
[13] ASTM International (2006). Standard Practice for Classification of Soils for Engineering Purposes (Unified Soil Classification System), pp 12.
[14] BS 1377-1:1990. Methods of test for soils for civil engineering purposes. General requirements and sample preparation.
[15] AASHTO Guide for Design of Pavement Structures (1993): American Association of State Highway and Transportation Officials.
[16] Federal Ministry of Works and Housing. (1997). General Specification for Roads and Bridges, Volume II, Federal Highway Department, FMWH: Lagos, Nigeria, pp317.

NIPES Conference Proceedings
The 1st International Conference of the Nigerian Institution of Professional Engineers and Scientists 7th-8th Oct. 2021: 144-159
www.nipesjournals.org.ng

Serverless Computing Technology: Issues Toward its Adoption

F. O. Oliha*

Department of Computer Science, University of Benin, Nigeria. e-mail: oliha_festus@uniben.edu

Abstract

The pay-as-you-go model of existing cloud services has flagged the necessity for serverless technology as an extension of the cloud computing paradigm to provide support for building cloud applications as functional units executed per running time. The transition from cloud-based to serverless is somewhat slow sequel to inadequate techno-exposure, the swift techno-emergence, and the tech-know-how to deploy serverless applications by cloud solution developers and service consumers. To plug these techno-barriers, the paper explores and exposes the foundations of serverless computing with objectives to combine, explicate, and buttress trending research with ample clarity, a vital point of view on serverless technologies, their impact, services, applications, deployment, and challenges toward adoption by developers and consumers of cloud application services. A sample walkthrough of a serverless application was built to demonstrate the technical know-how of serverless technologies to fascinate cloud-based application developers towards embracing its services in building cloud applications as function units deployed and billed per-use-time contrary to the conventional pay-as-you-go model.

***Keywords*:**
Services Computing, Cloud Computing, Serverless Computing, FaaS, Serverless Architecture, Serverless Application

1. Introduction

Cloud services have over time been credited with increasing competitiveness through cost reduction, elasticity, greater flexibility, and optional resource utilization thereby adapting consumable platforms with easy and readily available services. Interestingly, Cloud Computing has gained popularity by its virtualization of computing resources for cloud application developers. Resources like Infrastructure, Platforms, and Software have been virtualized as services thereby increasing consumers' services options toward many resources without up-front cost or elasticity [1]. The pas-as-you-go model is being powered by cloud service and providers – Amazon, Google, IBM, Adobe (AWS, GCP, IBMC. ACC), etc., and more are in the technological advancement.

Users are opened to several solutions for the deployment of their cloud applications at a scalable dependent service. One major concern hitherto is the cost of idleness in running their cloud applications; on the other hand, cloud developers are saddled with the burden of scaling in regards to operations, management, availability, and fault tolerance. These challenges have given rise to Serverless computing – the extension of the cloud computing model to provide support for the development of scalable independent microservices without having to worry about provisioning and utilization of cloud resources [1,2].

Serverless Computing extends the promises of Cloud Computing – the pay-as-you-go model, to deliver a true pay-only model for consumed services with almost infinite scalability while hiding the details of resource provisioning and utilization. It favors cloud developers with the provision of small self-contained units of computation to easily manage and scale in the cloud. This indicates that serverless means pay on delivery and not paying for idleness. Recent studies exposed that Serverless Computing is witnessing technological advancement across the entire cloud computing paradigm and it has emerged as a fresh paradigm for developers of cloud applications to deploy applications as containers or microservices. [1,2,3,4,5].

A lot of cloud developers are exploring the emerging serverless technology with apt benefits in deploying cost-effective services on the cloud. Developing serverless services allows developers

to reduce server-related overheads and reclaim resources with focuses on core development and a cultivated deployment initiative. The advantage it brings to the computing paradigm is visible in its pay-per-running-time model, and it has been the key indicator in adopting the paradigm for developers and service consumers. With its containerization approach, developers now deploy cloud applications as a piece of code running as functions. Thus, serverless technologies have broadened cloud application services and the invocation of serverless functions has increased with a remarkable transactional use but the shift towards its adoption is yet a challenge for many developers in the transitional chain to serverless computing paradigm. This paper focuses on its technologies and issues affecting its adoption despite what it has to offer. The remaining sections discuss milestones in achieving the study's objectives.

2. Review of Concepts

This section discusses reviews on serverless computing with respect to granular knowledge on its definitions, technologies, platforms, and architecture. Serverless Computing is the emerging trend birthed from cloud computing and it has received various but similar views in recent times. With regards to event-based server-side code and stateless functions, its concepts have been defined in similar ways while projecting its prospects in varying articles and literature.

2.1 Serverless Computing

Defining Serverless Computing, [4] referred to it as "FaaS – Function as a Service, which is essentially a stateless computing container that is event-triggered and lasts for a single invocation". This definition was based on resource provisioning, allocation and function invocation. On the notion of server scaling, [1], noted that *"Serverless computing is a platform that hides server usage from developers and runs code on-demand automatically scaled and billed only for the time the code is running"*. They emphasized two key aspects in their view of definition which pinpoints cost and elasticity. Cost – denoting that services are only billed at times when running and unbilled when idled. Elasticity – denoting the scaling of servers by cloud providers which is abstract to developers.

In the views of [6], "*Serverless Computing, also known as Functions as a Service, is a new approach to cloud computing that allows programmers to run event-driven functions in the cloud without the need to manage resource allocation or configure the runtime environment*". In their view, they emphasized the technology's capabilities to easily write robust and large-scale web services – microservices to be deployed as serverless functions. Also, [7], summarized that Serverless Computing "is an event-driven computing model or code execution where underlying infrastructure (including physical and virtual hosts, virtual machines, containers as well as operating systems) is abstracted from the developer and the service consumer". In this view, cloud applications execute as stateless containers running on the instance of an event triggering where their logics are encapsulated and deployed as functions running on the cloud provider's containers.

On a contrary view, [8], emphasized that *"serverless computing provides a programming model that is not simply elastic, in the sense that humans or scripts can add and remove resources as needed*". Their emphases were centered on "autoscaling" and that a serverless application is not just FaaS-based but with a supported standard/proprietary library. On the latter, they stressed that serverless computing has brought about a step forward and two steps backward as they quibbled its autoscaling potentials in current computing trends. However, this paper sees Serverless Computing as small stateless and event-driven functions as a service where computational services are deployed as a unit of functions in the cloud. Its FaaS nature conceptualizes services as

functions for consumers at the expense of running time only. Thus, a look at its architectural build-up will broaden the comprehension.

2.2 Serverless Architecture and Computing Technologies

From a developer's perspective, serverless architecture entails applications built using custom code (functions) that run on a stateless, managed FaaS platform, and typically orchestrated by events [5] Figure 1 depicts components of the architecture.

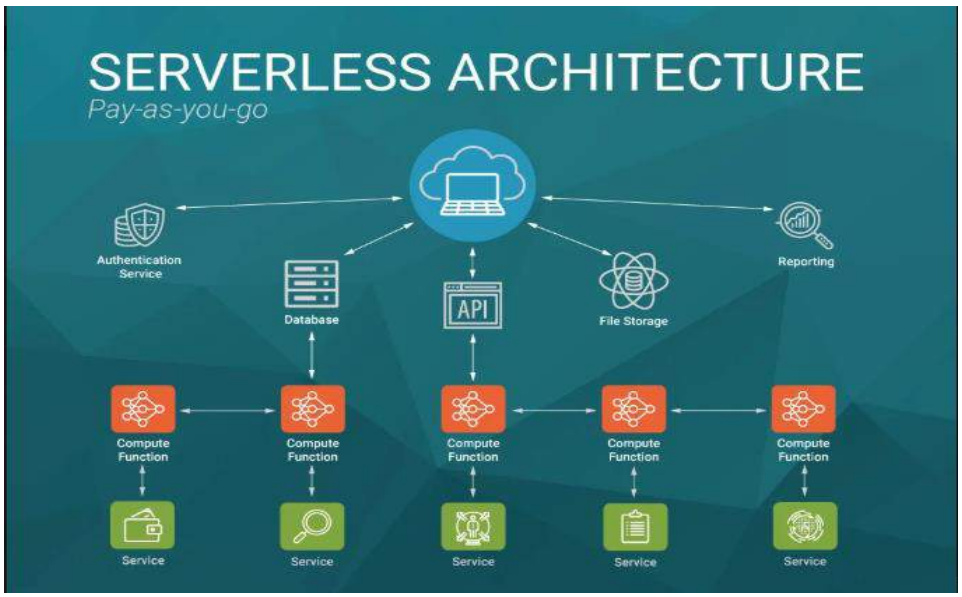

Figure 1. Serverless Architecture [18].

The building blocks of serverless computing has been highlighted in work of literature [5,9,10]: "API Gateways – *a communication layer between the frontend and the FaaS layer*; Backend as a Service (BaaS) – *is essentially a cloud-based distributed NoSQL database which essentially removes database administration overheads.* BaaS *features include cloud storage, push notifications, server code, user and file management, and many other backend services*; FaaS – *is the layer that executes specific business logic (or code) with the cloud provider providing the level of abstraction in terms of executing the business logic"*. It is seen as the core of serverless computing and is sometimes interchangeably used.

2.3 Platform Providers for Serverless Computing

Different cloud providers have emerged to provide environments in aiding cloud developers in deploying successful serverless applications. [10], noted that "major serverless platform providers are:

i. **Amazon Lambda**: This is a serverless function platform provided by Amazon Web Service (AWS). Amazon Web Services introduced the first serverless computing platform, AWS Lambda, in 2014, and similar abstractions are now available from all major cloud providers[6]. Amazon Lambda is the most mature serverless platform on the market. It supports a variety of programming languages including Java, Python, and Node.js. Lambda takes advantage of most AWS services and allows developers to apply its functions as event handlers as well as to provide glue code when composing services [10].

ii. **Microsoft Azure Functions:** This serverless platform is provided by Microsoft. It lets developers write code for functions like processing images, sending emails, and maintaining files that are executed on schedule or when needed. The platform provides HTTP webhooks, integration with Azure, and support for such programming languages as .NET, Go, Node.js, Python, PHP, and Java. The runtime code is open-source and is available on GitHub under an MIT License [10].

iii. **Google Cloud Functions:** It is a computing platform that provides basic FaaS functionality to run serverless functions written in Node.js in response to HTTP calls and events from Google Cloud services. It provides development tools such as prediction APIs, translation APIs, and data storage [10].

iv. **IBM Cloud Functions:** This is another serverless deployment that acts as an event action platform for creating composite functions. It supports Node.js, Java, Swift, Python, and arbitrary binaries embedded in a Docker container. Cloud Function is based on OpenWhisk, which is available on GitHub under an Apache open-source license".

Several other emerging serverless providers are shown in Figure 2.

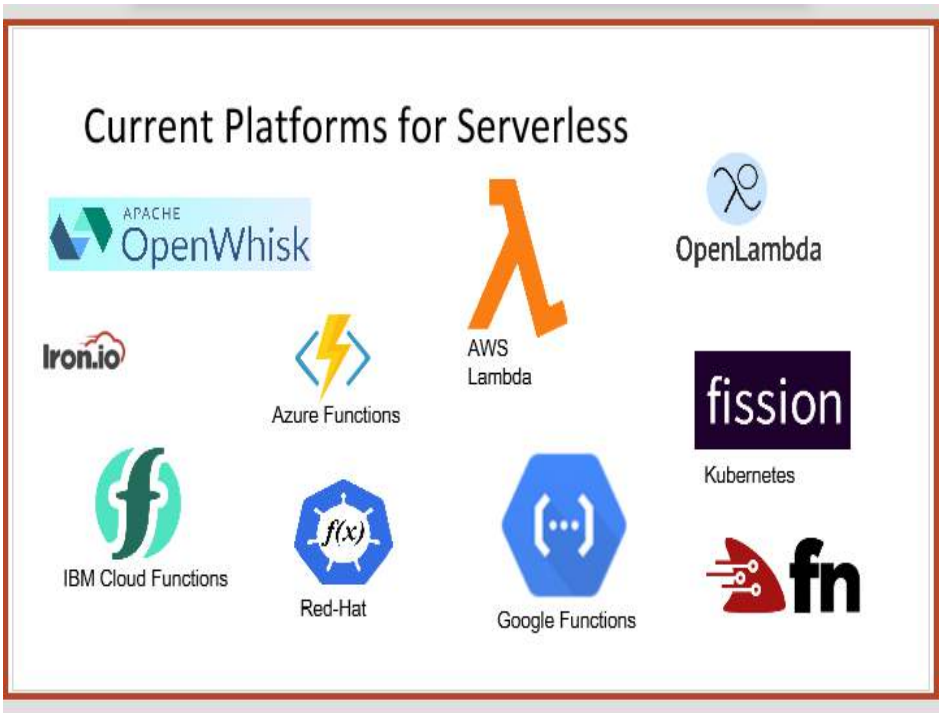

Figure 2. Platform Providers for Serverless Computing [11].

3. Technological Applications and Issues

3.1 Serverless Application Use Cases

Several use-cases have experienced computing edges via serverless approaches as a result of their economical simplicity [12]. Serverless architecture is applied in developing serverless specific applications and commonly used cases are as depicted in Figures 3 - 5.

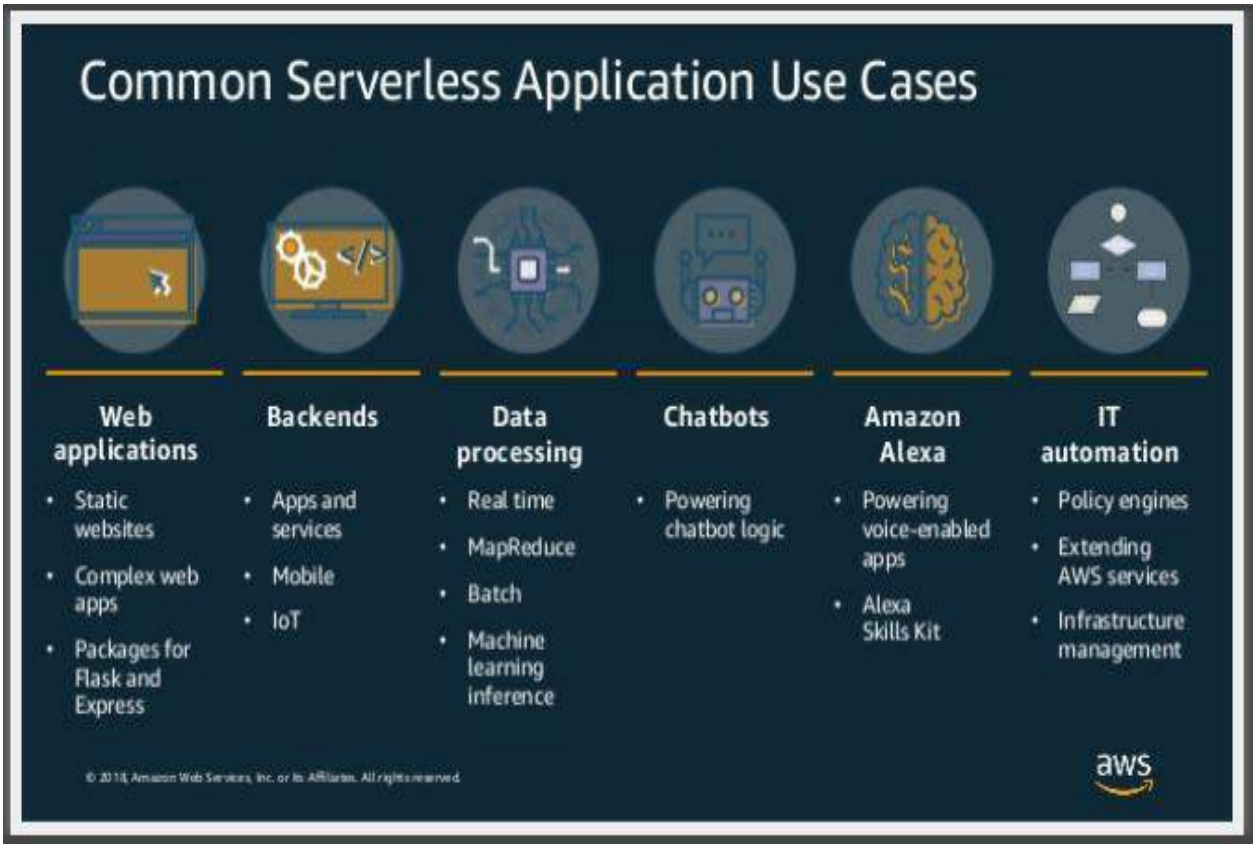

Figure 3. Serverless Application Use-Cases [11].

According to [4] "FaaS-suggested usages are similar across providers and can be generalized into *data-processing* and *backends.* Specifically, the following use cases are mapped to the provider's capabilities:

i. The advertised solutions for **AWS Lambda** are data real-time file processing, real-time stream processing, data transformations, and backends for Internet-of-Things, mobile, or web applications.

ii. Based on Microsoft's suggestions, **Azure Functions** can be used to implement web applications, APIs, microservices, machine learning workflows, data processing pipelines, and real-time processing applications.

iii. **Google Cloud Functions** are suitable for implementing application backends, real-time data processing systems, and intelligent applications".

Each serverless platform provider is dominant in application-specific domains peculiar to their platform capability. Despite serverless applications in dominant use cases like web applications, backends, data processing, chatbots, Amazon Alexa, and IT automation; there are instances where serverless can and cannot be applied as captured in Figure 5. It is most suitable for ephemeral stateless event-driven applications and practically not too suitable for long-lasting stateful applications. Figure 6 shows its building blocks and services.

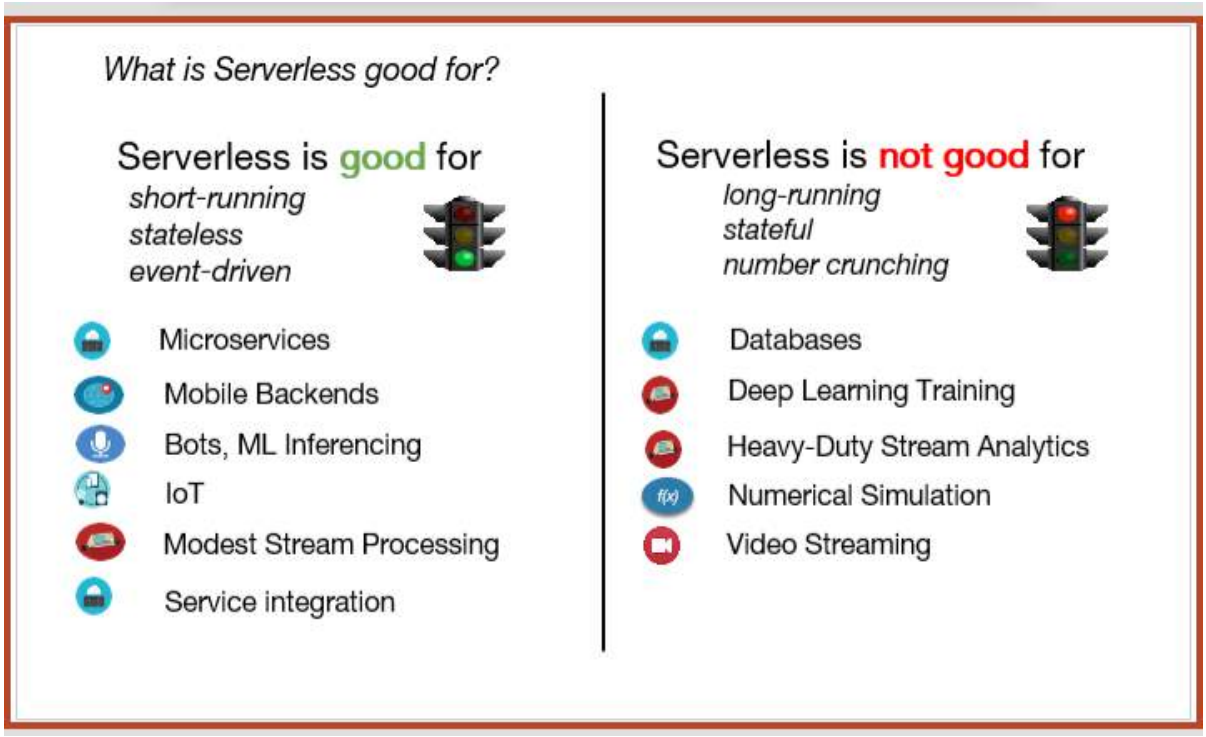

Figure 5. Serverless Application Use Cases [11].

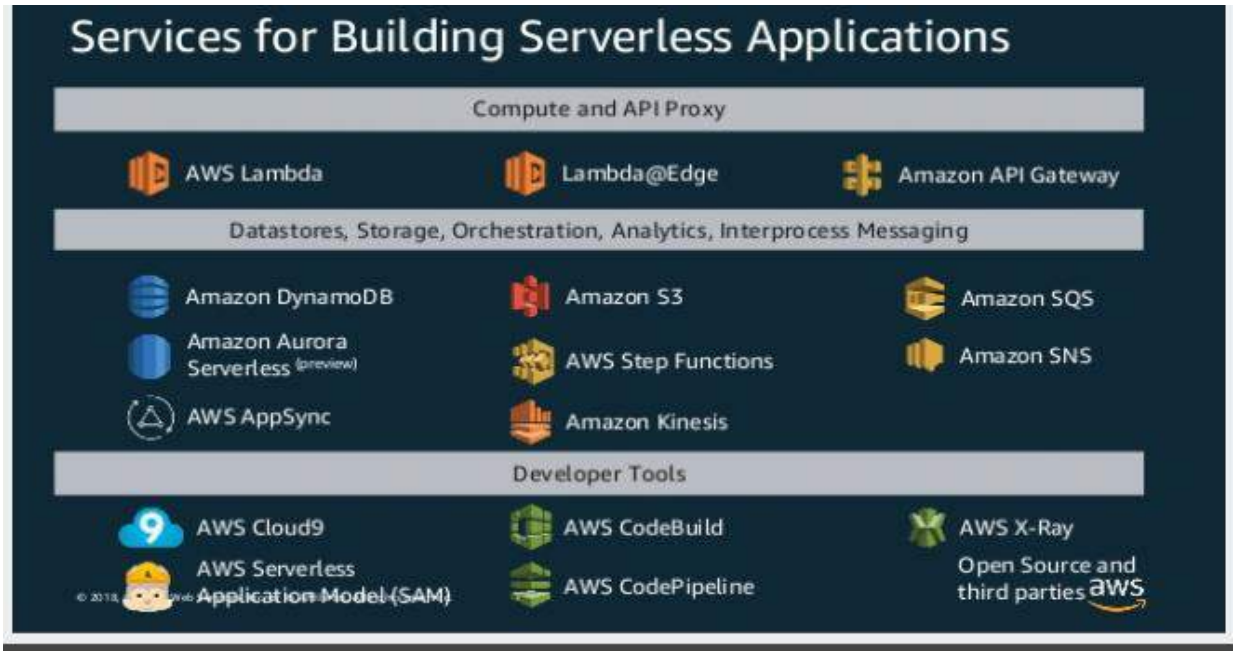

Figure 6. Service for Building Serverless Applications [11].

3.3 Open Challenges Toward its Adoption

The serverless architecture, regardless of its benefits, is associated with some concerns for developers and service consumers, making it a challenge for its slow adoption for building a true pay-as-you-use application for cloud services. These concerns are identified in works of literature and are categorized as follows [1,2,8,12]:“

i. **Vendor lock-In:** This is a portability concern where a serverless application running on one provider's serverless infrastructure will require additional re-engineering to be transferred to another provider's serverless infrastructure. Portability needs requirement change for multitenancy operations. That is, a serverless application written in the AWS platform can only run in such provider's platform, except it is modified to run in another. This issue is a major challenge to developers, and the thought of rewriting or modifying functions to run on multiple platforms is weighing on its fast adoption.

ii. **Tools and Frameworks:** another issue affecting the adoption is that of technologies and frameworks which are yet flexible and open-sourced to many developers. As serverless is an emerging technology, the development frameworks are yet unpopular, which raises great concern for application developers. According to [12], *The lack of proper modeling paradigms leads to non-unified development approaches which will reduce the quality of the code and also complicate collaborations of developers in long term.* Thus, tools and frameworks are yet ready to support the shift from traditional cloud-based applications to serverless applications for developers.

iii. **Startup Latency and Cold Starts:** Startup latency in FaaS is usually a result of a cold or warm start. When events are triggered, concerns are usually on cold start startup latency due to the creation of a new function instance. Also, with serverless ability to scale to zero to avoid payment for idle time, there may be overhead in invocation latency resulting from a cold start. These incur overhead usually vary from [9]: the language you use, how many libraries you're using, how much code you have, the configuration of the serverless function environment itself.

iv. **Data Loss:** It is easy to write a serverless function that produces incorrect results or leaks confidential data when reused. Terminate function instances when they are idle can lead to data loss if the programmer is not careful [6].

v. **Resource Limits:** Serverless computing imposes limits on memory, function execution time, bandwidth, and CPU usage. For instance, the maximum execution time per request is 300 seconds (or 5 minutes) for Azure Functions and AWS Lambda.

vi. **Increased Security Concerns**: There are high-security risks in a serverless environment, as many users run their functions on a shared platform. Thus, if someone loads malicious code, it may negatively affect all cloud users.

vii. **Function State:** While real applications require state, it's not clear how to manage state in serverless functions, as they're stateless. FaaS is stateless because it can't be guaranteed that the state is persistent across multiple invocations.

viii. **Multi-tenancy Concerns**: In addition to your application, a serverless provider also supports other clients. Thus, there's a risk that your software will be placed on the server along with function-heavy applications that may cause slow performance.

ix. **Sharing and Intra-communication**: Serverless applications are composed of functions that need to work together to achieve the application's desired functionality. In today's serverless infrastructures, two (Lambda) functions can only communicate through an autoscaling intermediary service; today, this means a storage system like S3 which is radically slower and more expensive than point-to-point networking [8]". There is bound to be a function addressing problem and that of Intra-communication for functions.

3.4 Remedies for Concerns

As at the time of this work, some of the suggested remedies but not limited to help hasten the adoption were highlighted as follows:

- **Function Instance Reuse:** A cold startup latency can be curbed as a "warm start" and can be introduced as a remedy. This according to [9], "involves the reuse of an instance of a serverless function and its host container from a previous event". Practically, the reuse of an instance of the same function can help to reduce latency in any serverless environment.

- **Availability of Skills**: as an emerging technology, cloud developers are still in the grey to shift to serverless applications as [9], stressed also that "serverless computing is a fairly new business, so there's a lack of developers on the market with skills in serverless programming. Software companies may have to invest in training their developers to catch up with new business trends".

- **Persistent State:** [13], opined that "Storing state external to a stateless FaaS could enable many important applications and allow big datasets to trigger multiple microservice-based FaaS invocations".

These are a few of the many setbacks that have led to the slow adoption of serverless computing by cloud developers. However, its benefits outweigh these setbacks.

3.3 Benefits

Unburdened in brevity by the highlighted issues in the prior section compared to other cloud computing services, serverless computing offers different tradeoffs regarding cost, control, and flexibility [2]. These tradeoffs provide consumers (cloud developers) the advantage of putting more focus on business logic instead of provisioning and managing servers, amongst other things. In addition, other benefits identified in the literature have been highlighted as follows [2,5,9,14]:

i. **Reduced Costs:** According to [14], "Serverless computing reduces the cost of developing and deploying features because it reduces operational and development costs, lowers the cost to scale applications and provides a more dynamic pay-as-you-go model. Serverless computing is based on the principle of pay-as-you-go. It costs nothing when your application doesn't run. Developers pay only for the time when their application executes a user's functions in response to specific events or requests. This model greatly benefits developers, as they can significantly save ***cloud costs***. It also aids in reducing ***development costs*** for developers as there's no need to handle updates or infrastructure maintenance.

ii. **Elastic Scalability:** Developers no longer need to purchase additional infrastructure for handling unexpected growth as serverless architecture can scale up and down according to application workload, this is achieved by replicating functions. The cloud service provider manages infrastructure, which means services can scale faster than before, automatically scaling up to accommodate many concurrent users and scale down when traffic subsides.

iii. **Improved Resource Management**: Applications developed in serverless environments are more fine-grained. This means that the cloud provider can closely match abstract demand to actual system resources. When an application doesn't run, the cloud provider distributes the server resources among other running applications. Once a triggering event appears, resources are allocated to execute the function. There will be no extra resources so you do not need to pay for resources not used.

iv. **Fewer Responsibilities for Developers**: In the serverless model, the cloud provider has more control over resources and more insight into the context of application behavior. Developers don't need to care about workload intensity, resource distribution, scaling, and application deployment as these issues are in the hands of the cloud provider.

v. **Faster Releases and Reduced Time to Market:** To deploy new functions, developers just need to compile their code, zip it, and upload it to the serverless platform. There's no need to write any scripts to deploy functions. This leads to faster releases and time-to-market reductions of up to two-thirds according to a study by Microsoft.

vi. **Agile-friendly Development:** Serverless computing allows developers to concentrate on application code rather than infrastructure maintenance. Moreover, it benefits developers through reduced software complexity and better code optimization. For instance, if an application usually takes one second to execute an operation with a hardware server, in a serverless environment it may take only 200 milliseconds, so developers can save 80 percent of their costs.

vii. **Multi-language Support**: Currently, some serverless platforms support multiple programming languages, so developers can choose the most convenient for them.

viii. **Built-in Logging and Monitoring Mechanisms**: Serverless providers have developed their solutions for user logging and monitoring that eliminate the need for developers to purchase third-party tools for similar purposes. In addition, serverless providers offer function-level auditing that ensures the application data privacy that's necessary for full GDPR compliance".

To justify the serverless extension of the cloud computing technology and expose its benefits over the challenges, a sample walkthrough of a serverless application was built to demonstrate functions as services in emerging computing technology.

4. Building a Serverless Application – A Sample Walkthrough

AWS is considered for this walkthrough as it is the most popular and widely used serverless platform by developers. AWS provides several services in order to build and deploy a serverless application. Figure 7 shows the steps required in deploying a serverless application.

```
# Step 1. Install serverless globally
$ npm install serverless -g
# Step 2. Login to your Serverless account
$ serverless login
# Step 3. Create a serverless function
$ serverless create --template hello-world
# Step 4. Deploy to cloud provider
$ serverless deploy
# Your Function is deployed!
$ http://xyz.amazonaws.com/hello-world
```

Figure 7. Steps in Building and Deploying a Serverless Application [11].

To demonstrate a sample walkthrough of a serverless web application, using AWS Platform, the following services will be highlighted [11] – "AWS CodeStar, AWS Cloud9, and Node.js:

- **Cloud9** is a cloud IDE for writing, running, and debugging code. Cloud9 comes prepackaged with essential tools for many popular programming languages (JavaScript, Python, PHP, etc.) so you don't have to tinker with installing various compilers and toolchains.

- **AWS CodeStar** is a software development tool that enables you to quickly develop, build, and deploy applications on AWS. With CodeStar, you can set up your continuous delivery toolchain in minutes, allowing you to start releasing code faster.

- **Node JS** is an open-source platform for building server applications with JavaScript with support for writing command-line tools for server-side scripting, typically to create dynamic web pages [15]. The advantage of using Node.js for serverless application development is centered on the fact that, when you deploy a Node.js application as a serverless function, resources are allocated on the fly to run your code when a specific event is triggered. You don't have to provision or pay for server resources upfront — these resources will be created for you by your cloud provider when, and only when, your code needs to run".

4.1 Creating a Default Serverless Application Using AWS Platform and Resources

To use this platform,

- Get a user account and role in AWS which are required in gaining access to AWS Lambda Functions. Obtaining this access, navigate to the AWS console to access your CodeStar IDE and select your project to start your application development with the support of creating a service role for you.

- Select the template with AWS Lambda and Node.Js for building web apps as depicted in Figure 8.

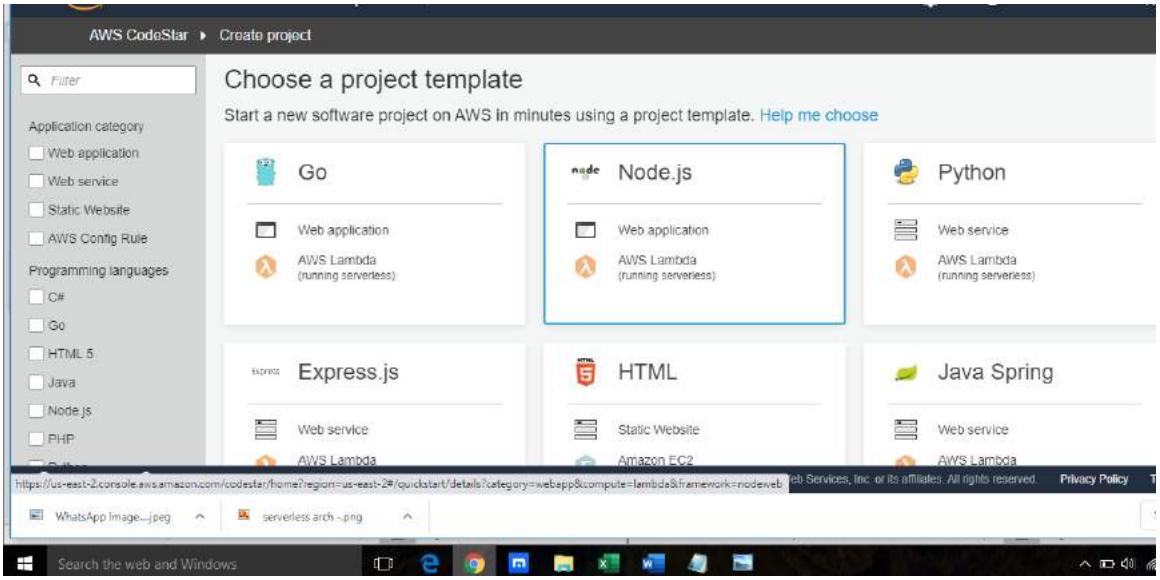

Figure 8. Project Template.

- enter Project Details – enter *obuaya-nodejs-sls-app* for the name of the project and select **AWS CodeCommit**, then select Next and select **Create Project**, afterwards, select **AWS Cloud9** as your editor on the Set-up tool. With this, an instance of the project application is generated – ***t2.micro*** as depicted in Figure 9. The Cloud9 IDE will run on this instance and it will be accessible via a client web browser.

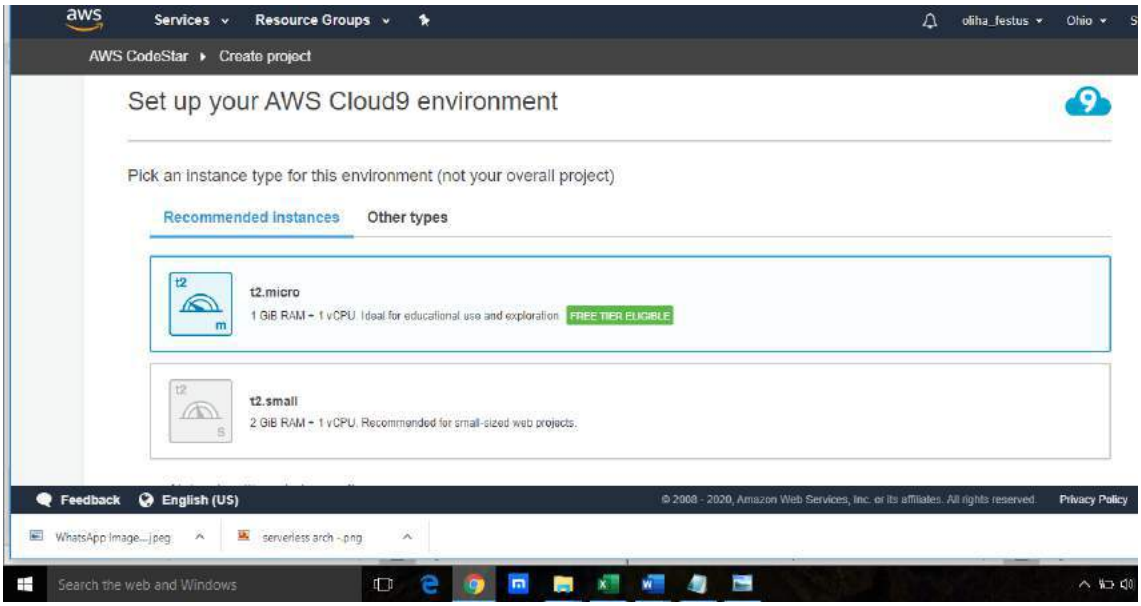

Figure 9. Configure Cloud9 Editor with an Instance of the Application.

- The project is then set up in connection to an IDE – Cloud9, by CodeStar. The setup is a complete continuous integration pipeline using CodeCommit for version control, AWS CodeBuild to build and test, and AWS CloudFormation for deployment to Lambda. Additionally, CodeStar will use Amazon CloudWatch to monitor your application.

- In a few minutes, the name of the project (*obuaya-nodejs-sls-app*) with complete set up for runtime and editor are all generated with an application service endpoint or API which in this case is "https://8uhuqvfurj.execute-api.us-east-2.amazonaws.com/Prod/". This serverless app is ready and executed via the endpoint in a web browser as seen in Figure 10.

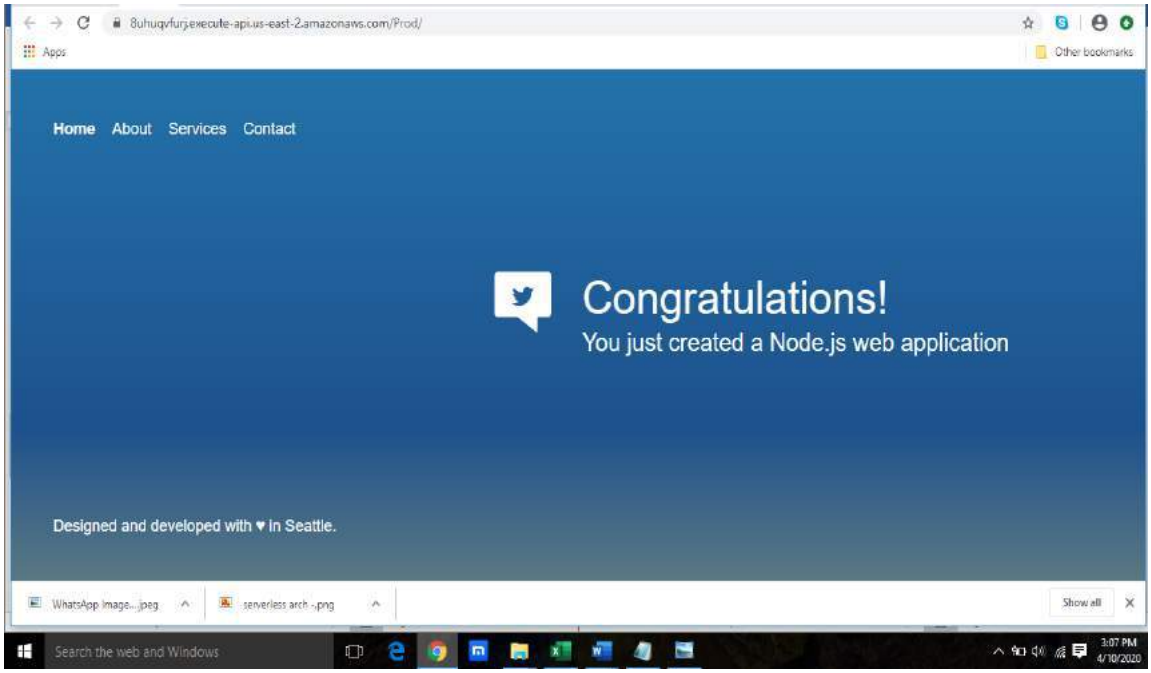

Figure 10. Serverless Application Deployed

4.2 Modifying the Default Serverless Application

This section is vital for developers in order to make suitable changes to the default Node.Js serverless application. Modification can be done on the Cloud9 IDE environment by following the steps below:

- Select the **start coding** from the CodeStar Dashboard to enable a git repository clone of the application into the coding environment via the command - *cd /home/ec2-user/environment/obuaya-nodejs-s*. Highlight the *index.html* file and the Cloud9 IDE imports it to a coding interface with your global username and email as depicted in Figure 11.

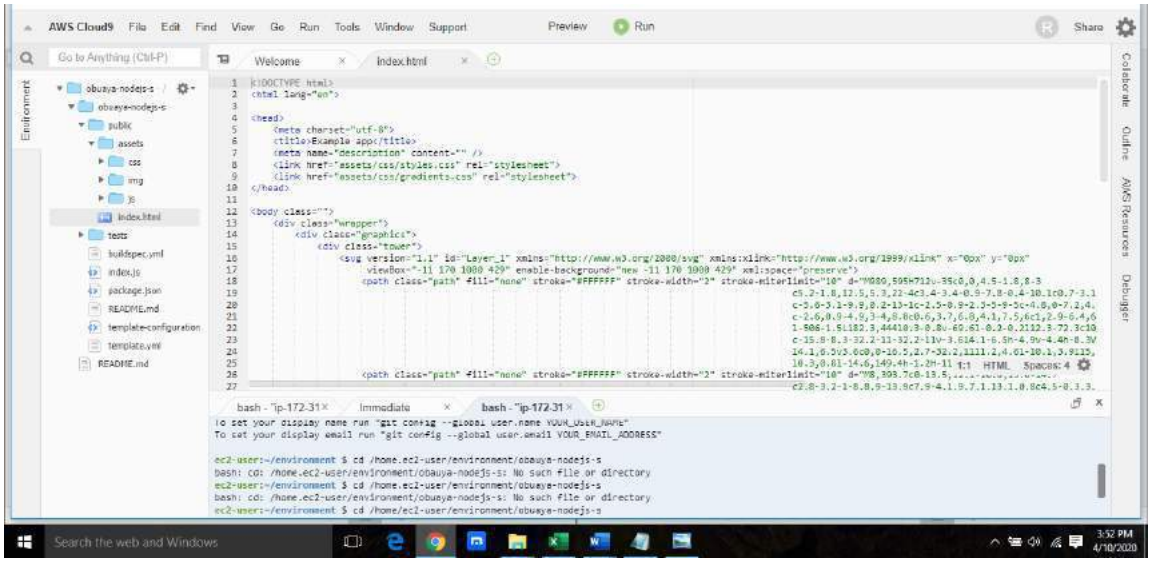

Figure 11. Index Page of the Application.

- add and save modifications by doing the steps:

- enter the command *git status*. If git returns *modified: public/index.html* in red, you have successfully saved your changes;

- stage your changes, commit your changes, and push the changes to the master branch in git on CodeCommit using the following command:

git add public/index.html

git commit -m modified index page

git push origin master"

- If successfully pushed, navigate to the **Pipeline History**, then click on it to see how your function was triggered as an AWS event by CloudWatch as shown in Figure 12.

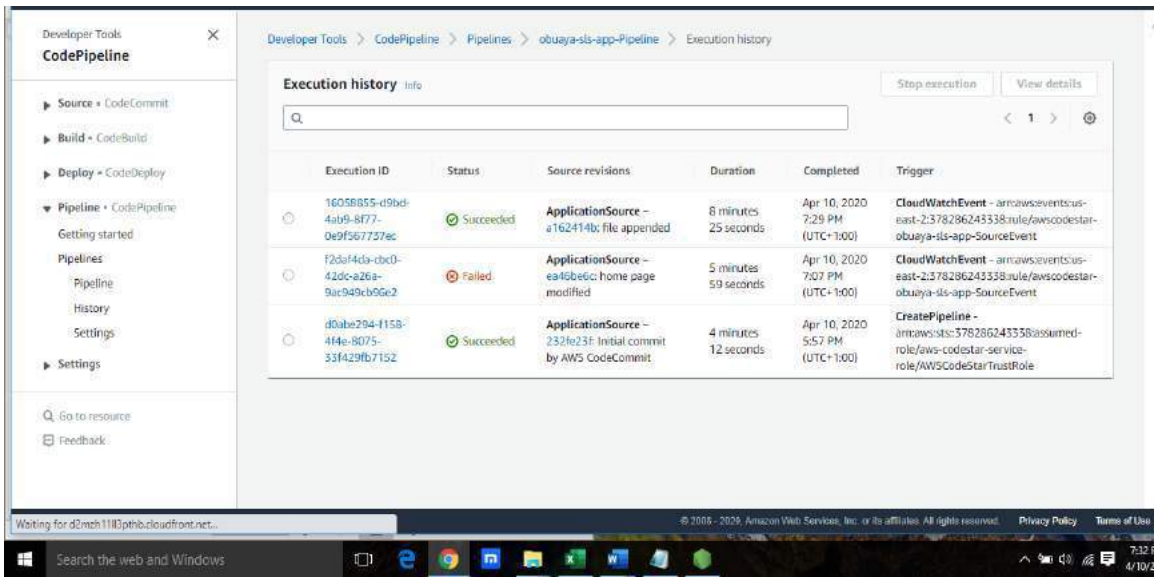

Figure 12. CodePipeline Execution History.

It is evident that it committed and was successfully built. The chart for continuous deployment from how it moved from one stage to another was captured in Figure 13.

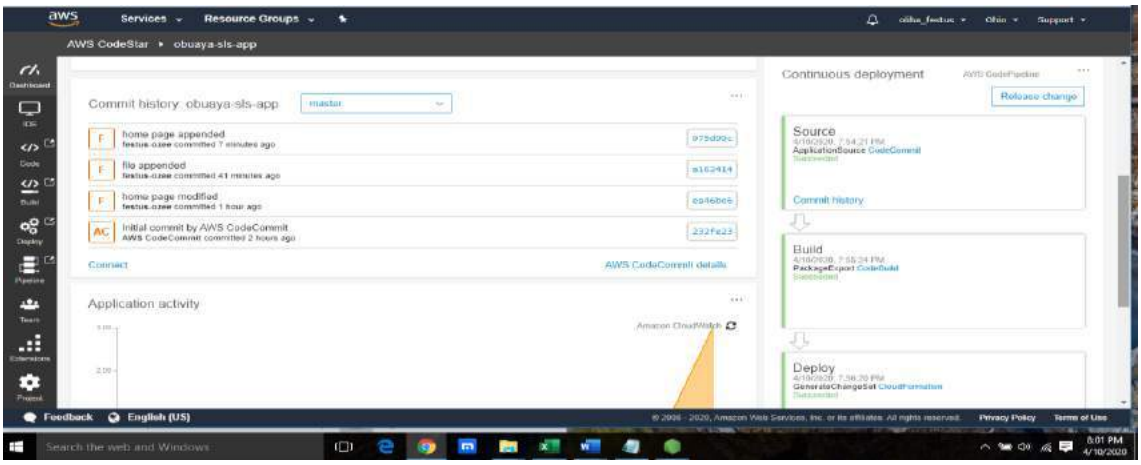

Figure 13. Continuous Deployment Chart

It is advised to terminate all project resources to avoid being charged. Project resources can be accessed via the project settings and it will display all resources used for deployment and invocation as shown in Figure 14.

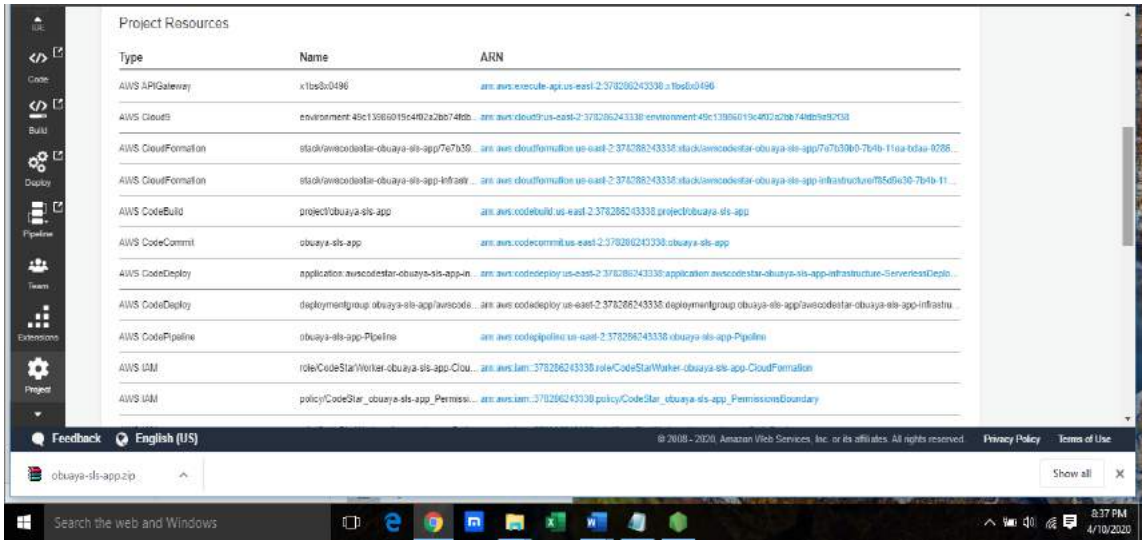

Figure 14. Project Resources.

4.3 Discussion

Despite the variance in the literature about the concept of serverless computing, it is pertinent to agree that it has a lot to offer and contrary conceptual views are as a result of its infancy and emerging technologies are usually concordant with open challenges as noted in the work of [16]. As an emerging trend in cloud computing, it holds the key architectural patterns for services computing in the cloud. The extension of cloud services by this technology is to be welcomed with an optimistic assertiveness by developers to enable worthy efforts on application logic. These service attitudes and patterns were also detailed in [17].

Exploring the functionality of serverless computing via its building blocks and services, the architecture provides developers with computing resources to improve their efficiencies and productivity. The technology of serverless computing comes with challenging concerns notwithstanding its juicy advantages. Stressing concerns peculiar to developers are those of the limiting resources such as the execution time of serverless functions associated with function providers like Azure and Lambda (AWS). Another alarming concern that had imposed drawbacks on developers on its adoption is tied to security. Developers may write function services and deploy them in a shared serverless platform – this exposes the application to the risk of being maliciously attacked and denied invocation or access to their apps. Additionally, due to FaaS stateless nature, there is the challenge of guaranteeing doggedness of their states across multiple invocations and besides, multiple platform challenge restricts supports for other clients' collaboration.

Emerging technologies are always susceptible to challenges and remedies are spawned accordingly as it trends. Associated open challenges of this technology were considered with remedies: to reuse function instances and its domicile host service containers to reduce startup latencies; software firms to train developers with skills to build microservices that support FaaS invocation on shared and intra-serverless platforms. Adding to this, the sample walkthrough

demonstrated an exploratory use of serverless computing technologies and services in building a serverless application in an AWS platform, to obviate server-related burdens and focus only on application logic – thus, to encourage and expedite developers towards its adoptions. Significantly, serverless technology offers an easier, cheaper, and faster way to deploy cloud-based applications and doesn't require developers to focus their time resources on how their backbends will work. These are beneficial in hastening its adoption to building applications on the FaaS platform.

5. Conclusion

Objectively, serverless computing has been explored and exposed towards its adoption by cloud developers. Being an emerging cloud computing technology, the exploratory efforts in this paper revealed that the issues limiting full serverless technology adoption were open challenges, and research experts are relentlessly on deck to proffer solutions to most of the open challenges to enable a rapid shift for developers towards adopting serverless functions for cloud applications. The impact of this study is noteworthy for foundational knowledge on serverless computing as a trending technology towards expediting its adoption by cloud application developers. The outcome will encourage prospective and cloud developers in building serverless applications taking cognizance that, its benefits still outweigh the challenges. Though still in an emerging phase, serverless computing and its technologies will indeed become the next evolution of services computing in the cloud.

References

[1] P. Castrol, V. Ishakian, V. Muthusamy, and A. Slominsky, (2019). The Rise of Serverless Computing", RIGHTSLINK, ACM, Vol 62(12), pp. 44-54. doi:10.1145/3368454.

[2] I. Baldini, P. Cheng, S.J Fink, N. Mitchell, V. Muthusamy, R. Rabbah, P. Suter, and O. Tardieu, (2017). Serverless computing: Current trends and open problems, Research Advances in Cloud Computing, Springer, pp. 1–20.

[3] T. Wagner (2018). How Serverless Impacts Startups, Investors, and the Business Economics of the Future, Amazon Web Services, Inc, 21 pp.

[4] C. Ivan, R. Vasile, and V. Dadarlat, (2019). Serverless Computing: An Investigation of Deployment Environments for Web APIs, Computers, Vol. 8(50), MDPI, pp. 1-18. doi:10.3390/computers8020050.

[5] A. Muralidharan, and R. Thiyagarajan (2017). Serverless Computing – A Compelling Option for Today's Digital Enterprise, White Paper, Demystifying a Complex Technology Landscape, Trigent Overcoming Limits, 6 pp.

[6] A. Jangda, D. Pinckney, Y. Brun, and A. Guha, (2019). Formal Foundations of Serverless Computing, Proc. ACM Program. Lang. 3, OOPSLA, Article 149, 26 pp. https://doi.org/10.1145/3360575.

[7] Deloitte, (2018), Serverless Computing – Architectural Considerations & Principles, Deloitte Touche Tohmatsu, India, 12 pp

[8] J.M. Hellerstein, J. Faleiro, J.E. Gonzalez, J. Schleier-Smith, V. Sreekanti, A Tumanov, and C. Wu (2019). Serverless Computing: One Step Forward, Two Steps Back", CIDR19, 9th Biennial Conference on Innovative Data Systems Research, Asilomar CA, USA, Online Proceedings, 9 pp.

[9] M. Robert, (2018). Serverless Architectures. Retrieved April 2020. Available @ https://martinfowler.com/articles/serverless.html.

[10] A. Bryk, (2020). Serverless Computing: Architecture, Challenges, and Prospects. Retrieved April 2020. Available @ https://www.apriorit.com/dev-blog/551-serverless-computing#

[11] AWS (2018). "Serverless: Changing the Face of Business Economics – A Venture Capital and Startup Perspective", Amazon Web Services, Inc, 21 pp.

[12] H. Shafiei, A. Khonsari, and P. Mousavi (2019). Serverless Computing: A Survey of Opportunities, Challenges and Applications, 13 pp.

[14] Innovative Committee, (2018). White Paper: Demystifying Noops and Serverless Computing, Federal Information Technology, CIO Council. 9 pp.

[15] G.D. Maayan (2014). How to Create Serverless Node.js Apps with AWS Lambda, CloudBoost. Available @ https://blog.cloudboost.io/how-to-create-serverless-node-js-apps-with-aws-lambda-d5ab23be0cfb.

[16] P.K. Gadepalli, G. Peach, L. Cherkasova, R. Aitken, G. and Parmer (2019). Challenges and Opportunities for Efficient Serverless Computing at the Edge, 38th Symposium on Reliable Distributed Systems, pp. 261-265.

[17] D. Taibi, N. El-Ioini, C. Pahl, and J.R.S. Niederkofler, (2020). Patterns for Serverless Functions (Function-as-a-Service): A Mjultivocal Literature Review, CLOSER Proceedings of the 10th International Conference on Cloud Computing and Services Science, Vol. 1, pp. 181-192.
[18] IP Specialists, (2019). Serverless Architecture. Retrieved March 2020. Available @ https://medium.com/@ipspecialist/serverless-architecture-19b5aceece86.

NIPES Conference Proceedings
The 1st International Conference of the Nigerian Institution of Professional Engineers and Scientists 7th-8th Oct. 2021: 160-167
www.nipesjournals.org.ng

Bacterial Bio-Calcination on the Mechanical Property of Cement Mortar

Aruwan, F. S.[a], Kaura, J. M.[b], Ocholi, A.[c,*]
[a,b,c]Department of Civil Engineering, Ahmadu Bello University, Zaria, Nigeria.

Abstract
This work investigated the effect of growth media on the strength development and microstructure of cement mortar. The bacterium called Bacillus Coagulans was incorporated at different cell concentrations of $1.5x10^8$, $6.0x10^8$ and $1.2x10^9$ suspension density with varying percentage replacement of Nutrient Broth Medium (NBM) at 30%, 40% and 50% and mixing water to the dry mix of cement and sand (fine aggregate). Mix ratio of 1:3 was used with water cement (w/c) ratio of 0.5. To establish the objective of gain in strength, mortar cubes were tested at 3, 7, 14 and 28 curing duration and the results compared with controlled cement mortar. Compressive strength obtained for control cement mortar was 24.08N/mm^2 and optimal bio-cement mortar was 28.02N/mm^2 at 28days curing age was achieved with the addition of $1.5x10^8$B. Coagulans suspension density with 50% NBM. The strength improvement is due to the growth of calcite crystals within the pores of the cement sand matrix as indicated from the microstructure obtained from Scanning Electron Microscopy (SEM) examination. It also indicates 3.46% improvement of water absorption at 28days for $1.5x10^8$ B. Coagulans suspension density with 50% NBM as against 5.98% water absorption at 28days curing age for control.

***Keywords*:**
Bacillus Coagulans, Bio-cement mortar, Compressive strength, Nutrient Broth growth Medium (NBM), Scanning Electron Microscopy (SEM).

1.0 Introduction

Today, due to increase in population and urbanization, the need to provide safe and environmentally friendly structures have become a necessity. Concrete is widely used as construction material around the world because of its resistance, durability and low cost in comparison with other construction material [1, 2]. Cement is one of the most important components of the concrete, which provides properties of compaction. Modernization and industrialization have increased the demand for cement and the world attention has been focused on environmental preservation due to the alarming depletion of ozone layer as a result of pollution resulting from manufacturing processes. Cement production accounts for about 5-7% of global Carbon dioxide (CO_2) emission [3]. As demand for supplementary cementitious materials is increasing day by day, it is very important to find a suitable technology to ensure the improvement of properties of structures.

Bio-cement a recently discovered novel product of bio-mineralization based microbial induced calcite precipitation (MICP) process, is widely used to improve the durability of concrete [4]. To date, several studies have demonstrated the positive influence of microbial compounds on cement mortar and concrete properties. The MICP process is an effective and eco-friendly technology that can be applied to solve various environmental problems [5, 6, 7, 8, 9, 10, 11, 12]. MICP refers to the formation of calcium carbonate from a super saturated solution due to the presence of their microbial cells and biochemical activities [13]. Calcium carbonate is one of the most well know mineral that bacteria deposit by the phenomenon called bio-cementation or MICP. Such deposits have recently emerged as promising binders for protecting and consolidating various building materials [14]. It should be noted that bacteria have been in existence, however many of their biotechnological applications are not yet widespread [15]. Although most researchers are concerned in the calcite precipitation and the process is not yet clear and defined. The effect of multi-component growth media, containing germination and sporulation aids for the bacteria aerobic oxidation pathway, on the basic properties of fresh and hardened cement mortar instead of the potential self-healing efficiency in a structural service was investigated by [16] and also [17]

altered the chemical dosage proportions of the nutrient growth medium to achieve early strength in concrete.
NUB enhance the germination of bacterial cells, sporulation of bacteria and precipitation of calcite within the pores of the cement-sand matrix, which typically consist of calcium, carbon and nitrogen sources. Thus, in this study, the microbially induced calcite precipitation process is utilized in cement mortar to improve its compressive strength.

2.0 Materials and Method

2.1 Materials
2.1.1 Microorganism
In order to stimulate calcite mineralization, which is a by-product of microbial metabolic activity, a urease producing bacteria was used to induce the calcite precipitate. This MICP process is known as Urea Hydrolysis. The bacteria specie used for the study was *Bacillus Coagulans.* It is classified as ATCC 7050 in the American Type Culture Collection, endospore-forming (spore is formed within the cell) bacteria, it is a Gram-positive rod-shaped bacterium, grows optimally at 37°C and pH in the range 5.5 to 6.2. It is obtained from the Department of Microbiology laboratory Ahmadu Bello University, Zaria which was isolated from lateritic soil.

2.1.2 Nutrient Broth Growth Medium
The growth medium was prepared using a mixture of chemicals at varying proportions which is based on initial microbiological studies [18]. Chemical used include the following per liter of distilled water: 3g of nutrient broth (Bacto); 20g of urea; 10g of NH_4Cl and 2.12g (equivalent to 25.2mM) of $NaHCO_3$.

2.1.3 Cement and Sand
The cement used in this research work was 42.5N Portland Limestone Cement conforming to BS EN [19]. Locally available clean, well graded, natural river sand having fineness modulus of 2.76 and nominal maximum size of 5mm was used conforming to BS EN [20].

2.2 Method
2.2.1 Preparation of Microbial cement mortar
The mortar was prepared using cement sand ratio of 1:3 by weight. On 76mm cubic molds were prepared. Cement and sand were thoroughly mixed, adding along with grown culture at w/c ratio of 0.5 of different cells concentration of *B. Coagulans* corresponding to $1.5x10^8$cells/ml, $6.0x10^8$cells/ml and $1.2x10^9$cells/ml, which the nutrient growth medium was also added at varying percentage (%) replacement of w/c ratio (30%, 40% & 50%). Cubes were cast and compacted using rammer. After demolding all specimens were cured until compressive strength at the intervals of 3, 7, 14 and 28 days. Control specimens were also prepared in similar way.

2.2.2 Compressive Strength
Compressive strength test was carried out on harden cement mortar and bio-cement mortar in accordance to BS EN [20]. The compressive strength test was conducted on cubes of 76mm×76mm×76mm mixed mortar using the compressive testing machine (Denison) at the concrete laboratory of A.B.U, Zaria. The failure load was observed and recorded and the compressive strength in N/mm^2 was calculated from Equation (1.0).

$$\text{For mortar} \quad Rc = \frac{Fc}{76\times76} \tag{1.0}$$

Where, R_C is the compressive strength in newton per millimeters square, F_C is the maximum load at fracture, in newton and 76 x 76 is the area of the platens or auxiliary plates in square millimeters

2.2.3 Water Absorption

Water absorption test is carried out to determine the water absorption value of mortar, expressed in percentage. This property is particularly important in concrete used for water-retaining structure or watertight basement, as well as being critical for durability. This test was performed on 50mm x 50mm x 50mm cube specimens prepared in the laboratory. Water absorption measurements were done by weighing the saturated specimens (W_s) and dried specimens in oven at 110ºC for 24h (W_d) at curing times of 3, 7, 14 and 28 days.
The water absorption was calculated from Equation (2.0)

$$\text{Water absorption (\%)} = \left(\frac{W_s - W_d}{W_d}\right) \times 100 \qquad (2.0)$$

2.2.4 Scanning Electron Microscopy (SEM)

Scanning Electron Microscopy (SEM) has become an important tool for study of microstructures, hydration progress and structural morphology. This test was conducted to determine the microstructure of the sample and to examine it matrices. The mortar cubes considered for the test were control cement mortar cube for 28 days curing period and optimal bio-cement mortar cube for 28 days curing period. Which was conducted at the multipurpose laboratory of Umaru Musa Yar'adua University Katsina State using SEM with serial number MVE015707775 and model number 800-07334 (Phenom World made in the Netherlands).

3.0 Results and Discussion

3.1 Compressive Strength

The compressive strength results of the control cement mortar and the bio-cement mortar mixtures containing bacterial are shown in Fig. 1, 2 and 3. At 28 curing age, the compressive strength of the control cement mortar mixture was 24.08 N/mm^2, whereas that of the cement mortar mixtures for 1.5x10^{8}cells/ml are 24.53, 25.57 and 28.02 N/mm^2 respectively with varying proportioning of Nutrient Broth Medium (NBM) of 30% NBM, 40% NBM and 50% NBM. At 28 curing age, the compressive strength results of cement mortar mixtures of 30% NBM, 40% NBM and 50% NBM for 6.0x10^{8}cells/ml are 24.14, 24.18 and 25.33 N/mm^2 and that of 30% NBM, 40% NBM and 50% NBM for 1.2x10^{9}cells/ml are 24.21, 24.35 and 25.05 N/mm^2 respectively. The optimal compressive strength of 28.02N/mm^2 was obtained for 1.5x10^{8}cells/ml with 50% NBM.

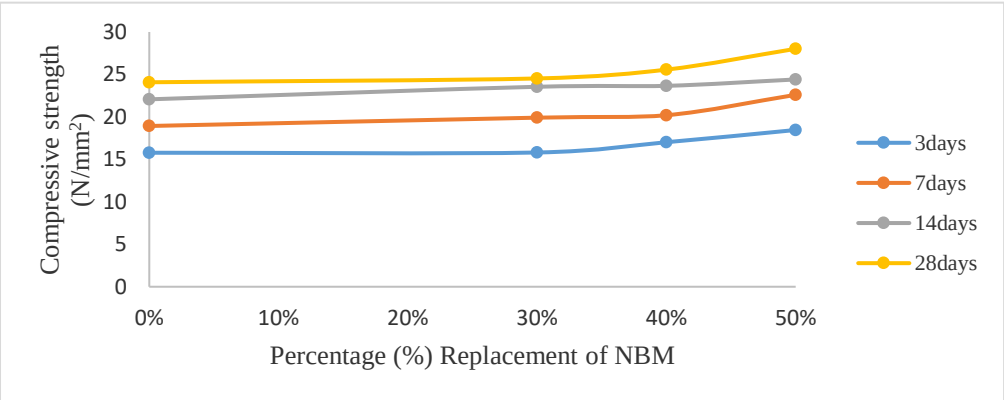

Fig. 1: Variation of Compressive Strength with NBM for 1.5x10^{8}cells/ml *B. Coagulans* Suspension density.

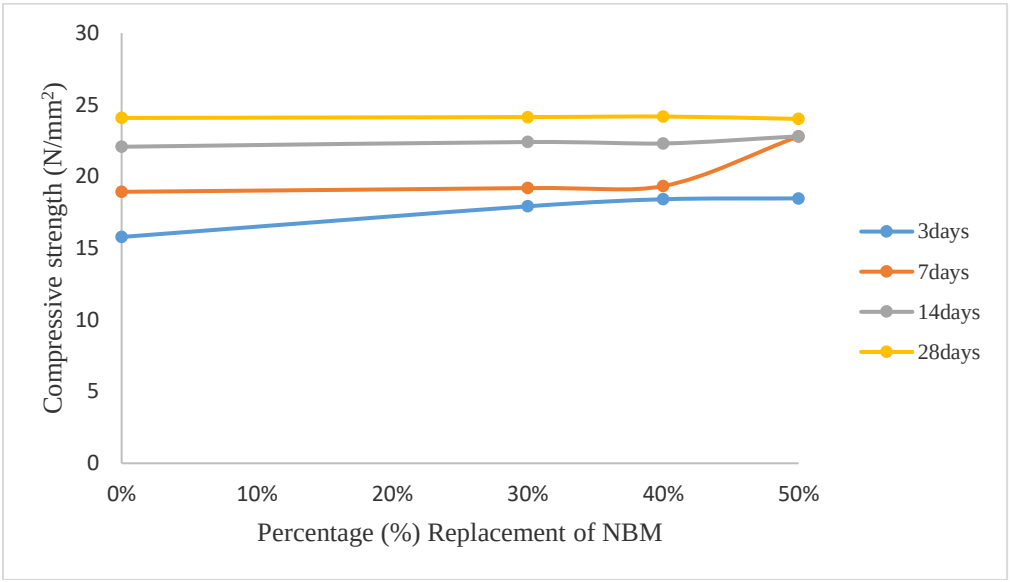

Fig. 2: Variation of Compressive Strength with NBM for 6.0x10^{8}cells/ml *B. Coagulans* Suspension density.

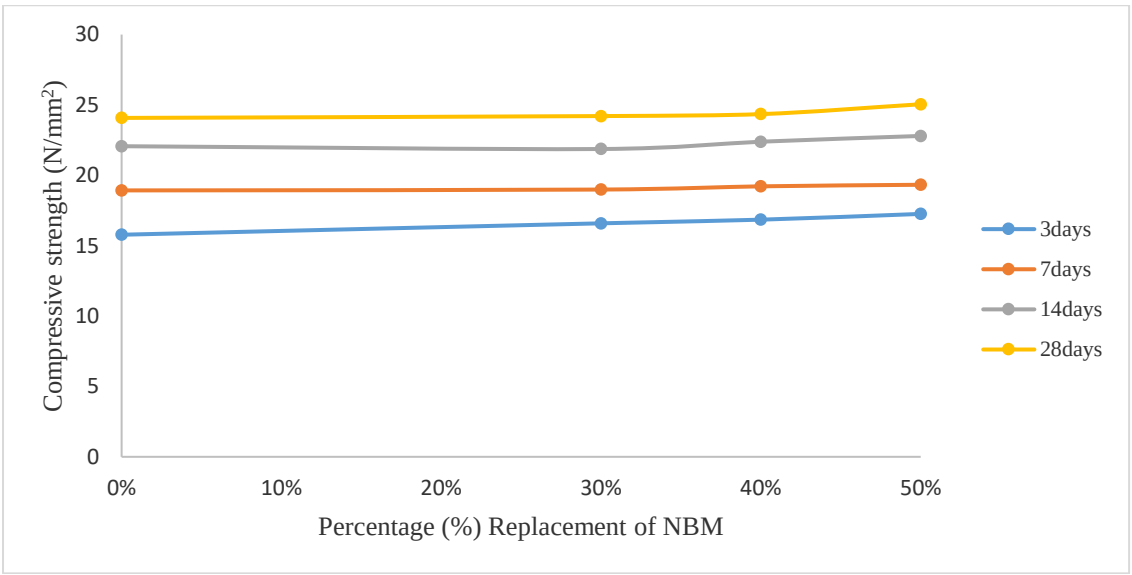

Fig. 3: Variation of Compressive Strength with NBM for 1.2x10^{9}cells/ml *B. Coagulans* Suspension density.

From the result shown in Fig. 1, 2 & 3 above, the compressive strength increases as curing age progresses, this is as a result of the specimens mixed with bacterial cells and might be attributed to the behavior of microbial cells within the cement mortar matrix and also the strength increases with percentage increment of NBM. This study is in agreement with the result reported [11, 16]. As genre *Bacillus*, such as *Sporosarcina pasteurii*, *B. Subtilis and B. Cereus* has been most commonly used in research studies because of their ability to precipitate calcium carbonate in calcite form which makes them suitable to use for strength improvement in cement mortar and concrete [5, 21, 22].

3.2 Water Absorption

The results shown in Fig. 4, 5 and 6 illustrates that the water absorption of cement mortar with or without bacterial cells decreases with time of curing up to 28 days, this is due to the continuous hydration and accumulation of hydrated products which fill the open pores of the specimens. Also,

the water absorption values of cement mortar specimens mixed with bacterial cells at $1.5x10^8$cells/ml, $6.0x10^8$cells/ml and $1.2x10^9$cells/ml are lower than those of control specimens. This is attributed to that bacterial biomass and microbial calcite precipitation within the pores and on the surface of cement mortar and also percentage replacement of the NBM with curing days had effect on the water absorption, compared to the control at either age. However, the improvement is attributed to the nitrogen and carbon source in the growth medium which permit the germination of bacterial spores, growth of bacterial cells, precipitation of calcite and sporulation of bacteria as seen in similar study [16].

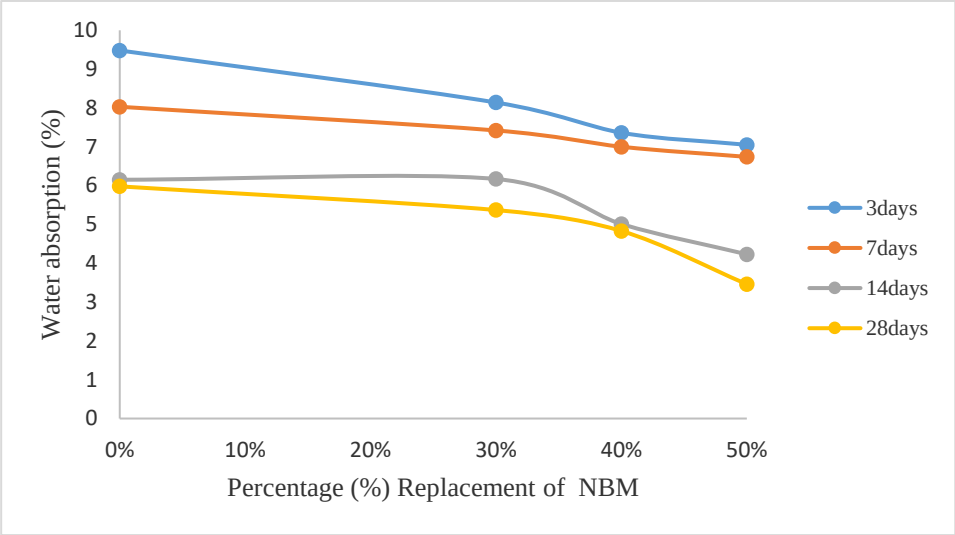

Fig. 4: Variation of Water absorption with NBM for $1.5x10^8$cells/ml *B. Coagulans* Suspension density

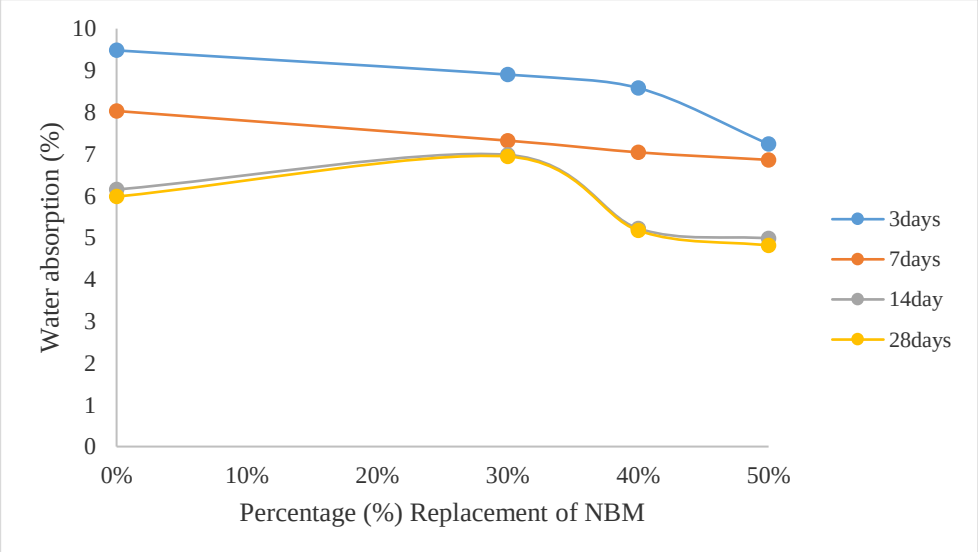

Fig. 5: Variation of Water absorption with NBM for $6.0x10^8$cells/ml *B. Coagulans* Suspension density.

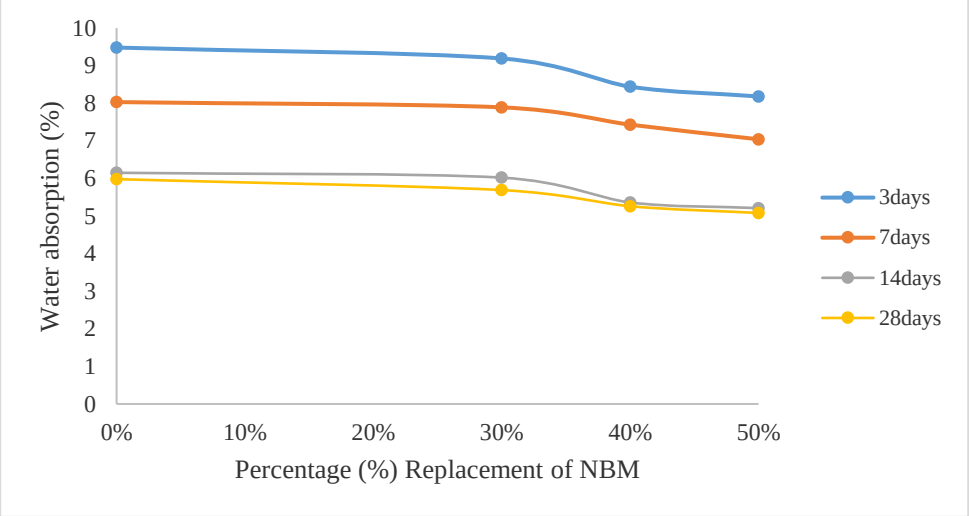

Fig. 6: Variation of Water absorption with NBM for 1.2x10^{9}cells/ml *B. Coagulans* Suspension density.

3.3 Scanning Electronic Microscopy (SEM)

To determine whether the increase in compressive strength of the specimens prepared with bacteria could be attributed to the microbial calcite precipitation, the mortar samples were taken off and examined under SEM. Plate 1 is a scanning electron micrograph of the matrix of bacteria-free cement mortar while Plate 2 shows micrographs of the specimen prepared with *Bacillus Coagulans*. The sample showed calcite crystals grown all over and precipitated.

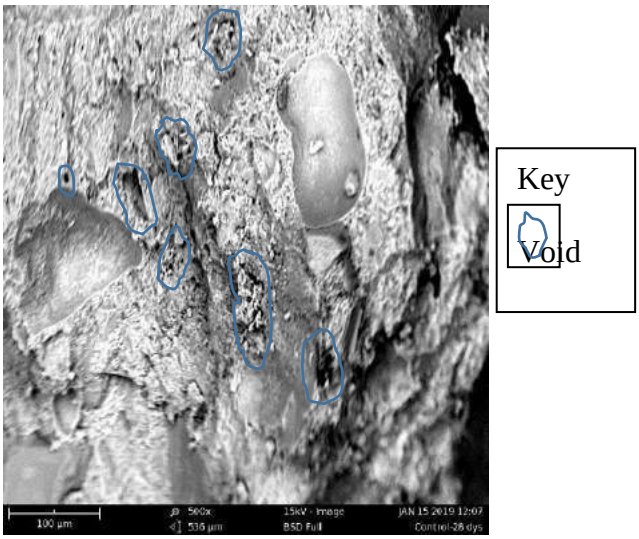

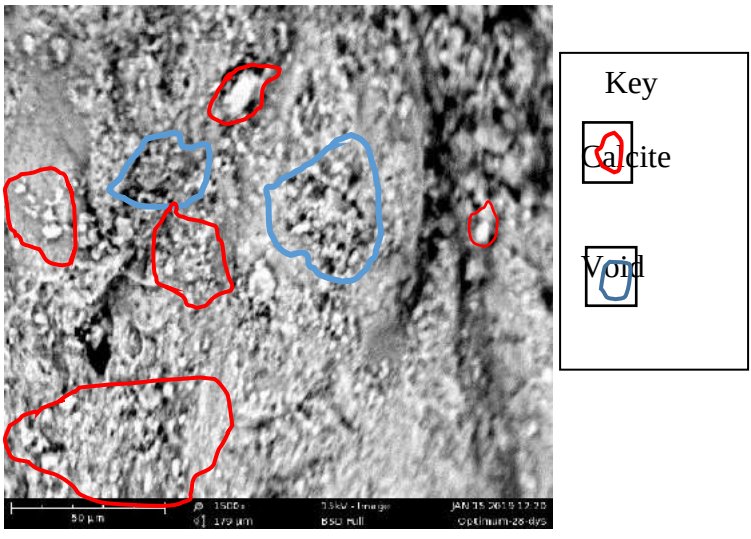

Plate 1: Cement Mortar at 28 days (Control)

Plate 2: Optimal Bio-Cement mortar

4.0 Conclusion

Based on the result of the study, it is concluded that the compressive strength of the bacteria modified cement mortar were improved due to the deposition of the calcite by the bacterial activity. The compressive strength increases with concentration of bacterial cells while a decrease in strength improvement was observed when cement mortar mixed with 6.0x10^{8}cells/ml and 1.2x10^{9}cells/ml. The addition of bacterial cells with increment of the Nutrient Broth growth Media (NBM) to the cement mortar improves the compressive strength of the mortar with respect to control. Therefore, the optimum bacterial cells concentration which leads to the highest

improvement in cement mortar gives higher compressive strength of 28.02N/mm^2 at 28days is 1.5x10^{8}cells/ml with 50% growth media. The compressive strength of the bacteria modified cement mortar were improved due to the deposition of the calcite within the pores of the cement-sand matrix as indicated from the microstructure obtained from scanning electron microscopy (SEM) examination. Based on the result of the study, it is concluded that the water absorption of the bacteria modified cement mortar were improved due to the deposition of the calcite by the bacterial activity. The water absorption decreases with concentration of bacterial cells while an increase in water absorption improvement was observed when cement mortar mixed with 6.0x10^{8}cells/ml and 1.2x10^{9}cells/ml. The addition of bacterial cells with increment of the Nutrient Broth growth Media (NBM) to the cement mortar improves the water absorption of the mortar with respect to control. Therefore, the optimum bacterial cells concentration which leads to the highest improvement in cement mortar gives lower water absorption of 3.46% at 28days is 1.5x10^{8}cells/ml with 50% growth media.

References

[1] Khaliq, W., & Ehsan, M. B. (2016). Crack healing in concrete using various bio influenced self-healing techques. *Construction and Building Material, 102*(1), 349-357.

[2] Siddique, R., Nanda, V., Kadri, E. H., Khan, M. I., Singh, M., & Rajor, A. (2016). Influence of bacteria on compressive strength and permeation properties of concrete made with cement bag house filter dust. *Construction and Building Materials, 106*, 461-469.

[3] Hassanbeigi, A., Price, L., & Lin, E. (2012). Emerging energy-efficiency and CO_2 emmission-reduction technologies for cement and concrete production: a technical review *Renew Sustainable Energy Rev, 16*(8), 6220-6238.

[4] Achal, V., Mukherjee, A., & Reddy, M. S. (2011). Effect of calcifying bacterial on permeation properties of concrete structures. *J Ind Microbiol Biotechnol, 38*, 1229-1234.

[5] Abdulkareem, M., Ayeronfe, F., Abd Majid, M., Mohd.Sam, A., & Jay Kim, J. (2019). Evaluation of effects of multi-varied atmospheric curing conditions on compressive strength of bacterial (bacillus subtilis) cement mortar. *Construction and Building Material, 218*, 1-7.

[6] Achal, V., Pan, X., Zhang, D., & Fu, Q. (2012). Bioremediation of Pb-contaminated soil based on microbially induced calcite precipitation. *Journal Microbiol. Biotechnol., 22*(2), 244-247.

[7] Aggarwal, M., & Pandey, M. (2018). Ureolytic Bacteria Effect Analysis for Mechanical Properties Enhancement of Cement Mortar. *International Journal of Applied Engineering Research., 5*(11), 9145-9153.

[8] Anbu, P., Kang, C., Shin, Y., & So, J. (2016). Formation of Calcium Carbonate Minerals by Bacteria and its Multiple Applications. *SpringerPlus Journal, 5*, 250, 1-26.

[9] De Muynck, W., De Belie, N., & Verstraete, W. (2010). Microbial Carbonate precipitation in construction materials: a review. *Ecological Engineering, 36*, 118-136.

[10] Mitchell, A. C., Dideriksen, k., Spangler, L. H., Cunningham, A. B., & Gerlach, R. (2010). Microbially enhanced carbon capture and storage by mineral-trapping and solubility-trapping. *Environmental Science Technology, 44*(13), 5270-5276.

[11] Schwantes-Cezario, N., Porto, M. F., Sandoval, G. F. B., Nogueira, G. F. N., Couto, A. F., & Toralles, B. M. (2019). Effect of Bacillus Subtilis biocementation on the mechanical properties of mortars *IBRACON STRUCTURES AND MATERIALS JOURNAL, 12*(1), 31-38.

[12] Shashwati, S. P., & Sunita, S. (2019). Strength improvement of cement mortar by the Addition of Ureolytic Microorganism. *Sustainable Construction and Building Materials*, 887-895.

[13] Bosak, T. (2011). Calcite precipitation, microbially induced. *In: Reitner J, Thiel V, editors. Encyclopedia of earth sciences series. Netherlands: Springer*, 223-227.

[14] Achal, V., Mukherjee, A., & Reddy, M. S. (2010). Microbial Concrete: Way to enhance the durability of building structures. *Journal Material Civil E ngineering, 23*, 730-734.

[15] Bang, S. S., Galinat, J. K., & Ramakrishnan, V. (2001). Calcite Precipitation induced by polyurethane-immobilized *Bacillus pasteurii*. *Enzyme and Microbial Technology, 28*, 404-409.

[16] Xin Chen, Jie Yuan, & Alazhari, M. (2019). Effect of microbiologibal growth components for Bacteria-Based Self-Healing on the properties of cement mortar. *Materials, 12*(1303), 1-15.

[17] Chidara, R., Nagulagama, R., & Yadav, S. (2014). Achievement of Early Compressive Strength in Concrete Using Sporosarcina pasteurii Bacteria as an Admixture. *Advances in Civil Engineering, 7*.
[18] Chahal, N., & Siddique, R. (2013). Permeation properties of concrete made with fly ash and silica fume: Influence of urealytic bacteria. *Construction and Building Materials., 49*, 161-174.
[19] BS EN 197-1 (2000): Composition, Specifications and Conformity criteria for common cements, British Standards Institution. www.bsi-global.com
[20] BS EN 196-1 (2005): Methods of testing cement. Determination of strength, British Standards Institution. www.bsi-global.com
[21] Li, M., Zhu, X., Mukherjee, A., Huang, M., & Achal, V. (2017). Biomineralization in metakaolin modified cement mortar to improve its strength with lowered cement content. *Journal of Hazardous Materials.*, 1(35), 1-28.
[22] Abo-El-Enein, S. A., Ali, A. H., Talkhan, F. N., & Abdel-Gawwad, H. A. (2013). Application of microbial biocementation to improve the physico-mechanical properties of cement mortar. *HBRC Journal., 9*, 36-40.

NIPES Conference Proceedings
The 1st International Conference of the Nigerian Institution of Professional Engineers and Scientists 7th-8th Oct. 2021: 168-174
www.nipesjournals.org.ng

Hybrid Alternative Energy System Potentials in Remote Areas of Delta State, Nigeria

Onwuamaeze, I.P.[a], Idim, A. I.[b], Salisu, S.[a]
[a]Department of Mechanical Engineering, Petroleum Training Institute, Effurun, Nigeria.
[b]Department of Electrical and Electronics Engineering, Petroleum Training Institute, Effurun, Nigeria.

Abstract

The traditional, classical or conventional energy system such as the use of hydropower plant has been used extensively to support electricity in some parts of the state. This in no doubt is not adequately sufficient to meet the increasing demand for electricity in Delta State, Nigeria. Consequently, this study is focused on the investigation of a hybrid alternative by taking into consideration the accessible renewable resources (majorly biomass, solar and wind) these resources are readily available in remote area of the state. To achieve this, a techno-economic analysis is conducted. The results demonstrate showed that the hybrid system produces a robust output power with adequate raw materials available. Moreover, considering the hybrid system, the efficiencies of the solar PV, wind and biomass are 32%, 41.6% and 42% respectively. The estimated total capital cost of the whole system is satisfactory and greatly economical. Conclusively, the results obtained showed that Delta State, Nigeria has adequate resources in terms of required renewable energy to produce power that can be used to supplement the conventional systems. The findings also reveal that encouraging the hybrid alternative energy system will be useful for off-grid power in Delta State of Nigeria. This will help create job for young people, reduce the rate of crime and also improve education system in the country.

***Keywords*:**
Hybrid Alternative Energy, Techno economic Analysis, Renewable Energy, Remote areas, Conventional systems

1. Introduction

Nigeria is one of the developing countries in Africa. There are thirty six states in Nigeria. Delta State is in the South East of Nigeria and the population of Nigeria has risen greatly in recent times [1]. The demand for the local energy source is common in the Eastern Part of Nigeria where majority does not have access to electricity. The most affected are the people living in villages and rural communities, in such locations, lantern, candles and head torches are used extensively. Few populations living in urban settings are known for using popular clean cooking fuels and other renewable energy technologies, like the cooking gas etc. While the majority use firewood, charcoal and other sources of local fuel as their primary cooking fuel [2]. In Lusaka, 96% of rural areas use a solar panel for lighting, while some households use torch as their source of lighting. In a previous study, [3] interviewed the people in Lusaka about electricity access. In the case of household without a grid connection, a participant in the study explained that although she had the capacity and willingness to pay tariffs if she were to use electricity just for lighting, but she could not afford the connection fee. Other researchers are of the opinion that the use of electricity for lighting depend on equipment such as refrigerator and/or television. For cooking, electricity is used only sparingly and then only for quick tasks such as boiling an egg because the tariffs are unaffordable.

In Nigeria, there are abundant materials which are very useful sources of energy in underutilised form in hydro power form and other forms. Moreover, the available renewable energy resources

such as solar, biomass, wind, and geothermal are under-utilised. The aim of the present study is to harness the potential of these energy resources to increase access to electricity in rural areas, especially in Delta region of Nigeria. Delta State of Nigeria has great population. The study also investigates the technoeconomic feasibility of these renewable energies in a combined hybrid system. Based on the energy resources and household energy demand in Delta State Nigeria, according to the 2016 projected populations, the total population as that year was estimated as presented in Table 1. Row 12 of the table shows the population of Delta State as at 2016. This year 2021 the population in the state has gone far higher as a result of the new revolution.

Table 1: States in Nigeria and Population in 2006 and 2016 Respectively

Rank (2006)	State	Population (2006)	Population (2016)
1	Kano State	9,401,288	15,076,892
2	Lagos State	8,113,605	12,000,598
3	Kaduna State	6,113,503	8,252,366
4	Katsina State	5,801,584	7,831,319
5	Oyo State	5,580,894	7,840,864
6	Rivers State	5,198,605	7,303,924
7	Bauchi State	4,653,066	6,537,314
8	Jigawa State	4,361,002	5,828,163
9	Benue State	4,253,641	5,741,815
10	Anambra State	4,177,828	5,527,809
11	Borno State	4,171,104	5,860,183
12	Delta State	4,112,445	5,663,362

13	Niger State	3,954,772	5,556,247
14	Imo State	3,927,563	5,408,756
15	Akwa Ibom State	3,178,950	5,482,177
16	Ogun State	3,751,140	5,217,716
17	Sokoto State	3,702,676	4,998,090
18	Ondo State	3,460,877	4,671,695
19	Osun State	3,416,959	4,705,589
20	Kogi State	3,314,043	4,473,490
21	Zamfara State	3,278,873	4,515,427
22	Enugu State	3,267,837	4,411,119
23	Kebbi State	3,256,541	4,440,050
24	Edo State	3,233,366	4,235,595
25	Plateau State	3,206,531	4,200,442
26	Adamawa State	3,178,950	4,248,436
27	Cross River State	2,892,988	3,866,269
28	Abia State	2,845,380	3,727,347
29	Ekiti State	2,398,957	3,270,798

30	Kwara State	2,365,353	3,192,893
31	Gombe State	2,365,040	3,256,962
32	Yobe State	2,321,339	3,294,137
33	Taraba State	2,294,800	3,066,834
34	Ebonyi State	2,176,947	2,880,383
35	Nasarawa State	1,869,377	2,523,395
36	Bayelsa State	1,704,515	2,277,961
–	Federal Capital Territory	1,405,201	3,564,126

2. Renewable Energy Potential and Conversional Methods

Researchers and strategist in energy field tend to explore the potentials of renewable energy using the classical and global approach. This section shall focus on exposition to biomass energy, solar energy PV and hybrid renewable energy system.

2.1. Biomass Energy- Biomass can be used in solid or gasified form for heating or energy generation. It can also be transformed to liquid or gaseous fuels. Biomass can be used as a source of renewable energy either directly through combustion for the production of heat or indirectly through the transformation of biomass into various forms of biofuels [4]. The biofuel can be used in a gas turbine to generate electricity, a heat-producing boiler, or a combined heat and power plant (CHP) to generate both heat and power. Various methods for converting biomass to biofuel exist, and they are broadly classed as physical-chemical, combustion, thermochemical, and biochemical transformations [5]. Presently, woody biomass and charcoal are projected to provide roughly 90% of the resources used by most African Country households [6]. The vast nature of most forest in terms of landscape is roughly about sixty six percent of the country's total land area, this is vanishing as a result of the rising energy demand. One of the reasons for investing in renewable fuels like biogas and biofuels is as a result of the strain on the forest resource. There are so many feedstocks which can support the production of biogas like the sun flower seed, Jatropha, water hyacinth, cottonseed, soy seeds are all potential biofuel feedstocks available in most African Countries [6]. According to research conducted by [7] focused on information obtained from the Ministry of Energy, there are currently three hundred and forty one thousand biogas digesters in use. Equally, [8] is of the opinion that sugar cane as a feedstock is another source of biomass

energy currently in use to complement one of the African country's - Nigeria's energy needs [7][8].

2.2. Solar Energy Photovoltaics (PV) and solar thermal systems are two ways in which energy can generated from solar energy. when the energy radiating from the sun makes impact with the solar cell, it causes the electrons to flow around, resulting in electricity. An electric current is started by the action of electrons. The conversion of sunlight to energy occurs invisibly and quickly. There are no moving parts to break down. The concentrated solar power (CSP) utilizes solar radiation to generate electricity in a similar way as solar cells, but in a different method. Most solar thermal systems employ a mirrored solar collector to direct sunlight onto a receiver that heats a liquid. In the same way that coal plants operate, the super-heated liquid is utilized to create steam to generate electricity [9]. Nigeria has a year-round average of 2,000 to 3,000 hours of sunshine. Global horizontal irradiation is 5.5 kWh/m2 /day on average. The areas with the highest Global Horizontal Irradiation (GHI) are the south-west part of Western Province. The south-south part of Nigeria has an average daily amount of sunshine exceeding 6.3 kWh/km2 (yearly total around 2300 kWh/km^2) and more [10][11]. C. Wind Energy A wind turbine is a revolving mechanism that converts mechanical energy from the wind's kinetic energy. The propeller-like blades of a turbine are turned by the wind around a rotor, which spins a generator, and generates power [12]. Wind speeds has an average of 2.5 m/s at 10 m above the ground (a speed that is mainly suitable for mechanical applications). The Department of Energy has drawn plans to develop a wind atlas to identify areas where electricity can be generated from wind. Seven areas in Nigeria have been identified as viable for off-grid wind power generation [7]. D. Hydro Energy To generate electricity using hydropower energy, water must be in motion. This is kinetic (moving) energy. When flowing water turns the blades in a turbine, its form is changed to mechanical (machine) energy.

The turbine then turns the generator rotor which converts this mechanical energy into another energy form (electricity). Since water is the initial source of energy, this is called hydroelectric power [13]. Presently, Nigeria has an installed large hydro power generation capacity of 2,350 MW. In the future, the projected capacity is about 6,000 MW [14]. The country depends on hydropower for power generation which accounts about 95% of total generation [7][8].

2.3. Hybrid Renewable Energy System - The configuration of the hybrid renewable consists of three different technologies such as solar PV, wind, and biomass. The mode of operation of this system begins when biogas (from organic waste) was fed into the generator. Subsequently, AC electricity was produced and stored in a 1 kWh LA battery. A 1kW flat plate photovoltaic and a generic 10 kW wind turbine are also coupled to the system to supplement the power produced. The generated electricity in the PV system was DC, while AC electricity is generated from the wind turbine system.

Table 2. Energy Consumption Rate

Consumption	kWh/yr	%
AC Primary Load	72,125	100
DC Primary Load	0	0
Deferrable Load	0	0
Total	72,125	100

Table 3. Component Cost

Component	Capital Cost (NGN)	Replacement (NGN)	Operating and Maintenance Cost (NGN)	Total (NGN)
Wind	20,000,000	1,785,504	2,585,200	24,370,704
Solar PV	11,366,400	40,000	587,600	11,994,000
Biogas Generator	16,000,000	4,847,540	7,425,200	28,272,740
Converter	63,702,400	3,542,800	13,035,312	80,123,214

Table 2-3 present the dataset in terms of obtained dataset and information based on component efficiency, cost and energy consumption rate of the system. A summary of the total net cost in the present system is presented in Table 2. The major cost of the hybrid renewable energy system is the capital cost, followed by the replacement cost and the operating and maintenance cost. The total capital cost is NGN63,702,400 while the replacement cost goes for NGN3,542,800 and operating cost equal to NGN13,035,312.

3. Conclusion

This paper investigates a hybrid system consisting of solar PV, biomass, and wind generators. The study found that Nigeria has enough renewable resources to generate electricity in Nigeria, particularly in the Delta State of Nigeria. From the analysis, it is a clear indication that biomass for bioenergy, solar PV and wind energy are sufficient with available feedstocks and sufficient as alternative energy source in Nigeria. Moreover, considering the hybrid system, the efficiencies of the solar PV, wind and biomass are 32%, 41.6% and 42% respectively. The estimated total capital cost of the whole system is satisfactory and greatly economical. The outcome of this study also revealed that by increasing the uptake of off-grid projects in Africa, could bring many benefits to the rural and urban areas. Some of these benefits are improved education, time saving, and job creation.

References

[1] R. E.O. Ojo, E. F. Oyawale (2019) Initial assessment of reuse of sustainable wastes for fibreboard production: the case of waste paper and water hyacinth. Journal of Material Cycles and Waste Management, Springer.

[2] MO. Okwu, Otanocha O. Balogun P., Tega.O. (2018) Comparative Performance of Load Bearing Characteristics of Biogas and Gasoline Fuelled Electric Generator, International Journal of Ambient Energy.DOI:10.1080/01430750.2018.1517669

[3] O.J. Oyejide, M.O. Okwu, L.K.Tartibu (2019). Adaptive Design and Development of a Modular Water Hyacinth Briquette Stove Energy Sources, Part A: Recovery, Utilization, and Environmental Effects, DOI: 10.1080/15567036.2019.1675808

[4] A. Steinhauser, Biomass to Biofuels Nanotechnology for the Energy Challenge Biofuels Catalysis for Renewables Energy Demand and Climate Change. 2011.

[5] Uyanga Kindness A. O. Adeoye, S. E. Ogbeide, (2018**).** Production and Characterization of organic Solar Cells. World Journal of Engineering, Emerald Publishing group. Vol 15 (4) 540-548)

[6] Okwu M.O. Samuel O.D., Otanocha O., L.K. Tartibu, Omoregbee H.O., Mbachu V.M. (2021) Development of Tenary Models for Prediction of Biogas Yield in a Novel Modular Biodigester: A Case of Fuzzy Mamdani Model (FMM), Artificial Neural Network (ANN) and Response Surface Methodology (RSM). ***Biomass Conversion and Bio refinery, Springer.***

[7] O. Adewale, S. Kaunda, M. Morel, and M. Mtawali, "The State of the Energy Sector in Nigeria," no. October, 2013.
[8] J. Abass, M. Mwanza, J. Chachak, N. S. Çetin, and K. Ülgen, "Assessment of solar energy source distribution and potential in Nigeria," Period. Eng. Nat. Sci., vol. 5, no. 2, pp. 103– 116, 2017.
[9] "How Does Solar Work? | Department of Energy." [Online]. Available: https://www.energy.gov/eere/solar/howdoes-solar-work. [Accessed: 10-Jun-2021].
[10] M. Woods, R. Barua, and D. Kabira, "Nigeria: Solar PV and Hydro Mini-Grids," 2019.
[11] W. B. Group, "Solar Modeling Report," 2014.

[12] "How Do Wind Turbines Work? | Department of Energy." [Online]. Available: https://www.energy.gov/eere/wind/how-dowind-turbines-work. [Accessed: 10-Jun2021].
[13] U.S Department of the Interior Bureau of Reclamation Power Resource Office, "Hydroelectric Power," 2005.
[14] J. Axelsson, "Master Thesis Energy Technology for Sustainable Developent Design of a Hybrid Renewable Energy System Isolated From the Power Grid in a Rural Community in Zambia Acknowledgement," 2019.
[15] D. Ribó-Pérez, Á. Herraiz-Cañete, D. Alfonso-Solar, C. Vargas-Salgado, and T. Gómez-Navarro, "Modelling biomass gasifiers in hybrid renewable energy microgrids; a complete procedure for enabling gasifiers simulation in HOMER," Renew. Energy, vol. 174, pp. 501–512, 2021.

NIPES Conference Proceedings
The 1st International Conference of the Nigerian Institution of Professional Engineers and Scientists 7th-8th Oct. 2021: 175-185
www.nipesjournals.org.ng

Ratio Estimators of Finite Population Mean Using Gini's Mean Difference

J. O. Muili[a]*, T. O. James[b], and I. A. Yunusa[c]
[a, b]Department of Mathematics, Kebbi State University of Science and Technology Aliero, Nigeria
[c]Department of Mathematics and Statistics, Federal Polytechnic Nasarawa, Nasarawa State, Nigeria

Abstract
A class of ratio-type estimators of finite population mean has been proposed. The properties of the proposed estimators i.e. Bias and Mean Square Error were obtained up to first order of approximation using Taylor's Series Expansion and the condition for their efficiency over some existing estimators were also established. The efficiency of proposed estimators showed significant improvement over the estimators considered in the study. The results of the empirical study showed that the proposed estimators are more efficient than existing estimators based on the comparison criteria measures

***Keywords*:**
Gini's Mean Difference, Mean Square Error, Auxiliary variable, Ratio estimator.

1. Introduction

It is well observed and confirmed that the appropriate use of auxiliary information in sample survey result to reduction of variance or mean square error of the estimators. The auxiliary variables are the population parameters such as populations' coefficient of variation, coefficient of kurtosis, skewness, median, decile, quartile, correlation, etc. Efficiency of estimators of the population parameters can be increased by the appropriate use of auxiliary information in relationship with auxiliary variable. [1] was the first that made used of auxiliary variable and came up with what is known as ratio-type estimator for estimating the population mean which is more efficient than the sample mean. Many authors have used different auxiliary variables in modifying estimators of population mean in return to increase the precision of the estimators by using prior knowledge of population parameters. Authors like [2, 3] developed classes of ratio estimators for the estimation of population mean using known auxiliary information on coefficient of kurtosis, coefficient of variation and coefficient of variation. [4] also proposed set of ratio-type estimators for the population mean using non-conventional location parameters like mid-range, and tri-mean as auxiliary information. Other researchers are [5], [6], [7], [8, 9, 10, 11], [12] and [13]. In this study, our concern is estimating the population mean using known auxiliary information.

The main purpose of this study is to develop a new set of ratio-type estimators to improve the precision of the estimates of population mean in simple random sampling without replacement. The auxiliary information used in this study is gini's mean difference (G). Gini's Mean Difference (G) is a measure of variability which is less sensitive to outliers. The presence of extreme values or outliers in the observation of the study variable will have little or no effect on the other estimate.
Let $U=\{U_1,U_2,...,U_N\}$ be a finite population having N units and each $U_i=(X_i, Y_i)$, $i=1,2,3,...,N$ has a pair of values. Y is the study variable and X is the auxiliary variable which is correlated with Y, where $y=\{y_1, y_2,..., y_n\}$ and $x=\{x_1, x_2,..., x_n\}$ are the n sample values. $\bar{y}$ and $\bar{x}$ are the sample means of the study and auxiliary variables respectively. S_y^2 and S_x^2 are the population mean squares of Y and X respectively and s_y^2 and s_x^2 be respective sample mean squares based on the random sample of size n drawn without replacement.

1.2 Literature Review

The ratio estimator for estimating population mean $(\bar{Y})$ of the study variable (Y) is given as:

$$\hat{\bar{Y}}_r = \frac{\bar{y}}{\bar{x}}\bar{X} = \hat{R}\bar{X} \quad (1)$$

where $\hat{R} = \frac{\bar{y}}{\bar{x}}$

$$Bias\left(\hat{\bar{Y}}\right) = \gamma\frac{1}{\bar{X}}\left(RS_x^2 - \rho S_x S_y\right) \quad (2)$$

$$MSE\left(\hat{\bar{Y}}_r\right) = \gamma\left(S_y^2 + R^2 S_x^2 - 2R\rho S_x S_y\right) \quad (3)$$

where $R = \frac{\bar{Y}}{\bar{X}}$

[4] proposed a class of ratio type estimators for finite population mean using known values of decile mean $\left(DM\right)$, and coefficient of variation $\left(C_x\right)$ as auxiliary information, the biases, constants and mean square errors are given as:

$$\hat{\bar{Y}}_1 = \frac{\bar{y} + b\left(\bar{X} - \bar{x}\right)}{\left(\bar{x} + DM\right)}\left(\bar{X} + DM\right) \quad (4)$$

$$\hat{\bar{Y}}_2 = \frac{\bar{y} + b\left(\bar{X} - \bar{x}\right)}{\left(\bar{x}C_x + DM\right)}\left(\bar{X}C_x + DM\right) \quad (5)$$

$$\hat{\bar{Y}}_3 = \frac{\bar{y} + b\left(\bar{X} - \bar{x}\right)}{\left(\bar{x}\rho + DM\right)}\left(\bar{X}\rho + DM\right) \quad (6)$$

$$Bias\left(\hat{\bar{Y}}_i\right) = \gamma\frac{S_x^2}{\bar{Y}}R_i^2, \qquad where\ i = 1,2,3 \quad (7)$$

$$MSE\left(\hat{\bar{Y}}_i\right) = \gamma\left(R_i^2 S_x^2 + S_y^2\left(1 - \rho^2\right)\right) \qquad where\ i = 1,2,3 \quad (8)$$

$$R_1 = \frac{\bar{Y}}{\bar{X} + DM},\ R_2 = \frac{\bar{Y}C_x}{\bar{X}C_x + DM},\ R_3 = \frac{\bar{Y}\rho}{\bar{X}\rho + DM}$$

[14] proposed a class ratio type estimators using the values of median $\left(M_d\right)$, quartile deviation $\left(QD\right)$, gini's mean difference $\left(G\right)$, downton's method $\left(D\right)$, probability weighted moments $\left(S_{pw}\right)$, and their linear combination with correlation coefficient $\left(\rho\right)$ and coefficient of variation $\left(C_x\right)$ as auxiliary information given as:

$$\hat{\bar{Y}}_4 = \frac{\bar{y} + b\left(\bar{X} - \bar{x}\right)}{\left(\bar{x} + \psi_1\right)}\left(\bar{X} + \psi_1\right) \quad (9)$$

$$\hat{\bar{Y}}_5 = \frac{\bar{y} + b\left(\bar{X} - \bar{x}\right)}{\left(\bar{x} + \psi_2\right)}\left(\bar{X} + \psi_2\right) \quad (10)$$

$$\hat{\bar{Y}}_6 = \frac{\bar{y} + b\left(\bar{X} - \bar{x}\right)}{\left(\bar{x} + \psi_3\right)}\left(\bar{X} + \psi_3\right) \quad (11)$$

$$\hat{\bar{Y}}_7 = \frac{\bar{y} + b\left(\bar{X} - \bar{x}\right)}{\left(\bar{x} + \psi_4\right)}\left(\bar{X} + \psi_4\right) \quad (12)$$

$$\hat{\bar{Y}}_8 = \frac{\bar{y} + b\left(\bar{X} - \bar{x}\right)}{\left(\bar{x} + \psi_5\right)}\left(\bar{X} + \psi_5\right) \tag{13}$$

$$\hat{\bar{Y}}_9 = \frac{\bar{y} + b\left(\bar{X} - \bar{x}\right)}{\left(\bar{x} + \psi_6\right)}\left(\bar{X} + \psi_6\right) \tag{14}$$

$$\hat{\bar{Y}}_{10} = \frac{\bar{y} + b\left(\bar{X} - \bar{x}\right)}{\left(\bar{x}\rho + \psi_1\right)}\left(\bar{X}\rho + \psi_1\right) \tag{15}$$

$$\hat{\bar{Y}}_{11} = \frac{\bar{y} + b\left(\bar{X} - \bar{x}\right)}{\left(\bar{x}\rho + \psi_2\right)}\left(\bar{X}\rho + \psi_2\right) \tag{16}$$

$$\hat{\bar{Y}}_{12} = \frac{\bar{y} + b\left(\bar{X} - \bar{x}\right)}{\left(\bar{x}\rho + \psi_3\right)}\left(\bar{X}\rho + \psi_3\right) \tag{17}$$

$$\hat{\bar{Y}}_{13} = \frac{\bar{y} + b\left(\bar{X} - \bar{x}\right)}{\left(\bar{x}\rho + \psi_4\right)}\left(\bar{X}\rho + \psi_4\right) \tag{18}$$

$$\hat{\bar{Y}}_{14} = \frac{\bar{y} + b\left(\bar{X} - \bar{x}\right)}{\left(\bar{x}\rho + \psi_5\right)}\left(\bar{X}\rho + \psi_5\right) \tag{19}$$

$$\hat{\bar{Y}}_{15} = \frac{\bar{y} + b\left(\bar{X} - \bar{x}\right)}{\left(\bar{x}\rho + \psi_6\right)}\left(\bar{X}\rho + \psi_6\right) \tag{20}$$

$$\hat{\bar{Y}}_{16} = \frac{\bar{y} + b\left(\bar{X} - \bar{x}\right)}{\left(\bar{x}C_x + \psi_1\right)}\left(\bar{X}C_x + \psi_1\right) \tag{21}$$

$$\hat{\bar{Y}}_{17} = \frac{\bar{y} + b\left(\bar{X} - \bar{x}\right)}{\left(\bar{x}C_x + \psi_2\right)}\left(\bar{X}C_x + \psi_2\right) \tag{22}$$

$$\hat{\bar{Y}}_{18} = \frac{\bar{y} + b\left(\bar{X} - \bar{x}\right)}{\left(\bar{x}C_x + \psi_3\right)}\left(\bar{X}C_x + \psi_3\right) \tag{23}$$

$$\hat{\bar{Y}}_{19} = \frac{\bar{y} + b\left(\bar{X} - \bar{x}\right)}{\left(\bar{x}C_x + \psi_4\right)}\left(\bar{X}C_x + \psi_4\right) \tag{24}$$

$$\hat{\bar{Y}}_{20} = \frac{\bar{y} + b\left(\bar{X} - \bar{x}\right)}{\left(\bar{x}C_x + \psi_5\right)}\left(\bar{X}C_x + \psi_5\right) \tag{25}$$

$$\hat{\bar{Y}}_{21} = \frac{\bar{y} + b\left(\bar{X} - \bar{x}\right)}{\left(\bar{x}C_x + \psi_6\right)}\left(\bar{X}C_x + \psi_6\right) \tag{26}$$

where

$$\psi_1 = \left(M_d + G\right),\ \psi_2 = \left(M_d + D\right),\ \psi_3 = \left(M_d + S_{pw}\right),\ \psi_4 = \left(QD + G\right),\ \psi_5 = \left(QD + D\right),\ \psi_6 = \left(QD + S_{pw}\right)$$

$$Bias\left(\hat{\bar{Y}}_j\right) = \gamma \frac{S_x^2}{\bar{Y}} R_j^2, \qquad where\ \ j = 4,5,...,21 \tag{27}$$

$$MSE\left(\hat{\bar{Y}}_j\right) = \gamma\left(R_j^2 S_x^2 + S_y^2\left(1 - \rho^2\right)\right) \qquad where\ \ j = 4,5,...,21 \tag{28}$$

$$R_4 = \frac{\bar{Y}}{\bar{X} + \psi_1},\ R_5 = \frac{\bar{Y}}{\bar{X} + \psi_2},\ R_6 = \frac{\bar{Y}}{\bar{X} + \psi_3} R_7 = \frac{\bar{Y}}{\bar{X} + \psi_4},\ R_8 = \frac{\bar{Y}}{\bar{X} + \psi_5},\ R_9 = \frac{\bar{Y}}{\bar{X} + \psi_6},$$

$$R_{10}=\frac{\bar{Y}\rho}{\bar{X}\rho+\psi_1},\ R_{11}=\frac{\bar{Y}\rho}{\bar{X}\rho+\psi_2},\ R_{12}=\frac{\bar{Y}\rho}{\bar{X}\rho+\psi_3}R_{13}=\frac{\bar{Y}\rho}{\bar{X}\rho+\psi_4},\ R_{14}=\frac{\bar{Y}\rho}{\bar{X}\rho+\psi_5},\ R_{15}=\frac{\bar{Y}\rho}{\bar{X}\rho+\psi_6}$$

$$R_{16}=\frac{\bar{Y}C_x}{\bar{X}C_x+\psi_1},\ R_{17}=\frac{\bar{Y}C_x}{\bar{X}C_x+\psi_2},\ R_{18}=\frac{\bar{Y}C_x}{\bar{X}C_x+\psi_3}R_{19}=\frac{\bar{Y}C_x}{\bar{X}C_x+\psi_4},\ R_{20}=\frac{\bar{Y}C_x}{\bar{X}C_x+\psi_5},\ R_{21}=\frac{\bar{Y}C_x}{\bar{X}C_x+\psi_6}$$

2. Methodology

2.1 Proposed Estimator

Motivated by the work of Subzar *et al*. (2018), we proposed ratio-type estimators for estimating population mean using value of gini's mean difference as:

$$\hat{\bar{Y}}_{p1}=\frac{\bar{y}+b\left(\bar{X}-\bar{x}\right)}{\left(\bar{x}+\eta_1\right)}\left(\bar{X}+\eta_1\right) \tag{29}$$

$$\hat{\bar{Y}}_{p2}=\frac{\bar{y}+b\left(\bar{X}-\bar{x}\right)}{\left(\bar{x}+\eta_2\right)}\left(\bar{X}+\eta_2\right) \tag{30}$$

$$\hat{\bar{Y}}_{p3}=\frac{\bar{y}+b\left(\bar{X}-\bar{x}\right)}{\left(\bar{x}+\eta_3\right)}\left(\bar{X}+\eta_3\right) \tag{31}$$

$$\hat{\bar{Y}}_{p4}=\frac{\bar{y}+b\left(\bar{X}-\bar{x}\right)}{\left(\bar{x}+\eta_4\right)}\left(\bar{X}+\eta_4\right) \tag{32}$$

$$\hat{\bar{Y}}_{p5}=\frac{\bar{y}+b\left(\bar{X}-\bar{x}\right)}{\left(\bar{x}+\eta_5\right)}\left(\bar{X}+\eta_5\right) \tag{33}$$

$$\hat{\bar{Y}}_{p6}=\frac{\bar{y}+b\left(\bar{X}-\bar{x}\right)}{\left(\bar{x}+\eta_6\right)}\left(\bar{X}+\eta_6\right) \tag{34}$$

$$\hat{\bar{Y}}_{p7}=\frac{\bar{y}+b\left(\bar{X}-\bar{x}\right)}{\left(\bar{x}\rho+\eta_1\right)}\left(\bar{X}\rho+\eta_1\right) \tag{35}$$

$$\hat{\bar{Y}}_{p8}=\frac{\bar{y}+b\left(\bar{X}-\bar{x}\right)}{\left(\bar{x}\rho+\eta_2\right)}\left(\bar{X}\rho+\eta_2\right) \tag{36}$$

$$\hat{\bar{Y}}_{p9}=\frac{\bar{y}+b\left(\bar{X}-\bar{x}\right)}{\left(\bar{x}\rho+\eta_3\right)}\left(\bar{X}\rho+\eta_3\right) \tag{37}$$

$$\hat{\bar{Y}}_{p10}=\frac{\bar{y}+b\left(\bar{X}-\bar{x}\right)}{\left(\bar{x}\rho+\eta_4\right)}\left(\bar{X}\rho+\eta_4\right) \tag{38}$$

$$\hat{\bar{Y}}_{p11}=\frac{\bar{y}+b\left(\bar{X}-\bar{x}\right)}{\left(\bar{x}\rho+\eta_5\right)}\left(\bar{X}\rho+\eta_5\right) \tag{39}$$

$$\hat{\bar{Y}}_{p12}=\frac{\bar{y}+b\left(\bar{X}-\bar{x}\right)}{\left(\bar{x}\rho+\eta_6\right)}\left(\bar{X}\rho+\eta_6\right) \tag{40}$$

$$\hat{\bar{Y}}_{p13}=\frac{\bar{y}+b\left(\bar{X}-\bar{x}\right)}{\left(\bar{x}C_x+\eta_1\right)}\left(\bar{X}C_x+\eta_1\right) \tag{41}$$

$$\hat{\bar{Y}}_{p14}=\frac{\bar{y}+b\left(\bar{X}-\bar{x}\right)}{\left(\bar{x}C_x+\eta_2\right)}\left(\bar{X}C_x+\eta_2\right) \tag{42}$$

$$\hat{\bar{Y}}_{p15} = \frac{\bar{y} + b\left(\bar{X} - \bar{x}\right)}{\left(\bar{x}C_x + \eta_3\right)}\left(\bar{X}C_x + \eta_3\right) \tag{43}$$

$$\hat{\bar{Y}}_{p16} = \frac{\bar{y} + b\left(\bar{X} - \bar{x}\right)}{\left(\bar{x}C_x + \eta_4\right)}\left(\bar{X}C_x + \eta_4\right) \tag{44}$$

$$\hat{\bar{Y}}_{p17} = \frac{\bar{y} + b\left(\bar{X} - \bar{x}\right)}{\left(\bar{x}C_x + \eta_5\right)}\left(\bar{X}C_x + \eta_5\right) \tag{45}$$

$$\hat{\bar{Y}}_{p18} = \frac{\bar{y} + b\left(\bar{X} - \bar{x}\right)}{\left(\bar{x}C_x + \eta_6\right)}\left(\bar{X}C_x + \eta_6\right) \tag{46}$$

where

$$Bias\left(\hat{\bar{Y}}_j\right) = \gamma \frac{S_x^2}{\bar{Y}} R_j^2, \qquad where\ \ j = 4,5,...,21 \tag{47}$$

$$MSE\left(\hat{\bar{Y}}_j\right) = \gamma\left(R_j^2 S_x^2 + S_y^2\left(1-\rho^2\right)\right) \qquad where\ \ j = 4,5,...,21 \tag{48}$$

where $\eta_1 = \left(M_d + G^2\right),\ \eta_2 = \left(M_d + D \times G\right),\ \eta_3 = \left(M_d + S_{pw} \times G\right),\ \eta_4 = \left(QD + G^2\right),$
$\eta_5 = \left(QD + D \times G\right),\ \eta_6 = \left(QD + S_{pw} \times G\right)$

In order to obtain the bias and MSE, we define $e_0 = \frac{\bar{y} - \bar{Y}}{\bar{Y}}$ and $e_1 = \frac{\bar{x} - \bar{X}}{\bar{X}}$ such that
$\bar{y} = \bar{Y}\left(1 + e_0\right)$ *and* $\bar{x} = \bar{X}\left(1 + e_1\right)$, from the definition of e_0 and e_1, we obtain

$$\left.\begin{aligned} &E\left(e_0\right) = E\left(e_1\right) = 0,\ E\left(e_0^2\right) = \gamma C_y^2 \\ &E\left(e_1^2\right) = \gamma C_x^2,\ E\left(e_0 e_1\right) = \gamma C_{yx} = \gamma\rho C_y C_x \end{aligned}\right\} \tag{49}$$

$$Bias\left(\hat{\bar{Y}}_{Pi}\right) = \gamma \frac{S_x^2}{\bar{Y}} R_{Pi}^2, \qquad \left(i = 1,2,...,18\right) \tag{50}$$

$$MSE\left(\hat{\bar{Y}}_{Pi}\right) = \gamma\left(R_{Pi}^2 S_x^2 + S_y^2\left(1-\rho^2\right)\right), \qquad \left(i = 1,2,3,...,18\right) \tag{51}$$

where $R_{p1} = \frac{\bar{Y}}{\bar{X} + \eta_1},\ R_{p2} = \frac{\bar{Y}}{\bar{X} + \eta_2},\ R_{p3} = \frac{\bar{Y}}{\bar{X} + \eta_3} R_{p4} = \frac{\bar{Y}}{\bar{X} + \eta_4},\ R_{p5} = \frac{\bar{Y}}{\bar{X} + \eta_5},\ R_{p6} = \frac{\bar{Y}}{\bar{X} + \eta_6},$
$R_{p7} = \frac{\bar{Y}\rho}{\bar{X}\rho + \eta_1},\ R_{p8} = \frac{\bar{Y}\rho}{\bar{X}\rho + \eta_2},\ R_{p9} = \frac{\bar{Y}\rho}{\bar{X}\rho + \eta_3} R_{p10} = \frac{\bar{Y}\rho}{\bar{X}\rho + \eta_4},\ R_{p11} = \frac{\bar{Y}\rho}{\bar{X}\rho + \eta_5},\ R_{p12} = \frac{\bar{Y}\rho}{\bar{X}\rho + \eta_6}$
$R_{p13} = \frac{\bar{Y}C_x}{\bar{X}C_x + \eta_1},\ R_{p14} = \frac{\bar{Y}C_x}{\bar{X}C_x + \eta_2}, R_{p15} = \frac{\bar{Y}C_x}{\bar{X}C_x + \eta_3},\ R_{p16} = \frac{\bar{Y}C_x}{\bar{X}C_x + \eta_4},\ R_{p17} = \frac{\bar{Y}C_x}{\bar{X}C_x + \eta_5},$
$R_{p18} = \frac{\bar{Y}C_x}{\bar{X}C_x + \eta_6}.$

2.2 Efficiency Comparisons

Efficiencies of the proposed estimators are compared with efficiencies of the existing estimators in the study

The $\hat{\bar{Y}}_{pi}$ – *family* of estimators of the finite population mean are more efficient than $\hat{\bar{Y}}_r$ if,

$$MSE\left(\hat{\bar{Y}}_{pi}\right) < MSE\left(\hat{\bar{Y}}_{r}\right) \qquad i = 1,2,...,18$$

$$\left(R_{pi}^2 S_x^2 + S_y^2\left(1-\rho^2\right)\right) < \left(S_y^2 + R^2 S_x^2 - 2R\rho S_x S_y\right) \tag{52}$$

The $\hat{\bar{Y}}_{pi} - family$ of proposed estimators of the population mean are more efficient than $\hat{\bar{Y}}_{j}$ if,

$$MSE\left(\hat{\bar{Y}}_{pi}\right) < MSE\left(\hat{\bar{Y}}_{j}\right) \qquad i = 1,2,...,18 \;\; j = 1,2,3$$

$$\left(R_{pi}^2 S_x^2 + S_y^2\left(1-\rho^2\right)\right) < \left(R_j^2 S_x^2 + S_y^2\left(1-\rho^2\right)\right) \tag{53}$$

The $\hat{\bar{Y}}_{pi} - family$ of proposed estimators of the population mean are more efficient than $\hat{\bar{Y}}_{j}$ if,

$$MSE\left(\hat{\bar{Y}}_{pi}\right) < MSE\left(\hat{\bar{Y}}_{j}\right) \qquad i = 1,2,...,18 \;\; j = 4,5,...,21$$

$$\left(R_{pi}^2 S_x^2 + S_y^2\left(1-\rho^2\right)\right) < \left(R_j^2 S_x^2 + S_y^2\left(1-\rho^2\right)\right) \tag{54}$$

When conditions (52), (53) and (54) are satisfied, we can conclude that the proposed estimators are more efficient than some selected existing estimators.

2.3 Numerical Illustration

In order to show the merits of the proposed estimator, we have considered the real populations as:

Table 1: Characteristics of Populations [14]

Parameter	Population I	Population II	Population III
N	34	34	80
n	20	20	20
$\bar{Y}$	856.4117	856.4117	5182.637
$\bar{X}$	199.4412	208.8823	1126.463
ρ	0.4453	0.4491	0.941
S_y	733.1407	733.1407	1835.659
C_y	0.8561	0.8561	0.354193
S_x	150.2150	150.5059	845.610
C_x	0.7531	0.7205	0.7506772
β_2	1.0445	0.0978	-0.063386
β_1	1.1823	0.9782	1.050002
M_d	142.5	150	757.5
MR	320	284.5	1795.5
TM	165.562	162.25	931.562
HL	320	190	1040.5
QD	184	80,25	588.125
G	162.996	155.446	901.081
D	144.481	140.891	801.381
S_{pw}	206.944	199.961	791.364
DM	206.944	234.82	1150.7

Table 1 consists of the Population Parameters.

Table 2: Constant and Bias of Some Selected Existing and Proposed Estimator

Estimator	**Constant**			**Bias**		
	Pop-I	**Pop-II**	**Pop-III**	**Pop-I**	**Pop-II**	**Pop-III**
$\hat{\bar{Y}}_r$	4.294	4.100	4.601	4.940	4.270	60.877
$\hat{\bar{Y}}_1$	2.107	1.9301	2.276	2.137	2.2087	26.800
$\hat{\bar{Y}}_2$	1.806	1.6013	1.949	1.483	1.3964	19.650
$\hat{\bar{Y}}_3$	1.289	1.1703	2.206	0.800	0.7459	25.188
$\hat{\bar{Y}}_4$	1.6960	1.6651	1.9813	1.5604	1.5098	20.312
$\hat{\bar{Y}}_5$	1.7606	1.7136	2.0598	1.6815	1.599	21.953
$\hat{\bar{Y}}_6$	1.5602	1.5324	2.0681	1.3205	1.2788	22.129
$\hat{\bar{Y}}_7$	1.8955	1.9263	1.8608	1.9490	2.0207	17.916
$\hat{\bar{Y}}_8$	1.9764	1.9915	1.9299	2.1191	1.9915	2.1598
$\hat{\bar{Y}}_9$	1.7274	1.751	1.9371	1.6187	1.6696	19.416
$\hat{\bar{Y}}_{10}$	0.9671	0.9633	1.7938	0.5074	0.5053	16.650
$\hat{\bar{Y}}_{11}$	1.0148	0.9997	1.8622	0.5586	0.5443	17.942
$\hat{\bar{Y}}_{12}$	0.8701	0.8666	1.8693	0.4107	0.409	18.079
$\hat{\bar{Y}}_{13}$	1.1177	1.1672	1.9130	0.6777	0.7419	18.936
$\hat{\bar{Y}}_{14}$	1.1818	1.2211	1.9909	0.7577	0.8121	20.508
$\hat{\bar{Y}}_{15}$	0.9902	1.0283	1.9991	0.5318	0.5758	20.677
$\hat{\bar{Y}}_{16}$	1.4153	1.3533	1.5540	1.0866	0.9973	12.495
$\hat{\bar{Y}}_{17}$	1.4752	1.3979	1.6184	1.1806	1.0642	13.552
$\hat{\bar{Y}}_{18}$	1.2908	1.2329	1.6252	0.9038	0.8278	13.666
$\hat{\bar{Y}}_{19}$	1.6021	1.5977	1.6667	1.3923	1.3901	14.373
$\hat{\bar{Y}}_{20}$	1.6793	1.6603	1.7410	1.5298	1.5011	15.684
$\hat{\bar{Y}}_{21}$	1.4444	1.4326	1.7489	1.1317	1.1176	15.825
$\hat{\bar{Y}}_{p1}$	0.0282	0.0296	0.0097	0.0004	0.0005	0.0005
$\hat{\bar{Y}}_{p2}$	0.0318	0.0326	0.0110	0.0005	0.0006	0.0006
$\hat{\bar{Y}}_{p3}$	0.0223	0.0231	0.0111	0.0003	0.0003	0.0006
$\hat{\bar{Y}}_{p4}$	0.0282	0.0295	0.0097	0.0004	0.0005	0.0005

$\hat{\bar{Y}}_{p5}$	0.0318	0.0325	0.0110	0.0005	0.0006	0.0006
$\hat{\bar{Y}}_{p6}$	0.0223	0.0230	0.0111	0.0003	0.0003	0.0006
$\hat{\bar{Y}}_{p7}$	0.0283	0.0297	0.0097	0.0004	0.0005	0.0005
$\hat{\bar{Y}}_{p8}$	0.0319	0.0327	0.0110	0.0006	0.0006	0.0006
$\hat{\bar{Y}}_{p9}$	0.0224	0.0231	0.0111	0.0003	0.0003	0.0006
$\hat{\bar{Y}}_{p10}$	0.0283	0.0297	0.0097	0.0004	0.0005	0.0005
$\hat{\bar{Y}}_{p11}$	0.0319	0.0327	0.0110	0.0006	0.0006	0.0006
$\hat{\bar{Y}}_{p12}$	0.0223	0.0231	0.0111	0.0003	0.0003	0.0006
$\hat{\bar{Y}}_{p13}$	0.0283	0.0296	0.0098	0.0004	0.0005	0.0005
$\hat{\bar{Y}}_{p14}$	0.0319	0.0327	0.0110	0.0006	0.0006	0.0006
$\hat{\bar{Y}}_{p15}$	0.0223	0.0231	0.0111	0.0003	0.0003	0.0006
$\hat{\bar{Y}}_{p16}$	0.0282	0.0296	0.0098	0.0004	0.0005	0.0005
$\hat{\bar{Y}}_{p17}$	0.0318	0.0326	0.0110	0.0005	0.0006	0.0006
$\hat{\bar{Y}}_{p18}$	0.0223	0.0231	0.0111	0.0003	0.0003	0.0006

Table 2 shows Constant values and Bias of the proposed and some existing estimators for the three Populations. The result revealed that the proposed estimators have least constant values and bias compared to the existing estimators

Table 3: MSE and PRE of the existing and proposed estimators

Estimator	**MSE**			**PRE**		
	Pop-I	**Pop-II**	**Pop-III**	**Pop-I**	**Pop-II**	**Pop-III**
$\hat{\bar{Y}}_r$	10960.76	10539.27	189775.1	100	100	100
$\hat{\bar{Y}}_1$	10934.74	10571.58	153292.6	100.238	99.69437	123.7993
$\hat{\bar{Y}}_2$	10386.83	10030.11	116239.3	105.5256	105.0763	163.2624
$\hat{\bar{Y}}_3$	9644.04	9472.95	144936.7	113.6532	111.2565	130.9365
$\hat{\bar{Y}}_4$	10208.16	10333.07	119741.5	107.3725	101.9955	158.4873
$\hat{\bar{Y}}_5$	10311.83	10203.59	128249.9	106.2931	103.2898	147.9729
$\hat{\bar{Y}}_6$	10002.72	9929.39	129161.3	109.5778	106.1422	146.9288
$\hat{\bar{Y}}_7$	10540.91	10564.74	107326.5	103.9831	99.75892	176.8204
$\hat{\bar{Y}}_8$	10686.6	10683.87	114349.5	102.5655	98.64656	165.9606
$\hat{\bar{Y}}_9$	10258.09	10264.06	115098.9	106.8499	102.6813	164.88

$\hat{\bar{Y}}_{10}$	9306.32	9266.94	100762.1	117.7776	113.7298	188.3398
$\hat{\bar{Y}}_{11}$	9350.19	9300.31	107457.3	117.225	113.3217	176.6051
$\hat{\bar{Y}}_{12}$	9223.53	9184.47	108172.8	118.8348	114.751	175.437
$\hat{\bar{Y}}_{13}$	9452.18	9469.56	112609.8	115.9601	111.2963	168.5245
$\hat{\bar{Y}}_{14}$	9250.70	9529.64	120761.3	118.4857	110.5946	157.1489
$\hat{\bar{Y}}_{15}$	9327.27	9327.31	121636.1	117.5131	112.9937	156.0187
$\hat{\bar{Y}}_{16}$	9802.37	9688.30	79228.58	111.8174	108.7835	239.5286
$\hat{\bar{Y}}_{17}$	9882.86	9745.56	84709.31	110.9068	108.1443	224.031
$\hat{\bar{Y}}_{18}$	9645.86	9543.10	85298.12	113.6318	110.4386	222.4845
$\hat{\bar{Y}}_{19}$	10064.19	10024.69	88963.27	108.9085	105.1331	213.3185
$\hat{\bar{Y}}_{20}$	10181.93	10119.77	95756.01	107.6491	104.1454	198.1861
$\hat{\bar{Y}}_{21}$	9841.01	9791.32	96489.29	111.3784	107.6389	196.680
$\hat{\bar{Y}}_{p1}$	8872.134	8834.561	14473.36	123.5414	119.2959	1311.203
$\hat{\bar{Y}}_{p2}$	8872.233	8834.648	14474.03	123.5400	119.2947	1311.142
$\hat{\bar{Y}}_{p3}$	8871.994	8834.401	14474.11	123.5434	119.2981	1311.135
$\hat{\bar{Y}}_{p4}$	8872.133	8834.56	14473.36	123.5414	119.2959	1311.203
$\hat{\bar{Y}}_{p5}$	8872.232	8834.647	14474.03	123.5401	119.2947	1311.142
$\hat{\bar{Y}}_{p6}$	8871.994	8834.400	14474.11	123.5434	119.2981	1311.135
$\hat{\bar{Y}}_{p7}$	8872.136	8834.564	14473.36	123.5414	119.2959	1311.203
$\hat{\bar{Y}}_{p8}$	8872.237	8834.652	14474.03	123.5400	119.2947	1311.142
$\hat{\bar{Y}}_{p9}$	8871.996	8834.402	14474.11	123.5433	119.2981	1311.135
$\hat{\bar{Y}}_{p10}$	8872.135	8834.563	14473.36	123.5414	119.2959	1311.203
$\hat{\bar{Y}}_{p11}$	8872.236	8834.651	14474.03	123.5400	119.2947	1311.142
$\hat{\bar{Y}}_{p12}$	8871.995	8834.402	14474.11	123.5434	119.2981	1311.135
$\hat{\bar{Y}}_{p13}$	8872.135	8834.562	14473.36	123.5414	119.2959	1311.203
$\hat{\bar{Y}}_{p14}$	8872.235	8834.65	14474.03	123.5400	119.2947	1311.142
$\hat{\bar{Y}}_{p15}$	8871.995	8834.401	14474.11	123.5434	119.2981	1311.135
$\hat{\bar{Y}}_{p16}$	8872.134	8834.561	14473.36	123.5414	119.2959	1311.203
$\hat{\bar{Y}}_{p17}$	8872.234	8834.649	14474.03	123.5400	119.2947	1311.142

$\hat{\bar{Y}}_{p18}$	8871.994	8834.401	14474.11	123.5434	119.2981	1311.135

Table 3 shows Mean Square Errors (MSE) and Percentage Relative Efficiency (PRE) of the proposed and some existing estimators for the three Populations. The result revealed that the proposed estimators have least MSE and highest PRE compared to the existing estimators. This implies that the proposed estimators are more efficient than sample mean, [4] and [14].

3. Results and Discussion

A class of ratio estimators of population mean is proposed and the performance of the proposed estimators over the existing estimators were established. Tables 2 and 3 show the results of the Constant, Bias, Mean Square Error (MSE) and Percentage Relative Efficiency (PRE) of the proposed and existing estimators considered in the study for all the populations used. The results revealed that the proposed estimators have the least MSE and highest PRE than other estimators. The results also show that the average dispersion of the proposed estimators gives better estimates on the average than the existing estimators considered in the study.

4. Conclusion

Going by the results in Table 3, the proposed estimators performed better than the existing estimators considered in the study. It is clear that the proposed estimators do better than the existing estimators having minimum Mean Square Error (MSE) and the highest Percentage Relative Error (PRE). We therefore recommend the proposed estimators for use in practical applications for estimating population mean.

Nomenclature

N:	Population size
n:	Sample size
Y:	Study variable
X:	Auxiliary variable
$\bar{Y}, \bar{X}$:	Population means of study and auxiliary variables
ρ:	Coefficient of correlation
C_y, C_x:	Coefficient of variations of study and auxiliary variables
Q_3:	The upper quartile
QD:	Population Quartile Deviation
β_1:	Coefficient of skewness of auxiliary variable
β_2:	Coefficient of kurtosis of auxiliary variable
TM:	Tri-Mean
M_d:	Median of the auxiliary
MR:	Population mid-range
HL:	Hodges-Lehman estimator
G:	Gini's Mean Difference
D:	Downton's Method
S_{pw}:	Probability weighted moments

References

[1] W.G Cochran (1940). Sampling Techniques, 3rd Edition. Wiley Eastern Limited, India.
[2] C. Kadilar and H. Cingi (2004). Ratio Estimators in Simple Random Sampling. Applied Mathematics and Computation Vol. 151, pp. 893 – 902.
[3] C. Kadilar and H. Cingi (2006). An Improvement in estimating the population mean by using the correlation coefficient. Hacettepe Journal of Mathematics and Statistics. Vol. 35, pp. 103 – 109.
[4] M. Abid, N. Abbas, H.Z Nazir, and Z. Lin (2016). Enhancing the Mean Ratio Estimators for Estimating Population Mean Using Non-Conventional Location Parameters. Revista Colombiana de Estadistica. Vol. 39(1), pp. 63 – 79.
[5] L.N Upadhyaya and H.P Singh (1999). Use of Transformed Auxiliary Variable in Estimating the Finite Population Mean. Biometrical Journal. Vol. 416, pp.27 – 636.
[6] R. Tailor and B. Sharma (2009). AModofied Ratio-cum-product Estimator of Finite Population Mean Using Known Coefficient of Variation and Coefficient of Kurtosis. Statistics in Transition-New Series. Vol. 10(1), pp. 15 – 24.
[7] Z. Yan and B. Tian (2010). Ratio Method to the Mean Estimation using Coefficient of Skewness of Auxiliary Variable. In: Information Computing and Applications. ICICA.
[8] J. Subramani and G. Kumarapandiyan (2012a). A Class of almost Unbiased Modified Ratio Estimators for Population Mean with known Population Parameters. Elixir Statistics. Vol. 44, pp. 7411 – 7415.
[9] J. Subramani and G. Kumarapandiyan (2012b). Estimation of Population Mean using Co-efficient of Variation and Median of an Auxiliary Variable. International Journal of Probability and Statistics. Vol. 1, pp.111 – 118.
[10] J. Subramani and G. Kumarapandiyan (2012c). Modified Ratio Estimators using known Median and Co-efficient of Kurtosis. American Journal of Mathematics and Statistics. Vol. 2, pp. 95 – 100.
[11] J. Subramani and G. Kumarapandiyan (2012d). Estimation of Population Mean using known Median and Co-efficient of Skewness. American Journal of Mathematics and Statistics. Vol. 2, pp. 101 – 107.
[12] M.I Jeelani, S. Maqbool and S.A Mir (2013). Modified Ratio Estimators of Population Mean using Linear Combination of Estimators of Population Mean using Linear Combination of Coefficient of Skewness and Quartile Deviation. International Journal of Modern Mathematical Sciences. Vol. 6, pp. 174 – 183.
[13] A. Nasir, A. Muhammad, T. Muhammad, A. Nasir, and H. Zawar (2018). Enhancing Ratio Estimators for Estimating Population Mean using Maximum value of Auxiliary Variable. Journal of the National Science Foundation of Sri Lanka. Vol. 46(3), pp.453 – 463.
[14] M. Subzar, S. Maqbool, T.A Raja, K.P Surya and P. Sharma (2018). Efficient Estimators of Population Mean Using Auxiliary Information Under Simple Random Sampling. Statistics in Transition new series. Vol. 19(2), pp.1 – 20.

Appendix

$$\bar{X}=\frac{1}{N}\sum_{i=1}^{N}X_i,\quad \bar{Y}=\frac{1}{N}\sum_{i=1}^{N}Y_i,\quad \bar{x}=\frac{1}{n}\sum_{i=1}^{n}x_i,\quad \bar{y}=\frac{1}{n}\sum_{i=1}^{n}y_i,\quad \gamma=\frac{1-f}{n},$$

$$TM=\frac{\left(Q_1+2Q_2+Q_3\right)}{4}, s_y^2=\frac{1}{n-1}\sum_{i=1}^{n}\left(y_i-\bar{y}\right)^2,\quad s_x^2=\frac{1}{n-1}\sum_{i=1}^{n}\left(x_i-\bar{x}\right)^2, S_y^2=\frac{1}{N-1}\sum_{i=1}^{N}\left(Y_i-\bar{Y}\right)^2,$$

$$S_x^2=\frac{1}{N-1}\sum_{i=1}^{N}\left(X_i-\bar{X}\right)^2, MR=\frac{X_{(1)}+X_{(N)}}{2}, HL=Median\left(\frac{\left(X_i+X_j\right)}{2}, 1\le i\le j\le N\right)$$

$$G=\frac{4}{N-1}\sum_{i=1}^{N}\left(\frac{2i-N-1}{2N}\right)X_i, D=\frac{2\sqrt{\pi}}{N\left(N-1\right)}\sum_{i=1}^{N}\left(i-\frac{N+1}{2}\right)X_i, S_{pw}=\frac{2\sqrt{\pi}}{N^2}\sum_{i=1}^{N}\left(2i-N-1\right)X_i$$

$$QD=\frac{Q_3-Q_1}{2}$$

NIPES Conference Proceedings
The 1st International Conference of the Nigerian Institution of Professional Engineers and Scientists 7th-8th Oct. 2021: 186-203
www.nipesjournals.org.ng

Development of a Foot Operated Soap and Water Dispenser

Onochie U. P [a], Onwurah C [b], Obilikpa S. C [c], Ani E. O [d], Kwasi-Effah C. C [e], Okoroafor S. P [f], Isaac-Uzaye V. U [g]
[a,b,d,f,g] Department of Mechanical Engineering, Faculty of Engineering, Alex Ekwueme Federal University, Ndufu Alike, Ebonyi State, Nigeria
[c] Department of Mechatronics Engineering, Faculty of Engineering, Alex Ekwueme Federal University, Ndufu Alike, Ebonyi State, Nigeria
[e] Department of Mechanical Engineering, Faculty of Engineering, University of Benin, Benin City, Edo State, Nigeria
Corresponding Author: onochieuche@yahoo.com, Phone No: 08023778718

Abstract
Hand washing and sanitizing has become a very essential part of our daily life especially in the era of COVID-19 pandemic. Most of the existing hand washing facilities on campuses is such that, the hands of the user are recontaminated after using the dispenser due to the use of hand for turning off the running tap after use. In this study, a pedal driven dispenser for hand washing and sanitizer is developed. The objective of this project is to reduce the risk of contracting or transmitting bacteria and virus during hand washing and to promote effective hand washing practice across university campuses in line with COVID-19 protocols. The machine was designed based on a simple working principle to accommodate a person at a time. All necessary engineering design specifications were considered. An average standard height was used to position the tap at a height of 1.25m. The mechanism is very easy to operate due to the simplicity of the foot pedal press. Hence, it can be conveniently used by almost everyone regardless of their height. The performance evaluation of the machine was analyzed using computer aided design software called Autodesk Inventor software for simulation to outline the places that stress and strain would occur as regards to force application. This dispenser will replace the conventional veronica bucket (hand-operating tap) popularly used on campuses. It is also very effective and will help to stop the spread of the COVID-19 infections and promote good personal hygiene.
***Keywords*:**
Design, Dispenser, Simulation, Fabrication, Water, Soap

1. Introduction

The whole world has been engulfed in a pandemic since the recent emergence of the Corona virus. According to [1], the novel corona virus also known as SARS-CoV-2 is responsible for corona virus disease (COVID-19) pandemic which emerged in late December 2019 in Wuhan, in Hubei province of China, and within three months, had spread globally, prompting the World Health Organization (WHO) to declare it a threat to world health [2]. SARS-CoV-2 belongs to the family Corona viridae (of the order Nidovirales, large, positive single-stranded RNA viruses), which are important human and animal viruses, in permanent circulation with four members of this family causing respiratory infections (common cold) worldwide [3]. It is a beta corona virus that causes fever, headache, and respiratory problems such as cough and shortness of breath. Globally, there have been 116,135,492 confirmed cases of COVID-19, including 2,581,976 deaths, reported by WHO. According to the Centers for Disease Control and Prevention [4], Nigeria had 158,000 confirmed cases of COVID-19 with 1,964 deaths. 138,000 patients have so far recovered from the virus. As of 7 March 2021, a total of 249,160,837 vaccine doses have been administered.

In [5], it was reported that COVID-19 is transmitted from person to person through respiratory droplets and close contact, as previously seen in SARS-CoV and MERS-CoV [6], the two other zoonotic corona viruses. The necessity of practicing respiratory hygiene and hand hygiene, and using appropriate personal protective equipment has been highlighted. On 29 December 2019, the

first four cases of an acute respiratory syndrome of unknown ethology among people linked to a seafood market ("wet market") were reported in Wuhan city, Hubei province, China. This has brought upon emergency lockdowns globally and its effects on health, wellbeing, business, and other aspects of daily life are felt throughout the society. There has been a direct detrimental impact to the global economy, raising concerns about the financial sustainability with effects predicted to continue as the virus fails to be contained. With the number of confirmed cases and its continuous spread, the priority is to reduce the rate of infection and prevention of infection seems to be the best approach. To reduce the rate at which the Corona virus spreads, the world health organization (W.H.O) has given directives to improve our daily hygiene routines, such as frequent and correct washing of hands with soap under running water, use of hand sanitizers after every contact with people or surfaces, use of nose mask to prevent the virus infection through the mouth and nose and while carrying out these measures social distancing is a priority to stop the further spread from one person to another.

According to [7], the most common way to transmit this virus would be through contact and every day, our hands are exposed. Hands act as a medium for exchange of microbes between the organism and its environment. The skin of the hands breeds a variety of organisms such as pathogens. Therefore, adequate hand hygiene can greatly reduce disease transmission. [8] also reported that hand hygiene comprises various processes such as hand washing, cleansing or disinfection. Hand washing is done with soap and water and aims at mechanical removal of dirt and microorganisms. Shaking of hands was a very widely practice, but today there are restrictions to this now. Hand washing should be most highly practiced by all and in doing this, more convenient methods and machines has to be designed to enable ease and help stop the continuous spread of this virus, improving the hygiene practice through technology.

According to [9], the US Centre for Disease Control and Prevention, reported that to prevent the spread of germs during the COVID-19 pandemic, it is essential for everyone to cultivate the habit of hand washing with soap and water for at least 20 seconds or use hand sanitizer with at least 60% alcohol to clean hands before and after touching your eyes, nose, or mouth, touching your mask, entering and leaving a public place. Touching an item or surface that may be frequently touched by other people, such as door handles, tables, gas pumps, shopping carts, or electronic cashier registers/screens the single most important way of preventing the spread of infections is through Hand washing; hands unwashed or poorly washed are very common way of spreading many diseases such as: cold, flu, ear infections, strep throat, diarrhea and other intestinal problems. By handling food, touching door knobs, shaking hands and putting mouths on a telephone receiver, germs and viruses causing these diseases are passed on by such routine. Either in the offices, at home, in the market places, in the classroom and so on in our daily activities we practice one of these. Good hand washing practices have also been known to reduce the incidence of other diseases, notably pneumonia, trachoma, scabies, skin and eye infections and diarrhea-related diseases like cholera and dysentery [10].

Foreign developed countries have produced advance hand washing machines which are expensive for developing countries, there is need to design low cost and efficient machines to fight and contain the spread of COVID-19. A water and soap dispenser machine with contactless mechanism is ideal in limiting the transfer of the virus from one person to another [10]. The foot

operated soap and water dispenser machine is designed and fabricated to eliminate the risk of spreading COVID-19 when an infected person is about to wash off their hands from a tap. This dispenser machine is designed to be used in any place a thorough hygiene routine and COVID19 protocol is observed such as in offices, classrooms, hostels, churches, public restrooms as well as domestic places. Ideally the cap of the soap container and the water tap head needs to be opened before one can be able to wash off their hands [10]. The design is made in such a way that a contactless mechanism is possible using pedals and tension springs to link the components of mechanism. Adopting a contactless way of washing our hands can help enormously in fighting against the spread of the Corona virus, saving lives and maintaining a high level of hygiene in the society today.

According to [11], it was reported that due to the ongoing fight against the COVID-19, there is need to introduce new and convenient way of reducing the spread of the virus through contactless way of hand washing without being hindered with the challenges that comes with power supply normally associated with automated hand washing machines. From our day-to-day activity, living a contactless lifestyle is hard and next to impossible because traditionally, there must be an interaction between oneself and his/ her environment. This seems to be a bit of a challenge because there's no way one can even maintain a good hygiene through washing of hands without having contact with the tap head to release water. The hand washing facilities that is commonly used and available requires contact and the ideal purpose of its use to help stop the spread of the Corona virus is not solely achieved. This basically means that when a person possibly with the virus on their hands tries to wash it off with soap and water, they still need to turn off the tap which most possibly has the virus on it, transferred before tap is opened. In this scenario, once he/she tries to close the tap to stop water from running, the virus is most likely to be transferred back to the same person as its being closed or the next person that would use the tap.

2. Materials and Method

The selection of material for any application is often based on the material's properties, suitability of use in the environment of operation, performance, design consideration, cost, and usability owing to their strength, durability, weight, and other mechanical properties. All the materials used were sourced locally such as the mild steel square pipe, angle iron, spring, sink, water container, water hose, push valve and tap, etc. The machine was designed based on a simple working principle to accommodate a person at a time. An average standard height was designed to position the tap at a height of 1.25m. Hence it can be conveniently used by almost everyone regardless of their height. The working diagram for fabricating the machine frame and other components is shown below. The various components welded and coupled together to make the machine are listed and explained in the section below. The design process of the hand washing machine was based on the functionality of individual parts.

2.1 Mechanical Design of the Dispenser

The components that make up the machine are mainframe, angle iron, 2-inch square pipes, 1-inch square pipes, water container, push valve, tap, sink, water hose, push angle valves, spring and

pedals. The mainframe was first designed using CAD software (Autodesk Inventor). It has a dimension of 0.61mx0.64mx1.01m as depicted in the top and side views presented in Fig. 1.

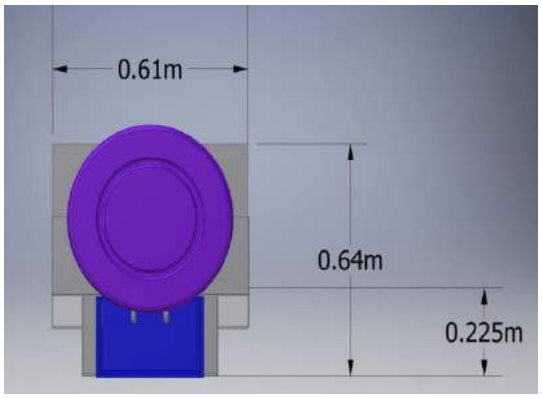

(a)Top View

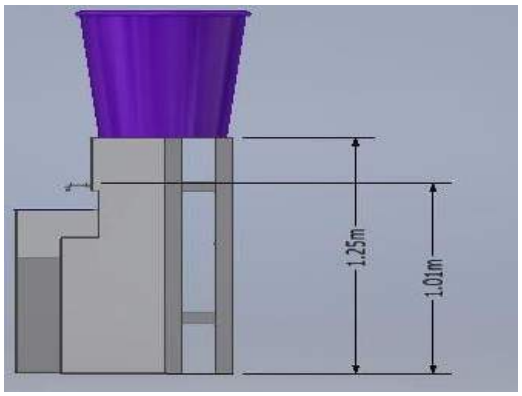

(b) Side View

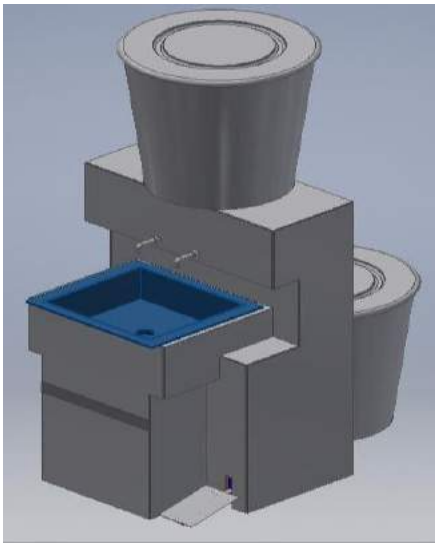

(C) Isometric View of the CAD Model

Fig. 1: Top, Side, and Isometric Views of the Dispenser

Soap and Water Translating pipes illustrated in fig.2 are stationed near the frame having a translational movement inside a 2-inch square pipe fixed to the frame. As the inner pipe moves in a vertical linear motion, there is frictionless constraint applied to make sure the mechanism works as designed. These pipes are coated with water-resistant paints that increase their durability.

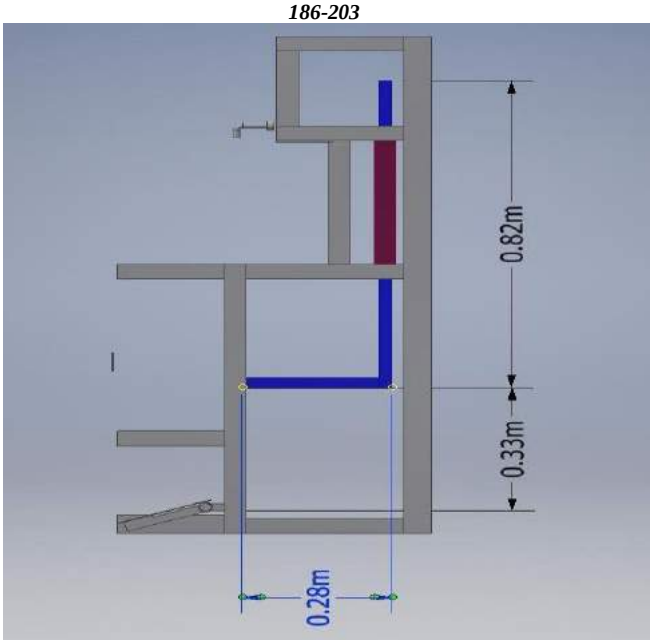

Fig. 2: Soap and Water Translating Pipes

2.2 Working Principle of the Machine

The machine was designed and fabricated to operate based on a simple mechanism. The foot operated machine is basically made of metal and other non-metal materials. For the soap dispenser, the cap is operated by pressing the pedal with the foot. On pressing the pedal, the tension spring attached to the inner movable pipe and outer fixed pipe gets extended/elongated. In order to bring the inner movable pipe downwards, when the inner movable pipe pulls downward the outer fixed pipe remains in position holding the soap dispensing container. For this action to take place, the inner movable pipe should move downwards, causing contact between the bottle and the extended part which presses the cap. As the inner movable pipe moves downwards, the pressure is applied on the cap and the bottle starts dispensing soap through the tap head on the sink. The soap is able to come out of the nozzle because its viscosity is reduced making it easy to flow. The dispensing action of the soap bottle comes to an end when the pump is brought back to its original position by removing the force applied. When the force from the pedal is lifted, the pedal returns to its original position, so does the spring and the translating pipe. Thus, it returns to its initial position and stops dispensing soap. When soap is received from one tap head at the sink, the operator/user moves across and makes a press with his/her foot on the second pedal which controls the flow of clean water for washing the hands. Once the foot is pressed on the pedal, the translating pipe which seats on the push angle valve, presses the valve head downwards to allow the flow of water through the valves to the basin where the contaminated hands are washed. After washing the hands, the tap is closed by the same spring action when the foot is released.

2.3 Design Calculations

2.3.1 Forces acting on the Machine

a. Load on machine

Force acting on the machine as load from the volume of water container placed on top of the machine is given by 30 litres.

If 1litre = 1kg, therefore, 30 litres = 30kg

Also 1kg = 10N, 30kg = 300N

But 1N = 0.225 lbf, 300N = 67.4427 lbf

b. Forces on pedal

Assuming that the pedal is acted upon by five different forces,

Forces applied on the pedal (F_p) = Mass x Acceleration due to gravity (1)

Force 1:

Given that Mass = 1.6 kg and acceleration due to gravity = 9.81m/s^2, we have that

F_{p1} = 1.6 x 9.81 = 15.696 kgm/s^2 = 15.696 N

Force 2:

Given that Mass = 1.8 kg and acceleration due to gravity = 9.81m/s^2, we have that

F_{p2} = 1.8 x 9.81 = 17.658 kgm/s^2 = 17.658 N

Force 3:

Given that Mass = 2 kg and acceleration due to gravity = 9.81m/s^2, we have that

F_{p3} = 2 x 9.81 = 19.62 kgm/s^2 = 19.620 N

Force 4:

Given that Mass = 2.2 kg and acceleration due to gravity = 9.81m/s^2, we have that

F_{p4} = 2.2 x 9.81 = 21.582 kgm/s^2 = 21.582 N

Force 5:

Given that Mass = 2.4 kg and acceleration due to gravity = 9.81m/s^2, we have that

F_{p5} = 2.4 x 9.81 = 23.544 kgm/s^2 = 23.544 N

2.3.2 Calculation for Spring Stiffness

Since the applied force at the pedal is proportional to the force required to stretch the spring fixed at the top of the soap and water shaft linkages, we calculate the spring stiffness from Hook's law of elasticity given by;

$F = F_S = -K.\Delta E$ (2)

Where FS= Spring force, K = Spring Stiffness and ΔE = Displacement/ change in translational distance and the negative sign showing work is done against the restoring force.

From evaluation, the tension spring suitable for the machine mechanism has a spring stiffness of 25N/M

2.3.3 Displacement along the Translating Pipes

Considering that the spring used is made of high carbon steel with spring stiffness of 25N/M, hence, from equation 2,

Displacement 1:

F_{S1} = 15.696 N, -K = 25N/M

From equation 2; ΔE_1 = 0.62784 m

Displacement 2:

F_{S1} =17.658 N, -K = 25N/M

ΔE_2 = 0.70632 m

Displacement 3:

F_{S1} = 19.620 N, -K = 25 N/M

ΔE_3 = 0.7848 m

Displacement 4:

F_{S1} = 21.582 N, -K = 25N/M

ΔE_4 = 0.86328 m

Displacement 5:

F_{S1} =23.544 N, -K = 25N/M

ΔE_5 = 0.94176 m

Table 1 show the comparison between the different theoretical displacements gotten from the value of the different forces on the pedal

Table 1: Applied force -Displacement

S/N	Applied force (N)	Theoretical Displacement (mm)
1	15.696	0.62784
2	17.658	0.70632
3	19.620	0.78480
4	21.582	0.86328
5	23.544	0.94176

2.4 Finite Element Analysis

This is a numerical method used to ascertain information on how a part, component or machine behaves under some given conditions. It gives other valuable information such as the displacement, factor of safety, contacts which were produced in the simulation report.

3. Results and Discussion

3.1 Simulation and Performance Analysis of Machine

The performance evaluation of the machine was analyzed using computer aided design software called Autodesk Inventor software for simulation to outline the places that stress and strain would occur as regards to force application.

3.1.1 Soap Dispenser Pipe Analysis

Different forces were used to execute the stress analysis on the soap dispenser pipe. The results presented are as a result of different forces on the pedal for soap dispenser pipe.

1. **Displacement Simulation result**

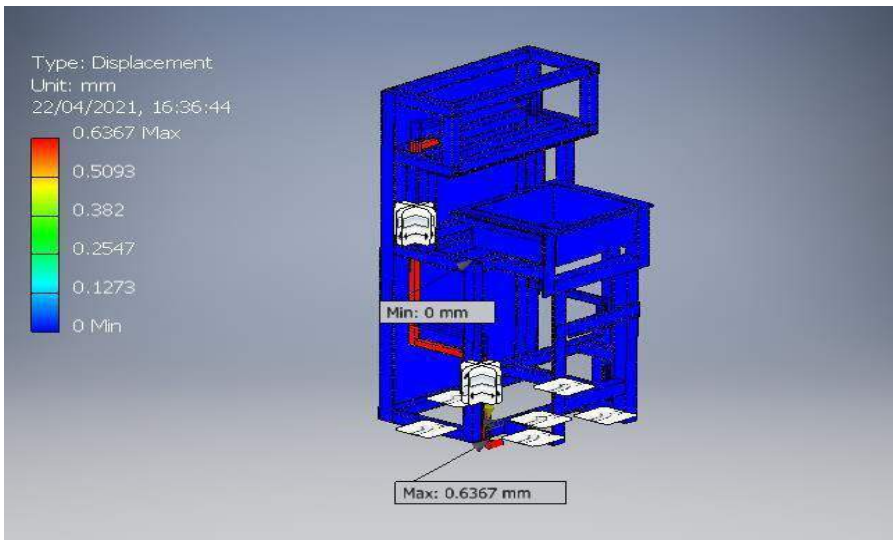

Fig 3: Simulation showing displacement

2. **Stress Simulation result at XX axis**

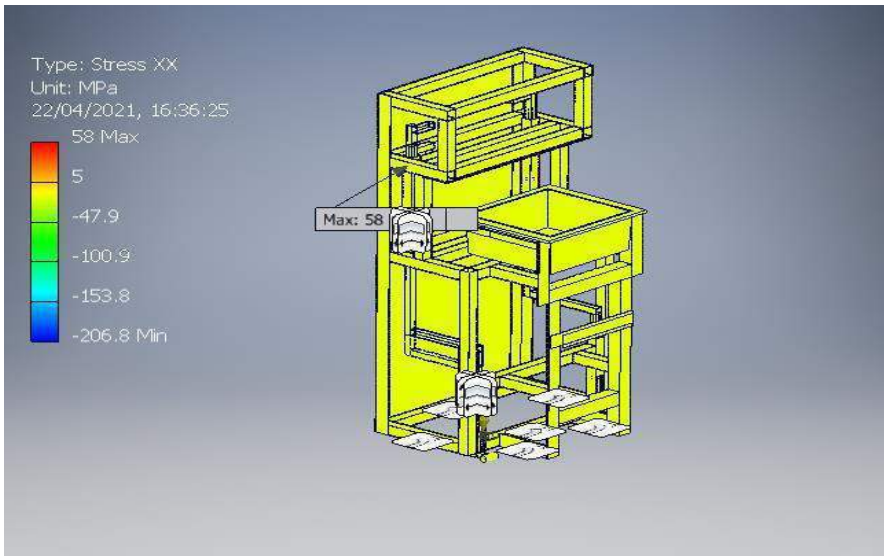

Fig 4: Simulation showing stress at xx axis

3. Von Mises Stress Simulation result

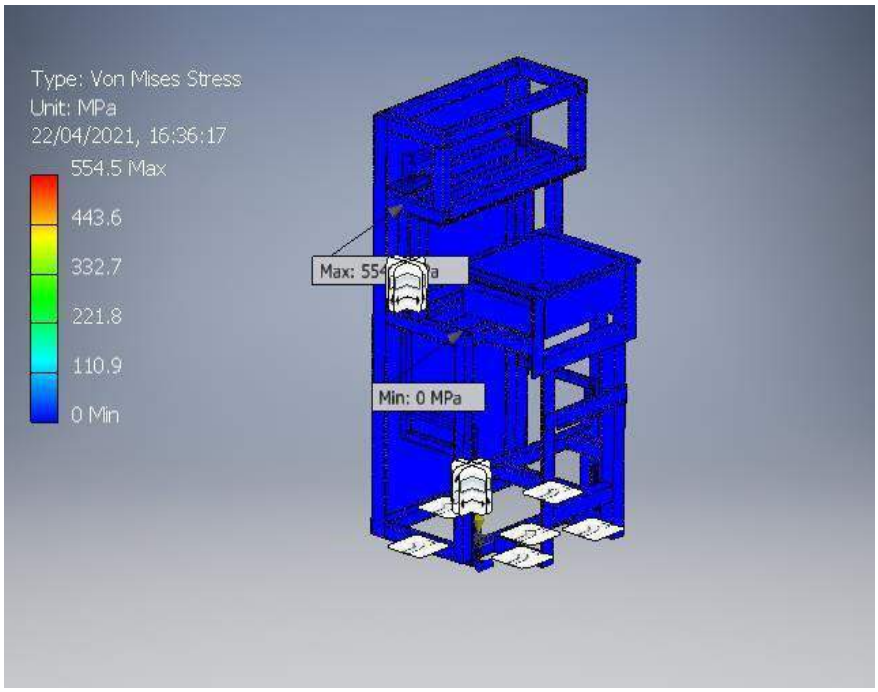

Fig 5: Simulation showing von mises

4. Safety factor simulation result

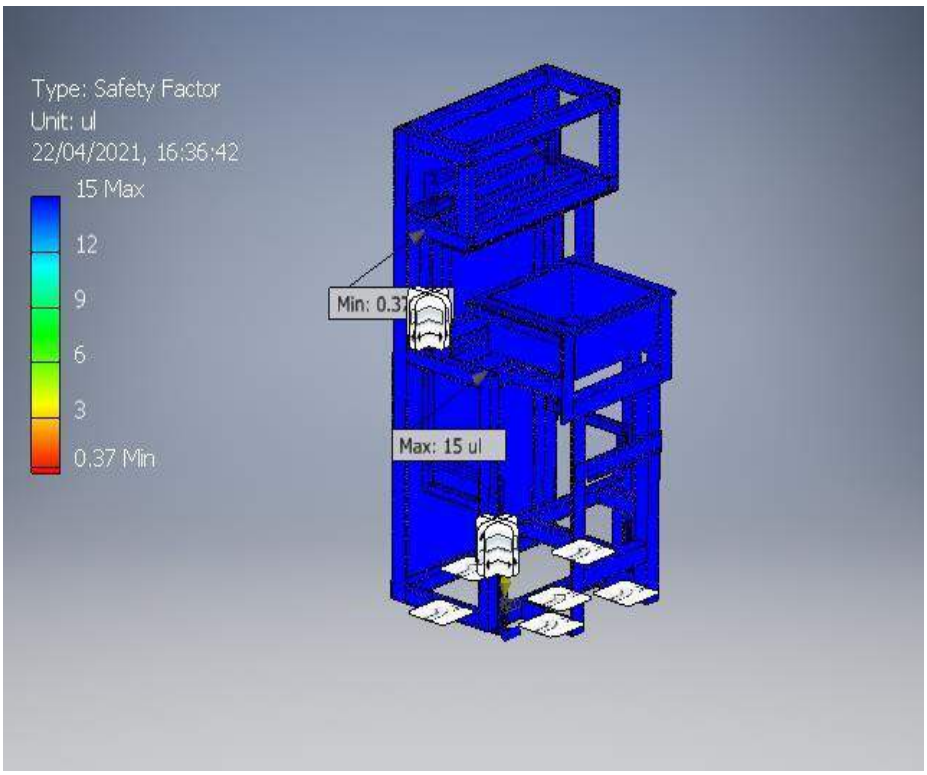

Fig 6: Simulation showing safety factor

5. Simulation showing principal stress

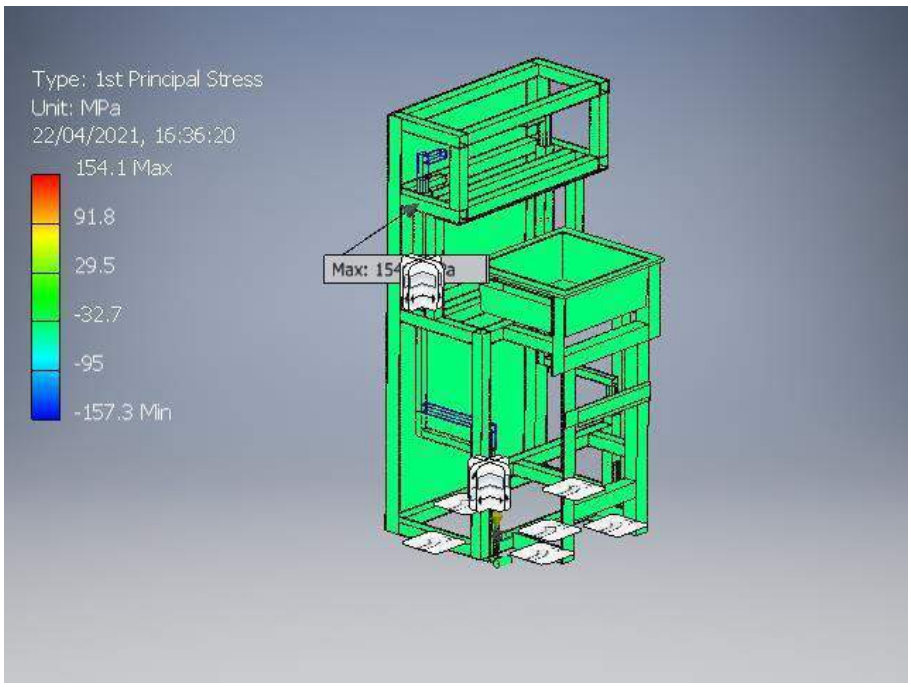

Fig 7: Simulation showing principal stress

6. Simulation showing principal strain

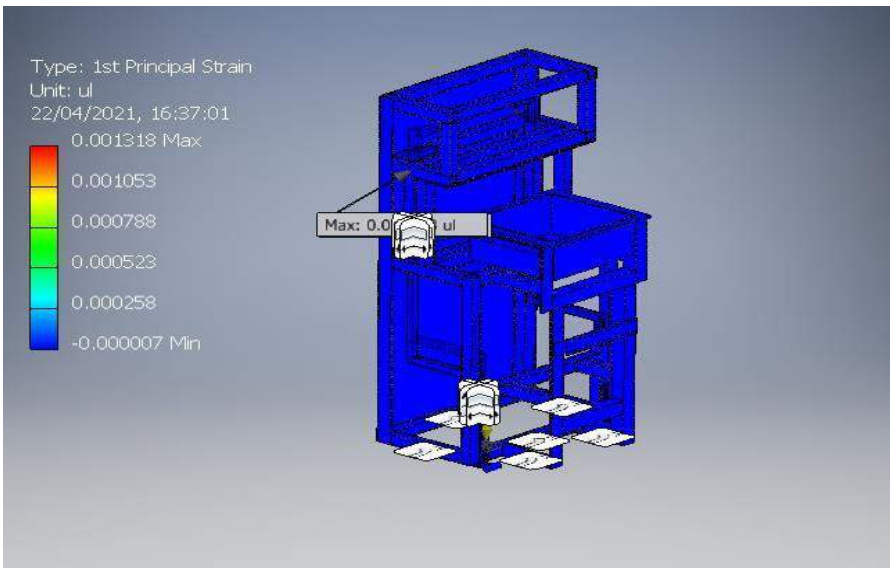

Fig 8: Simulation report diagram showing principal strain

7. Strain simulation on xx axis

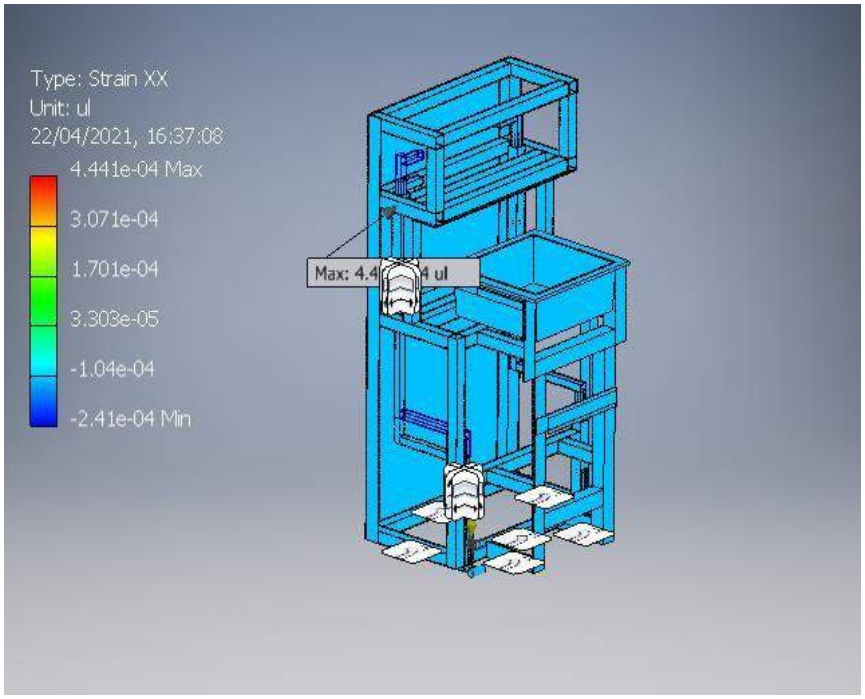

Fig 9: Simulation showing strain on xx axis

8. Contact pressure simulation

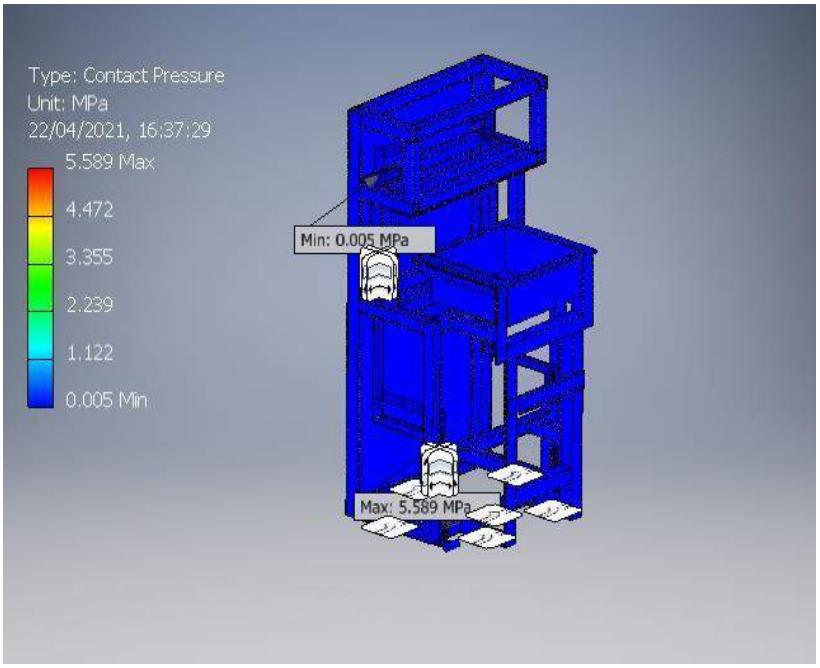

Fig 10: Simulation showing contact pressure

9. Equivalent strain simulation

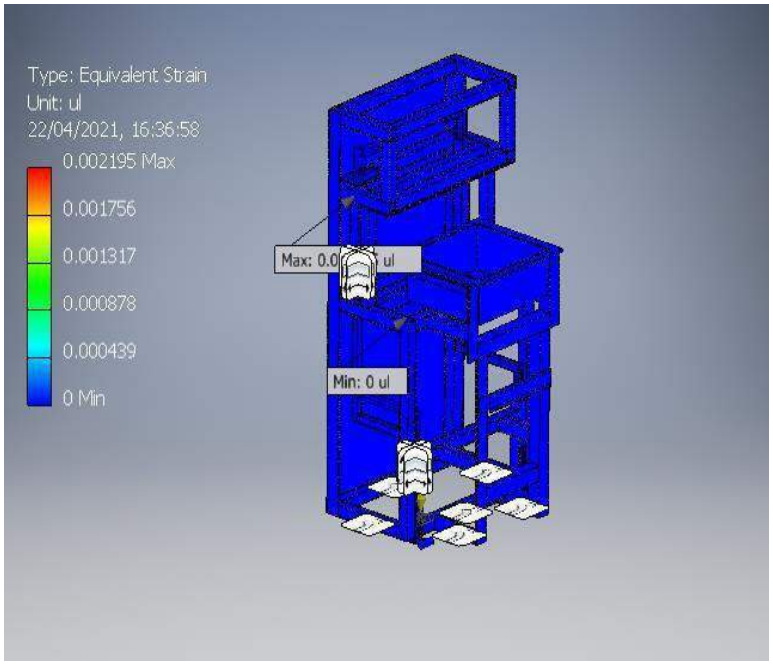

Fig 11: Simulation showing equivalent strain

3.2.1 Water Dispenser Pipe Analysis

Different forces were used to execute the stress analysis on the water dispenser pipe. The results gotten are as a result of different forces on the pedal for water dispenser pipe.

1. Displacement Simulation

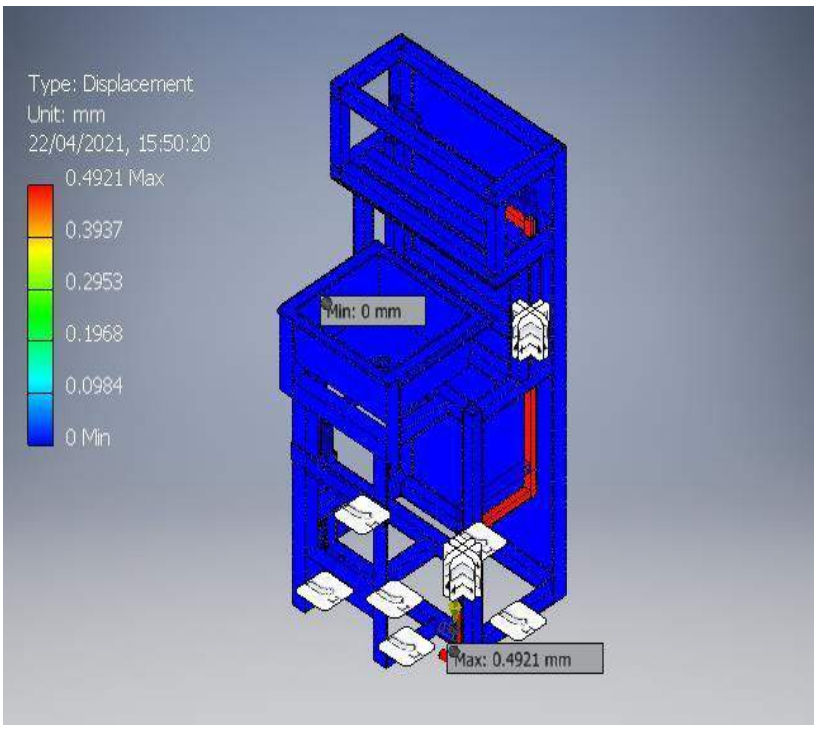

Fig 12: simulation showing displacement

2. Stress simulation on xx axis

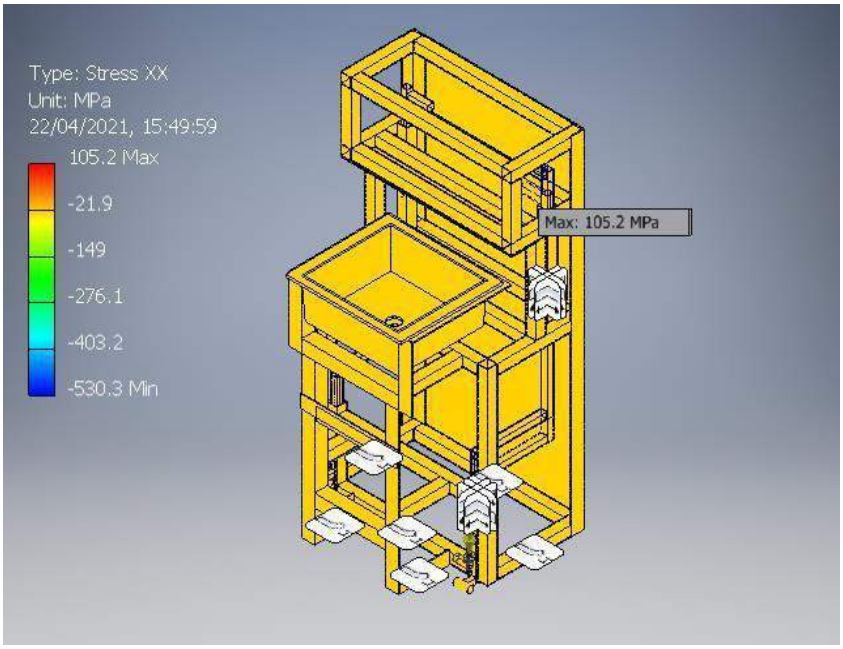

Fig 13: simulation showing stress on xx axis

3. Von mises stress simulation

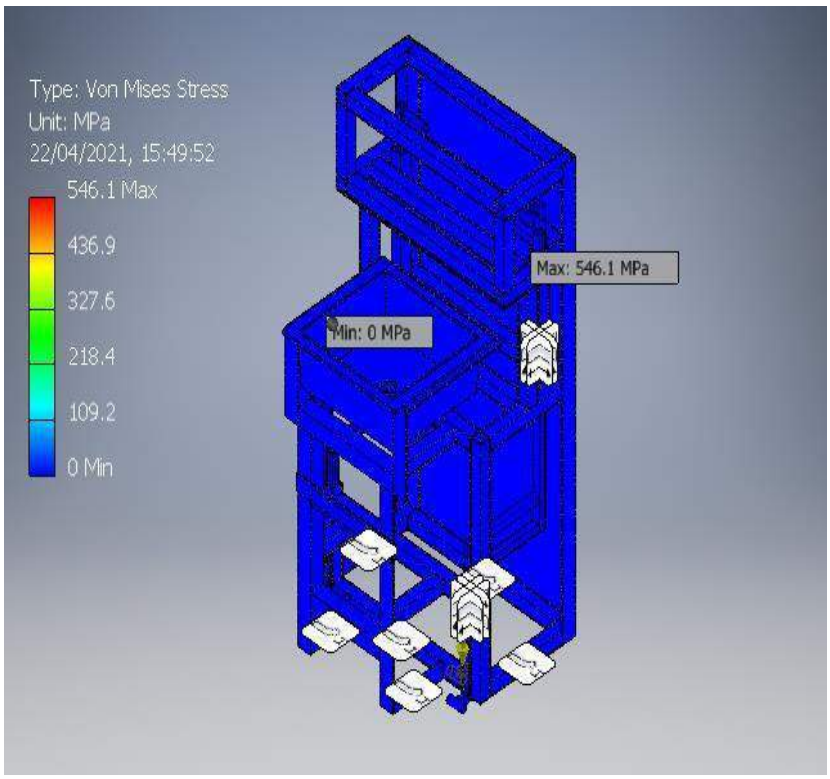

Fig 14: Simulation showing von mises stress

4. Safety factor simulation

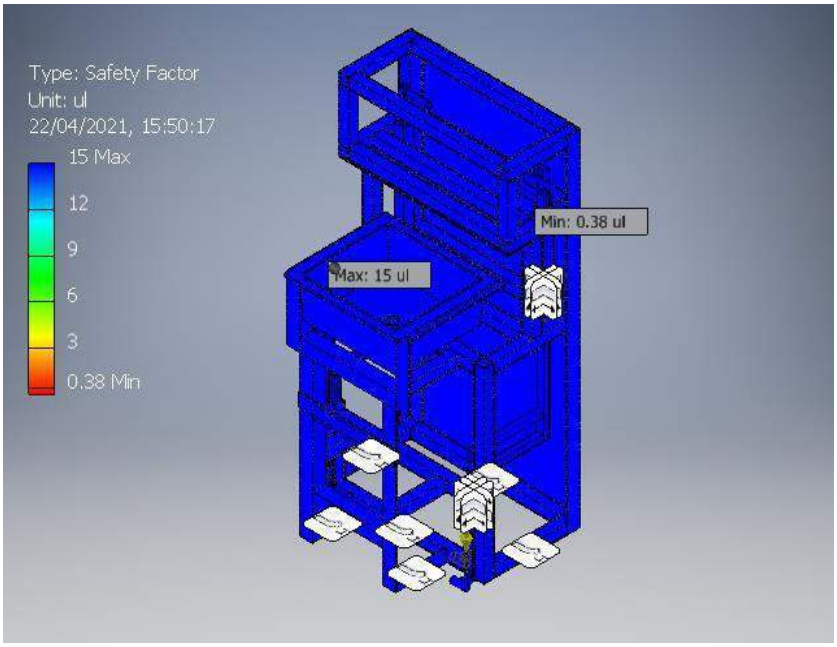

Fig 15: Simulation showing safety factor +

5. Principal strain simulation

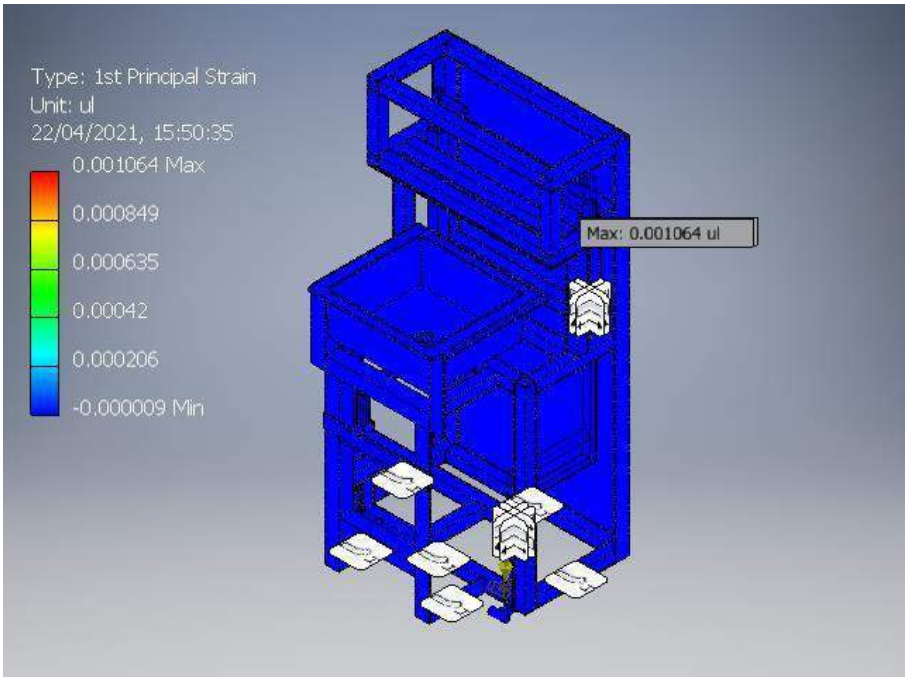

Fig 16: Simulation showing principal strain

6. Strain on strain xx axis

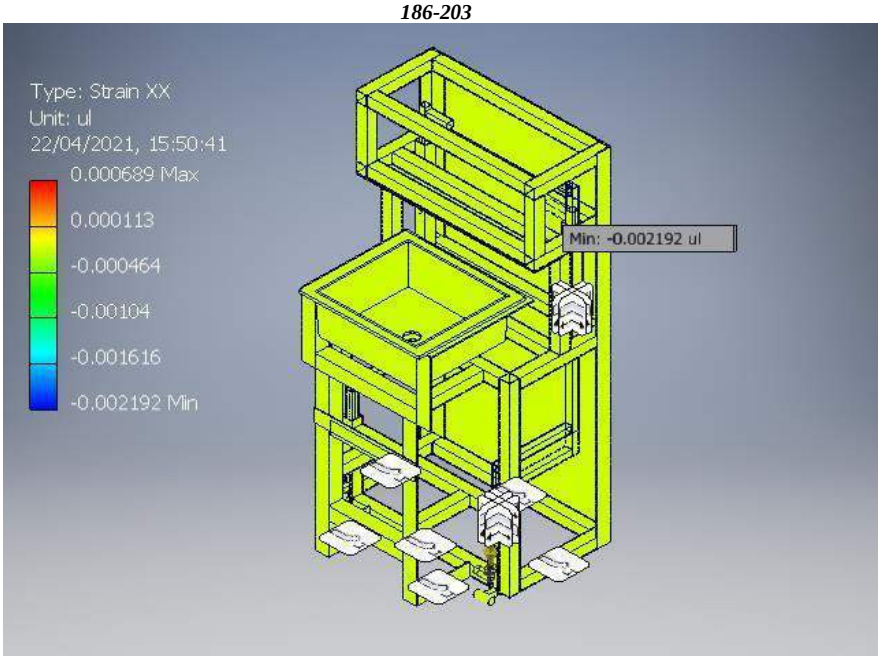

Fig 17: Simulation showing strain on xx axis

7. Contact pressure Simulation

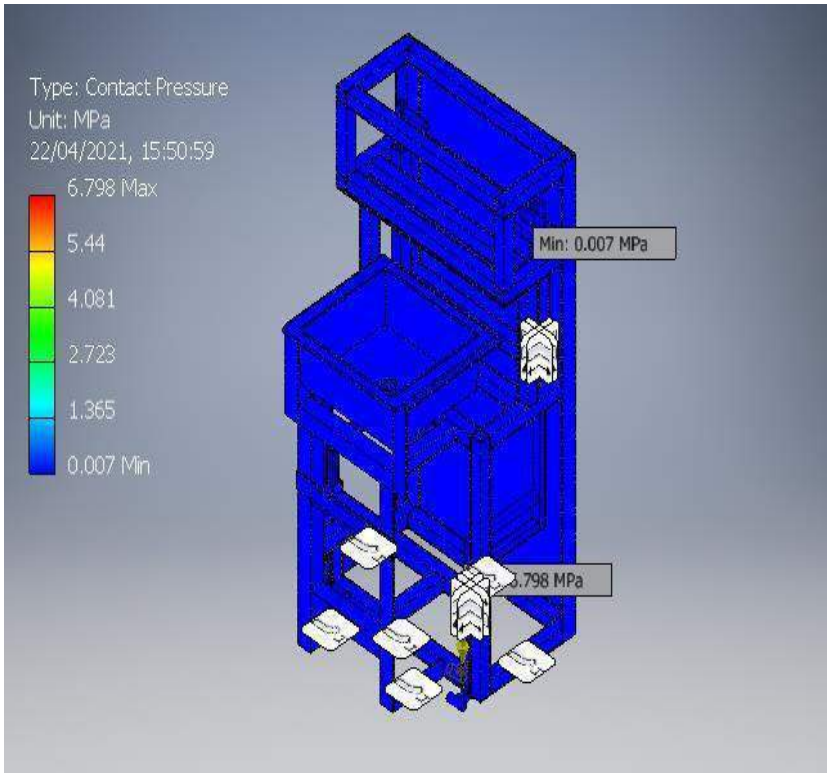

Fig 18: Simulation showing contact pressure

8. Equivalent strain simulation

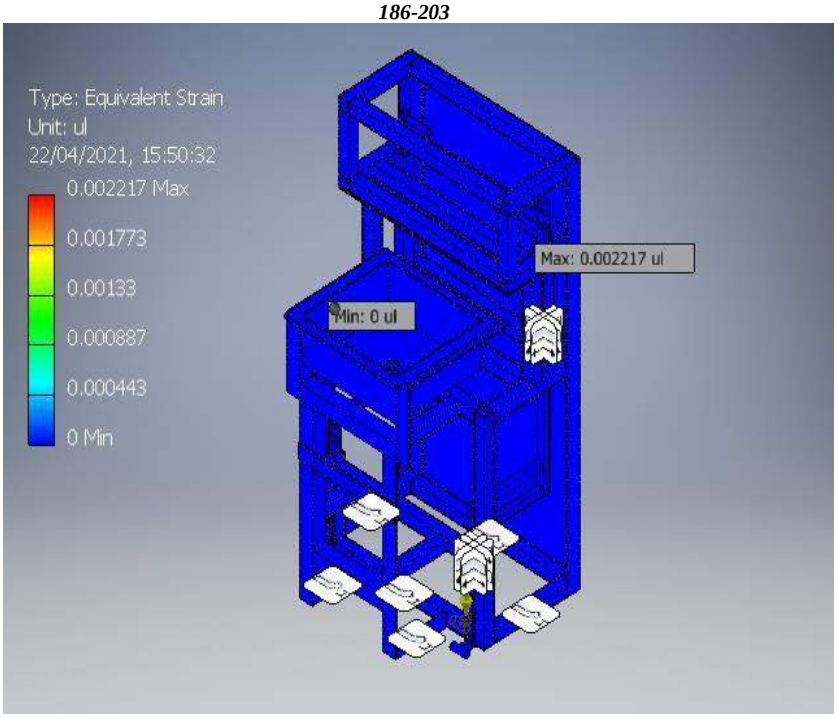

Fig 19: Simulation showing equivalent strain

3.3 Interpretation of Analysis

From the simulation analysis of the soap pedal translating pipe and the water pedal translating pipe, the following were deduced;

1. The increase in force leads to increase in translational displacement.
2. The increase in force leads to increase in the stresses on the soap and water pedal translating pipes.
3. The increase in force leads to increase in the strain on the soap and water pedal translating pipes.
4. The increase in force leads to increase in the von mises stresses on the soap and water pedal translating pipes.
5. The increase in force leads to increase in the principal stresses on the soap and water pedal translating pipes.
6. The increase in force leads to increase in the principal strains on the soap and water pedal translating pipes.
7. The increase in force leads to increase in the contact pressure on the soap and water pedal translating pipes.
8. The increase in force leads to increase in the equivalent strain on the soap and water pedal translating pipes.
9. The increase in force leads to decrease in the safety factor of the translating pipes.

3.4 Comparing Displacement Values

From the Table 2, it can be seen that the theoretical displacement values are similar to the displacement values gotten from the finite element analysis of the translating pipes. This shows that the results of the analysis are correct and obtainable.

Table 2: Theoretical displacement-FEA displacement

THEORETICAL DISPLACEMENT (mm)	FINITE ELEMENT ANALYSIS DISPLACEMENT (mm)	
	SOAP	**WATER**
0.62784	0.636687	0.592125
0.70632	0.716251	0.608231
0.78480	0.795814	0.675156
0.86328	0.875377	0.839390
0.94176	0.954941	0.934542

4. Conclusion

The need for a contactless way of maintaining hygiene through hand washing cannot be overemphasized. A foot operated hand washing machine capable of dispensing liquid soap and water for hand washing was designed and fabricated. The mechanism utilized is simple and made from durable material, it is easy to operate and has low cost of maintenance. This is an advantage over other designs with complicated mechanisms. It was observed from experimental analysis that force on the pedals leads to the translational motion which dispenses liquid soap and water. Therefore, it can be concluded that the force which serves as the work input affects the displacement which leads to the dispensation of liquid soap and water. The operating efficiency of the machine is 90% and can be used in any firm or institution for the fight of COVID-19 and maintaining hand washing practices for personal hygiene.

References

[1] C. Huang, Y. Wang, X. Li, L. Ren, J. Zhao, Y. Hu (2019). “Clinical Features of Patients Infected with 2019 Novel Corona Virus in Wuhan, China”. Lancet. 395(10223):497-506.

[2] C. Sohrabi, Z. Alsafi, N. O’Neill, M. Khan, A. Kerwan, A. Al-Jabir, C. Iosifidis, R. Agha, (2020). World Health Organization declares global emergency: A Review of the 2019 Novel Corona virus (COVID-19). Int. J. Surg. 76, 71–76.

[3] Y. Roussel, A. M Giraud-Gatineau, M. T Jimeno, J. M Rolain, C. Zandotti, P. Colso, D. Raoult (2020). SARS-CoV-2: Fear Versus Data. Int. J. Antimicrob. 105947.

[4] Centers for Disease Control and Prevention CDCP (2020). "Coronavirus Disease 2019 (COVID-19)".https://www.cdc.gov/coronavirus/2019-ncov/prevent-gettingsick/disinfecting-your-home

[5] X. Peng, X. Xu, Y. Li, L. Cheng, X. Zhou, B. Ren (2020) Transmission Routes of 2019nCoV and Controls in Dental Practice. Int. J. Oral Sci. 12.

[6] D. K Chu D, E. A Aki, S. Duda, K. Solo, S. Yaacoub, H. J Schünemann (2020). Physical Distancing, Face Masks, and Eye Protection to Prevent Person-to-Person Transmission of SARS-CoV-2 and COVID-19: A Systematic Review and Meta-Analysis. Lancet. 395:197387

[7] M. Gupta, A. Abdelmaksoud, M. Jafferany, T. Lotti, R. Sadoughifar, M. Goldust M. (2020). COVID-19 and Economy. doi:10.1111/dth.13329 https://www.cdc.gov/handwashing/when-how-handwashing.html

[8] C. Huang, W. Ma, S. Stack (2012). "The Hygienic Efficacy of Different Hand-Drying Methods: A Review of the Evidence". Mayo Clinic Proceedings. 87 (8): 791–8. doi:10.1016/j.mayocp.2012.02.019. PMC 3538484. PMID 22656243.

[9] P. Sun, X. Lu, C. Xu, W. Sun, and B. Pan (2020). Understanding of COVID-19 Based on Current Evidence. J Med Virol.

[10] WHO. (2020).”Infection Prevention and Control During health Care When Novel Coronavirus (nCoV) Infection is Suspected”. https://apps.who.int/iris/rest/bitstreams/1266296/retrieve.

[11] J. Witt Huberts, K. Greenland, W. P Schmidt, V. Curtis (2016). Exploring the potential of antimicrobial hand hygiene products in reducing the infectious burden in low-income countries: An integrative review. Am J Infect Control; 44:764-71.

NIPES Conference Proceedings
The 1st International Conference of the Nigerian Institution of Professional Engineers and Scientists 7th-8th Oct. 2021: 204-210
www.nipesjournals.org.ng

Policy and Standards for Energy Efficiency in Nigeria - A Systematic Review

Akinfaloye Oluwabusayo Akinyemi
Department of Mechanical Engineering, Petroleum Training Institute, Effurun, Nigeria.

Abstract
Energy issues is a global concern in this era of Industry 4.0. This systematic review presents policy and standards for energy efficiency in Nigeria. This issue has become very significant especially as government, researchers, strategists and professionals continue to combat climate change. The issue of climate change in Nigeria is on the increase as a result of inefficient use of energy especially in the oil and gas sector. This has led to increase in environmental pollution, amount of greenhouse gases, and general health issues. This must be significantly reduced to embrace green environment and sustainable energy process. Nigeria is still struggling with the energy sector because there are energy obstacles to be eradicated. These barriers to energy efficiency include hoary technology, inefficient electrical facilities, thermal utilities, power infrastructure, and others. To achieve sustainable standard for energy efficiency, energy analysis and auditing, energy modelling, and energy monitoring are usually implemented. This can be deterministically analyzed and presented in four major areas which include: standards for energy efficiency management, climate change and energy efficiency, possible barriers to energy efficiency, and policies for energy efficiency. In this study, further elaboration of the enlisted areas are detailed focusing on the standard put in place for sustainable energy efficiency, and possibility of boosting and implementing energy efficiency.

***Keywords*:**
Global concern, Policies, Standards for Energy Efficiency, Energy Sustainability

1. Introduction

The need to conduct global research on Energy efficiency is the focus of researchers especially in this era of Industry 4.0. This is clearly a suggestion focused on how effective and efficient energy can be converted from one form to another. Regrettably, some of the energy which transforms from one form to another is lost in the form of heat energy. Energy efficiency is defined in a simple term as the sum of all the useful energy and wasteful energy. As the energy efficiency of a system increases, there is tendency for lower emission which is produced by the source of available energy, when this happens then there is tendency for reduced hazard in terms of health and environmental hazards [1]. One of the Social Development Goals is universal access to modern energy and clean cooking, which is critical for modern living and a higher level of living. As a result, the need for energy efficiency policies and standards in Nigeria, as well as the rest of the world, should be carefully examined, formulated, and implemented in order to reduce the negative effects of energy waste on the environment, health, atmosphere, and less-than-optimal resource use, among other things. Renewable energy sources and alternative energy technologies produce zero or extremely low emissions and have minimal influence on the environment and human health, hence energy efficiency policies and regulations should be developed to encourage their use. Greenhouse gases such as carbon (IV) oxide and carbon (II) oxide, heavy metals such as lead and mercury, pollution and contaminants such as ashes, and radioactive waste such as alpha particles, beta rays, gamma rays, radioactive by-products, and so on are all examples of these emissions. These emissions can also cause disease conditions related to cancers, red blood cell, food poisoning, water system contamination. This important relationship between energy access and its health implications creates a platform; The SDGs presents a very good platform and opportunity to apply a connection or series of connections between modern energy access and health. Thus, the knowledge of energy efficiency and energy saving opportunities is important in producing a good energy standards and policy.

2. Review Focused on Energy Supply in Facilities

The gap between energy demand and supply is widening in Nigeria, where affordable electricity is neither sufficient nor reliable. The Nigerian Energy Sector Study demonstrates the critical necessity for energy efficiency regulations as a partial solution [2]: According to the Nigerian Electricity Regulatory Commission (NERC), gas-based power plants account for 80% of real generation capacity in 2015, with hydro power plants accounting for the remaining 20%. Gas power plants account for 84 percent of installed capacity, while hydro power plants account for 16 percent. Plants built before the 1990s and plants built (or being built) during the mid-1990s make up the current fleet of power plants. The available generating capacity was just under 6200 MW in 2012 and has climbed to only 6840 MW in 2015. This is due to the older thermal power stations' poor maintenance. However, a lack of gas and a water shortage severely limit power plant performance, and grid constraints have a significant impact on electricity supply security. Peak demand is estimated to be over 12,800 MW, while peak generation is at best around 5000 MW, and the only way to make up for this massive shortfall is to rely on off-grid power. According to a poll conducted in 2013, almost 80% of Nigerians use alternative energy sources such as generators or solar inverters. According to estimates, the country now has between 8 and 14 GW of decentralized generating capacity (diesel and gasoline).

Furthermore, it is projected that 86 percent of Nigerian businesses own or share a generator, with these private generators covering 48 percent of the country's overall electricity demand. Nigeria is Africa's largest generator importer, with millions of privately installed diesel generators. This form of energy generation, on the other hand, is clearly problematic, not only because of the obvious detrimental impact on people's health as a result of constant air pollution and noise, but also because of the lack of fuel supply stability. Despite the fact that Nigeria is the largest African OPEC crude oil production, its refinery capacity is limited and the majority of petrol and diesel must be imported [3]. Because oil exports account for an average of 80% of government revenue, extreme fluctuations in oil prices, such as from USD147 in July 2008 to below by December 2008, and from in the second quarter of 2014 to below USD 30 in January 2016, have had a significant impact on Nigeria's budget. Furthermore, pipeline infractions as a result of the Delta region's independence movement have had a severe influence on production capacity [4,5].

3. Formulating and Implementing Energy Efficiency Regulations

It is obvious that fuel subsidies have been scrutinized and attempts made to reduce them. However, as a result of this, prices doubled, causing severe social unrest [6]. The reason for formulating and implementing energy efficiency regulations, as well as vigorous efforts to enhance the availability of inexpensive electricity, whether on-grid or off-grid, is evident. Using energy efficiency to its greatest capacity reduces energy demand and, as a result, relieves strain on the energy supply sector. Building construction in Nigeria necessitates a massive effort required in building construction to meet up with the estimated deficit of seventeen million housing units. While it is critical to provide homes for the population, it is also evident that without strong regulations promoting energy efficiency and decentralized renewable energy use, construction activities would inevitably put additional strain on the existing energy supply system [2]. Despite the fact that grid energy supply is erratic or failing, and fuel scarcity makes running private generators difficult, new buildings are largely designed in what is known as a "international style of architecture."

This design strategy ignores the energy-related aspects of a building's location, instead balancing local conditions with increased use of building services associated with massive amounts of

energy for air-conditioning and lighting, resulting in higher energy costs [7]. There appears to be a general lack of awareness in Nigeria about the direct relationship between building design and technologies, as well as their impact on energy efficiency in state-of-the-art building design. Traditional construction materials and conceptions that respond to local climatic circumstances are typically regarded backwards, but modern materials and building designs from elsewhere are sought, resulting in designs that demand a lot of energy, particularly for cooling and lighting [1]. Despite the fact that there are a number of well-tested and advanced tactics that would suit the climate (e.g., phase change materials, thermal mass activation), these measures are not well established because there is no local precedent.

However, because neither systematic data collecting on the technical characteristics of the building stock nor data on actual electricity usage related to building types are available, assessments of the status quo rely on expert judgments, case study analyses, and general observations. The existence of suppressed energy demand, the practice of so-called estimated billing (households are charged based on estimates rather than actual consumption due to the lack of meters), electricity theft, and the fact that private generators take over in the event of grid failure all complicate the assessment of baseline data. When it comes to residential building usage, Nigerians prefer to rent or build their homes, rather than own them. Rent is usually paid in advance for a period of twelve or even twenty four months. Apart from the difficulty in acquiring a large sum of money at once, this technique also means that building owners are less likely to resolve problems that arise in the buildings because they have already been paid and hence have little motivation to do so.

The above status quo description clearly demonstrates that energy efficiency measures must address the building sector in a way that begins the necessary widespread paradigm shift toward energy efficient building design, construction, and use. It does, however, show that the obstacles are immense, owing to a serious lack of understanding among architects, engineers, builders, and clients, as well as the fact that reliable data is virtually non-existent.

4. Challenges for Policy Makers

Suppressed Electricity Demand, Urbanization, and Housing Deficit. The problems outlined above are made considerably worse by rural-urban migration, which leads to massive urbanization and adds to Nigeria's massive housing shortage. Because of the development of the service sector on the one hand, and the increasing demand for energy services such as refrigeration, lighting, and cooling in the residential sector on the other, urbanization leads to higher power consumption in buildings. In emerging countries, urban buildings account for around half of total national power use. At present, forty percent of the population in Africa currently live in the urban area, there is every tendency of further increase in movement of people from rural to urban area by sixty percent on or before 2050 [8].

In terms of the situation in Nigeria, the rural population fell to 52 percent in 2015, down from 85 percent previously [9]. The rural population refers to persons who live in rural areas as defined by national statistical offices. Nigeria, which has a population of over 190 million people, is one of nine countries where half of the world's population growth is predicted to be concentrated between 2017 and 2050 [10]. The primary difficulty with power availability is seen when population increase is compared to current average electricity usage per capita and the UN Sustainable Development Goals: In comparison to other countries, energy consumption indicators are quite low. According to the indicator International Energy Agency (IEA), In Nigeria, the latest available statistics at a national level looking at the timeline from 2015 is 140

kWh electricity consumption per capita, excluding privately generated electricity [11]. This means that as soon as energy is available at a reasonable price, people will use it to meet their needs, such as for domestic hot water preparation to improve hygienic standards, for cooking hot meals more than once per day, for electricity consumption for ventilation, air-conditioning, and lighting, or for electronic devices. The fact that an increase in per capita electricity consumption will almost probably be required to meet the UN Sustainable Development Goals underscores the critical importance of energy efficiency programs in general, and specifically in the building sector [12]. In light of rapid population growth, on-going rural-urban migration, and projected increases in energy consumption, it is clear that energy efficiency potentials associated with building designs must be fully exploited in order to reduce electricity demand for ventilation, air conditioning, and lighting to the greatest extent possible. In this regard, the energy building code has been identified as a key policy tool, provided that the code can be applied to mass housing.

5. Analysis and Solution Procedure

In Nigeria, energy has become a global concern; the need to conduct global research on energy efficiency has become very necessary. Good number of research fellows is currently conducting research in the field of renewable energy [13]. The global energy policy has been viewed and perceived as a solution procedure in the energy space. This is necessary as it will help solve problems in the rural and urban centres. This will help liberate the people of the rural area and urban households [6]. As a result, this research work will focus majorly on four sections: energy efficiency management standards (EEMS), energy efficiency and climate change (EECC), energy efficiency hurdles (EEH), and energy efficiency policies (EEP). From previous research paper, the device of the energy system was classified using the framework: Performance efficiency (Pe), Operation Efficiency (Oe), Equipment efficiency (Ee) and Technology efficiency (Te), the aforementioned reveal chances to improve energy efficiency with a scholarly conclusion provided at the end of the research.

5.1. Framework of Energy Efficiency Standards and Policy

5.1.1. Energy efficiency management standards

Energy efficiency standards give organizations an opportunity to achieve and maintain optimum level of efficiency in their productive activities [14]. To achieve energy efficiency management standards, energy modelling, energy analysis, energy auditing, and energy monitoring are used. Over the years, standards and policy have been developed to maintain energy efficiency and they include American National Standards Institute and Management System for Energy (ANSI/MSE). This can be implemented in Nigeria as standard for energy efficiency.

5.1.2. Energy efficiency and climate change

Due advancement in technology, increased human industrialization and exploitation of natural resources, poor energy efficiency management, there is an increase in the adverse effects of pollution in the global environment which include the water systems of the world, land, and the climate [15]. This section analyzes the relationship between energy efficiency and the climate change. Globalization is good for humanity because it reduces the effort human put in to doing a particular task and improves modern living. However due to the type of energy source used in the world today being fossil fuel, biomass, fuel wood and methane gas, the emission released by these energy sources include but not limited to Carbon (IV) Oxide, Carbon (II) Oxide, Nitrogen (IV) oxide and others. These gases are called Green House Gases (GHGs), and they cause

greenhouse effects which include global warming, rise in sea level (some countries will disappear if this trend is unchecked), health hazard, fire hazard, acid rain etc. To reduce this climate change problem, the methodology to mitigate these issues is that the energy consume from the various energy sources like fossil fuel, fuel wood, and biomass fuel must be reduced or at best eliminated. One of the ways of reducing energy consumption is through increasing energy efficiency.

5.1.3. Barriers to Energy

Barriers to energy are defined as the predicted mechanism that prevents investment in sciences and technologies for efficient use of energy and also prevents it from being economically efficient [17]. The energy barriers could be because of institutional barriers, economic barriers, and behavioral barriers. In summary, it could be classified as institutional barriers, economic barriers and behavioral barriers [16]. For example, some countries are reluctantly encouraging the switch to renewable energy resource due to economic reasons and fear that their economy which is dependent on the export and proceeds from crude oil or other exhaustible resources will stagnate. This forms an economic barrier to energy.

5.1.4. Energy efficiency policies

These are various policies put in place to mitigate energy problems through energy efficiency management programs. As explained in section one of this paper, some national and international standard policy is in place to deal with many aspects of energy efficiency. Globally, the current change in the international energy preference results into two important, yet largely unforeseen events like the shale energy prospects. Decarbonization policy is a policy that encourages the use energy sources that are low in carbon like (solid coal, liquid kerosine, and diesel) and therefore emit less GHGs [17]. High combustion efficiency, particulate filter (filtering Nitrogen (IV) Oxide, Sulphur (IV) Oxide, Lead), presence of catalyst, is incorporated in equipment that use biomass or fossil fuel energy sources to reduce Carbon (II) Oxide and other environmentally and unfriendly particles from fuel combustion. Carbon (II) Oxide from an incomplete combustion of fuel wood, biomass, and fossil fuel, is a dangerous gas that reacts with red blood hemoglobin (an iron complex protein compound) to form an irreversible complex compound called carboxyhemoglobin that can cause syncope and death in few minutes.

6. Conclusion

This paper detailed a review of the various opportunities for energy efficiency management through some energy management systems and policies globally and suggestions was made for implementation in Nigeria. Energy management is indispensable in reducing cost of production, maintaining high quality of life, and reduction in the use of energy. It also prevents avoidable deaths and creates more opportunities. There are some social, economic, and behavioral aspects in shaping energy policy. Nigeria will save enough money for investment in other priority area if energy efficiency standards are followed and energy efficiency policies implemented. Improved health because of efficient use of energy will reduce absence in workplace, and increase productivity. This was analysed and presented in four major areas which include: standards for energy efficiency management, climate change and energy efficiency, possible barriers to energy efficiency, and policies for energy efficiency. Further elaboration of the enlisted areas were detailed focusing on the appropriate standard for sustainable energy efficiency and energy boosting.

References

[1] C. X. Jiang, Z. L. Li, Y. Qian, and X. C. Lu, "Towards low emissions and high thermal efficiency of gasoline compression ignition engine under high loads by modulating the fuel reactivity and injection strategy," Sci. China Technol. Sci., vol. 63, no. 1, 2020, doi: 10.1007/s11431-019-1436-y.

[2]. GIZ NESP. The Nigerian Energy Sector: An Overview with a Special Emphasis on Renewable Energy, Energy Efficiency and Rural Electrification, 2nd ed. June 2015. Available online: https://www.giz.de/en/downloads/giz2015-en-nigerian-energy-sector.pdf; Energy Platform Nigeria: http://www.energyplatformnigeria.com/index.php/overarching (accessed on 8 April 2018).

[3]. OPEC. Annual Statistical Bulletin 2017. Available online: http://www.opec.org/opec_web/flipbook/ASB2017/ASB2017/assets/common/downloads/ASB2017_13062017.pdf (accessed on 10 May 2018).

[4]. Yusuf, M. An Analysis of the Impact of Oil Price Shocks on the Growth of the Nigerian Economy, 1970–2011. Afr. J. Bus. Manag. 2015, 9, 103–115.

[5]. Offiong, A.I.; Atsu, I.A.; Ajaude, E.; Ibor, B.I. The Impact of Oil Price Shocks on the Economic Growth and Development of Cross River State, Nigeria. Int. J. Financ. Res. 2016, 7.

[6]. Rentschler, J. Incidence and impact: The regional variation of poverty effects due to fossil fuel subsidy reform. Energy Policy 2016, 96, 491–503.

[7]. Todd, J.A.; Geissler, S. Regional and Cultural Issues in Environmental Performance Assessment for Buildings. Build. Res. Inf. Int. J. Res. Dev. Demonstr. Innov. 1999, 27, 247–256.

[8]. Habitat, U.N.; Cities and Climate Change Initiative. Regional Roll-Out Strategy for Africa 2012–2021. 2011. Available online: http://mirror.unhabitat.org/list.asp?typeid=3&catid=550&RecsPerPage=ALL (accessed on 8 April 2018).

[9]. World Bank. Indicator Rural Population: World Bank Staff Estimates Based on United Nations, World Urbanization Prospects. 2016. Available online: http://data.worldbank.org/indicator/SP.RUR.TOTL.ZS?end=2015&locations=NG&page=2&start=1960&view=chart (accessed on 8 April 2018).

[10]. DESA. World Population Prospects Key, Findings and Advance Tables; Revision, Working Paper No. ESA/P/WP/248; Department of Economic and Social Affairs of the United Nations Secretariat: New York, NY, USA, 2017.

[11]. IEA. Indicator kWh Electricity Consumption per Capita: Based on IEA data from IEA Statistics © OECD/IEA. 2014. Available online: http://data.worldbank.org/indicator/EG.USE.ELEC.KH.PC?locations=NG; (accessed on 29 June 2018).

[12]. United Nations. Resolution Adopted by the General Assembly on 27 July 2012 [without Reference to a Main Committee (A/66/L.56)] 66/288; The Future We Want; USA. 2012.

[13] Uyanga Kindness M.O.Okwu, A. O. Adeoye, S. E. Ogbeide, (2018). Production and Characterization of organic Solar Cells. World Journal of Engineering, Emerald Publishing group. Vol 15 (4) 540-548) https://doi.org/10.1108/WJE-06-2017-0136

[14] E.O. Ojo, M.O.Okwu, E. F. Oyawale (2019) Initial assessment of reuse of sustainable wastes for fibreboard production: the case of waste paper and water hyacinth. Journal of Material Cycles and Waste Management, Springer. https://doi.org/10.1007/s10163-019-00871z.

[15] N. Rehmatulla and T. Smith, "Barriers to energy efficiency in shipping: A triangulated approach to investigate the principal agent problem," Energy Policy, vol. 84, 2015, doi: 10.1016/j.enpol.2015.04.019.

[16] M.O. Okwu, Otanocha O. Balogun P., Tega.O**. (2018)** Comparative Performance of Load Bearing Characteristics of Biogas and Gasoline Fuelled Electric Generator, International Journal of Ambient Energy.DOI:10.1080/01430750.2018.1517669

[17] M. A. Zahed, S. Salehi, R. Madadi, and F. Hejabi, "Biochar as a sustainable product for remediation of petroleum contaminated soil," Current Research in Green and Sustainable Chemistry, vol. 4. 2021, doi: 10.1016/j.crgsc.2021.100055.

NIPES Conference Proceedings
The 1st International Conference of the Nigerian Institution of Professional Engineers and Scientists 7th-8th Oct. 2021: 211-215
www.nipesjournals.org.ng

Investigation of Microbial Fuel Cell Power Potential from Abattoirs in Effurun, Delta state, Nigeria

Essang N.P.[a] and Oyejide, O. J.[b*]
[a]Department of Petroleum and Natural Gas Processing Engineering, Petroleum Training Institute, Effurun, Nigeria
[b]Department of Mechanical Engineering, Federal University of Petroleum Resources, Effurun, Nigeria

Abstract
In order to reduce the effect of the extensive consumption of fossil fuels energy on our planet, renewable energies exploitation and research need to be revived. Microbial fuel cells are indeed a renewable energy technology and a potential alternative that have a double function: to produce electricity while intensifying wastewater treatment processes by accelerating the degradation of organic matter. This research work therefore focuses on the investigation of microbial fuel cell power potential from abattoir in Effurun. Microbial Fuel Cell was built and assessed in terms of their performance. Different concentration of diluted abattoir wastewater was used as substrates. Important parameters including the maximum power density, average power and voltage were calculated and measured in order to compare the Microbial Fuel Cells where different substrates concentration is used. The results were promising, as we could obtain a significant power of 92.16 mW, power density of 1.233 mW/mm^2, current of 168.1 mA, and voltage of 14.4 v. The results confirm the principle that controls electric generators, when put in series, the voltage adds up and the current increases.

Keywords**:** *Abattoir, Power, Voltage, Electrode, Microbial Fuel Cell*

1. Introduction

Energy is expended and waste generated with every human activity ranging from breathing which produces carbon monoxide (gaseous waste) to excreting which is an organic solid waste. Waste generated can be gaseous such as carbon dioxide (CO_2), hydrogen sulphide (H_2S), carbon monoxide (CO); liquid waste (e.g. industrial effluents) or solid waste (e.g. municipal waste). All these wastes are released into the environment which is harmful to it by altering the energy balance of nature which has impacted negatively on the environment. Incidentally, it is harmful to life (both human, plant and animal) as these are part of the environment [1]. With the increasing rate of rural-unrban migration, there is a corresponding increase in the amount of both domestic and industrial waste generated [3]. The improper waste management in the Nigerian society can lead to a high risk of human exposure to epidemics [5] [6]. The economy of a nation is fundamentally linked and largely dependent on environmental health but policymakers often overlook this. Decree No. 58 of 1988 (as amended) of the Federal Environmental Protection Agency (FEPA), Nigeria confers what is now the Federal Ministry of Environment (FME) with the responsibility of the protection and development of the environment.
Energy has always played a key role in the development of both natural and artificial elements. Earth has different forms of energy which it constantly recycles to maintain the energy balance needed for the sustenance of life. As global fossil fuel depletes and energy demand increases, there is a demand for clean energy, scientists worldwide are now researching for renewable, reliable and sustainable source of energy to meet demand. Researchers have begun developing technology and harnessing the stored energy in readily available sources such as wind, light, organic matter, etc. in the pursuit of clean energy and a sustained environment. One of such technological devices is the Microbial Fuel Cell (MFC). The Microbial Fuel Cell (MFC) is a device which converts the chemical energy in organic matter directly to electrical energy [8]. Membraneless MFC is a bioreactor which converts the stored chemical energy in organic matter directly to electricity in a single chamber [2].
The microbial fuel cell is a bioreactor which converts the chemical energy stored in the bonds of organic matter into electricity through the biocatalysis of microorganisms. The higher the number

of microbial fuel cells, the higher the voltages, currents and power generated [7]. There are basically two methods and designs in which an MFC bioreactor can be achieved; the single chamber system and the two-chamber system as shown in Fig 1 and Fig 2.
The single chambered MFC is simpler in design, cost effective and there is no need for aerating the cathode chamber like that of the two-chamber MFCs [8]. Fig. 1 shows the schematic diagram of a single chamber MFC. Unlike the two-chamber MFC, it is not essential to have the cathode electrode filled with liquid catholyte or in a separate chamber. The cathode can be in direct contact with air either in the presence or absence of a membrane [2].
Fig. 2 shows the basic configuration of a two-chamber MFC. The main components include the anode chamber and cathode chamber separated by a proton exchange membrane (PEM). Microbes decompose the substrate in the anodic chamber producing electrons, protons and carbon dioxide (CO_2). The electrons are transferred to the cathodic chamber via a conducting wire and the protons are also transferred to the cathodic chamber via the PEM.
The use of a microbial fuel cell finds economic importance in environmental waste management, health, agriculture and power. One major product from the technology of the MFC from the anaerobic decomposition of organic waste is methane gas (CH_4). CH_4 is a greenhouse gas which is in every regard not environmentally friendly. The prevention of CH_4 from escaping into the environment reduces the risk of natural disaster from the depletion of the ozone layer of the earth. Other benefits include the reduction of nitrogen leaching into ground and surface waters; improve hygiene through the reduction of pathogens, worm eggs, and flies. Also, it reduces odour by 80%; controlled recycling/reduction of organic waste; reduces deforestation by providing renewable alternative to wood fuel and charcoal. CH_4 burns "cleaner" than wood fuel, kerosene, and undigested bio waste. It also creates an integrated waste management system which reduces the likelihood of soil and water pollution compared to the disposal of untreated bio wastes hence a better and healthy environment for all life.

2. Materials and Method

2.1 Materials

In this section, the materials and components used in the design and fabrication of the system is discussed here. A single chambered Microbial Fuel Cell was designed and fabricated using locally, cheap and readily available materials. The single chambered MFC was joined together to form a stacked MFC. The following materials and equipment were used in the fabrication and performance evaluation of the system;

i. PET Bottles
ii. Electrical multimeter.
iii. Electrodes (graphite rods and aluminium plates)
iv. Waste water from abattoir
v. LED bulbs
vi. Flexible wire
vii. Digital pH metre.

2.2 Method

2.2.1 Description of the Microbial Fuel Cell

Fig. 1 shows the double chambered MFC with each chamber made from plastic. One the chamber serves as the anodic chamber where the anode electrode is placed and is air-tight for anaerobic digestion to take place. The system has an opening at the top which pave way for easy feed-in opening and at the bottom which allow discharge opening. With this arrangement, charging and discharging of unused and used feedstock was achieved. More so, the second chamber serves as the cathode chamber where the cathode electrode is placed. At the top of this chamber is a port allowing oxygen (O^{2+}) to come in and react with the hydrogen ions (H^{+}) to produce water to be

collected at the bottom side. The two chambers are separated by a proton electron membrane. Fig. 3 shows the isometric view of the microbial fuel cell.

2.2.2 Test and Evaluation of Microbial Fuel Cell (MFC)

The testing stage involves the following steps;

(A) Arrangement of electrodes in the MFC

The electrodes were arranged in the MFC as depicted in Fig. 4.

(B) Charging with Abattoir Waste Water

Fig. 5 shows the charging processes setup.

3.Results and Discussion

The results of the performance test evaluation of the microbial fuel cell having twelve (12) electrodes each connected in series is shown in Table 1. The cathode is graphite and the anode aluminium. The electrolyte was abattoir waste water. As shown in Table 1, an average power of 92.16 mW, power density of 1.233 mW/mm^2, current of 168.1 mA, and voltage of 14.4 v were obtained. These are all indications that power can be generated from abattoir waste water through microbial fuel cell.

Table 1. Results of Performance Test Evaluation of Microbial Fuel Cell

Day	pH	Volt (V)	Current (mAmp)	Power (mW)	Power Density (mW/mm^2)
1	5.42	0.73	10.87	7.94	0.106
2	5.57	0.72	10.53	7.58	0.101
3	5.71	0.71	10.46	7.42	0.099
4	5.96	0.65	8.63	5.61	0.075
5	6.03	0.67	6.12	4.1	0.055
6	6.14	0.68	6.2	4.22	0.057
7	6.38	0.65	5.87	3.82	0.051
8	6.41	0.65	4.81	3.13	0.042
9	6.59	0.65	4.39	2.85	0.038
10	6.71	0.6	4.2	2.52	0.034
11	9.39	0.6	7.26	4.36	0.058
12	9.17	0.55	6.38	3.51	0.047
13	8.92	0.54	6.83	3.69	0.049
14	8.83	0.53	6.67	3.54	0.047
15	8.55	0.51	6.11	3.12	0.042
16	8.31	0.5	6.53	3.27	0.043
17	8.16	0.49	5.7	2.79	0.037
18	7.97	0.48	5.4	2.59	0.035
19	7.68	0.41	5.23	2.14	0.029
20	7.42	0.41	5.59	2.29	0.031
21	7.31	0.4	5.43	2.17	0.029
22	7.25	0.39	4.32	1.68	0.023
23	7.18	0.36	4.88	1.76	0.024
24	7.14	0.35	5.21	1.82	0.024
25	7.11	0.32	3.63	1.16	0.016

26	7.09	0.32	3.72	1.19	0.016
27	7.06	0.27	3.93	1.06	0.014
28	7.04	0.26	3.2	0.83	0.011
Total		14.4	168.1	92.16	1.233

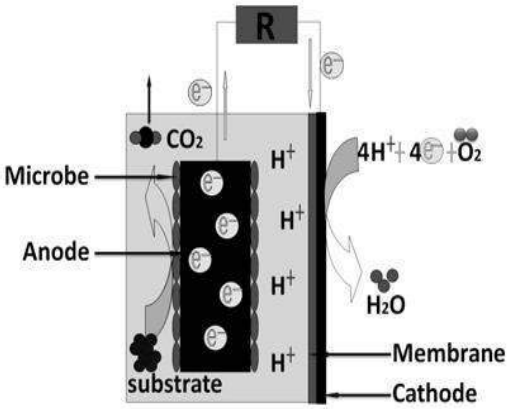

Figure 1. Schematic diagram of a single chamber MFC [8]

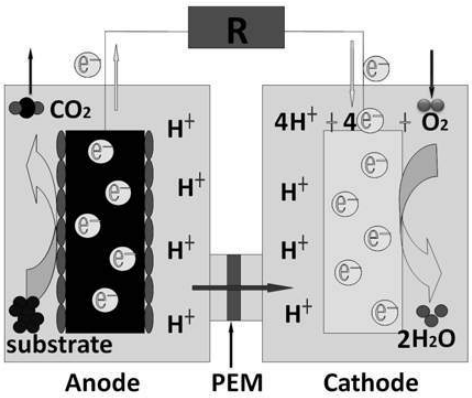

Figure 2. Schematic diagram of a typical two-chamber MFC [8]

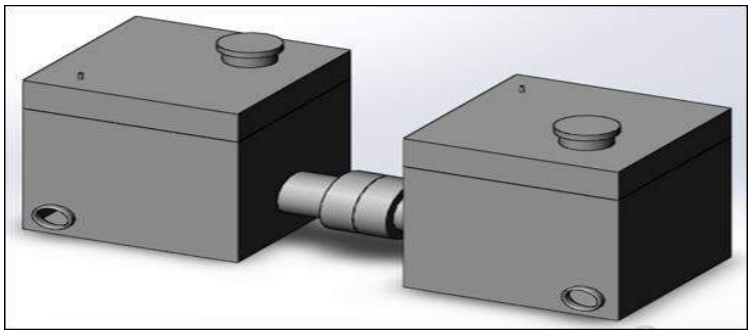

Figure 3. Isometric view of microbial fuel cell

Figure 4. Arrangement of electrodes in the MFC

Figure 5. charging Microbial Fuel Cell with abattoir waste water

Figure 6. Performance Test Evaluation

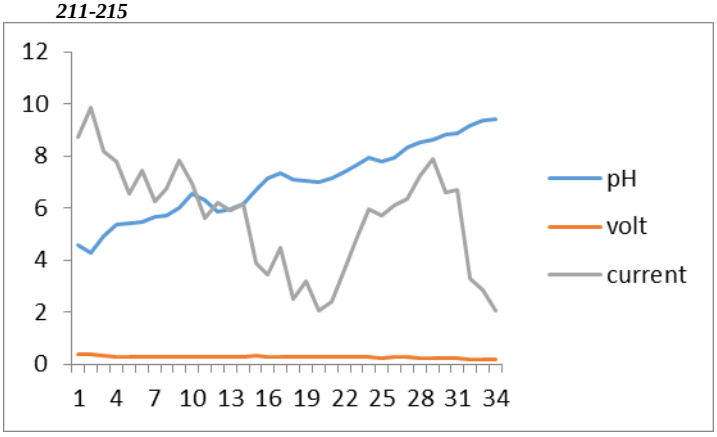

Figure 7. Graph of pH, voltage and current readings

Figure 6 shows the results of performance test evaluation. The system was able to power the LED bulb, thus with more connections of cell together, the system can power some home appliances. As shown in Fig 7, the voltages recorded for MFCs was uniform throughout and with a steady rise in pH readings tending towards strong alkalinity which favour power generation.

4. Conclusion

With the high population and inadequate power supply in Nigeria, alternative means of power is urgently needed. Adequate power supply is the bedrock of any society for development and sustenance. The Microbial Fuel Cell is a suitable source of clean and renewable energy fit for the Nigerian society. Clean fuels, specifically fuel cells and biofuels are sources of energy from organic matter without any pollution are suitable replacements for traditional fossil fuels.

References

[1] Scherr, S.J and Sthapit. S., 2009. "Mitigating Climate Change through Food and Land Use". Ecoagriculture Partners and Worldwatch Institute. ISBN: 978-1-878071-90-0.

[2] Logan, B.E., Hamelers, B., Rozendal, R., Schröder, U., Keller, J., Freguia, S., Aelterman, P., Verstraete, W., Rabaey, K. (2006). "Microbial Fuel Cells: Methodology and Technology". Environmental Science and Technology 40, 5181-5192.

[3] M. K. C. Sridhar and T. B. Hammed (2014). "Turning Waste to Wealth in Nigeria: An Overview". Journal of Hum Ecol, 46(2): 195-203

[4] N. Njoku, J. Lamond, G. Everett and P. Manu. "An Overview of Municipal Solid Waste Management in Developing and Developed Economies: Analysis of Practices and Contributions to Urban Flooding in Sub-Saharan Africa". University of West England. 2015. (pages 203-204).

[5] N. Mokhtarian, Rahimnejad, G. D. Najafpour, Wan Ramli Wan Daud, A. A. Ghoreyshi (2012). "Effect of Different Substrate on Performance of Microbial Fuel Cell". African Journal of Biotechnology Vol. 11(14), pp. 3363-3369, 16 February.

[6] Orhorhoro, EK; Ebunilo, POB; Sadjere, EG (2017). Determination and Quantification of Household Solid Waste Generation for Planning Suitable Sustainable Waste Management in Nigeria. Inter. J. of Emerg. Engr. Rese. and Tech. 5(8):1-9

[7] Oyejide O.J., Orhorhoro E.K., Salisu S. (2018); 'Analysis and Performance Evaluation of Microbial Fuel Cells for Electricity Generation.' Journal of Applied Sciences and Environmental Management. 22(7): 1025-1029. DOI: 10.4314/jasem.v22i7.5.

[8] Kun Guo, Daniel J. Hassettb and Tingyue Guc (2012). "Microbial Fuel Cells: Electricity Generation from Organic Wastes by Microbes". ISBN: 978-1845939564, pp 164-189. CAB International, Oxon. United Kingdom.

NIPES Conference Proceedings
The 1st International Conference of the Nigerian Institution of Professional Engineers and Scientists 7th-8th Oct. 2021: 216-222
www.nipesjournals.org.ng

Estimation and Empirical Modelling of Solar Radiation from Tilted Surfaces

Eghosa Omo-Oghogho*, Ikpe Aniekan Essienubong, Collins Kwasi-Effah and Sadjere Ejuvwedia Godwin
Department of Mechanical Engineering, University of Benin, P.M.B 1154, Benin City, Nigeria

Abstract
Interest in solar energy has prompted the accurate measurement and mapping of solar energy resources of the globe. Solar radiation data are available in several forms. Most radiation data available for horizontal surfaces include both direct and diffuse radiation. This is normally done by using solar-meters. Most solar-meters measurements are recorded simply as total energy (global radiation) incident on the horizontal surface; other measurements separate the direct (beam) and the scattered (diffuse) radiation. Radiation data are the best source of information for estimating average incident radiation and for the proper designing of a solar water heating system. A precise analysis and design of a solar water heating system requires knowledge of the solar energy obtained from the sun and the availability of global solar radiation and its components at the location of project site. Since the solar radiation reaching the earth's surface depends upon climatic conditions of the place, a study of solar radiation under local climatic conditions is essential. Solar radiation data were obtained through the use of an empirical model to predict and estimate solar radiation. The highest value of solar radiation were obtained in April, 2018 and the average horizontal radiation on a surface and radiation on a tilted surface was found to be 966.12W/m^2 and 1055.99W/m^2 respectively.

Keywords: *Solar radiation, Solar energy, Tilted surfaces, horizontal surface, Solar collector*

1.0 Introduction
Energy and its different forms are fundamental to human existence and the economic development of any country. Nigeria with its increasing population needs alternative source of energy to support its growing population. Currently there is a lot of over dependence on fossil fuel and environmental pollution caused by fossil fuel combustion, chlorofluorocarbons, other chemicals and organic materials [1]. Researches are being conducted towards addressing this problem, these includes the use of solar energy through collectors, optical, thermal and thermodynamic analysis, coupled with the use of optimum tilt angle for maximum insolation across different locations. Solar radiation from the sun that keeps our planet warm exceeds by far the current primary energy supply used by mankind for its comfort, leisure and economic activities. It also exceeds vastly other energy sources at ground level such as geothermic or tidal energy, nuclear power and fossil fuel burning. Sunrays also drive hydraulics, wind, wave power and biomass growth. The global warming crisis as a result of the depletion of the ozone layer caused by the emissions of CFC'S (chlorinated and brominates organic compounds) and NOx has led to many researches on alternative renewable sources of energy like the sun, hydro, wind and geothermal. Most countries in the world have realized the need for reduction of gas emissions to contrast the adverse global climatic change, encouraging the use of renewable and fully sustainable sources of energy [2].

The solar radiation from the sun coming through the atmosphere to the earth can be anticipated with a high accuracy. The amount of solar energy depends basically on the astronomical geometric parameter such as the actual distance from sun to earth, since the earth moves around the sun on an elliptical orbit, the sun-earth distance is a function of the day. With regard to the mean value of the earth-sun distance, the sum of energy per unit area obtained from the sun exterior of the earth's atmosphere, known as the solar constant, is approximately

1367W/m^2 [3]. The earth's cross-sectional area is estimated to be 127400000km^2 and the total power released to the earth by the sun is estimated to be 1.75 × 1014 kW [3].

The solar radiation reaching the earth's surface is sometimes difficult to estimate because of the interaction with the atmosphere and the different soil surfaces in contact. The mean solar radiation is a function of various statistical data which cannot be predicted with a high precision. While passing through the atmosphere a major part of the incident energy from the sun is suppressed by reflection, scattering or absorption by air molecules, clouds and particulate matter also called aerosols. Due to this only 60% (approximately 1.05×10^{14} kW) of sunlight from the sun to the earth's atmosphere reaches the earth's surface [4]. Notwithstanding, the total annual solar radiation falling on the earth's surface is approximately more than 7500 times the world's total annual primary energy consumption of 450 EJ [5].

The energy generated within the inner core of the suns solar sphere having temperatures of approximately many millions of degrees must be transferred out to the surface and then be radiated into space. A combination of radiative and convective processes occur with successive emission, absorption and radiation. The radiation in the sun's core is in the x-ray and gamma-ray parts of the spectrum, with the wavelengths of the radiation increasing the temperature drops at larger radial distances [3].

The surface of the sun consists of granules (irregular convection cells), with a measurement of between 1000 to 3000 km and having a lifetime cell of a few minutes. Other features of the sun's solar surface are small dark areas called pores which are of the same size in magnitude as the convective cells and the larger dark areas called sunspots which vary in size. The convective zone has an outer layer called the photosphere. It is essentially opaque and also consist of gases that are composed of strongly ionized particles that are able to absorb and emit a continuous spectrum of radiation. The source of most solar radiation is the photosphere [6].

Apart from the photosphere, a less transparent solar atmosphere can be observed during total solar eclipse or by an instrument known as the solar disk. The photosphere is immediately below a layer of gases that are cooler and several hundred kilometers deep called the reversing layer. Chromosphere is another layer that is close to the photosphere having a depth of about 10,000 km and this is a gaseous layer with temperatures higher than that of the photosphere but with lower density [7]. Also there is a layer called corona, which is far from the photosphere and it is a zone of very low density with a very high temperature of about 10^6 K. The sun showing its physical structure, temperature and density gradients will serve as a basis for acknowledging that the sun does not in fact function as a blackbody radiator at a fixed temperature [8]. The radiation aspect from the sun that is not reflected or scattered and reaches a specific surface directly from the sun is known as the direct or beam radiation. The scattered radiation which reaches a specific surface from all directions is known as diffuse sky radiation. The total radiation incident on a horizontal surface consist of diffuse sky and direct radiation and is known as the global or total horizontal radiation. The total radiation incident on a non-horizontal or tilted surface is a combination of the direct radiation, diffuse sky radiation, and another form of radiation that is reflected from the ground surface and is known as the global tilted radiation [9].

Some factors that determines the availability of the solar radiation in specific locations are climate conditions formed by geographical factors including latitude, size of lands and seas, sea tides, height above sea level and land formation. The latitude is of great importance since the angle of the incidence of the solar radiation causes the lower irradiance at higher latitudes. According to solar radiation travels through a distance in the atmosphere before reaching the earth and at higher latitudes the distance is longer resulting in the increased absorption and reflection of the solar radiation before reaching the earth. The other one is that the higher angle of incidence results in the lower irradiance on the horizontal ground surface [10].

Solar energy is a form of energy obtained from the sun and it is a type of renewable energy. The energy from the sun can be used to generate thermal energy or heat energy for use in our residential homes and industry respectively. Solar radiation varies with location and it is important to known the quantity of solar energy that can be obtained in a particular location, this can be measured and also estimated for. Due to the issues of faulty equipment and maintenance of research centers that can store this information, it is important to also obtain this solar radiation data by empirical and angular solar relations.

The aim of this work is to determine theoretically reliable solar radiation data that can be used for research purpose and the design and fabrication of solar machines and equipment.

2.0 Methodology

This study compares its obtained data with that measured from National Centre for Energy and Environment, University of Benin, Benin City, Edo State, Nigeria (longitude and latitude of 6.33°N, 5.61°E) for the project location. Data obtained from the energy center was from the period of 2012 to 2017. Solar radiation data available at the agency is only global radiation (a combination of both the direct and diffuse radiation).

In order to properly estimate the total solar radiation on a tilted surface, angular solar relation like the incident angle, hour angle, altitude angle, zenith angle, azimuth angle and the declination angle were calculated respectively.

Collectors were installed horizontally at an angle to increase the amount of radiation intercepted by the surface of the collector. In order to obtain the radiation on a tilted surface, angular relations of solar radiation were estimated for. The surface absorbs beam, diffuse and ground reflected solar radiation. Also the amount of solar radiation received per unit area by a surface held perpendicular to the sun rays comes in straight line from the direction of the sun at its current position in the sky and this was determined with the aid of Equation (1).

$$I_n = A \exp\left(-\frac{B}{cos\theta_Z}\right) \quad (1)$$

Where I_n is the normal solar radiation intensity in W/m^2, A and B are constants (1230 and 0.142 were obtained from [11]).

$$I_b = I_n \cos\theta_Z \quad (2)$$

$$I_d = I_n C \quad (3)$$

Where I_b is the beam radiation, $\cos\theta_Z$ is the zenith angle, I_d is diffuse radiation and C is a constant (0.058 was obtained from [11, 12]).

$$\theta_z = 90 - \alpha \quad (4)$$

Where α is the altitude angle.

$$\text{Sin}\alpha = \text{cosL}\,\text{cos}\omega\,\text{cos}\delta + \text{sinL}\,\text{sin}\delta \quad (5)$$

Where L is the latitude of the site, ω is the hour angle and δ is the declination angle respectively.

$$\omega = (\text{ST} - 12)15 \quad (6)$$

Where ST is the solar time and it is from 1 to 24 hours.

$$\delta = 23.45 \sin\left(360\frac{284+\text{n}}{365}\right) \quad (7)$$

Where n is for the number of days.

$$R_b = \frac{\cos\theta_Z}{\text{Cos}\theta} \quad (8)$$

where θ is the anle of incidence.

$$\text{Cos}\theta = \cos\theta_Z\,\text{cos}\beta + \sin\theta_Z\,\text{sin}\beta \quad (9)$$

where α is the altitude angle, γ is azimuth angle and β is the tilt angle respectively.

$$\beta = \text{lattitude} + 5^o \quad (10)$$

$$\gamma_s = \text{sign}(\omega)\left|\cos^{-1}\left(\frac{\cos\theta_z \sin\text{L} - \sin\delta}{\sin\theta_z \cos\text{L}}\right)\right| \quad (11)$$

Where γ is the azimuth angle.

$$I_T = I_b R_b + \text{I}_\text{d}\left(\frac{1+cos\beta}{2}\right) + I_b R_b \rho_g \left(\frac{1-cos\beta}{2}\right) \quad (12)$$

Where I_T is the total solar radiation on a tilted surface and ρ_g is ground reflectance.

Data source was generated using Equations (1) to (12), this is to ensure that at any point in time of a particular day and time, when the tilt angle is altered, horizontal radiation and radiation on a tilted surface is obtained for that location and time. This data sheet could be readily available for solar energy research and for the purpose of weather forecast.

3.0 Results and Discussion

The amount of solar energy obtained in a particular location depends on the angular solar relations, analysis of the solar flat plate collector considering the location, tilt angle and ambient conditions of the site under study.

3.1 Angular relations of solar radiation

Solar energy availability was determined considering some conditions, these conditions are ambient conditions, tilt angle, the location (longitude and latitude) of study and the mid-month in each month. The mid-months (nth) are recommended average days of various months. A particular day in each month was chosen (mid-month), this day has approximately the average solar radiation which is equal to the monthly mean value for that particular month as shown in Table 1, with this the total radiation on an horizontal and tilted surface were obtained respectively as shown in Table 2 and 3 using Equations 1 to 12.

Table 1: Angles of solar relations from January to December 2018 in Benin City, Edo State.

Mid-Month	No of Days(n)	Declination (d)	Altitude angle	Zenith angle	Azimuth angle	Incident angle
17 Jan 2018	17	-20.92	49.86	40.13	46.44	29.13
16 Feb 2018	47	-13.61	54.14	35.85	56.06	24.85
16 Mar 2018	75	-2.42	58.79	31.21	74.61	20.21
15 April 2018	105	9.42	60.15	29.87	97.88	18.87

15 May 2018	135	18.79	58.26	31.74	115.88	20.74
11 June 2018	162	23.09	56.62	33.37	123.26	22.37
17 July 2018	198	21.21	57.40	32.60	120.08	21.60
16 Aug 2018	228	13.46	59.63	30.37	105.87	19.37
15 Sept 2018	258	2.221	59.80	30.19	83.48	19.19
15 Oct 2018	288	-9.60	56.13	33.87	62.19	22.87
14 Nov 2018	318	-18.92	51.12	38.88	48.90	27.88
10 Dec 2018	344	-23.05	48.48	41.51	43.96	30.52

Table 1 shows the obtained solar declination angle, altitude angle, zenith angle, azimuth angle and incident angle respectively from January to December 2018 for Benin City, Edo State, the mid-month, latitude, number of days and hour angle were considered during the analysis. This analysis enabled the estimation of the radiation on a horizontal surface and the radiation on a titled surface respectively.

Table 2: Radiation on a Horizontal surface from January to December 2018 of Benin City, Edo State

Months	I_b**(W/m²)**	I_d**(W/m²)**	I_{TH}**(W/m²)**
January	781.04	59.25	840.29
February	836.73	59.87	896.60
March	891.09	60.43	951.52
April	905.55	60.57	966.12
May	885.16	60.40	945.56
June	866.56	60.19	926.75
July	875.51	60.27	935.78
August	900.20	60.51	960.71
September	902.09	60.53	962.62
October	860.68	60.13	920.81
November	797.87	59.45	857.32
December	761.90	59.02	820.92

Table 2 shows the direct solar radiation, diffuse solar radiation and the total solar radiation on a horizontal surface for a period of one year for Benin City, Edo State, Nigeria considering the location and site of study. This obtained data will enable researchers estimate the total radiation on a tilted surface and also enhance solar energy researches due to the fact that parameters/data for solar energy are scarce.

Table 3: Radiation on a tilted surface from January to December 2018 of Benin City, Edo State

Months	I_{bt}**(W/m²)**	I_{dt}**(W/m²)**	I_g**(W/m²)**	I_{TH}**(W/m²)**
January	892.31	67.69	1.54	961.54

February	936.72	67.03	1.65	1005.40
March	977.72	66.30	1.75	1045.77
April	988.12	66.09	1.78	1055.99
May	973.38	66.39	1.73	1041.51
June	959.55	66.64	1.70	1027.89
July	966.25	66.52	1.72	1034.49
August	984.30	66.17	1.77	1052.24
September	985.66	66.14	1.77	1053.57
October	955.12	66.72	1.69	1023.53
November	905.96	67.50	1.58	975.03
December	876.59	67.90	1.51	945.99

Table 3 shows the direct solar radiation, diffuse radiation, ground reflected radiation and the total solar radiation on a tilted surface for a period of one year for Benin City, Edo State, Nigeria considering the location and site of study. This data was obtained considering a tilt angle of 11^{o} (11 degree), the computation was done so as to allow for varying climatic condition for optimum performance of the solar system under study. The solar radiation obtained was compared to the solar radiation data obtained from National Centre for Energy and Environment, University of Benin, Benin City, Edo State, Nigeria as shown in Figure 1 for 2017.

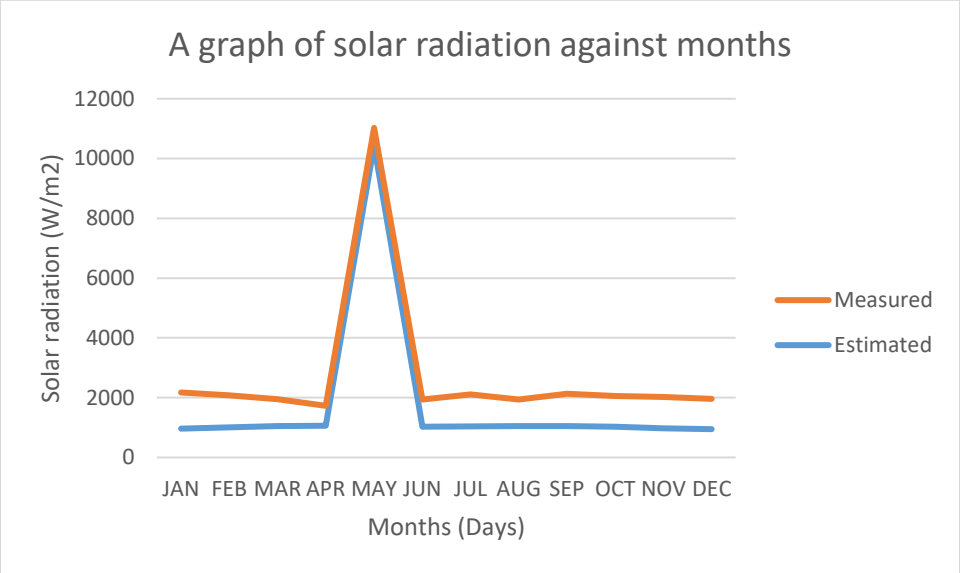

Figure 1: A graph of measured and estimated solar radiation against months.

The graph shows the interaction between the estimated and measured solar radiation of 2017 (obtained from the National Centre for Energy and Environment) with the number of days, from the above it shows there is a good agreement between the measured and estimated solar radiation. Therefore, proving that the accuracy of the estimated solar radiation obtained by empirical equations could be relied on.

4.0 Conclusion

A procedure was developed to determine the solar radiation on a horizontal surface and on a tilted surface. A solar radiation data of Benin City, Edo State was generated with respect to various input parameters (time, day, hour angle, latitude and longitude, tilt angle and angular solar relations respectively) so that when the input parameters are altered or varied, output parameters like solar radiation on a horizontal surface and on a tilted surface can be obtained. The highest form of solar radiation obtained were 966.12W/m^2 and 1055.99W/m^2 respectively for the month of April, 2018.

Reference

[1] Dare A. A, Odufa K. M, Ajuka L. O, Oyedepo S. O and Adeaga O. A (2017), Estimation of insolation of a flat plate solar collectors in selected cities in Nigeria, International Journal of Computational Engineering Research (IJCER).
[2] Dincer, I. and Rosen, M. A (1998), A worldwide perspective on energy, environment and sustainable development.
[3] Duffie, J. A. and Beckman, W.A. (2013), Solar Engineering of Thermal Processes. John Wiley and sons, inc., New York.
[4] Kalogirou, S. A (2009), Solar Energy Engineering: Processes and Systems. Elsevier, U.S.A.
[5] Thirugnanasambandam, M., Iniyan, S., Goic, R. (2010): A review of solar thermal technologies. Renewable and Sustainable Energy Reviews 14, pp. 312–322.
[6] Anderson, E. E. (1982): Fundamentals of Solar Energy Conversion, Addison-Wesley, Reading, MA.
[7] Coulson, K. L. (1975): Solar and Terrestrial Radiation, Academic, New York.
[8] Robinson, N. (ed.), (1966): Solar Radiation, Elsevier, Amsterdam.
[9] Quaschning V. (2005): Understanding Renewable Energy Systems. Earthscan, London.
[10] Kjellson, E. (2009): Solar Collectors Combined with Ground-Source Heat Pumps in Dwellings. Analyses of System Performance. Ph.D. thesis, Lund University.
[11] ASHRAE (2005): "Handbook of Heating and Ventilation of Air Conditioning Applications", Atlanta.
[12] Igboanugo A. C., Kwasi-Effah C. C., Ogbeide O. O (2016) A Factorial Study of Renewable Energy Technology in Nigeria International, Journal of Environmental Planning and Management Vol. 2, No. 4, 2016, pp. 36-44

NIPES Conference Proceedings
The 1st International Conference of the Nigerian Institution of Professional Engineers and Scientists 7th-8th Oct. 2021: 223-240
www.nipesjournals.org.ng

Design, Modelling and Construction of a Shell and Tube Heat Exchanger for Laboratory Experiments

O.J Unuareokpa, J.C Madu, S.A. Edo-Taiwo S.D Peters
Department of Mechanical Engineering University of Benin, Benin City, Edo State, Nigeria

Abstract

Heat transfer instruction lessons has been a mainstay in the curriculum of undergraduate and postgraduate programs in mechanical and chemical engineering disciplines in higher institutions across the world. This paper presents the design and fabrication of a shell and tube heat exchanger (STHE) for laboratory experiments. A detailed thermal design using the Kern's approach was adopted for the thermal design of the heat exchanger. Thereafter, a mechanical design was carried out employing the TEMA standards and the ASME BPVC. It was then modeled before its fabrication. A water retention mechanism was designed using PVC pipes and 90˚ bend connectors to form a U-shaped apparatus to ensure efficient exchange of heat between both streams of fluid.

Keywords: Heat, Heat Exchanger, Shell and Tube Heat Exchanger, Heat Transfer, Laboratory, Kern's Approach, Thermal Design, Fabrication.

1. Introduction

Heat exchangers are one of the most widely used equipment in the process industries [1]. A heat exchanger is an equipment that provides the platform for the transfer of heat from a stream of fluid to another. Heat exchangers are widely used in automobile radiators, domestic and industrial air-conditioners and refrigerators [2-4]. They are used in power generation plants, engineering thermo-fluid laboratories, fast moving consumer goods (FMCG) industries such as breweries, pharmaceuticals and food industries [5-9].

The different forms of heat exchangers may be classified based on the configuration of the direction or path of fluid flow and by their various applications. The majority of the heat exchangers that are grouped based on the configuration of direction of fluid flow are further sub-classified into four (4) major categories: Parallel (concurrent) Flow, Counter (countercurrent) Flow, Cross-Flow, and Multi-Pass Cross-(hybrid) Flow [10]

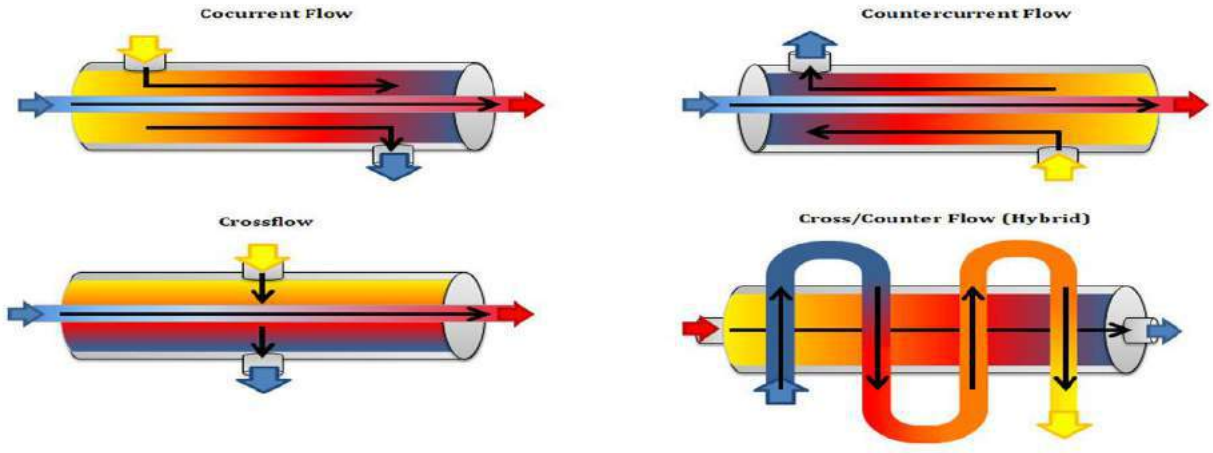

Figure 1: Classification of heat exchangers based on fluid flow [30]

However, there are basically eight (8) major types of heat exchangers and all these employs one or more of the aforementioned configurations of fluid flow. They include: shell and tube heat exchanger, plate heat exchanger, plate and shell heat exchanger, adiabatic wheel heat exchanger, plate fin heat exchanger, pillow plate heat exchanger, fluid heat exchanger, waste heat recovery unit heat exchanger. Among these basic types of heat exchangers, the shell and tube heat exchanger is the most versatile [11].

The shell and tube heat exchanger as the name implies consist of cylindrical or rectangular cross sectional tubes that are mounted in a shell (a large vessel) which could have any arbitrary shape at its cross-section. One stream of fluid runs (flows) through the tubes often referred as the tube side flow, while the other stream of fluid flow over the bundle of tubes (inside the shell) and is often referred to as the shell side flow. By these means, heat is transferred from one stream of fluid to another. Hence, heat transfer instruction lessons has been a mainstay in the curriculum of undergraduate and postgraduate programs in mechanical and chemical engineering disciplines in higher institutions across the world [12].

In order to carryout requisite laboratory experiments, many indigenous institutions in Nigeria import laboratory equipment including heat exchangers [11]. Process and petrochemical industries in Nigeria also have their heat exchangers imported. Therefore, designing and fabricating a shell and tube heat exchanger would go a long way in addressing the problems currently faced by engineering colleges in many tertiary institutions in Nigeria, while boosting the economy by virtue of a potential market and exporting these equipment to other countries and therefore promoting local content inclusion.

1.2 Shell and Tube Heat Exchangers

The shell and tube heat exchangers are arguably the most versatile type of heat exchangers in use. Shell and tube heat exchangers are known to possess somewhat large ratios of heat transfers to volume and weight of the streams they carry. They are designed to offer prime flexibility; of which easy cleaning is a key characteristic. It is interesting to note that they can also be designed for high pressures relative to the atmosphere or environment and also high-pressure differences between the fluid streams [13].

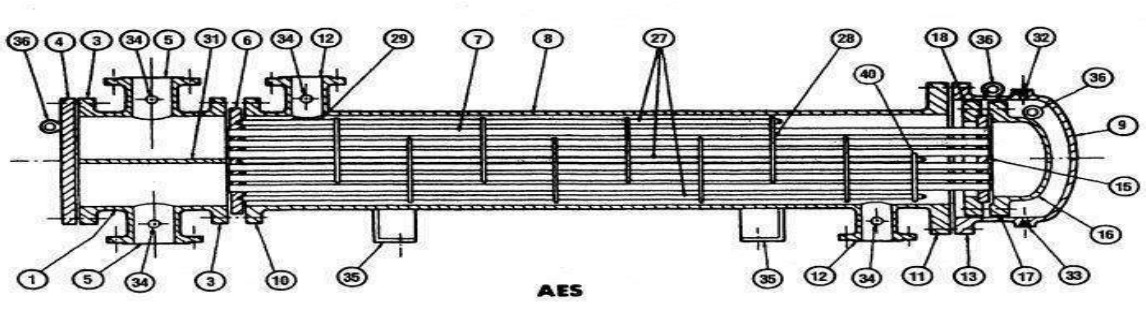

Figure 2: Typical parts of a heat exchanger and connections: (1) Stationary head-channel; (2) Stationary head-bonnet; (3) Stationary Head Flange-Channel or bonnet; (4) Channel cover; (5) Stationary head nozzle; (6) Stationary tubesheet; (7) Tubes; (8) Shell cover; (9) Shell flange-stationary head end; (11) Shell flange-rear head end; (12) shell nozzle; (13) Shell cover flange; (14) Expansion joint; (15) Floating Tubesheet; (16) Floating head cover; (17) Floating head cover flange; (18) Floating head backing device; (19) Split shear ring; (20) Slip-on backing flange; (21) Floating head cover-external; (22) Floating tubesheet

skirt; (23) Packing box; (24) Packing; (25) Packing gland; (26) Lantern ring; (27) Tierods and spacers; (28) Transverse baffles or support plates; (29) Impingement Plate; (30) Longitudinal baffle; (31) Pass partition; (32) Vent connection; (33) Drain connection; (34) Instrument connection; (35) Support Saddle; (36) Lifting lug; (37) Support bracket; (38) Weir; (39) Liquid level connection; (40) Floating Head support. Source: [24]

As seen from Figure 2, the shell and tube heat exchanger is made up of many parts. They main parts include:

I. Shell: container for the shell fluid and it houses the tube bundle that is placed inside of it. The shell diameter to be chosen in such a way that it gives a close fit to the tube bundles. TEMA provides shell types that are already standardized.
II. Baffles: these are plates positioned along the length of the shell at right angles (for transverse baffles) to the tubes axes used to induce greater turbulence. They are also subdivided into segmental, disc-and-doughnut and orifice baffles.
III. Tubes: these are mostly circular or rectangular cross-sectional vessels that run inside the shell. They are arranged uniformly to a pattern and held firm by the tube sheet (s).
IV. Tube sheets: the tube sheet is a flat circular plate circular plate that contains regular patterns of drilled holes according to the tube sheet pattern. The tubes are connected to the tube sheet. The tube sheet in conjunction with the shell and the channel forms the primary barrier for the inter-mixing between the tube side flow and the shell side flow.
V. Tie rods: they are used to provide structural support for the tube bundles in the shell.
VI. Heads: Heat exchangers typically have two types of head; the rear head and the front head. The different types of standard heads have been computed by (TEMA).
VII. Nozzles and Openings: the shell side flow and the tube side flow enter the heat exchangers by means of nozzles and openings. These entry cavities must be able to withstand pressures.

[14] made a simplified approach to effectively design a shell and tube heat exchanger for beverage and process industry application. [15] designed and fabricated a small shell and tube heat exchanger prototype as an auxiliary cooling system for the radiator of a 30 KVA generator for an engineering outlet in Kano North Western Nigeria as a means to improve the efficiency of the cooling process. [16] did a study on the performance analysis of a shell and tube heat exchanger. They aimed at varying different constructional parameters to get performance review under varying conditions. In a bid to achieve this, they developed a Microsoft Excel program to make calculations and getting results after varying parameters easier. [17] performed another heat analysis on a shell and tube heat exchanger with a bundle arrangement consisting of a rotated square pitch and rotated triangle pitch. The analysis was done considering water as the tube side stream and steam on the shell side stream, with subsequent substitution of carbon-dioxide and sulphur-dioxide gases as the tube side stream. [18] undertook a study aimed to fabricate the optimum design for a shell and tube heat exchanger as a condenser with correspondingly high productivity of drinking water for portable solar water distiller. Because of the nature of the purpose of the heat exchanger which was to condense drinking water, stainless steel was chosen as the material to fabricate the heat exchanger. [19] designed a shell and tube heat exchanger to be used in Nitric acid manufacturing plants. The heat exchanger was designed to cool the tail gas using the output gaseous stream from the reactor. [20] made a simplified approach to design a Shell and Tube heat exchanger for use in hydraulic oil and process industry application. The temperature and pressure of hydraulic oil data where duly obtained from an

existing industrial hydraulic power pack machine. [21] designed and fabricated a shell and tube heat exchanger for use as a testing model for laboratory work. For easy accessibility and low-cost, the material chosen for the shell construction was polyvinyl chloride (PVC) while galvanized steel was chosen as the material to fabricate the tubes, baffles, nozzles and tube sheet. [22] designed and fabricated a shell and tube heat exchanger for practical applications in the department of Mechanical Engineering Technology, Federal Polytechnic Ede, Nigeria employing the Kern's approach for the thermal design.

[11] designed and fabricated the a shell and tube heat exchanger in the department of Mechanical Engineering, Imo State University, Owerri. The project was aimed at using the shell and tube heat exchanger for laboratory use. The Bell Delaware's approach was used in the thermal design and no-phase change assumption was also adopted.

2. Methodology

The heat exchanger could be considered as a pressure vessel. Since they operate under thermodynamics and heat transfer principles, its design is much more than the conventional mechanical design [23]. The successful design of a shell and tube heat exchanger can be subdivided into two main phases;

(i) Thermal design
(ii) Mechanical design.

2.1 Thermal Design

There are many approaches to the thermal design of a shell and tube heat exchanger. The most popular include the Kern's methods, Dell-Delaware method, and the Stream Analysis method. For the sake of this design, the Kern's approach was adopted. The Kern's method is based on correlations developed based on experimental data for typical heat exchangers. It attempts to correlate data from heat exchangers by a simple equation analogous for flow in tubes. The disadvantage of this approach is that it is restricted to a baffle cut of (25%), and therefore, cannot completely account for tube-baffle and baffle-shell leakages. Also its prediction of pressure drop is less satisfactory. Regardless of the obvious disadvantages, the Kern's method allows for quick calculation of the shell-side coefficients and pressure drop, gives reasonable accuracy for preliminary design, and provide simplicity [13].

Table 1: Initial Design Data

SHELL SIDE	TUBE SIDE
Internal Diameter (ID) = 6 in	Outer Diameter of tube (OD) = ¾ in
Number of passes = 1	Number of passes (n) = 4
Configuration TEMA-Shell type E	Configuration : BWG 18, 1 in Triangular pitch
Mass flow rate ($\dot{m}_s$) = 0.5 Kg/s	Mass flow rate ($\dot{m}_t$)= 1.75 Kg/s
Flow allocation: Hot fluid	Flow Allocation : Cold fluid
Inlet Temperature (T_1) = 100 ^{O}C	Inlet Temperature (t_1) = 23 ^{O}C
Outlet Temperature (T_2) = 65 ^{O}C	Outlet Temperature (t_2) = ?
Fluid Allocation: Water	Fluid Allocation: Water

2.1.1 Heat Balance

The heat balance equation is given by;

$$Q = \dot{m}_s \times C_{ps} \times (T_1 - T_2) = \dot{m}_t \times C_{pt} \times (t_2 - t_1) \quad (1)$$

The unknown outlet temperature is calculated from Equation (1).

2.1.2 Determination of LMTD

The counter-flow arrangement will be adopted for this design. Therefore, the Logarithmic Mean Temperature Difference (LMTD) is given by

$$\text{LMTD} = \frac{(T_1 - t_2) - (T_2 - t_1)}{\ln \frac{(T_1 - t_2)}{(T_2 - t_1)}} \quad (2)$$

Since the number of tube passes is two (2), we employ the LMTD correction factor; F_T from A.1. Therefore, the true or correct temperature difference, $\Delta_t = \text{LMTD} \times F_T$ (3)

2.1.3 Determination of the number of tubes required.

To determine the number of tubes required for the heat exchanger, the overall design heat transfer coefficient U_D needs to be assumed. According to [25], The overall heat transfer coefficient, U_D, for water-water heat exchanger has an equivalent value of 1418W/m^2 K to 2837 W/m^2 K. Therefore, we assume U_D to be = 2000 W/m^2 K and substitute in equation (4).

The heat transfer rate is given by $Q = U_D A \Delta T_m$ (4)

The tubes heat transfer surface area, A is given by $A = N_t \times L \times a''$ (5)

Therefore, the number of tubes, N_t is obtained from equation (5)

2.1.4 Tube - Side Design

The Internal flow area for the tube side (a_t) is expressed as

$$a_t = \frac{N_t \times a'_t}{n} \quad (6)$$

The mass velocity of tube-side flow is given by; $G_T = \frac{\dot{m}_t}{a_t}$ (7)

The velocity at the tube – side flow is given by; $v_t = \frac{G_t}{\rho}$ (8)

To calculate for the tube – side Reynolds number; $Re_t = \frac{G_t \times d_i}{\mu}$ (9)

The tube-side film heat transfer coefficient (h_i) for water flowing in tubes has been computed by [26] the data is given A.3.

The corrected coefficient is given as $h_{io} = h_i \times ID/OD$ (10)

2.1.5 Shell - Side Design

The shell side flow area is given by; $a_s = \frac{ID \times C'B}{P_T}$ (11)

Shell side mass velocity, is given by; $G_s = \frac{\dot{m}_s}{a_s}$ (12)

The velocity at the shell – side flow is given by; $v_s = \frac{G_s}{\rho}$ (13)

To calculate for the shell – side Reynolds number (Re_s); $Re_s = \frac{G_s \times D_e}{\mu}$ (14)

Where, D_e is the shell equivalent diameter. The shell equivalent diameter depends on the tube configuration [25]. Hence for a triangular pitch configuration, A.2 gives the equivalent diameter for common configurations.

The shell-side film heat transfer coefficient (h_o) is given by;

$$h_o = j_H \frac{k}{D_e} \left(\frac{c_p \mu}{k}\right)^{\frac{1}{3}} \quad (15)$$

Where, $j_H = \frac{h_o D_e}{k} \left(\frac{c_p \mu}{k}\right)^{-\frac{1}{3}} \left(\frac{\mu}{\mu_w}\right)^{-0.14}$ (16)

j_H is a factor obtained from A.4 with the aid of the shell side Reynolds number while viscosity ratio, $\left(\frac{\mu}{\mu_w}\right)^{-0.14}$ can be assumed to be equal to be 1, because of the low viscosity of water [25].

2.1.6 Clean Overall Heat Transfer Coefficient

The clean overall heat transfer coefficient U_C is given by;

$$U_C = \frac{h_{io} \times h_o}{h_{io} + h_o} \quad (17)$$

Since U_C is greater than U_D, the assumption was appropriate and there would be no need for further iterations with subsequent values of U_D.

2.1.7 Fouling Resistance

The fouling resistance, R_d is given by;

$$R_d = \frac{U_C - U_D}{U_C \times U_D} \quad (18)$$

2.1.8 Tube Side Pressure Drop

The pressure due to friction can be calculated with the equation (19)

$$\Delta p_t = \frac{f G_t L n}{5.22\times10^{10}\, D_e s \emptyset_t} \quad (19)$$

The direction of change introduces further pressure drop Δp_r called the return loss, it is given as;

$$\Delta p_r = \frac{4n}{s} \times \frac{v^2}{g'} \quad (20)$$

Hence, total tube side pressure loss is given by;

$$\Delta p_T = \Delta p_t + \Delta p_r \quad (21)$$

2.1.9 Shell Side Pressure Drop

[25] provided a more accurate equation in determining the pressure drop on the shell-side, it is given by;

$$\Delta p_s = \frac{f {G_t}^2 D_s (N+1)}{5.22\times10^{10}\, D_e s \emptyset_s} \quad (22)$$

2.2 Mechanical Design

As mentioned in section 2 after successful thermal design the mechanical design is the next stage in the design of a shell and tube heat exchanger.

2.2.1 Design Pressure

The design pressure plays a very major role in determining the minimum thickness required for the pressure parts. According to section VIII division 1, of the rules for construction of pressure vessels by [27], a pressure vessel shall be designed of at least the most severe condition of coincident pressure. Generally too, the design pressure is 10% greater than the maximum allowable working pressure. Therefore tube-side pressure which is higher is given by;

$$P_T = G_t \times v_t \quad (23)$$

2.2.2 Design Temperature

The design temperature for a non-directly heated body like the heat exchanger is given by an addition of 10˚C to the maximum temperature of any component in the heat exchanger. In this design, the maximum fluid temperature occurs at the inlet to the shell with water at 100˚C. Therefore, the design temperature of 110˚C is adopted.

2.2.3 Shell Wall Thickness

According to section UG-27 of [27].

The minimum wall thickness $t_s = \frac{PR}{SE-0.6P}$ (24)

2.2.4 Tube Sheet Design

Generally, tube sheets less than 100 mm are made from plate materials [28, 29]. The minimum tube sheet thickness due to bending t_{ts} is given by;

$$t_{ts} = \frac{FG_p}{3}\sqrt{\frac{P_t}{kf}}\ [24] \quad (25)$$

2.2.5 Headers

For the sake of simplicity and ease of construction and maintenance, the A-type; channel and removable cover head is used. Likewise for the rear head, the L-type; fixed tubesheet like "A" stationary head is used.

2.3 Material Selection

Of course, it may not be possible for every component to be made of one material, often though, the best is chosen with considerations also given to the cost, availability and machinability.

2.3.1 Shell Material

The material chosen was ASTM A285 Grade C carbon steel. This grade of steel is effective at low pressure conditions. They have intermediate to low yield strength, hence these properties make them useful in structural, mechanical and other engineering applications especially in pressure vessels like steel tanks and boilers and heat exchangers.

2.3.2 Tube Material

The material chosen for the tube is copper type-L. This is because they have a very high thermal conductivity of 385 W/mk. They have high resistance to pitting, crevice erosion, stress corrosion cracking, corrosion fatigue and erosion hence they are suitable for the tube side flow.

2.3.3 Baffle and Tubesheet Material

The baffles and tube sheet materials were made of stainless steel. This is because stainless steels are corrosion resistant; possess high tensile stress, very durable, temperature resistance and easy formability and fabrication.

2.3.4 Headers

The material used for both headers was ASTM A285 grade C carbon steel.

2.4 Design Drawings

The design drawings were all done with Dassault systemes SOLIDWORKS.

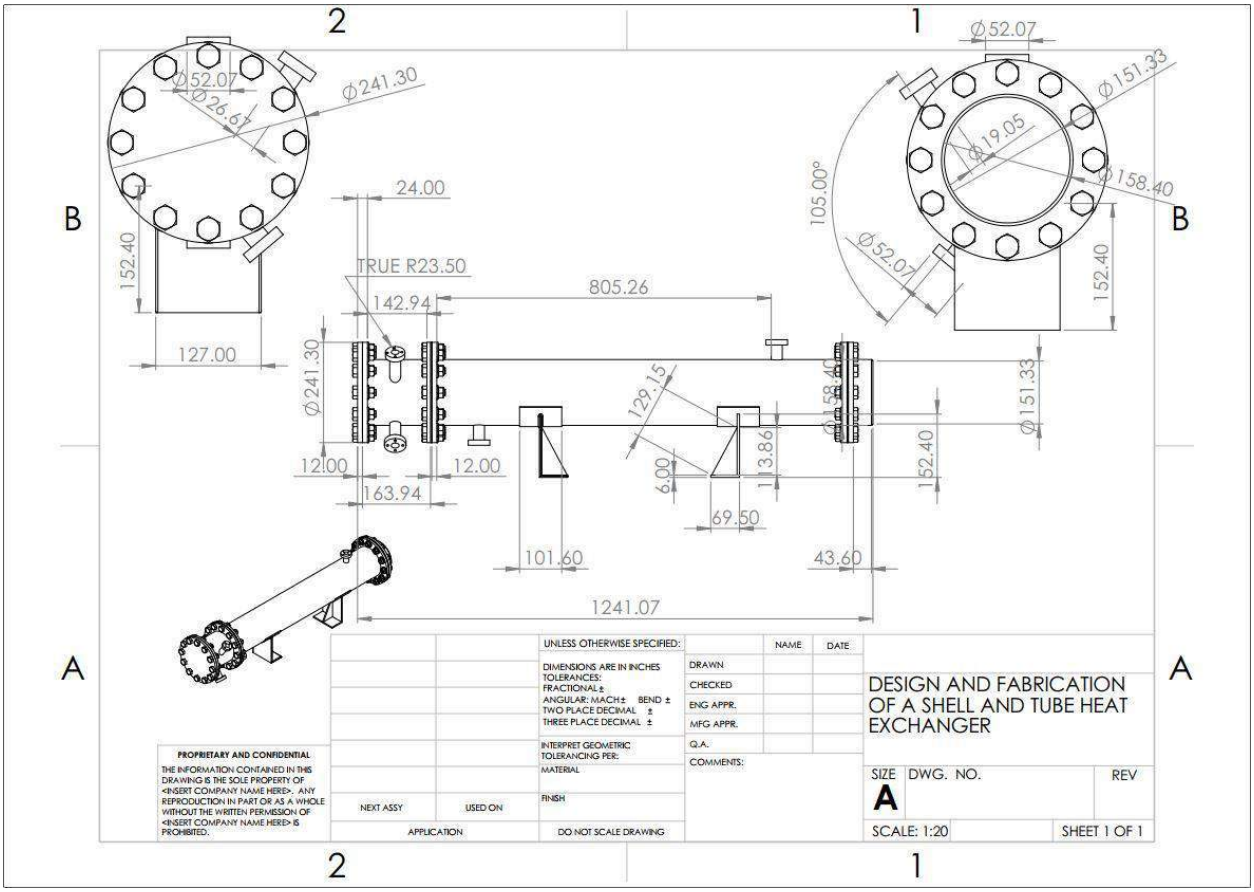

Figure 3: Design 2D drawings of the heat exchanger.

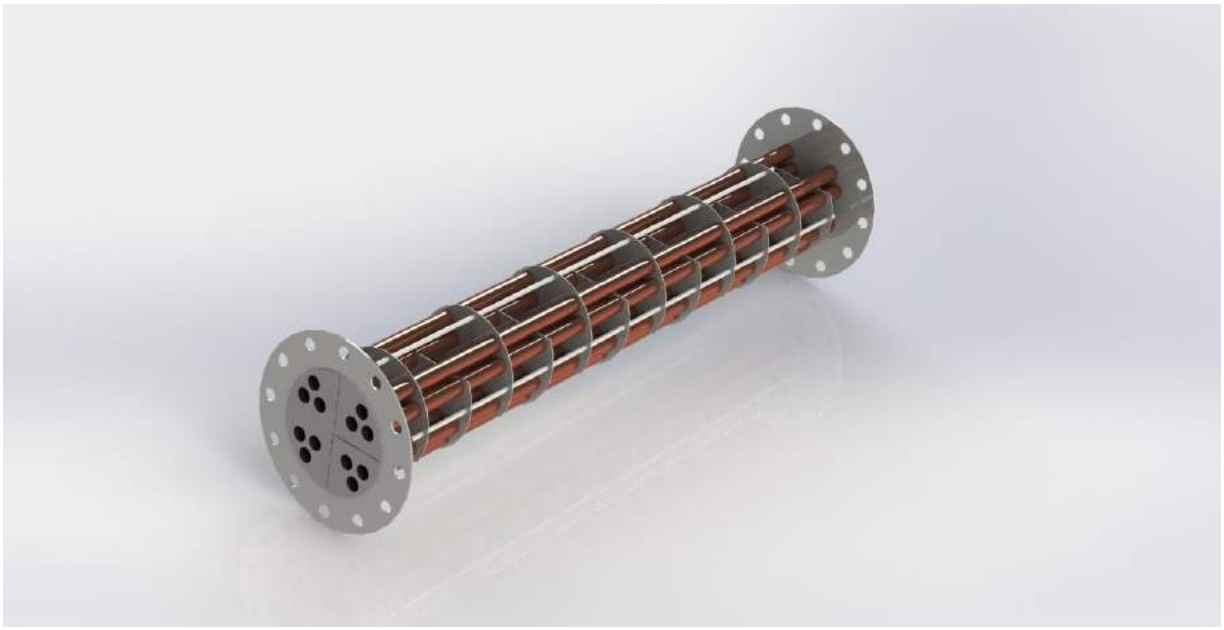

Figure 4: Pictorial 3D rendition of the tube bundle

Figure 5: Pictorial 3D rendition of the assembled shell and tube heat exchanger

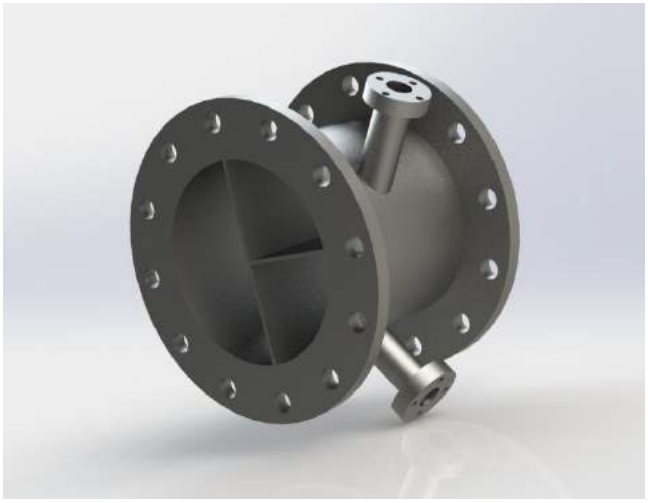

Figure 6: Pictorial 3D rendition of the front head partition.

2.5 Design Summary

Table 1 provides the design summary of both the thermal and mechanical design.

Thermal Design		
Parameters	**Equation used**	**Values**
Log Mean Temperature Difference (LMTD)	3	53.53 ^{O}C

Corrected LMTD	3	51.40 ^{O}C
Tube-side Reynolds number	9	54,432
Tube-side transfer surface area	5	0.718 m^2
Tube-side mass velocity	8	2707.13 Kg/m^2s
Tube-side film heat transfer coefficient	10	10, 198.75 W/m^2
Shell-side mass velocity	12	164.05 Kg/m^2s
Shell-side film heat transfer coefficient	15	2599.5 W/m^2 K
Clean overall heat transfer coefficient	17	2010.1164 W/m^2 K
Fouling resistance	18	0.0000025164 m^2 K/W
Tube-side pressure drop	21	85.191 kPa
Shell-side pressure drop	22	27.5 kPa
Heat load	1	73.185 kW
Internal flow area per tube	6	6.464×10^{-4} m^2
Shell-side flow area	11	3.048×10^{-3} m^2

Mechanical Design		
Parameters	**Equation used**	**Values**
Design pressure	23	80.61 kPa
Tubesheet thickness	25	2 mm
Shell wall thickness	24	5 mm
Number of tubes	5	12
Thickness of tube		1.2446 m
Baffle spacing		8 cm
Design Temperature		110 ^{O}C
Number of Baffles		12

2.6 Fabrication

After the completion of the mechanical design, the fabrication drawings were used to construct the heat exchangers. The process of fabrication, involved several processes such as:

I. Measurement of materials
II. Cutting of sheet metals and shell tubes
III. Brazing of copper tubes to the tubesheet
IV. Welding of components
V. Assembly of components using mechanical fasteners
VI. Painting

Figure 7: Flange welding to front head and shell in progress.

Figure 8: Completely fabricated and painted shell and tube heat exchanger.

3. Results and Discussions

The shell and tube heat exchanger was designed and fabricated to be used in laboratory experiments in tertiary institutions for thermal power and heat transfer courses. The heat exchanger is easy and safe to operate. It is also compact and has mounting brackets which make them easy to mount on a skid and to reposition to choice locations.

One prolific feature of the design is the use of copper tubes as tube material. [19] Fabricated the tubes of a heat exchanger using SA-179 carbon steel finned tubes because of cost implication while [18] used stainless steel because of the purpose of the heat exchanger in condensing drinking water. While the choice of the number of tubes for this design is 12 as gotten from the

thermal design, the number of tubes used ranges from 2 [18] to 1782 [19]. The length of the copper tubes used was 1000 mm. [18] used length of 400 mm, while [14] used tube length of 10,000 mm.

During the performance test of the shell and tube heat exchanger, experiments were carried out with different mass flow rates. An average flow rate of 1.0316 kg/s with temperature of 20°C of water was passed through the tube-side inlet. This was similar to [11] that passed water of 15°C at 2.58 kg/s.

3.1 Water Retention Apparatus

For there to be efficient exchange of heat between the both streams of fluid, it is necessary for both streams to be in thermal contact for a considerable period of time. To achieve this, Pascal's law which states that pressure applied to an enclosed fluid will be transmitted without a change in magnitude to every point of the fluid and to the walls of the container was applied. The pressure at any point in the fluid is equal in all directions [29, 31].

To achieve this, a water retention mechanism was designed using PVC pipes and 90° bend connectors to form a U-shaped apparatus as shown in Figure 9.

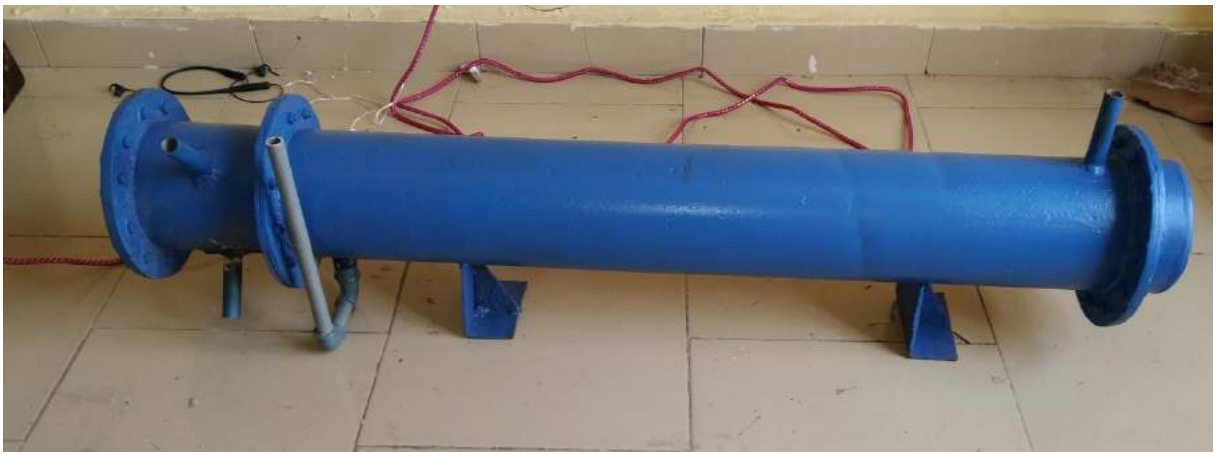

Figure 9: Fabricated Heat exchanger with water retention apparatus incorporated.

4. Conclusion

This paper has presented a study on the design and fabrication of a shell and tube heat exchanger (STHE) for laboratory experiments in Nigerian tertiary institutions. After an extensive literature review and study of past similar works, a detailed thermal design using the Kern's approach was adopted for the thermal design of the heat exchanger. Thereafter, a mechanical design was carried out using the TEMA standards and the ASME BPVC. Thereafter, Dassault systemes SOLIDWORKS was used to model the heat exchanger before its fabrication. Testing of the heat exchanger was successfully carried out; however, the results are beyond the scope of this work.

A water retention mechanism was designed using PVC pipes and 90˚ bend connectors to form a U-shaped apparatus to ensure efficient exchange of heat between the both streams of fluid.

Nomenclature

Q The heat flow rate

F_T LMTD correction factor

LMTD Logarithmic Mean Temperature Difference (LMTD)

U_D Assumed overall heat transfer coefficient

A Tube heat transfer surface area

N_t The number of tubes

L Length of tubes

a" The total external surface per tube

G_T Tube side mass velocity

a_t Internal flow area for the tube side

ρ Water density

μ Dynamic viscosity of the fluid at caloric temperature

d_i Internal diameter of tubes

Re_t Tube side Reynolds number

h_{io} Corrected tube-side film heat transfer

h_i Tube-side film heat transfer coefficient

ID Internal diameter of tube

OD Outer diameter of tube

P_T Tube pitch

B Baffle Spacing

a_s Shell side flow area

$\emptyset_s$ Shell side viscosity ratio

f Friction factor

N Number of baffles

n Number of tube passes

g' Acceleration due to gravity

s Specific gravity

$\emptyset_t$ Tube side viscosity ratio

C' Adjacent tube clearance

v_s Shell side velocity

D_e Shell equivalent diameter

Re_s Shell side Reynolds number

G_s Shell side mass velocity

h_o Shell-side film heat transfer coefficient

j_H Dimensionless heat transfer factor

U_C Clean overall heat transfer coefficient

Δp_t Pressure due to friction

Δp_r Return loss

Δp_T Total pressure drop

Conflict of Interest

The authors wish to state that there is no conflict of interest in this paper.

References

[1] Patel, D.S., Parmar, R.R., Prajapati V.M (2015): CFD Analysis of Shell and Tube Heat Exchangers. International Research Journal of Engineering and Technology. Vol 2 (9): pp 2231- 2235.
[2] Zohuri, B. (2017) Heat Exchanger Types and Classifications. In: Compact Heat Exchangers. Springer, Cham. https://doi.org/10.1007/978-3-319-29835-1_2
[3] Permana, I., Ajiwiguna, T.A., Kirom, M.R. (2018): Journal of Physics: Conference Series Vol 1153.
[4] Zohuri, B., McDaniel, P. (2019) Heat Exchangers. In: Thermodynamics in Nuclear Power Plant Systems. Springer, Cham. https://doi.org/10.1007/978-3-319-93919-3_13
[5] Prasad, A.K and Anand, K., 2020: Design & Analysis of Shell & Tube Type Heat Exchanger, International Journal of Engineering Research & Technology (IJERT). Vol 9 (1).
[6] Little, C., Hayes, J., LeFemina, L., McDonald, L., Alnahri, W. (2019): Thermofluids Laboratory; Heat Exchangers. New York Institute of Technology. Technical Paper.
[7] Mathew, S.U., Tamzor, L.A. (2020): Heat Exchanger Process Optimization in a Typical Brewery Plant. European Journal of Engineering Research and Science. Vol 5 (1): pp 76-81.
[8] Master, B.I., Chunangad, K.S., Boxma, A.J., Kral, D., Stehlik, P. (2007): Most Frequently Used Heat Exchangers from Pioneering Research to Worldwide Applications. Heat Transfer Engineering. Vol 27 (6): pp 4-11.
[9] Dhumal, A.H., Kerkal, G.M., Pawale, K.T. (2017): Heat Transfer Enhancement for Tube in Tube Heat Exchanger Using Twisted Tape Inserts. International Journal of Advanced Engineering Research and Science. Vol 4 (5): pp 89-92.
[10] Sachchidanand, J., Nimankar, J., Dahake, S.K (2016): Review of Heat Exchangers. Global Journal of Engineering Science and Researchers. Vol 3(12) pp 81-92.
[11] Chukwudi B.C and Ogunedo M.B (2018): Design and Construction of a Shell and Tube Heat Exchanger. Elixir Mechanical Engineering. Vol 118: pp 50687-50691

[12] Parikh, S.E. (2011): Characterizing Expert and Novice Differences in Problem Solving in Heat Transfer. Stanford University.
[13] Kakac, S., Liu, H., & Pramuanjaroenkij, A. (2012): HEAT EXCHANGERS, Selection, Rating, and Thermal Design. CRC Press.
[14] Gawande, S. H., Wankhede, S. D., Yerrawar, R.N., Sonawane, V.J., & Ubarhande, U.B. (2012): Design and Development of Shell & Tube Heat Exchanger for Beverage. Modern Mechanical Engineering, pp 121-125.
[15] Araromi, O.O. (2013): Design and Development of a Small Heat Exchanger as Auxiliary Cooling System for Domestic and Industrial Applications. International Journal of Engineering Trends and Technology (IJETT), V(6), 314-319.
[16] Bhatt, D., & Javhar, P. M. (2014): Shell and Tube Heat Exchanger Performance Analysis. International Journal of Science and Research, III(9), 1872-1881.
[17] Shukla, A., Kumar, P., & Tiwari, D. D. (2015): Design Procedure of Shell and Tube Heat Exchanger. International Journal of Engineering and Technical Research (IJETR), 116-119.
[18] Adam, N., Abduhamed, A., Hairuddin, A., and Kareem, H. (2016): Design and fabrication of a heat exchanger for portable solar water distiller system. International Food Research Journal, 15-22.
[19] Ahmed, M. (2017). Heat Exchanger. Moratuwa: University of Moratuwa. Technical Paper.
[20] Taware, S.R., Patil, D. S., and Arakerimath, D.R. (2017): Design, Fabrication and testing of Shell and Tube Heat Exchanger for Heat Recovery from Hydraulic Oil. Internatiion Journal of Engineering Research & Technilogy, 505-512.
[21] Scott-Emuakpor, C. (1982): Design, Construction, and Testing Of a Model Heat Exchanger. Technical Paper.
[22] Abdulmumuni, B., Adedeji, M., & Ologunye, O. (2017): Design and Fabrication of Shell and Tube Heat Exchanger for Practical Applications. Federal Polytechnic Ede. Technical paper.
[23] Peters, M., Timmerhaus K.D., & West, R. (2003): Plant Design and Economics for Chemical Engineers. New York: McGraw-Hill.
[24] Tubular Exchanger Manufacturers Association, INC. (1999): Standards of The Tubular Exchanger Manufactures Association (8th ed.).
[25] Kern, D. Q. (1983): Process Heat Transfer. Mcgraw-Hill International Book Company.
[26] Eagle, A., & Ferguson R.M. (1930): On the coeeficient of heat transfer from the internal surface of tube walls. Proccedings of The Royal Society A.
[27] American Society of Mechanical Engineers. (2013): 2013 ASME Boiler & pressure Vessel Code: V111 Rules for Construction of Pressure Vessels (13th ed.). New York.
[28] Golder, K., & Gound, V. (2013): Mechanical design of Heat Exchangers . National Programme on Technology Enhanced (NPTEL).
[29] Kwasi-Effah C. C.1, Obanor A. I., Aisien F. A., Ogbeide O.(2016) Review of Existing Models for Stirling Engine Performance Prediction and the Paradox Phenomenon of the Classical Schmidt Isothermal Model, International Journal of Energy and Sustainable Development Vol 1(1) 6-12
[30] Fanchi, J. R. (2010): Integrated Reservoir Asset Management. Gulf Professional Publishing.
[31] Ronquillo, R. (2019): Understanding Heat Exchangers. Retrieved March 4, 2020, from Thomas Industry Update:https://www.thomasnet.com/articles/process-equipment/understanding-heat-exchangers/

Appendix

A.1 LMTD correction factors for 1-2 heat exchangers

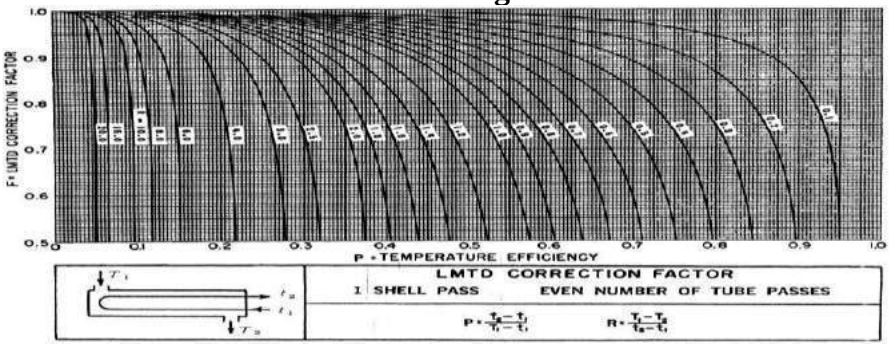

Source: [24]

A.2 Heat exchanger and condenser tube data.

Tube OD, in.	BWG	Wall thickness, in.	ID, in.	Flow area per tube, in.²	Surface per lin ft, ft²		Weight per lin ft, lb steel
					Outside	Inside	
½	12	0.109	0.282	0.0625	0.1309	0.0748	0.493
	14	0.083	0.334	0.0876		0.0874	0.403
	16	0.065	0.370	0.1076		0.0969	0.329
	18	0.049	0.402	0.127		0.1052	0.258
	20	0.035	0.430	0.145		0.1125	0.190
¾	10	0.134	0.482	0.182	0.1963	0.1263	0.965
	11	0.120	0.510	0.204		0.1335	0.884
	12	0.109	0.532	0.223		0.1393	0.817
	13	0.095	0.560	0.247		0.1466	0.727
	14	0.083	0.584	0.268		0.1529	0.647
	15	0.072	0.606	0.289		0.1587	0.571
	16	0.065	0.620	0.302		0.1623	0.520
	17	0.058	0.634	0.314		0.1660	0.469
	18	0.049	0.652	0.334		0.1707	0.401
1	8	0.165	0.670	0.355	0.2618	0.1754	1.61
	9	0.148	0.704	0.389		0.1843	1.47
	10	0.134	0.732	0.421		0.1916	1.36
	11	0.120	0.760	0.455		0.1990	1.23
	12	0.109	0.782	0.479		0.2048	1.14

Source: [24]

A.3 Tube-side water-heat-transfer curve

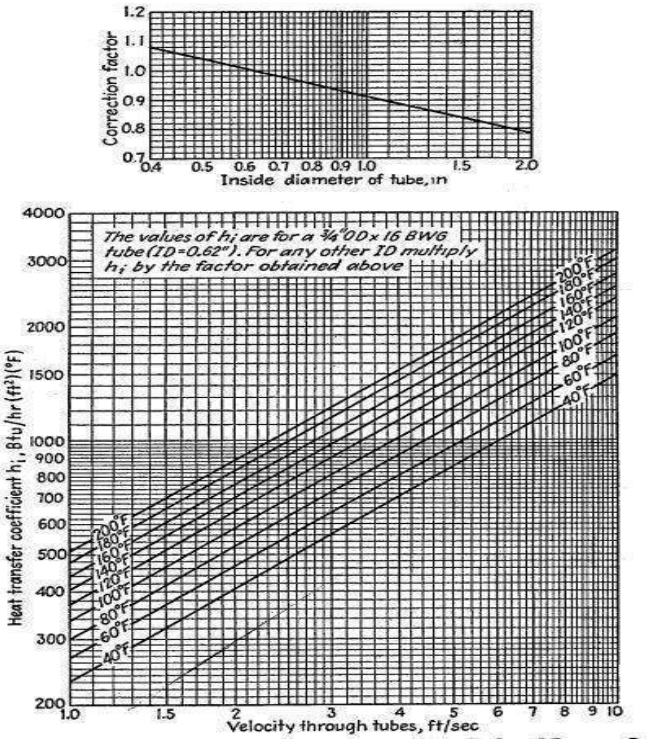

Source: [26]

A.4 Shell-side heat transfer curve for bundles with 25% cut segmental baffles

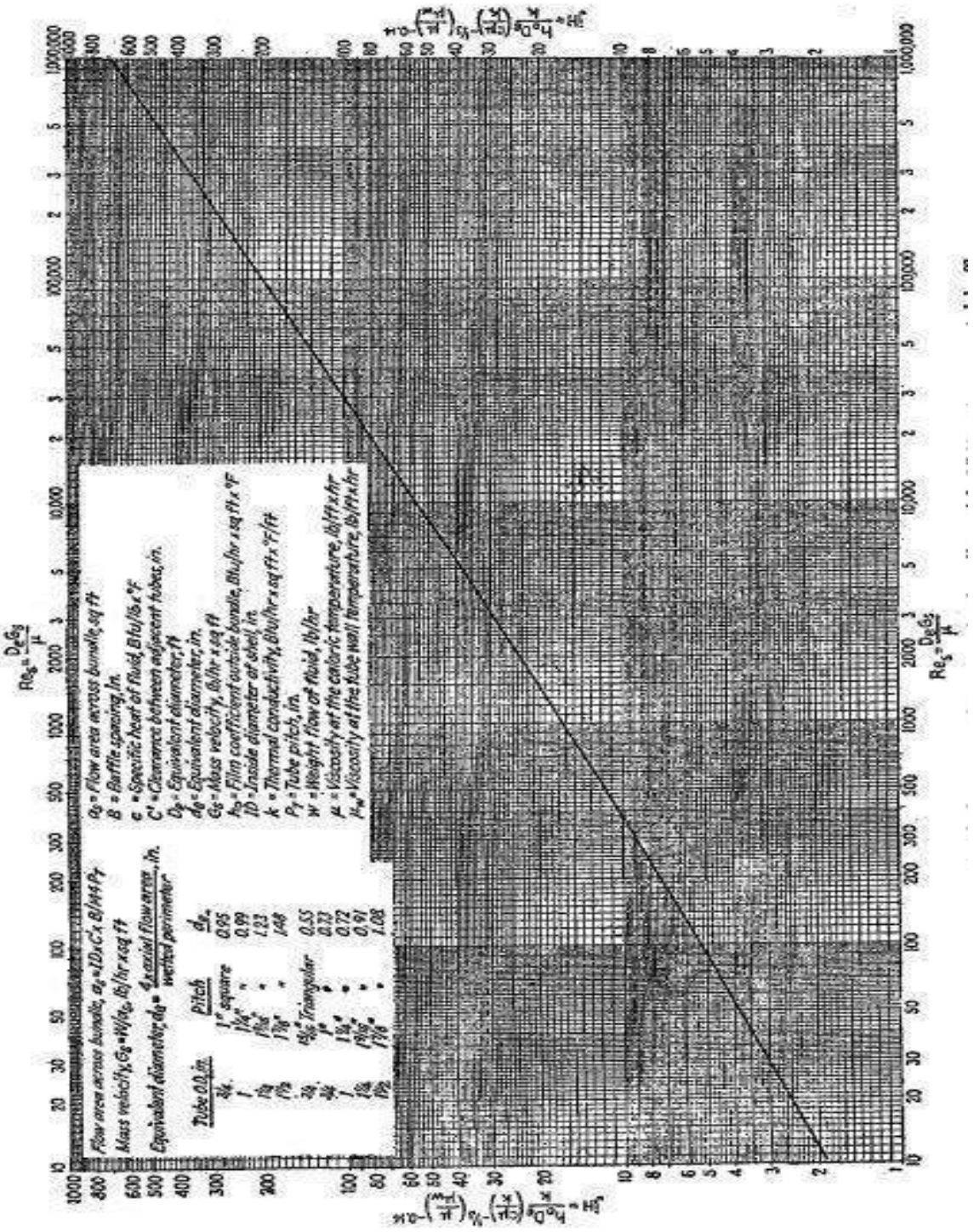

Source: [25]

NIPES Conference Proceedings
The 1st International Conference of the Nigerian Institution of Professional Engineers and Scientists 7th-8th Oct. 2021: 241-258
www.nipesjournals.org.ng

Static and Dynamic Analysis of a UFAA-19 Series Hybrid Electric Vehicle

C.C. Kwasi-Effah[a], U.E. Igbeka[b], B.C. Ataman[c], A.I. Emenime[d], F. Max-Eguakun[e]
Department of Mechanical Engineering, University of Benin, Ugbowo, Benin City, 300283, Nigeria

Abstract
Due to the ongoing control on emission levels and increase in fuel prices in many countries, it has become imperative for vehicle manufacturers to develop more fuel efficient drivetrain technologies. Hybrid electric vehicles are viewed as short- to mid-term solutions for reducing emissions and fuel consumption while maintaining vehicle performance. This paper presents a design of a UFAA-19 Series Hybrid Electric Vehicle to reduce the dependency on fossil fuels in Nigeria. A CAD model of the hybrid system was developed, afterwards, static and dynamic analyses were then carried out. Mild steel was the material used for the design and simulation of the model. The results from the static analysis showed that the model was stressed within permissible limits. The dynamic analysis showed that a 750W BLDC motor was sufficient for providing the low-speed torque for the mini hybrid system. The vehicle reached speeds of up to 17km/hr. Results also showed that an IC engine rated at 3.5kW would provide sufficient power for the system to reach up to speeds of 70km/hr. The hybridization factor for the system was found to be 17.6% which makes it a mild hybrid vehicle.

Keywords**:** *Hybrid vehicle, emission, modelling UFAA, Dynamic, Static*

1. Introduction

With the introduction and widespread adoption of Nicolas Otto's Internal Combustion Engine for use in vehicles, air pollution from exhaust became a problem as harmful amounts of carbon monoxide and carbon dioxide were released into the atmosphere as well as smog [1]. In the world currently, 60% of CO emissions, 50% of NO emissions, and 30% of HC emissions are caused by automobiles [2].To address the issue, automakers are being forced to shift a portion of their production from internal combustion engines to hybrid systems or pure electric vehicles. An electric vehicle that has zero fossil fuel by-products, also known as Zero-Emission Vehicles (ZEV), will provide a solution to this problem; however, the energy capacity and weights of electric batteries are still insufficient for replacements of internal combustion engines. The hybrid system is thus viewed as a suitable alternative.

Hybrid electric vehicles, HEVs, according to the International Electrotechnical Commission, are vehicles with propulsion energy from two or more sources, stores, or power converters and have at least one that's converted directly to electrical energy. Based on this definition, HEVs could be classified based on their source of power as battery and gasoline ICE, battery and diesel ICE, battery and capacitors, and battery and flywheel [3]. This definition of HEVs is generally not accepted by ordinary people and as such a more suitable definition is required.

A hybrid vehicle combines more than one power source. It most commonly refers to vehicles that use both an internal combustion engine and an electrically powered motor, a Hybrid Electric Vehicle (HEV). HEVs can perform at least one of the following functions:

- engine idle start and stop
- energy recuperation (regenerative braking)
- electric torque assist
- electric driving
- battery charging (from the drive)
- battery charging (from the grid)

The emissions of Hybrid Electric Vehicles (HEVs) are generously less when contrasted with that of the Internal Combustion Engine Vehicles (ICEVs). Significant advantages of HEVs over ICEVs include better mileage, high efficiency, and improved productivity, less reliance on petroleum, reduced pollution because of the halfway or complete traction given by the electric motors.

The components providing a pathway for mechanical power in hybrid vehicles include the internal combustion engine, the transmission, the drivetrain, electric motors, and the alternator. For electrical power, we have the battery packs, the electric motors, the alternator, and the bidirectional power converter. Based on the arrangements of these components, HEVs can be classified into Series Hybrids, Parallel or Series-Parallel Hybrids, and Complex Hybrids (CHEV). [4].

Hybridization of an electric vehicle is the degree to which the vehicle's power is being assisted by a secondary power source such as an ICE. Hybridization factor is a measure of this power assist. It is represented as the ratio between the electric motor power and the sum of the total power input to the vehicle. It can be expressed mathematically as:

$$Hybridization\ factor, HF = \frac{Motor\ power}{Motor\ power + Engine\ power} \quad (1)$$

A summary of the different characteristics of the different classes of hybrid electric vehicles by hybridization degree is presented in Table 1.

Table 1: Comparison of different HEVs by the degree of hybridization

Hybrid Type	Micro Hybrids	Mild Hybrids	Full Hybrids
IC engine	Conventional	Downsized	Downsized
Motor power	3 to 5kW	7 to 15kW	30 to 50kW
Motor voltage	12V	60 to 200V	200 to 600V
Hybridization factor	< 10%	10 to 30%	> 40%
Energy saving	5 to 10%	20 to 30%	30 to 50%
Functions	Idle start/stop Regenerative braking Accessory powering	Idle start/stop Regenerative braking Torque assist	Idle start/stop Regenerative braking Electric traction
Relative cost	Low	Medium	High
Example	Mercedes Smart	Honda Civic	Toyota Prius

Modern HEVs use efficiency-enhancing technologies like regenerative breaking where the vehicle's kinetic energy is converted to electric energy to charge batteries as opposed to heat energy as seen in conventional brakes. Many HEVs shut down the ICE at idle and at low speeds restarting it when necessary reducing idle emissions; this is called a start-stop system. Also, as HEVs have smaller engines than ICEVs the gear ratio can be adjusted for maximum efficiency to further improve economic fuel usage [5].

1.2 Vehicle Dynamics

The free-body diagram of a vehicle accelerating up an inclination is as shown in Figure 1.
The diagram shows the vehicle accelerating with an instantaneous velocity, V, up a slope, θ, against a wind velocity, V_w. From Newton's second law of motion, the net force exerted on the vehicle is equal to the product of its mass and acceleration.

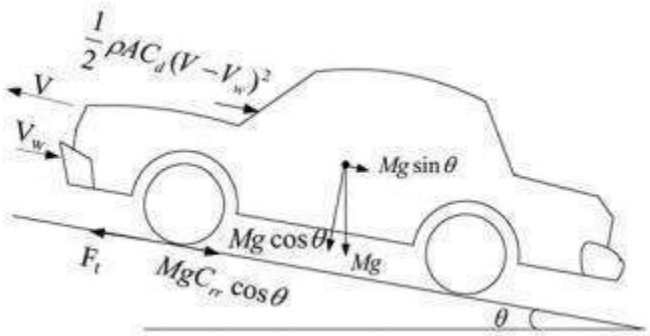

Figure 1: Free body diagram of a vehicle accelerating up an inclination

$$F_t - \sum F_r = f_m M \propto$$

Where F_t = Traction force acting on the vehicle

ΣF_r = Sum of all the resisting forces (drag, frictional and component of the vehicle's weight in its direction motion)

M = Overall mass of the vehicle

α = Acceleration of the vehicle

f_m = mass factor for converting the rotational mass of the rotating components into translating mass

$$\sum F_r = F_D + F_f + Mg\sin\theta$$

$$= \frac{1}{2}\rho AC_d(V - V_w)^2 + MgC_{rr}\cos\theta + Mg\sin\theta$$

Where A = Frontal area of the vehicle

ρ = Density of air

C_d = Drag coefficient

C_{rr} = Coefficient of rolling resistance

The total propulsion force is then given by

$$\Rightarrow Traction\ force, F_t = f_m M$$

$$\propto + \frac{1}{2}\rho AC_d(V - V_w)^2 + MgC_{rr}\cos\theta + Mg\sin\theta \quad (2)$$

The power required to drive the vehicle at a speed, V, is given by the

$$Power, P = F_r \times V = f_m M \propto V + \frac{1}{2}\rho A C_d V(V - V_w)^2 + MgVC_{rr}\cos\theta + MgV\sin\theta$$

1.3 Literature Review

Balasubramani N. et al. designed and fabricated a two-wheeler hybrid electric system and studied its performance characteristics. The two-wheeler vehicle was powered in the front by an electric motor which was the hub motor and in the back by an IC engine. They tested the system in 3 modes; engine mode, electric mode, and hybrid mode, and compared the results with that gotten from a conventional two-wheeler system. They found out that the system gives twice the mileage as a conventional vehicle when the electric motor was used at start-up for generating high torque and the IC engine for sustaining the cruising speed. They also found out the hybrid system emitted 50% less pollution [6].

Grundit E. et al. modelled and simulated a series hybrid car, Smarter, using the MATLAB/Simulink graphical modelling software for competing in the 2009 Shell Eco-marathon competition. They varied the components of the drivetrain and investigated its effect on fuel efficiency. Although the model was never verified with a physical model, they found out that the car, Smarter, would cover 255km per litre of fuel and place 10th in the competition. They however discovered that further modification of the drivetrain parameters yielded little change in the vehicle's fuel efficiency and suggested that the parallel hybrid system be investigated [7].

Chuddy et al. carried out a study on the performance of a parallel and series hybrid system using a flexible Advanced Vehicle Simulator (ADVISOR). They studied the fuel economy of the two IC systems working independently and compared that with the savings from the parallel and series systems. The fuel economy was found to be 24% better than the IC engine running alone and 4% better than the series hybrid system [8].

Lukic et al. presented a study on the effect of hybridization on the fuel economy and dynamic performance of a vehicle. They studied the 3 different hybrid classes; micro, mild and full hybrid system for a conventional passenger vehicle. Their studies show that an acceptable level of fuel economy at a low price can be provided for by vehicles with a low hybridization factor. They also found out the optimum level of hybridization ranges between 30 to 50% and depends on the power requirement of the vehicle [9].

Kwasi-Effah et al. carried out a study on the fuel savings from a hybrid electric vehicle. They created a MATLAB/Simulink model of the hybrid system based off on the Toyota Prius series-hybrid vehicle. The fuel consumption of the model was studied when it was subjected to the Urban Dynamometer Driving Schedule (UDDS) and the Highway Fuel Economy Test (HWFET) drive cycle data. They found out that the vehicular emission for the series-parallel system reduced by over 60% with emissions of 75g/km for CO_2, 0.096g/km for HC, 1.362g/km for CO, and 0.066g/km for NO_x [10, 11, 12].

Ceraolo M. et al. studied the problem of optimizing energy consumed by a hybrid system while considering two drivetrain configurations: the series and parallel drivetrains. For each configuration, the effect of the functions of different management strategies was considered (full

electric drive, plug-in capabilities, etc.). They found out that the parallel hybrid system was superior to the series hybrid system [13, 14, 15].

2. Methodology

The model considered in this work was based on a go-kart. These are small open-wheeled suspension-less vehicles that are usually used for racing (karting). A conventional go-kart has 5 components: Chassis, steering system, power system, drivetrain, and braking system.

2.1 Conceptual Design

Vidyanandan, K V. [12] presented the different drivetrain configurations for hybrid vehicles. The concept chosen for this project was based off on the parallel hybrid drivetrain configuration. This configuration was chosen as opposed to the simpler series hybrid drivetrain because of the following reasons:

1. Compact design
2. High efficiency
3. Low cost
4. Low power requirements (i.e. smaller battery packs)

The low cost of the parallel hybrid drivetrain is due to the fewer number of components (when compared with the series-parallel and complex drivetrains) and their relatively small sizes (when compared with the series drivetrain). One of the reasons for this is due to the recycling of their motor for regenerative braking. We decided to capitalize on this and went with the conventional hybrid design as opposed to the plug-in hybrid design. Thus, we rely solely on regenerative braking to charge for batteries as well as the torque from the IC engine during the vehicle's cruising speed.

Since the target vehicle for this project is a go-kart, the rear-wheel-drive transmission system was chosen. Rear-wheel drive systems are favoured by racing cars of which a go-kart is one. As earlier stated, go-karts, aside from those used for recreational purposes, are usually designed for racing (karting).

In summary, the conceptual design we went with was that for a conventional parallel hybrid electric vehicle

2.2 Design Specification

We wanted to build a simple but practical model of the parallel hybrid go-kart with the following specifications

1. Lightweight for better mobility
2. Low power requirement
3. Low cost
4. Durable

We were looking at reaching speeds up to 70km/hr (19.4m/s) with the mass of the system (kart and driver) not exceeding 180kg.

2.2.1 Preliminary Analysis

In other to proceed with a detailed design of the system, a preliminary analysis is presented below which would serve as the minimum specification for the kart. This section aims to estimate the minimum power needed by the electric motor in other to propel the kart.

2.2.1.1 Assumptions

1. The effect of drag is neglected
2. The kart is assumed to move through still air
3. The body is assumed to be a point mass

2.2.1.2 Parameters

Vehicle mass (kart + driver), M = 180kg
Top speed for EM, V = 15km/hr (4.12m/s)
Acceleration time, t = 10s
Maximum incline angle, $\theta = 2^{\circ}$
Working surface = concrete
Coefficient of rolling resistance, $C_{rr} = 0.01$

2.2.1.3 Calculations

From equation 1.2, neglecting air drag, the traction force is given by

$$F_t = M \propto +MgC_{rr}\cos\theta + Mg\sin\theta$$

From the kinematic equations of motion,

$$Acceleration, \propto = \frac{\Delta V}{t}$$

$$\therefore Traction\ force, F_t = M\left(\frac{V}{t} + gC_{rr}\cos\theta + g\sin\theta\right)$$

$$= 180\left(\frac{4.12}{10} + 9.81 \times 0.01 \times \cos 2° + 9.81 \times \sin 2°\right)$$

$$\therefore Traction\ force, F_t = 154.3N$$

The power required to sustain this speed by the EM is given by

$$Power, P = F_t \times V$$

$$= 154.3 \times 4.12$$

$$\Rightarrow Power\ required, P = 643W$$

Therefore, the least rating for the electric motor should be **643W**. This also sets the limit of the value for the rating of the IC engine to be used for the mini hybrid system.

2.3 Detailed Design

The goal in this section is to present the processes and analysis carried out in creating the form representing the mini hybrid system. It also entails the details carried out in sizing some of the critical components of the system. A CAD model of the mini hybrid system was created in Solidworks 2018. Mathematical models representing some of the dynamic systems of the model were created and simulated in Simulink. Mild steel was chosen as the material for the design and analysis. This is due to its high strength, availability and low cost. The material properties of mild steel are shown in Appendix A1.

2.3.1 Design of Static Components

The static components of the go-kart design are the front and rear chassis. The type of chassis that we went with was the open chassis design. This is because this type of kart design offers the least drag due to its low frontal area. Also, it has a good combination of simplicity and strength. The kart design was based off on the fixed axle go kart plans from KartFab.com. The two parts of the chassis were connected by hinges.

The front chassis of the go-kart provides support for the driver, the front axle and the steering system. The rear chassis houses the propulsion system and the rear shaft. The kart chassis were separated into these two compartments in other to isolate the propulsion system, which is the most critical system, from the rest components of the kart.

The strength was the most important criterion considered during the design of the kart. Also, the system was designed so that the number of weld joints would be kept to a minimum. This is to reduce the site of stress concentrations.

Figure 2: CAD model of front and rear chassis

2.3.2 Design of Dynamic Components

The dynamic components of the go-kart are the steering system and the electrical and IC propulsion systems.

2.3.2.1 Steering System

The Ackermann steering geometry was employed for the steering system. This was achieved with the help of a four-bar mechanical linkage consisting of a track rod, a tie rod, steering column and front axle. The steering column transfers the angular rotation of the steering to the pitman arm at its base. The tie rod forms a connection between the steering column and one of the front axles. It transmits the angular rotation of the steering column to the axle. The two front axles are connected by the track rod which enables the axles to rotate together.

Figure 3: CAD model of the steering system

2.3.2.2 Electrical Propulsion System

From the results of the preliminary analysis, it can be seen that the rating of the electric motor should be greater than 643W. A 760W BLDC motor was selected for the hybrid system. In other to properly size the batteries, a simulation was carried out in the Simscape workspace of Mathlab. The schematic for the model is as shown in Figure 4.

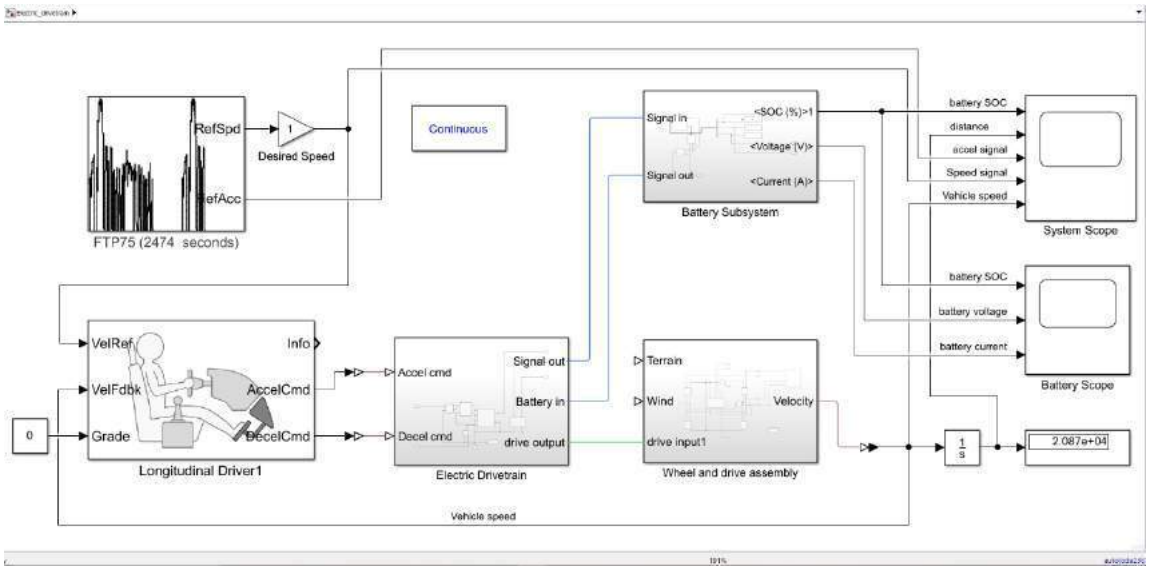

Figure 4: Model of the Vehicle showing the Electrical drivetrain

A breakdown of the different components of the model is presented as follows:

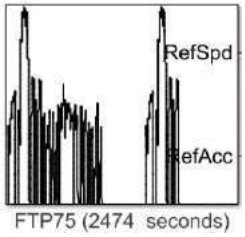

1. Drive Cycle:

This block generates a standard or user-specified longitudinal drive cycle. The block output is the vehicle longitudinal speed. This model makes use of the FTP75 drive cycle.

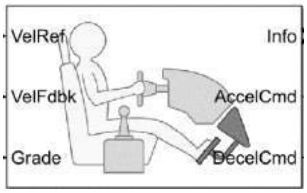

2. Longitudinal Driver:

This is a parametric longitudinal speed tracking controller for generating normalized acceleration and braking commands based on reference and feedback velocities.

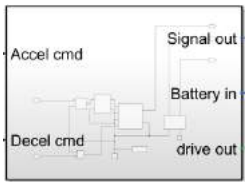

3. Electric Drivetrain:

This subsystem handles translating the acceleration and brake signals from the driver and translating that to mechanical torque signals to the vehicle.

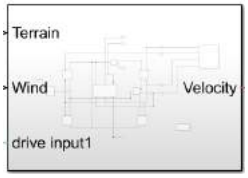

4. Wheel And Drive Assembly:

This contains the components that model the vehicle's body and the wheels.

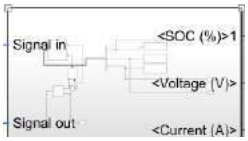

5. Battery Subsystem:

This subsystem models the battery. Discharge, State of Charge, current and voltage values can be simulated with the input signal from the H-Bridge.

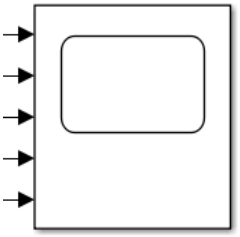

6. Scopes:

These are placed with the components to monitor the values and plot a graph of these against time. The scopes in this system monitor the vehicle's speed, distance travelled, and the battery's state of charge, voltage and current.

2.3.2.2 Working of the System

Reading off velocity values from the drive cycle input, the longitudinal driver sends either an acceleration signal or a brake signal to the drivetrain. This gets converted by the H-Bridge block to a Pulse-Width Modulated (PWM) voltage signal which is to be applied across the motor's terminals.

This output signal from the H-Bridge is first fed to the battery where the appropriate voltage, current and state of charge changes are applied. Then a lead from the battery supplies power to the DC Motor in the drivetrain.

The motor, once excited, applies a torque to the rear shaft of the vehicle through a chain drive (sprocket and chain) where a reduction ratio of 37:14 is applied. This torque on the shaft moves the rear wheels and the vehicle body. The velocity of the vehicle is measured and fed back to the longitudinal driver forming a closed-loop control system.

2.3.2.3 IC Propulsion System

Once the rating of the electric propulsion system was determined, an IC engine was selected based on vehicle rating proposed vehicle top speed. A Simulink model was created, and the ratings of the IC engine was varied.

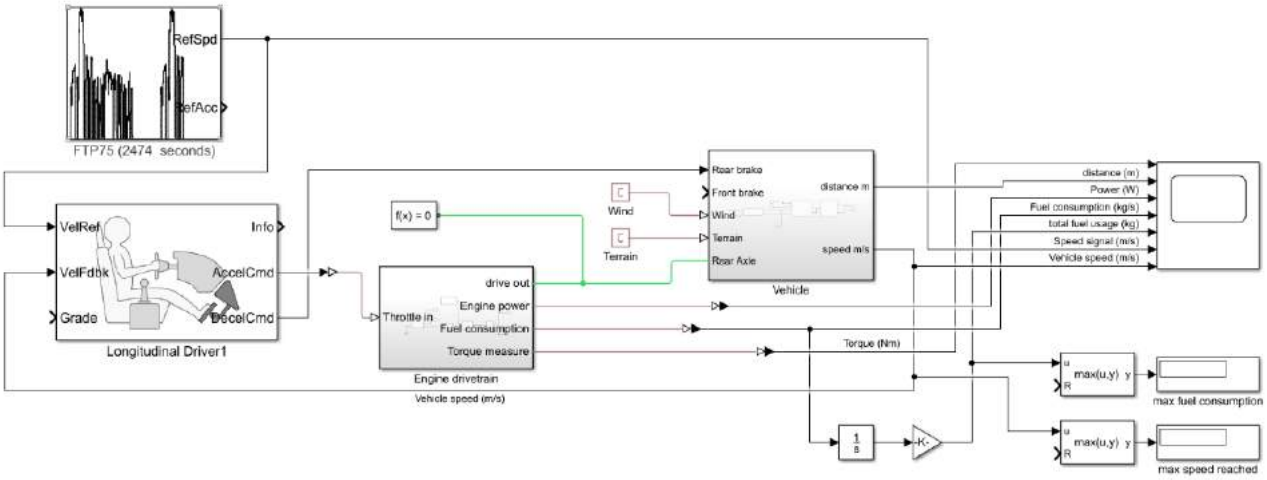

Figure 5: Model of the Vehicle showing the mechanical drivetrain

2.4 Detailed Drawing

ITEM NO.	PART NUMBER	QTY.
1	front_chassis	1
2	5972K44	4
3	front_axle	1
4	steering_column	1
5	tyre_assembly	4
6	818.22M - Plain washer, 14 mm, regular	2
7	818.2.2.4M - Hex flange nut, M16 x 2 --S	2
8	base_plate	1
9	rear_axle	1
10	7835152	3
11	rear_chassis	1
12	hinge	2
13	front_axle_L	1
14	track_rod	1
15	48V_750W_BLDC_Motor_Assembly	1
16	2299K35	1
17	2299K37	1
18	60cc Assembly	1
19	6261K441	28
20	6261K441	28
21	tie_rod	1
22	battery	2

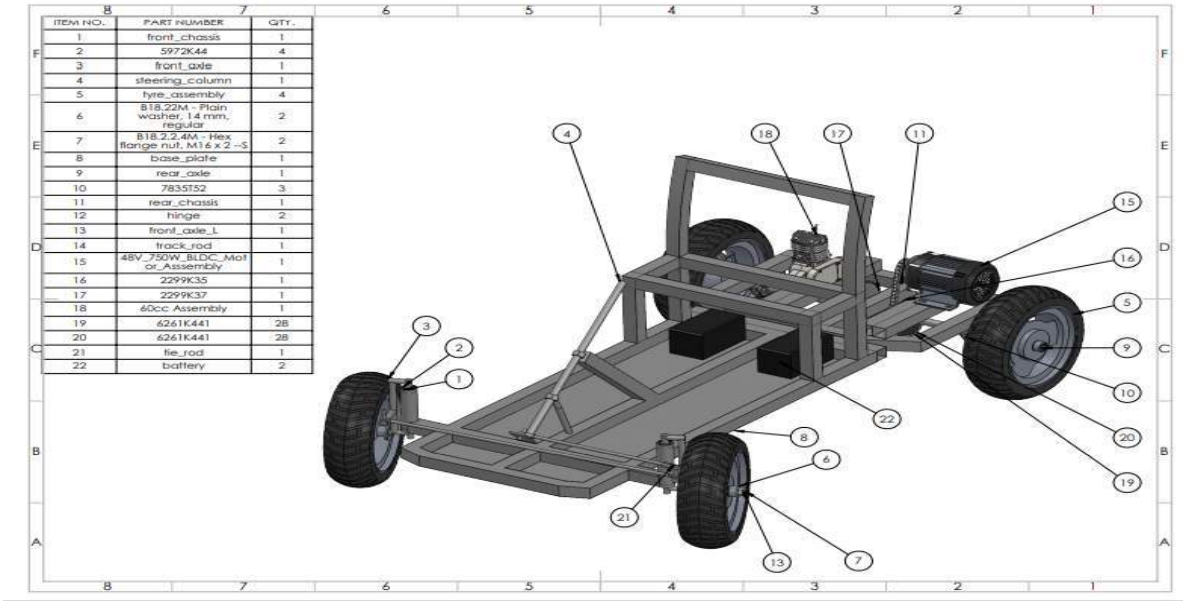

Figure 6: 3D model of the mini hybrid system showing its BOM

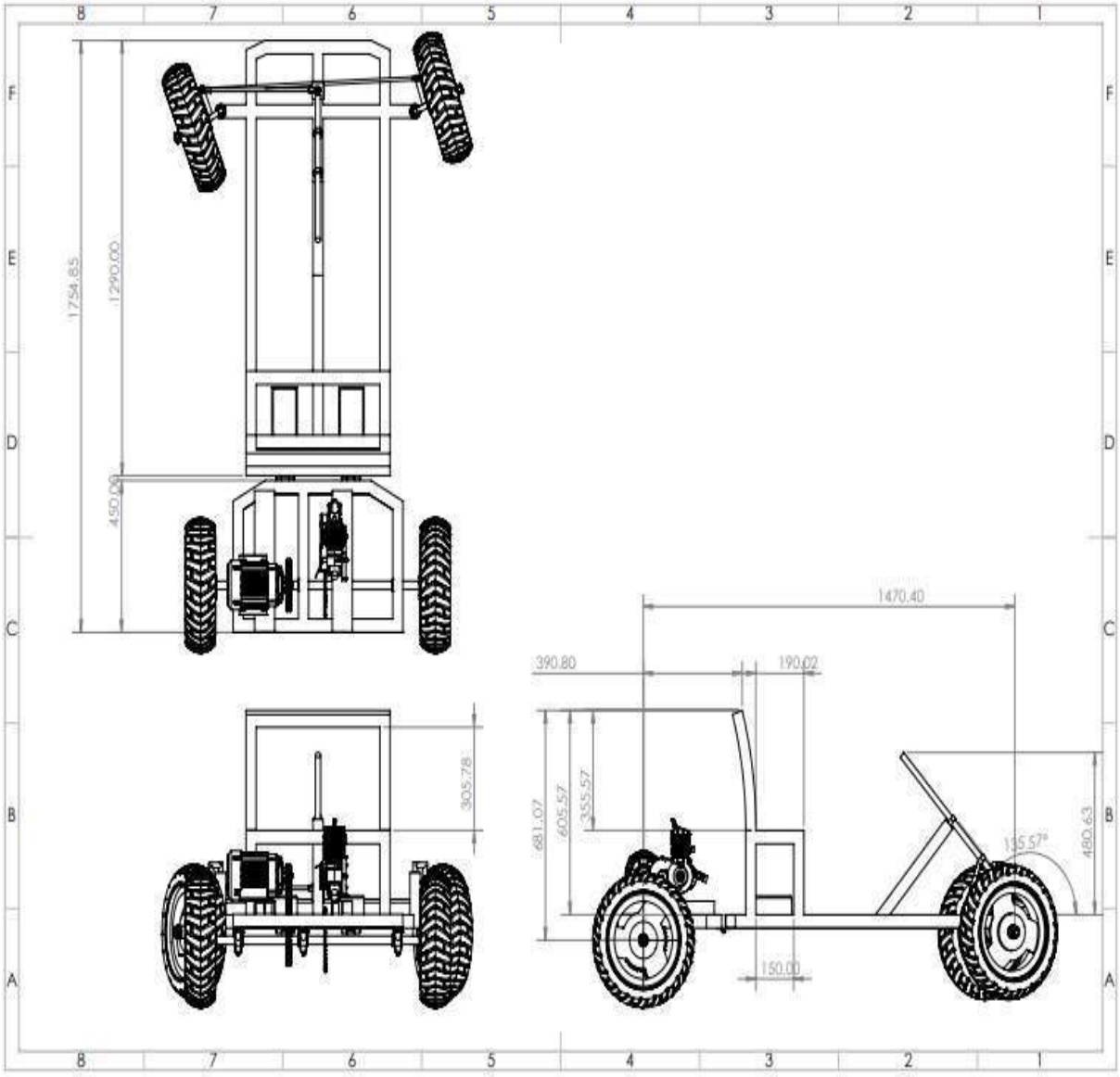

Figure 7: Detailed drawing of the mini hybrid electric vehicle

3.0. Results and Discussion

3.1 Static Analysis

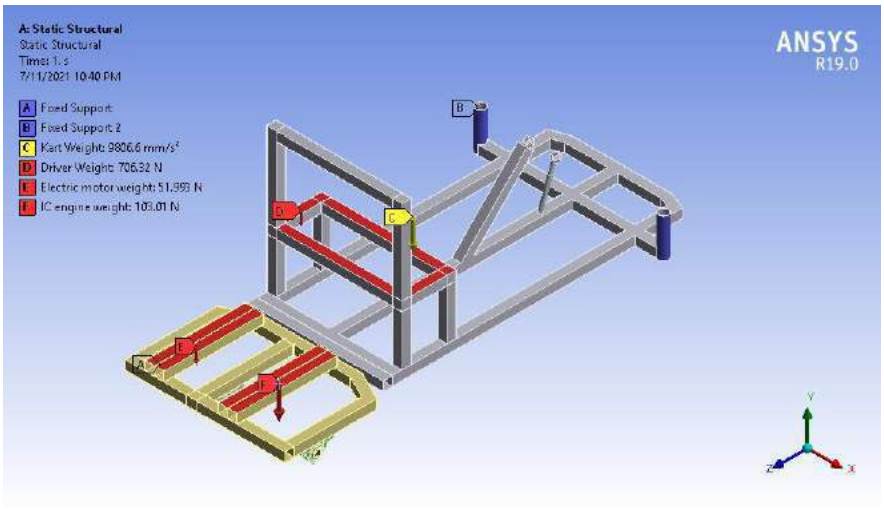

Figure 8: Constraints and loading for frame analysis

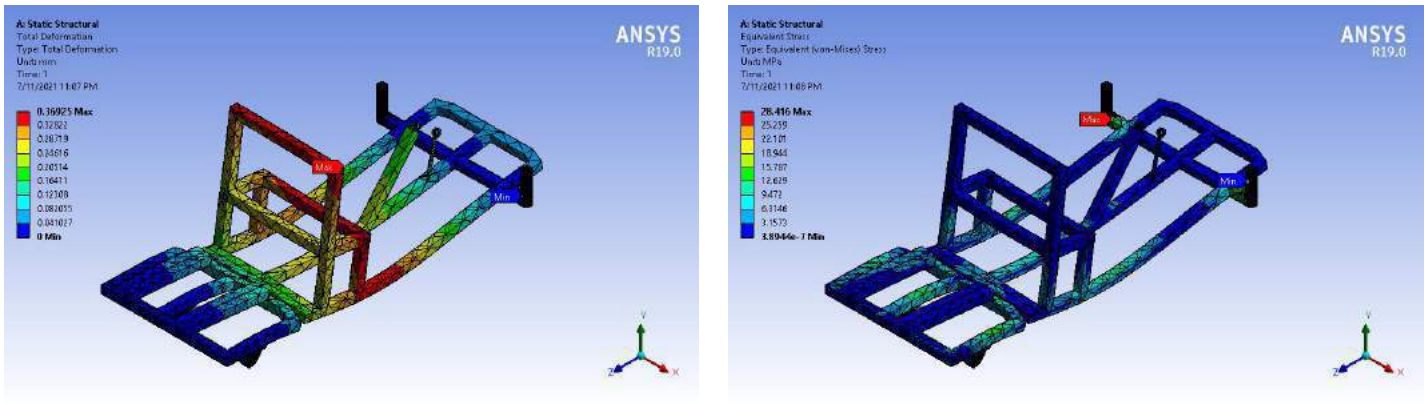

Figure 9: Total deformation and equivalent stress results for frame analysis

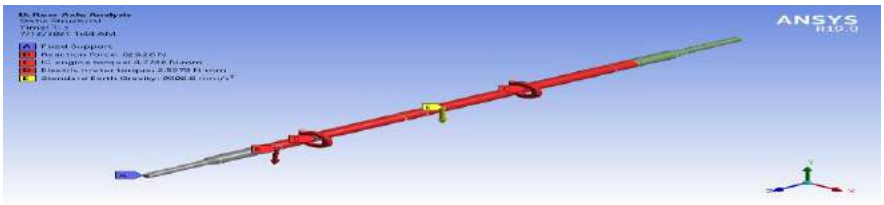

Figure 10: Constraints and loading for rear shaft analysis

Table 1: Summary of the simulated frame

Maximum Deformation	0.36925mm
Maximum equivalent stress	28.416MPa

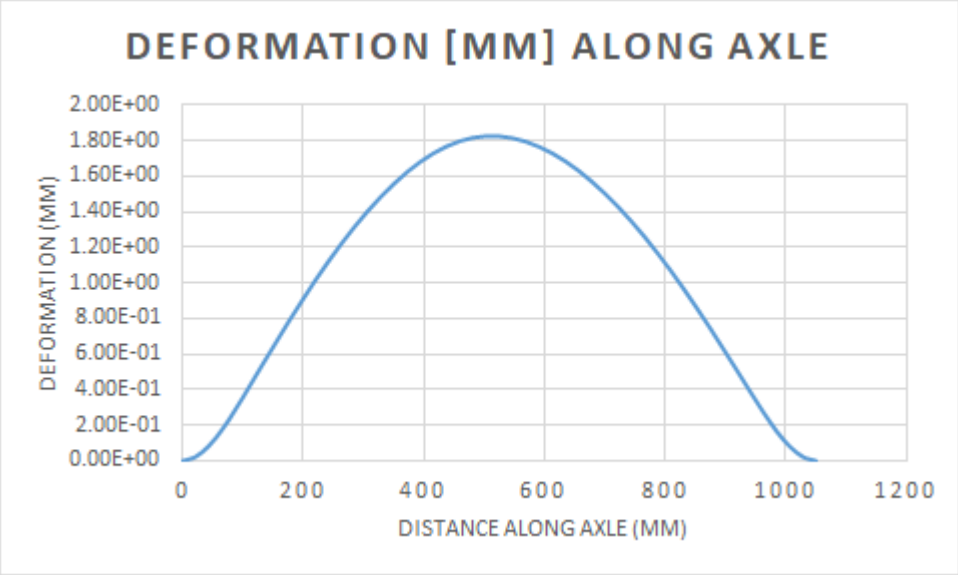

Figure 11: Graph of deformation along the rear shaft

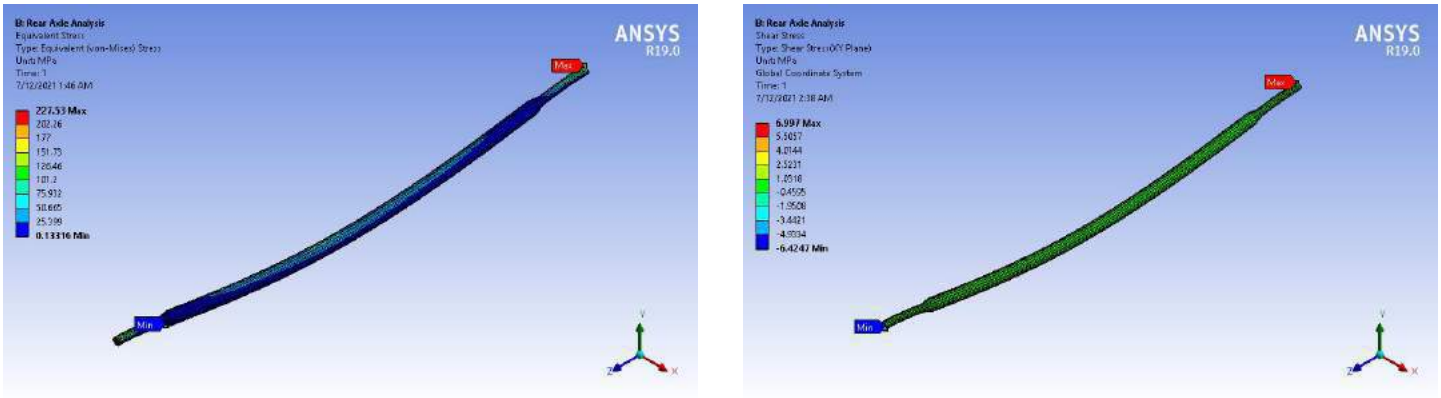

Figure 12: Equivalent stress and shear stress results for the rear shaft analysis

Table 2: Summary of simulation results for rear shaft analysis

Maximum deformation	1.8256mm
Equivalent stress	227.53MPa
Maximum shear stress	6.997Mpa

From Figure 11, maximum deformation occurs in the driver's seat. Also, maximum Von Mises stress would occur in the front chassis close to the left housing for the front axle. It can also be seen that the maximum stress (28.4MPa) induced in the model didn't exceed the yield stress for its material (370MPa). This implies that the chassis would be able to withstand the loads imposed on it.

From Figure 12, the maximum deformation occurs at the centre of the rear shaft. Also, the maximum equivalent and shear stresses induced in the shaft are less than the yield tensile stress (370MPa) and shear strength (80GPa) for mild steel. This maximum stress occurs at the corner of the shaft close to the IC engine. The reason for this is because the corner is a sharp edge that tends to build up stresses (has high-stress concentrations) when the model is subjected to a deforming load.

3.2 Dynamic Analysis

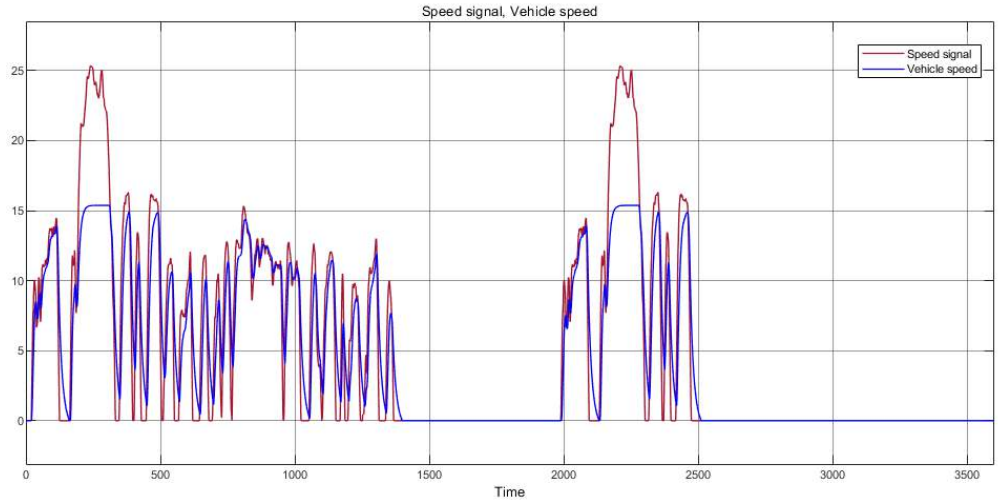

Figure 13: Reference and actual velocity (km/hr) of the vehicle based off the FTP75 drive cycle running on electric propulsion alone

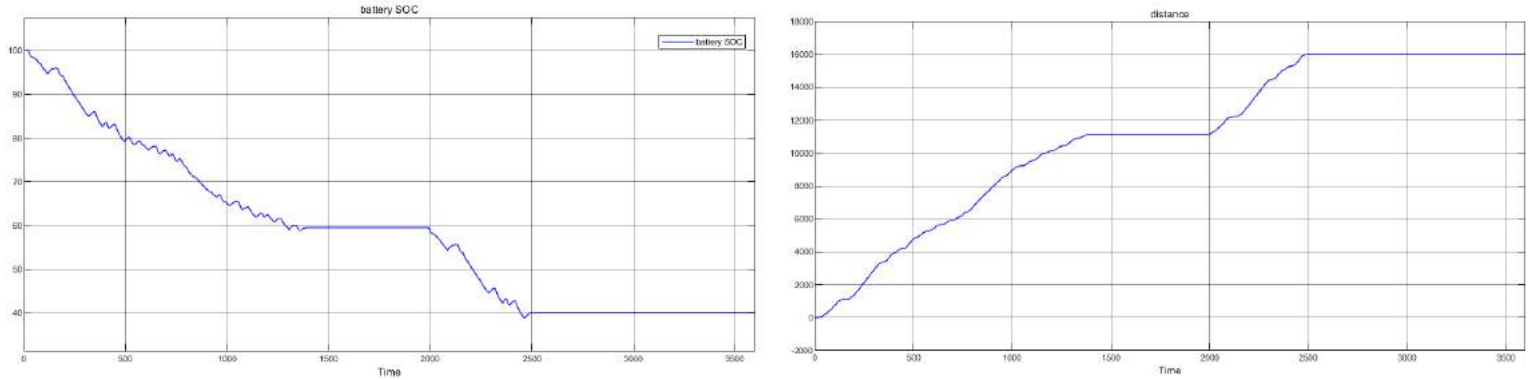

Figure 14: Graphs of battery SOC (%) and distance (m) against time for the hybrid system running on electric propulsion alone

Table 3: Summary of fuel consumption and max. speed for different IC engine

Power (kW)	Max Speed (m/s)	Fuel Consumption (x 10^{-4}kg)
0.75	14.35	3.5098
1.00	14.35	3.5098
1.50	14.35	4.0759
2.00	14.39	4.4342
2.50	16.36	4.7019

3.00	18.05	4.907
3.50	19.52	5.060

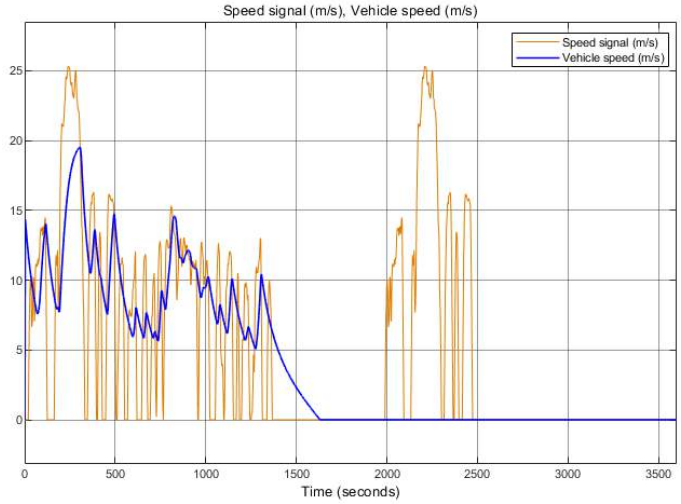

Figure 15: Reference and actual velocity response for the hybrid system running on the 3.5KW engine alone

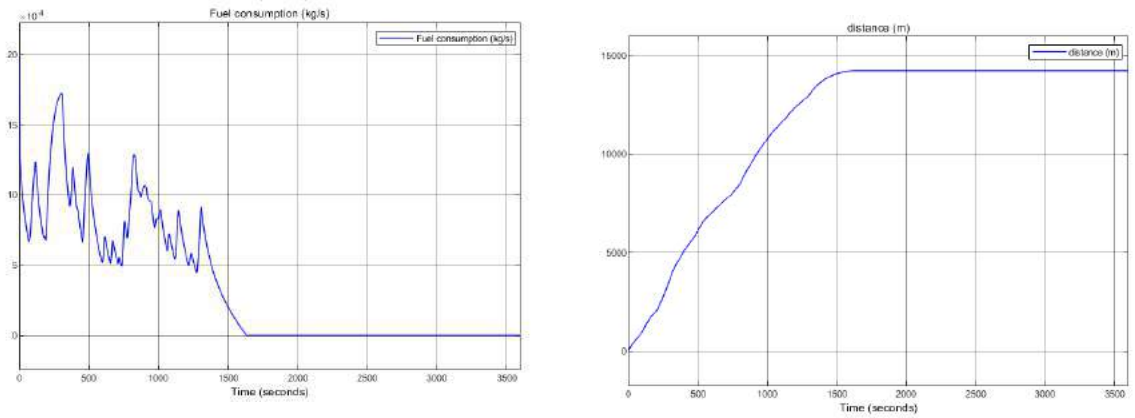

Figure 16: Graphs of fuel consumption (kg) and distance covered (m) vs time (s) for the hybrid system running on the 3.5KW engine alone

From Figure 14, the vehicle developed a top speed of **17km/hr** while running on electrical propulsion alone which is consistent with the preliminary analysis presented in section 2.2.1.2. Also, the vehicle covered 16000m during its motion while attaining a SOC of 40% at the end as shown in Figure 15.

Table 3 shows the result from the analysis of the hybrid system running on IC propulsion alone for different engine power ratings. It can be seen that an engine with a rating of **3.5KW** would satisfy our requirements for the engine speed. The dynamic characteristics of the vehicle, when powered by this engine, is as shown in Figures 15 and 16.

3.3 System Analysis

From Equation1, the hybridization factor, HF, is given by

$$Hybridization\ factor, HF = \frac{Motor\ power}{Motor\ power + Engine\ power}$$

From the analysis presented above

Motor power = 0.75kW

Engine power = 3.5kW

$$HF = \frac{0.75}{0.75 + 3.5}$$
$$= 17.6\%$$
$$\Rightarrow \boldsymbol{Hybridization\ factor\ \ HF = 17.6\%}$$

Since the hybridization factor is greater than 10% but less than 30%, as shown in Table 1, the mini hybrid system is a **mild hybrid vehicle**.

4. Conclusion

A 3D representation of the mini hybrid system was created in Solidworks. Static and dynamic analysis of the computer model was carried out in Ansys and Simulink respectively and the results were presented in their respective sections.

Overall, it was found that the chassis and the rear shaft were stressed within acceptable limits. A **750W** BLDC motor was shown to be feasible for providing the low-speed torque with the vehicle reaching up to speeds of **17km/hr**. It was also shown that a **3.5kW** IC engine would be feasible for the high-speed requirements of the vehicle which was found to be **70km/hr**. The system was found to be a **mild hybrid vehicle** with a hybridization factor of **17.6%**.

4.1 Recommendations

1. The results from the simulation should be validated by building a physical model based on the specifications provided above and running it on a standard track with the FTP-75 as the reference drive cycle.
2. The fuel savings and overall efficiency of the hybrid should be determined and compared with that for the IC system working alone.
3. More complex systems like the series-parallel hybrid and the complex hybrid vehicles should be studied and compared with results from this study.
4. A stronger but lighter material other than mild steel should be investigated

Nomenclature

CAD	Computer-Aided Design
HEV	Hybrid Electric Vehicle
ZEV	Zero-Emission Vehicles
HC	Hydrocarbon
ICEV	Internal Combustion Engine Vehicles
ICE	Internal Combustion Engines
IC	Internal Combustion
HF	Hybridization Factor
SOC	State of Charge
AC	Alternating Current
DC	Direct Current
BLDC	Brushless DC
UDDS	Urban Dynamometer Driving Schedule
HWFET	Highway Fuel Economy Test
EM	Electric Motor
PWM	Pulse Width Modulation

References

[1] K. C. Prajapati, R. Patel, R. Sagar, B. T. Mechanical, and E. Student, "Hybrid Vehicle : A Study on Technology," *International Journal of Engineering Research & Technology (IJERT)*, vol. 3, no. 12, pp. 1076–1082, 2014.

[2] N. Ha, "Comparative environmental impacts of Internal Combustion Engine Vehicles with Hybrid Vehicles and Electric Vehicles in China - Based on Life Cycle Assessment," *E3S Web of Conferences*, vol. 118, no. 2019, 2019, doi: 10.1051/e3sconf/201911802010.

[3] C. C. Chan, "The Stae of the Art of Electric Vehicles," *Journal of Asian Electric Vehicles*, vol. 2, no. 2, pp. 579–600, 2004, doi: 10.4130/jaev.2.579.

[4] A. Zia, "A comprehensive overview on the architecture of hybrid electric vehicles (hev)," in *2016 19th International Multi-Topic Conference (INMIC)*, 2016, pp. 1–7.

[5] M. Kebriaei, A. H. Niasar, and B. Asaei, "Hybrid electric vehicles: An overview," in *2015 International Conference on Connected Vehicles and Expo (ICCVE)*, 2015, pp. 299–305. doi: 10.1109/ICCVE.2015.84.

[6] N. Balasubramani, prasath S. Hari, K. A. Jagadeesh, P. S. Karna, and prasath D. Karun, "Fabrication and Performance Analysis of Hybrid Two Wheeler," *International Research Journal of Engineering and Technology (IRJET)*, vol. 5, no. 3, pp. 3672–3676, 2018.

[7] E. Grunditz and E. Jansson, "Modelling and Simulation of a Hybrid Electric Vehicle for Shell Eco-marathon and an Electric Go-kart," *Power Engineering*, 2009.

[8] K. Tammi, T. Minav, and J. Kortelainen, "Thirty years of electro-hybrid powertrain simulation," *IEEE access*, vol. 6, pp. 35250–35259, 2018.

[9] S. M. Lukic and A. Emadi, "Effects of drivetrain hybridization on fuel economy and dynamic performance of parallel hybrid electric vehicles," *IEEE Transactions on Vehicular Technology*, vol. 53, no. 2, pp. 385–389, 2004, doi: 10.1109/TVT.2004.823525.

[10] Collins C. Kwasi-Effah and Timon Rabczuk , "Dimensional Analysis and Modelling of a Lithium-Ion Battery. Journal of Energy Storage, Vol 18, pp308-315 2018, https://doi.org/10.1016/j.est.2018.05.002

[11] Kwasi-Effah C.C, Obanor A.I "Simulation of the Emission Impact of a Hybrid-Electric Vehicle" International Journal of Engineering & Technology Sciences (IJETS) 1 (5): 251-259, 2013

[12] C.C Kwasi-Effah, AI Obanor " Modeling and Simulation of a Gasoline-Electric Vehicle" International Journal of Engineering & Technology, 1(4) 163-176, 2013

[13] CC Kwasi-Effah, AI Obanor, OO Ogbeide "Performance Investigation of a Series-Parallel Petrol-Electric Vehicle" International Journal of Oil, Gas and Coal Engineering,Vol 5(4): 54-60, 2017

[14] M. Ceraolo, A. Di Donato, and G. Franceschi, "A general approach to energy optimization of hybrid electric vehicles," *IEEE Transactions on vehicular technology*, vol. 57, no. 3, pp. 1433–1441, 2008.

[15] K. V Vidyanandan, "Overview of Electric and Hybrid Vehicles," 2018. [Online]. Available: https://www.researchgate.net/publication/323497072

Appendix

Table A1. Material properties for mild steel

Chemical composition	Carbon, C	0.14 - 0.20%
	Iron, Fe	98.81 – 99.26%
	Manganese, Mn	0.60 – 0.90%
	Phosphorus, P	≤ 0.040%
	Sulphur, S	≤ 0.050%
Density		7.87×10^5 kg/m^3
Ultimate tensile strength		440Mpa
Yield tensile strength		370Mpa
Modulus of elasticity		205Gpa
Bulk modulus		140Gpa
Poisson ratio		0.290
Shear modulus		80Gpa

NIPES Conference Proceedings
The 1st International Conference of the Nigerian Institution of Professional Engineers and Scientists 7th-8th Oct. 2021: 259-269
www.nipesjournals.org.ng

Development and Evaluation of a Manual Dewatered Cassava Mash (DCM) Sieving Machine

A. A. Ahiakwo[a], j. Osere[a] and A. B. Odinwa[a]
[a] Department of Agricultural Education, Federal College of Education (Tech.) Omoku

Abstract
Traditional sieving of dewatered cassava mash (DCM) using plant, synthetic or metallic material as the sieving surface with the arbitrary aperture fixed by the local developers and to be used with the awkward posture of processors, produces poor results as the sieving process exposes the users to musculoskeletal discomfort affecting their back, neck, shoulder and arm during the sieving process. Other factors that affect the sieving process besides the arbitrary fixing of the aperture, include lack of consideration of ergonomic and anthropometry of the user groups in the sieve development. To address this anomaly, this paper focuses on developing an improved dewatered cassava mash sieving machine incorporating ergonomic and anthropometric data of user groups as well as a modified sieve aperture. The machine was evaluated with respect to throughput capacity and exposure to musculoskeletal discomfort. The result showed an increase in throughput capacity from 35 to 59kg/h with a decrease in exposure to musculoskeletal discomfort from 66% to 47%. Adopting this improved machine will improve the livelihood of cassava farmers in this unit operation and add to a systematic change in sustainable development and ecologically smart future

Keywords:
Traditional sieve, ergonomic consideration, sieving posture, improved sieve, reduction in discomfort

1. Introduction
Cassava is a popular food item in Africa and one among the unpreserved tubers, deteriorating within two days once harvested [1]. Additionally, the tubers need to have the cyanogenic glucocides reduced to a level which is acceptable and safe for consumption [2,3]. For these reasons, cassava is usually sold in processed form as garri, cassava bread, farinha, etc. [4,5]. When harvested, cassava undergoes the processes of peeling, washing, grating, fermentation and dewatering; the resulting cassava mash is a conglomeration of bonded particles. Sieving is carried out not only to reduce the dewatered mash into fine particles (undersize) which drifts through the sieve, but to also separate the coarse particles (oversize) which are removed after a cycle of sieving [1].

[2], showed that sieving process will involve the breaking of cassava mash lump if it were to consist only of the starchy flesh and also if grating efficiency were to be close to hundred percent (100%). Unfortunately, this ideal situation is not attainable due to the inefficiency of the grating system. Besides, cassava tuber consists of the central vascular fibre as expressed in Figure 1

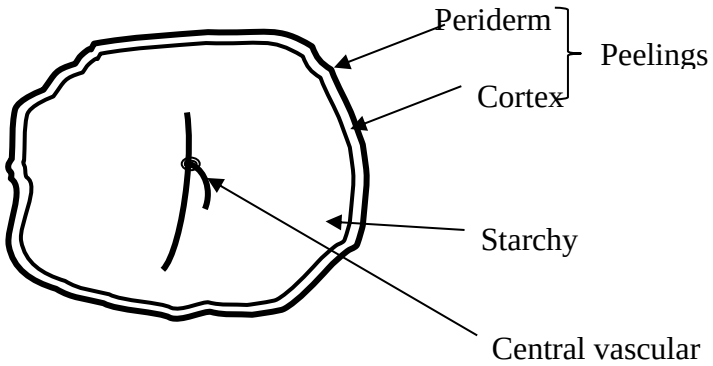

Figure 1: Cross Section of Unpeeled Cassava Tuber (Source: [2])

[6], found that this separation creates uniformity in particle size which is important because it enhances uniform garri frying of individual particles during the frying operation especially as smaller particles take less time and energy to fry.

[7],[8],[9] and [10] from their research showed that traditional sieve users are at high risk of developing musculoskeletal disorders with time as they are exposed to a discomfort level of 66% on quick ergonomic checklist rating and production losses as the process consumes time. [11],[12] and [7] reported that sieving process is currently carried out manually using the traditional sieve made of raffia plant with highlighted problem of drudgery, ergonomic challenges, high energy and time input. A few motorized sieving machines according to [13] and [14] developed to address the problems of sieving are still under trial. It has also been shown [7] that designing a sieve for cassava processing without adequate consideration to mesh number and aperture has resulted to the discomfort of the processors particularly in traditional method of sieving and hence has modified the current sieve aperture from the 2.87 average to 5mm with positive results.

[15] in their research on anthropometry of processors for ergonomically designing of improved dewatered cassava mash (DCM) sieving machine subjected important body parts necessary for adjustment of the traditional sieving process for improvement to measurement. The following results on the parameters measured for the 5th, 50th and 95th percentile of the generated data were: elbow height sitting (D) of 15.00, 19.23 and 22.67; lower leg length (E) of 38.80, 44.03 and 48.87, elbow to fingertip (F) of 38.27, 48.23 and 52.43; thigh clearance (H) of 9.83, 13.17 and 18.00; hip breadth (J) of 28.33, 32.83 and 42, respectively in centimeters. They recommended that the following ergonomic dimensions: 72cm for machine height, 53 cm for machine width, 68cm for machine length, and a sitting range of 36-50 cm will yield a more comfortable posture for developing an improve sieving machine. It is the objective of this research to develop a manual improved dewatered cassava (DCM) sieving machine using ergonomic and anthropometric data of the user groups.

2. Methodology

The manual sieving machine was conceptualized (Figure 2) and consisted of the following parts: platform hopper, DCM sieving platform, platform auxiliary components; frame and support.
During sieving process, the processor loads about 10kg of DCM into the platform hopper (item 1) in Figure 2. With item 2 (access to DCM) he picks bits of DCM and sieves on the sieving platform (item 3) without bending down each time. The overflow is pushed into the oversize entrance (item 4) while the undersize passes through to undersize chamber (item 5). The undersize are collected at the undersize exit (item 6) while the oversize are collected at the oversize exit (item 7). The process is repeated when the load on item 1 (the platform hopper) is exhausted.

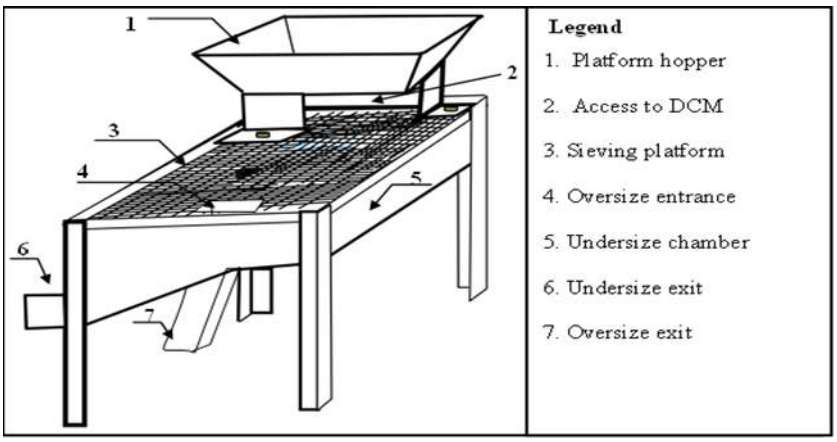

Figure 2: Operating concept of the manual sieving machine

2.1 The platform hopper

The platform hopper was made of galvanized metal formed into a trapezoidal shape welded to a square base frame and screwed onto the sieving platform.

2.12 The DCM sieving platform

The DCM sieving platform consists of a sieve made of perforated round hole of 5 mm diameter [8], welded to a frame of 25.4 mm angle iron of dimension 68 x 53 cm. A 10 mm steel rod was welded length and crosswise to the angle iron to support and prevent the sieve from the effect of compressive force during sieving process.

2.13 Platform auxiliary components

The platform auxiliary components are the part that receives the sieved DCM and transfers to exit terminals and includes the undersize collector chamber/exit compartment and the oversize entrance and exit compartment. Both compartments were made of 1 mm galvanized metal with undersize collector chamber/exit compartment tilted to 42^o angle of repose and welded to the four leg supports and covered on top by the DCM sieving platform.

2.14 The Frame Support

The frame support consists of four angle iron of length 72 cm each. It provided the base upon which the DCM sieving platform and the auxiliary compartments were welded to. The dimension for building the machine was derived from [15] and shown in Table 1.

Table 1: Recommended dimension for developing the improved DCM sieve

Machine parts to be dimensioned	Processor's parts singly or combined measured	Designed dimension (cm) Established	Dimension source
Sitting height	**Lower leg** length E	An adjustable seat of height range (35 – 50)	5th percentile men– 95th percentile women zone B
Task height h_p	**Lower leg** length + **Elbow** height sitting (E + D)	72	95th percentile E (women) + 95th percentile D (men) zone B
Machine width W_p	**Elbow to** fingertip (F)	53	95th percentile F (women) Zone C
Machine length L_p	Hip breadth J x 2	68	50th percentile Jx2, women zone B
Leg entrance h_e	E+ H	64	50th percentile E and 95th H (men) Zone C.
Collector chamber h_c	hc = D – H	16	95th percentile D (Female) zone A – 5th percentile H (male) Zone C

Source: [15]

2.2 Design Consideration

The following ergonomic design consideration was made based on the concept in Figure 2:

1. The user's back was designed to be at neutral position while performing the sieving task instead of being in the bent posture of the traditional sieving process to prevent induced stress.
2. Shoulder/arm was designed to be at neutral position, as it rest at an angle of 90^o on the sieving platform to keep the back at the neutral position.
3. The hopper was on the platform for easy access to DCM without bending at the end of each sieving cycle.

4. Coarse particle exit outlet was also at the platform for easy discharge of coarse particle without bending to discharge at the end of each sieving cycle.

2.3 Force analysis of machine members

The machine design considered two major forces namely: the force due to the weight of the DCM contained in the hopper which is assumed to act at the centre of the hopper from the right end of the machine and the force due to the sample of DCM collected each time from the hopper and the compressive and shearing force on the collected sample during sieving process which act at the centre of the machine. The machine was therefore designed against tilting of machine due to the hopper load and bending of the sieve due to both compressive and shearing force during sieving of the DCM and the reaction at the support is shown in Figure 3. The weight of the hopper 5kg and the contained mash 10kg, a total of 15kg acts 15cm from the right of the sieve platform. It is assumed that in a single cycle of sieving, 1kg of DCM is lifted and sieved on the sieving platform and act at 36 cm from the right side of the sieve platform.

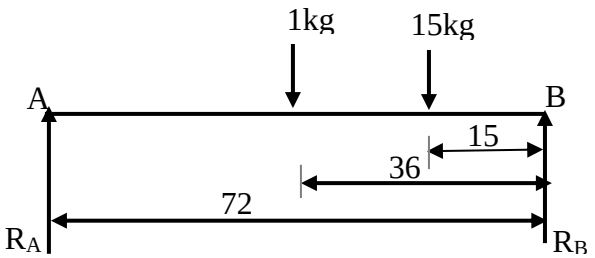

Figure 3: Force analysis of the manual sieving machine

Taking moment about A and summing forces, the reactions at the supports were calculated and shear force and bending moment drawn as shown in Figure 4.

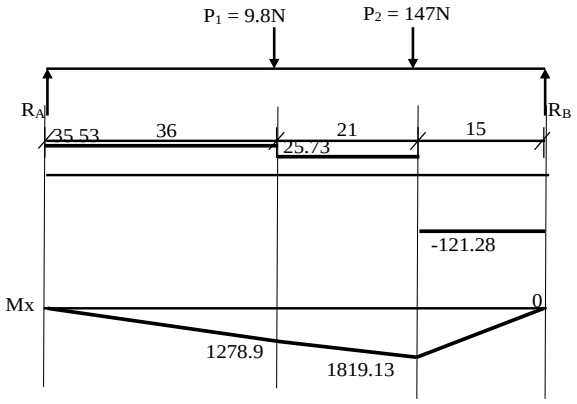

Figure 4: Shear force and bending moment diagram

2.4 Hopper design

The hopper to hold the DCM during sieving process comprised of two parts, the tapered welded to a rectangular base of total volume derived from the expression [16]:

$$V = {}^{H}/_{3}\left[\frac{(X^2Y - x^2y)}{(X-x)}\right] + xyh \qquad 1$$

Where: H = height of the tapper part,
X = length of the upper hoper

Y = width of upper hopper
χ = length of the lower part of the tapper hopper
y = width of lower part of the tapered hopper
h = height of the rectangular base

The hopper was scaled up from a sample hopper of volume 5,300 cm^3 that was occupied 1.5kg of DCM. It took an average of 2 minutes to sieve 2kg of DCM on a 5 mm perforated sieve aperture [17]. The hoper was therefore designed to hold 10 kg of DCM at a given instant, to be exhausted within 10 – 13 minutes. This time interval was to enable the processor to rise and refill the hoper as the time lapses thereby relieving or neutralizing buildup of stress on the processor during the sieving process.

2.5 Angle of repose for undersize exit chamber

The slope of the undersize exit chamber - angle of repose (θ) was established using equation:

$$\theta = \tan^{-1} 2h/D, \qquad 2$$

The angle of repose θ was obtained by filling a sample of DCM into a cylindrical and inverting the container, allowing the sample from the inverted container to fall by gravity slowly. After four replications, average height of the conical shape of the DCM measured using a metre rule was 8.50cm and the average diameter was 19 cm. Using equation 2 yielded the angle of repose of 42^o at 46% mc. The orthographic projection of the improved manual DCM machine is shown in Figure 5.

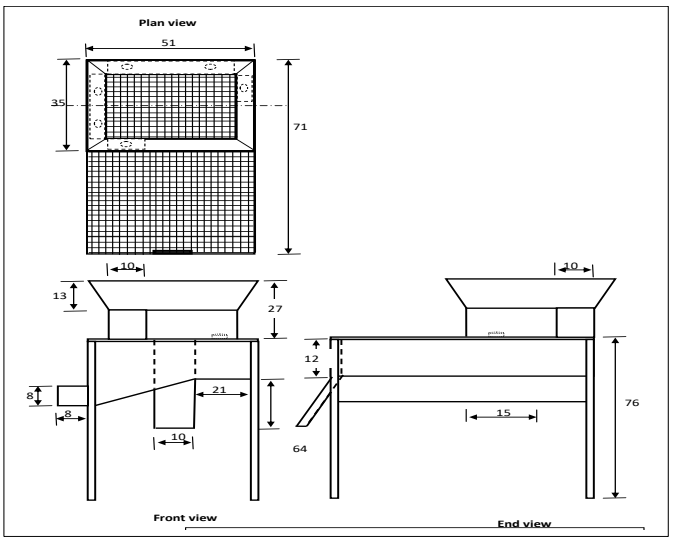

Figure 5: Orthographic projection of the improved DCM sieve

2.6 Evaluation of the improved DCM sieving machine

The improved DCM machine was evaluated with respect to change in throughput capacity and exposure to musculoskeletal discomfort when compared to the traditional sieve.

2.61 Evaluation base on throughput capacity

2kg of dewatered cassava mash was sieved on both the improved sieve and the traditional sieve and replicated 4 times. The time to completely sieve the given sample in each case was recorded

2.62 Evaluation base on musculoskeletal discomfort

Quick Exposure Checklist (QEC) was used to evaluate the developed improved DCM sieve with respect to change in Musculoskeletal Discomfort (MSD) risk (Figure 6) compared to the traditional sieve. The following three namely: Observers' (researchers'), the workers (processors') were used in the evaluation in consideration of (QEC) action level.

2.63 Observer's and processor's assessment

2.64 Observer's assessment

Under this assessment, the researcher observed 36 different processors (14 male and 22 females) carry out the task of sieving dewatered cassava mash using the improved DCM sieve as shown in Figure 6 through one complete cycle of sieving operation.

Figure 6: Evaluation of the improved DCM sieving machine

During the assessment, the researchers observed and measured the angle of deviation (^{o}) of the processors back from normal, processors back movement (number of times the back moves) in a sieving cycle, processors shoulder arm task position (mm), processors wrist arm deviation from normal (^{o}) and motion pattern per minute.

2.65 Processor's Assessment

Under this assessment, 36 different processors (14 male and 22 females) carried out the task of sieving dewatered cassava mash using the improved DCM sieve. They were each provided with 2kg of DCM and time to sieve this quantity was recorded. From this the total time spent in sieving a given quantity was recorded. The force required to carry out this sieving process was also recorded. The Overall exposure or total exposure after intervention "E_i" was computed using equation 3 given by [18]Neville et al (2005): $E_i = \frac{x}{\times_{max}} \times 100\%$ 3

Where:

E_i = Overall exposure

$\varkappa$ = actual total exposure score

X_{max} = maximum possible total exposure {X_{maxMH} = 176%for manual handling, [18](Neville et al, 2005)}

3. Results and Discussion

3.1 Result of force analysis of the sieving machine

The force analysis revealed reactions at the support R_A and R_B as 35.53N and 121.28N respectively. With the difference in reaction at the support the sieve platform will tilt to the right and on an unpaved ground, the force per unit area will be high causing the angle iron legs to bore into the ground. In a paved floor, the supports at the righthand side of the platform will be severely under stress. To overcome this, ends of the supports were braced to increase surface area and reduce the force on the floor. For this reason, the machine support was made of the different thickness with angle iron of 0.2 x 5 x 5cm at the side of high force concentration. Also the force analysis of the

sieving process through the bending moment diagram reveal that the sieve will bend or sag over time as shown in the bending moment diagram. To forestall this occurrence a 10mm steel rod was welded crosswise under the platform frame.

3.2 Results of Evaluation and Inferences

The following results were obtained after evaluation based on throughput capacity and assessment of musculoskeletal discomfort.

3.21 Result of evaluation based on throughput capacity.

Table 2 shows the throughput capacity of the improved DCM sieving machine compared to that of the traditional sieve.

Table 2: Throughput of the improved sieve compared to the traditional sieve.

Treatment on	Replications					
Sieve type/2kg	1	2	3	4	Total	Mean (kg/h)
Traditional (3mm aperture)	32	33	37	39	141	35
Improved (5 mm aperture)	54	55	64	62	235	59

From the table the use of the improved DCM sieving machine increased the throughput capacity 35 to 59kg/h.

3.3 Results of Observers assessment

Table 3 shows the result of the observers' assessment of 14 male and 22 female processors who were used to test the improved DCM sieve. The average back postures are 2.40^{o} and 2.93^{o} respectively. There was no noticeable back and forth movement, given number of back movements as 0 respectively. The sieving task was performed at a height of 72 mm which is the height of the sieving platform from the floor. The average wrist hand deviation was 1.5^{o} and 1.9^{o} respectively from normal and the average motion pattern of hand was 20.30 and 19.30 times per minutes respectively.

3.4 Results of Processor's Assessment

Table 4, shows the results of assessment of 14 male and 22 male processors selected for testing the improved sieving machine. The maximum weight handled in this test was 2kg for a sieving cycle, average time processors spent while using the sieve was 3.7hrs and 3.3hrs respectively. Response as to difficulty in keeping with the task and how stressful the task was are medium and mild respectively for both cases.

Because the back postures of both the male and female processors were at a deviation $< 20^{O}$, the back posture used in this improved DCM sieve was almost neutral and classified using QEC rating as A1. Because there was no observable back movement while using the improved DCM sieve, the back movement was considered static and classified using QEC as B2.

The processors arm was at 72 mm and above the waist height, the task therefore was performed at chest height and classified as C2. Shoulder and arm were observed to move 19 times per minute during the sieving process. The shoulder and arm movement were therefore considered to be repeated frequently, and classified as D2. The wrist/hand was at $1.6^{0} < 15^{0}$. The task was therefore performed with almost straight wrist and classified as E1. The processors move their hand an average of 19 times per minute while sieving the DCM using the improved DCM sieve. Therefore, the task was performed with similar repeated motion between 11 to 20 times per minutes and classified as F2. However, the head and neck were at $\theta < 20$. This means that head and neck was not bent excessively and classified as G1 [7, 18].

Table 3: Observers assessment

Parts assessed	Male Processors Mean	Female Processors Mean
Back posture θ)	2.40º	2.93º
Back movement (no. of times)	0	0
Shoulder arm task position(mm)	72	72
Wrist hand deviation (θ)	1.6º	1.9º
Motion pattern per minute	20.30	19.30

Table4: Processors average assessment

Parts Assessed	Male Processors Mean	Female Processors Mean
Max. weight handled (kg)	2	2
Average time spent per day (hr.)	3.7	3.3
Max force exerted (kg)	1.5	1.5
Difficult keeping with task	sometime	sometime
How stressful task is	Mildly stressful	Mildly stressful

3.5 Inference on observers' assessment of improved DCM sieve

Table 5 shows the deduction of findings of observers' assessment in table 3 with respect to quick exposure checklist (QEC) for observers' assessment.

Table 5: Inference on observer's assessment and QEC rating

Parts assessed	**Observation**	**Inference**	**QEC Rating**
Back	1) Back at $\theta < 20^0$	Back almost neutral	A1
	2) Back movement was nil	Back was static	B2
	3) Task height at 72, above waist height	Task was performed at chest height	C2
	4) Shoulder arm moved about19 times per minute	Shoulder arm movement is repeated frequently	D2
Wrist/hand	1) Wrist was at 1.6^o	Task was perform with almost straight wrist	E1
	2) Task was repeated 19 times per minute	Task is performed with similar repeated motion between 11 and 20 times per minute	F2
Head/neck	$\theta < 3^0$	Head and neck was bent not excessively	G1

3.6 Inference on processors assessment of improved DCM sieve

Table 6 shows the inference drawn from Table 4.

Table 6: Inference on worker assessment and QEC rating

Assessment	Assessment result	Inference	QEC Rating
Maximum weight handled	2kg	Maximum weight handled was light (5kg or less)	H1
Average time spent on task per day	3.7hrs	Task was performed 2 to 4hrs	J2
Maximum force level exerted by one hand	2kg	Force exerted by one hand is medium (1 to 4kg)	K2
Visual demand	Low	Almost no need to view fine details	L1
Difficult keeping with task	workers response	sometimes	P2
How stressful task is	worker response	mildly stressful	G2

The maximum weight handled in this task was 2kg, this falls below 5kg. This maximum weight is considered light and rated H1. As can be deduced from the table, average time spent on task per day is 3.7hours. From QEC, the task is performed between 2 to 4 hours and is rated J2. The maximum force level exerted by one hand is 1.5kg. From QEC this falls between 1 – 4kg and is rated K2. Visual demand was low because there was no need to view fine detail hence the rating is L1. Workers response with respect to difficulty keeping with the task was mildly and rated G2.

3.7 Ergonomic exposure scores for improved sieving method

Table 7 shows the scores of the combined rating of observers and processors assessment for the various body parts involve in DCM sieving process using the improved DCM sieve.

Table 7: Exposure score-Improve sieving machine

	Back	Shoulder/arm	Wrist/hand	Neck	Work pace	Stress
	A1H1= 2 A1J2 = 4 J2H1 = 4 B2J2 = 6 D2J2 = 6	C2H1 = 4 C2J2 = 6 J2H1 = 4 D2H1= 4 E1J2 = 4	F2K2 = 6 F2J2 = 6 J2K2 = 6 E1K2 =4	G1J2 = 4 L1J2 = 4	P2= 4	Q2= 4
Total	16	24	26	8	4	4

The total back score is 16, should/arm 24, wrist/hand 26, neck 8, workspace 4 and stress 4 given a total exposure score of 82. Figure 7 shows a comparison of levels of exposure of processors to sieving discomfort while using the traditional and the improved sieve.

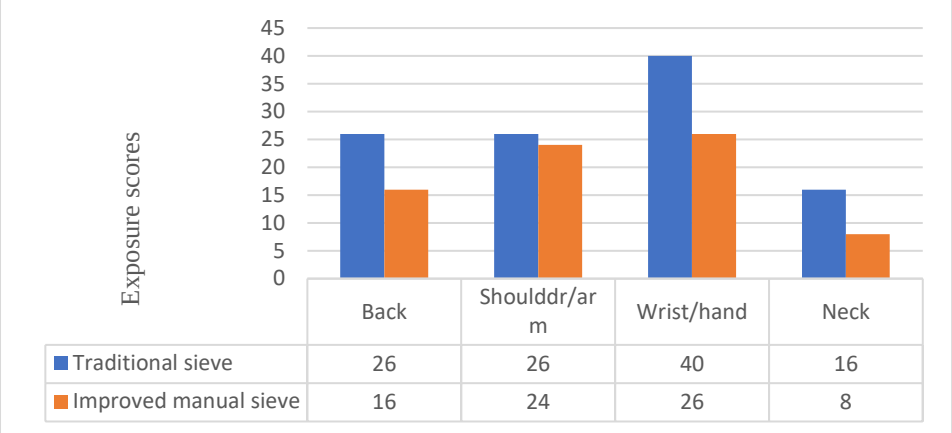

Figure7: Comparison of levels of exposure to sieving discomfort using traditional and improved sieve

From the scores, the total exposure "E" for processors using the improved DCM is computed as 47%, which is a reduction compared to 66% level of exposure obtained when using the traditional sieve [7].

Figure 7: Completed improved manual DCM sieving device after evaluation

4. Conclusion

Traditional dewatered cassava mash sieving device was improved, this was made possible by consideration of ergonomic factors and the anthropometry of the user groups. The resulting dimensions improved the siting and sieving posture of the processors thereby reducing musculoskelectal discomfort during sieving process and by encoporating a modified sieve size there was an increase in throughput capacity. Encouraging cassava farmers and processors to adapt to this innovation is an approach toward achieving systematic change in sustainable development and ecologically smart future.

References

[1] A.A Ahiakwo., C.B. Isirimah and D.G Inimgba (2015). Appraisal and projection of dewatered cassava mash sieving technology. Net journal of agricultural science, Vol.3(2), pp55- 59.

[2] **R.** Debbie., F. Graham and O. John (2012). Crop Post-Harvest: Science and Technology, John wily and sons Publishers Ltd. West Sussex, UK.

[3] F.S. James (2012). Screening Theory and Practice Triple/S Dynamics, In. pp1-7, 12-20

[4] C. A. Onyenwoke, and K. J. Simonyan (2014). Cassava post-harvest processing and storage in Nigeria: A review. African journal of agric. research, Vol.9(53), pp3853-3863.

[5] K. A. Thomas and O. N. Philips (2015). Assessment of food safety practices among cassava processors in selected rural communities of Oyo State, Nigeria. Afr. J. of food, agric., Nutri and Develp. Vol15(4), pp112-117.

[6] O. L. Peter., A. Leo., O. A. Simeon (2010). Sustaining world food security with improved cassava processing technology: , available Online at www.mdpi.com/journal/sustainability , accessed on 4 July 2021.

[7] A. A. Ahiakwo., K. J. Simonyan. and A. B Eke (2019). Assessment of workers' level of exposure to work-related musculoskeletal discomfort in dewatered cassava mash sieving process, Arid Zone J. of Engrg, Tech. and Environment (AZOJETE), Vol 15(3), pp 648 – 661.

.[8] T. M. Samue., O. O. Aremu., I. O. Salami., B. O. Adetifa and L. I. Onu (2016). Anthropometric studies for designing to fit Gari-frying Workers. Agric. Engrg International CIGR Journal, Vol.18(1), pp180-191

[9] O. A. Bukola., O. D. A. Akinfoye and O. J. Olufemi (2015). Comparative assessment of two methods in the production of fermented cassava flour (láfún) on manual energy expended, Intl. J.of Agric. Sc.. Vol. 4(9), pp 628-641

[10] M. McNeill (2005). Ergonomics in post-harvest agro-processing, Afr. Newsletter on occupnal Health , Vol.15(7), pp11–13.

[11] B. S. Ogunsina., L. A. Sanni and C. Oladigbo (2008). Development of a rotary pulverizer for cassava cake in garri production. J. of Food Process Engineering, Vol.13(8), pp 783–797.

[12] W. B. Asiru., J. C. Igbeka. and T. M. A. Olayanju., (2010). Energy expenditure in garri processing activities by Nigerian Women, Journal of Natural Sciences, Engineering and Technology,Vol.9(2), pp149-157

[13] R. M. Davies., M.O. Olatunji and Burubai, W (2008). A Survey of cassava processing machinery in Oyo State. Intl. J. of Agricultural Sciences, Vol.4(3), pp 337 – 340.

[14] T. A. Adekanye., S. I. Ogunjimi and O. A. Ajala (2013). An assessment of cassava processing plants in Irepodun local govern area of Kwara State, Nigeria. World J. of agric. research Vol. 1 (1), pp 14-17.

[15] A. A. Ahiakwo., J. Osere and N. J. Chijioke-Eke, N. J. (2021). Determination of anthropometry of processors for designing ergonomically improved dewatered cassava mash sieving machine. Global J. of Engrg. and Tech. advances, Vol.6(1), pp015 – 025.

[16] V. Taylor (2018). How to calculate the volume of a Tapered Hopper. Available Online at: www.hunker.com/ 13425784/how-to-calculate-the-of-a-tapered-hopper. Accessed on December 9, 2021.

[17] A. A. Ahiakwo,, K. J. Simonyan. and A. B. Eke (2019). Effects of sieve aperture modification on dewatered cassava mash sieving process, Nig. J. of Technology. (NIJOTECH), Vol.38 (2), pp512 – 519.

[18] S. Neville., H. Alan., B. Karel, S. Eduardo and H. Hal (2005). Quick exposure checklist (QEC) for the assessment of workplace risks for work related musculoskeletal disorders (WMSDs). In: Handbook of Human Factors and ergonomics methods. CRC Press New York, Washington, D.C.

NIPES Conference Proceedings
The 1st International Conference of the Nigerian Institution of Professional Engineers and Scientists 7th-8th Oct. 2021: 270-279
www.nipesjournals.org.ng

Suitability Assessment for Genetic Algorithm Optimal Wireless Sensor Node Network Deployment in the University of Benin Using Geographic Information System

Okosun. O[1] and Omoifo O. I [2]
[1,2]Department of Computer Engineering, Faculty of Engineering, University of Benin, Benin City
Corresponding Author: Email: oduware.aghama@uniben.edu
+2348065771616, 08056820122

Abstract

The paper compares a genetically optimized node deployment scheme for a ZigBee wireless sensor network with Geographical Information System for a tropical environment. The development of a model for maximum connectivity and full area coverage with parameters such as isolated nodes and minimum islands. Optimal positions of the sensor nodes were achieved using a heuristic tool Genetic Algorithm (GA) that operates on encoding of the decision variables with the Genetic Algorithm optimization tool set. Global Positioning System (GPS) coordinates of positions within the work area were taken and positions of the sensor nodes were achieved using Graphical Information System (GIS) tool to determine possible influences of the University of Benin tropical environment to the node deployment scheme.

Keywords: Zigbee, Genetic Algorithm (GA), Coverage, Connectivity, sensor network, Graphical Information system (GIS)

1. Introduction

Advancements in sensing electronic technology have attracted tremendous research over the years in networks such as Wireless Sensor Network (WSN) [3]. Coverage and connectivity are two most fundamental issues of wireless sensor network. Coverage can be treated as a measure of quality of service in a sensor network which shows how well each point in a region is covered and the accuracy of the information gathered by the nodes [4]. Connectivity shows how well a sensor device communicates with other devices. Hence, coverage and connectivity design issues are non-trivial problems taken into consideration in order to ensure an efficient security network for Wireless Sensors [7]. Genetic Algorithm (GA) which is one of the most powerful heuristics for solving optimization problems based on natural selection was adopted because it mimics biological evolution and does not require derivative information. Only the objective function and the corresponding fitness levels influence the directions of its search. The Genetic Algorithm process leads to the evolution of populations of nodes that are better suited to their environments [6]. Okosun and Omoifo in 2019 proposed a full area coverage and connectivity model using closed form solutions that showed unique characteristics of a Toeplitz matrix for node placement to achieve coverage and adjacency matrix for connectivity. The characteristics of a good wireless sensor network include power efficiency, scalability, responsiveness, reliability and mobility. A wireless sensor network with these features can prove to be very beneficial and if not followed or ensured can result in a network that suffers from overhead thus negating its applicability [15].Ren in (2013) designed a ZigBee Network model with reliable communication in order to get the model he built two zigbee test beds, one with a gateway and the other without a gateway to test whether the network model based on gateway has function to enhance the reliability of Zigbee network. The result showed that weather has a big effect on the stability of network, and gateway can enhance the reliability of data communication but it will add cost to the network. But the test beds were not specific to a geotropic region. The geographical topology of the system where sensors are placed is essential to planning of

educated deployments of sensor networks for infrastructural security and the database for the geographical topology continues to increase with increase in new applications.

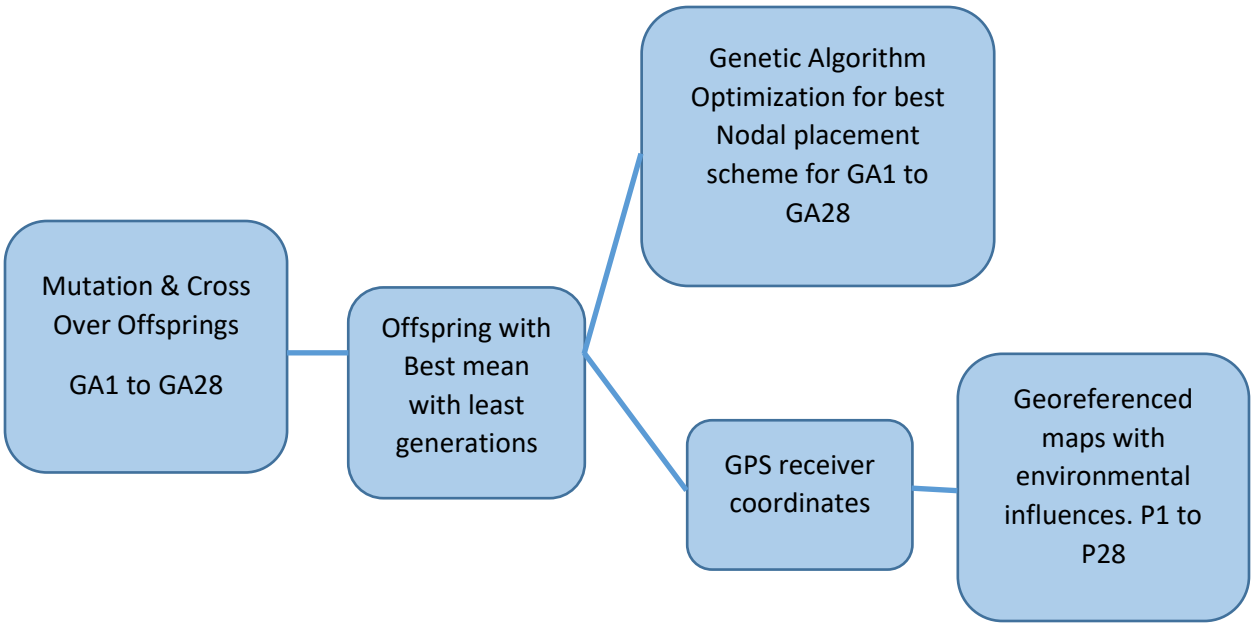

Figure 1: Figure 1: Optimization Methodology Flow Process Chart

2. Materials and Method

A point is covered by a sensor if the Euclidean distance between the point and the sensor is no more than the sensing range 'rs' according to the disk/Boolean sensing model by [7]. A measurement campaign for determining the communication distance between two ZigBee modules was carried out by [9] within the department of Computer Engineering, University of Benin. An effective communication distance of 22.86 meters approximately 23 meters ranked best with the acceptable packet error rate of two-bit errors and eighty -seven percent performance rating.

2.1. Unoptimized System

The standard unoptimized system is a grid framework which completely covers the entire work area. A work area of 500m by 500m within the region of interest is measured. Intersection within the grid is separated by the communicating distance of 23 meters [9] and it resulted to a 22 row × 22 column. A deterministic placement approach was adopted while positioning nodes at every intersection of the grid framework to exert control of the system and avoid clustering. Having control of the system enables the optimization parameters meet desired performance goals through careful planning with the least number of nodes to ensure connectivity, coverage and yield uniform node density with reduced cost.

2.2. The Objective fitness function

To minimize redundancy of devices in setting up of a network within a region of interest, the objective fitness function in Equation one (1) subject to the coverage and connectivity models by [10] is adopted.

$$f = \min \sum_{i=1}^{t} p_i \quad (1)$$
$$subject\ to: Z \times p \geq b$$

$$(B + I)^d = M$$

Where $'p_i'$ is the optimization parameter. Genetic algorithm is used to solve the minimization problem.

A population of node is fed to the MatLab software and the global minimum of GA1 to GA28 Mutation & Cross Over Offspring nodes positioning scheme is generated. A Global Positioning System receiver is used to determine coordinates of various points within the region of interest for offspring with best mean. These coordinates are fed into a Geographical Information System for the evaluation of the node positions of best mean Mutation & Cross Over Offspring nodes coordinates generated. A three dimension view of the landform surface is carried out on the region of interest terrain for more informed decision and planning of the node deploymment scheme.

2.3. GA Best Offsprings

Table A1 in Appendix A shows the various combinations of offspring, which the optimization tool box is applied to generate the desired node schemes. The Optim tool box 7.2 is setup with the following optimization parameters. Solver:- GA-Genetic Algorithm, Fitness Function:- Optimization Parameter 'P', Number of Variables:- total number of nodes in the region of interest (*t*), Bounds:-Upper Bound 1, -Lower Bound 0, Non Linear Constraint function:- coverage model and connectivity model, Integer Variable Indices:- was selected to make integers constrained in the range within the bounds, Population type:- Double vector was selected because it is required when there are integer constraints and a Population size of 50 was selected.

2.4. Measurement of GPS coordinates

Coordinates of various positions within the region of interest measured with the Garmin-eTrex-10 hand held device is shown in Table 1.

Coordinates gotten from the region of interest is used to generate high resolution satellite imagery of 16 January, 2016 which was downloaded from Google Earth Desktop application, exported into Arc GIS 10.1 environment and georeferenced using Latitude Longitude Geographic coordinate (1984 World Geodetic System (WGS)). Shape files representing roads, buildings, tree canopies and nodes were created in Arc Catalog. On-screen digitizing is deployed to digitize roads, buildings and tree canopies from the georeferenced high-resolution satellite imagery and nodes. Create spatially balanced random point algorithm is also used to create four sets of 284 random points each representing the network nodes generated from the four simulations and equally spaced at 23meters (75feets) apart. Attribute database was created from the nodal layer. However, to ascertain nodes with/or without possible interference with land use/environmental factors, the nodes were overlaid with building and trees canopy layers (representing land use/environmental factors). The symbology algorithm is deployed to reclassify the four sets each of the 284 nodes that fall within buildings and tree canopies. Similarly, contours are lines joining places of equal height (elevation). The procedure deployed in creating the relief and contours commenced by building a database using 284 spatially spread nodal point layer. The 284 spatially spread nodal

point layer is used in extracting elevation values from a 30 X 30 meters resolution United States Geological Surveys (USGS) digital elevation model (DEM). DEM is a grid dataset containing elevation information and very useful in relief mapping. Inverse distance weighting (IDW) algorithm was used to interpolate the point layer and the output reclassified to form the shaded relief classes. An Interpolated grid file is used to extract contour lines

using contour extraction algorithm. The contour, spaced at 1meters apart is overlaid with shaded relief and road network, nodes, building and trees canopy layers in Arc Map 10.1 software

Table 1:Coordinates of Positions within the Region of Interest

S/ No	Names of Positions within Faculty of Engineering	Latitude	Longitude	Elevation (meters)
1	Tree 1 by field	6.40272^{O} N	5.61499^{O} E	112
2	Electrical Engineering LT Building Edge	6.40288^{O} N	5.61503^{O} E	111
3	DO4 Building by Field	6.40276^{O} N	5.61539^{O} E	117
4	Computer Engineering Walkway	6.4025 ^{O} N	5.61533^{O} E	110
5	Electrical Engineering Car Park Midpoint	6.40281^{O} N	5.6147 ^{O} E	112
6	Electrical Engineering Building Edge/Car Park	6.40309^{O} N	5.61442^{O} E	114
7	Electrical Engineering Car Park Edge	6.40292^{O} N	5.61434^{O} E	113
8	Electrical Engineering Car Park Corner	6.40275^{O} N	5.61428^{O} E	112
9	Electrical Engineering Tree 2 by Car Park	6.40271^{O} N	5.6144 ^{O} E	113
10	Electrical Engineering Tree 3 by Car Park	6.40263^{O} N	5.6147 ^{O} E	114

3. Results

Result of the GA2, GA8, GA9, GA12 optimization process shows crossover and mutation offspring with best means of 284 nodes which converges at the 57th , 56th , 62nd ,and 57th generation respectively.

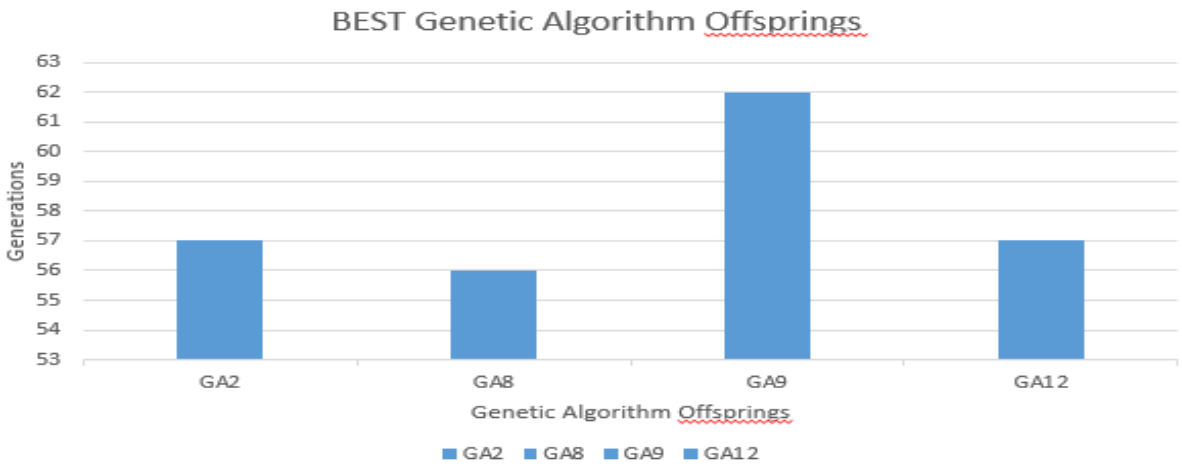

Figure 2: Genetic Algorithm best Offsprings

3.1. Optimal Node Positioning Schemes

The deployment of 284 nodes on the grid is shown in Figures 3,4, 5 and Figure 6 as ‘‘GA12’’ ‘‘GA9’’, ‘‘GA8’’ and ‘‘GA2’’ respectively.

3.2. Georeferenced Map for GA2

GA OFFSPRINGS	NODE DEPLOYMENT SCHEMES
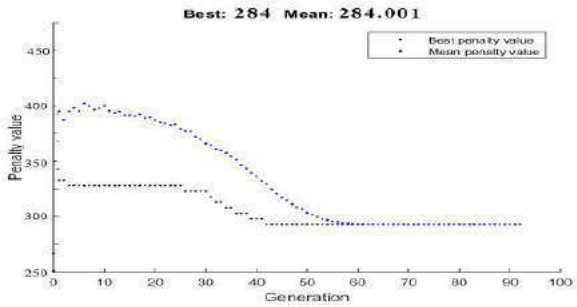 Figure 3:GA 12 = Single Point Crossover function with Adaptive Feasible Mutation function	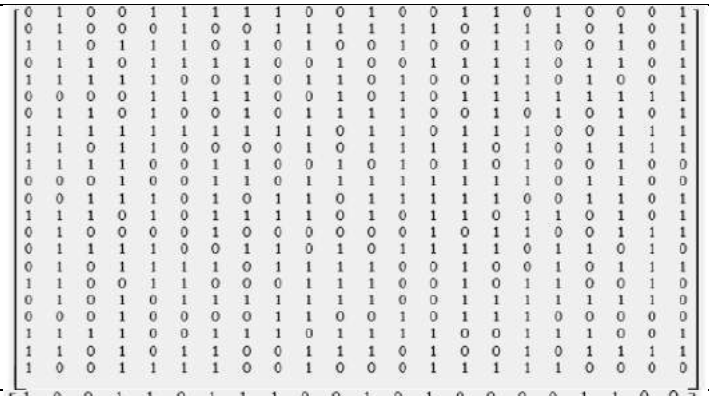
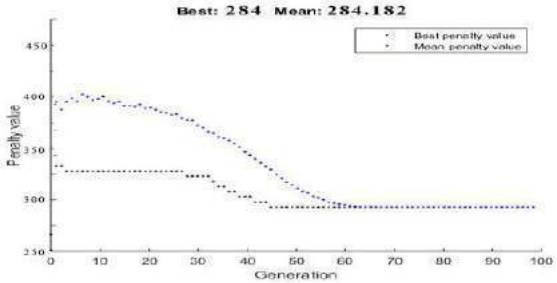 Figure 4:GA 9 = Single Point Crossover function with Constraint Dependent Mutation function	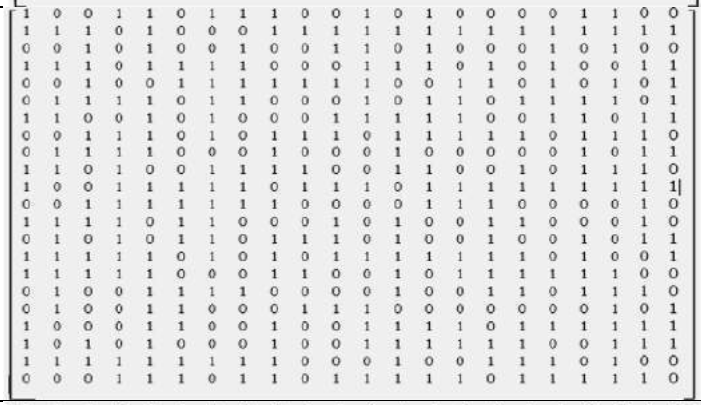
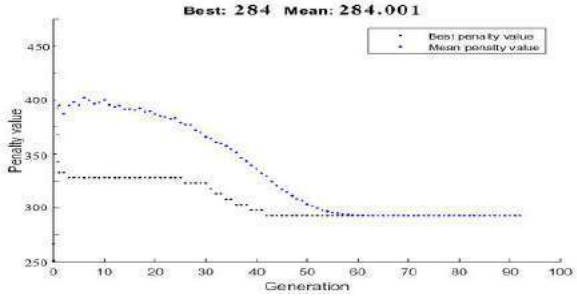 Figure 5:GA 8 = Scattered Crossover function with Adaptive Feasible Mutation function	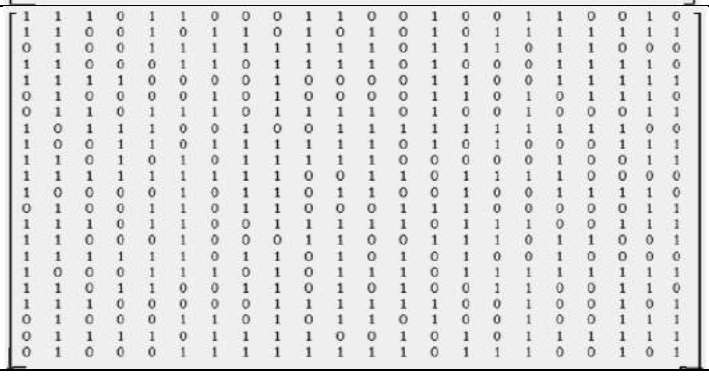

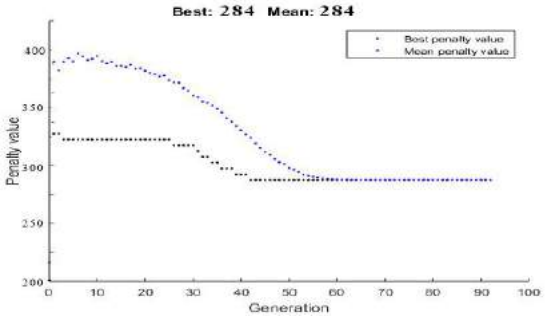

Figure 6:GA 2 = Constraint Dependent Crossover function with Gaussian Mutation function

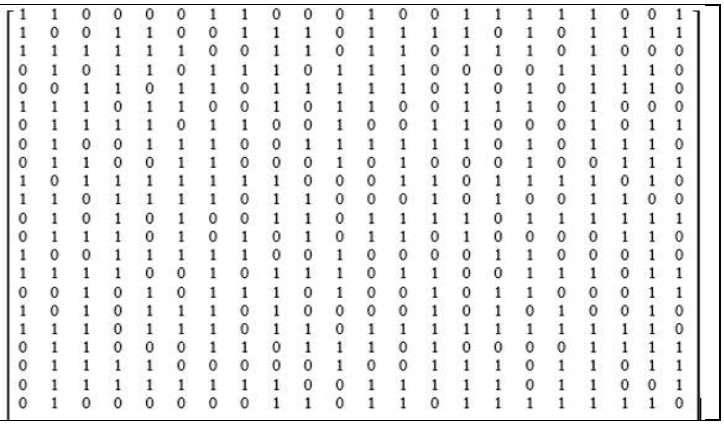

The Figure 7 show a georeferenced map P2 for GA2 which has 222 nodes without any influence, 37 Nodes likely to be influenced by buildings and 25 Nodes likely to be influenced by trees canopy. The outcome for the Average Nearest Neighbor Analysis of GA2 georeferenced nodes is shown in Table 3 and the data set of the elevation information is shown in Table 4, for the georeferenced map P2 generated from the Arc GIS 10.1 tool.

A Nearest Neighbor Ratio of 1.590481 and a p-value of 0 from the table is within the 0.01>2.58 critical value and this indicates that there is less than 1% likelihood that the dispersed pattern could be the result of random chance.

3.3. Georeferenced Map for GA8

The Figure 8 show a georeferenced map for P8 which has 218 nodes without any influence, 34 Nodes likely to be influenced by buildings and 32 Nodes likely to be influenced by trees canopy. The outcome for the Average Nearest Neighbor Analysis of GA8 georeferenced nodes is shown in Table 5 and the data set of the elevation information is shown in Table 6, for the georeferenced map P8 generated from the Arc GIS 10.1 tool.

A Nearest Neighbor Ratio of 1.589546 and a p-value of 0 from the table is within the 0.01>2.58 critical value and this indicates that there is less than 1% likelihood that the dispersed pattern could be the result of random chance.

3.4. Georeferenced Map for GA9

The Figure 9 show a georeferenced map P9 for GA9 which has 217 nodes without any influence, 37 Nodes likely

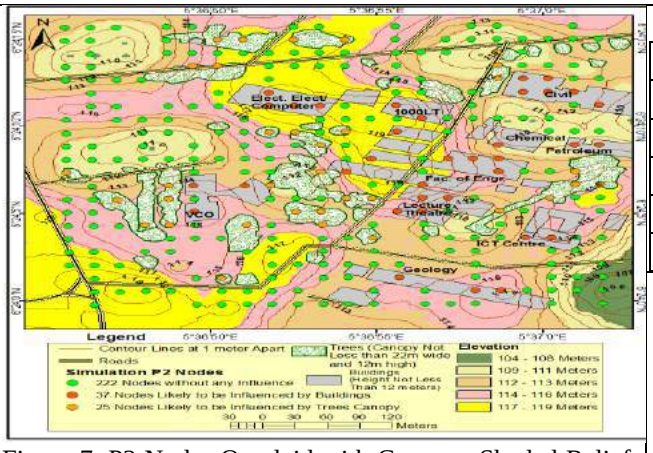

Figure 7: P2 Nodes Overlaid with Contour, Shaded Relief and Land Use

Table 3: Average Nearest Neighbor Summary for P2	
Observed Mean Distance:	23.225277 Meters
Expected Mean Distance:	14.602677 Meters
Nearest Neighbor Ratio:	1.590481
z-score:	19.036883
p-value:	0.000000

Table 4: Data Set Information	
Input Feature Class:	Nodal_Points_SimulationP2
Distance Method:	EUCLIDEAN
Study Area:	242238.559375
Selection Set:	False

to be influenced by buildings and 29 Nodes likely to be influenced by trees canopy. The outcome for the Average

Nearest Neighbor Analysis of GA9 georeferenced nodes is shown in Table 7 and the data set of the elevation information is shown in Table 8, for the georeferenced map P9 generated from the Arc GIS 10.1 tool.

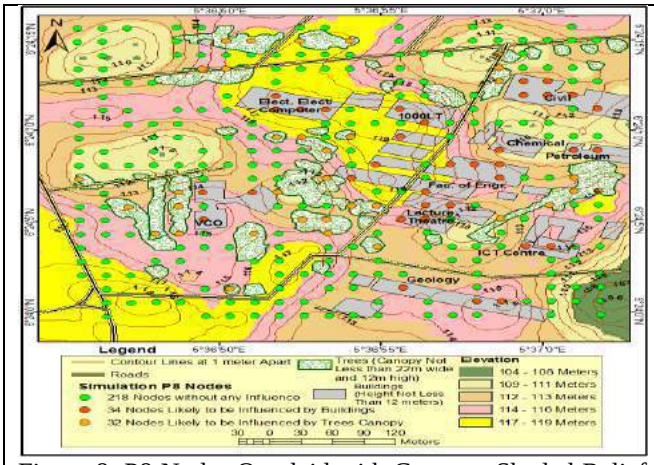

Figure 8: P8 Nodes Overlaid with Contour, Shaded Relief and Land Use

Table 5: Average Nearest Neighbor Summary for P8	
Observed Mean Distance:	23.216494 Meters
Expected Mean Distance:	14.605743 Meters
Nearest Neighbor Ratio:	1.589546
z-score:	19.006732
p-value:	0.000000

Table 6: Data Set Information for P8	
Input Feature Class:	Nodal_Points_SimulationP8
Distance Method:	EUCLIDEAN
Study Area:	242340.291828
Selection Set:	False

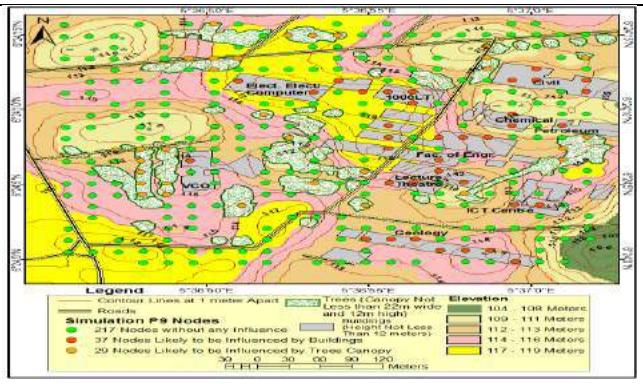

Figure 9: P9 Nodes Overlaid with Contour, Shaded Relief and Land Use

Table 7: Average Nearest Neighbor Summary for P9	
Observed Mean Distance:	23.261753 Meters
Expected Mean Distance:	14.629063 Meters
Nearest Neighbor Ratio:	1.590105
z-score:	18.991257
p-value:	0.000000

Table 8: Data Set Information for P9	
Input Feature Class:	Nodal_Points_SimulationP8
Distance Method:	EUCLIDEAN
Study Area:	242258.740103
Selection Set:	False

A Nearest Neighbor Ratio of 1.590105 and a p-value of 0 from the table is within the 0.01>2.58 critical value and this indicates that there is less than 1% likelihood that the dispersed pattern could be the result of random chance.

3.5. Georeferenced Map for GA12

The Figure 10 show a georeferenced map for P8 which has 212 nodes without any influence, 38 Nodes likely to be influenced by buildings and 34 Nodes likely to be influenced by trees canopy. The outcome for the Average Nearest Neighbor Analysis of GA12 georeferenced nodes is shown in Table 9 and the data set of the elevation information is shown in Table 10, for the georeferenced map P12 generated from the Arc GIS 10.1 tool.

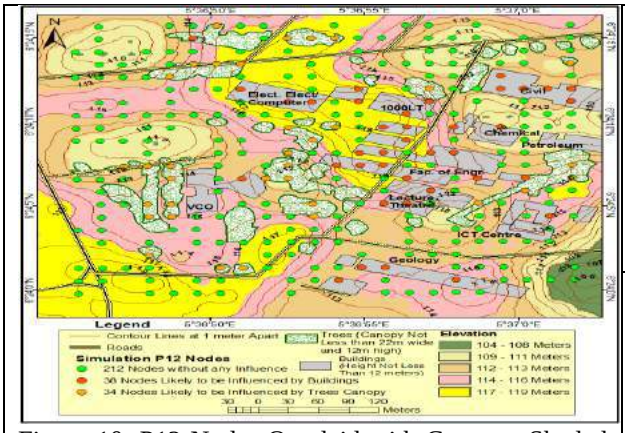

Figure 10: P12 Nodes Overlaid with Contour, Shaded Relief and Land Use

Table 9: Average Nearest Neighbor Summary for P12	
Observed Mean Distance:	23.229675 Meters
Expected Mean Distance:	14.598354 Meters
Nearest Neighbor Ratio:	1.591253
z-score:	19.061778
p-value:	0.000000

Table 10: Data Set Information for P12	
Input Feature Class:	Nodal_Points_SimulationP8
Distance Method:	EUCLIDEAN
Study Area:	242095.160384
Selection Set:	False

A Nearest Neighbor Ratio of 1.591253 and a p-value of 0 from the table 5.20 is within the 0.01>2.58 critical value and this indicates that there is less than 1% likelihood that the dispersed pattern could be the result of random chance.

3.6. Discussion

This research work has shown that the application of the coverage model and connectivity model in GA node placement can lead to the proper positioning of nodes with minimal geological influences. In order to appreciate the implemented model in theory, the optimization results and the theoretical predictions are evaluated in Table 1.

Table 11: Implemented model versus the GIS theoretical Predictions

Optimization Results (nodes)	**GIS Theoretical Predictions (nodes)**	**Error Rate Of Implemented Deployment**	**Percentage Rating (100%)**
(GA)	**Georeferenced map (P)**		
GA2	**P2**		
284	222	0.2183	21%
GA8	**P8**		
284	218	0.2323	23%

GA9	**P9**		
284	217	0.2359	23%
GA12	**P12**		
284	212	0.2535	25%

The comparism between the georeferenced results from ARC GIS maps and the theoretical implementation from the GA optimization show that P2 node positioning scheme is most suitable for deployment within the university of Benin area due to its larger number of 222 nodes without any influence at a 0.2183 percentage of error rate.

5. Conclusion

GA-generated designs with the coverage model and connectivity model as optimization constraints compared favorably to GIS theoretical deterministic designs for positioning of nodes dispersedly. A Nearest Neighbor Ratio within the 0.01>2.58 critical value and a p-value of zero (0) indicates that there is less than 1% likelihood that the dispersed pattern could be the result of random chance. This implies that the coverage-connectivity algorithm for this research deployed nodes intelligently (deterministically).

References

[1] Abidin, H. Z. (2013). "Deterministic Static Sensor Node Placement in WSN based on territorial predator scent marking behaviour". *International Journal of Communication Networks and Information Security*, 186-191.

[2] Alliance. (2003). *"Using Smart Card for Secure Physical Access".* New Jersey: Smart Card Alliance.

[3] Bhondekar, A. P. (2009). "Genetic Algorithm Based Node Placement Methodology For Wireless Sensor Networks". *International Multiconference of Engineers and Computer Scientists*, (pp. 18-20). Hong Kong.

[4] Chaudhary, N. (2015). "A Survey on Coverage Problem in Wireless Sensor Network". *Journal of Engineering and Computer science*, 11952-11955.

[5] Duncan, A. (2004). "Powers of Adjacency matrix and the walk matrix". *Oar//handle/123456789/24439*, pp. 1-8.

[6] Dunning, T. (2008). "Recorded Step Directional Mutation for Faster Convergence". *https://www.researchate.net*, DOI: 10.1007/BFb0040808.

[7] Gosh, A., & Sajal, k. (2008). "Coverage and connectivity issues in wireless sensor networks". *Pervasive and Mobile Computing 4*, 303–334.

[8] krohn, A., B, M., D, C., & R, T. (2006). Increasing Connectivity in Wireless Sensor Network Using Cooperative Transmission. *The 3rd International Conference on Networked Sensing Systems(INSS)*, 31.

[9] Okosun, O., & Edeoghon, I. (2020, July). Design and Construction of a Wireless Fingerprint Attendance management System Based on ZigBee Technology. *Journal of Civil and Environmental Systems Engineering, 18*(1).

[10] Okosun, O., & Omoifo, O. (2019). ‘‘Genetic Algorithm Based Minimal Node Placement For Full Coverage In A Wireless Sensor Network. *Journal of the Nigerian Association of Mathematical Physics*, 177-120.

[11] Penrose. (1997, june). "The longest edge of the random minimal spanning tree". *The Annals of Applied Probability*, 340–361.

[12] Ren, Y. (2013). "The Zigbee network model with reliable communication". *2nd International Conference on Next Generation Computer and Information Technology* (pp. 25-30). china: SERSC.

[13] Tamminen, J., Lee, K.-C., & Piche, R. (2013). Graph. In K. Ruohonen, *Graph Theory* (p. 1). columbia.

[14] vaishyampayan J., T. K. (2017). A Review of Node Deployment Techniques in Wireless Sensor Networ. *International Research Journal of Engineering and Technology*, 2395-0072.

[15] YongMin, L., ShuCi, W., & Xiao, N. (2009). "The Architecture and Characteristics of Wireless Sensor Network". *IEEE International Conference on Computer Technology and Development (ICCTD)* (pp. 561-565). DOI: 10.1109ICCTD.2009.44.

APPENDIX A

Table A1: Combinations of Crossover and mutation function Offspring

Genetic Algorithm optimization	**Genetic Algorithm Methodologies**
GA1	Constraint Dependent Crossover function with Constraint Dependent Mutation function
GA2	Constraint Dependent Crossover function with Gaussian Mutation function
GA3	Constraint Dependent Crossover function with uniform Mutation function
GA4	Constraint Dependent Crossover function with Adaptive Feasible Mutation function
GA5	Scattered Crossover function with Constraint Dependent Mutation function
GA6	Scattered Crossover function with Gaussian Mutation function
GA7	Scattered Cross Over function with Uniform Mutation function
GA8	Scattered Crossover function with Adaptive Feasible Mutation function
GA9	Single Point Crossover function with Constraint Dependent Mutation function
GA10	Single Point Crossover function with Gaussian Mutation function
GA11	Single Point Crossover function with Uniform Mutation function
GA12	Single Point Crossover function with Adaptive Feasible Mutation function
GA13	Two Point Crossover function with Constraint Dependent Mutation function
GA14	Two Point Crossover function with Gaussian Mutation function
GA15	Two Point Crossover function with Uniform Mutation function
GA16	Two Point Crossover function with Adaptive Feasible Mutation function
GA17	Intermediate Crossover function with Constraint Dependent Mutation function
GA18	Intermediate Crossover function with Gaussian Mutation function
GA19	Intermediate Crossover function with Uniform Mutation function
GA20	Intermediate Crossover function with Adaptive Feasible Mutation function
GA21	Heuristic Crossover function with Constraint Dependent Mutation function
GA22	Heuristic Crossover function with Gaussian Mutation function
GA23	Heuristic Crossover function with Uniform Mutation function
GA24	Heuristic Crossover function with Adaptive Feasible Mutation function
GA25	Arithmetic Crossover function with Constraint Dependent Mutation function
GA26	Arithmetic Crossover function with Gaussian Mutation function
GA27	Arithmetic Crossover function with Uniform Mutation function
GA28	Arithmetic Crossover function with Adaptive Feasible Mutation function

NIPES Conference Proceedings
The 1st International Conference of the Nigerian Institution of Professional Engineers and Scientists 7th-8th Oct. 2021: 280-295
www.nipesjournals.org.ng

Development and Reliability of a Smart Door

Osaretin Osaro* and Sufianu A. Aliu
Department of Mechanical Engineering, University of Benin, Benin City, Nigeria.
*Email:sufianu.aliu@uniben.edu, osaroretin43@gmail.com

Abstract
An automatic suspended sliding door was designed and fabricated using materials sourced locally. Also, reliability analysis and availability analysis were carried out on the smart door. Most of the challenges associated with manually operated doors can be solved through the use of an automatic door. The automatic sliding door was tested after fabrication. The system was certified to have functioned properly as desired. The design values of the parameters were compared with the actual values measured from the system while in operation. The percentage deviation of the actual values from the design values of the parameters such as the door opening time, the door delay time, the door maximum velocity, the door minimum velocity, and the total time taken for the door to complete one operational cycle are 7.69%, 3.15%, 3.53%, 14.89%, and 6.51% respectively. The deviations of the actual values from the design values are negligible. Also, from reliability analysis and availability analysis, it shows that the system is 94.3% reliable and 99.17% available. Therefore, the design and fabrication, availability analysis and the reliability analysis of a functional smart door was successfully executed.
***Keywords*:** *Sliding door, automation, design, fabrication, reliability analysis and availability analysis*

1.0 Introduction

This work puts forward a smart door system that works with a passive infrared sensor based on human movement near the door. It contains the design and fabrication, availability analysis, reliability analysis, and the functionality of a smart door. This smart door can also be referred as a self-opening and closing door. A self-opening and closing door is an intelligent door which opens on its own by sensing or detecting the presence of a living being approaching the door and closes after a predetermined time-delay if there is no person within its range. This functionality will be achieved through the use of PIR sensors. PIR sensor means passive infrared sensors. PIR sensor is a motion detector which sense the presence of somebody through the heat energy emitted by the person approaching the door. Since humans emit energy in the form of infrared radiation, the PIR sensor detects the presence of a living being within the sensor's range and sends out a command or signal to a microcontroller which controls an electric bidirectional motor which in turn actuates the movement of the door. The door then automatically closes when a specific time-delay has elapsed and if there is no motion near the door. This door can also be called an automatic door or intelligent door. The automatic door is an electro-mechanical door [1]. Intelligent doors are doors whose components and elements communicate to each other and work in conjunction to perform a predetermined function. Intelligent doors use smart lock.

Fast and efficient movement of persons, goods and services are needed in modern days' work schedules. Doors are placed between these schedules and it plays an important role in making the work environment conducive. Any obstruction to effective movement is detrimental to the efficiency of the organization or industry and must be removed. The conventional manual door may be a barrier to effective movement [2]. Overtime, it has been a challenge for people living with disabilities to use the door without the help of someone. For persons in wheelchairs and other disabled persons, automatic doors are an immense boon, since conventional doors can be very difficult to work with [3, 4].

The use of manual doors in some places such as shopping malls, banks, hospitals, scientific laboratories and other traffic characterized firms, poses some challenges. These challenges ranges from the risk of cross-contamination due to door-to-human contact, loss of man-hour (or reduction in speed at work) due to the time spent at doorpost, difficulties encountered by physically challenged

persons at the doorpost, extra cost for hiring persons whose duty is to open door for clients. All these challenges can be overcome through the use of a smart door. This door is also designed to be sensitive to obstacles on the doorway. This is to ensure that the door doesn't close on somebody which happens to be on the path of the doorway The safety of the automatic door is enhanced by this safety measure [5].

2.0 Methodology

This entails design considerations, material selection, design process and fabrication processes.

2.1 Design Considerations

When there is nonexistence of friction between a machine and the people at the point of contact (That is, if the people are made more comfortable, safer, and more efficient when using the machine), then the designer can be said to have been succeeded [5]. As a result, several considerations need to be made in the design of a system. Some of these considerations are sustainability, reliability, corrosion resistance, low cost, simplicity, high efficiency, maintainability, and producible with locally available materials.
The operational requirements are; the door should always open when a person or persons moves towards the door and also close after a predetermined time, must be noise free during operation and must be able to work properly in all atmospheric conditions. The functional requirements are the design should provide a safe means of access, should be capable of providing an airtight environment, should provide privacy, and the material of door should have a good thermal resistance.

2.2 Materials

With regards to the various requirements, reliable materials were selected for each component. These components and the materials selected are:

1. **Chain drive:** A chain drive is a mechanical drive system that is used to transmit mechanical power or motion from one shaft to another. It consists of a chain wrapped round two sprockets. A chain is a series of links connected by pin joints [6]. The material selected for the roller chain and sprockets is alloy steel. The sprockets are tempered and case hardened at the tooth area in order to increase or enhance the wear resistance of the material. Alloy steel was selected as the material both for the chain and sprockets on the standpoint of wear resistance and strength.
2. **Roller bearings**: The bearing is a machine element which support another moving machine element. It allows relative motion between the contact surfaces of the members, while carrying the load. [7]. The material of the rollers selected is cast nylon. Cast nylon was selected because of its advantages which include: low rolling resistance, it generates low or no noise when in operation, and its ability to absorb shock and vibration.
3. **Door panel:** Glass door panel was selected because it is an excellent insulator, resistance to most chemicals, light in weight, attractive appearance, and high compressive strength ($1000N/mm^2$).
4. **Door frame and the structure:** The structure contains the door frame and other supports for the components of the system. The material selected for the structure and the frame is medium carbon steel because of its high mechanical strength, ductility, and its relative low cost.

5. **Track:** The track acts as the runway for the bearing. The material of the track is steel. Steel was selected because of its high strength and ductility, corrosion resistance, and durability.
6. **Electric motor:** The electric motor is used to produce or generate rotational motion which is being transmitted to the glass door through the chain drive. The electric motor is a bidirectional electric motor which can rotate both in clockwise direction and counterclockwise direction. The rotation of the motor opens or closes the door in response to the signal received from the microcontroller.
7. **Microcontroller:** The microcontroller is the central controlling unit of the whole system (the smart door). It controls the rotation of the electric motor. This is achieved through the signal received by the controller from the sensor.
8. **PIR sensors:** The PIR sensor receives the heat energy radiated by an individual moving towards the door and sends a signal to the controller. This heat energy is sensed by the sensor only when the person is within the sensor's range. Moreover, the sensor's range can be adjusted to meet the need of the system.
9. **Limit switches:** Limit switches are used to automatically detect the presence of an object or monitor the movement of an object. It helps to indicate that the movement limit of the door has been reached.
10. **Relays:** Relay is an electromechanical device that uses an electromagnet to operate a pair of movable contacts from an open position to a closed position. The advantages of relay is that it takes a relatively small amount of power to operate the relay coil. It can be used to control motors, heaters, lamp etc.
11. **Batteries:** The battery stores DC electrical energy which can be used to power the system when there is a power outage or failure from the national grid. There are ten in number. Each of the battery has a voltage rating of 6 volts. Both batteries are connected in series to supply a voltage of 12 volts.
12. **Timer:** The timer controls the delay time at the fully opened position before the door closes.
13. **Switch:** The switch is a manually operated device used to control the supply of voltage. This is achieved by making a circuit either open or closed.
14. **Light-emitting diode (led):** LED is a semiconductor light source that emits light when current flows through it. It can be used to indicate whether a circuit is closed or open.

2.3 Design of the system components

The design of the system involves the following processes;

2.3.1 The door panel

The door panel is the movable part of the system that slides sideways to give access to persons that want to use the door. In order to achieve the desired design requirement, the following door dimensions were used.
Height of the door panel (H) = 2000 mm
Width of the door panel (b) = 840 mm
Thickness of the door panel (t_h) = 12 mm
As obtained from https://uk.saint-gobain-building-glass.com, the density of the door panel material (glass) is given as;
Mass density of the door panel material (ρ) $= 2500\ kg/m^2$

The mass of the door can be obtained from Equation (1) [8];
Mass of the door panel (M_g) $= \rho \times \mathrm{H} \times b \times t_h$ (1)

Mass of the door panel (M_g) = 2500 × 2 × 0.84 × 0.012

Mass of the door panel (M_g) = 50.4 kg

Weight of the door panel (W_g) = (Mg)×g (2)

= 50.4×9.81

= 494.424 N

2.3.2 The door frame

The material of the frame is medium carbon steel and its dimensions are given as Rectangular hollow section of (40×20×3)mm.

Mass per unit length = 2.36 kg/m. [9]

Total length of the steel material (L) =2H + 2b (3)

= 2×2000 + 2×840 = 5680mm 5.68m

Total mass of the frame (M_f) = 2.36 × 5.68 = 13.4 kg

Weight of the frame (W_f) = M_f × g (4)

= 13.4 × 9.81 = 131.5 N

Total weight of the door (W) = $W_g + W_f$ (5)

= 494.424 + 131.5 = 625.925 N ≅ 626 N

2.3.3 Force analysis for the door

The force analysis of the door was done in the manner of [10].

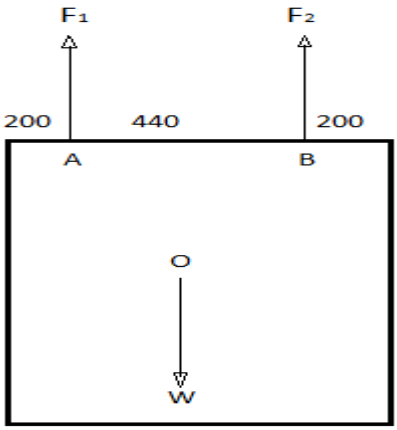

Figure 1 Free body diagram of the door

Where W is the weight of the door,

F_1 and F_2 are the forces acting on the two hinge joints.

$\sum F_y = 0$

$F_1 + F_2 - W = 0$

$W = F_1 + F_2$ (6)

Taking moment about point A

$\sum M_A = 0$

$F_2 \times 440 = W \times 220$

$F_2 = \frac{220W}{440} = \frac{220 \times 626}{440} = 313$ N

Assuming that the mass of the door is evenly distributed.

Then, $F_1 = F_2 = 313$ N

2.3.4 Selection of roller from manufacturer's catalogue

Dongguan Kentie Bearing Co. catalogs and technical brochures was used for the roller selection. The process of roller selection process was done in the manner of [6]. Radial load (Fr) = 313 N, Axial load (Fa) = 0, Bore diameter (d) 10 mm (assumed), Speed (N) = 229.18 rpm, Rated life of the bearing (L10h) = 60000 hours, Race-rotational factor (υ) = 1.2. The bearing is subjected to only radial load. Thus,

Dynamic load (P_l) = $\upsilon \times$ Fr (7)

= 1.2 × 313 = 375.6 N

The rating life of the bearing (L10) = $\frac{60 \times N \times L_{10h}}{10^6}$ (8)

L10 = $\frac{60 \times 229.18 \times 60000}{10^6}$ = 825.059 million revolutions

Dynamic load capacity (C) = P(L_{10})1/3 (9)

C = 375.6(825.059)1/3 = 3522.79 N

From manufacturer's catalogue, for bore diameter of 10 mm;

Bearing number 6000 is suitable for this application.

Bearing number 6000 has the following specifications:

Bore diameter (d) = 10 mm, Outer diameter (D_o) = 26 mm, Axial width of the bearing (B) = 8 mm

2.3.5 Force analysis for the rollers

The force analysis for the rollers was done in the manner of [11].

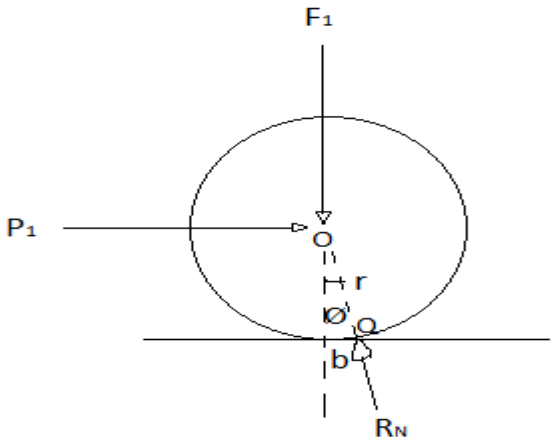

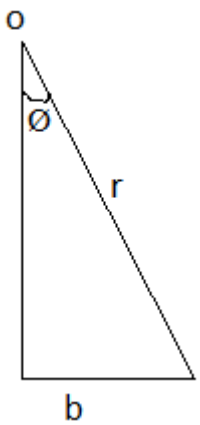

Figure 2 Free body diagram of the roller

Where F_1 is the force or load on the roller, P_1 is the force required to overcome rolling resistance, and R_N is the normal reaction.

$\sum F_y = 0$

$R_N \times \cos(\emptyset) - F_1 = 0$

$F_1 = R_N \times \cos(\emptyset)$ (10)

$\sum F_X = 0$

$P_1 - R_N \times \sin(\emptyset) = 0$ (11)

$P_1 = R_N \times \sin(\emptyset)$ (12)

Dividing equation (12) by Equation (13) gives

$$\frac{P_1}{F_1} = \frac{R_N \times \sin(\emptyset)}{R_N \times \cos(\emptyset)}$$

$$\frac{P_1}{F_1} = \tan\emptyset \quad (13)$$

The value of $\emptyset$ is small since the area of contact of the roller with the track is small. Thus,

$\tan\emptyset \cong \sin\emptyset$

$$\sin\emptyset = \frac{b}{r} \quad (14)$$

From Equation (13) and (14)

$$\frac{P_1}{F_1} = \frac{b}{r}$$

$$P_1 = F_1 \times \frac{b}{r} \quad (15)$$

The radius of the bearing (r) = $\frac{D}{2} = \frac{26}{2}$ = 13 mm.

The distance (b) is called the coefficient of rolling friction.

The value of b for cast nylon roller on steel track is 0.027 inches (0.6858 mm) [12, 14]

$\therefore P_1 = 313 \times \frac{0.6858}{13}$ = 16.512 N

The total force required to overcome rolling resistance on both rollers (P) = $2P_1$

P = 2 × 16.512 = 33.024 N

The force (P) is the force required to sustain its motion.

The value or magnitude of the kinetic frictional force, that acts when there is motion, is usually less than the maximum magnitude of the static frictional force that must be overcome to start motion. [13].

The force (Fa) required to start or initiate its motion is generally 2 to 2.5 times the force (P) required to sustain its motion. [12]. That is;

Fa = 2P (16)

= 2 × 33.024 = 66.048 N

2.3.6 The drive system (chain drive)

The chain and sprocket was selected from RENOLD Superior Chain Technology catalog, and this was done in the manner of [6].

2.3.6.1 Selection of chain

Maximum velocity of the sliding door (V_{max}) = $\frac{S}{t}$ (17)

Where S is the distance covered at maximum velocity (S = 740 mm), and t is the time taking (t = 4.5 seconds).

From equation (17), $V_{max} = \frac{0.74}{4.5} = \frac{0.74}{4.5} = 0.164$ m/s

The maximum velocity of the door is 0.164m/s.

The minimum velocity of the door at the extreme positions (fully closed and opening positions) is;

Minimum velocity of the door ($\boldsymbol{V_{min}}$) = $\frac{S_2}{t_2}$

Where S_2 is the distance covered by the door with the minimum velocity, and t_2 is the time taking

Dimensions:

S_2 = 100 mm (assumed)

t_2 = 2.5 seconds (assumed)

Minimum velocity of the door ($\boldsymbol{V_{min}}$) = $\frac{0.1}{2.5}$ = 0.04 m/s

The total time taken for the door to get to its fully opened or closed position is the sum of the taking for during the maximum velocity and the time taking for during the minimum velocity. That is;

Total time = 4.5 + 2.5 = 7 seconds

The power required to accelerate the door = Fa × V (18)

= 66.048 × 0.164 = 10.83 W

Transmission efficiency (η_T) = $\frac{P_{out}}{P_{in}}$

$P_{in} = \frac{P_{out}}{\eta_T}$ (19)

Where P_{in} is the power input into the drive system from the motor, and P_{out} is the power output from the drive system to accelerate the door.

The efficiency of a well lubricated chain drive is of the range: 96% to 98%. [6].

Using an efficiency of 97% (assumed)

And P_{out} = 10.83 W

From equation (19), $P_{in} = \frac{10.83}{0,97}$ = 11.165 W

The input power (P_{in}) is the power to be transmitted by the chain drive or the transmitted power (TP).

Rating power (RP) = $\frac{TP \times K_s}{K_1 \times k_2}$ (20)

Transmitted power (TP) = 11.165 W

Using a pinion (driving sprocket) with 15 teeth. (assumed)

According to [6].

For electric motor as the input power and smooth driven load, the Service factor (ks) is 1.0

For chain with single strand, the Multiple strand factor (k1) is 1.0

For pinion with 15 teeth, the Tooth correction factor (k2) is 0.85

From equation (20), Rating power (RP) = $\frac{11.165 \times 1}{1 \times 0.85}$ = 13.135 W = 13.135 W

Chain tension (Pc) = $\frac{RP}{V}$ (21)

Where V is the maximum velocity of the chain, which is equal to the maximum velocity of the door (V = 0.164 m/s).

From equation (21), Chain tension (Pc) = $\frac{13.135}{0.164}$ = 80.09 N

The driving sprocket (pinion) rotate at the same speed with the spindle of the motor (That is, Pinion speed (Np) = 229.18 rpm). The closest higher speed in table 14.2 [6] is 300 rpm. At pinion speed of 300 rpm, the most suited chain drive is 06B. Chain number 06B has a speed of 300 rpm and power rating of 0.61 KW.

Chain number 06B has the following dimensions and breaking load;

Pitch (p) = 9.525 mm, Roller diameter (d1) = 6.35 mm, Width (b1) = 5.72 mm, Breaking load (WB) = 8900 N.

Number of links in the chain (Ln) = $2(\frac{a}{p}) + (\frac{Z_1+Z_2}{2}) + (\frac{Z_2-Z_1}{2\pi})2 \times (\frac{p}{a})$ (22)

Where Pitch (p) = 9.525 mm, Number of teeth of the driving sprocket (pinion) (Z1) = 15 teeth, Number of teeth of the driven sprocket (Z2) = 15 teeth, and Using a center distance (a') of 1550 mm. (assumed)

From equation (22), Number of links in the chain (Ln) = $2(\frac{1550}{9.525}) + (\frac{15+15}{2}) = 340.46$

Since the number of links must be even, then, Number of links in the chain (Ln) = 340 mm

Actual center distance (a) between the driving sprocket and the driven sprocket is given as

a = $\frac{p}{4}\{[Ln - (\frac{Z_1+Z_2}{2})] + \sqrt{([Ln - (\frac{Z_1+Z_2}{2})]2 - 8[\frac{Z_2-Z_1}{2\pi}]2)}\}$ (23)

a = $\frac{9.525}{4}\{[340 - (\frac{15+15}{2})] + [Ln - (\frac{15+15}{2})] = 1547.8$ mm

length of the chain (Lc) = Ln × p (24)

= 340 × 9.525 = 3238.5 mm

2.3.6.2 Selection of sprocket

Both the driving sprocket and driven sprocket have the same dimensions, Number of teeth of the driving sprocket (pinion) (Z1) = 15 teeth. (assumed), Number of teeth of the driven sprocket (Z2) = 15 teeth. (assumed), Chain pitch (p) = 9.525 mm. (gotten from calculation), Roller diameter (d1) = 6.35 mm. (gotten from calculation), and Width between inner plates (b1) = 5.72 mm. (gotten from calculation)

Dimensions of the sprockets:

Pitch circle diameter (D) = $\frac{p}{\sin\frac{180}{Z}}$ (25)

= $\frac{9.525}{\sin\frac{180}{15}}$ = 45.81 mm

Top diameter (Da);

(Da)max = D + 1.25p – d1 (26)

= 45.81 + 1.25(9.525) – 6.35 = 51.366 mm

(Da)min = D + p(1 - $\frac{1.6}{Z_1}$) – d1 (27)

= 45.81 + 9.525(1 - $\frac{1.6}{15}$) - 6.35 = 47.969 mm

∴ Top diameter (Da) = $\frac{51.366 + 47.969}{2}$ = 49.67 mm

Roller seating radius (ri) = 0.505(d1) + 0.069($\sqrt[3]{d1}$) (28)

= 0.505(6.35) + 0.069($\sqrt[3]{6.35}$) = 3.33 mm

Root diameter (Df) = D – 2ri (29)

= 45.81 – 2(3.33) = 39.15 mm

Tooth width (bf) = 0.93(b1) (30)

Tooth width (bf) = 0.93(5.72) = 5.3 mm

2.3.7 Selection of electric motor

2.3.7.1 Power rating of the motor

The angular velocity of the motor (ω) can be obtained from the relationship below; [6].

V = ω × r (31)

Where V is the maximum velocity of the chain (V = 0.164 m/s), and r is the pitch circular radius of the sprocket (r = 22.905 mm).

From equation (31), $\omega = \frac{V}{r} = \frac{0.164}{22.905 \times 10^{-3}}$ = 7.1616 rad/s

The speed (N) required can be obtained from equation (32);

$\omega = \frac{2\pi N}{60}$ (32)

N = $\frac{60\omega}{2\pi} = \frac{60 \times 7.1616}{2\pi}$ = 68.39 rpm

The motor power required is the power to be transmitted by chain drive or the input power (Pin) into the drive system as obtained from Equation (19).

Thus, the power rating of motor (Pm) is 11.165 W.

The torque (T) required can be obtained from Equation (33), [6].

Pm = T × ω (33)

T = $\frac{P_m}{\omega} = \frac{11.165}{7.1616}$ = 1.56 Nm

2.3.7.2 Motor Efficiency

The motor efficiency analysis was done in the manner of [14].

Motor Efficiency, $\eta_m = \frac{W_{mech.}}{W_{elect.}}$ (34)

Motor efficiency is usually between 70% and 96%. [14].

Where $W_{mech.}$ is the mechanical work output from the motor, and $W_{elect.}$ is the electrical work input to the motor.

From Equation (34), $W_{elect.} = \frac{W_{mech.}}{\eta_m}$

Using a motor efficiency of 85% (Assumed), and $W_{mech.}$ of 11.165W

$W_{elect.} = \frac{11.165}{0.85}$ = 13.14W

2.4 Duration of operation of the door with battery

To ensure a continuous operation of the smart door when there is a power outage from the main power source, an alternative source for electric power supply has to be made through the use of batteries. A set of ten batteries with voltage rating of 6v and battery capacity of 5Ah each, was selected to serve as a backup for the system. The analysis and the formulas in this section were in the manner of [15]. These batteries are connected in series.

Total output voltage (V) = $V_1 + V_2 + \ldots + V_{10}$ (35)

Where $V_1 = V_2$ = 6 volts

∴ V = 10 × 6 = 60 volts

The duration (Time, t) of operation of the smart door using battery as alternative source of power supply is calculated as follows;

Power (Ps) = IV (36)

Where V is the voltage to be supplied by the battery (60V), Ps is the power required by the system (15W), and I is the current.

From Equation (36); I = $\frac{Ps}{V} = \frac{15}{60}$ = 0.25A

Battery capacity (C_b) = It (37)

t = $\frac{C_b}{I}$

where battery capacity (C_b) = 5Ah, Current (t) = 0.25A, Time (t) =?

∴ t = $\frac{5}{0.25}$

t = 20h

The duration of operation of the door with battery is 20 hours.

2.5 System efficiency

System efficiency, $\eta_s = \frac{W_{output}}{W_{input.}}$ (38)

Where W_{output} is the work output from the system (10.83W), $W_{input.}$ is the electrical work input to the system (15W)

Then, System efficiency, $\eta_s = \frac{W_{output}}{W_{input.}} = \frac{10.83}{15} = 0.722$

The efficiency of the system is 72.2%.

2.6 Projections

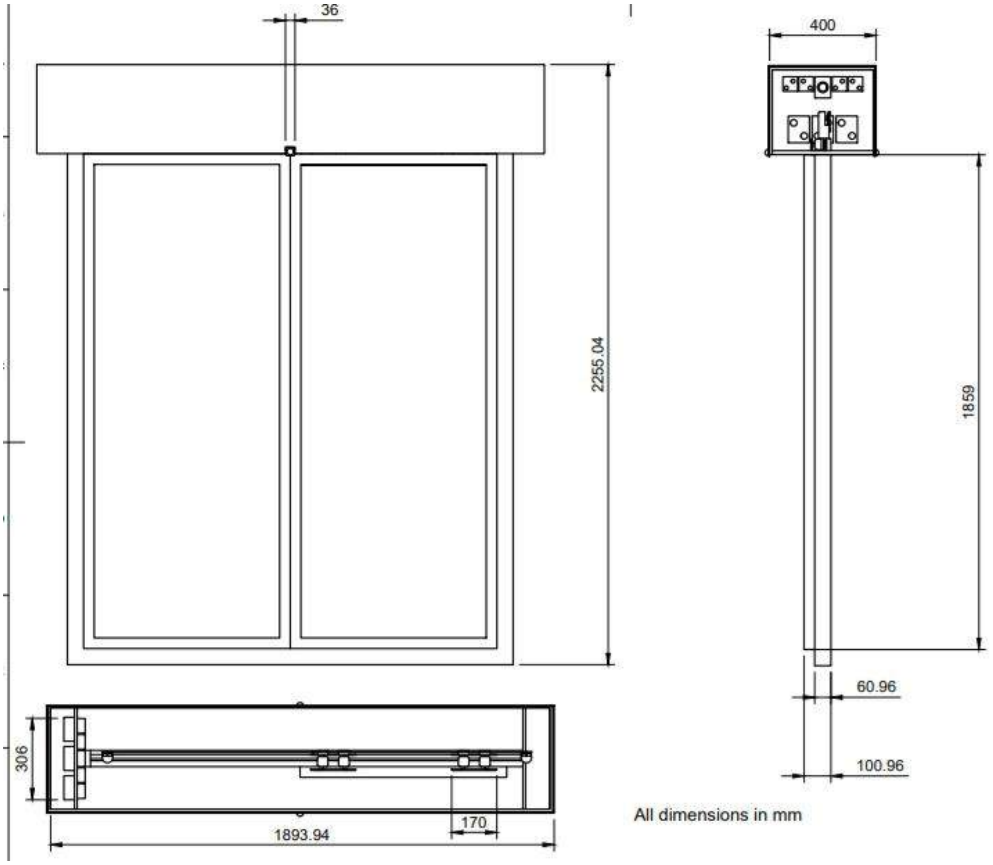

Figure 3 Orthographic views of the smart door.

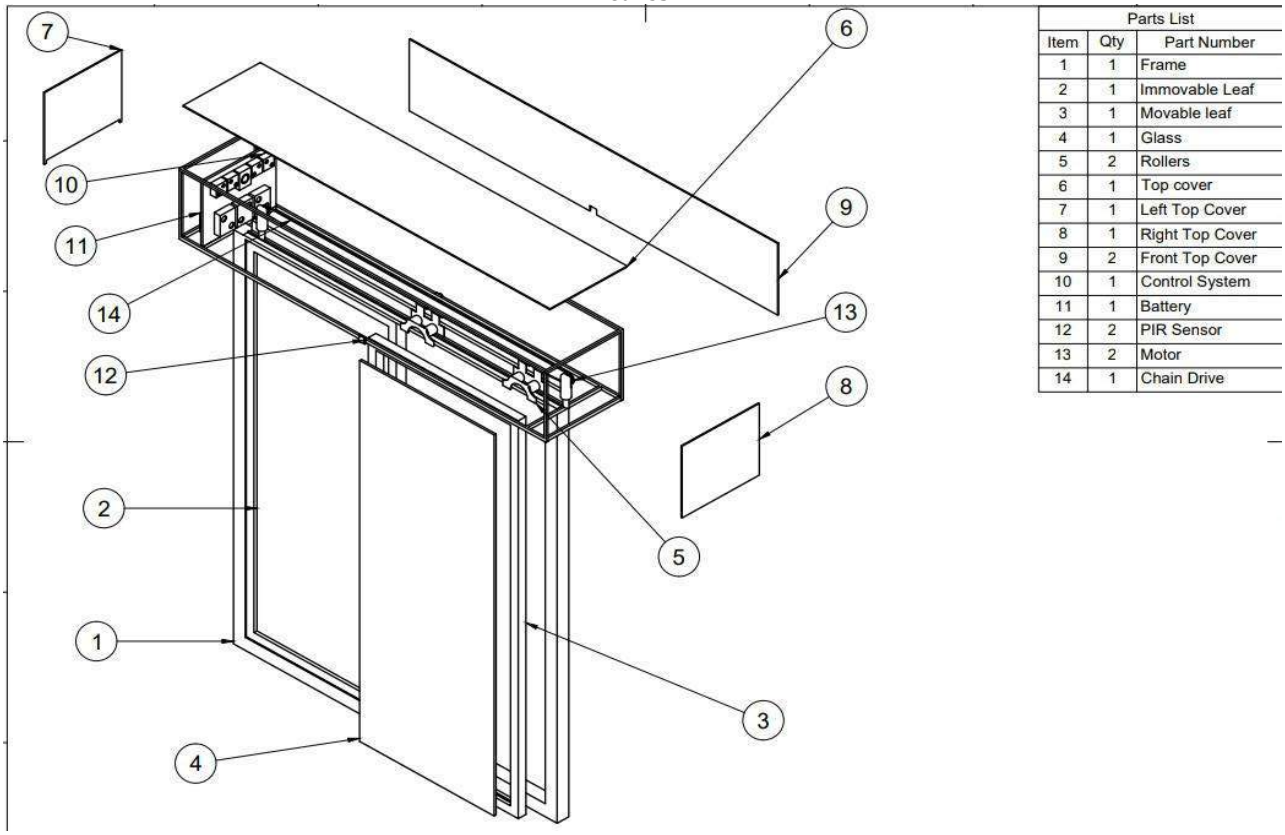

Parts List		
Item	Qty	Part Number
1	1	Frame
2	1	Immovable Leaf
3	1	Movable leaf
4	1	Glass
5	2	Rollers
6	1	Top cover
7	1	Left Top Cover
8	1	Right Top Cover
9	2	Front Top Cover
10	1	Control System
11	1	Battery
12	2	PIR Sensor
13	2	Motor
14	1	Chain Drive

Figure 4 Exploded view of the self-opening and closing door

2.6 Operating process of the self-opening and closing door

The smart door is an automated door system which senses the motion of a person approaching the door. The motion of the person is detected by a passive infrared sensor (PIR Sensor) mounted at the top of the door frame. The PIR sensor detects the motion of the person, within the sensor's field of view, through the thermal energy radiated from the person. The signal from the sensor is sent to the microcontroller which then initiate the rotation of the motor. The rotational motion of the motor is transmitted through the chain drive (a roller chain and two sprockets of the same specifications) to the door. This transmitted motion causes the door to slide open. The door remains opened for a predetermined period of time (4 seconds), called the delay-time, to allow the person to fully pass through the door before shutting or closing. This delay-time is adjustable. The sliding door starts its motion with a maximum velocity and gradually come to rest with a lesser velocity. This functionality was achieved through the use of limit switches. There are two sets of limit switches used to achieve this process. The first set are contact sensors (two in number) installed at both extreme of the track. The other set are proximity sensors (two in number) installed in between the two contact sensors. The proximity sensors are installed at a distance of 100mm from each of the contact sensors. The door starts its motion with a maximum velocity and switches to a lower velocity on getting to the proximity sensor. When the door gets to the position of the proximity sensor, the sensor sends a signal to the microcontroller which switches the velocity of the door to a lower velocity through a set of relays. The door comes to rest, slowly, when it gets to the contact sensor. The contact sensor sends signal to the microcontroller which switches the velocity of the door to zero through a relay. The door remains stationary at the fully open position for 4seconds (which is the delay-time) to allow the person to pass through the entryway. This delay-time can be adjusted using the timer. After which, the timer sends signal to the microcontroller which changes the

velocity of the door from zero to a maximum velocity through the relay. The maximum velocity of the door changes to a lower velocity on getting to the second proximity sensor at the other end of the track. Gradually, the door comes to rest at the fully closed position with the lower velocity on getting to the second contact sensor. This whole process is repeated when the PIR sensor detects the motion of a person approaching the door.

3.0 Result and Discussion

The results gotten from the test carried out on the self-opening and closing door are discussed as follows;

The highest distance from the door in which a person's movement can be detected by the system was measured to be 410cm.

The time taken for the door to become fully opened (the door opening time) when someone walks towards the door was measured (Table 1) and the average was taking to be 6.5 seconds.

Table 1 Door Opening Time.

S/N	Door Opening Time (t_o) (seconds)
1	6.50
2	6.80
3	6.35
4	6.70
5	6.40
6	6.55
7	6.30
8	6.40

The time taken for the door to returned from its fully opened position to its fully closing position after an individual has passed through the door was measured (Table 2) and the average was taking to be 6.27 seconds.

Table 2 Door Closing Time.

S/N	Door Closing Time (t_c) (seconds
1	6.41
2	6.13
3	6.30
4	6.40
5	6.25
6	6.35
7	6.20
8	6.15

The door delay time at the fully opened or closed position was measured (Table 3) and the average was taking to be 4.13 seconds.

Table 3 Delay Time.

S/N	Delay Time (t_d) (seconds)
1	4.03
2	4.30
3	4.23
4	4.05
5	4.15
6	4.10
7	4.20
8	4.00

The door maximum velocity was obtained from the ratio of the distance covered by the door to the time it takes, at high velocity. The maximum velocity is 0.170m/s. Also, the door minimum velocity was obtained from the ratio of the distance covered (0.1m) by the door to the time it takes (2.15 sec.), at a lower velocity. The minimum velocity is 0.047m/s. The time taken for the door to complete its operational cycle is the total time taken by the door to move from its closed positon to the fully opened position and return back to its fully closed position. Its value was obtained to be 16.90 sec. The desired or design value of some of the design parameters were compared with their actual values. The actual values were obtained from the test results. Table 4 shows the deviation of the actual values from the design values.

Table 4 Deviation of the Actual values from Design values of some Design Parameters.

S/N	Design Parameters	Design Value	Actual Value	Deviation	Percentage Deviation
1	Door opening time	7.00 s	6.50 s	0.5 s	7.69 %
2	Delay time	4.00 s	4.13 s	0.13 s	3.15 %
3	Maximum velocity	0.164 m/s	0.170 m/s	0.006 m/s	3.53 %
4	Minimum velocity	0.04 m/s	0.047 m/s	0.007 m/s	14.89 %
5	Total time	18.00 s	16.90 s	1.1 s	6.51 %

From Table 4, it is obvious that the deviations of the actual values from the design or desired values are small. Thus, the deviations can be considered negligible.

4.0 Availability analysis and Reliability analysis

4.1 Availability analysis

The availability analysis of the door was done in accordance to [16]. Considering a period of 30 days (720 hours), the availability analysis of the smart door is as follows
Time spent during preventive maintenance = 4 hours and the Breakdown time = 2 hours. Therefore,
System downtime = 4 + 2 = 6 hours
System uptime = 720 – 6 = 714 hours

Availability, $A = \frac{uptime}{uptime+downtime}$ ……(4.1)

Availability, $A = \frac{714}{714+6} = 0.9917$

Therefore, the availability of the system within a period of 30 days (720 hours) is 99.17%.

4.2 Reliability analysis

The availability analysis of the was done in accordance to [17, 18]. The reliability analysis for the door system for a period of 30 days (720 hours) is as follows;
Period under consideration (time), t = 30 days, Initial number of live components (at time, t = 0), N_i= 34 components, Number of survived live components (after time, t), N_s = 32 components, and Number of failing components (after time, t), N_f = 2 components.

Failure rate, $\lambda = \frac{N_f}{N_i \times t}$ …… (4.2)

$= \frac{2}{34 \times 30} = 1.961 \times 10^{-3}$ per day

Reliability, $R = e^{-\lambda t}$ …….... (4.3)

$= e^{-(1.961 \times 10^{-3} \times 30)} = 0.943$

The reliability of the door system is 0.943. Thus, the system is 94.3% reliable.

5.0 Conclusion

A smart door was successfully design, fabricated, and tested. The smart door was able to eliminate the difficulties encounter by physically challenge persons when using manually operated doors, the risk of cross-contamination (due to human-to-door contact) in places like laboratories, hospitals etc., the cost of hiring persons to open doors for clients, and to enhance the ease and speed of human and goods movement in work places since there is no obstruction to movement. Also, the availability and reliability analysis was carried out. The smart door is 94.3% reliable and 99.17% available.

Nomenclature

H	Height
b	Width
t_h	Thickness
M_g	Mass of door panel
W_g	Weight of door panel
L	Total length of steel material
M_f	Mass of frame
W_g	Weight of frame
W	Total weight of the door
F_1	Force on hinge A
F_2	Force on hinge B
P_l	Dynamic load
C	Dynamic load capacity
L10	Rating life of bearing
υ	Race-rotational factor
Fr	Radial load
d	Bore diameter
D_o	Outer diameter
B	Bearing axial width
V_{max}	Maximum velocity
$\boldsymbol{V_{min}}$	Minimum velocity
P_{in}	Input power
P_{out}	Output power
RP	Rating power

TP	Transmitted power
K1	Multiple strand factor
K2	Tooth correction factor
Pc	Chain tension
Ln	Number of links
p	Pitch
Z	Number of teeth
a	Center distance between sprockets
Lc	Length of chain
r	Pitch circular radius
D	Pitch circular diameter
Pm	Motor power rating
N	Speed
T	Torque
$W_{mech.}$	Mechanical work output
$W_{elect.}$	Electrical work input
Ps	System power
V	Output power
I	Current
C_b	Battery capacity
t	Time
N_s	Number of survived live components
N_i	Initial number of live components
N_f	Number of failing components
R	Reliability
A	Availability
t_o	Door opening time
t_c	Door closing time
t_d	Delay time
R_N	Normal reaction
P	Rolling resistance
Fa	Accelerating force

Greek letters

ρ	Mass density
η_T	Transmission efficiency
ω	Angular velocity
η_m	Motor efficiency
η_s	System efficiency
λ	Failure rate
∅	Angle

References

[1] Oladumoye m., Oluwatobi A.A. and Obakin O. (2014). Design and Construction of an Automatic Sliding Door using Infrared Sensor. Computing, Information System, Development Informatics and Allied Research Journal. Vol 5, no 4. Retrieved September 20, 2015 from www.cisdijournal.net.

[2] Dikio C. Idoniboyeobu. Development of Automatic Door System. American Journal of Engineering Research (AJER), Vol 7, no 5, 2018, pp.168-173.

[3] Zungeru A. M. et at, (2012). Design and Implementation of a low cost Digital Bus Passenger Counter.
[4] PO Olagbegi, CC Kwasi-Effah, BA Ugbi (2013) Contemporary Issues on Office Environment. International Journal of Engineering Sciences, 2(7), Pages: 292-296
[5] Webster J. G., While (1999). Encyclopedia of Electrical and Electronics Engineering, Vol 4. New York: John Wiley and son, Inc.
[6] Henry D. (1967). Machine design "The Profile of Industrial Designer.
[7] Bhandari. V.B. (2009). Design of Machine Elements. Third edition.
[8] Kkurmi R. S. and Gupta J. K. (2005). A Textbook of Machine Design. Fourteenth Edition. Eurasia Publishing House (PVT) Ltd. Ram Nagar, New Delhi -110 055.
[9] Khurmi. R. S., (2008). Strength of Materials (Mechanics of Solids). Third edition. ISBN: 81-219-2822-2.
[10] https://www.ssabwebsitecdn.azureedge.net. (10/01/2021).
[11] Hibbeler R.C. (2010). Engineering Mechanics (Statics). Twelfth edition. ISBN-10: 0-13-607791-9.
[12] Beer F. P., Johnson E. R, Mazurek D. F. and Eisenberg E. R. (2010). Vector Mechanics for Engineers (Statics). Ninth edition. ISBN 978-0-07-352923-3, volume 1.
[13] Dave Lippert and Jeff Spekter. (2007). Rolling Resistance and Industrial Wheels. Hamilton White Paper, No. 11, (2013).
[14] Halliday David and Resnick Robert, (2007), Fundamentals of Physics, Tenth Edition, ISBN: 978-1-118-23072-5.
[15] Olagbegi P.O, Kwasi-Effah C.C, Ugbi B. A (2013). An Experimental Access Control System for Enhancing Security and Safety in University Campuses Scholars Journal of Engineering and Technology (SJET); 1(3):172-176
[16] Yasar Demirel. (2018).Comprehensive Energy System. ISBN: 978-0-12-814925-6
[17] Theraja B. L. and Theraja A. K. (2005), A Textbook of Electrical Technology, volume 1, First multicolor edition, ISBN: 81-219-2440-5.
[18] www.fiixsoftware.com. (15/03/2021).

NIPES Conference Proceedings
The 1st International Conference of the Nigerian Institution of Professional Engineers and Scientists 7th-8th Oct. 2021: 296-308
www.nipesjournals.org.ng

Assessment of the Corrosion Behaviour of Epoxy-Eggshell Ash Nanoparticle Coating for Mild Steel

*Oisakede M. O, Orumwense F.F.O. Sadjere E. G., Ebunilo P. O. B
Department of Mechanical Engineering, University of Benin, P.M.B 1154, Benin City, Nigeria
*maureen.oisakede@uniben.edu

Abstract

Mild steels are increasingly being imported and locally produced in Nigeria as a result of industrialization. They are useful in various applications like railway, buildings, bridges, port construction e. t. c. where they may be subject to corrosion attack. Corrosion can be controlled or reduced through the use of suitable and locally available coatings. Nanoparticles due to their large surface areas have been shown to be excellent materials as they are good absorbents of coating pigments. Egg shells are readily available and easily accessible in Nigeria and they contain calcium which easily combine with epoxy to give compounds resistant to corrosion attack. The effect of the addition of eggshell ash nanoparticles (ESAnp) in epoxy as a coating for mild steel was studied. 1, 2, 3 and 4wt% Eggshell ash nanoparticles were added to epoxy. The coating was done using spraying method Corrosion protection efficiency of 95.42% was obtained for the mild steel when coated with epoxy-4wt%ESAnp. The substrate showed more tendencies to pitting than the coated samples. This study has established that epoxy-4wt%ESAnp have good anti-corrosion properties.

Keywords: Mild steel, Nanoparticles, Epoxy, Eggshell ash, Corrosion protection.

1. Introduction

In recent times several techniques have been used to protect metals from corrosion which include polymeric coatings are most widely used technique to control corrosion of metal structures due to their ease of application at reasonable cost. The coating efficiency is mostly dependent on basic properties of the organic film like barrier effect and the presence of inhibitors or sacrificial pigments and the interface interaction in terms of adherence [1]. Epoxy has been widely used as a coating material to protect the steel reinforcement in concrete structures, because of its outstanding processability, excellent chemical resistance, good electrical insulating properties, and strong adhesion/affinity to heterogeneous materials. Epoxy coatings generally reduces the corrosion of a metallic substrate subject to an electrolyte in two ways. First, they act as a physical barrier layer to control the ingress of deleterious species. Second, they can serve as a reservoir for corrosion inhibitors to aid the steel surface in resisting attack by aggressive species such as chloride anions [2].

Nanoparticles are generally considered to be a number of atoms or molecules bonded together with radius of 100nm. Nanoparticles find relevance in corrosion resistant, erosion-resistant and wear-resistant environments [3].

Nanoparticles are being incorporated into epoxy matrices as filler to improve the mechanical, rheological, anticorrosive, and light-resistance properties. Especially nano metal oxides such as TiO_2, Fe_2O_3, ZnO, SiO_2, Al_2O_3, $CaCO_3$ and zirconia have been used as nano filler for corrosion protection on mild steel for more than a decade [4]. Eggshells are mainly composed of calcium carbonate and the membrane contains protein [5].

The objective of this work is to evaluate corrosion performance of epoxy-egg shell ash nanoparticle coating for mild steel being that egg shell contains calcium carbonate in high proportion. The produced nanoparticles were characterized using XRF (X-ray fluorescence), FT-IR (Fourier transform infrared spectroscopy), XRD (X-ray diffraction), and SEM (Scanning electron microscopy) techniques.

2. Materials and Method

2.1 Materials

The eggshells were obtained from a local tea seller in Benin City, Nigeria, the epoxy (LY 556), chemically belonging to the epoxide family was used in the present work. Its common name is *Bisphenol-A-Diglycidyl-Ether*. hardener tri-ethylene-tetramine (TETA) designation HY 951 was purchased from Chemical shop in Warri Delta State Nigeria.

Figure 1: Eggshell

2.2 Method

To detach the membranes from the shells, the eggshells were washed using water and thereafter dried and ball milled into eggshell powder particles and then they was packed in a graphite crucible before firing in a carbolite electric resistance furnace at a temperature of 500°C for 4hrs to produce carbonized eggshell ash [6]. Mild steel with compositions shown in Table 1 was used in this work. The mild steel was grit blasted at a pressure of 3 kg/cm^2 using alumina grits having size of around 60 μm size. The grit blasted sample was cleaned in an ultrasonic cleaner and the weight of each cleaned specimen was taken by using a precision electronic balance with ± 0.1 mg accuracy.

Table 1: Chemical composition of the mild steel

	Metal Elements	Percentage (%)
1.	C	0.130
2.	Si	0.153
3.	Mn	0.630
4.	P	0.060

5.	Cu	0.040
6.	Al	0.030
7.	S	0.010
8.	Cr	0.010
9.	Ni	0.020
10.	Mo	0.01
11.	W	0.088
12.	Fe	balance

2.3.3 Production of the Nanoparticles

The sol gel method was used in the production of egg shell ash nanoparticle. Particle size and morphology of produced nanoparticles was examined by TEM (Jeol, JSM2010) using a 200 keV electron beam. Mini Pal compact energy dispersive X-ray spectrometer (XRF) was used for the elemental analysis of the produced nanoparticles. The eggshell ash nanoparticles were continuously sonicated in ethanol solvent by ultrasonic waves using sonicator equipped with a titanium probe with a diameter =13 mm) for 15 minutes. The uncured epoxy (LY556) and its corresponding hardener (HY 951) were mixed in a ratio of 2:1 by weight as per recommendation. Then 1, 2, 3 and 4wt% ESA nanoparticles was added to the epoxy mixture and stirred up to a speed of 1200 rpm for 15 minutes, then the coating mixture was applied to the steel substrate by using spray gun and then kept in a dry place at room temperature for 7 days to allow full curing. (Figure 2).

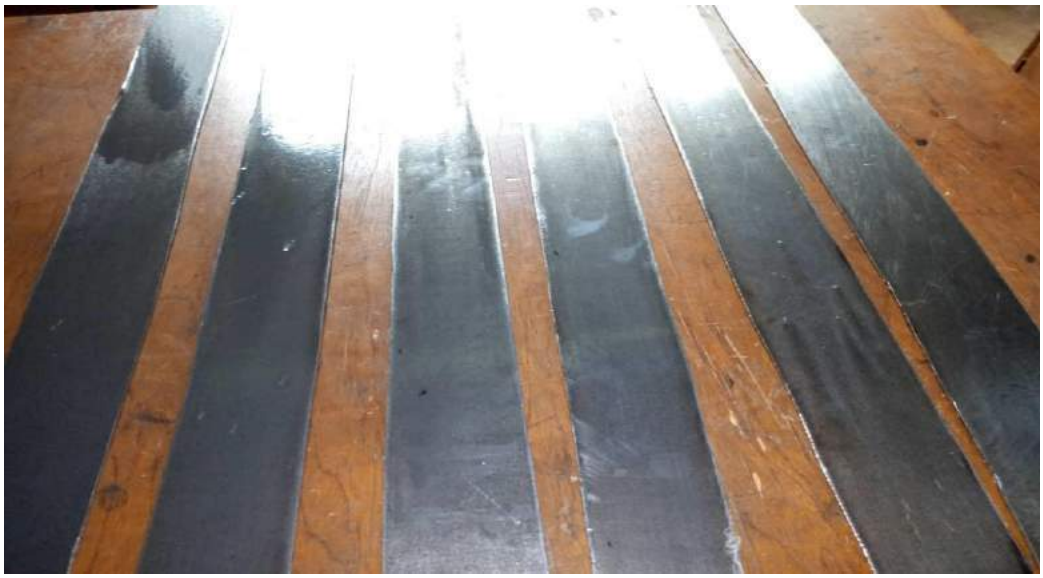

Figure 2: Photograph of the coated samples

The thickness of the coatings was measured by cutting each sample into two halves (perpendicular to its length) using a TechCut 4 low speed saw from Allied High Tech. Productions Inc. The thickness of the coatings was calculated by taking the mean of three thickness values on each sample. The X-ray diffraction (XRD) patterns of the samples were determined by X‟PertPro PANalytical, LR 39487C. XRD diffractometer using Cu Kα radiation (40 kV, 40 mA). The surfaces of the coating specimens were examined directly by scanning electron microscope. The specimens were cleaned thoroughly with acetone before being

observed under scanning electron microscope. The portable Rockwell hardness machine was used to determine the hardness values of the samples. The coating adhesion strength was determined using universal testing machine PC-2000 Testometric testing machine.

3. 0 Results and Discussion

The morphologies of the Eggshell ash nanoparticles by transmission electron microscope/ energy dispersive spectrometry (TEM/EDS) is shown in Figures 3. The nanoparticles were observed to be solid in nature, but irregular in size. Spherical shape particles can also be seen. The average particle size obtained was 91.34nm.

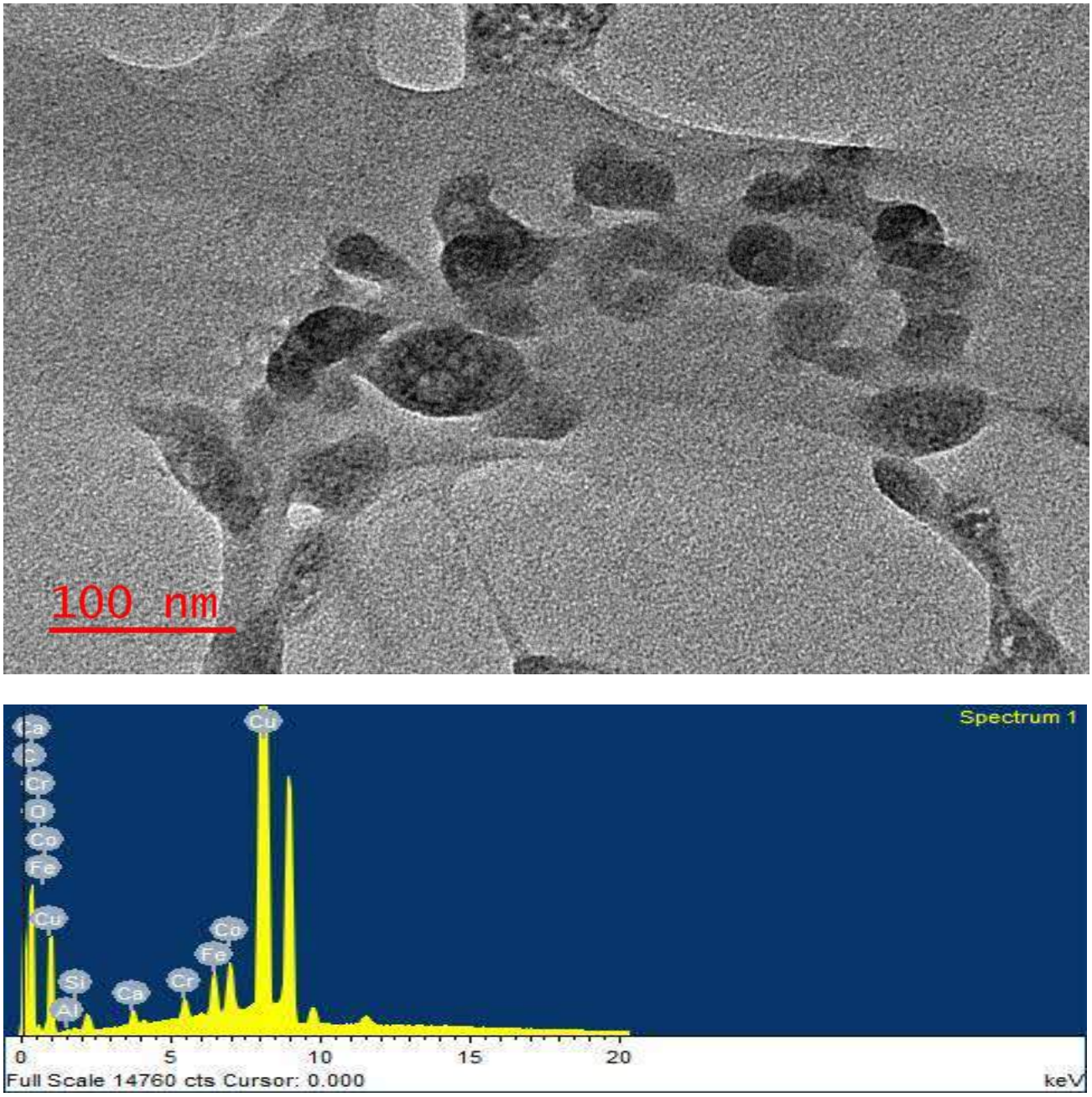

Figure 3: TEM/EDS of the Microstructure of the ESAnp

It was observed that the micro-analysis of the EDS of the ESAnp revealed the presence of C, Al, Ca and O. The higher peak of calcium (Ca) and in Figure 3 was as a result of the fact that the major constituent of ESAnp which is calcium. Also the presence of high peak of oxygen (O) may confirm that the various elements in the egg shell ash and palm kernel ash are not pure. The high carbon obtained in both samples is due to the effect of carbonization at high temperature. This is similar to the work of [7].

Figure 4 displayed the percentage by weight gain of the coating samples, while Figure 5 and give the coating thickness of the coated samples. Figure 4 it was observed that the weight increases as the wt% of ESAnp was increased, that is weight gained of: 1.92, 2.36, 2.38 2.71, 2.83% was obtained with epoxy/ESAnp coating. Similar pattern was obtained for the coating thickness. A 99.6, 130, 135, 170, 184.6 µm was obtained with epoxy/ESAnp coating. Increases in both weight gain and coating thickness could be attributed to the facts that ESAnp was able to cover the surface of the mild steel.

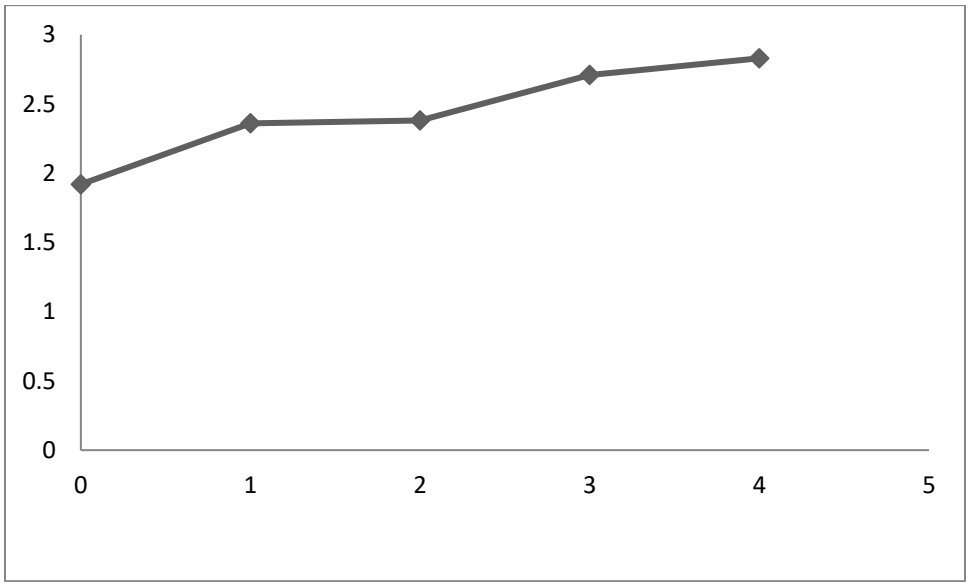

Figure 4: Percentage by weight gain of the sample

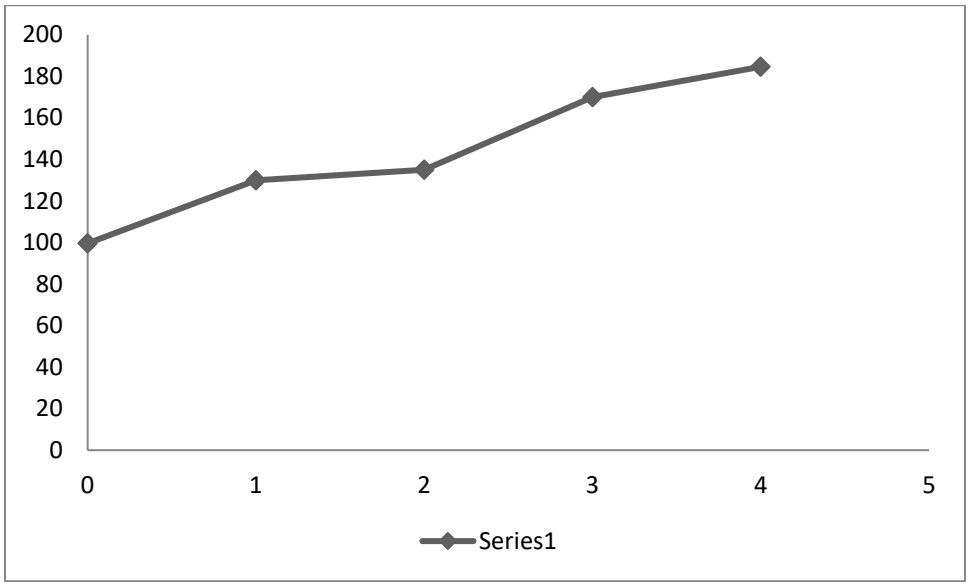

Figure 5: Coating thickness of the sample

In the Open-Circuit Potential plots shown in Figure 6, the mild steel without coating was observed to have the lowest potential of all the samples. Disparity was observed in the potential of the mild steel and the coated specimens, with that of the coated specimens tending with respect to the positive axis and that of mild steel tending with respect to the negative axis.

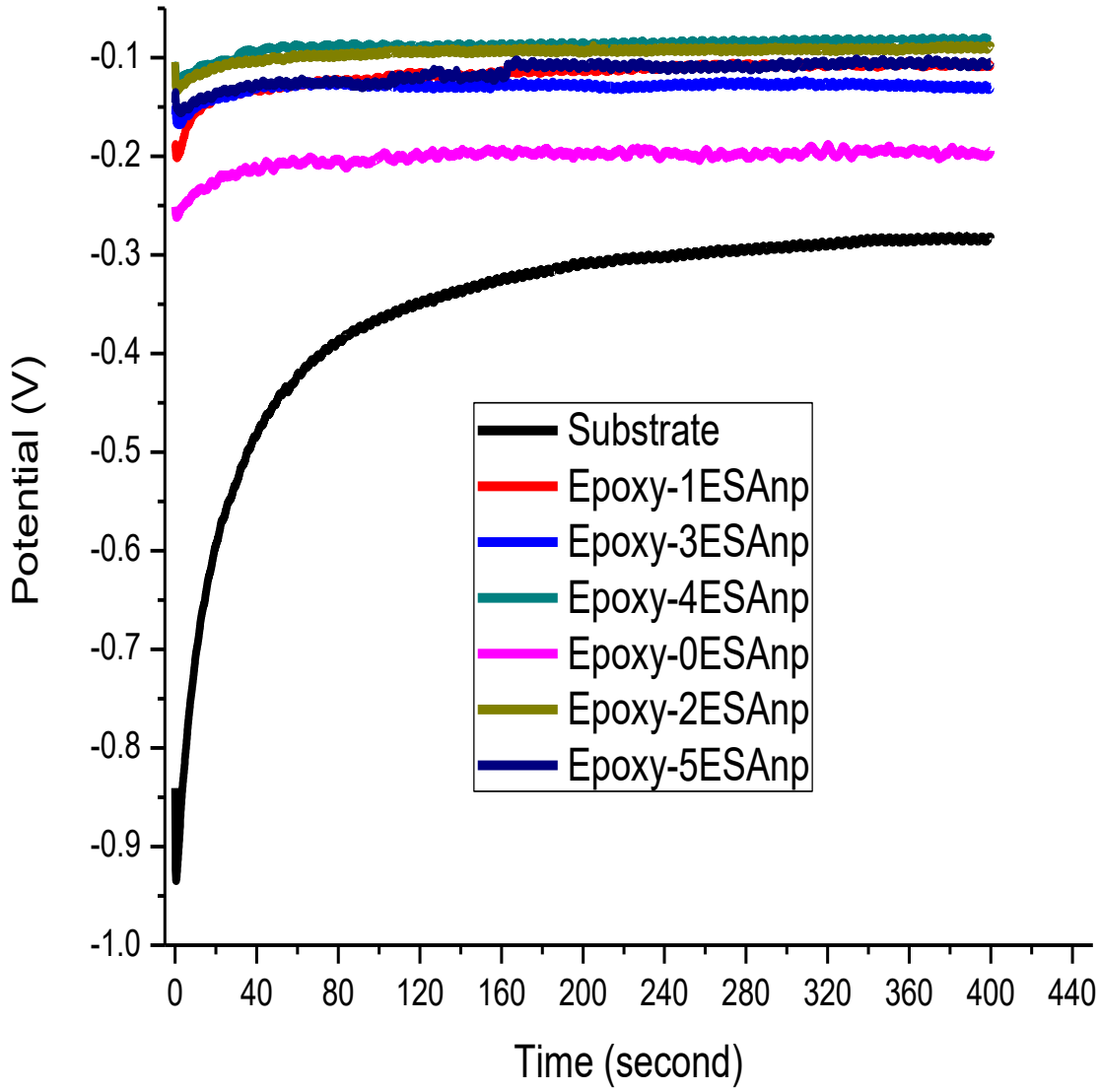

Figure 6: Open circuit potential for epoxy- egg shell ash nanoparticles coating

The investigation of the corrosion rate of the coating was carried out in simulated sea water using Tafel polarization curve. The Tafel polarization curve is shown in Figures 7 and the outcomes obtained are shown in Table 2. From Table 2, it was observed that corrosion current of the samples coated was lesser than that of mild steel alone, and the potential samples coated tending with respect to the positive axis and that of mild steel tending with respect to the negative axis of the graph. This established that the developed coating can improve the corrosion protection of the sample. From Figures 7, the observation showed that the mean potential for mild steel moved towards a lesser potential and elevated current density. With increase in %weight Eggshell ash

nanoparticles, the corrosion potential as well as the corrosion resistance of the samples increased.

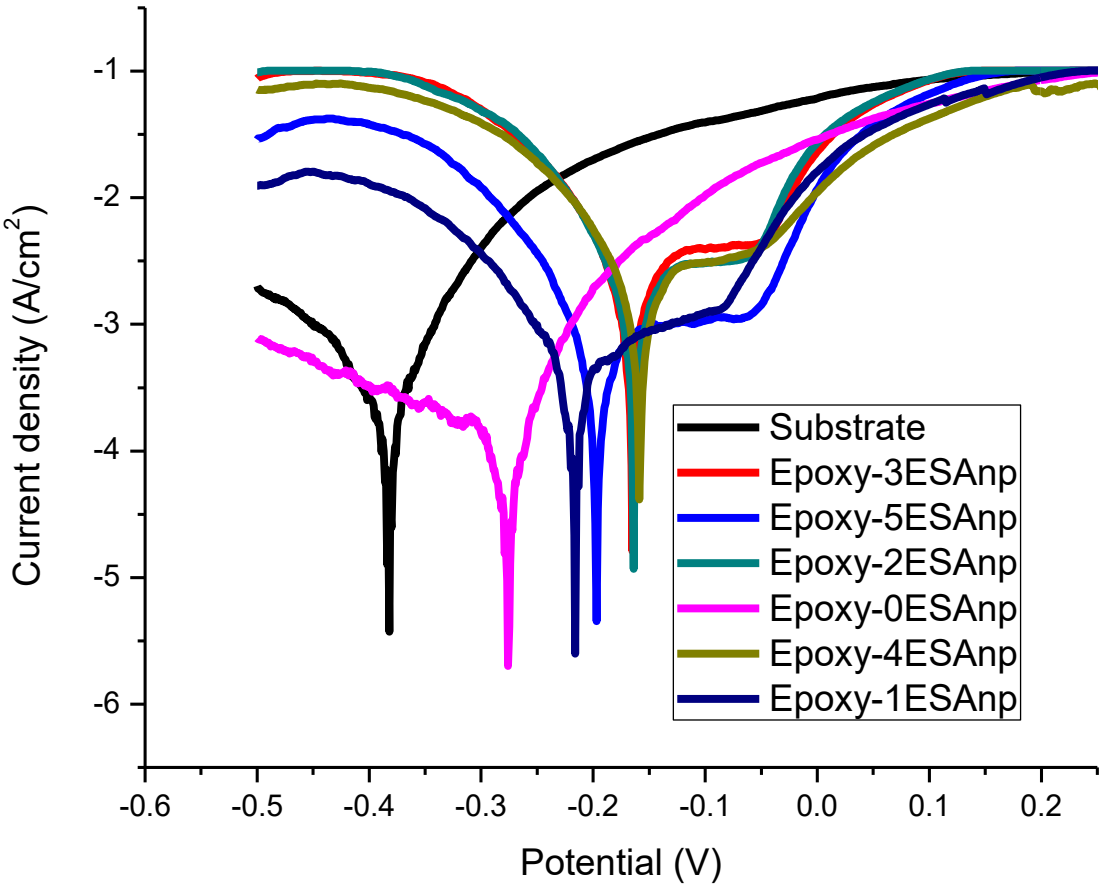

Figure 7: Tafel polarization curves for epoxy-eggshell ash nanoparticles composite coating

From Figures 8-11 shows the corrosion potential, current density, polarisation resistance and corrosion rate of the samples. Comparing Figure 8 and Figure 9, it can be seen that there is a comparable drift, meaning the higher the polarisation and potential resistance the lesser the corrosion rate and current density. This trend was anticipated since the lesser the potential the higher the predisposition for corrosion to occur. For mild steel, the corrosion potential was -0.385 the values increased to -0.289, -0.197, -0.165, -0.164 and -0.159 for epoxy-egg shell ash nanoparticles at 0, 1, 2, 3, and 4wt% (Table 2). Furthermore, the corrosion rate of the mild steel was 1150mpy this decreased to 921, 775, 293.8, 111.7 and 52.66 for epoxy- Eggshell ash nanoparticles at 0, 1, 2, 3 and 4wt%. A corrosion protection efficiency of 95.42 was obtained for the mild steel when coated with epoxy-4%wt Egg shell ash nanoparticles.

Table 2: The Tafel extrapolation results of the specimens

Specimen	Ecorr(V)/ Ag/AgCl	Icorr A/cm^2	Bc	Ba	Rp(Ω.cm^2)	CR(mpy)
	Epoxy- Egg shell ash nanoparticles coating					
Mild steel	-0.385	3.84E-3	5.810	10.757	8.7	1.150E3
Epoxy-0%wt Egg shell ash nanoparticles	-0.289	2.13e-3	8.671	4.938	9.8	9.21E2
Epoxy-1%wt Egg shell ash nanoparticles	-0.197	1.319E-3	8.719	0.971	10	7.75E2
Epoxy-2%wt Egg shell ash nanoparticles	-0.165	5.164E-4	9.559	1.099	31	2.938E2
Epoxy-3%wt Egg shell ash nanoparticles	-0.164	5.061E-4	9.434	2.996	52.3	1.117E2
Epoxy-4%wt Egg shell ash nanoparticles	-0.159	2.36E-4	3.152	9.857	141.3	5.266E1

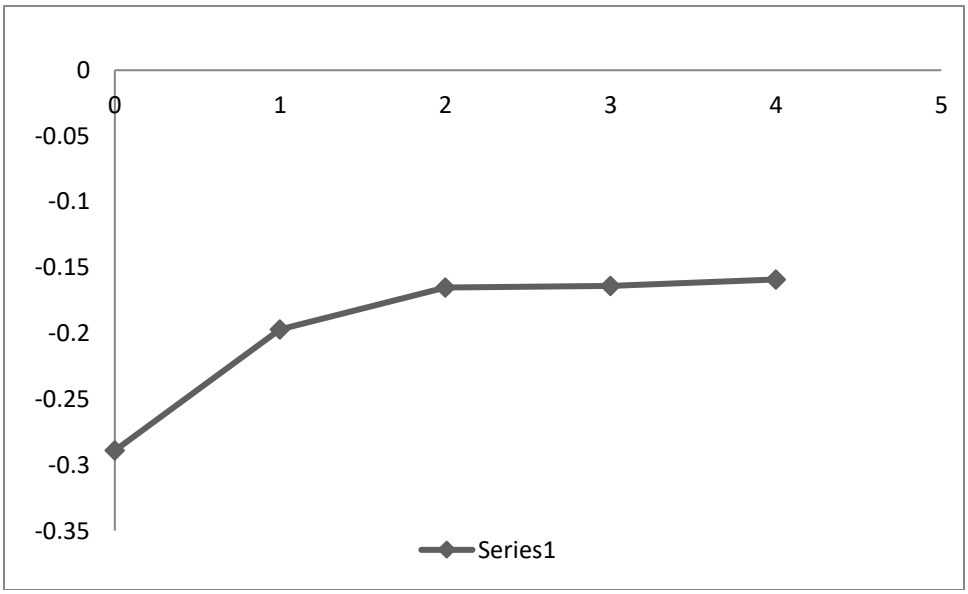

Figure 8: Variation of corrosion potential with percentage weight of coating materials

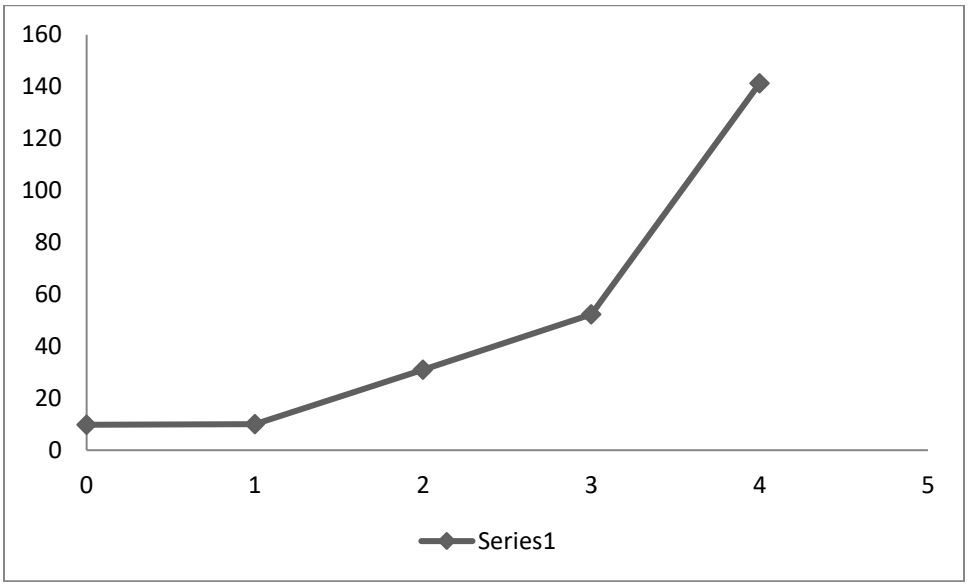

Figure 9: Variation of corrosion resistance with percentage weight of coating materials

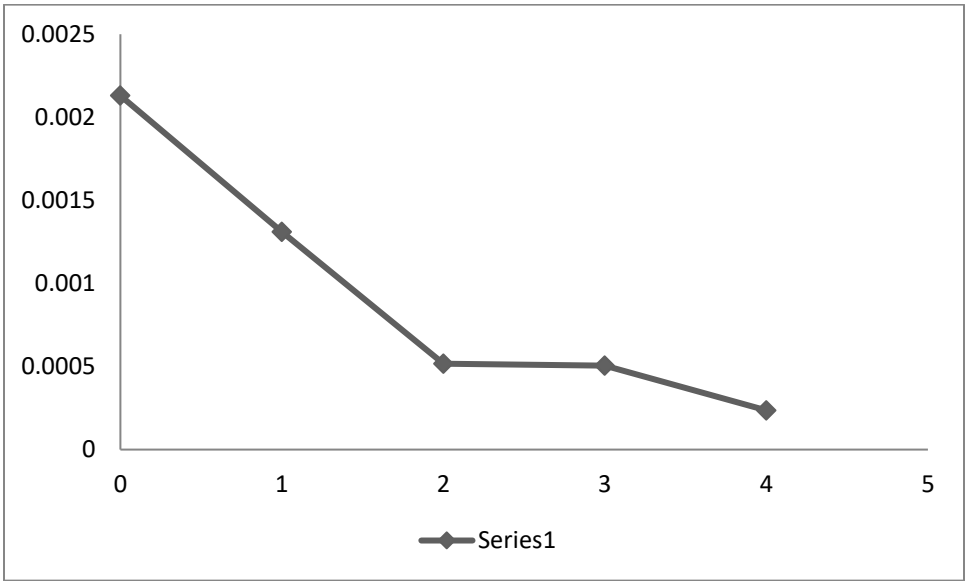

Figure 10: Variation of corrosion current density with percentage by weight of coating materials

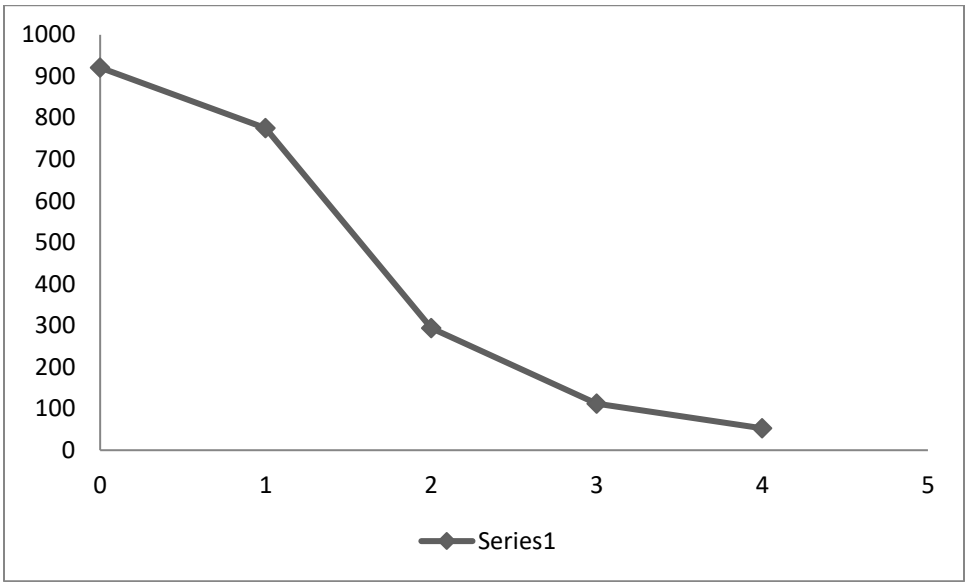

Figure 11: Variation of corrosion rate with percentage weight of coating materials

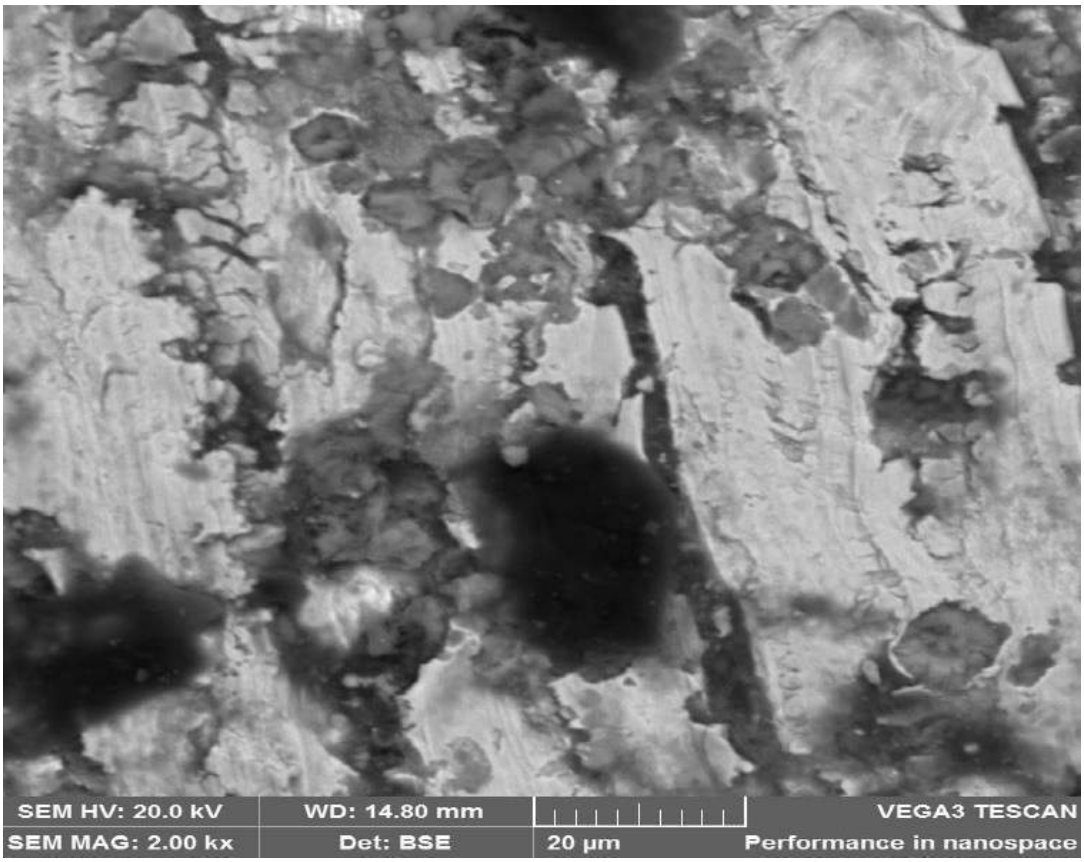

Figure 12: Scanning Electron Microscopy corrosion worn surface of the uncoated mild steel

In studying the corrosion surface of mild steel as well as its composite coatings at 0wt% and 4%wt Egg shell ash nanoparticles formulation, scanning electron microscope was used. It was seen that mild steel showed higher tendency to pitting corrosion than the samples that are coated (Figure 12).

The corroded surface of the coated sample revealed that the coating was not detached from the surface of the mild steel as a result of corrosion attack. The coating helped to cover the surface of the mild steel and made it passive to corrosion attack. (Figures 13).

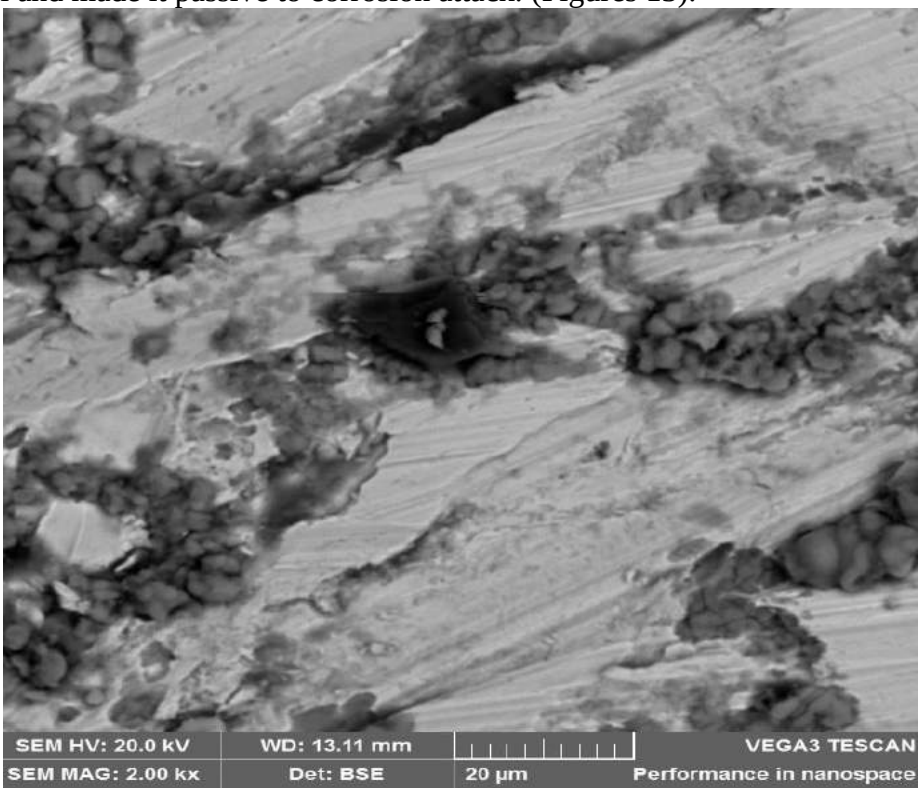

Figure 13: Scanning Electron Microscopy corrosion worn surface of the epoxy-4%wt Egg shell ash nanoparticles coated mild steel

The method of the corrosion of materials in sea water involves vigorous disbanding of mild steel in subsea water as well as electron discharge [8]. This is shown in Equations 1-2

$Fe + H_2O + Cl^-$----------$[FeClOH]_{ads}$ (1)

$[FeClOH] + H^+$ ----------$Fe^{2+} + Cl^- + H_2O$ (2)

There was a hug**e** amount of pits enveloped by iron oxide film showing that pit creation under these circumstances occurred at some point in the exposure time while iron oxide built up on the surface (Figure 12).

The sample of the composite coating contained hard phases and made the degree of damage on the sample surface low (Figure 13).

4. Conclusion

Eggshell ash was successful developed as nanoparticles using the sol-gel method, Characterization of the nanoparticles as well as the coating of the mild steel was also successfully done and the following conclusions were obtained:

1. The coating thickness increases with increases in weight percent of Eggshell ash nanoparticles
2. The coating helped to cover the surface of the mild steel and made it passive to corrosion attack
3. A Corrosion protection efficiency of 95.42% was obtained for the mild steel when coated with epoxy-4%wt Eggshell ash nanoparticles.

Acknowledgement

The first author wishes to specially acknowledge Prof. F. F. O. Orunmwense, Prof. P. O. B. Ebunilo and Dr. E. G. Sadjere for the success of this research work. My thanks also goes to all members of staff of the Mechanical Engineering Department, Faculty of Engineering, University of Benin, Benin City for the success of this work.

6. Conflict of Interest

There is no conflict of interest associated with this work.

References

[1] Ayman M. A., Hamad A. A., Ashraf M. E., Ahmed M. T. and Mohamed H. W., (2017). Effect of Titanium Dioxide Nanogel Surface Charges and Particle Size on Anti-Corrosion Performances of Epoxy Coatings, *International Journal of Electrochemical Science*, 12 (2), 959 – 974.

[2] Bagherzadeh M. R. and Mahdavi F. (2007) Preparation of Epoxy- clay nanocomposite and investigation on its anti-corrosive behavior in epoxy coating. *Progress in organic coating.* 60(2), 117-120.

[3] Durodola, B.M., Olugbuyiro, J.A.O., Moshood, S.A. Fayomi, O.S.I. and Popoola, A.P.I. (2011). Study of Influence of Zinc Plated Mild Steel Deterioration in Seawater Environment. *International Journal of Electrochemical Science.* 6, 5605-5616

[4] Ehsan B., Ali J., Zahra R., Sarah S., Mohammad R. S. (2014). Anti-corrosion hybrid coatings based on epoxy–silicanano-composites: Toward relationship between the morphology and EIS data. *Progress in Organic Coatings.* 77 (7), 1169–1183.

[5] Gleiter. H. (2000). Nanostructured materials; Basic concepts and microstructure *Acta Materialia*, 48(1), 1-29.

[6] Gohil, S.K, Chandra, R., Chalke, B., Bose, S. and Ayyub, P. (2007). Sputter deposition of self-organised nanoclusters through porous anodic alumina templates. *Journal of Nanoscience and Nanotech*nology. 7 (2), 641-6.

[7] Hassan S.B., Aigbodion V.S, and Patrick S.N. (2012) Development of Polyester/Eggshell Particulate Composites. *Tribology in Industry*. 34(4), 217-225.

[8] Hassan, S. B., and Aigbodion, V. S. (2015). Effects of eggshell on the microstructures and properties of Al–Cu–Mg/eggshell particulate composites. *Journal of King Saud University - Engineering Sciences.* 27(1), 49–56. doi:10.1016/j.jksues.2013.03.001

NIPES Conference Proceedings
The 1st International Conference of the Nigerian Institution of Professional Engineers and Scientists 7th-8th Oct. 2021: 309-317
www.nipesjournals.org.ng

Sustainable Energy Mix in Subnational and Municipal Public Infrastructure Projects

Kingsley- Omoyibo, Queeneth Adesuwa
Department of Mechanical Engineering, College of Engineering, Igbinedion University Okada, Okada Town, Edo State, Nigeria.
Email: queeneth.omoyibo@iuokada.edu.ng
Phone: +234 8141391481

Abstract
The aim of this study is to comprehensively investigate the public-private partnership (PPP) model that can be used to fund subnational and municipal public infrastructure projects as well as using it as a veritable tool for a sustainable energy mix in the contemporary socio-political era. Concurrent Triangulation Design (CTD) was used to gather data, analyze and merge final results. The model had phase 1 and 2 comprising of the quantitative and qualitative phases respectively. The four PPP models: Design, Build Finance Operator and Transfer (DBFOT), Operate Maintain and Transfer (OMT), Build Lease Operate and Transfer (BLOT) and Build Operate and Transfer (BOT) selected were analyzed using regression coefficient. A Standard deviation of 0.19508 shows that the Standard Deviation is less than 1, Coefficient of Variation < 1. The low variance recorded showed that DBFOT recorded the highest response showing that DBFOT model as the chosen in the model can be used as a veritable tool for a sustainable energy mix in municipal public private infrastructure project. DBFOT recorded 83.92% of respondents, BLOT had 8.93%,OMT had 5.36% and BOT had 1.79%, of respondents. The established funding model DBFOT in this study will be adequate in constructions of industrial waste facility, operate, maintain and provide a sound financial mechanism for industrial waste project.

Keywords**:** *Sustainable energy mix, PPP: Public-private partnership, DBFOT: Design Build Finance Operate and Transfer, BLOT: Build Lease Operate Transfer, OMT: Operate Maintain Transfer, BOT: Build Operate Transfer and Concurrent triangulation design (CTD)*

1.0.Introduction

Public-private partnership model is a funding model that finances projects. Financing waste to-energy projects with service provided by the private sector entity using the facility for a long term with operations standards [1]. In terms of energy mix, circular economy and energy recycling in Europe looked into municipal solid-waste management and waste to energy issues in terms of public-private partnership. Waste facilities were constructed, and a good financing mechanism was structured [2]. Public-private partnership has revolutionized the world through provision of infrastructure and project management [3]. The development of the urban environment using land property or facilities controlled by public sector and provision of funding by the private sector, have developed the urban environment and improved infrastructures. Public-private partnerships in urban waste water management was investigated using Adelaide experience and lessons for developing countries [4]. Research was done on PPP relationship building and how the romance of public – private partnership can be kept alive to improve infrastructural development and funding mechanisms of industrial projects [5]. China has done a lot in the area of Public – Private Partnership for improving the waste-to-energy incineration industry. The status of waste-to-energy, the opportunities from waste-to-energy as it impacts the Chinese economy and the challenges of waste-to-energy incineration were critically looked into [6]. The reason for public private partnership, viewing the policy perspective and the prospects of PPP were critically examined by looking into the 'what' and 'why' of PPP policy perspective. Issues of operating services, operating standards and pricing were resolved [7].

1.2. Municipal Public Infrastructural Projects: Public infrastructure procurement practice and challenges as studied by [8], revealed that public infrastructure plays a pivotal role in eradicating poverty and development of human capacity, owners were advised to release contract finds early enough for proper execution of projects. The law No. 73/7 of 7th December, 1973 on the preferential

claim of the treasury to safeguard public funds by municipal councils should be effectively implemented.

1.3. Gaps of Present Research: Some study examined the matrices of performance for the existing energy resource in terms of a sustainable energy solution for an envisaged energy market. A side from funding, energy is a vital agent in public-private partnership as power drives the industrial sector. This study seeks to investigate the public-private partnership (PPP) model that can be used to fund subnational and municipal public infrastructure projects as well as using it as a veritable tool for a sustainable energy mix in the contemporary socio-political era.

1.4. Energy mix

Energy mix is all direct use of energy in housing, use of energy in industrialization, energy sources from coal, oil, gas, nuclear, hydropower, solar etc. Energy mix of Nigeria is the specific combination of the different sources of energy used to meet her energy consumption needs especially for industrial purposes. Energy consumption needs: Energy used for industry purposes as PPP is a partnership before the public and private sector.

The present energy scenario and future energy mix of Bangladesh and her indigenous fuels, played a major role in electricity generation which led to the diversifiable of existing primary energy mix for ensuring long-term energy security. Bangladesh utilized renewable energy (solar energy) and imports large hydropower from neigbhouring countries through grids in the regions [11].

The study examined the matrices of performance for the existing energy resource. A long term sustainable energy solution in Bangladesh's energy market was envisaged. A side from funding, energy is a vital agent in public-private partnership power drives the industrial sector. Fossil fuels are the main source of energy for generating electricity. Industrial projects need sustainable energy (power) to function effectively. Sustainable energy mix is all renewable energy-hydroelectricity-wind biomass– wave/tidal that are of different energy sources used to meet energy needs in a region (generating power) to generate electricity supply to industries that can be replenished within a lifetime with no damage on the long run, to the planet.

1.5. Public private partnership models

Public-private partnership modes are models of funding public infrastructure project. The main principles of PPP are investing in projects, using main power, materials, budget and knowledge [9]. The private and public partners contribute to the society and do soon a commercial note. PPP are beneficial in a number of usage which are: Risk sharing, completing projects on a timely basis, funding some of the demerits are: limited influence by public sector, models adopted and investigated in this research are: Build Lease Operate Transfer (BLOT)., Design Build, Finance, Lease, Operate and Transfer (DBFLOT) and Operate Maintain and Transfer (OMT) and Build Operate and Transfer (BOT).

1.6. Build Lease Operate and Transfer (BLOT): A public private partnership model Build Lease Operate and Transfer (BLOT) is a model where a private contractor builds, handle the industrial municipal infrastructure project on a leaded public land and operates the facility for the duration of the lease once the lease is complete, and ownership is transferred to the public entity or client. A private organization designs the finance and builds a facility on a leased public land for the duration of the lease and then transfer ownership to the public organization.

BLOT model is transparent in operations and focus on core business of the cheat BLOT is a strategic partnership where a multi-disciplinary team with skill sets come together to operate and transfer. One may transfer the team to one's location and place the workforce on one payroll at the end of the project option 1 for option 2, one may continue with some contract and option 3. The team may be transferred to one's payroll and continue to lease the facility the BLOT model.

1.7. Design Build Finance, Operate and Transfer Model (**DBFOT**) Project delivery scheme involving designing building an infrastructure, operating this structure for a specific time frame and transferring the ownership of the project to the government after specific time frame. It involves a private sector awarded a contract to design, construct, finance, and operate a major project with conditions of agreement with considerations as: The private sector may be paid by the government agency from fees collected from the projects. End users while government retains ownership of the projects. It transfers procurement route is a PPP which involves private finance initiative (PFI). For design, a public body enters into a single contract, construction and full/partial private financing of a public-private facility over a contractual defined term. The main contractor is appointed to design and construct the works as opposed to a traditional contract, where the client appoints consultants to design, and the contractor assigned to construct the works.

1.8. Operate Maintain and Transfer (OMT): Operate maintain and transfer (OMT) model uses a tender process, toll contractors are appointed on an annual basis.
BLOT Build Lease Operate and transfer is a PPP model where a private contractor finances the building of an industrial waste management project on behalf of a public sector partner and thereafter, lease out the project to the client for a predetermined period or lease period.
The client occupies the project and pays rent to the contractor for a minimum term under a lease hold agreement. The level of the rent is generally a function of the total development costs including acquisition of the land, design, constructing and operating cost of the project. The contract transfers the ownership of the project to the client for a price that was agreed on previously. During the lease period, the client handles operations while the contract handles maintenance at the end of the agreement, maintain reverts back to the client.

1.9. Build operate and Transfer (BOT): Build operate transfer is a method of delivering a project for an infrastructure project of a large scale. The public sector gives concession to a private entity to construct, design, finance, own and operate the project as stated in the concession contract.

2.0. Methodology

This survey adopted a survey research design sorted to examine four PPP models namely DBFOT, BLOT, OMT and BOT, and how an established PPP model can be used as a veritable tool for sustainable energy mix in sub-national and municipal public infrastructure project. It made use of both qualitative and quantitative methods using primary data from a three (3) months extensive field investigation through administering of questionnaires, in-depth interviews on focus groups, and use of secondary data from journal articles, books, and internet to explore the research findings.

2.1. Concurrent Triangulation Design

The concurrent triangulation design (CTD) was used to analyze data in this study where both quantitative analysis using closed ended questions structured in a questionnaire survey and qualitative analysis using in-depth interview method with a thematic analysis.

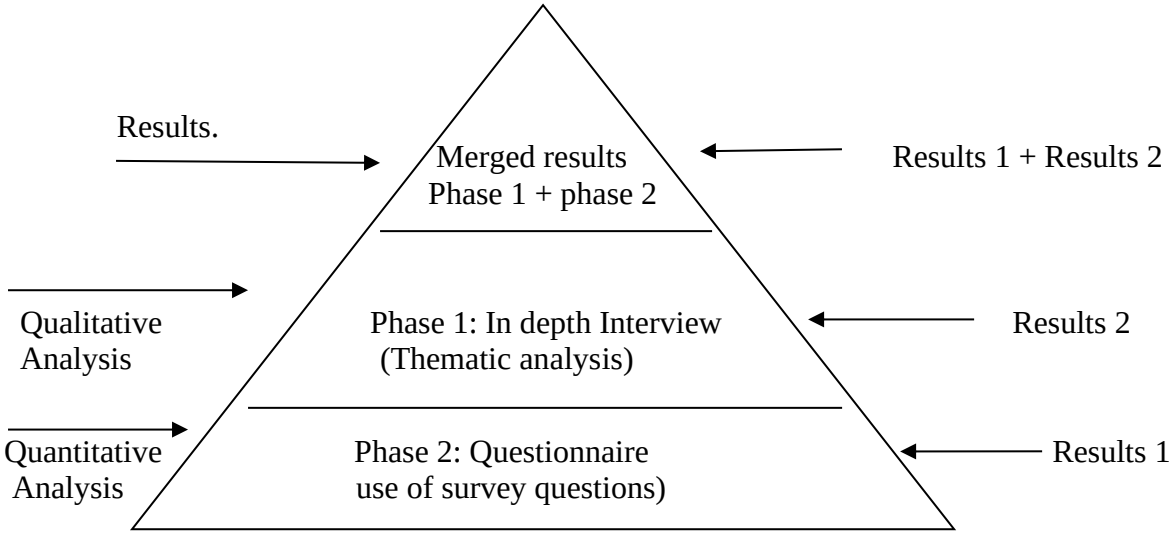

Figure 1: Concurrent Triangulation Design (CTD) source: [7]
A dedicated e-mail address was uploaded with a list of 3000 recipients imported from a CSV file closed ended questions in a questionnaire was distributed.

Phase 1: Quantitative analysis was carried out for a population of 300 respondents. 300 questionnaires were administered; only 260 questionnaires were answered and returned with 40 questionnaires unanswered.

Phase 2: For the qualitative analyses, in-depth interviews were conducted for a sample size of 30 respondents. Only 20 in-depth interviews were recorded and analyzed.
A total of 280 responses were merged, analyzed and recorded. A five point likert scale of strongly Agreed (1), Agreed (2), disagreed (3), strongly disagreed (4) and Undecided (5) were used to check for consistency of respondents on subject matter and validation was carried out. The data collected was in two sections. Section A contained socio-demographic characteristics of the respondents and section B examined the industries in Benin metropolis of Edo State, Nigeria.

3.0 Results

Table 1: Table of questionnaires and in-depth interviews found useable for PPP models. Concurrent triangulation design (CTD) (merged results (R_1 + R_2)

S/N	PPP models	Respondents	%
1.	BLOT	25	8.93
2.	DBFLOT	235	83.92
3.	OMT	15	1.79
4.	BOT	5	1.79
	Total	280	100%

Table 2: Questionnaires (R_1)

S/N	PPP models	Respondents	%
1.	BLOT	24	9.23
2.	DBFLOT	208	80.00
3.	OMT	13	5.00
4.	BOT	5	1.92

	Total	260	100%

Table 3: In-depth Interview (R_2)

S/N	PPP models	Respondents	%
1.	BLOT	1	5
2.	DBFOT	17	85
3.	OMT	2	10
4.	BOT	0	0
	Total	20	100%

Table 4: Section A: Socio-demographic Characteristics of respondents (280 persons)

	Response	Frequency	Percentage
Age as at last birthday	28 – 37	05	1.786%
	38 – 47	166	59.285%
	48 – 57	70	25.000%
	58 – 67	20	7.143%
	Above 68 years	19	6.786
		280	100%
Educational Qualification	OND	10	3.571%
	HND	40	14.285%
	B.SC	200	71.428%
	Masters	10	3.571%
	Ph.D.	20	7.145%
		280	100%
Religious affiliation	Christianity	210	75.00%
	Islam	65	23.210%
	Traditional religion	5	1.790
		280	100%

Field work, 2021

Objective 1: To examine the perceptions of engineers on public – private partnership models in the area of municipal public infrastructure projects.
Objective 2: To determine the PPP model that can be used to achieve a sustainable energy mix for municipal projects.
Section B: Selecting the most appropriate PPP model that will be a veritable tool for sustainable energy mix for municipal public infrastructure project.

Table 5: Perceptions of Engineers on the public – private partnership models

	Responses	Frequency	Percentage
Have you heard of public – private partnership (PPP)	Yes	274	97.86
	No	6	2.14
If yes, what is PPP	A partnership plan for infrastructure development, using private funding	201	71.8
	A partnership plan that encourages innovations utilizes assets and contributes to societal development	40	14.3
	A partnership that involves government and private person working together to deliver infrastructural projects and developing human capacity.	39	13.9
		280	**100%**
PPP models. DBFOT – Design Build Finance, Lease Operate and Transfer	Yes	277	98.93

BLOT – Build Lease Operate and Transfer BOT – Build Operate Transfer OMT – Operate maintain and transfer	No - -	3 - -	1.07 - -
Have you heard of these models? Which of these models is ideal for industrial development	DBFOT BLOT OMT BOT	225 35 15 5	
		280	**100%**
The DBFOT uses the private finance initiative (PFI). The private sector is highly involved.	Yes No	280 0	100 0
		280	**100%**

In support of the result in Table1, a participant gave her opinion thus: The Design Build Finance, Lease Operate and Transfer PPP model deals strictly with the private sector initiative. It has a time frame, and transfers the ownership of the infrastructure to the government after specific time frame. The main contractor, designs, builds and constructs the project. (In depth Interview word in Florson PVC Industries 20/6/2021).

Another respondent said: consultants do not design the projects and the clients do not appoint consultants to design the project and the private sector involved in the project may be paid by the government agency from monies collected from the project. (In depth interview from worker in Mouka Foam Manufacture Industries, 20/6/2021).

Objective 3: Impact of energy mix on the four PPP to examine the models DBFOT, BLOT, OMT, BOT and on municipal public infrastructure projects.

Table 6: Responses

	Response	Frequency	Percentage
What is energy mix?	Energy mix is all direct use of energy. Combination of different sources of energy to meet energy consumption needs for industrial purposes.	80 200	28.57 71.43
		280	**100%**
Energy mix has impact on the PPP models that later impacts on industrial projects?	Yes No	271 9	96.79 3.21
		280	**100%**
If yes, what are the impact	Industrial projects need sustainable energy to function effectively	11	3.92
	A sustainable energy mix using all renewable energy from different energy sources like solar, wind, tidal etc that can be replenished within a lifetime, has an impact on the function ability of the PPP models and the municipal public infrastructure project.	269	96.07
		280	**100%**

Field work 2021.

Table 7: Types of PPP models available to be used as a veritable tool for a sustainable energy mix in municipal public infrastructure projects.

	Response	Frequency	Percentage
How many types of PPP model do you know?	5 types	56	20
	4 types	96	34
	7 types	100	35
		280	**100%**
What is the type of PPP model that is common in PPP practices in Nigerian infrastructure projects sponsored using PPP?	DBFLOT BLOT OMT BOT	248 12 10 10	88.57 42.9 3.57 3.57
		280	**100%**
Which of these PPP model have been executed and seen to be most function for Nigerian government as regards PPP?	DBFLOT BLOT OMT BOT	199 31 10 10	71.07 11.07 3.57 14.29
		280	**100%**
Do you think that DBFLOT has worked, for all PPP contracts executed in Nigeria for infrastructure development?	Yes No	272 08	97.14 2.86
		280	**100%**
Have you seen project that were executed using the DBFLOT	Yes No	276 04	98.57 1.43
		280	**100%**

Field work 2021.

Table 8: Socio-economic and political impact of PPP models used for infrastructure development

	Response	Frequency	Percentage
The issue of contractors not being paid is a political issue.	Yes	274	97.86
	No	06	2.14
		280	**100%**
	Yes No	211 19 50	75.36 6.79 17.85
		280	**100%**
	Yes No	249 31	88.93 11.07
		280	**100%**
Do you think the government and private sector can always do a lot in the area of PPP?	Yes No	251 29	89.64 10.36
		280	**100%**
What can be done to improve on industrial development as regards building more infrastructures? Which of these PPP model is most preferred?	-1. DBFLOT -2. BLOT -3. OMT -4. BOT	110 77 93 0	39.29 27.50 33.21 0
		280	**100%**
Does private partnership impact on government projects?	Yes No	271 19	96.70 3.21
Do you think the private sector should passively invest on government projects?	Yes No	261 19	93.21 6.70
		280	**100%**
	Yes	219	78.21

Should the private sector initiative transfers ownership of infrastructure to government after time frame?	No	61	21.79
		280	**100%**
Do you think consultants should design project?	Yes	270	96.43
	No	10	3.57
		280	**100%**
Government should provide a sound financing mechanism for government projects and build sustainability.	Yes	269	96.07
	No	11	3.93
		280	**100%**

Field work, 2021

3.1. Hypothesis Testing:

Objective 1:

To examine the perception of engineers in the area of municipal public infrastructure projects on public – private partnership model: Design Build Finance Operate and Transfer.

With regards to PPP projects financing, assets, utilization, construction, operations and maintenance of public infrastructure projects. It looked into the area if the model selected helping to attract technical expertise for industrial development. Engineers from their perspectives, showed that PPP models are important parameters and majority of them agreed that PPP models was ideal with positive perceptions.

Objective 2:

To determine the PPP model that can be used to achieve a sustainable energy mix for municipal public infrastructure projects. From results, advocacy have been provided for makers of policy in the area of PPP models selecting and DBFOT model was the PPP model selected by most respondents as the appropriate model to faster sustainable energy mix, boost private finance initiative, government owning projects after executing of projects, the funding will provide.

Objective 3

To examine the impact of energy, mix on the four PPP models: BLOT, DBFOT, OMT, BOT and how each model impacts on municipal public infrastructure projects.

Objective 4

To identify mechanism to ensure that the four PPP models: BLOT, DBFOT, OMT and BOT are used as prompt intervention for assist. Energy mix in sub-national and municipal public infrastructure projects.

3.2 Findings

1. This study has comprehensively enlightened engineers on the subject Public Private Partnership (PPP) Models: BLOT, DBFOT, OMT and BOT, with regards to financing, assets utilization, operations and maintenance of public infrastructures.
2. Examinations of the perception of engineers in the area of municipal public infrastructure projects on public – private partnership model: Design Build Finance Operate and Transfer were carried out.
3. The PPP model that can be used to achieve a sustainable energy mix for municipal public infrastructure projects was determined. From results, advocacy have been provided for makers of policy in the area of PPP models selection. DBFOT model was the PPP model selected by most respondents as the appropriate model to foster sustainable energy mix and boost private finance initiative.

4. Examination of the impact of energy mix on the four PPP models: BLOT, DBFOT, OMT, BOT and how each model impacts on municipal public infrastructure projects have been carried out. Mechanism to ensure that the four PPP models: BLOT, DBFOT, OMT and BOT are used as prompt intervention for energy mix in sub-national and municipal public infrastructure projects have been identified.

4.0 Conclusion

The perceptions of engineers on public – private partnership models in the area of municipal public infrastructure projects were examined. The PPP model that can be used to achieve a sustainable energy mix for municipal projects have been determined. The impact of energy mix on the four PPP models: BLOT, DBFOT, OMT, BOT and how each model impacts on municipal public infrastructure projects has been examined. The mechanism to ensure that DBFOT, BLOT, OMT and BOT are used as prompt interventions for a sustainable energy mix in a sub-national and municipal public infrastructure project has been identified. The mechanisms are: Planning, outlining the business case, publication of tender notice, prequalification of bidders, shortlisting bidders, negotiation, receipt of bid, issue of bid as regards best offer and final offer and invitation to tender. The most appropriate PPP model that will be a veritable tool for sustainable energy mix for municipal public infrastructure project has been selected to be the Design, Build, Finance, Operate and Transfer (DBFOT) Model as it impacts on energy positively. This model will be able to deliver improved services and produce better value for money by encouraging innovation, greatest asset utilization and integrated white whole-of-life management.

Conflict of interest

There is no conflict of interest.

References

[1] Caiyun Cui, Yong Liu, Bo Xia, Xiaoyan Jiang, Martins Skotmore (2020) overview of public private partnership in the waste- to- energy incineration industry in china: status, opportunities and challenge International journal of strategic reviews vol 32 (I): 3-14

[2] Finlayson, J. (2002), Urban development through PPPs in the Euro – Mediterranean region, Journal of Environmental Quality Vol 17 (5): pp599 – 610.

[3] Ganesh Keremane (2012) Public Private Partnership in Urban Waste water managements: The Ade/ aide experience and lesson for developing countries. Economic Journal of development issues vol 13 & 14 No1-2 (combined issues) pp 34- 50.

[4] Gregor Schwerhoff (2018) Renewable energy potentials and achieving sustainable energy in Africa. Canadian journal of Economics vol 51(1): pp 236 – 274.

[5] Huang, J. (2018) creating an enabling environment for public- private partnership in waste-to-energy projects No58 December Asian Development Bank for sustainable development working paper series.

[6] Jeff Delmont (2021) ppp relationship building keep the romance alive Elsevier Journal. pp 101.

[7] Kingsley – Omoyibo, Q. A: Concurrent triangulation Design (CTD) diagram (2020). Unpublished

[8] Malinauskaite J. Spencer, N. (2017) municipal solid waste management and waste-to-energy in the context of a circular economy and energy recycling in Europe Journal of energy. Science direct.com Vol 14; pp 2013 – 2044.

[9] Nong, H.N., Fombe, L.F, Achankong E, Fombe, G.M (2021) public infrastructure procurement Practice and Challenge in the Bamenda municipality North West region Cameroun journal of Advancement in social science research vol 18 (4): pp 646- 661.

[10] N.K. Das and Martin, M.A. (2020) present energy scenario and future energy mix of Bangladesh International Journal of energy strategy reviews vol 32 (1): pp 100576.

[11] United Nation Developments programs (1999) public private partnership for the urban environment UNDP/ PPPUE Conference paper series, vol III: UNDP, New York.

[12] Wolf, P.E & Palaniappan, M (2004) public or private water management? Culturing the Gordian knot. Journal of water resources planning of management vol 130(I) pp. 1- 3.

NIPES Conference Proceedings
The 1st International Conference of the Nigerian Institution of Professional Engineers and Scientists 7th-8th Oct. 2021: 318-335
www.nipesjournals.org.ng

Quantitative Analysis of Phytochemical Constituents and Invitro Antioxidant Potentials of Poly-Herbal Formulation

Oshomoh, E. O., Uwaya, D. O. and Uzama-Avenbuan, O.

Department of Science Laboratory Technology, Faculty of Life Sciences, University of Benin. Edo State. Nigeria.
Corresponding Author: Oshomoh, E. O. E-mail: emmananuel.oshomoh@uniben.edu; Tel: 08055452141

Abstract

Plants of medicinal value have contributed to the health of many individuals and to the world in general. Vernonia amygdalina, Greenwayodendron suaveolens, Euphorbia heterophylla and Xylopia aethiopica are all known to have medicinal values varying in their effect. The quantitative analysis of phytochemical constituents and some invitro antioxidant properties of Greenwayodendron suaveolens, Vernonia amygdalina, euphorbia heterophylla and Xylopia aethiopica leaves were determined. Phenols, flavonoids, tannins, saponins and tannins were the phytochemicals detected from the plants. The determination of the macro and micro elements such as iron, manganese, potassium, calcium, magnesium, copper, lead, cadmium, chromium, and nickel was made directly on each final solution using flame photometer and a Bulk Scientific 210 VGP, atomic absorption spectroscopy (AAS). The 1, 1-Diphenyl-2-picrylhydrazyl (DPPH), 2, 2-azino di-(3-ethylbenzothiazoline- 6-sulfonic acid) (ABTS), hydroxyl free radical (OH-) and ferric reducing antioxidant power (FRAP) were analyzed using one way analysis of variance (ANOVA), $P<0.05$ was obtained. In DPPH, ABTS, FRAP and OH- scavenging activities, Vernonia amygdalina, Greenwayodendron suaveolens and Euphorbia heterophylla was found to have scavenging activities which increased as their concentrations increase. The medicinal potential of these plants could be as a result of their phytochemicals, micro and macro elements and their free radical scavenging abilities. More research needs to be carried out to further prove their anti-oxidative potentials.

Keywords: Invitro, antioxidant, poly-herbal, phytochemical, mineral elements

1.0 Introduction

Medicinal plants have contributed to the health of many people and throughout the world due to the presence of biologically active ingredients such as alkaloids, tannins, flavonoids and phenolic compounds. Many of these native medicinal plants are used as herbs and food in order to achieve specific physiological effects in the individual body. Pregnant and lactating women sometimes eat it because of its medicinal properties [1]. The four plants used to formulate the poly-herbal drugs are *Greenwayodendron suaveolens, Xylopia aethiopica, Vernonia amygdalina* and *Euphorbia heterophylla. Greenwayodendron suaveolens* is a species of plant in the genus *Greenwayodendron*, and a member of the Annonacea family. It is a monophyletic tree genus from tropical Africa. It is widely distributed in Western and Central Africa from Ivory Coast to Angola [2]. It is deciduous, medium sized to fairly large tree up to 35-45 meters tall, has bole branches for up to 25 m, straight, cylindrical and sometimes grooved at the base [3].

The plant is used alone or in mix with other plants for the treatment of various diseases, including parasitic diseases such as uncomplicated malaria and Helminthiasis [4]. In general, this plant is used as a water extract or as an enema for back pain, sexual weakness, headaches, malaria, loss of appetite, snake pain, pelvic pain, hepatitis, epilepsy, insanity, rheumatism, constipation, abdominal pain, pain gear and many more [5]. Despite its bitter taste, the leaves are sometimes eaten by several species of monkeys, as reported by some Nkundo hunters. In some areas in the Central African Republic and in Cameroon, the leaves of this forest tree, also called "ancient tobacco" or "forest tobacco", are used and evaluated as cigarettes [6,7].

Xylopia aethiopica belongs to the kingdom Plantae, Division Tracheophyta (vascular plant), Class Magnoliopsida, Family Annonaceae and Genus Xylopia. It is fragrant tree with a height of more than 20 m and a diameter of 60 to 75 cm. The fruit is cylindrical pods which are attached with a width of 2 to 3 mm. It is a native of the lowland rainforest and moist fringe forests in the savanna zones of Africa. Its common names are Ethiopian pepper, negro-pepper and spice tree [8].

Plate1: *Greenwayodendron suaveolens* plant

Plate 2: *Xylopia aethiopica*

Plate 3: *Vernonia amygdalina* plant

Plate 4: *Euphorbia heterophylla* plant

Xylopia aethiopica grows in Tropical Africa, in forest areas and especially in rivers and in arid regions [9].

A number of studies have confirmed the anti-inflammatory and antipyretic properties of this herb. The seeds of *Xylopia aethiopica* are known for their many medicinal properties. In Africa, it is used as a spice and local medicine to treat diarrhea, colic, snake disease, cardiovascular disease, diabetes, treatment and treatment of sexually transmitted infections in southern Nigeria [10].In Nigeria, fruit extracts and bark extracts are used to treat bronchitis, bile and dysentery. Fruits are used to neutralize karmic pain and laxatives, and are believed to increase fertility and provide assistance [11]

Vernonia amygdalina, belongs to the kingdom Plantae, phylum tracheophytes, Class Angiosperm, Order Asterales, Family Asteraceae and Genus *Vernonia*. It is a small shrub that grows in tropical

Africa to a height of 2-5 m. The leaves are elliptical and up to 20 cm in length and also have a rough bark [12] It is commonly called bitter leaf in English due to its bitter taste. Other common names include grawa (Amharic), ewuro (Yoruba), etidot (Ibibo), onugbo (Igbo), ityuna (tiv), oriwo (Edo), awonwono (Akan), chusar-doki (Hausa), mululuza (Luganda), labwori (Acholi), olusia (Luo) and ndoleh (Cameroon) [13]

V. amygdalina is a native plant that is widely used in Nigeria for therapeutic and nutritional purposes. It grows in a number of ecological zones in Africa, producing large amounts of food and is drought resistant [14]. Bitter taste is caused by nutrient inhibitors such as alkaloids, saponins, tannins, and glycosides [15].

Macerated leaves from plants are consumed as vegetables and herbs, while water extracts serve as a tonic for the prevention of several diseases. It has been reported that *V. amygdalina* is used by wild chimpanzees for the treatment of parasitic diseases in Tanzania [16]. Philips *et al.* (1993) reported the antiplasmodial effects of the lactone and steroid sesquiterpene constituents of *V. amygdalina* were also effective against *Plasmodium falciparium* invitro. *V. amygdalina* (Bitter leaf tea) is also used throughout West Africa for the treatment of diabetes and other metabolic diseases related to the liver [17]. This plant has recently gained special importance because it has been shown to be active in the treatment of humans against HIV/AIDS and has strong antimalarial and anthelmintic properties [18] and antitumorigenic properties [19]. In Ghana, young leaves rather than old ones have been proven with animal models to have antidiabetic and anti-inflammatory activities [20]. Pharmacological studies also show that leaf extracts have hypoglycemic and hypolipidemic properties in experimental animals and can thus be used to treat diabetes [21]. Uhegbu and Ogbechi (2004) reported the antidiabetic effect of water extracts from the leaves of *Vernonia amygdalina.* Sesquiterpene lactone extract from leaves has an anti-hepatotoxic effect in rats on carbon tetrachloride (CCl_4) induced liver damage. *Euphorbia heterophylla* belongs to the kingdom: Plantae, phylum: tracheophytes, Class: Angiosperm, Class: Eudicots, Order: Malpighiales, Family: Euphorbieae, Genus: *Euphorbia* [22]. Some of the common names are Mexican fireplant, Japanese poinsettia, fire on the mountain, painted spurge, milkweed and kaliko plant. It grows between 30 and 100 cm tall and has hollow stems that may branched or with simple ribs that are angular in shape [23].

In general, Euphorbia with around 1,600 species, have adhesives such as latex milk [24]; some are carcinogenic, very irritating to the skin and toxic to livestock and humans [25]. Euphorbia plants are widely distributed in nature, ranging from plants and shrubs to trees in tropical and temperate regions of the world [26].

Euphorbia heterophylla leaf is used in traditional medical practice as a laxative, anti-gonorrhoea, migraine, and wart. Plant lattices have been used as fish poisons, insecticides, and poisons [27]. In some parts of Kogi, Nigeria, the leaves are used as an anticonvulsant and cough medicine. It has been reported that *E. heterophylla* leaves contain quercetin [28] and diterpenoids in the roots [29] *E. heterophylla* leaves have also been reported to have skin irritation, antitumor / anticancer which stimulates tumors and, more recently, anti-HIV euphorbia activity [30] *E. heterophylla* is a medicinal herb commonly referred to as "weed bush". It grows in semi-humid places, especially in cassava, grape and soybean plantations. However, chemical research reports about *E. heterophylla* are rare. It is known that the leaves have an antibacterial effect [31]. In the Nigerian

Igbo community, *E. heterophylla* is used as a scavenger. Extracts for exfoliation of leaves are also used to treat respiratory infections and asthma by traditional medical practitioners [32].

The aim of this current study is to evaluate the antioxidant properties of *Greenwayodendron suaveolens, Vernonia amygdalina,* and *Euphorbia heterophylla,* elemental analyses and phytochemical studies on *Greenwayodendron suaveolens, Vernonia amygdalina, Euphorbia heterophylla and Xylopia aethiopica*.

2.0. Materials and Method

2.1. Sample Collection and Identification

Greenwayodendron suaveolens plant was obtained from the Department of Plant Biology and Biotechnology, Faculty of Life Sciences, University of Benin, Benin City. *Vernonia amygdalina* plant was collected from Ikpoba Hill in Ikpoba Okha Local Government Area, Edo State. *Xylopia aethiopica* plant was collected from Uselu market in Egor Local Government Area, Edo State. *Euphorbia heterophylla* plant was collected from Afeye Okpameri, Akoko-Edo Local Government Area, Edo state.

2.2. Plant Sample Treatment

The plant sample was washed thoroughly in clean water, the fruits of *Xylopia aethiopica* and the leaves of *Vernonia amygdalina, Greenwayodendron suaveolens,* and *Euphorbia heterophylla* plant were destalked and air-dried at room temperature for two weeks to achieve a sum total drying of the leaves and then pulverized into fine powder and weighed with standard weighing scale.

2.3. Method of Extraction

A total of 1000 g of powdered leaves of *Greenwayodendron suaveolens,* 1000 g of *Vernonia amygdalina,* 250 g of *Euphorbia heterophylla* and 310 g of *Xylopia aethiopica* were dissolved in 10 litres, 10 litres, 2.5 litres and 3.1 litres of distilled water respectively. The mixtures were left to stand for four (4) days with continuous stirring, after which they were filtered and the filtrates of each was concentraed and stored in the fridge.

2.4. Determination of antioxidant properties.

The antioxidant property was carried out on the aqueous extracts of *Vernonia amygdalina, Greenwayodendron suaveolens,* and *Euphorbia heterophylla* only.

2.5. DPPH (1, 1-Diphenyl-2-picrylhydrazyl) Scavenging Activity

The scavenging ability of the natural antioxidants of the plants extracts towards the stable free radical of DPPH was measured by the method of [33].

2.6. ABTS [2, 2-azino di-(3-ethylbenzothiazoline- 6-sulfonic acid)] Scavenging Activity

The stock solutions included 7.4 mM $ABTS^{+}$ solution and 2.6 mM potassium persulfate solution. 2, 2-azino di-(3-ethylbenzothiazoline- 6-sulfonic acid). The working solution of ABTS was obtained by the stock in methanol to give absorbance of 0.70 at 734 nm. ABTS was measured by the method of [34, 35]

oh^- free radical
OH^- free radical scavenging method was described by Elizabeth and Rao (1990) with modified by [36].**FRAP** (Ferric Reducing Antioxidant Power) FRAP was measured with the method described by [37].

2.7. Quantitative Phytochemical Composition of Aqueous Extracts of *Greenwayodendron suaveolens, Vernonia amygdalina, Euphorbia heterophylla and Xylopia aethiopica*

2.8. Total Phenolic Content Determination
The amount of total phenolics in extract was determined according to the method of [38] with slight modification using tannic acid as a standard.

2.9. Alkaloids Content Determination
The total alkaloid content was measured using the method described by Harborne in 1973.

2.10. Flavonoid Content Determination
The flavonoid content was determined on triplicate aliquots of the homogenous cabbage extract (1.5 g) [39].Thirty-microliter aliquots of the methanolic extract were used for flavonoid determination. Samples were diluted with 90 µl methanol, 6 µl of 10 % Aluminum chloride ($AlCl_3$), 6 µl of 1mol/l Sodium acetate (CH_3CO_2Na) were added and finally 170 µL of methanol was added. The absorbance was read at 415 nm after 30 min. Quercetin was used as a standard for calculating the flavonoid content (Ug Qe/g).

2.11. Total Saponins Content Estimation
Estimation of total saponins content was determined by the method described by Makkar *et al in* 2007 based on vanillin-sulphuric acid colorimetric reaction with some modifications.

2.12. Tannins Content Determination
Exactly 0.20 mL of sample was added to 20 mL of 50% methanol and placed in a water bath at 77 ^{0}C – 80 ^{0}C for 1 hour and shaken. The extract was quantitatively filtered using a double layered Whatman No.1 filter paper and 20 mL of distilled water, 2.5 mL Folin-Denis reagent and 10 mL 17% Na2CO3 were added and mixed. The mixture was allowed to stand for 20 min. A series of standard tannic acids solutions were prepared in methanol and their absorbance as well as samples was read after colour development on a UV/ Visible spectrophotometer at a wavelength of 760 nm. Total tannin content was calculated from calibration curve.

2.13. Determination of Total Nitrogen
A modified method of micro-Kjeldahl as described by [40] was used for crude protein determination. Procedure for digestion: Three grams each of the defatted samples were separately weighed on pre-weighed into micro-Kjeldahl digestion flask together with few anti-bumping granules. Two grams of catalyst mixture ($CuSO_4$: Na_2SO_4: SeO_2, 5:1:0_2 w/w) was added to each flask and then 10 mL nitrogen free concentrated H_2SO_4 also added to each flask. The flasks were placed in inclined position on a heating mantle in a fume cupboard. Digestion was started at temperature of 30 ^{0}C until frothing ceased and then heating was increased to 50 ^{0}C for another 30 mins and finally at full heating (100 ^{0}C) until a clear solution was obtained. Simmering was continued below boiling point for another 30 min to ensure complete digestion and conversion of nitrogen to ammonium sulphate. After digestion was completed, samples were allowed to cool and

then transferred quantitatively to 100 mL volumetric flasks with washing and cooling to room temperature. Volumes were made up to mark with distilled water.

1. 5 ml of the filtrate from the digest was transferred with the aid of a 10 ml pipette into a 25 ml standard flask. 2.5 ml of the Alkaline Phenate was added and the solution shaken to mix properly. Then 1 ml of Sodium Potassium Tartarate was added, shaken properly followed by the addition 2.5 ml of sodium hypochlorite. There after the solution was made up to the 25 ml mark with distilled water and the absorbance of the resultant solution measured with the aid of UV/Visible Jenway6715 Spectrophotometer, at 630 nm. The Nitrogen standards were treated the same way with the sample.

$$N\ (mg/kg) = \frac{\text{Instrument Reading } \mathbf{X} \text{ Slope Recip } \mathbf{X} \text{ Color Vol. } \mathbf{X} \text{ Digest Vol.}}{\text{Weight of Sample } \mathbf{X} \text{ Aliquot Taken}} \quad (1)$$

2.14. Digestion of Samples

The digestions of the samples were done in accordance with the method described by Akan *et al in* 2013, with little modification.

2.15. Metals Analysis

The metals of interest in this study are Iron, Manganese, potassium, calcium, magnesium, copper, lead, cadmium, chromium, and nickel. The determination of these metals in the samples was made directly on each final solution using Flame Photometer and a Bulk Scientific 210 VGP, and Atomic Absorption Spectroscopy (AAS).

2.16. Statistical Analysis

The data were expressed as mean ± standard error of mean (SEM) and 'n' represents the number of replicates. One way Analysis of Variance (ANOVA) was performed with Newman Keul's post hoc test. All data were analyzed using graph Pad Prism (UK) software version 6. $P<0.05$ indicates significant difference between compared data.

3.0. Results

Table 1: Quantitative analysis of Phytosterols present in *Greenwayodendron suaveolens, Vernonia amygdalina and Euphorbia heterophylla* and *Xylopia aethiopica*.

Samples	Total tannin (ug/ml)	Total flavonoid (ug/ml)	Total phenols (ug/ml)	Total saponin (ppm)	Total alkaloid (%)
Greenwayodendron suaveolens	6.575	20.323	20.330	2.259	1.600
Vernonia amygdalina	8.493	44.839	25.275	2.657	0.800

Euphorbia amygdalina	8.356	33.065	17.033	1.904	1.200
Xylopia Aethiopica	12.468	41.935	24.835	3.096	0.600

Table 2: Elemental analysis of Macro and Micro nutrients of the aqueous extract of *Greenwayodendron suaveolens*, *Vernonia amygdalina*, *Euphorbia heterophylla* and *Xylopia aethiopica*.

S/N	Parameters	A	B	C	D
1	Calcium (Mg/Kg)	75.00	48.00	56.00	15.00
2	Copper (Mg/Kg)	0.2	0.24	0.21	0.28
3	Iron (Mg/Kg)	4.800	3.400	2.900	10.500
4	Magnesium (Mg/Kg)	70.10	63.00	112.00	83.01
5	Manganese (Mg/Kg)	0.73	0.66	1.19	0.86
6	Cadmium (Mg/Kg)	0.1	BDL	BDL	0.1
7	Chromium (Mg/Kg)	0.05	0.09	0.01	0.03
8	Lead (Mg/Kg)	BDL	BDL	BDL	BDL
9	Potassium (Mg/Kg)	136.2	177.1	80.2	74.10
10	Nickel (Mg/Kg)	BDL	BDL	BDL	0.1
11	Nitrogen (%)	0.5690	0.3456	0.2950	0.2571
12	Phophorus (Mg/Kg)	54.404	56.411	18.135	54.404

Keys: A= *Greenwayodendron suaveolens;* B= *Vernonia amygdalina*; C= *Euphorbia heterophylla*; D= *Xylopia aethiopica;* BDL= Below Detection Limit.

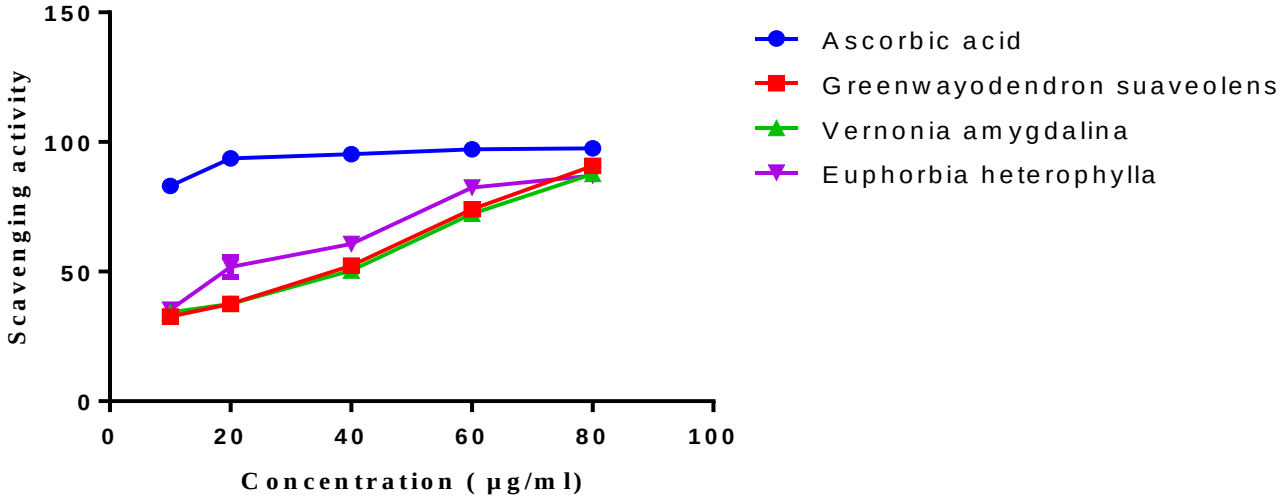

Figure 1: DPPH scavenging activity of Ascorbic acid, *Greenwayodendron suaveolens, Vernonia amygdalina and Euphorbia heterophylla*.

Greenwayodendron suaveolens, Vernonia amygdalina and Euphorbia heterophylla shows DPPH scavenging activities. The scavenging power of the plants increases as the concentration increases. At 80µg/ml, the scavenging activities of the plants are comparable to that of ascorbic acid.

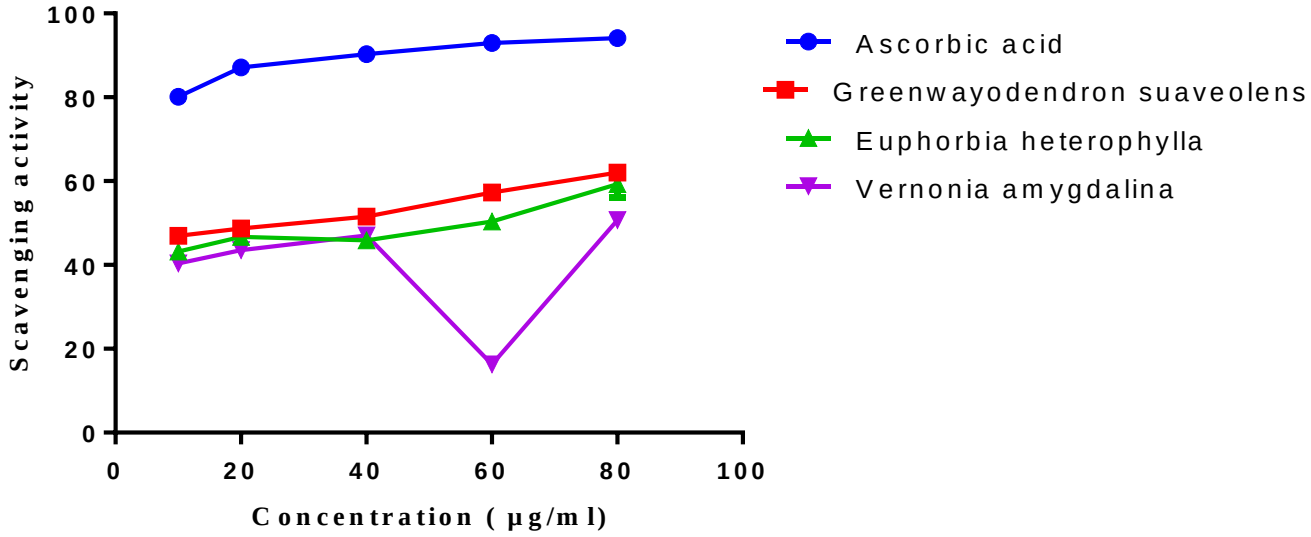

Figure 2: ABTS scavenging activity of Ascorbic acid, *Greenwayodendron suaveolens, Vernonia amygdalina and Euphorbia heterophylla*.

Greenwayodendron suaveolens, Vernonia amygdalina and Euphorbia heterophylla shows ABTS radical scavenging activities. The scavenging power of the plants increases as the concentration

increases. However, the scavenging activities of the plants are not comparable to that of ascorbic acid.

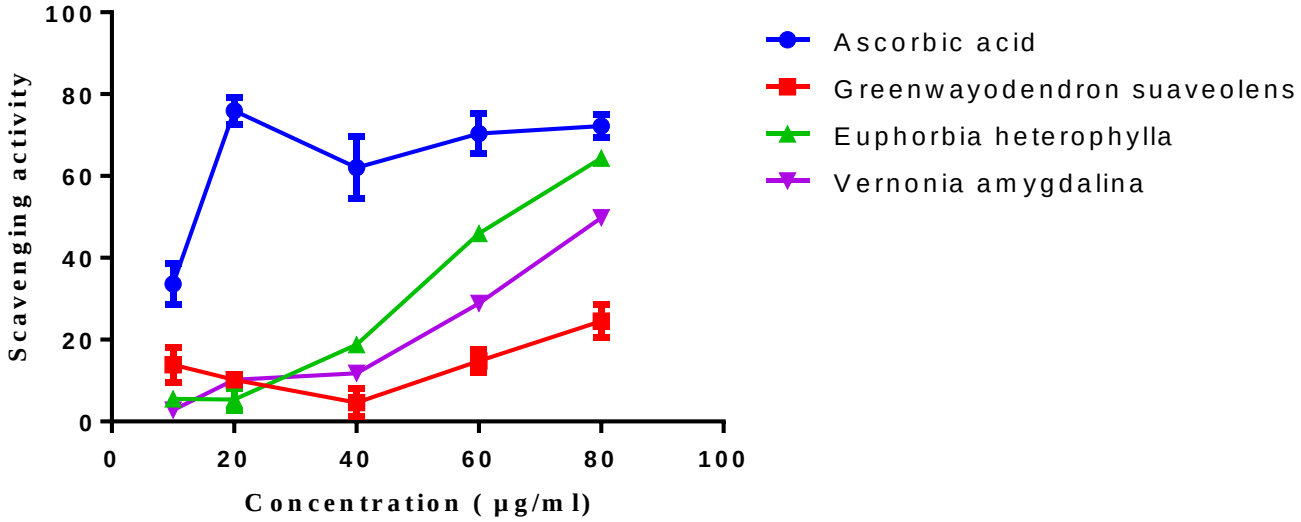

Figure 3: OH^- free radical scavenging activity of Ascorbic acid, *Greenwayodendron suaveolens, Vernonia amygdalina and Euphorbia heterophylla*.

Greenwayodendron suaveolens, Vernonia amygdalina and Euphorbia heterophylla shows OH^- free radical scavenging activities. The scavenging power of the plants increases as the concentration increases. However, the scavenging activities of the plants are not comparable to that of ascorbic acid.

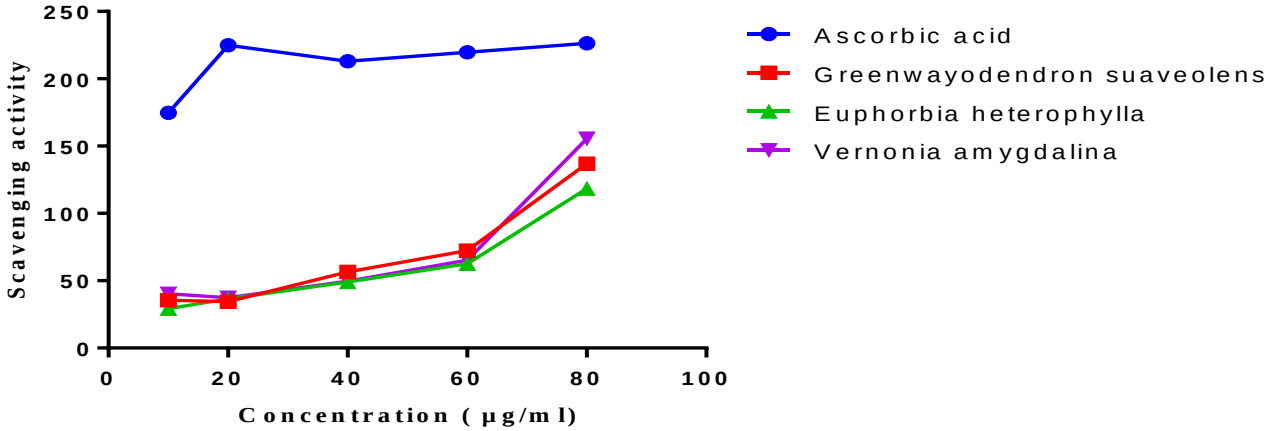

Figure 4: FRAP scavenging activity of Ascorbic acid, *Greenwayodendron suaveolens, Vernonia amygdalina and Euphorbia heterophylla*.

Greenwayodendron suaveolens, Vernonia amygdalina and Euphorbia heterophylla shows OH^- free radical scavenging activities. The scavenging power of the plants increases as the

concentration increases. However, the scavenging activities of the plants are not comparable to that of ascorbic acid.

3.1. Discussion

Plants have been used for centuries in the treatment of various ailments. Research has shown that the medicinal effects of plants are based on their phytochemicals and non-phytochemical constituents [42]. This study shows the quantitative phytochemical and non- phytochemical constituents of *Greenwayodendron suaveolens, Vernonia amygdalina, Euphorbia heterophylla and Xylopia aethiopica* (Tables 1 and 2). Total tannins composition *in G. suaveolens, V. amygdalina, E. heterophylla and X. aethiopica* were 6.575, 8.493, 8.356 and 12.468 respectively. Tannins is used in medicine, especially in the treatment of Asian (Japanese and Chinese) naturopathy. Herbal extracts containing tannins are used as a diuretic strengthening agent [43] as a diuretic, [44] against gastric and duodenal tumours [45] and as an anti-inflammatory, antiseptic, and hemostatic drug [46]. Total flavonoids composition in *G. suaveolens, V. amygdalina, E. heterophylla and X. aethiopica* were 20.232, 44.839, 33.065 and 41.935 respectively (Table 1). Flavonoids are intended to function as insect repellents, natural fungicides (phytoalexins) and potential regulators of the indole acetic acid plant hormones [47]. Phenols composition in *G. suaveolens, V. amygdalina, E. heterophylla and X. aethiopica* were 20.330, 25.275, 17.033 and 24.835 respectively. The presence of phenols and flavonoids in the extract can help prevent oxidative stress by scavenging free radicals and bioactivation of carcinogens for excretion in the liver [48]. Total saponins composition in *G. suaveolens, V. amygdalina, E. heterophylla and X. aethiopica* were 2.259, 2.657, 1.904 and 3.096 respectively. Saponins are used in preparation and development of vaccines [49]. Total alkaloid composition in *G. suaveolens, V. amygdalina, E. heterophylla and X. aethiopica* were 1.600, 0.800, 1.200 and 0.600 respectively. Alkaloids have a broad spectrum of pharmacological activities, including antimalarial, anti-asthmatic, antiarrhythmic, analgesic, antihyperglycemic and antibiotic agents [50].

G. suaveolens, V. amygdalina, E. heterophylla and X. aethiopica showed that they contained both macro and micro elements including calcium, copper, iron, magnesium, manganese, chromium, potassium, nitrogen and phosphorus. Cadmium is present in *V. amygdalina* and *E. heterophylla* and absent in both *G. suaveolens* and *X. aethiopica*. Nickel is absent in *G. suaveolens, V. amygdalina, E. heterophylla* and present in *X. aethiopica*. Lead is absent in all four plants. From the result the plants can supply calcium for normal growth and development of the skeleton and regulates muscle contraction such as the cardiac muscles and also aid normal blood clotting as supported by [51]. According to [52], calcium can be used for treating osteoporosis and osteopenia. Copper, though present in all four plants is shown in little quantities. It is reliable in the treatment of copper deficiency as it is required in trace quantities. According to [53] copper is very important as a trace element for all living organisms because it is a key component of the respiratory enzyme and cytochrome C oxidase required for metabolism. According to [54], iron is useful in the synthesis of haemoglobin and myoglobin and also in the treatment of iron deficiencies such as iron deficient anaemia, hence, these plants may be used in both nutritive and treatment regimens. The medicinal importance of magnesium in accordance with US National Institutes of Health (2016) is used medically as ordinary laxatives, antacids and to stabilize abnormal nerve excitation or vascular spasms in diseases such as eclampsia. According to [55], manganese is an essential human dietary element which is present as a coenzyme in several biological processes including macronutrient metabolism, bone formation, and free

radical defense systems. According [56], cadmium has no known biological functions in higher organisms, but according to [57], administration of cadmium to cells causes oxidative stress and increases the levels of antioxidants to protect the cells against macro molecular damage. Chromium is accepted by the U.S. National Institutes of Health as a trace element for its roles in the action of insulin, a hormone critical to the metabolism and storage of carbohydrate, fat and protein. The precise mechanisms of its actions in the body, however, have not been fully defined, leaving the question whether chromium is essential for healthy people [58]. In medicine, the benefits of potassium are resting cellular-membrane potential and the propagation of action potentials in neuronal, muscular and cardiac tissue. Due to the electrostatic and chemical properties, K^+ ions are larger than Na^+ ions, and ion channels and pumps in cell membranes can differentiate between the two ions, actively pumping or passively passing one of the two ions while blocking the other, hormone secretion and action, vascular tone, systemic blood pressure control, gastrointestinal motility, acid–base homeostasis, glucose and insulin metabolism, mineralocorticoid action, renal concentrating ability, fluid and electrolyte balance as supported by [59, 60]. Only *X. aethiopica* is known to contain nickel, though the US Institute of Medicine has not confirmed that nickel is an essential nutrient for humans, so neither a recommended dietary allowance (RDA) nor an adequate intake have been established. According to [61, 62], when ammonia is extracted from plants, it is used for protein synthesis. Phosphorus plays a major role in the structural framework of DNA and RNA. Living cells use phosphate to transport cellular energy with adenosine triphosphate (ATP), necessary for every cellular process that uses energy. Calcium phosphate is used for the reinforcement of bones.

From the results, *G. suaveolens, V. amygdalina and E. heterophylla* has DPPH scavenging activities (Figure 1), ABTS scavenging activities (Figure 2), OH scavenging activities (Figure 3) and Ferrric Reducing Antioxidant power (figure 4). DPPH is a radical widely used in food industry to evaluate scavenging activities of food product [63]. ABTS method is easy, accurate and rapid. It presents numerous advantages since it avoids unwanted side-reactions, high temperatures are not required to generate ABTS radicals and antioxidant activity can be studied over a wide range of pH values. This method is capable of determining both hydrophilic (in buffered media) and lipophilic (inorganic media) antioxidant properties **(2000)**. The ability of the plants to scavenge DPPH radical and ABTS radical indicates that the plants have antioxidant properties. Hydroxyl radicals functions as highly reactive species as primary poisons and as sources of secondary toxic substances. Free radicals have been implicated in causation of ailments such as cancer, inflammation, diabetes, liver cirrhosis, cardio vascular disease, Alzheimer's, aging and acquired immunodeficiency syndrome. It has been reported that OH- free radical is the chief cause of inflammation [54]. Natural antioxidant substances are believed to play a potential role in interfering with the oxidation process by reacting with free radicals, chelating catalytic metals and scavenging oxygen in biological systems [55]. Hydroxyl radicals produced in or near DNA have contributed to significant biological effects such as mutagenesis and cytotoxicity. The scavenging activity of OH^- by *G. suaveolens, V. amygdalina and E. heterophylla*, finds application in prevention of cancer from DNA mutation. Ferrozine [63], a compound closely related to TPTZ, has been widely used, with excess ascorbic acid, to measure iron limiting factor of Fe (II)-TPTZ, and hence, colour formation is the reducing ability of the sample. This assay is commonly used to measure the antioxidant content in industries and solvent systems including ethanol, aqueous acetone, methanol, aqueous alcohol, and benzene [62]. The quantitative phytochemical constituents, non- phytochemical constituents and scavenging activity of the plants gave evidence

that these plants are used in the treatment of gastric and duodenal tumours, inflammation, lung cancer, stomach cancer, ovarian cancer and estrogen-dependent breast cancer in humans. They are also known to reduce blood cholesterol levels by inhibiting intestinal cholesterol absorption [61].

4.0 Conclusion and Recommendation

This research was carried out *invitro* and it has been established that the plants can be used to treat diseases especially those due to oxidative stress. It is therefore recommended that more research need to be carried out *Invivo* to further prove their anti-oxidative potentials.

References

[1] Abosi, A. O. and Raseroka, B. H. (2003). Invivo antimalarial activity of *Vernonia amygdalina*. *Britain Journal of Biomedical Science.* **60**(2): 89-91

[2] Akah, P. A. and Okafor, C. I. (1992). Blood sugar lowering effect of *Vernonia amygdalina* (Del) in an experimental rabbit model. *Phytotherapy Research.* **6**: 171-173.

[3] Appiah, K. (2018). Medicinal plants used in Southern Ghana: An Ethnobotanical Study. *Medicines.* **6**(1): 1-27.

[4] Asante, D. (2016). Antidiabetic Effect of Young and Old Ethanolic Leaf Extracts of *Vernonia amygdalina*: A Comparative Study. *Journal of Diabetes Research.* **85**: 85.

[5] Asante, D. (2019). Anti-inflammatory, anti-nociceptive and antipyretic activity of young and old leaves of *Vernonia amygdalina. Biomedicine and Pharmacotheraphy.* **111**: 1187-1203.

[6] Asekun, O. T. and Adeniyi, B. A. (2004). Antimicrobial and cytoxic activities of fruit essential oil of *Xylopia aethiopica* from Nigeria. *Fitoterapia.* **75**(34): 368-370.

[7] Benzie, I. F. F. (1996) *Clinical Biochemistry.* **29:** 111–116.

[8] Berry, M. I. (1984). Fever few faces the future. *Pharmacology Journal.* **232**: 611.

[9] Bonsi, M. L. K.; Osuji, P. O.; Tuah, A. K. and Umunna, M. N. (1995). *Vernonia amygdalina* as a supplement of teff straw (Eragrostis tef) fed to Ethiopian Menz. Sheep. *Agroforestry systems.* **31**(3): 229-244.

[10] Bremer, K. (1994). *Asteraceae cludistics* and classification. Timber press, Portland, Oregon.

[11] Burkill, H. M. (1985). *The useful plants of west tropical Africa*. **1**: 130-132.

[12] Butler, G. W. and Bailey, R. W. (1973). *Chemistry and Biochemistry of herbage*. Vol. 1, Accident Press, London and New York.

[13] Cheng, Z.; Moore, J.; and Yu, L. (*2006). High-throughput relative DPPH_ radical assay. Journal of Agriculture Food Chemistry*. **54**: 7429–7436.

[14] Choi, J.; Lee, E.; Lee, H.; Kim, K.; Ahn, K. and Shim, B. (2007). Identification of campesterol from Chrysanthemum coronarium L and its antiangiogenic activities. *Phytothermal Reserve.* **21**: 954-959.

[15] Dauby, G.; Duminil, J.; Heuertz, M. and Hardy, O. J. (2010). Chloroplast DNA polymorphism and phylogeography of a central African species widespread in mature rainforest: *Greenwayodendron suaveolens* (Annonaceae). *Tropical Plant Biology*. **3**: 4-13.

[16] *Dunal, A. R. (2007). "Xylopia aethiopica"* African plant database. Conservatoire et Jardin botaniques de la Ville de Geneve. Retrieved 1 January 2013.

[17] Erikson, K. M. and Ascher, M. (2019). "Chapter 10. Manganese: It's Role in Disease and Health". In: Sigel, A.; Freisinger, E.; Sigel, R. K. O.; Carver, P. L. (Guest editor) (eds). *Essential Metals in Medicine; Therapeutic Use and Toxicity of Metals ions in the Clinic*. Metal Ions Life Sciences. **19**. Berlin de Guyter, GmbH. pp 253-266.

[18] European Food Safety Authority (2014). Scientific Opinion on Dietary Reference Values for chromium. *EFSA Journal. **12**(10): 3845.*

[19] Falodun, A. and Agbakwuru, E. O. P. (2004): Phytochemical analysis and laxative activity of Euphorbia heterophylla linn (*Euphorbiaceae*) Pakistan Journal of Science Resources. **47**(5) 345-348.

[20] Falodun, A.; Agbakwuru, E. O. P. and Ukoh, G. C. (2003). Antibacterial activity of *Euphorbia heterophylla linn* (family *Euphorbiaceae*). *Pakistan Journal of Science Resources.* **46**(6): 471-472.

[21] Food and Agricultural Organizations of the United Nations (2017). "Plant Production and Protection Division". *www.fao.org* Retrieved July 17, 2017.
[22] Gbadamosi, I. T. and Egunyomi, A. (2014). Ethnobotanical Survey of Plants Used for the Treatment and Management of Sexually Transmitted Infections in Ibadan. *Nigerian Ethnological Research Application.* **12**: 659-669.
[23] Greenwood, N. N. and Earnshaw, A. (1997). Chemistry of the Elements (2nd Edition), Butterworth-Heinmann. Oxford. Pp 459-472.
[24] Harborne, J. B. (1973). "Phenolic compounds" In: *Phytochemical Methods*. Chapman and Hall, London. Pp 52-80.
[25] Harborne, J. B. (1973). "Flavonoids" In: *Phytochemistry* (L. P. Miller, ed), Vol. 2. Van Nostrand Reinhold Co., Newyork. pp 344-380.
[26] Haslam, E. (1989) Plant Polyphenols – Vegetable Tannins Revisited – Chemistry and Pharmacology of Natural products, *Cambridge University Press*, Cambridge. pp.165.
[27] Hatano, T.; Yazaki, K.; Okonogi, A. and Okuda, T. (1991). *Chemistry and Pharmacy Bulletin*. **39**: 1689.
[28] Hogan, C. Michael (2010). Heavy metal. Encyclopedia of Earth. National Council for Science and the Environment. E. Monosson and C. Cleveland (eds.). Washington DC.
[29] Hostettmann, K. and Marston, A. (2005). *Saponins.* Cambridge University Press, Cambridge.
[30] Huffman, M. A. and Seifu, M. (1989). Observations on the illness and composition of a possibly medicinal plant *Vernonia amygdalina* (Del.) by a wild chimpanzee in the Mohale Mountains National Park, Tanzania. *Primates.* **30**(1): 51-63.
[31] Hurrell, R. F. (1997). Bioavailability of iron. *European Journal of Clinical Nutrition.* **51**:4–8.
[32] Ilahy R., Hdider C., Lenucci M.S., Tlili I., Dalessandro G. (2011). Antioxidant activity and bioactive compound changes during fruit ripening of high-lycopene tomato cultivars. *Journal of Food Composition and Analysis*. 24:588-595.
[33] Institute of Medicine (1997). Dietary reference intake: calcium, magnesium, phosphorus, vitamin
[34] Izevbige, E. B.; Bryant, T. L.; Walker, A. (2004). A novel natural inhibitor of extracellular signal regulated kinases and human breast cancer cell growth. *Experimental Biology and Medicine*. **229**(2): 163-169.
[35] Johnson, M. D. (2008). "Copper". Merck manual Home Health handbook. (Larry, E., editor), Merck Sharp and Dohme Corporation, a subsidiary of Merck and Co., Inc. Retrieved April 7, 2013.
*[36]Kannnan, M. (2010). Cadmium-induced oxidative stress in Saccharomyces cerevisiae. Indian Journal of Biochemistry and Biophysics. **47**(6): 383-387.*
[37] Khanna A. K., Rizvi F. and Chander R. (2002). Lipid lowering activity of Phyllantus niruri in hyperlipideamia rats. *Journal of Ethanopharmacol*, 82 (1): 19-22.
[38] Leonard, B. S.; Karen, L. L.; Bruce, B.; Thomas, F. K. and Jay, H. H. (2002). Complementary and alternative medicine in chronic liver disease. *Hepatology.* **34**(3): 595-603.
[39] Makkar H. P., Siddhuraju P., Becker K. (2007). Methods in molecular biology: plant secondary metabolites, Totowa: Human Press; p. 93-100.
[40] *Malnic, G.; Giebisch, G.; Muto, S.; Wang, W.; Bailey, M. A. and Satlin, L. M. (2013). "Regulation of K+ excretion". In Alpern, R. J.; Caplan, M. J. and Moe, O. W. (eds.). Seldin and Giebisch's the kidney: physiology and pathophysiology (5th ed.). London: Academic Press. Pp 1659–1716.*
[41] Mato, K .B. (2005). *Savoir-faire local dans la périphérie de la partie Sud-Ouest du Parc National de la Salonga*. Mémoire DEA en Biologie. Université de Kinshasa .91 p.
[42] Melton, L. J.; Chrischilles, E. A.; Cooper, C.; Lane, A. W. and Riggs, B. L. (1992). How many women have osteoporosis? *Journal of Bone Mineral Reserves* **7**: 1005-1010.
[43] Mitich, L. W. (1992). Tansy. *Weed Technology.* **6**:242.
[44] Mols, J. B.; Gravendeel, B. and Chatrou, L. W. (2004). Identifying clades in Asian Annonaceae: monophylectic genera in the Polyphylectic Miliueae. *American Journal of botany.* **90**: 590-600.
[45] Okwu, D. E. (2001). Evaluation of the chemical composition of indigenous spices and flavouring Agents. *Global Journal of Pure Applied Science.* **7**(3): 455-459.
[46] Philipson, J. D.; Wright, C. W.; Kirby, C. C. and Warhust, D. C. (1993). *Phytochemistry of some plants used in traditional medicine for the treatment of protozoal diseases*. Abstracts, international symposium of the phytochemical society of Europe, University of Lausanne, Switzerland. p13.
[47] Roulette, C. J.; Mann, H.; Kemp, B. M.; Remiker, M.; Roulette, J. W.; Hewlett, B. S.; Kazanji, M.; Breurec, S.; Monchy, D.; Sullivan, R. J. and Hagen, E. H. (2014). Tobacco use *vs*. helminths in Congo basin hunter-gatherers: self-medication in humans? Evolution and Human Behaviour.

[48] Rowan, N. G. and Onwukaeme, D. N. (2001). Deterpenoid esters of *Euphorbiaceae* in *Euphorbia hyles. Nigerian Journal of Pharmacology.* **32**: 60-64.
[49] *Russo, P.; Frustaci, A.; Del Bufalo, A., Fini, M. and Cesario, A. (2013). "Multitarget drugs of plants origin acting on Alzheimer's disease". Curriculum of Medical Chemistry. **20**(13): 1686–1693.*
[50] Ryan, E.; Galvin, K.; O'Connor, T. P.; Maguire, A. R. and O'Brien, N. M. (2007). Phytosterol, squalene, tocopherol content and fatty acid profile of selected seeds, grains, and legumes. *Plant Foods and Human nutrition.* **62**: 85-91.
[51] Sajeeth, C. I.; Manna, P. K. and Manavalan, R. (2011). *Der Pharmacia Sinica.* **2**(2): 220-226.
[52] Shiv, k. (2011). *Advances in Applied Science Research.* **2**(1):129-135.
[53] Simpson, M. G. (2010). "Chapter 1 plant Systematics: an Overview" In: *Plant systematics* (2nd ed.) Academic Press.
[54] Singleton, V .L. and Rossi, J. A. (2005). Colorimetry of total phenolics with phosphomolybdic-phosphotungstic acid reagents. *Am J Enol Vitic* **16**: 144-58.
[55] Stookey, L. L. (1970). *Analytical Chemistry.* **42:** 779–783.
[56] Tsabang, N.; Tsouh Fokou, P. V.; Tchokouaha, Y. L. R.; Noguem, B.; Bakarnga-Via, I.; Dongmo Nguepi, M. S., Nkongmeneck, B. A. and Boyom, F. F. (2012). Ethnopharmacological survey of Annonaceae medicinal plants used to treat malaria in four areas of Cameroon. *Journal for Ethnopharmacology.* **139**:171–180.
[57] Uhegbu, F.O. and Ogbuehi, K. J. (2004). Effect of aqueous extract (crude) of leaves of *Vernonia amygdalina* (Del) on blood glucose, serum albumin and cholesterol levels in diabetic albino rats. *Global Journal of Pure and Applied Sciences.* **10**(1): 189-194.
[58] US National Institutes of Health (2016). "Dietary Supplement Fact Sheet: Magnesium". Office of Dietary Supplements, Retrieved 13 October, 2016.
[59] Varady, K. A.; Houweling, A. H. and Jones, P. J. (2007). Effect of plant sterols and exercise training on cholesterol absorption and synthesis in previously sedentary hypercholesterolemic subjects. *Translavania Reserve.* **149**: 22–30.
[60] Wee, S. C. and Wee, K. Y. (2011). *Advances in Applied Science Research.* **2**(3): 418-425.
[61] Weiner, I. D.; Linus, S. and Wingo, C. S. (2014). "Disorders of potassium metabolism". In Freehally, J.; Johnson, R. J. and Floege, J. (eds.). *Comprehensive clinical nephrology* (5th ed.). St. Louis: Saunders. p. 118.
[62] Williams, C. A.; Hault, J. R. S.; Harbone, J. B. and Grenenham, J. (1995). *Phytochemistry.* (1):267
[63] Yoshida, T.; Ohbayashi, H.; Ishihara, K.; Ohwashi, W.; Haba, Okano, Y.; Shingu, T. and Okuda, T. (1991). *Chemistry and Pharmacy Bulletin.* **39**: 2233.

Appendices

Appendix 1

The scavenging activity of *Greenwayodendron suaveolens, Euphorbia heterophylla and Vernonia amygdalina* of DPPH scavenging activity.

Sample	**Concentation**	**Absorbtion 1**	**Absorbtion 2**	**Absorbtion 3**
Ascorbic acid	10	83.07	83.22	82.93
	20	92.81	93.51	94.78
	40	94.92	94.08	96.76
	60	97.74	96.76	96.90
	80	97.46	97.60	97.74

Greenwayodendron suaveolens	10	33.57	32.16	32.44
	20	36.81	38.22	37.66
	40	51.62	53.31	52.05
	60	73.91	73.48	74.61
	80	90.13	91.96	90.41
Euphorbia heterophylla	10	33.85	36.53	35.40
	20	55.01	56.28	44.29
	40	61.21	60.37	60.51
	60	81.95	82.09	83.22
	80	86.60	87.59	87.17
Vernonia amygdalina	10	34.98	32.58	35.26
	20	37.94	37.66	37.09
	40	51.20	51.06	48.94
	60	73.34	70.80	72.92
	80	89.99	86.46	86.60

Appendix 2

The scavenging activity of *Greenwayodendron suaveolens, Euphorbia heterophylla and Vernonia amygdalina* of ABTS scavenging activity.

Sample	**Concentration**	**Absorbtion 1**	**Absorbtion 2**	**Absorbtion 3**
Ascorbic acid	10	80.49	79.95	79.95
	20	87.14	87.25	86.92
	40	90.19	90.86	89.86
	60	93.03	93.03	92.81
	80	93.79	94.77	93.79

Greenwayodendron suaveolens	10	47.03	47.03	46.81
	20	48.77	48.77	48.67
	40	51.61	51.39	51.50
	60	57.06	57.38	57.38
	80	62.18	62.07	61.96
Euphorbia heterophylla	10	42.89	43.11	43.54
	20	47.56	46.27	46.27
	40	45.83	46.16	45.61
	60	50.41	50.41	50.30
	80	62.62	52.73	62.62
Vernonia amygdalina	10			
	20	43.65	43.00	44.09
	40	47.03	47.14	46.92
	60	16.40	16.19	16.40
	80	50.95	50.12	51.06

Appendix 3

The scavenging activity of *Greenwayodendron suaveolens, Euphorbia heterophylla and Vernonia amygdalina* of OH- scavenging activity.

Sample	**Concentration**	**Absorbtion 1**	**Absorbtion 2**	**Absorbtion 3**
Ascorbic acid	10	23.40	38.55	38.88
	20	80.55	77.77	69.44
	40	72.22	66.66	47.22
	60	61.11	72.22	77.77

	80	75.00	75.00	66.66
Greenwayodendron suaveolens	10	22.22	11.11	8.33
	20	11.11	11.11	8.33
	40	11.11	0.00	2.77
	60	10.00	14.28	20.00
	80	32.07	18.18	23.40
Euphorbia heterophylla	10	5.55	5.55	5.55
	20	0.00	8.10	8.10
	40	18.18	18.18	20.00
	60	46.26	46.26	45.45
	80	63.26	65.04	64.71
Vernonia amygdalina	10	2.77	2.77	2.77
	20	8.33	13.88	8.33
	40	11.11	12.19	12.19
	60	30.76	30.76	25.00
	80	50.00	50.00	49.29

Appendix 4

The scavenging activity of *Greenwayodendron suaveolens, Euphorbia heterophylla and Vernonia amygdalina* of Ferric Reducing Antioxidant Power.

Sample	**Concentation**	**Absorbtion 1**	**Absorbtion 2**	**Absorbtion 3**
Ascorbic acid	10	175.04	174.44	174.84
	20	225.24	224.84	224.84
	40	212.84	213.24	212.84
	60	219.44	219.64	220.04

	80	224.84	228.84	225.24
Greenwayodendron suaveolens	10	34.84	35.64	35.84
	20	34.64	34.44	34.44
	40	57.24	56.24	56.44
	60	73.26	70.84	73.04
	80	136.44	137.24	137.04
Euphorbia heterophylla	10	29.64	29.84	28.04
	20	36.44	36.84	36.64
	40	49.44	49.24	48.64
	60	63.24	62.64	62.04
	80	117.64	118.84	118.64
Vernonia amygdalina	10	40.64	40.04	40.04
	20	36.64	37.64	37.84
	40	48.04	47.64	53.64
	60	64.84	65.44	65.64
	80	155.04	155.84	155.44

NIPES Conference Proceedings
The 1st International Conference of the Nigerian Institution of Professional Engineers and Scientists 7th-8th Oct. 2021: 336-349
www.nipesjournals.org.ng

Assessment of Noise Pollution in Oba Market, New Benin Market & Oregbeni Market, Benin City, Edo State

Ogbeifun, Nowamagbe Prince[1] and Njokede, Fortune .O.[2]
[1, 2] Department of Civil Engineering, University of Benin, Benin City, Nigeria.

Abstract
Increase in workplace stress, loss of sleep and anger may not be unconnected to the level of noise exposure an individual is subjected. Three major markets in Benin City namely Oba market, New Benin Market and Oregbeni market, being workplaces, were examined to determine their noise levels with a view to ensuring that shoppers and vendors carrying out their business in a healthy environment. The noise levels in these markets were measured between 8 – 11am, 12 – 3pm and 4 – 7pm daily spanning 7days at each market. Questionnaires were distributed to market stakeholders to get a glimpse of the sources of noise in the markets and the adverse health effects arising from prolonged exposure to the prevailing noise. Results showed that the average noise in the markets is between 77.00 to 89.20dB in the morning; 74.30 to 90.20dB in the afternoon and 83.30 to 90.90dB in the evening. Oba market has the highest mean noise (86.76dB), occurring predominantly in the evenings, followed by New Benin market which has the highest mean noise in the morning (84.73dB) and in the afternoon (85.55dB). Oregbeni market is the least noisy market in the pack even though it sometimes experiences sudden short and loud sound. Traffic activities, grinding machine and generator operations constitute the major sources of noise even as respondent acknowledged that they experience many of the adverse health effects associated with noise in the markets under review. Proper market administration, siting and layout structuring will be helpful towards reducing noise in the markets.

Keywords: *Oba Market, New Benin Market and Oregbeni Market, noise, Benin City, morning, afternoon and evening, respondents*

1.0 Introduction

Noise pollution has been found to be one of the major environmental hazards and social discomforts in major cities of the world, particularly in recent times [1]. It is difficult to pinpoint the exact history of noise pollution, but known problems associated with noise in urban environments go as far back as ancient Rome. Due to the clattering of their wheels on paving stones, chariots in ancient Rome were banned from the streets at night to prevent the noise that interrupted sleep and caused annoyance to the residents. Times later, some cities in Medieval Europe either banned horse drawn carriages and horses from the streets at night or covered the stone streets with straw to reduce noise and to ensure a good night sleep for the residents [2].

In 18th Century Philadelphia, lawmakers covered nearby cobblestone streets with earth to prevent noise-induced interruptions in their important work. The above events showcased two major effects of noise from which men of all ages have required relief: interruption of sleep, and interference with work that requires concentration [2]. It is fascinating that noises originating from the various types of transport system in contemporary society are still among the principal sources of environmental noise, even though the types of noise are not the same as those that existed in Rome, Medieval Europe, or 18th century Philadelphia [2, 3].

Modern transport systems (including road, rail, and air) and the products of modern-day technology produce growing levels of unwanted noise of different types and intensities throughout the day and night that disturb sleep, concentration, and other activities [4, 5]. This noise affects us without our being consciously aware of it. Unlike our eyes, which we can close to eliminate undesirable visual input, we cannot willingly shut our ears to exclude unwanted auditory input; at least not without the

help of ear plugs. Our hearing organs are constantly active and aware of sound, even when we are asleep or in a coma [6].

According to World Health Organization [7], noise must be recognized as a major threat to human wellbeing. In fact, noise is no longer regarded as a mere irritation; it is now found to be quite harmful, posing grave threat to human life especially in the urban environment [8]. Like deforestation, the release of harmful wastes in to the environment or poisonous gases into the atmosphere, the adverse effect of Noise may not immediate; however sustained exposure over a certain time period may be as lethal or worse as any of the other global environmental hazards [9].
Given the rise in urban development, and the effect of noise pollution on healthy and maintainable living within cities, this study examines urban market noise pollution levels in Benin City, Nigeria. This is with a view to establishing the extent of the problems towards mitigating noise pollution.

1.1 Environmental Noise

According to Akhtar [10] sound may be defined as an audible vibration that travels through the air while noise is a sounds that are disagreeable or unpleasant, produced by acoustic waves of random intensities and frequencies which adversely affect the physiology or psychological well-being of an individual. Recent studies showed that noise is now recognized as a serious health problem in contemporary societies [11]. Noise is a prominent feature of the environment and its sources include but not limited to noise from transportation, industrial and community environment. Community noise, domestic noise and workplace noise all constitute environmental noise. The main form of environmental noise in Nigeria is from transportation, primarily motor vehicles. Others include electro-acoustic noise from various sources such as generators, blenders, loudspeakers, noise produced by aircraft, church, mosque and from pets like dogs [12].

1.1 Noise Pollution

Noise pollution, otherwise called sound pollution, is the production of noise with varying effects on the actions of human or animal life, a large portion of them unsafe to a certain extent. One of the environments most influenced by man and his activities are urban settlements [13-16].
Preethi, Sravani [17] and World Health Organization [7] described Noise pollution as the unwanted and disturbing sound which is above the traditional level of sound comfortable to the human ear and features a negative effect on people and society. Practically all human activities create noise albeit at a differing limits. Those noise exceeding extant levels are acknowledged as causing distress to such as expose to the noise. Table 1 is the WHO guideline for community noise in specific environment.

Table 1: Guideline Values for Community Noise in Specific Environments [18]

Specific environment	**Critical health effect(s)**	**LA_{eq}[dB(A)]**	**Time base [hours]**	**LA_{max} fast [dB]**
Outdoor living area	Serious annoyance, daytime and evening	55	16	-
	Moderate annoyance, daytime and evening	50	16	-
Dwelling, indoors	Speech intelligibility & moderate annoyance,	35	16	-
Inside bedrooms	daytime & evening	30	8	45

Specific environment	Critical health effect(s)	LA_{eq}[dB(A)]	Time base [hours]	LA_{max} fast [dB]
	Sleep disturbance, night-time			
Outside bedrooms	Sleep disturbance, window open (outdoor values)	45	8	60
School class rooms & pre-schools, indoors	Speech intelligibility, disturbance of information extraction, message communication	45	During class	-
Pre-school bedrooms, indoor	Sleep disturbance	30	Sleeping time	45
School, playground Outdoor	Annoyance (external source)	55	During play	-
Hospital, ward rooms, indoors	Sleep disturbance, night-time Sleep disturbance, daytime and evenings	30 30	8 16	40 -
Hospitals, treatment rooms, indoors	Interference with rest and recovery	#1		
Industrial, commercial shopping and traffic areas, indoors and outdoors	Hearing impairment	70	24	110
Ceremonies, festivals and entertainment events	Hearing impairment (patrons:<5 times/year)	100	4	110
Public addresses, indoors and outdoors	Hearing impairment	85	1	110
Music and other sounds through headphones/ earphones	Hearing impairment (free-field value)	85 #4	1	110
Impulse sounds from toys, fireworks and firearms	Hearing impairment (adults) Hearing impairment (children)	- -	- -	140 #2 120 #2
Outdoors in parkland and conservations areas	Disruption of tranquillity	#3		

where
#1: As low as possible.
#2: Peak sound pressure (not LAF, max) measured 100 mm from the ear.
#3: Existing quiet outdoor areas should be preserved and the ratio of intruding noise to natural background sound should be kept low.
#4: Under headphones, adapted to free-field values.

Unlike other environmental problems, noise pollution continues to grow and associated with an increasing number of complaints from people exposed to the noise, even though such complaints are often ignored [19, 20]. The growth in noise pollution need curtailing is at it brings about direct, as well

as cumulative adverse health effects. It also adversely affects future generations and has socio-cultural and economic effects [21]. In addition to creating a nuisance to the urban environment, noise pollution has been associated with psychological defects [22, 23], physiological defects [24-26], and physical defects on the exposed populace [27-29]. In specific terms, deafness, tinnitus, cardiac problems, such as hypertension, ischemic heart disease and vasoconstriction, sleep interferences, headaches, fatigue, stomach ulcers, vertigo, and aggression have been attributed to noise pollution [30, 31].

The increase in environmental noise pollution in Nigerian urban areas has been found to be dependent on increase in population, commercial activities as well as road traffic volume [32]. In Nigeria, the problem of noise pollution is wide spread. Several studies report that noise level in metropolitan cities in Nigeria exceeds specified extant limits [33] and the extent of discomfort associated with noise on residents is well documented [1, 34-36].

Oviasogie and Ikudayisi [33] examined noise levels within the Government Residential Area (GRA) and Ogbe quarters in Benin City and compared them with current standard levels. The result showed that 5 of 6 points, in each of the Government Residential Area (GRA) and Ogbe quarters, the noise level exceeded the recommended limit of 60dB(A) by values of 1-27dB(A), with the maximum recorded noise level of 88.3dB in Ogbe quarters. Oviasogie and Ikudayisi (2019) also showed the statistically significant difference in noise sources from generators, market and vehicular activities across the locations considered, using the Mann-Whitney Test. It was found that generator was the dominant source of noise in GRA while market noise was the most prominent noise at Ogbe quarters. These suggests that growing economic activities, means of transportation, household security and power source often determine, to a greater extent, the level of noise in urban areas. Crowded cities and towns, automated means of transport, new developments for recreation and entertainment are polluting the atmosphere with their nonstop noise [3, 5, 30].

Oyedepo [1] examined the noise levels of Ilorin metropolis, Nigeria by residential density. High density residential areas had noise levels higher than 70dB while most locations in the low-density residential areas had the least noise levels within the acceptable 55dB limit.

1.2. A-Weighting

A-weighting is applied to instrument-measured sound levels in an effort to account for the relative loudness perceived by the human ear, as the ear is less sensitive to low audio frequencies. It is employed by arithmetically adding a table of values, listed by octave or third-octave bands, to the measured sound pressure levels in dB. The resulting octave band measurements are usually added (logarithmic method) to provide a single A-weighted value describing the sound; the units are written as dB(A) [37]. The table below shows some examples of noise sources and their corresponding decibel effects on man's hearing.

Table 2: Examples of Noise Sources and Decibel Effects [8, 38]

Noise Source	Decibel (dbA)	Decibel Effect
Jet take-off (at 25 meters) Recommended product: Outdoor Noise Barriers	150	Eardrum rupture
Aircraft carrier deck	140	
Military jet aircraft take-off from aircraft carrier with afterburner at 50 ft (130 dB).	130	
Thunderclap, chain saw. Oxygen torch (121 dB).	120	Painful. 32 times as loud as 70 dB.

Noise Source	Decibel (dbA)	Decibel Effect
Steel mill, auto horn at 1 meter. Turbo-fan aircraft at takeoff power at 200 ft (118 dB). Riveting machine (110 dB); live rock music (108 - 114 dB).	110	Average human pain threshold. 16 times as loud as 70 dB.
Jet take-off (at 305 meters), use of outboard motor, power lawn mower, motorcycle, farm tractor, jackhammer, garbage truck. Boeing 707 or DC-8 aircraft at one nautical mile (6080 ft) before landing (106 dB); jet flyover at 1000 feet (103 dB); Bell J-2A helicopter at 100 ft (100 dB).	100	8 times as loud as 70 dB. Serious damage possible in 8 hr exposure.
Boeing 737 or DC-9 aircraft at one nautical mile (6080 ft) before landing (97 dB); power mower (96 dB); motorcycle at 25 ft (90 dB).	90	4 times as loud as 70 dB. Likely damage in 8 hour exposure.
Garbage disposal, dishwasher, average factory, freight train (at 15 meters). Car wash at 20 ft (89 dB); propeller plane flyover at 1000 ft (88 dB)	80	2 times as loud as 70 dB. Possible damage in 8 hour exposure.
Passenger car at 65 mph at 25 ft (77 dB); freeway at 50 ft from pavement edge 10 a.m. (76 dB). Living room music (76 dB); radio or TV-audio, vacuum cleaner (70 dB).	70	Arbitrary base of comparison. Upper 70s are annoyingly loud to some people.
Conversation in restaurant, office, background music, Air conditioning unit at 100 feet.	60	Half as loud as 70 dB. Fairly quiet.
Quiet suburb, conversation at home. Large electrical transformers at 100 feet.	50	One-fourth as loud as 70 dB.
Library, bird calls (44 dB); lowest limit of urban ambient sound	40	One-eighth as loud as 70 dB.
Quiet rural area.	30	One-sixteenth as loud as 70 dB. Very Quiet.
Whisper, rustling leaves	20	
Breathing	10	Barely audible

2.0 Materials & Method

2.1 Study Area Description

For this study, three major markets in Benin City, Edo State were examined to determine their noise levels. These markets include Oba Market, New Benin Market and Oregbeni Market. Figure 1 is a map of the markets showing their proximity to each other. These markets constitute the major markets in Benin City known for their affordable price of consumables and non-consumable goods for retail and wholesale purchases.

Fig 1: Map of Benin City, Edo State, showing the Study Markets

2.1.1 Oba Market

The Oba market is located at the heart of the city centre close to the revered Oba Palace. The centre of the market is around cordinates 6°20'5"N and 5°37'11"E beside the Oredo Local government secretariat. While the Main Market was properly delineated, the market has however extended into Mission Road and Forestry road that leads to New Benin Market. Shopping within this expansion has exacerbated the noise levels in the markets. The main market beside the secretariat is renowned for affordable food items (mostly perishable items), textile materials and make-up items. The other axes of the market are known for wholesale groceries, beverages, books and stationeries and some electronics. Shops selling clothing and sewing accessories also make the trader pack of the extended axes of the market.

As the market is located near major intersection, some of the noise associated with the market include horns from vehicles; outdoor speakers for advertising items or other promotional displays; hawkers drawing attentions to their wares; grinding machines at work to mention but a few. This noise varies and often asynchronous.

2.1.2 New Benin Market

New Benin Market located at along New Lagos Road that connects Akpakpava road and Benin Lagos road. The market has a midpoint around cordinates 6.3448° N and 5.6340° E. The market is at the intersection between mission road and New Lagos road. The market is currently expanding from the intersection along the connecting roads in all direction. The market is renowned for affordable food and household items mostly for retail purchases. Major dealers of used electronics, traditional beads and clothing also abound in the market. The predominant noise in the market includes vehicle horns, bells of sellers drawing attentions to their wares, and shopping transactions.

2.1.3 Oregbeni Market

Oregbeni market, also known as Ikpoba-Hill market, is located at Ramat park junction connecting Akpakpava and Benin-Asaba Express road in Ikpoba–Okha Local Government Area with midpoint around cordinates 6°20'56"N and 5°39'33"E. while Business activities occurs every day at the market, the highest form of activities causing noise occurs at the days designated as market as '***Oregbeni Market day***' that takes place at least once in a week. On these market days, traders from the nearby villages and communities bring their farm produce to the market to sell at very affordable price for fairly large quantities. This correspondingly attracts patronages from distant customers who troupe to the market in large number either for consumption or resell. This increased beehive of activities leads to an increased noise level causing grave discomfort to those in around the market.

2.2 Sampling Points

A total of twelve (12) noise monitoring stations were carefully selected to represent all the noise-producing segments of the markets. OB, NB and OR were chosen to refer to Oba market, New Benin market and Oregbeni market respectively for noise point source identification. Points of interest for noise measurement include road intersections and sections within the markets near the major roads that are opened for business on almost a daily basis and other obvious noise locations from morning to evening. Table 3 states the position and description of the noise points for which measurements was performed.

Table 3: Sampling Stations and their Cordinates and Descriptions.

Noise Point ID	Northing	Easting	Description
OB1	6°20'07.7"	5°37'11.2"	The road intersection at the main entrance into the market, opposite the statue of Queen Iden.
OB2	6°20'06.0"	5°37'12.2"	The grinding machines section of the market.
OB3	6°20'06.2"	5°37'10.3"	The local food stuffs section of the market where food stuffs such as okra, crayfish, tomatoes etc are sold.
OB4	6°20'05.9"	5°37'13.1"	Along the walkway of the cosmetics section of the market.
NB1	6°21'02.0"	5°37'54.8"	The road intersection at one of the entrances of the market
NB2	6°21'04.2"	5°37'52.2"	The clothing section of the market on the left side.
NB3	6°21'01.8"	5°37'51.7"	The inner section of the market where fresh foods are sold.
NB4	6°21'05.1"	5°37'53.9"	The electronics section of the market.
OR1	6°21'00.5"	5°39'33.0"	The road intersection at the entrance of the market, opposite Ramat Park.
OR2	6°21'00.2"	5°39'32.8"	The inner section of the market where food stuffs such as groundnut oil are sold.
OR3	6°21'00.3"	5°39'33.1"	The provisions store section of the market.
OR4	6°21'00.1"	5°39'32.6"	The section of the market where thrift items are sold during market day.

2.3 Decibel-X Pro

"Decibel-X PRO" is a paid sound meter apps available on Google play store that is reliably pre-calibrated and supports frequency weightings in the region of ITU-R 468, A and C. With ability for trim calibration from -15 dB to 15 dB and standard measurement range from 30 dBA up to 130 dBA. This noise meter app when installed in a smartphone device perfectly serves as a professional noise meter measuring

ambient sound pressure levels (SPL) of its sphere of operation. This mobile noise meter application was selected based on certain criteria with occupational relevancy such as its ability to:

a) support A-weighted sound levels,
b) report average sound level as a numeric value
c) be accessible for public use being available in major digital app distribution platforms such as Apple Store and Google Play Store.

2.4 Noise Measurement Procedures

Measurements were conducted over a period of three weeks in the three different markets. The utilized Smartphone (LG v40 ThinQ) was removed from its protective case to ensure maximum access to the microphone. To ensure consistency of measurements, the phone was held at arm's length (0.6m) and at shoulder's height (1.5m) as the recording position for the duration of each sample. Phone was laid flat in the palm of the hand, screen facing up and microphone facing away from the body at a 180^o angle. It should be noted that the measurements were altered for some locations due to space and location limitations outlined below.

A-weighted instantaneous sound pressure level (LAi) measurements with a calibration of ±0.00, were taken for a period of four days per market and 6 hours per station, bringing the total periods of reading to 12 days within a span of three weeks. This procedure was carried out for morning (8:00 - 11:00 a.m.), afternoon (12:00 - 3:00 p.m.) and evening (4:00 - 7:00 p.m.). Two subsequent recordings were performed and recorded at each site for each sample within a 120-minute period, with each recording lasting one hour in duration. Each recording within the two hour period was averaged together to provide a more accurate representation of each time period. The mean noise levels at each market were obtained as thus [23, 30]:

$$\text{Mean noise Level } \left(LA_{eqA}\right) = \frac{\sum LA_{eqA}}{n} \qquad (1.0)$$

Where n is the number of noise source points per market

2.5 Distribution of Structured Questionnaire

Structured questionnaires were prepared and given to shop owner and residents near the markets. The shops and homes severely impacted by the noise were about 43, 38 and 42 in Oba markets, New Benin market and Oregbeni market respectively. Women comprise about 60% of respondents of the study. This was aimed at accessing the level of discomfort of the noise levels in the market at various times of the day. The results of the questionnaire were graphically depicted and statistically analyze using Microsoft excel.

3.0 Results and Discussion

3.1 Daily Summary of Noise level in the Markets

The daily summary of sound measurement using decibel X-Pro is presented in tables 4 – 6 comprising Morning, afternoon and evening sound levels.

Table 4: Distribution of the Average, Minimum and Maximum Noise Levels in dB (A) during Morning Period

Point ID	Average	Min.	Max.
OB1	89.40	44.55	120.60
OB2	77.00	45.25	96.80
OB3	89.20	45.65	109.30
OB4	86.80	54.15	96.30
NB1	82.90	40.35	96.30
NB2	83.25	47.70	103.65
NB3	87.65	50.75	105.25
NB4	85.10	55.45	99.30
OR1	83.65	45.50	96.05
OR2	88.80	36.80	109.45
OR3	83.10	53.90	96.25
OR4	74.75	41.20	91.60

Table 5: Distribution of the Average, Minimum and Maximum Noise Levels in dB (A) during Afternoon Period

Point ID	Average	Min.	Max.
OB1	86.30	53.00	99.95
OB2	79.80	45.85	99.40
OB3	89.80	50.40	106.75
OB4	82.45	46.05	97.90
NB1	87.50	54.15	107.80
NB2	81.85	39.85	98.50
NB3	90.20	50.15	105.60
NB4	82.65	43.90	100.35
OR1	90.00	44.35	109.45
OR2	83.60	53.55	94.60
OR3	84.40	46.30	97.35
OR4	74.30	42.15	86.75

Table 6: Distribution of the Average, Minimum and Maximum Noise Levels in dB (A) during Evening Period

Point ID	Average	Min.	Max.
OB1	90.20	59.65	109.70
OB2	83.60	38.50	97.45
OB3	88.85	57.35	101.60
OB4	84.40	46.20	103.35
NB1	89.20	51.25	105.55
NB2	85.55	41.90	104.70
NB3	86.75	54.20	102.45
NB4	84.80	42.65	100.50
OR1	90.90	51.45	103.85
OR2	84.95	49.75	102.20
OR3	83.30	44.80	93.80
OR4	80.10	50.45	96.95

In the morning periods, records show that Oba Market has the highest noise level of 89.40 dB(A) with an average noise level of 84.59 dB(A); while New Benin Market has the highest average noise value of 84.73 dB(A) within the period of 8am to 11am. Oregbeni market recorded the lowest mean noise level of 74.75 dB(A) within this period morning noise measurement. In the markets, the predominant noise section is those dealing with foodstuff items, with Oregbeni market having the maximum value of 109.45dB. This is predominantly human-induced noise with associated desperation of shoppers to purchase goods before they are sold to another buyer. The noise form is usually chaotic in nature

The highest mean in the markets in the afternoon were 89.90 dB, 90.20 dB and 90.00 dB at OB3, NB3 and OR1 respectively. The peak maximum noise value was found at Oregbeni market section near the road intersection with a value of 109.45 dB. Similar scenario also occurred at the New Benin market while the food section at Oba market accounted for the Peak noise level in the afternoon

For the three markets under review, the shop closest to the road experienced the highest average and loudest noise in the evening. The highest mean noise and loudest noise of 90.20dB and 109.70dB respectively was found in Oba market; 89.20dB and 105.55dB respectively for New Benin Market and 90.90dB and 103.85dB at Oregbeni market. This is not too surprising considering that shoppers are hesitant to enter the interior section of the market in the evening coupled market closure policy by the regulating authority in evening period.

3.2 Mean Noise Levels at the Markets

The mean noise levels at each of the market, putting together all the noise producing section of the markets is shown in figure 2.0

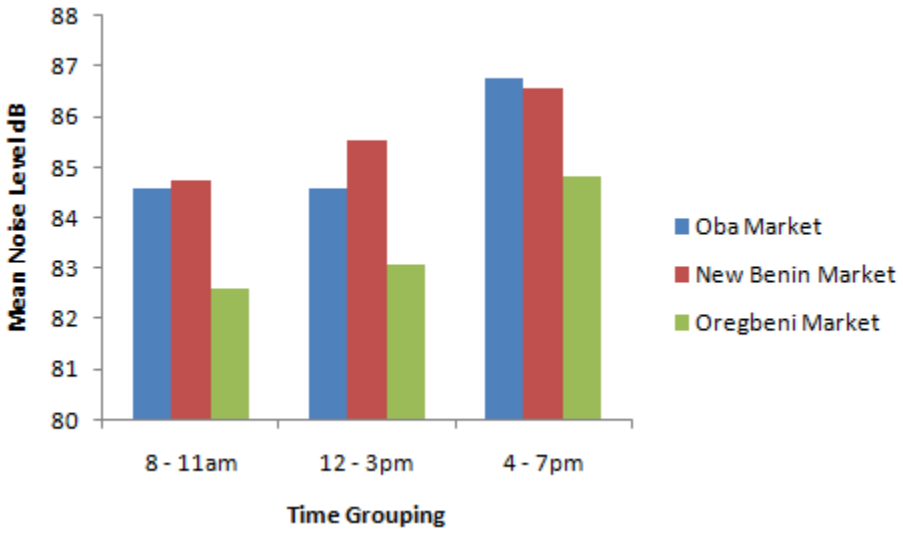

Figure 2.0: Mean Noise Levels of the Markets and Designated Time Periods

Figure 2.0 indicates that Oba Market produced the overall highest mean noise level of 86.76 dB(A) particularly in the evening while New Benin Market produced the highest mean noise level during the morning and afternoon sessions with 84.73 dB(A) and 85.55 dB(A) respectively. Oregbeni market produced the least mean noise levels within the period under review for the three markets examined.

3.3. Deliverables from Questionnaire Studies

Questionnaire studies revealed about seven noise sources in the markets abound. These include Traders Negotiating, Loud speakers, Grinding Machine, traffic, worship centres, generators and live-animals such as chickens, goats and other animals for sales but not slaughtered. Worship centre in this context indicate those make shift place of worship, particularly in the mornings, where traders congregate. The percentage of noise emanating from theses sources in each of the markets examined are shown in Table 7.

The survey showed that in Oba market, traffic activities produce the loudest noise followed by generators producing electricity with traders negotiating purchases coming as the third highest noise sources in the market. The least source of noise was found to be un-slaughtered animals in the market.

similar to Oba market, New Benin market has traffic activities has the major source of noise followed in equal measure by noise from advert-calling loud speakers (81.6%) followed by make shift worship centres in the market (73.7%). The principal source of noise at Oregbeni market is grinding machine (90.7%) followed by generators (88.4%) and in equal measure, traders negotiating purchases and traffic activities (86%). The least noise from Oregbeni market is worship centres (53.5%). Overall, traffic activities featured as the major source of notice in three markets examined.

Table 7: Distribution of Major Noise Sources in Each Market

SOURCES	Oba Market (%)	New Benin Market (%)	Oregbeni Market (%)
Traders Negotiating	83.3	76.3	86.0
Loud speakers	76.2	81.6	67.4
Grinding Machine	69.0	60.5	90.7

Traffic	95.2	89.5	86.0
Worship Centres	50.0	73.7	53.5
Generators	88.1	81.6	88.4
Un-slaughtered Animals	42.9	44.7	72.1

3.4 Measure of Noise-induced discomfort in the markets

With the questionnaire, measure of discomfort arising from noise was grouped into three classes namely: low, moderate and high discomforts. From Table 7, the level of noise induced discomfort at Oba market is generally low up to 11am from which it becomes moderate up 1pm, after which it becomes highly discomforting up to 5pm and remain moderate until the close of business. Similar trend occurred at New Benin market except that towards the close of business, the discomfort arising from noise is low at the close of business each day. Oregbeni market attains two noise peaks daily between 9am to 11am and 3pm to 5pm. For the rest of the day, the level of discomfort is generally moderate.

Table 8: Period of Noise-Induced Discomforts in the markets

Time	Oba Market (%)			New Benin Market (%)			Oregbeni Markets (%)		
	Low	Moderate	High	Low	Moderate	High	Low	Moderate	High
7am-9am	66.7	26.2	8.1	68.4	31.6	-	76.7	16.3	7
9am-11am	45.2	40.5	14.3	52.6	42.1	5.3	16.3	25.6	58.1
11am-1pm	26.2	52.4	21.4	28.9	47.4	23.7	20.9	41.9	37.2
1pm-3pm	16.7	38.1	45.2	18.4	34.2	47.4	27.9	39.5	32.6
3pm-5pm	11.9	28.6	59.5	13.2	39.4	47.4	9.3	25.6	65.1
5pm-7pm	21.4	45.3	33.3	13.2	50	36.8	23.3	39.5	37.2
7pm-9pm	16.7	42.9	40.4	47.4	31.6	21	20.9	46.5	32.6

3.4 Adverse Effects of noise in the Markets

The adverse effects of noise incorporated into the questionnaire for the three markets examined include disturbance, irritation, headache, loss of concentration, loss of hearing and stress, loss of sleep, anger, loss of appetite. As in noise induced discomfort, these adverse effects were grouped into three classes: low, moderate and high and shown in table 8. Respondents acknowledged that they experience high adverse effects arising from disturbance, irritation, headache, loss of concentration, loss of hearing and stress in the majority of cases in the markets examined. Loss of appetite appears not to be an issue with noise level by the respondents.

Table 9: Measure of Adverse effects of noise by respondents in the markets

Time	Oba Market (%)			New Benin Market (%)			Oregbeni Markets (%)		
	Low	Moderate	High	Low	Moderate	High	Low	Moderate	High
Disturbance	7.1	23.8	69.1	13.2	23.7	63.1	9.3	30.2	60.5
Irritation	11.9	35.7	52.4	10.5	39.5	50.0	14	39.5	26.5
Headache	19.1	45.2	35.7	15.8	39.5	44.7	23.3	37.2	39.5
Loss of Concentration	26.2	26.2	47.6	23.7	26.3	50.0	18.6	32.5	48.8

Loss of Hearing	21.4	35.7	42.9	13.2	34.2	52.6	23.3	34.8	41.9
Stress	33.3	28.6	38.1	31.6	21.1	47.3	25.6	39.5	34.8
Loss of Sleep	26.2	19.1	54.7	31.6	42.1	26.3	18.6	23.3	58.1
Anger	19.1	38	42.9	23.7	36.8	39.5	21	32.5	26.5
Loss of Appetite	54.7	28.6	9.7	50	36.8	13.2	60.5	30.2	9.3

4.0 Conclusion and Recommendation

The noise level effect at 70dB is considered annoying[38] and is regarded as the noise level stipulated for commercial areas such as markets. WHO [7, 18] posited that prolonged exposure to this noise level leads to hearing impairment. While intermittent period low noise abound in the markets under review, the average noise levels in the markets is between 77.00 to 89.20dB in the morning; 74.30 to 90.20dB in the afternoon and 83.30 to 90.90dB in the evening. While the adverse effects of noise may not be immediate, it is often irreversible from prolonged exposure to high decibel noise. It was noticed that New Benin market has the highest mean noise in the morning and afternoon while Oba market has the highest noise in the evening even as Oregbeni market sometimes experience occasional sharp and low noise hence accounting for its high average noise in afternoon and evening.

Questionnaire study revealed that traffic activities accounts for the major source of noise at New Benin market and Oba market while grinding machine is the principal source of noise at Oregbeni market. The period of highest discomfort associated with noise is between 1pm to 5pm at Oba market and New Benin market, while Oregbeni market has two peaks between 9-11am and 3 - 5pm. With the exception of loss of appetite, respondents acknowledged the various adverse effects of noise such as irritation, loss of sleep, headaches etc

While it may not be entirely possible to shut out noise in markets, with proper control, the effects of noise can be brought to a manageable level to make the environment more convenient for both sellers and shoppers. The following recommendations are considered:

1. Relocate the market to a land some distance from the market to control traffic noise. The markets, by virtue of their locations, aggravate the noise (usually from vehicle horns) from traffic activities.
2. Provide a dedicated power supply to the market to reduce dependence on generators
3. Grinding machine vendors should be clustered and taken to a secluded area of the market where there would be mandatory use of ear muff.
4. More civilised purchasing methods should be adopted where the minimum price tags are placed on items to avoid prolonged bargaining.
5. Restriction on the use of loudspeakers over a prolonged period in the market environment should be enforced.
6. Proper layout planning of market to ensure ease of movement of goods and people within the market space should be considered. Overcrowding in the market often contribute, immensely, to increased market noise.
7. Further studies on noise pollution in other markets or commercial hubs in Benin City, Edo state and the nation at large should be carried out to increase the level of awareness of the harmful effects of noise pollution to the general public

References

[1.] Oyedepo, S.O.*(2012).Noise pollution in urban areas: The neglected dimensions* Environmental Research Journal. **6**(4).35-45

[2.] Berglund, B. and Lindvall, T. (1995), *Community Noise* World Health Organization: Archives of the Center for Sensory Research. p. 1-195.

[3.] Kryter, K. (1985), *The effects of noise on man.*, Academic Press: New York. p. 389-393.

[4.] Bluhm, G., Nordling, E. and Berglind, N.*(2004).Road traffic noise and annoyance: an increasing environmental health problem.* **6**: p. 43-49.

[5.] Lee, C. and Fleming, G. (2002), *General Health Effects of Transportation Noise.*, U.S. Department of Transportation. : Washington, DC. p. RR297-LR2.

[6.] Babisch, W. (2005), *Noise and Health.* , Environ Health Perspective. p. A14-15.

[7.] World Health Organization (2001), *Occupational and community noise.* : London, United Kingdom.

[8.] Abel, A.A.*(2015).Urban Noise Pollution in Nigerian Cities: Imperatives for Abatement.* British Journal of Applied Science & Technology. **10**(6): p. 1-9.

[9.] Ijaiya, H.*(2014).The Legal Regime of Noise Pollution in Nigeria* Beijing Law Review. **05**: p. 1-6.

[10.] Akhtar, N.*(1996).Noise – Induced hearing loss in traffic police constables* Journal of College Physicians Surgical Pak. **6**(5): p. 265-268.

[11.] Stansfeld, S., Haines, M. and Brown, B.*(2000).Noise and health in the urban environment* Rev Environ Health. **15**: p. 43-82.

[12.] Oyedepo, O.S. and Saadu, A.*(2009).A comparative study of noise pollution levels in some selected areas in Ilorin Metropolis, Nigeria* Environmental monitoring assessment. **158**(1): p. 155-167.

[13.] Glaeser, E.L.*(2014).A World of Cities: The Causes and Consequences of Urbanization in Poorer Countries* Journal of European Economists Association. **12**: p. 1154–1199.

[14.] Scott, A.J. and Storper, M.*(2015).The Nature of Cities: The Scope and Limits of Urban Theory* International Journal of Urban Regulations. **39**: p. 1-15.

[15.] Solocki, W., Rosenzweig, C., Hammer, S. and Mehrotra, S. *(2013)* Responding to new global challenge from the urban transformation: Health, shelter and climate change. The urbanization of climate change, M. Stephen and T. Beatley. Abingdon, UK: Routledge. 107–116.

[16.] Zhao, J., Zhu, C. and Zhao, S.*(2014).Comparing the Spatiotemporal Dynamics of Urbanization in Moderately Developed Chinese Cities over the Past Three Decades: Case of Nanjing and Xi'an.* Journal of Urban Planning & Development.

[17.] Preethi, P.A., Sravani, M., Kumar, M.A., Sowmya, P., Siva, P.N., Manasa, G., Reddy, V.B. and Reddy, G.P.*(2016).Noise pollution and its impact on human health and social behaviour using systems approach-A case study in Kurnool City* Civil and Environmental Research. **8**(7): p. 70-80.

[18.] World Health Organization (1999), *Guidelines for Community Noise*, B. Birgitta, L. Thomas, and H.S. Dietrich, Editors, Stockholm University and Karolinska Institute: London, UK. p. 15-16.

[19.] Akande, T.M. and Ologe, F.E.*(2001).Awareness of commercial grinding machine operators in Ilorin to Noise induced hearing loss* Tropical Journal of Health Science. **8**: p. 28-31.

[20.] Aluko, E.O. and Nna, V.U.*(2015).Impact of Noise Pollution on Human Cardiovascular System* International Journal of Tropical Disease and Health. **6**(2): p. 35-43.

[21.] Yilmaz, H. and Ozer, S.*(2005).Evaluation And Analysis Of Environmental Noise Pollution In The City Of Erzurum, Turkey.* International Journal of Environment and Pollution. **23**(4): p. 438–448.

[22.] Singh, A., Bansal, A., Goel, S., Goel, P.K., Chhikara, P. and Singh, N.K.A.*(2015).Rapid Appraisal of Traffic Policemen about Auditory Effects of Traffic Noise Pollution from Ambala City.* Medical Journal. **8**: p. 5-12.

[23.] Tzivian, L., Winkler, A., Dlugaj, M., Schikowski, T., Vossoughi, M., Fuks, K., Weinmayr, G. and Hoffmann, B.*(2015).Effect of Long-Term Outdoor Air Pollution and Noise on Cognitive and Psychological Functions in Adults.* Int. Journal of Hygiene & Environmental Health. **218**: p. 1-11.

[24.] Basner, M., Babisch, W., Davis, A., Brink, M., Clark, C., Janssen, S. and Stansfeld, S.*(2014).Auditory and Non-Auditory Effects of Noise on Health* The Lancet **383**: p. 12-18.

[25.] Münzel, T., Gori, T., Babisch, W. and Basner, M.*(2014).Cardiovascular Effects of Environmental Noise Exposure.* European Heart Journal. **35**: p. 829–836.

[26.] Shahid, M.A.K., Bashir, H., Sabir, R. and Awan, M.S.*(2014).Physiological and Psychological Effects of Noise Pollution on Patients in Different Wards of Rabia Trust Hospital, Faisalabad* PJMMS. **2**(9-11).

[27.] Hammer, M.S., Swinburn, T.K. and Neitzel, R.L.*(2014).Environmental noise pollution in the United States: Developing an Effective Public Health Response* Environmental Health Perspective. **122**: p. 115–119.

[28.] Luo, J., Siemers, B.M. and Koselj, K.*(2015).How Anthropogenic Noise Affects Foraging* Global Change Biology.

[29.] Rider, C.V., Boekelheide, K., Catlin, N., Gordon, C.J., Morata, T., Selgrade, M.K., Sexton, K. and Simmons, J.E.*(2014).Cumulative Risk: Toxicity and Interactions of Physical and Chemical Stressors* Toxicology Science. **137**: p. 3-11.

[30.] Leval, K., Horvat, M. and Domitrović, H. *(2008)* In Effects Of Noise On Humans. 50, ELMAR. International Symposium. 333–336.

[31.] World Health Organization (2005), *United Nations Road Safety Collaboration: A Handbook of Partner Profiles*, W.H. Organization, Editor: Geneva, Switzerland.

[32.] Oyedepo, S.O. and Saadu, A.*(2010).Assessment of noise level in sundry processing and manufacturing industries in Ilorin metropolis, Nigeria.* Environmental monitoring assessment **162**: p. 453-464.

[33.] Oviasogie, A.C. and Ikudayisi, A.E.*(2019).Comparative Assessment Of Noise Sources In Two Residential Neighbourhoods In Benin City, Nigeria* International Journal of Environment and Pollution Research **7**(4): p. 1-28.

[34.] Ali, S.A.a.T., A.*(2003).Road traffic noise levels: Restrictions and annoyance in greater Cairo, Egypt.* Appl. Acoust. **64**(8): p. 815-823.

[35.] Olamijulo, J.O., Ana, G.R., and Morakinyo, O.M.*(2016).Noise from Portable Electric Power Generators in an Institutional Setting: A Neglected Risk Factor.* International Journal of Environmental Monitoring and Analysis. **4**(4): p. 115-120.

[36.] Weinhold, D.*(2015).Sick of Noise: The Health Effects of Loud Neighbours and Urban Din.* Grantham Research Institute on Climate Change and the Environment **Working Paper No. 213**.

[37.] Maisonneuve, N., Stevens, M., Niessen, M.E. and Steels, L.*(2009).Noise tube: Measuring And Mapping Noise Pollution With Mobile Phones* Information technologies in environmental engineering, Springer: p. 215-228.

[38.] Branch, M.C.*(1970).Outdoor Noise and the Metropolitan Environment*.

NIPES Conference Proceedings
The 1st International Conference of the Nigerian Institution of Professional Engineers and Scientists 7th-8th Oct. 2021: 350-359
www.nipesjournals.org.ng

Deployment of Machine Learning Models in Cybersecurity: A Review

***Osa E.*[a], *Ikponmwoba E. A*[b]**
[a]*Department of Electrical/Electronic Engineering, Faculty of Engineering, University of Benin, P.M.B. 1154, Benin City, Nigeria.*
[b]*Machine Learning Engineering, Rigr AI, Cork, Ireland.*

Abstract
From ARPAnet to the Internet, computer networks have entered the lives of a huge number of people way beyond the scientific community. They have connected more than 3 billion Internet users in more than 160 countries and regions around the world, greatly enriching the way people work and live. However, the ensuing cyber security problem is fast becoming the biggest destabilizing factor affecting the ubiquity of the network. It is grossly highlighted by the increasing number of malicious programs on the Internet, the continuous development of cyberattacks, the normalization of advanced persistent threats, the expansion of intelligent devices amongst others. Therefore, the development of related network security technologies continues to be the focus of research in the field of Network Security and Digital Forensics. Recent advances in Machine Learning provide novel solutions to the security problems encountered in computer networks. By making use of mathematical techniques across huge datasets, machine learning algorithms essentially build models of behaviour and utilizes these models for making future predictions based on new input data. Machine learning and recently Deep Learning techniques have found widespread applications and implementations in cyber security related issues. Many techniques, approaches, algorithms, methods and tools provided by Machine Learning sphere are successfully implemented and used by cybersecurity experts, digital forensic scientists and researchers to improve the security level of systems and networks as well as solve electronic crimes. This discourse serves to describe some Machine Learning models being deployed for the above purposes today

Keywords*: *Cyberspace, ARPAnet, Machine Learning, Cyberattacks, Cybersecurity.

1. Introduction

From ARPAnet to the Internet, computer networks have entered the lives of people way beyond the scientific community. It has connected more than 3 billion Internet users in more than 160 countries and regions around the world, greatly enriching the work and life of people around the globe. However, the ensuing cyber security problem is becoming the biggest destabilizing factor affecting the use of the network. It is highlighted by the increasing number of malicious programs on the Internet, the continuous development of cyberattacks, the normalization of advanced persistent threats, and the expansion of intelligent devices. Therefore, the development of related network security technologies has always been the focus of research in the field of network security. Recent advances in Machine Learning provide new challenges and solutions to the security problems encountered in applications, technologies and theories. Machine learning and recently especially Deep Learning techniques have found widespread applications and implementations in security-related issues. Many techniques, approaches, algorithms, methods and tools provided by Machine Learning are successfully implemented and used by security experts and researchers to improve the security level of systems and networks. Information is a backbone of modern society, and industry therefore protecting systems which process information is an important part of existence. Unfortunately, cybersecurity problems are evolving as fast as the technology changes and in the result, the number and the complexity of cyber attacks on information systems significantly increased within the last couple of years. The problem of cybersecurity is closely related to knowledge management problems. As these problems become more complex, protective measures have to benefit from developments in the fields of data mining and artificial intelligence to remain effective. The appeal and pervasiveness of machine learning (ML) is fast growing. Existing methods are being improved, and their ability to understand and answer real life issues is highly appreciated.

These achievements have led to the adoption of machine learning in several domains, such as computer vision, medical analysis, gaming and social media marketing [1]. In some scenarios, machine learning techniques represent the best choice over traditional rule-based algorithms and even human operators [2]. This trend is also affecting the cyber security field where some detection systems are being upgraded with ML components [3]. Although devising a completely automated cyber defence system is yet a distant objective, first level operators in Network and Security Operation Centres (NOC and SOC) may benefit from detection and analysis tools based on machine learning algorithms.

1.1. Taxonomy

1.1.1 Cybersecurity

Cyber security could be described as the aggregation of technologies and processes designed to protect computers, networks, programs, and data from attack, unauthorized access, change, or destruction. These systems are composed of network security and host security systems, every of those has a minimum firewall, antivirus computer code, associated with an intrusion detection system (IDS).

1.1.2 Cyberspace

This is a global domain within the information environment that consists of interdependent network of information systems infrastructure including the internet, telecommunications network, computer systems and embedded processors and controllers amongst others.

1.1.3 Artificial Intelligence

Artificial Intelligence (AI) has been considered the science of training machines in order to perform human tasks. There are many applications that AI has been involved in which include robotic vehicles, speech recognition, machine translation, and recently wireless communications [4].

1.1.4 Machine Learning

This is a specific subset of AI which includes techniques that are used for training machines in how to learn, without being explicitly programmed. Machine Learning (ML) is classified into supervised learning, semi-supervised learning, unsupervised learning, and reinforcement learning (RL) [4].

1.2. Rise of the (AI) Machines

Cisco's 2018 Annual Cybersecurity News Report found that nearly a third of Chief Information Security Officers (CISOs) have adopted AI as a way to improve the overall effectiveness of their cybersecurity strategy. Many security leaders reported that they were now "completely reliant" upon AI technologies to help protect their networks and sensitive data. As malicious programs have become more advanced, they have learned to hide themselves better and deeper. They can alter their own code, making it nearly impossible for older technology systems to detect them. AI-based cybersecurity solutions however can identify malicious behavior patterns in network traffic and in files and websites being introduced to a computer network. The catch is that AI algorithms alone can only identify what they have been trained to identify. While machine learning (a particular type of AI) makes it possible for an artificial intelligence system to grow and adapt over time, they are still limited by how they were initially set up and trained by a human operator. Through machine learning, the AI becomes smarter, learning to identify even more complex behavioral patterns. Machine learning can be used to tailor an AI-based solution to a specific network and environment

and can be used to identify progressively more complex threats as they are developed. But they need human guidance and course correcting to carry out their functions. However, security professionals are not the only ones using AI, malicious attackers are, as well. This has escalated into an arms race between the two sides, with both malicious programs and security solutions becoming steadily more intelligent.

1.3. AI for Cybersecurity

Artificial intelligence cannot do anything that humans cannot. After all the whole premise of AI is to create a machine that imitates human behavior. But it can do things faster, and can analyze large volumes of data that would be very time consuming for a human being. AI can automatically use complex pattern recognition tools to identify the hallmarks of a malicious program. While it is not all-powerful and cannot identify all threats, AI is an essential tool that reduces the amount of time that Information Technology (IT) professionals need to spend investigating attack alerts. This feature underlies perhaps the most important benefit of AI. Artificial intelligence can quickly detect many a cybersecurity threats, escalating the issues to the attention of human analysts. AI can also save human analysts significant amounts of time required to identify threats that they potentially would not have been able to. However, AI cannot completely replace dedicated IT professionals although it is increasingly being integrated into next-generation cybersecurity solutions [5]. A few of the major advantages of using AI for cybersecurity include handling large volume of data, AI cybersecurity can learn over time, Artificial intelligence identifies unknown threats (i.e., spot zero-day attacks).

2. Types of Cyber Attack

2.1 Vulnerability Scan

It is the scanning process for the detection of security vulnerabilities in the system. Software such as Nmap, Nessus, OpenVAS are frequently used for this process. This process could also involve collecting information about the target system and extracting network map of the target system. The first stage of the cyber attack architecture is vulnerability detection. After this stage, the attack methodology is determined by the attacker [6], [7].

2.2 Denial of Service (DoS)

It is the type of attack carried out by exploiting resource capacities of the target system such as RAM and CPU. In this type of attack, the target system is deactivated and the system cannot serve the intended purpose [8].

2.3 Distributed Denial of Service (DDoS)

They are the attacks intended to deactivate the target system much more quickly. DDoS attacks are carried out from multiple attack sources simultaneously. In DDoS attacks, in order to deactivate the target system, bandwidth is usually exploited or many connection requests are sent to the system at the same time. Thus, the system becomes unable to respond to incoming legitimate connections. This attack scenario is done by methods such as ICMP flooding, HTTP flooding, TCP flooding, etc. [9], [10].

2.4 Brute Force Attack

It is a type of attack designed to get full authority on the target system. The aim is mostly to obtain the password of the user, who is authorized to system. In order to obtain the login information of

the target system, data is uploaded to the target system. If there is no information available, different username and password combinations are tried in order to crack the password. This type of attack is frequently applied to network systems using protocols such as Remote Login, SSH, RDP, FTP, HTTP [11],[12].

2.5 Exploit

This is a type of attack on the target system designed to raise authority. The system is seized with pieces of code prepared for vulnerabilities in software or hardware in the systems. There are many types of exploits. But the most dangerous are the Zero Day Exploits because these exploits are written as soon as a security vulnerability is detected in the system and system administrators are not aware of the vulnerability [13], [14].

2.6 SQL Injection

This is mostly an attack on Web applications. Vulnerabilities in websites' databases are used to compromise the database. Thus, user information and confidential information on websites can be accessed. This type of attack ranks first in OWASP (Open Web Application Security Project), which deals with web applications security [15], [16].

3. Classification of Machine Learning Algorithms for Cyber Security

Machine learning includes a large variety of paradigms in continuous evolution, presenting weak boundaries and cross relationships. Furthermore, different views and applications may lead to different classifications of algorithms. Hence, we cannot refer to one fully accepted taxonomy from literature, but a taxonomy intended to capture the differences among the myriad of techniques that are being applied to cyber detection, is shown in Figure 1. This taxonomy is specifically oriented to security operators and avoids the ambitious goal of presenting the ultimate classification that can satisfy all AI experts. The first discriminant in Figure 1 is between the traditional ML algorithms, which today can be referred to as **Shallow Learning (SL)**, in opposition to the more recent **Deep Learning (DL)**. Shallow Learning requires a domain expert (that is, a **feature engineer**) who can perform the critical task of identifying the relevant data characteristics and categories before executing the SL algorithm. Deep Learning relies on a multi-layered representation of the input data and can perform feature selection autonomously through a process.

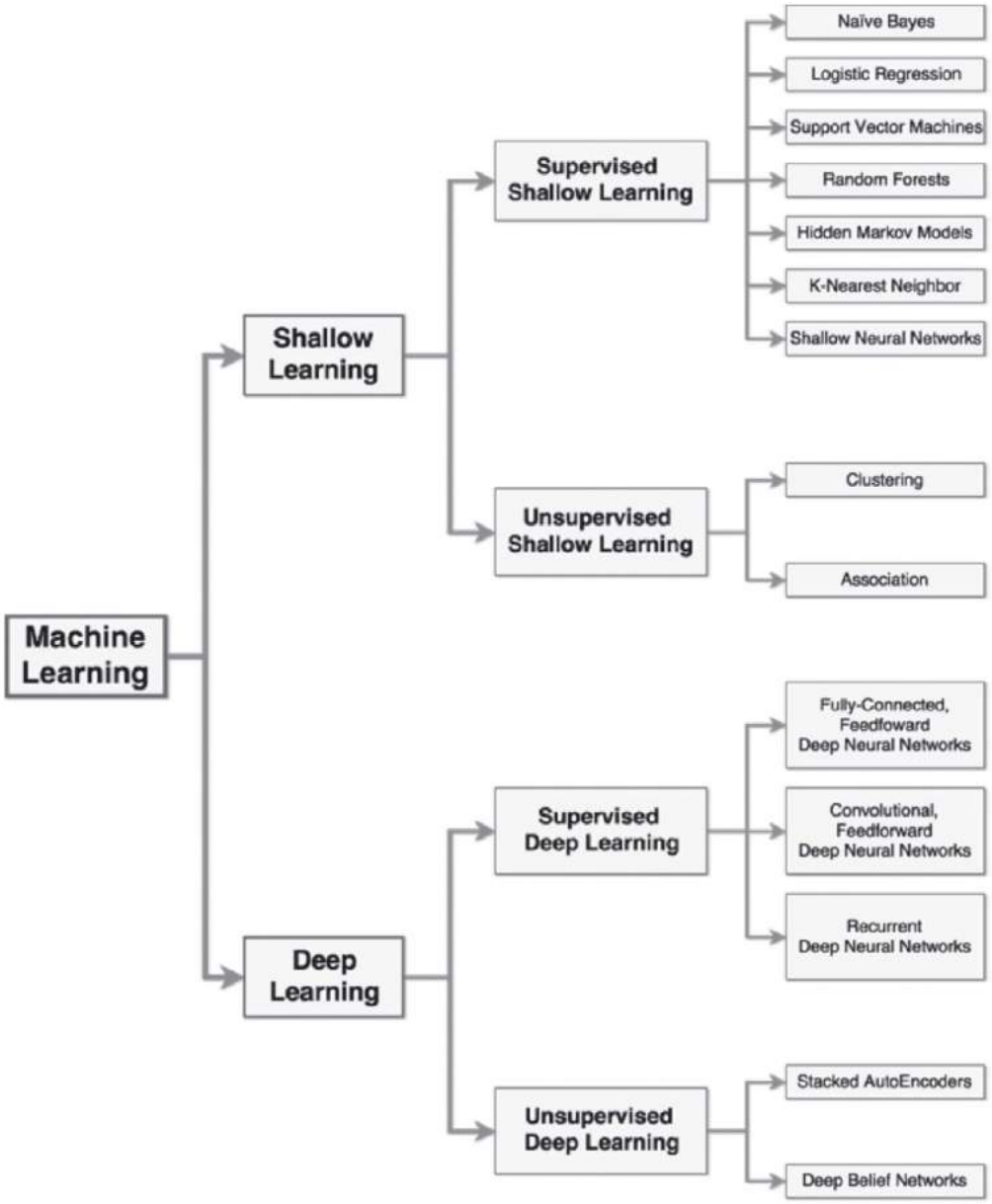

Figure 1. Classification of ML Algorithms for Cyber Security Applications [17]

SL and DL approaches can be further characterized by distinguishing between **supervised** and **unsupervised** algorithms. The **supervised** techniques require a training process with a large representative set of data that have been previously classified by a human expert or through other means. The **unsupervised** approaches do not require a prelabelled training dataset. In this section, we consider and compare the most popular categories of ML algorithms, in Figure 1. However, each category includes other different techniques.

3.1 Shallow Learning

3.1.1 Supervised SL algorithms

- **Naïve Bayes (NB)**

These algorithms are probabilistic classifiers which make the a-priori assumption that the features of the input dataset are independent from each other. They are scalable and do not require huge training datasets to produce any appreciable results.

- **Logistic Regression (LR)**

These are categorical classifiers that adopt a discriminative model. Like NB algorithms, LR methods make the a-priori independency assumption of the input features. Their performance is highly dependent on the size of the training dataset.

- **Support Vector Machines (SVM).**

These are non-probabilistic classifiers that map data samples in a feature space with the aim of maximizing the distance between each category of the samples. They do not make any assumption on the input features, but they perform poorly in multi-class classifications. Hence, they should majorly be used as binary classifiers. Their limited scalability might lead to longer processing times.

- **Random Forest (RF)**

A random forest is a set of *decision trees*, and considers the output of each tree before providing a unified final response of the entire process. Each decision tree is a conditional classifier: the tree is visited from the top and, at each node, a given condition is checked against one or more features of the analysed data. These methods are efficient for large datasets and excel at multiclass problems, but deeper trees might lead to overfitting.

- **Hidden Markov Models (HMM)**

These techniques model the system as a set of states producing outputs with different probabilities; the goal is to determine the sequence of states that produced the observed outputs. HMM are effective for understanding the temporal behaviour of the observations, and for calculating the likelihood of a given sequence of events. Although HMM can be trained on labelled or unlabeled datasets, in cyber security they have mostly been used with labelled datasets.

- **K-Nearest Neighbour (KNN)**

KNN are used for classification and can be used for multi-class problems. However, both their training and test data phase are computationally demanding as to classify each test sample, they compare it against all the training samples.

- **Shallow Neural Network (SNN)**

These algorithms are based on neural networks, which consist in a set of processing elements (that is, *neurons*) organized in two or more communicating layers. SNN include all those types of neural networks with a limited number of neurons and layers. Despite the existence of unsupervised SNN, in cyber security they have mostly been used for classification tasks.

3.1.2 Unsupervised SL algorithms

- **Clustering.**

These algorithms group data points that present similar characteristics. Well known approaches include k-means and hierarchical clustering. Clustering methods however have a limited scalability, but they represent a flexible solution that is typically used as a preliminary phase before adopting a supervised algorithm or for other purposes such as anomaly detection.

- **Association**

These algorithms aim to identify unknown patterns between data, making them suitable for prediction purposes. However, they tend to produce an excessive output of not necessarily valid rules, hence they must be combined with accurate inspections by a human expert.

3.2 Deep Learning (DL)

All DL algorithms are based on Deep Neural Networks (DNN), which are large neural networks organized in many layers capable of autonomous representation learning.

3.2.1 Supervised DL Algorithms

- **Fully-connected Feedforward Deep Neural Networks (FNN)**

These are a variant of DNN where every neuron is connected to all the neurons in the previous layer. FNN do not make any assumption on the input data and provide a flexible and general-purpose solution for classification, at the expense of high computational costs.

- **Convolutional Feedforward Deep Neural Networks (CNN)**

These are a variant of DNN where each neuron receives its input only from a subset of neurons of the previous layer. This characteristic makes CNN effective at analysing spatial data, but their performance decreases when applied to nonspatial data. CNN have a lower computation cost than FNN.

- **Recurrent Deep Neural Networks (RNN)**

These are a variant of DNN whose neurons can send their output also to previous layers; this design makes them harder to train than FNN. They excel as sequence generators, especially their recent variant, the **long short-term memory.**

3.2.2 Unsupervised DL algorithms

- **Deep Belief Networks (DBN)**

They are modelled through a composition of **Restricted Boltzmann Machines** (RBM) which is a class of neural networks without output layer. DBN can be successfully used for pre-training tasks because they excel in the function of feature extraction. They require a training phase, but with unlabeled datasets.

- **Stacked Autoencoders (SAE)**

They comprise multiple **Autoencoders**, a class of neural networks where the number of input and output neurons are equal. SAEs excel at pre-training tasks similarly to DBN, and achieve better results on smaller datasets.

4. Areas of Applications

There are three major areas where most cyber ML algorithms are finding application namely: **Intrusion detection, Malware analysis, and Spam detection**. An outline of each field is presented below.

4.1 Intrusion detection

It aims to discover illicit activities within a computer or a network through Intrusion Detection Systems (IDS). **Network** IDS are widely deployed in modern enterprise networks. These systems were traditionally based on patterns of known attacks, but modern deployments include other approaches for anomaly detection, threat detection and classification based on machine learning. Within the broader intrusion detection area, two specific problems are relevant to analysts: the detection of **botnets and of Domain Generation Algorithms (DGA).** A botnet is a network of infected machines controlled by attackers and misused to conduct multiple illicit activities. Botnet detection aims to identify communications between infected machines within the monitored network and the external command-and control servers. Despite many research proposals and commercial tools that address this threat, several botnets still exist. DGA automatically generate

domain names, and are often used by an infected machine to communicate with external server(s) by periodically generating new hostnames. They represent a real threat for organizations because, through DGA which relies on language processing techniques, it is possible to evade defences based on static blacklists of domain names.

4.2 Malware analysis

This is an extremely relevant problem because modern malware can automatically generate novel variants with the same malicious effects but appearing as completely different executable files. These polymorphic and metamorphic features defeat traditional rule-based malware identification approaches. ML techniques can be used to analyse malware variants and attribute them to the correct malware family.

4.3 Spam and phishing detection

It includes a large set of techniques aimed at reducing the waste of time and potential hazard caused by unsolicited emails. Nowadays, unsolicited emails, namely **phishing**, represent the preferred way through which an attacker establishes a first foothold within an enterprise network. Phishing emails include malware or links to compromised websites. Spam and phishing detection are increasingly difficult because of the advanced evasion strategies used by attackers to bypass traditional filters. ML approaches can improve the spam detection process [17].

5. Challenges to Machine Learning in Cybersecurity

However, machine learning is no silver bullet, not least for an industry still experimenting with these technologies in proof of concepts. There are numerous pitfalls. Machine learning systems sometimes report false positives (from unsupervised learning systems where the algorithms infer categories based on data), while some analysts have spoken candidly about how machine learning in security can represent a “black box” solution, where CISOs aren’t totally sure what’s “under the hood.” They are thus forced to place their trust and responsibility on the shoulders of the vendor – and the machines [18]. While AI is being leveraged in a wide number of areas, cybersecurity is one that has received special attention because of the rate at which threats are evolving and the volume of attacks. Organizations require a solution that can keep up. AI sometimes is championed as that solution – a silver bullet that will “solve” cybersecurity. While that isn’t the case, AI is an exciting technology that provides some real-world benefits today, and promises to have even greater potential for the future.

6. The Limitations of AI for Cybersecurity

Though AI is very powerful, it is still a relatively new technology when it comes to cybersecurity, and still has some limitations as stated below.

- **AI is not sophisticated enough to replace human analysts**

there’s still the potential for false positives and missed detection. AI is best used as a tool for human analysts to use – as it reduces the amount of time and resources that need to be spent evaluating potential threats – but not a tool to replace analysts.

- **Cyber threats are constantly evolving**

Bad actors are creative and have virtually unlimited resources; in some areas, cybercrime is an economy unto itself. As new threats emerge, security solutions that use artificial intelligence have to be re-trained in order to keep up.

- **Cybercriminals also use AI**

They are able to acquire AI-driven cybersecurity solutions and test their malicious programs against them. As a result, they can theoretically create an AI proof malware strain. They also use machine learning to understand what AI-based security systems are looking for, and then can either disguise their attack or pollute the sample so that their attack appears to be benign. Security is the only field where AI systems fight back.

- **It is better to be cautious**

AI systems are not yet advanced enough to be 100% accurate in distinguishing between malicious and benign activity. To protect a network and its applications and data, most cybersecurity solutions (including AI-based solutions) err on the side of caution. That is, when in doubt, they flag something as anomalous and potentially threatening. This creates alerts about anomalous activities that need to be investigated by human analysts and turn out to be benign. The alternative is to be cautious in order to minimize the number of false positives and risks of missing real attacks.

7. Conclusion

This paper presents a review of machine learning models being deployed for cybersecurity. Many algorithms and techniques which serve as platform for these models have also been described. Machine learning cold be highly beneficial to the cyber security industry when cyber attacks are treated as a data problem. It is recommended that the Nigerian Cyber security Industry research more and consequently deploy such models owing to the associated benefits.

References

[1] M.I. Jordan and T.M. Mitchell (2015) “Machine learning: Trends, perspectives, and prospects,” Science, 2015.
[2] Y. LeCun, Y. Bengio and Hinton, G. (2015) “Deep learning,” Nature, vol. 521, no. 7553, pp. 436–444, 2015.
[3] A. Buczak and E. Guven (2015). “A survey of data mining and machine learning methods for cyber security intrusion detection,” IEEE Communications Surveys & Tutorials, 2015.
[4] E. Alpaydin (2014). Introduction to Machine Learning; MIT Press: Cambridge, MA, USA.
[5] LASTLINE, (2018). AI and Cybersecurity: Understanding the Advantages and Limitations. https://www.lastline.com/author/jrivenbark.
[6] S. Wang, Y. Gong, G. Chen, Q. Sun and F. Yang (2013). Service vulnerability scanning based on service-oriented architecture in web service environments, J. Syst. Archit. (2013), https://doi.org/10.1016/j.sysarc.2013.01.002.
[7] A. Tantawy, S. Abdelwahed, A. Erradi and K. Shaban (2020). Model-based risk assessment for cyber physical systems security, Comput. Secur. (2020), https://doi.org/10.1016/ j. cose.2020.101864.
[8] C.L. Zhang, G.H. Yang and A.Y. Lu (2021). Resilient observer-based control for cyber-physical systems under denial-of-service attacks, Inf. Sci. (Ny). 545 (2021) 102–117, https://doi.org/10.1016/j.ins.2020.07.070.
[9] K.B. Virupakshar, M. Asundi, K. Channal, P. Shettar, S. Patil and D.G. Narayan (2020). Distributed denial of service (DDoS) attacks detection system for openstack-based private cloud, Procedia Comput. Sci. (2020), https://doi.org/10.1016/j. procs.2020.03.282.
[10] L. Barki, A. Shidling, N. Meti, D.G. Narayan and M.M. Mulla (2016). Detection of distributed denial of service attacks in software defined networks, *In: 2016 Int. Conf. Adv. Comput. Commun. Informatics, ICACCI, 2016, p. 2016*, https://doi.org/10.1109/ ICACCI.2016.7732445.

[11] M.M. Najafabadi, T.M. Khoshgoftaar, C. Kemp, N. Seliya and R. Zuech (2014). Machine learning for detecting brute force attacks at the network level, in: Proc. - IEEE 14th Int. Conf. Bioinforma. Bioeng. BIBE, 2014, p. 2014, https://doi.org/10.1109/ BIBE.2014.73.

[12] D. Stiawan, M.Y. Idris, R.F. Malik, S. Nurmaini, N. Alsharif and R. Budiarto (2019). Investigating brute force attack patterns in IoT network, J. Electr. Comput. Eng. (2019), https://doi.org/10.1155/2019/4568368.

[13] Exploit-db (2020). anatomy of exploit - world of shellcode, (n.d.) 35646. https://www.exploit-db.com/papers/35646 (accessed August 06, 2021).

[14] U.K Singh, C. Joshi and D. Kanellopoulos (2019). A framework for zero-day vulnerabilities detection and prioritization, J. Inf. Secur. Appl. (2019), https://doi.org/10.1016/j. jisa.2019.03.011.

[15] S.W. Boyd and A.D. Keromytis (2004). SQLrand: preventing SQL injection attacks, Lect. Notes Comput. Sci. (Including Subser. Lect. Notes Artif. Intell. Lect. Notes Bioinformatics). (2004), https://doi.org/10.1007/978-3-540-24852-1_21.

[16] W.G.J Halfond, J. Viegas and A. Orso (2008). A classification of SQL injection attacks and countermeasures.

[17] Apruzzese, G., Colajanni, M., Ferretti, L., Guido, A. and Marchetti, M. (2018). On the Effectiveness of Machine and Deep Learning for Cyber Security, *2018 10th International Conference on Cyber Conflict CyCon X*: Maximising Effects T. Minárik, R. Jakschis, L. Lindström (Eds.) 2018 © NATO CCD COE Publications, Tallinn.

[18] D. Drinkwater (2017). 5 Top Machine Learning Use Cases for Security. www.csoonline.com.

NIPES Conference Proceedings
The 1st International Conference of the Nigerian Institution of Professional Engineers and Scientists 7th-8th Oct. 2021: 360-371
www.nipesjournals.org.ng

Development and Application of a Deep Learning Based SMS Spam Detection Model

Osa E.[a] , Elaigwu. V.O[b]

[a]*Department of Electrical/Electronic Engineering, Faculty of Engineering, University of Benin, P.M.B. 1154, Benin City, Nigeria.*
[b]*Department of Electrical/Electronic Engineering, Faculty of Engineering, Benson Idahosa University, P.M.B. 1100, Okha, Benin City, Nigeria.*

Abstract
Antispam techniques have been developed for decades and many methods for mitigating spam emails have also been applied in the SMS domain. These include Artificial Intelligence techniques. This work is aimed at the development and subsequent deployment of a spam detection model using Deep Learning algorithms. Various Spam data repositories were scanned for usable data required to create the model. Packages such as Google Colab, Pandas, Seaborn, Matplotlib and Wordcloud were used for Expository data analysis to gain insight into the nature of the data. Packages such as Tensorflow, Python-dotenv, Scikit learn were used to create and evaluate the Deep Learning model. Finally, the model was deployed using Flask, a python library for web development. The web application was used to read SMS messages sent to a Twilio phone number which classified the messages into ***spam or ham****. The results showed an accuracy score of 98.3% which proves that the developed model is highly reliable for detecting SMS Spam messages.*
Keywords**:** *Spam, SMS, Python, Machine Learning, Deep Learning, Model.*

1. Introduction

One of the most popular and common communication services is the Short Message Service, known as SMS. SMS traffic volumes have risen from 1.46 billion in 2000 to 7.9 trillion in 2012 [1]. SMS-capable mobile phone users had reached 6.1 billion users by the year 2015 [2]. Short Message Service (SMS) is a service for transmitting short length messages of around 160 characters to various devices such as mobile phones, PDAs, Tablets, etc. utilizing certain standard protocols. It basically serves as an alternative means of communication to voice calls in situations where voice communication is not possible or is not desired. SMS is one of the most ubiquitous phone services with billions of people on the planet sending text messages every day. However, besides the legitimate use of such a communication service, criminals also take advantage of it for their nefarious activities. It is a major conduit for spam messages [3]. Spam refers to any kind of unwanted, unsolicited digital communication sent out in bulk (i.e. to multiple recipients who did not solicit for them). Unsolicited implies that the recipient did not grant verifiable permission for the message to be sent to him or her. Bulk implies that the message sent is part of a larger collection of messages which have virtually the same contents [4]. Spam is an issue about consent of the recipient and not necessarily message content. A message is said to be Spam only if it is both Unsolicited and Bulk. The problems caused by spam are due to the combination of the unsolicited and bulk nature of the messages. The quantity of the unwanted messages swamps messaging systems and drowns out the legitimate messages for recipients. Spam is commonly used as a medium for advertising products and services. According to [5], ninety-eight percent of all spam messages sent are a form of products or services advertisement which would apparently seem harmless while the remaining two percent pose the threat to the internet community and results in great losses. Spam instances include, Phishing mails that steal users login information and identities, Messages from internet fraudsters that mislead internet users to pay money in exchange for great riches or reward which are nonexistent, Malspam that intend to make users download malicious web content attached to the messages. However, Spam messages do not only appear in emails, they are also present in Internet forums, Text messages, Blog comments and other social media. Although SMS spam is less prevalent than email spam, it still accounts for roughly 1% of texts sent in the United States and 30% of text messages sent in parts of Asia. In the United States, SMS spam messages have been illegal under the Telephone Consumer Protection Act since 2004. Citizens who receive unsolicited

SMS messages can now bring the solicitors to small claims court. In 2009, China's three main mobile phone operators (China Telecom, China Mobile Ltd and China Unicom) signed an agreement to combat mobile spam by setting limitations on the number of text messages that could be sent each hour [6]. Spam first spread explosively as emails in the first decade of the 21th century as reflected by the statistical results in [7]. However, due to the fact that SMS is low-cost, bulk-sending, and reliably reaches intended recipients, spam began to gravitate towards this most popular and globally used communication service. Recently SMS is the recorded the most used data service in the world. In 2017 alone, the world sent 8.3 trillion SMS messages while the number of SMS messages sent monthly is 690 billion, this proves that SMS is important for business as well as other arenas of communications [8]. The companies hosting the bulk SMS sending service therefore have to continuously improve their spam filtering technology so as to combat spam SMS. This is however an arduous task as SMS contain limited words, abbreviations, etc. In addition, SMS spammers tend to use legitimate words to increase the rank of spam messages in spam filters and also use obfuscated words to confuse the spam filters. In order to address these deficiencies, Machine Learning algorithms which utilize Natural Language Processing should be implemented in Spam Detection and filtering.

1.2 An Overview of Spam

The history of spam dates back to 1864, over a hundred years before the advent of the Internet, with a telegram sent out en-masse to a number of British politicians. In a prescient sign of future developments, the telegram was an advertisement for a teeth whitening product. The first example of an unsolicited email dates back to 1978 and the precursor to the Internet—ARPANET. This proto-Internet spam was an advertisement for a new model of computer from Digital Equipment Corporation (DEC). However, it worked as many people bought the computers. By the 1980s, internet users came together on regional online communities, called bulletin boards (BBSes), that were administrated by hobbyists on their home servers. On a typical BBS, users were able to share files, post notices, and exchange messages online. During heated online exchanges, users would type the word "spam" over and over again to drown each other out. This was done in reference to a Monty Python sketch from the year 1970 in which *a husband and wife eating at a working-class café find that almost everything on the menu contains Spam. As the wife argues with the waitress over the preponderance of Spam on the menu, a chorus of Vikings drowns out the conversation with a song about Spam.* The use of the word "spam" in this context, i.e., loud annoying messaging, caught on much to the chagrin of ***Hormel Foods***, the maker of Spam recipe. Over on *Usenet*, a precursor to the modern day Internet (with functions much like today's Internet forums), **"spam"** was used to refer to excessive multiple posting across multiple forums and threads. The earliest Usenet spam included a fundamentalist religious tract, a political rant about the Armenian Genocide, and an advertisement for green card legal services. Spam did not start in earnest until the rise of the Internet and Instant email communication in the early 1990s. It however reached epic proportions with hundreds of billions of spam emails overwhelming inboxes. In 1999, ***Melissa***, the first virus that spread via macro-enabled Word documents attached to emails was let loose upon the digital world. It spread by ransacking victims' contact lists and spamming itself to everyone the contact list of the victim. *Melissa* resulted in $80 million in damages, according to the FBI (Federal Bureau of Investigation). Due to the absence of any anti-spam legislation, professional spammers rose to prominence, including the self-proclaimed "Spam King" Sanford Wallace. Wallace was at one time reckoned the biggest sender of spam emails and social media spam on websites like Myspace and Facebook. It was in the early 2000s that governments the world over began to get serious about regulating spam. Notable among them are all member countries of the European Union and the United Kingdom who have strict legislations in place to restrict spam. Likewise, in 2003 the United States enacted laws cheekily called the CAN-SPAM Act. These laws, in the United States and abroad, place restrictions on the content, sending behavior, and unsubscribe compliance of all

emails. Concurrently, top email providers such as Microsoft and Google worked hard to improve spam filtering technology. Microsoft's Bill Gates predicted spam would disappear by 2006. Under the influence of the enacted laws, a number of spammers, including the Spam King, were arrested, prosecuted and jailed for illicit activities online. In 2016, Sanford Wallace (aka Spam King) was convicted, sentenced to 30 months in prison, and ordered to pay hundreds of thousands in restitution for sending millions of spam messages on Facebook. Despite all the mitigation measures put in place, spam propagation is still an issue.

1.3 Types of Spam

Types of Spam include: Advance-fee scams, Phishing emails, Malspam and , Spam on mobile/Android devices [9].

1.4 Spam Text Messages and Phishing

Scammers usually send fake text messages to trick victims into giving personal information such as password, account number, or Social Security number. Once they lay hold on such information, they could gain access to email, bank, or other accounts of victims. They could also go ahead to sell information to other scammers or criminals on dark websites. The scammers use a variety of irreconcilable stories to try to rope in victims. They may promise free prizes, gift cards or coupons. Scammers also send fake messages that may state that they have some information about victim's account or transaction process. For instance, they may impersonate bank authorities and state that they have noticed some suspicious activity on victim's account. They may go ahead to claim there is a problem with payment details and send a fake invoice requesting victims to contact them if they did not authorize the purchase or send a fake package delivery notification to the victim. Other spam messages may install harmful malware on mobile phone of victims that steal personal information without victims realizing it [10].

1.5 Machine Learning

Arthur Samuel (1959) defined Machine learning as the field of study that gives machines the ability to learn without being explicitly programmed. Machine learning systems can be classified according to the amount and type of supervision they get during training as: Supervised learning, Unsupervised learning, Semi-supervised learning and Reinforcement learning.

1.5.1 Supervised Learning

In supervised learning, the training data contains both features and label. For example, predicting the price of a car given a set of features (mileage, age, brand, etc.). To train the model, we give the systems many examples of cars which include the features and the correct label. Some examples of supervised learning algorithms are k-Nearest Neighbors, Linear Regression, Logistic Regression, Decision Trees and Random Forest, Neural Networks.

1.5.2 Unsupervised Learning

In this type of machine learning, the training data is unlabeled. The system tries to learn without a "supervisor". Here the model tries to group similar data together: a form of clustering. Examples of unsupervised learning algorithms are K-means, DBSCAN, Hierarchical Cluster Analysis (HCA), Principal component analysis (PCA).

1.5.3 Semi-supervised learning

Labeling data is usually time-consuming and costly because sometimes the data could contain plenty of unlabeled data as well as labeled instances. Some algorithms can deal with data that is partially labeled. Most semi-supervised learning algorithms are a combination of unsupervised and supervised algorithms. For example, Deep Belief Networks (DBNs) are based on unsupervised components called Restricted Boltzmann Machines (RBMs) stacked on top of one another. RBMs are trained sequentially in an unsupervised manner and then the whole system is fine-tuned using unsupervised learning techniques.

1.5.4 Reinforcement Learning

In this kind of learning, the learning system called the Agent can observe the environment, select and perform actions, and get rewards in return. It must then learn by itself what the best strategy is (called a policy) to get the most reward over time. A policy defines what action the agent should choose when it is in a given situation.

In addition to these categories, machine learning can also be classified as either a Regression problem or a Classification problem. In Regression, continuous values are predicted, for example, the price of a house, quantity of goods to be sold in the coming month etc. For classification, discrete values are predicted, the model tries to predict the class of a particular feature for example, predicting breast cancer as either malignant or benign, classifying emails as either spam or non-spam. The Spam detection task falls under the natural language processing aspect of machine learning as the messages are text data. It is a binary classification task as we are predicting whether the message is either spam or ham.

1.6 Deep Learning

Deep learning is a class of the broad machine learning family based on artificial neural networks. It is inspired by the structure and function of the brain. Artificial neural network is a mathematical model that changes its structure during learning. In deep learning, a computer model learns from images, text, or sound. These models transform its input data into meaningful outputs, a process that is learned from exposure to known examples of inputs and outputs. Deep learning has experienced huge advancements in the artificial intelligence space and has been instrumental in many applications. Deep neural networks consist of multiple layers of interconnected nodes, each of which uses a progressively more complex deep learning algorithm to extract and identify features and patterns in the data. They then calculate the likelihood or confidence that the object or information can be classified or identified in one or more ways. The input and output layers of a deep neural network are called *visible* layers. The input layer is where the deep learning model ingests the data for processing, and the output layer is where the final identification, classification, or description is calculated. In between the input and output layers are *hidden* layers where the calculations of each previous layer are weighted and refined by progressively more complex algorithms to zero in on the final outcome. This movement of calculations through the network is called *forward propagation.* Another process called *back propagation* identifies errors in calculated predictions, assigns those weights and biases, and pushes them back to previous layers to *train* or refine the model. Together, forward propagation and back propagation allow the network to make predictions about the identity or class of the object while learning from inconsistencies in the outcomes. The result is a system that learns as it works and gets more efficient and accurate over time when processing large amounts of data.

2. Methodology

2.1 Importing Libraries & Data

The first step is to import libraries that we require to execute various codes. Thereafter the Data is imported. We treated the ham and spam message classification as a supervised machine learning problem. In a supervised machine learning problem, the inputs and the corresponding outputs are available during the algorithm training phase. During the training phase, the machine learning algorithm statistically learns to find the relationship between input texts and output labels. While testing, inputs are fed to the trained machine learning algorithm which then predicts the expected outputs without knowing the actual outputs. For supervised ham and spam message classification, we needed a dataset that contains both ham and spam messages along with the labels that specify whether a message is a ham or spam. In this paper, we used that open-source Spambase dataset from the UCI machine learning repository [11]. To import the above dataset into the work, we used the *read_csv()* method of the Pandas library as shown in appendix.

2.2 Data Exploration and Visualization

We explored the data to identify the target variables and do a bit of preprocessing on the dataset. Before application of machine learning algorithms to a dataset, it is always a good practice to visualize data to identify important data trends. We first plot the distribution of ham and spam messages in our dataset using a Bar chart. The dataset consists of 5569 messages of two classes: spam and ham messages. There are 745 spam messages (shown in Figure 1). The dataset comprises two columns, the message and the label. The label or target variable is what we are trying to predict (i.e., spam or ham).

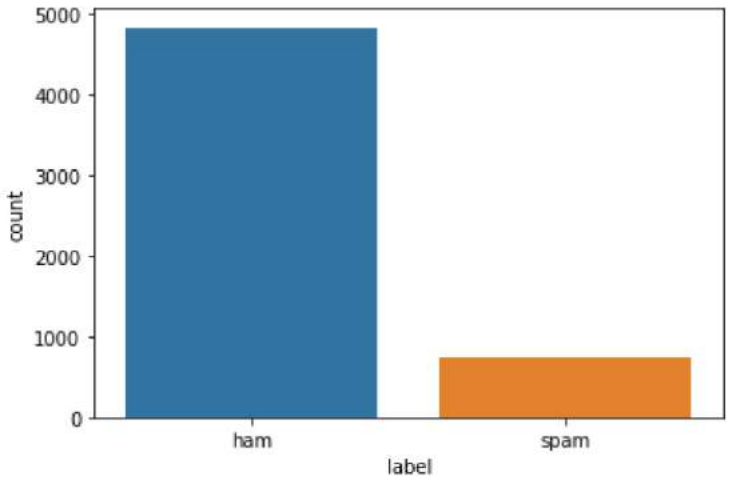

Figure 1: Bar Chart Visualizing Data Distribution.

2.3 Exploratory Data Analysis.

Exploratory Data Analysis is one of the most crucial steps in data science processes. It helps the scientist to understand and gain insight from the data. In this paper, we used Word Cloud, an open source tool for visualizing and analyzing the data. Wordclouds are a simple yet effective method of text visualization. The spam/ham messages were visualized using some wordclouds as shown in Figures 2a and b respectively. The frequency or importance of the words in the data is represented by the size of the text in the image.

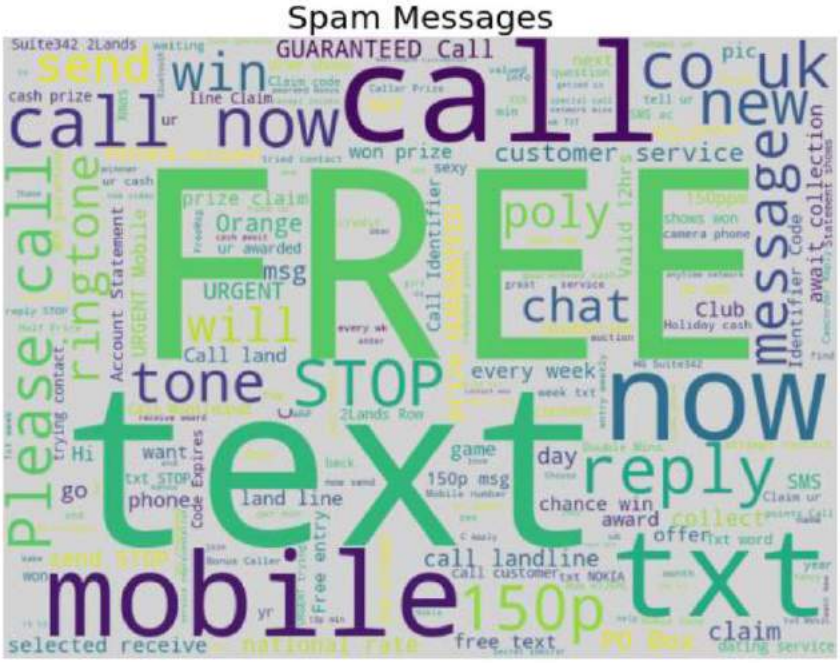

Figure 2a: WordCloud Spam Messages.

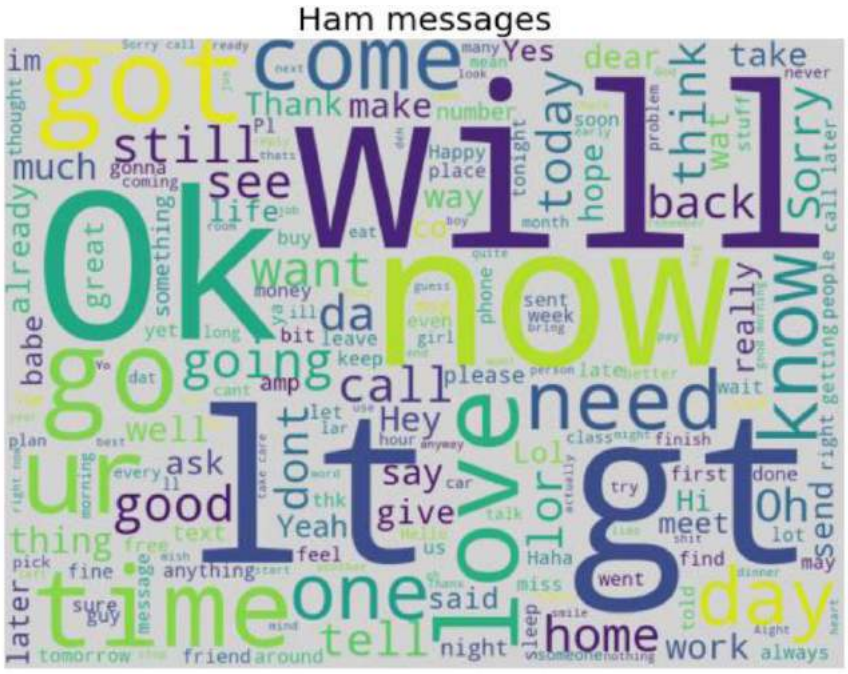

Figure 2b: WordCloud Ham Messages.

It is clearly seen from the visualizations above how the two categories of messages are differentiated.

• **Spam messages:** It can be noticed that in the spam messages, there is a higher frequency of "spammy" words such as: free, text, stop, call, message, etc. This gave our model better insight into what makes up a spam message.

• **Ham messages:** It is also noticed that Ham messages contain words such as love, time, home, work, etc.

2.4 Data Preprocessing

The datasets were collected from different sources without processed inputs for the machine learning algorithm. The first preprocessing step employed was cleaning the raw message data. This involved the following steps:

• **Converting to lower case (Case normalization)**: This was to capture the unique tokens and not differentiate between alphabet cases. Lowering the case of the text is essential because the word "SPAM", "Spam", "spam" all means the same thing and add the same value to the sentence but the model may see them different. Words that occur for a very few times or in a large number of documents are not very good for classification hence they were removed.

• **Removing special characters**: Special characters such as "", (),! , were also removed.

• **Removing stop words:** English stop words such as *a, to, i, am, is* were removed as they do not help much in classification procedure. The important words were the tokens other than the stop words. So, we removed the stop words from the messages as they do not represent any differentiating factor.

• **Removing hyperlinks.**
• **Removing numbers.**

• **Removing whitespaces**.

• **Word Stemming:** Stemming algorithms work by removing the end or the beginning of the words, using a list of common prefixes and suffixes that can be found in that language. We implemented stemming on words to bring them to their root form.

• **Word Lemmatization:** Lemmatization involves utilizing the dictionary of a particular language and trying to convert the words back to their base form. In the paper, the NLTK library in python was used to implement the Word Stemming and Word Lemmatization algorithms.

The next step after cleaning the data was to tokenize the cleaned data. Most deep learning algorithms do not work with texts and thus the data needs to be converted to numerical values. Tokenization is the process of splitting text into smaller chunks called tokens that can then be fed into the deep learning model as features.

2.5 Dividing Data into Training and Test Sets

Machine learning algorithms learn from the training set, and to evaluate how well the trained machine learning algorithms performs, predictions are made on the test set. It was therefore necessary to divide our data into the training and test sets. To achieve this, the train_test_split() method from the sklearn.model_selection module was implemented as shown in appendix.

2.6 Training the Deep Learning Model

Very simple neural network architecture was used in this work because of the small data size and to avoid over fitting. The input consists of an Embedding layer that takes integers as input, then looks up these integers in an internal dictionary, and returns the associated vectors. Summary of the model is

shown in the appendix. The model was thereafter fitted with the training set. The model trained for a number of epochs and stopped when there was no further improvement. This was made possible by the early stopping callback. The model training ran for about 11 or 12 epochs as shown in Figure 3. This variation was due to the stochastic nature of the model and even data splitting.

```
Epoch 1/50
140/140 [==============================] - 2s 9ms/step - loss: 0.3057 - accuracy: 0.8804 - val_loss: 0.0910 - val_accuracy: 0.9749
Epoch 2/50
140/140 [==============================] - 1s 7ms/step - loss: 0.0457 - accuracy: 0.9882 - val_loss: 0.1112 - val_accuracy: 0.9758
Epoch 3/50
140/140 [==============================] - 1s 7ms/step - loss: 0.0081 - accuracy: 0.9977 - val_loss: 0.1196 - val_accuracy: 0.9794
Epoch 4/50
140/140 [==============================] - 1s 7ms/step - loss: 0.0026 - accuracy: 0.9989 - val_loss: 0.1924 - val_accuracy: 0.9830
Epoch 5/50
140/140 [==============================] - 1s 6ms/step - loss: 6.4155e-04 - accuracy: 0.9996 - val_loss: 0.2298 - val_accuracy: 0.9830
Epoch 6/50
140/140 [==============================] - 1s 7ms/step - loss: 5.9977e-07 - accuracy: 1.0000 - val_loss: 0.3023 - val_accuracy: 0.9785
Epoch 7/50
140/140 [==============================] - 1s 7ms/step - loss: 2.4595e-05 - accuracy: 1.0000 - val_loss: 0.3369 - val_accuracy: 0.9803
Epoch 8/50
140/140 [==============================] - 1s 7ms/step - loss: 1.6828e-08 - accuracy: 1.0000 - val_loss: 0.3346 - val_accuracy: 0.9812
Epoch 9/50
140/140 [==============================] - 1s 6ms/step - loss: 1.6586e-09 - accuracy: 1.0000 - val_loss: 0.3401 - val_accuracy: 0.9821
Epoch 10/50
140/140 [==============================] - 1s 6ms/step - loss: 2.2260e-08 - accuracy: 1.0000 - val_loss: 0.3349 - val_accuracy: 0.9821
Epoch 11/50
140/140 [==============================] - 1s 7ms/step - loss: 5.0541e-10 - accuracy: 1.0000 - val_loss: 0.3412 - val_accuracy: 0.9830
Epoch 00011: early stopping
<tensorflow.python.keras.callbacks.History at 0x7f344a42b250>
```

Figure 3: Model Training with Epoch Display.

3. Results and Discussion

3.1 Evaluation of Algorithms

Once predictions were made, the next step was to evaluate the algorithm. Algorithm evaluation involved comparing actual outputs in the test set with the outputs predicted by the algorithm. Performance evaluation of a classification algorithm can be done using accuracy, F1, recall, and confusion matrix as performance metrics. In this paper, confusion matrix and accuracy were used as the performance metrics.

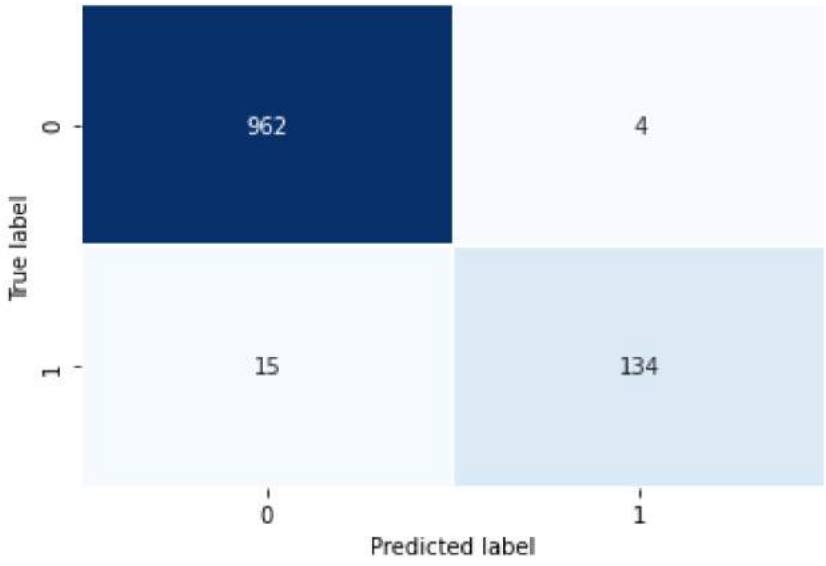

Figure 4: Confusion Matrix.

```
Classification Report
              precision    recall  f1-score   support

           0       0.98      1.00      0.99       966
           1       0.97      0.90      0.93       149

    accuracy                           0.98      1115
   macro avg       0.98      0.95      0.96      1115
weighted avg       0.98      0.98      0.98      1115

Accuracy : 0.9829596412556054
0.9829596412556054
```

Figure 5: Training Logs displaying Accuracy of Model.

The final accuracy for the validation set was around 98% (0.983) as seen in the training logs. The output shows that our algorithm achieves an accuracy of 98.3% for spam message detection which is impressive. The model was thereafter saved using the python pickle library.

3.2 Model Deployment

The model was finally deployed using **Flask**, a python library for web development. The web application reads SMS messages sent to a Twilio phone number and classifies them into spam or ham. The final result is displayed in an SMS dashboard as shown in the Figure 6.

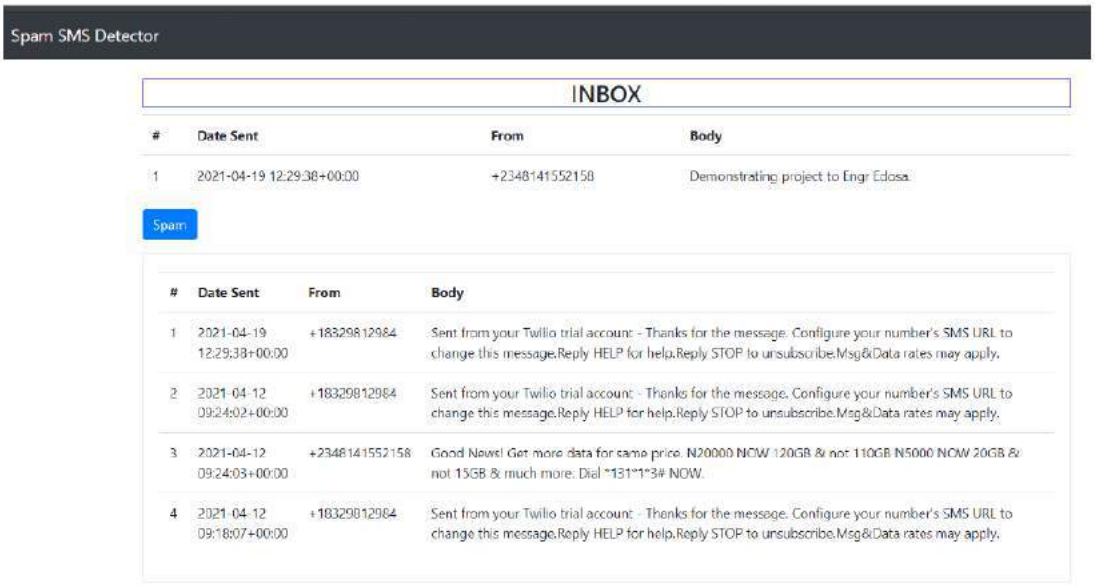

Figure 6: SMS Classification by Web Application.

4. Conclusion

Deep learning is a prominent algorithm employed in several cyber security areas. This work involved the development and application of an SMS Detection model using Deep Learning Algorithms. In this paper, a double layer Deep Learning Neural Network was applied to classify SMS messages as either Ham or Spam. Findings from result show that the developed model is highly accurate with a percentage of 98.3. For future improvements of this work, it is recommended that the model be integrated in form of an API (Application Programming Interface) for mobile and similar devices. The model can also be extended to accommodate online learning (i.e., continuous learning process while in operation).

References

[1] PortioResearch Worldwide A2P SMS Markets (2014–2017). Understanding and Analysis of Application to-Person Text Messaging Markets Worldwide; Portio Research Limited: Chippenham, UK, 2014.
[2] E. Ezpeleta (2017) Short Messages Spam Filtering Combining Personality Recognition and Sentiment Analysis. Int. J. Uncertain. Fuzziness Knowl.-Based Syst. 2017, 175–189.
[3] N. Choudhary and A.K Jain (2017). Towards filtering of SMS spam messages using machine learning based technique. Paper presented at the International Conference on Advanced Informatics for Computing Research.
[4] Spamhaus, (2021).The Spamhaus Project-The Definition of Spam. Available at: https://www.spamhaus.org.
[5] S. Forbes (2002). Web of deception: Misinformation on the Internet: Information Today, Inc. inc, c. s. (2018). Security report.
[6] TechTarget Contributor (2007). What is SMS spam (cell phone spam or short messaging service spam)? Available at: https://searchmobilecomputing.techtarget.com.
[7] V.V. Arutyunov (2013) Spam: Its past, present, and future. Sci. Tech. Inf. Process. 2013, 40, 205–211.
[8] M. Morreale (2017). Daily SMS Mobile Usage Statistics. 2017. Available online: https://www.smseagle.eu/2017/ 03/06/ daily-sms-mobile-statistics.
[9] Malwarebytes, (2021). SPAM: stupid pointless annoying…malware? https://www.malwarebytes.com.
[10] U.S. FEDERAL TRADE COMMISSION Consumer Information (2020). How to Recognize and Report Spam Text Messages. Available at: https://www.consumer.ftc.gov.
[11] Mark Hopkins, E. R., George, F. and Jaap, S. Classifying Email as Spam or Non-Spam. Retrieved from: http://archive.ics.uci.edu/ml/datasets/Spambase.

Appendix

ENTIRE CODE SNIPPETS

```
# -*- coding: utf-8 -*-
"""Copy of SPAM_DETECTOR.ipynb
Automatically generated by Colaboratory.
Original file is located at
https://colab.research.google.com/drive/1eCuG4ThRk2InjltJPKbMjfddw6gh_a_s
"""
import tensorflow as tf
print(tf.__version__)
# Commented out IPython magic to ensure Python compatibility.
# import libraries for reading data, exploring and plotting
import numpy as np
import pandas as pd
import seaborn as sns
import matplotlib.pyplot as plt
import wordcloud
from wordcloud import WordCloud, STOPWORDS, ImageColorGenerator
# %matplotlib inline
# library for train test split

from sklearn.model_selection import train_test_split
```

```
#deep learning libraries for text pre-processing
from tensorflow.keras.preprocessing.text import Tokenizer
from tensorflow.keras.preprocessing.sequence import pad_sequences
#Modeling
from tensorflow.keras.callbacks import EarlyStopping
from tensorflow.keras.models import Sequential
from tensorflow.keras.layers import Embedding, GlobalAveragePooling1D, Dense, Dropout, LSTM, Bidirectional,Flatten
url = 'https://raw.githubusercontent.com/ShresthaSudip/SMS_Spam_Detection_DNN_LSTM_BiLSTM/master/SMSSpamCollection'
messages = pd.read_csv(url, sep ='\t',names=["label", "message"])
messages.to_csv("drive/MyDrive/SpamDetector/spam.csv")
messages.head()
messages.describe()
messages.label.value_counts()
data = messages.copy()

sns.countplot(data['label'])
plt.show()
data['label'] = data['label'].map( (Wu et al., 2017) )
data_ham = data[data['label'] == 0].copy()
data_spam = data[data['label'] == 1].copy()
def show_wordcloud(df, title):
text = ' '.join(df.astype(str).tolist())
stopwords = set(wordcloud.STOPWORDS)
fig_wordcloud = wordcloud.WordCloud(stopwords=stopwords,background_color='lightgrey',
colormap='viridis', width=800, height=600).generate(text)
plt.figure(figsize=(10,7), frameon=True)
plt.imshow(fig_wordcloud)
plt.axis('off')
plt.title(title, fontsize=20 )
plt.show()
show_wordcloud(data_spam["message"],"Spam Messages")
show_wordcloud(data_ham["message"], "Ham messages")

"""Preparing Data for Training"""
X = data['message'].values
y = data['label'].values
X_train, X_test, y_train, y_test = train_test_split(X, y, test_size=0.20, random_state=42)
# prepare tokenizer
t = Tokenizer()
t.fit_on_texts(X_train)

# integer encode the documents
encoded_train = t.texts_to_sequences(X_train)
encoded_test = t.texts_to_sequences(X_test)
print(encoded_train[0:2])
# pad documents to a max length of 8words
max_length = 8
padded_train = pad_sequences(encoded_train, maxlen=max_length, padding='post')
padded_test = pad_sequences(encoded_test, maxlen=max_length, padding='post')
print(padded_train)

#model setup
vocab_size = len(t.word_index) +1

#define model
model = Sequential()
model.add(Embedding(vocab_size, 24, input_length=max_length))
model.add(Flatten())
```

```
model.add(Dense(500, activation='relu'))
model.add(Dense(200, activation='relu'))
model.add(Dropout(0.5))
model.add(Dense(100, activation='relu'))
model.add(Dense(1, activation='sigmoid'))

#compile model
model.compile(optimizer='rmsprop', loss='binary_crossentropy', metrics=['accuracy'])
model.summary()
early_stop = EarlyStopping(monitor='val_loss', mode='min', verbose=1, patience=10)
# fit the model
model.fit(x=padded_train,
y=y_train,
epochs=50,
validation_data=(padded_test, y_test), verbose=1,
callbacks=[early_stop]
)

from sklearn.metrics import classification_report, confusion_matrix, accuracy_score
def c_report(y_true, y_pred):
print("Classification Report")
print(classification_report(y_true, y_pred))
acc_sc = accuracy_score(y_true, y_pred)
print("Accuracy : "+ str(acc_sc))
return acc_sc
def plot_confusion_matrix(y_true, y_pred):
mtx = confusion_matrix(y_true, y_pred)
sns.heatmap(mtx, annot=True, fmt='d', linewidths=.5,
cmap="Blues", cbar=False)
plt.ylabel('True label')
plt.xlabel('Predicted label')
preds = (model.predict(padded_test) > 0.5).astype("int32")
c_report(y_test, preds)
plot_confusion_matrix(y_test, preds)
model.save("drive/MyDrive/SpamDetector/spam_model")

import pickle
with open('drive/MyDrive/SpamDetector/spam_model/tokenizer.pkl', 'wb') as output:
pickle.dump(t, output, pickle.HIGHEST_PROTOCOL)
"""<h1>Inference</h1>"""
s_model = tf.keras.models.load_model("drive/MyDrive/SpamDetector/spam_model")
with open('drive/MyDrive/SpamDetector/spam_model/tokenizer.pkl', 'rb') as input:
tokenizer = pickle.load(input)
sms = ["Congratulations! you just won 2 million dollars. Send you account details for processing "]
sms_proc = tokenizer.texts_to_sequences(sms)
sms_proc = pad_sequences(sms_proc, maxlen=max_length, padding='post')
pred = (model.predict(sms_proc) > 0.5).astype("int32").item()
print(pred)
```

NIPES Conference Proceedings
The 1st International Conference of the Nigerian Institution of Professional Engineers and Scientists 7th-8th Oct. 2021: 372-383

www.nipesjournals.org.ng

Smart Rack Protection Against Physical Insecurity and Privacy Intrusions of Mobile Phones in Examination Centers

Iwayemi, A.[a]*, Orisile, O. P.[a] and Okunola, I. O.[a]
[a]Department of Computer Engineering, School of Engineering, Federal Polytechnic, Ile-Oluji, Nigeria.

Abstract
Mobile phones are resources used for learning in our educational system. Online classes are accessed via mobile devices just like study materials in texts, images, audio, video and other file formats are stored and read via mobile phones. Most times, examination candidates at various levels especially in higher institutions keep assessing their preparatory resources (on mobile phones) till the moments they are called into the examination halls. Meanwhile, these important study aids are not allowed into examination halls so as to avoid examination malpractices. So, candidates are compelled to keep them in open places where they are unsafe, exposed to illegal accesses, privacy intrusion and often stolen. This paper presents an electronic framework towards ensuring the privacy and security of candidates' mobile phones during examinations. A smart rack protection against physical insecurity and privacy intrusions of mobile phones in examination centres was developed. A physical structure suitable for keeping series of mobile phones was constructed with doors that automatically lock after enrollment to secure the mobile phone(s). The enrollment involves a fingerprint based capturing system that was interfaced through programmed microcontroller which locks the rack to protect the mobile phones until the owner gets back to unlock it through their saved matching fingerprint data. Fingerprint R305 was interfaced with ATMEGA 328 Arduino microcontroller to activate the locking and unlocking processes while the software was written in C programming language. Once a registered fingerprint is placed on the sensor, access is granted to the user, the rack door opens automatically. During this process, the 16X2 LCD displays the registered user and if the user is not registered, the response will be: "finger not found". The results of testing this work yielded above 97% efficiency, a performance which secured candidates' mobile phones during examinations.

***Keywords*:** *security, mobile phones, microcontroller, fingerprint, examination*

1. Introduction

Security and privacy are essential needs in the fast growing population of the world today. Security has to do with the safekeeping of lives and properties against all sorts of attacks while Privacy, on the other hand, has to do with the confidentiality and secrecy of data and information. Intrusion against an individual's privacy or attack against their security is often seen as the greatest threat to life nowadays. The usages of mobile phones have increased and the type of information stored on these gadgets nowadays proves that an attack against mobile phone(s) is a major and irrecoverable one. There are several methods of securing mobile phones and ensuring privacy of data and information on it. As the number of mobile devices increases, the idea of mobile security has become of greater concern. Some of the trusted common means of achieving security within academic institutions include Codding Access Control (CAC), Image Censored, and Biometric Systems such as Fingerprint Recognition, Finger Geometry Recognition, Face Recognition Scanning (FRS), Eyes-Iris Recognition, Voice-Speaker Verification/Authentication, Signature Recognition, and so on.

1.1 Literature Review

One major goal of this work is to implement a method of securing and ensuring safety of mobile phones within public and private places especially academic institutions when

examinations are written. Humans are arguably the weakest link in any security strategy, and many people have neither the knowledge nor the time to track their devices if stolen. A student entering an examination hall often seeks for a place to keep their phone(s). This is because these phones are often medium of storage of their study materials. Online class materials and other resources used for preparation for examinations are stored on the phones. Hence, students, in a bit to refreshing their memories, keep their eyes at these materials on their mobile phones till the last minute before examination commences. The candidates are compelled to hand over these phones to unfamiliar individuals to hold for them while they write the examination. The alternative is for them to keep the mobile phones in their school bags that will be left in any open space at the examination hall or outside the center. All of these options expose the owners' phones to theft and privacy intrusions. In higher institutions in Nigeria, due to this challenge, examination period is an ample time for mobile phone thieves to dispossess phone owners of their phones. This system developed is targeted at helping in the security of mobile phones from theft, physical attack and privacy intrusion at this time. Meanwhile, the use of a biometric based system is an authentic way of security as used and proved in the article of many authors [1, 2, 3, 4, 5, 6, 7, 8, 9, 10, 11]. Face recognition and speech recognition are also effective ways of ensuring security as indicated in progressive researches [12, 13]. Also, the use of microcontroller based access control is a reliable way of ensuring security [14]. For instance, [15] presented fingerprint identification system using a pliable optical prism just like [16] presented similar system using graph matching both tending towards secured system easy to implement. The provision of fingerprint based system is a vital means of collecting authentic data. Fingerprint could be indexed based on multiple features [17]. [18] presented different stages of processing fingerprint with appropriate drawings. In addition, [19] presented an on-line fingerprint identification which proved to be a reliable system. It is not farfetched to say an automatic door is a smart system that could provide access control [20]. Since the issue of mobile phones theft is becoming too rampant in school premises, public and private sectors, especially at the times of examination, then it becomes essential to creatively apply these technological solutions to the safe keeping of mobile phones while examination is ongoing. This paper aimed at providing a smart mobile phone rack system towards ensuring privacy and security of mobile phones during examinations at examination centres using a microcontroller based fingerprint enrolment and authentication system.

2. Methodology

This section contains the step-by-step procedures of achieving this work. It includes each of the component units. Meanwhile the first step is the selection of design tools and materials necessary to achieve the goal. Then, the design procedure was enumerated including the block diagram of the system. The circuit diagrams of the power supply unit, the control unit and each of the other components were designed and reported. A complete circuit diagram of the entire work was also presented followed by the construction of the hardware, that is, the rack. The simulation process was also reported alongside the entire processes leading to the complete design. The flowchart of the software development was also reported appropriately.

2.1 Selection of Design Tools and Component

Selection of tools is pivotal to any engineering design as wrong tools will lead to wrong result and failure. Below is the list of some of the components selected for the design:

I. LM7805 Voltage Regulator
II. 12MHz Crystal Oscillator
III. Capacitor 22macroF
IV. AT mega 328p Microcontroller
V. 16x2 LED
VI. Buzzer Alarm
VII. Fingerprint sensor

2.2 System Design Procedure

The access control system consists of different parts, among which are: buzzer alarm D.C motor, LED, microcontroller and the fingerprint sensor. Once an authorized user places their print on the sensor, the door will automatically open and will be closed manually. If an unauthorized user places his/her print on the sensor, the user will be denied access and if the attempts is beyond three times, the alarm will trigger to alert the owner or security personnel. The access control system consists of the Input and output subsystem, the microcontroller unit and the power supply unit. The microcontroller unit resides in between the input and the output subsystems. The input subsystems include keypad buttons, fingerprint detection circuit. The output subsystem is interfaced on the output ports of the microcontroller unit. The output subsystems include: 24V relay, Celeron, status LED displays, buzzer alarm subsystem. The system should be able and capable of granting access to a registered user at any point in time and should be able to raise an alarm when an intruder is attempting to gain access. The hardware system consists of the Input and output subsystem, the microcontroller unit and the power supply unit. The microcontroller unit sits in-between the input and the output subsystems. The input subsystems include keypad buttons, fingerprint detection circuit. The output subsystem is interfaced on the output ports of the microcontroller unit. The output subsystems include: 12V relay, dc motor, status LED displays, buzzer alarm subsystem. Figure 1 shows the block diagram of the system. The block diagram shows how the following unit were integrated; Power supply unit, Sensory unit, Control unit, Display unit, Activator unit.

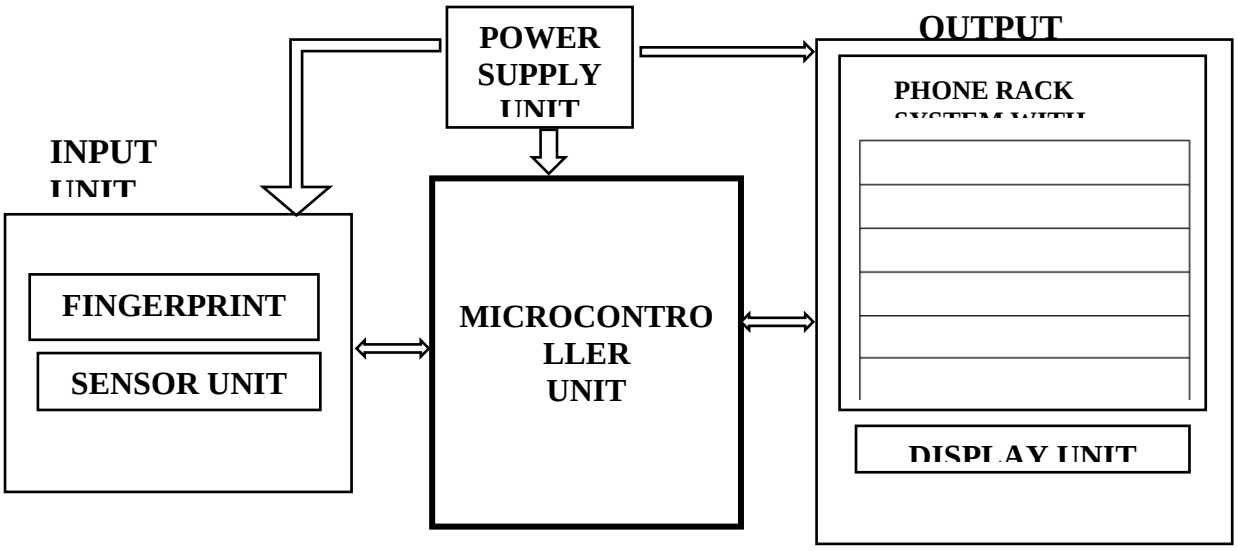

Figure 1: The block diagram

2.3 Design of the Power Supply

Generally speaking, the correct voltage supply is important for the proper functioning of the integrated circuit. For a proper function of any IC, it is necessary to provide a stable source of supply; According to technical specifications by the manufacturer of CD4001BE IC, supply voltage should move between 3 V to 18V. The controller requires the correct voltage levels for operation which is 5V supplied to the control panel, which is in turn distributed to the sensors.

The incoming 220V from the main supply is passed through a step-down transformer and rectified to get and output of smooth 5V supplied to the circuit.

Transformer

The local main is expected to deliver 240V, the system voltage requirement is 12V and 5V, therefore a 240V/15V transformer was used. The system input resistance is about 200Ω, therefore the expected load current is given by Equation (1)

$$I = V/R = 5/200 = 250 \text{ mA} \quad (1)$$

A transformer with the current rating of 500mA which is greater than load current was used. Thus the power rating of the transformer was completed to be Equation (2)

$$S = VI = 24 \text{ X } 500 \text{ mA} = 12VA \quad (2)$$

Filter

This is made up of capacitor connected across the output of the rectifier to smoothen the voltage to have the minimum ripple factor (at least 10% of the dc voltage). It is preferable to choose a filtering capacitor that will hold the peak-to-peak ripples at approximately 100% of the peak voltage.

The Voltage Regulator

The regulator is a single chip that regulates the ripple free rectified voltage to give a constant output voltage. Since the circuit needs a supply voltage of 24V and 5V, a 24V and 5V regulators were used. Figure 2 shows the circuit diagram of the power supply unit.

The percentage regulation or simply regulator of a power supply is given by Equations (3 and 4)

$$\% \text{ regulation} = [(V_{max} - V_{min})/V_{max}] \times 100 \quad (3)$$

Where;

V_{max} = maximum dc output voltage

V_{min} = minimum dc output voltage

in a general form

$$\% \text{ regulation} = [(V_{\text{no load}} - V_{\text{full load}})/V_{\text{full load}}] \times 100. \quad (4)$$

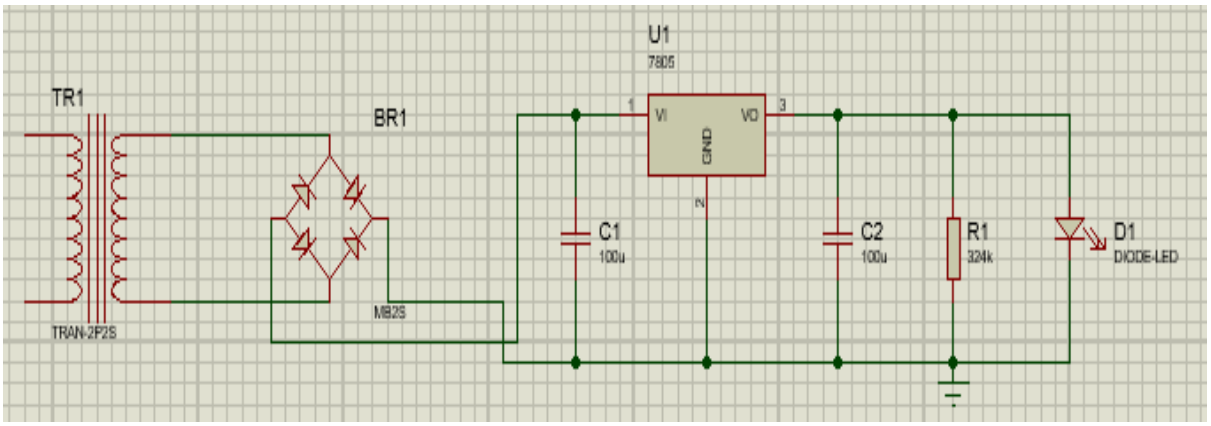

Figure 2: Power Supply Unit

2.4 Complete System

Figure 3 shows the complete circuit diagram of the entire system. This comprises the fingerprint unit, the LCD unit the enrolment unit, the indicator unit and the microcontroller unit. The fingerprint unit is connected to the microcontroller unit. The LCD is also conncted to the Microcontroller unit. The led indicator units and the enrolment unit are also connected to the appropriate pins of the microcontroller.

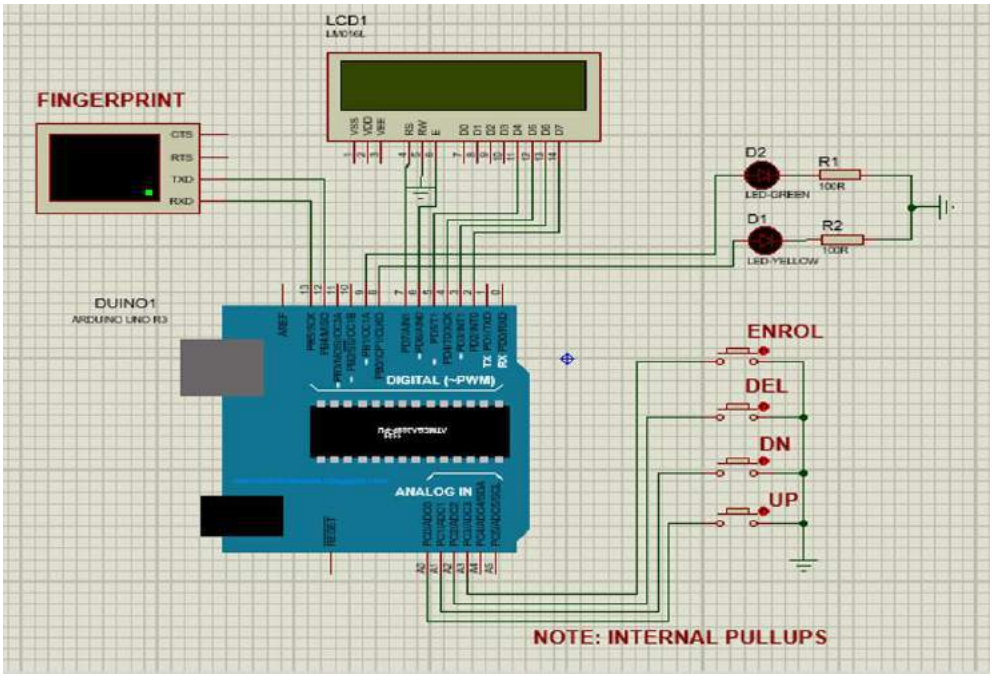

Figure 3: Complete Circuit Diagram

2.5 System Working Principle

The design of security door lock using the finger print technology was built around a Microcontroller unit, which reads in finger prints from finger print scanner and grants access, to a protected compartment, only to pre-registered finger prints. The finger print scanner serves as the main input into this embedded security system. Finger prints read are compared to those pre-programmed into the memory of the microcontroller. When a match is made, the microcontroller outputs a HIGH which activates the transistor-relay switching stage that controls opening and closing of the modeled motorized door granting access into the exact protected compartment in the rack. An alphanumeric liquid crystal display (LCD) is used in this design to show the operating status of this embedded security system. By default, it displays a welcome message requesting that the user should enter a finger print. And when a match is made, it displays "ACCESS GRANTED" otherwise it displays "ACCESS DENIED".

2.6 Software Design

Five stages of software were followed. They include the problem definition stage, the algorithm design stage, the coding stage, the testing and debugging stage and the documentation stage. The control program was written in C Programming language. The embedded C program implements the system flowchart. Simply put, it reads in binary patterns from the input subsystems and sends out binary patterns that would cause the required actions to be taken by the output subsystems. Figure 4 shows the flowchart.

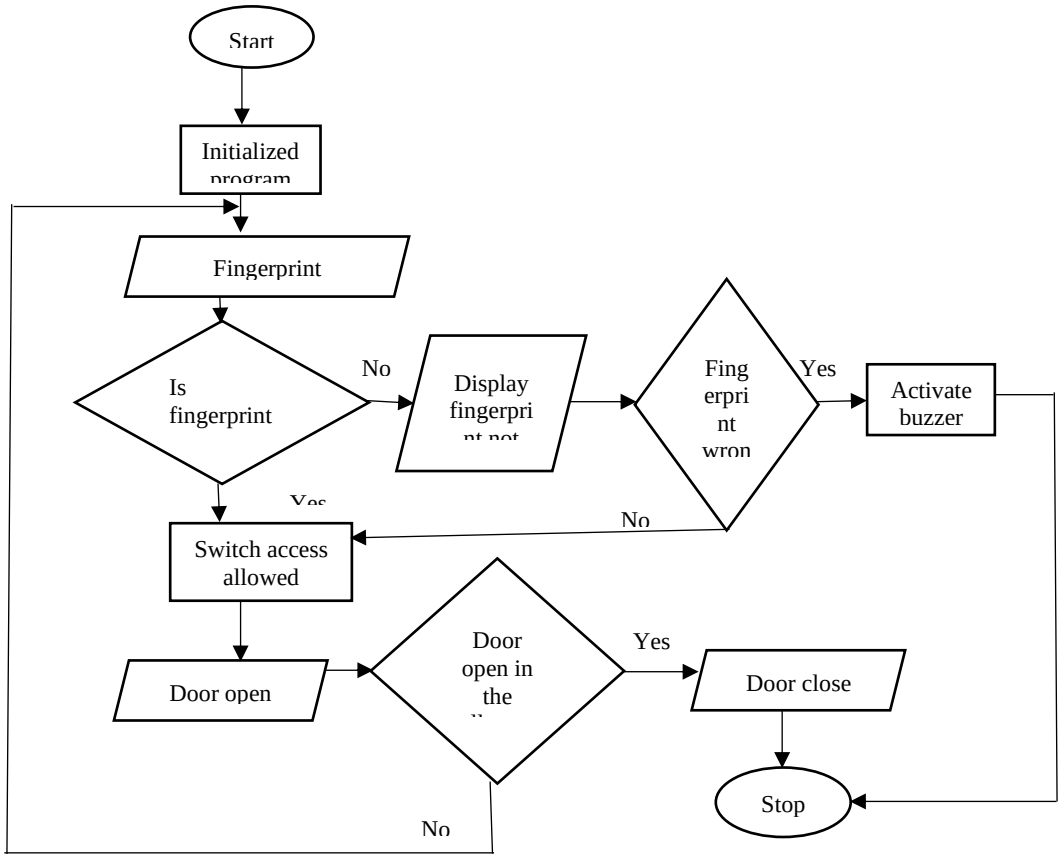

Figure 4: Flowchart of the operations

2.7 Simulation

The whole electronic/digital part of the work was simulated on PROTEUS simulation platform before the soldering work commenced to observe the operation before implementation.

2.8 Construction

The physical realization of the work is very vital. Here the layout is transformed into a finished hardware. After carrying out all the designed layout and analysis, the design was implemented, constructed and tested to ensure proper working condition. The construction of this work was done in four different stages.

I. The writing of the code (driver) which controls the Microcontroller using C language (ADAFRUIT ARDUINO INO).
II. The soldering of the circuits on board (as shown in Figure 5)
III. The coupling of the each compartments that form a mobile phone rack system.
IV. The connection with appropriate connectors and cables (Figure 6 shows the back view of the LCD indicating several connections)

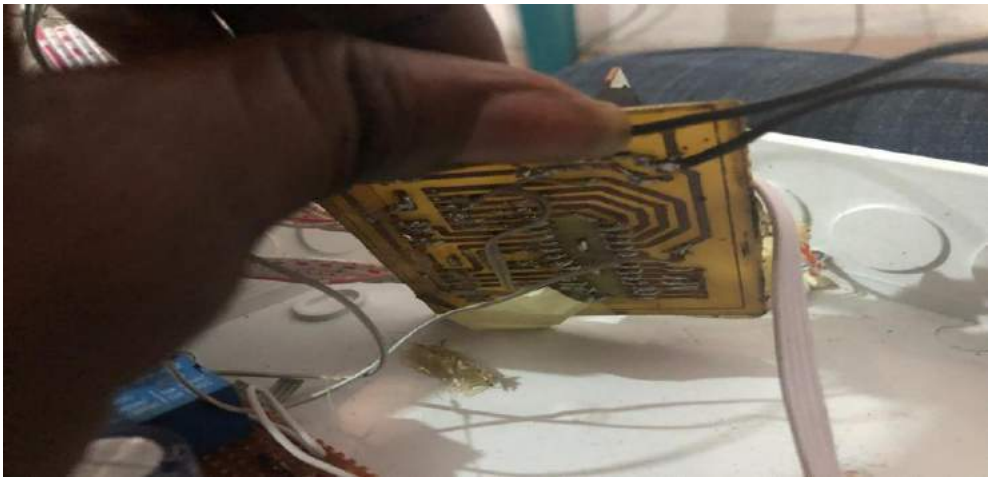

Figure 5: The PCB Layout after printing it on the board

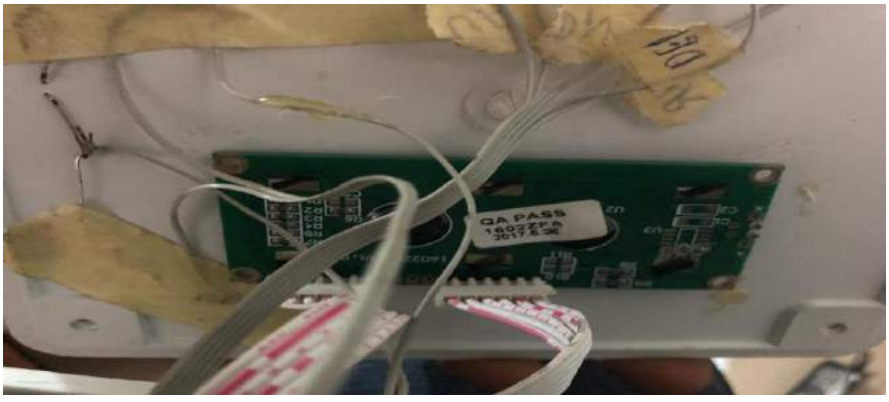

Figure 6: Back View of LCD display showing connections

2.9 Testing

Stage by stage testing was done according to the block representation on the breadboard before soldering of circuit on Vero board. The process of testing and implementation involved the use of some test and measuring equipment stated below.

I. **Bench Power Supply:** This was used to supply voltage to the various stages of the circuit during the breadboard test before the power supply in the work was soldered. Also during the soldering, the power supply was still used to test various stages before they were finally soldered.
II. **Oscilloscope:** The oscilloscope was used to observe the ripples in the power supply waveform and to ensure that all waveforms were correct and their frequencies accurate. The waveform of the oscillation of the crystal oscillator used was monitor to ensure proper oscillation at 4MHz.
III. **Digital Multi-meter:** The digital multi-meter basically measures voltage, resistance, continuity, current, frequency, temperature and transistor. The process of implementation of the design on the board required the measurement of parameters like, voltage, continuity, current and resistance values of the components and in some cases frequency measurement. The digital multi-meter was used to check the output of the voltage regulators used in this project.

3. Results and Discussion

User is asked to enroll his fingerprint. Therefore the user's identification is done .If the user is authorized, the door automatically opens. After igniting the phone rack, the door automatically opens. When destination is reached, after a set time delay, the door automatically closes when they kept phone has been removed. This system focuses on the use of fingerprints for securing phone through the door as barricade. The fingerprint recognition software enables fingerprints of valid users of the phone rack to be enrolled in a database. Before any user can use of the phone rack, the fingerprint image is matched against the fingerprints in the database while users with no matched record in the database are prevented from using the phone rack. A microcontroller stores the data equivalent of fingerprint of the master user. Comparison between this enrolled fingerprint and the fingerprint of the person who is about to use the phone rack is done by the microcontroller. If both the fingerprints are identical control circuitry of the microcontroller sends appropriate signals to the motor relays operating the door of the phone rack.

3.1 Result of Simulation

The simulation of the design was tested severally and yielded accurate results. The LCD displays the result appropriately. Figure 7 shows a result where the LCD displays a message.

3.2 Result of the Entire System

Figure 8 shows the result of the various stages of design enumerated in section 2which is a Smart Rack Protector against Physical Insecurity and Privacy Intrusion of Mobile Phones in Examination Centers. It is screwed or installed in an open place at an examination centre such that candidates holding mobile phones can enroll and safely keep their phone till the end of the examination. Each compartment has a space that is good enough for several phones in cases of one person having multiple phones or a set/group of individuals wanting to keep their phones in a single compartment to avoid individual enrolment. In that case, a representative of the set of candidates could collect the mobile phones from the members of their group, e=enroll through the fingerprint module of the system and safely keep the gadgets in a compartment until the end of the examination when they

will authenticate the enrolment, open the smart door to pick the phones and hand them over to members. Figure 9 shows the compartments with the smart doors.

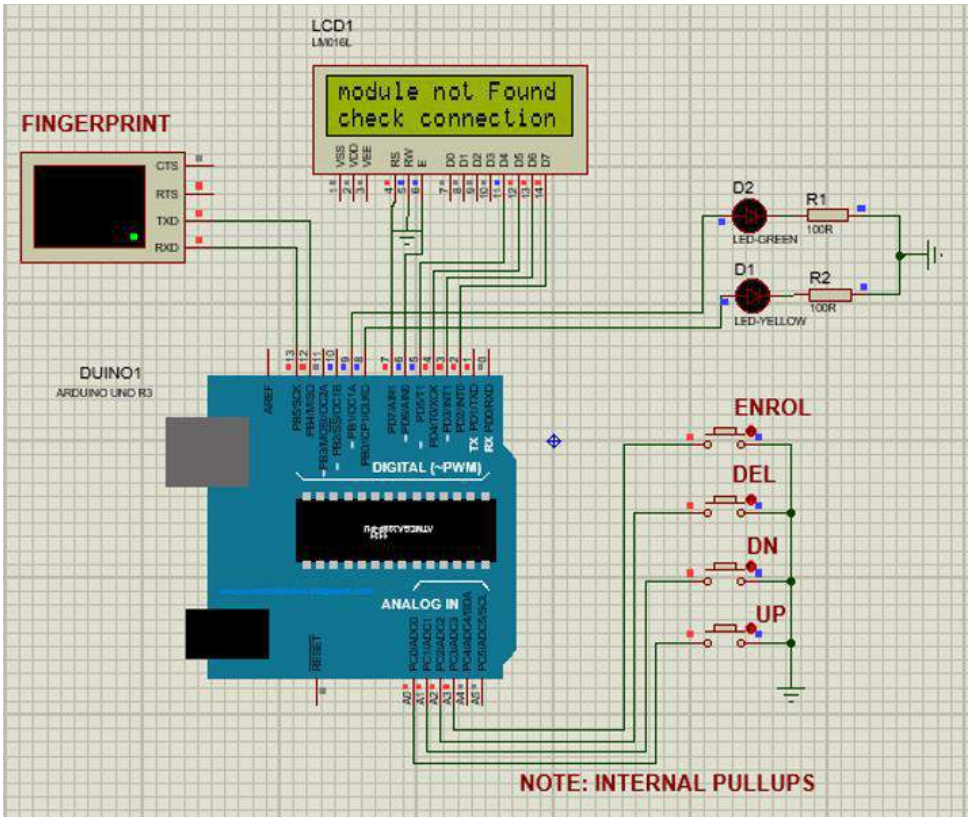

Figure 7: Simulation of the Design

Figure 8:Smart Rack Protector against Physical Insecurity and Privacy Intrusion of Mobile Phones

Figure 9: Compartments with Smart Doors

3.3 Performance Testing

Table 1 shows the results obtained as 110 students were able to register their finger in the system memory and 143 mobile phones belonging to the 110 candidates were physically secured and kept private. It should be noted that some of the candidates had more than one phones.

Table 1: Results of Testing Smart Doors in Five Centres with 110 Students

Test Centres	No of students	No of phones	No of attempted Locks	No Of Positive Locks	Undetected locks	No of attempted unlocks (N)	Detected No of wrong unlock attempts (M)	Detected No of Correct unlocks (T)	undetected Response (X)
LT1	20	44	48	44	4	72	20	44	8
LT2	20	20	20	20	0	30	10	20	0
LT3	30	35	35	35	0	43	8	35	0
LT4	24	24	24	24	0	34	10	24	0
LT5	16	20	16	16	0	28	12	16	0
TOTAL	110	143	143	139	4	207	60	139	8

Five examination centers (Lecture Theatres) namely LT1 and LT2, LT3, LT4 and LT5 were used. From Table 1, Equations (5-11) can be deduced:

SECURITY (LOCKING)

No of Times Lock was Attempted = 143 (5)

No of Times Lock was Positive = 139 (6)

Lock Efficiency = 139/143 * 100 (7)

Lock Efficiency >= 97% (8)

UNLOCKING

No of successful unlock, T = 139 (9)

No of positive unlock attempts, B = N – M – X (10)

= 207 – 60 - 8 = 139

Efficiency of Unlocking = (T/B) % (11)

= 139/139 * 100 = 100% Efficiency

4. Conclusion

The use of fingerprint identification in this work enhanced the security of the phone rack system and granted only registered users the privilege or access to compartments where their mobile phone(s) were saved. Thus, by implementing this reliable and easily replicable system in public places especially examination halls of Nigerian institutions which are currently in dire need of it, much greater security and privacy can be ensured. This is necessary because keeping them personally or in open places over the years exposed students' mobile phones physical insecurity, privacy intrusion and theft. The developed system is geared towards a robust and embedded real-time fingerprint based phone rack suitable for examination centres.

References

[1] Wahab, A., Chin, S. H., & Tan, E. C. (1998). Novel approach to automated fingerprint recognition. *IEE Proceedings - Vision, Image and Signal Processing, 145*(3), 160-166.

[2] Anil, K., Arun, R., & Salil, P. (2004). An introduction to biometric recognition. *IEE Transaction on circuit and system for video technology*, Vol *14* (2), 4-20.

[3] Pin, L. K. (2007). *Electronic Lock using usig fingerprint recognition*. Malaysia: University of Technology, Malaysia.

[4] Yugashini, I., Vidhyasri, S., & Devi, K. G (2013). Design and Implementation of Automated Door Accessing System with Face Recognition. *International Journal of Science and Modern Engineering* Vol 1(12), 10-13.

[5] Alshraf, E. S. (2011). Design and implementation of a biometrics access control using fingerprint for restricted area based on gabor filter. *International Arab Journal of Information Technologies*, Vol *8* (2), 353-363.

[6] Roy, R., &Sadlon, J. (2002, September 19). US20020133725A1 - Biometric access control and time and attendance network including configurable system-on-chip (CSOC) processors with embedded programmable logic - Google Patents. Retrieved from https://patents.google.com/patent/US20020133725

[7] Mary, R., & Dushyant, k. (2010).Fingerprint identification in biometry security system. *International Journal of Computer and Electrical Engineering*, 2(5), 853-855.

[8] Connell, J. H., Fred, A. M., & Ratha, N. K. (2018, September 6). Anonymizing Biometric Data for use in a Security System. Retrieved from http://patents.justia.com/patent/20180255056

[9] Wang, Y. A.,& Hu, J. (2011).Global ridge orientation modeling for partial fingerprint Identification.*IEE Transaction on pattern Analysis and Machine intelligence*, Vol 33(1), 1-18.

[10] Gupta, P., Ravi, S, Raghunathan, A., &Jha, N. K. (2005). *Efficient Fingerprint-based User Authentication for Embedded Systems*. Princeton, NJ: Dept. of Electrical Engineering, Princeton University, Princeton, NJ USA.

[11] Robert, W. D., Chinping, Y., & Chong, I. N. (2007, May 1). US7212658B2 - System for fingerprint image reconstruction based on motion estimate across a narrow fingerprint sensor - Google Patents. Retrieved from https://patents.google.com/patent/US7212658B2/en

[12] Hteik, H. L., Aung, S. K., & Hla, M. T. (2015). Automatic Door Access System Using Face Recognition. *International Journal of Scientific & Technology Research*, *4*(6), 294-299.

[13] Kavya, K., & Ramadeepti, M. P. (2015). Door Phone Embedded System for Voice and Finger print Based User Identification and Verification Platform. *International Research Journal of Engineering and Technology*, Vol *2*(8), 1272-1278.

[14] Oke, A. O., Omoniyi, O. M., Arulogun, O. T., & Olaniyan, O. M. (2009). Development of a microcontroller-controlled security door system. *Pacific Journal of Science and Technology*, Vol *10*(2), 394-403.

[15] Vito, D. A., & Raymond, W. K. (1978, October 17). US4120585A - fingerprint identification system using a pliable optical prism - google patents. Retrieved from https://patents.google.com/patent/US4120585

[16] Isenor, D. K., & Zaki, S. G. (1985, April 8). Fingerprint identification using graph matching. Retrieve from https://www.academia.edu/1384605/Fingerprint_identification_using_graph_matching

[17] Boer, J., Bazen, A. M., & Gerez, S. H. (2001). Indexing Fingerprint Databases Based on Multiple Features. In *ProRISC the 12th Annual Workshop on Circuits, Systems and Signal Processing Workshop* (pp. 300-306). Veldhoven, The Netherlands: STW.

[18] Tamori, T. (2003, February 25). US6523745B1 - electronic transaction system including a fingerprint identification encoding - Google Patents. Retrieved from https://patents.google.com/patent/US6523745

[19] Anil, J., Lin, H., & Ruud, B. (1996).On-line fingerprint *IEE Transactions on Pattern Analysis and Machine Intelligence*, 19(4),302-314.

[20] Anthony, R. R. (2004, June 22). US6751909B2 - Automatic door control system - Google Patents. Retrieved from https://patents.google.com/patent/US6751909B2/en

NIPES Conference Proceedings
The 1st International Conference of the Nigerian Institution of Professional Engineers and Scientists 7th-8th Oct. 2021: 384-396
www.nipesjournals.org.ng

Simulation of an Underwater Environment via Unity 3D Software

Osa E.[a], Orukpe P.E.[b]
[a]*Department of Electrical/Electronic Engineering, Faculty of Engineering, University of Benin, P.M.B. 1154, Benin City, Nigeria.*
[b]*Department of Electrical/Electronic Engineering, Faculty of Engineering, University of Benin, P.M.B. 1154, Benin City, Nigeria.*

Abstract
The ideal development platforms for underwater vehicle control systems are the physical vehicles themselves. However, limited availability of Underwater Vehicles (UVs) and the high costs associated with purchasing and maintaining them often call for the use of computer simulations as a more feasible and flexible development platform. The simulation must accurately emulate real world conditions and equipment to allow control software development in a virtual space. Unfortunately, simulations tend to be developed from the ground up for particular Underwater Vehicles and are thus idiosyncratic and difficult to reuse, and development time and cost can be substantial. It is therefore beneficial when developing simulation testbeds for intelligent control of UVs to utilize off-the-shelf, sophisticated simulation software namely, Game Engines. A game engine provides physics, modeling, and rendering capabilities that can significantly reduce simulator development time. The particular game engine utilized in this work is Unity 3D Game Engine. Various underwater scenarios were developed to prove the functionality of the underwater environment by creating C# scripts and utilizing the internal physics properties of Unity. A test object namely an autonomous underwater vehicle was deployed into the simulated environment to test the performance of the environment. Patrol scripts as well as obstacle avoidance scripts were written in C# to enable the underwater vehicle behave in the simulated environment. Results showed that the modelled underwater environment can serve the purpose of simulating various underwater scenarios such as navigation and patrol of Underwater Vehicles.
Keywords**:** *AUV, Simulation, Game Engine, Unity 3D.*

1. Introduction

Recent times have marked an increase in sub-sea exploration and marine research. Development of unmanned and autonomous underwater vehicles has facilitated the prospect of research in this domain. Unmanned Underwater Vehicles (UUVs) aid oceanographic research and perform underwater missions at reduced personal costs without risking human life. They are smaller, lighter and more portable compared to their counterpart submarines. Their robustness and navigational capabilities make them well suited for exploration of extreme environments in deep, uncharted territories. A key part to development of such vehicles is testing in underwater environments. Given the amount of effort and resources it requires, testing of such underwater vehicles and robots is an arduous task. Testing pools are usually not feasible due to space, cost and maintenance requirements. Water bodies such as lakes/ponds are usually remote and provide little control over the conditions. Conducting experiments and evaluations on a real physical system is not viable due to the possibility of physical strain and damage to the vehicle, limited resources, high costs associated with manufacturing, purchase and maintenance. Simulation modelling is the ideal solution in these circumstances. It involves development of a virtual prototype of a physical system and analyzing its performance in the real world. Simulation systems allow testing and validating the correctness of algorithms. They ensure the efficiency of physical design and accelerates testing procedures. Such frameworks help in detection and prevention of unnecessary hardware malfunctions and verifies the software architecture in a cost-effective way. They help in providing a platform for effective monitoring and debugging of robotic vehicles. By approximating the working conditions of real systems, simulation software can save time and resources spent in iterative cycles of building physical prototypes and can help in focusing on vehicular control mechanisms.

The design and development of intelligent controllers for autonomous underwater vehicles is a difficult, labor-intensive process that cannot be done in isolation from aspects of the AUV to be controlled. The best development system and testbed for such software is, of course, an actual AUV. However, this may not in most cases be the best first development system. Purchasing or (especially)

building an AUV is very costly, and there is significant cost involved in maintaining the vehicle and in the support needed for fielding it. In addition, the primary focus of intelligent control researchers is usually not fielding AUVs, and they often lack expertise in vehicle maintenance and operation. They may also be distant from collaborators who do have AUVs and the interest and expertise to operate them. And using an AUV for the early stages of prototyping and debugging control software can take the vehicle away from more productive work it could be doing using its existing software. Consequently, the best first testbed for intelligent control software is usually a simulator. Unfortunately, simulators have their own problems. Development of intelligent control software is often highly specific to the vehicle itself, and so there is limited availability of off-the-shelf simulations to suit the needs of a particular project.

Instead, these simulations are typically built from the ground up, with the emulated vehicle systems implemented by the artificial intelligence (AI) researchers themselves and customized to the target AUV. This involves the significant overhead of designing physics engines, model design, and building rendering mechanisms (or interfacing with existing ones, such as OpenGL) none of which directly contributes to the task of developing the control software itself. In addition, creation of a new simulator carries with it a significant commitment to maintaining the software and adding new technology and functionality to keep it up-to-date. Software maintenance is often estimated to take up to 90% of the total effort devoted to a piece of software. There are numerous off-the-shelf platforms that have capable physics engines, rendering, and modeling facilities that others have already committed to maintaining and extending: Game engines. As the name implies, these software systems are created for the design and development of modern 3D video games. Examples include Unity [1], Torque3D [2], Polycode [3] and CryEngine3 [4]. These range from well-maintained rendering and physics libraries to full toolkits that feature GUI-driven game world and object creation editors. Using these, a game designer can concentrate on the game itself and leave the physics and rendering to the engine.

1.2 Overview of Underwater Simulators

There have been many simulators developed over the years for AUV development, including those facilitating intelligent control development. An early example was the DIS-Java-VRML simulator from the Naval Postgraduate School, which had sophisticated physics and rendering capabilities, making use of hardware help from Silicon Graphics workstations. It was one of the first to use both standardized communication (Distributed Interactive Simulation [DIS] protocol [5] and a standardized modeling language (Virtual Reality Markup Language VRML) [6]. While it was a very advanced simulation for its time, it also was written entirely from the ground up and it relied on specialized hardware, and its age clearly shows, at least visually. Its descendant, the AUV Workbench [7] while more modern, also required substantial resources for maintenance and continuous modernization. Over the years more beneficial simulators began to evolve. The use of game engines for traffic and land vehicle simulation was carried out by [8]. [9] worked on GEAS. GEAS is a simulator for research in intelligent control of autonomous agents, especially AUVs. GEAS focuses on simulation at the level appropriate for high-level mission control software. It runs on a server machine, which may or may not be the same machine as the AUV controller (but usually will not be). Unity supports TCP sockets, and so GEAS can communicate with a server process that listens to a port for incoming connections. Authors in [10] presented URSim (Unity Ros Simulator), an open-source hybrid underwater simulator based on modular software framework - ROS (Robot Operating System) and a cross platform real-time game engine- Unity3D. It is an improvement on the above-named Simulators.

Our work is based on the URSim open-source framework, however it is unique in that it replaces the default capsule in URSim with a custom built Autonomous Underwater Vehicle, it has a custom

patrol script for navigation that was created via C# codes and custom scenes of underwater environment have been created.

1.3 Unity 3D Game Engine

Any coherent simulation system can be developed using a graphics rendering mechanism for creating a virtual environment with realistic 3D models and a computational back end system where the corresponding data is processed and respective commands are issued. Unity 3D, a game engine used to develop half of the world's games was the first choice for the virtual environment development. It acts as the face of the whole system, providing a platform to create a visually realistic environment where the UUV's algorithms and control structures can be tested and experimented with. Unity 3D [11] is a cross-platform game engine primarily used to create games. Its powerful graphics rendering, physics engines and intuitive development tools make it the preferred choice for developing realistic, efficient and easily deployable simulations. Unity provides a robust physics engine to simulate real world physics in the form of rigid body kinematics, fluid dynamics and collisions. The Unity Asset Store with wide variety of ready-made plugins and assets that can be imported to accelerate development. Unity is backed by a large, active community of developers that has been growing since 2005, providing support and making it more approachable for new developers. Games and simulations developed in Unity can be deployed on most platforms including Windows, MacOS and Android. The Unity engine supports C# (pronounced "C sharp") as the programming language and provides several APIs to simulate real world physics. The development environment provided by Unity and its intuitive work-flow makes it easier for developers to get started with developing games and simulations. Drag and drop mechanisms make it easy to import and position objects, add components and attach scripts. The aesthetic specifications of game environments can be controlled using materials, shaders and textures in Unity. Ready-made environment packages and a vast asset store aid the development process. Overall Unity provides ease and flexibility to design user virtual environments which can mirror a variety of realistic scenarios.

2. Methodology

The methodology adopted for modelling the simulation environment is broken into three steps namely; Underwater 3D Environment modelling, Mathematical Modelling and Hydrodynamic forces and collisions.

2.1. Underwater 3D Environment

The underwater environment of the simulation system has been developed keeping in mind the various capabilities of Underwater Vehicles in different underwater missions. There are four major sandboxing environments that have been created in this standing simulation. Each sandbox (test-beds) is unique in its own way. In order to create the underwater environment certain properties had to be configured appropriately namely: Main Camera, Right Perspective Camera, Non-Player Character, Floor, Directional Light, Top Camera, LocatorSphere, Pointers Patrol, Environmet, ColliderLevels, Water, Projectors, CaveLevelWalls.

Scripts for various configuration in C# programming language are contained in the Appendix Section.

2.1.1 Sandbox One

The environment developed as shown in Figure 1 acts a virtual test-bed for wholesome evaluation of the vehicle's capabilities and performance. It includes the simple horizontal terrain aimed at training the robot to execute a simple point-to-point navigation without patrol functions. Rocks and clear sea bed paths have been placed for obstacle avoidance training, a piping network for leakage detection and a geo-relative game object (Locator Sphere) with clear shaders has also been placed for target acquisition related tasks respectively.

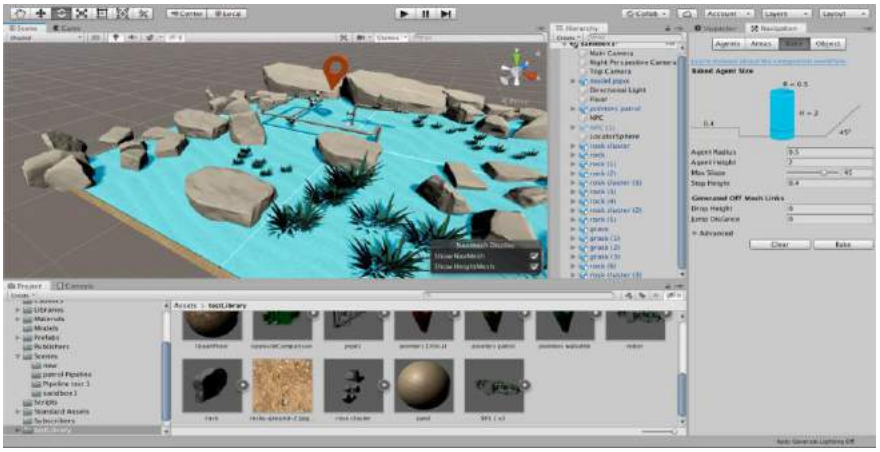

Figure 1: Sandbox one, simple point-to-point voyage

2.1.2 Sandbox Two

Unlike the previous sandbox, this one has a different pipping system with an attached patrol script (shown in appendix) for training in terms of leakage checks across serval points in the pipping system. The pipping network covers a much larger sea bed frame and wider placed seabed rocks for a more patrol-friendly environment.

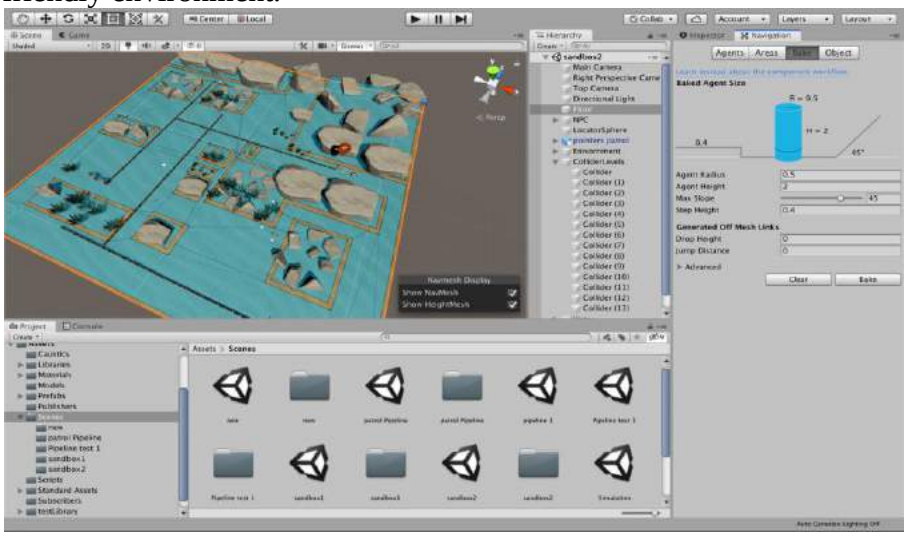

Figure 2: Sandbox two, larger piping network and patrol

2.1.3 Sandbox Three

This testbed (shown in Figures 3a and 3b) carries more advanced navigational approach to design. Its centers on maneuvering capability training for the underwater vehicle. Red and green hoops (circular gates) have been sunk into the ground for a training session where by the UV will autonomously navigate through green hoops and evades red loops during voyage. This test simply

points to the test for best voyage/navigation algorithm, to which collision avoidance and mapping training can be ascertained. Modulation and recurrent retaining of the UV via the navigation bake function provided by Unity3D enables the use of Artificial intelligence algorithms to surf through explicit options and concurrently helps in sensor functions whilst deciding which hoop is acceptable for navigation.

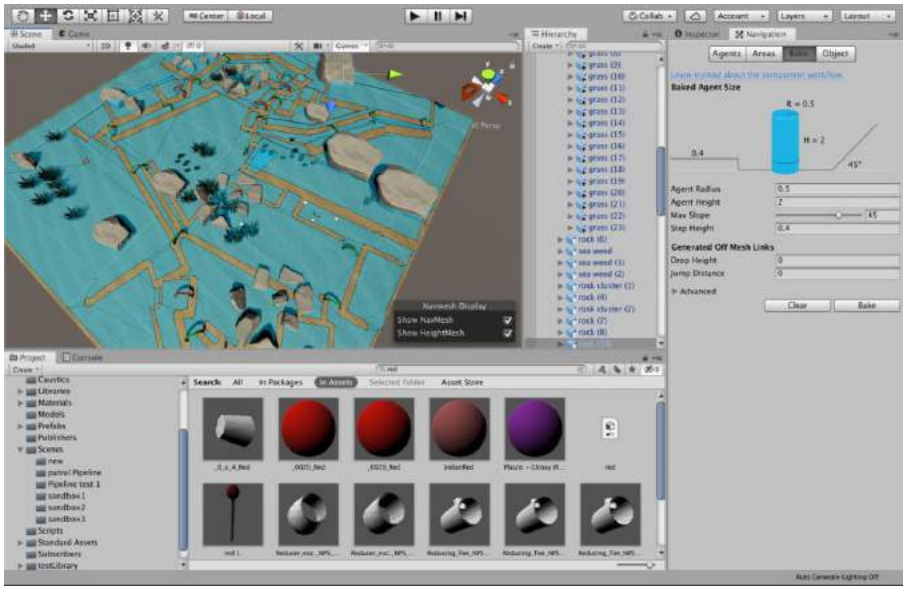

Figure 3a: Sandbox three, orthographic view of green-red hoop testbed

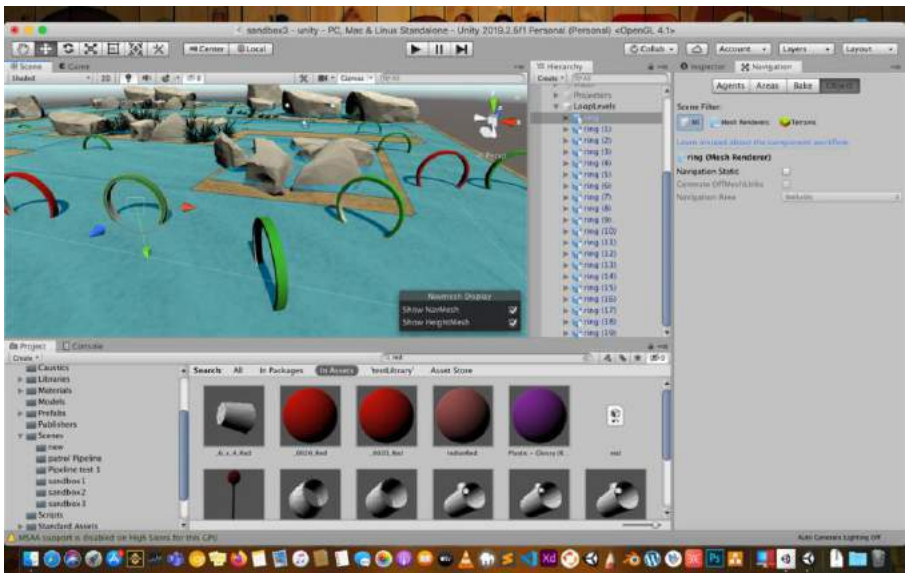

Figure 3b: Sandbox three, perspective view of colour-difference hoop.

2.1.4 Sandbox Four

As a hectic task, this sandbox was driven with complexity. It features a 3-level navigational course. It is primarily an underwater cave system that houses three lateral layers of navigable rock paths. Unlike, the other sandboxes; this fourth testbed was created to prove different depth navigation for an autonomous underwater vehicle.

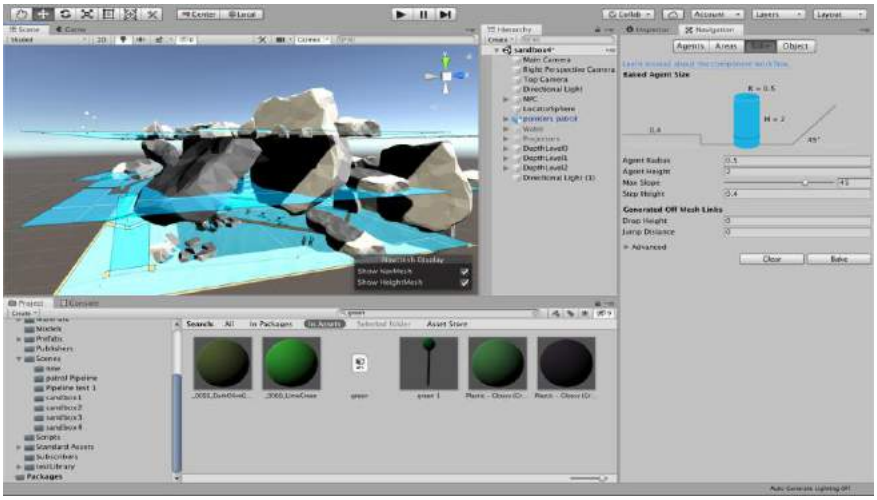

Figure 4: Sandbox four, underwater cave system.

2.2 Mathematical Modelling and Testing

Testing the model is very essential to avoid wrong building and misbehavior during voyage. For the successful voyage execution; the Modelling task is divided into two categories to develop the mathematical model of the vehicle - Kinematics and Dynamics. Fig. 5 shows a mathematical model of a six degrees of freedom (6DoF) vehicle. The vehicle is modelled to control heave (motion along z-axis), roll (rotation about x-axis), pitch (rotation about y-axis), yaw (rotation about z-axis), surge (motion along x-axis) and sway (motion along y-axis).

2.2.1 Dynamics

We further divide the dynamics of the vehicle based on two possible motions - Translational Motion and Rotational Motion. Unity physics engine account for several forces like hydrostatic, lift, drag, thrust, external forces acting on the vehicle simulating the motion.

2.2.2 Kinematics

To demonstrate the kinematics, we added two reference frames, body-fixed frame and the inertial frame. The body-fixed frame moves relative to inertial frame, hence simulating the linear and angular velocities. The position and orientation are described in reference to inertial frame thus simulating the degree of freedom of vehicle.

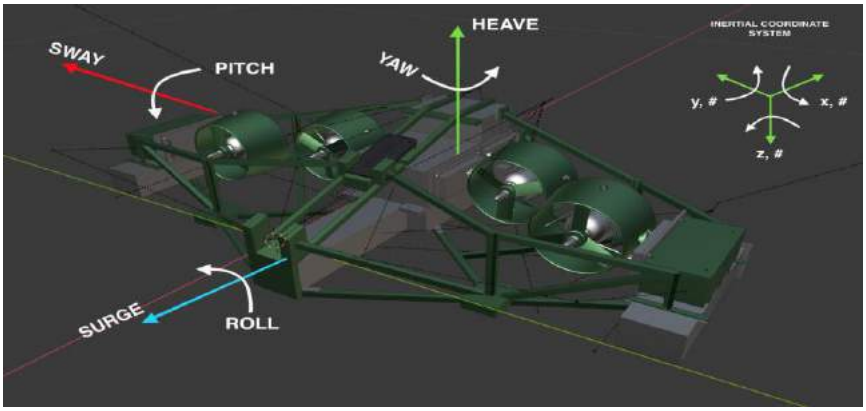

Figure 5: Vehicle modelling and testing.

2.3 Hydrodynamic forces and Collisions

Scenes in Unity are created using 3D or polygonal meshes. Meshes are the foundational structures of all games made in Unity. All objects in a scene are made up of meshes. Each mesh comprises of vertices and edges in 3D space that come together to form multiple triangles. Therefore, the surface of each Game Object can be considered to be made up of multiple small triangles.

Simulation of any force on an object requires application of force on the meshes' triangles. The proposed simulation system accounts for the various forces like buoyancy and drag that act on a solid body immersed underwater.

2.3.1 Buoyancy and drag

To enable a Game Object to experience physics-based forces, Unity provides Rigid body plugin. It allows the object to experience mass, velocity, gravity and drag. It can also be used to impose constraints on linear and angular movements and to detect collisions. To simulate buoyancy, corresponding C# scripts are attached to the Game Object to apply an upward force to the centers of all the submerged triangular faces of the vehicle's mesh.

$$B = \rho g v \text{ ---------- (1)}$$

$$\text{Where, } v = zS \text{ ---------- (2)}$$

In (1), the buoyant force B, can be calculated using the Archimedes principle while ρ represents the density of the liquid, g represents the gravitational acceleration and v represents the volume of the water above an individual triangle in the mesh. As demonstrated in (1) this volume can be calculated from (2) using the product of the surface area of the triangle, S, and the distance between the center of the triangle and the surface of the water, z. If this upward force is greater than the gravitational force, then the vehicle floats on the surface of the water plane. Simulation of the damping forces, drag and angular drag coefficients were specified using the Rigid body interface inside Unity platform.

3. Results and Discussion

The test of each scene as described in the methodology was carried out by trying out the navigation of a virtual Autonomous Vehicle in the respective scenes of the underwater simulation environment. This is shown in Figures 6 to 8. The Underwater Vehicle has an aerial and directional lamp added to it, to ensure proper navigation, scanning, visibility during voyage in terms of camera feedback and picture taking.

3.1 Parameters For Baked Test Agent In Unity

PARAMETER	VALUES
Agent Height	2
Agent Radius	0.5
Maximum Slope	45
Step Height	0.4

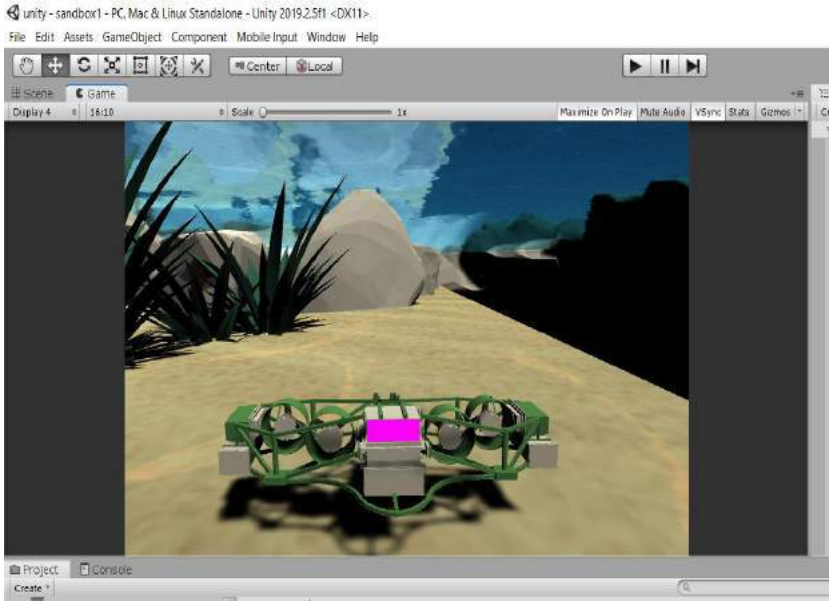

Figure 6: Test Case for Sandbox One

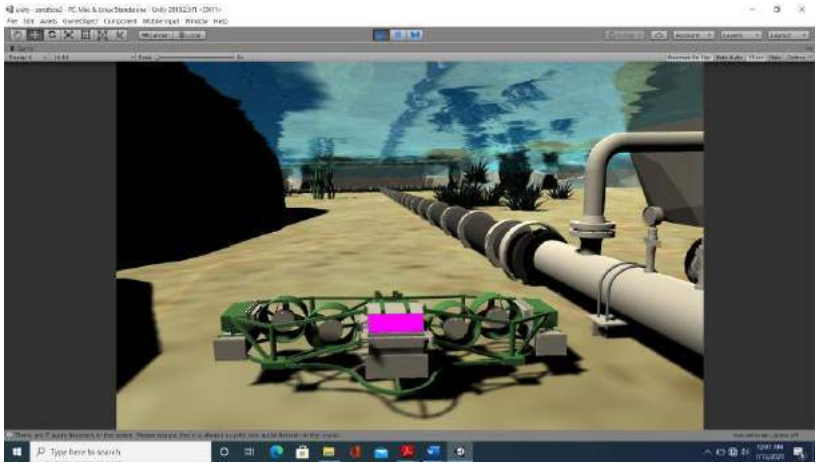

Figure 7: Test Case for Sandbox Two

Figure 8: Test Case for Sandbox Three

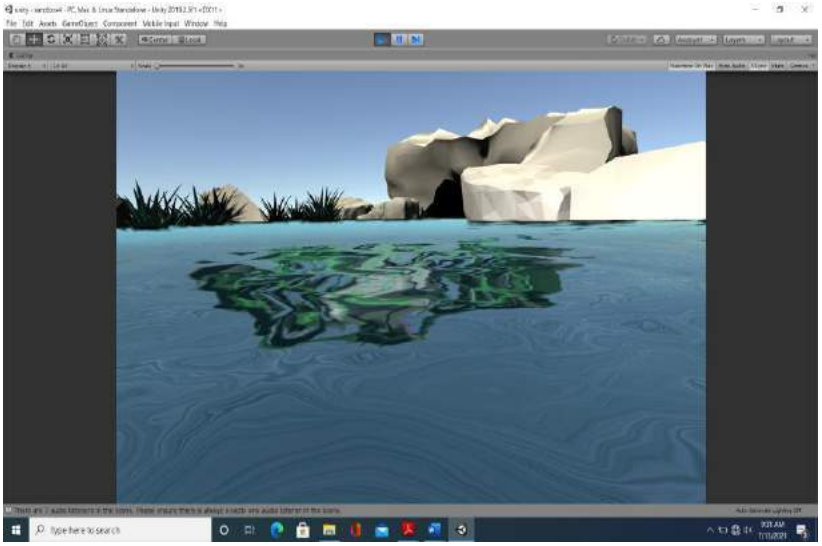

Figure 8a: Test Case for Sandbox Four Water Surface Level

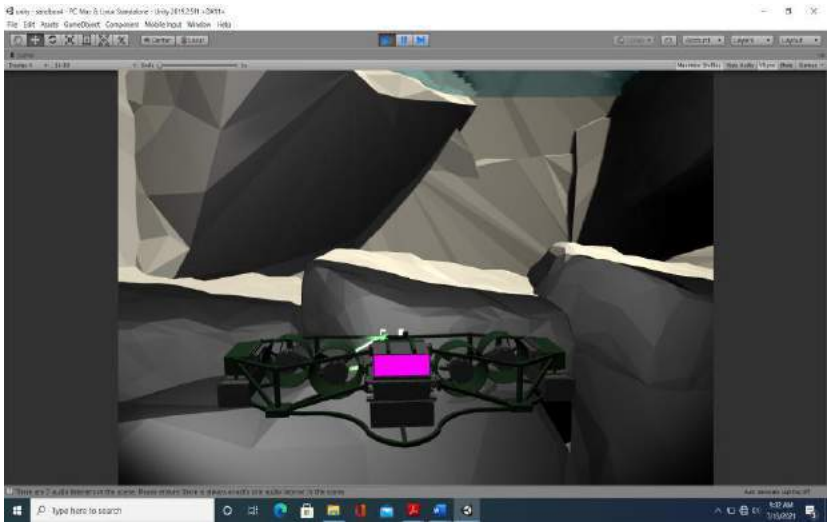

Figure 8b: Test Case for Sandbox Four Underwater Cave Level

3.3 Discussion

Figure 6 shows that the vehicle could perform simple navigation functions in the simulated environment which is the objective of Sandbox one. Figure 7 shows that the vehicle could perform patrol functions in the simulated environment of sandbox two. The vehicle can be seen patrolling an underwater piping network. Figure 8 shows that the UV can autonomously navigate through green hoops and evades red loops during voyage. This test simply points to the test for best voyage/navigation algorithm, to which collision avoidance and mapping training can be ascertained. Modulation and recurrent retraining of the UV via the navigation bake function provided by Unity3D enables the use of Artificial intelligence algorithms to surf through explicit options and concurrently helps in sensor functions whilst deciding which hoop is acceptable for navigation. In this scenario, the A* navigation algorithm has been deployed. As shown in Figure 8, Sandbox four proves different depth navigation for an autonomous underwater vehicle. It navigates the water surface and then descends below to lower cave levels.

4. Conclusion

This paper describes the simulation of an underwater environment. Such environments serve as low-cost arenas for experimenting underwater vehicles to ascertain their functionalities before actual

fabrication. Various tests prove that the simulation environment can serve for testing virtual underwater vehicles in terms of navigation, patrol, obstacle avoidance and other functions.
It is recommended that the academia namely Universities and other tertiary centres of learning adopt more of these procedures of employing simulation environments to test systems and machines before actual deployment. The huge advantage of low cost cannot be overemphasized especially in environments where it is seemingly difficult to get adequate equipment for carrying out experiments.

References

[1] W. Goldstone (2009). Unity Game Development Essentials. Packt Publishing Ltd.
[2] J. Lloyd (2004). The torque game engine. Game Development Magazine.
[3] I. Safrin (2013). Polycode web site. http://polycode.org, accessed 3/28/2013.
[4] H. Seeley (2007). Game technology 2007: Cryengine2. In ACM SIGGRAPH 2007 computer animation festival, page 64. ACM.
[5] D.A Fullford (1996). Distributed interactive simulation: its past, present, and future. In Proceedings of the 28th conference on Winter simulation, pages 179{185. IEEE Computer Society.
[6] J. Hartman and J. Wernecke (1996). The VRML 2.0 handbook: building moving worlds on the web. Addison Wesley Longman Publishing Co., Inc.
[7] D.T Davis and D. Brutzman (2005). The autonomous unmanned vehicle workbench: mission planning, mission rehearsal, and mission replay tool for physics-based x3d visualization. In Proceedings of the 14th International Symposium on Unmanned Untethered Submersible Technology.
[8] J.L Pereira and R.J Rossetti (2012). An integrated architecture for autonomous vehicles simulation. In Proceedings of the 27th Annual ACM Symposium on Applied Computing, pages 286{292. ACM.
[9] A.B Strout and R.M Turner (2013). A Game Engine-Based Simulator for Autonomous Underwater Vehicles. In the Proceedings of the 18th International Symposium on Unmanned Untethered Submersible Technology (UUST), Portsmouth, NH, August, 2013.
[10] Katara, P., Khanna, M., Nagar, H. and Panaiyappan, A. (2019) Open Source Simulator for Unmanned Underwater Vehicles using ROS and Unity3D.
[11] Unity3d", [online] Available: http://unity3d.com.

Appendix

AUV PATROL SCRIPT IN C#

```
using System.Collections;
using System.Collections.Generic;
using UnityEngine;
using UnityEngine.AI;
//AI patrol for AUV simulation.

public class NPCSimplePatrol : MonoBehaviour
{
   //Dictates whether the agent waits on each node
   [SerializeField]
   bool _patrolWaiting;

   //The total time we wait at each node
   [SerializeField]
   float _totalWaitTime = 3f;

   //The probability of switching direction.
   [SerializeField]
   float _switchProbability = 0.2f;

   //The list of all patrol nodes to visit.
   [SerializeField]
   List<Waypoint> _patrolPoints;

   //Private variables for base behaviour.
   [SerializeField]
   NavMeshAgent _navMeshAgent;
   int _currentPatrolIndex;
   bool _travelling;
   bool _waiting;
```

```
bool _patrolForward;
float _waitTimer;

// Use this for initialization
public void Start()
{
   _navMeshAgent = this.GetComponent<NavMeshAgent>();

   if (_navMeshAgent == null)
   {
      Debug.LogError("The nav mesh agent component is not attached to " + gameObject.name);
   }
   else
   {
      if(_patrolPoints != null && _patrolPoints.Count >= 2)
      {
         _currentPatrolIndex = 0;
         SetDestination();
      }
      else
      {
         Debug.Log("Insufficient patrol points for basic patrolling behaviour.");
      }

   }
}

public void Update()
{
   //Check if Robot is close to the destination.
   if(_travelling && _navMeshAgent.remainingDistance <= 1.0f)
   {
      _travelling = false;

      //if the robot is goint to wait, then wait.
      if(_patrolWaiting)
      {
         _waiting = true;
         _waitTimer = 0f;
      }
      else
      {
         changePatrolPoint();
         SetDestination();
      }
   }

   //Instead if we're waiting.
   if(_waiting)
   {
      _waitTimer += Time.deltaTime;
      if (_waitTimer >= _totalWaitTime)
      {
         _waiting = false;

         changePatrolPoint();
         SetDestination();
      }
   }
}

private void SetDestination()
{
   if (_patrolPoints != null)
   {
      Vector3 targetvector = _patrolPoints[_currentPatrolIndex].transform.position;
      _navMeshAgent.SetDestination(targetvector);
      _travelling = true;
```

```
        }
    }

    // <summary>
    // Selects a new patrol point in the available list, but
    // also with a small probability allows the robot to move forward or backwards.
    // </summary>
    private void changePatrolPoint()
    {
        if (UnityEngine.Random.Range(0f, 1f) <= _switchProbability)
        {
            _patrolForward = !_patrolForward;
        }

        if (_patrolForward)
        {
            /**
            _currentPatrolIndex++;

            if(_currentPatrolIndex >= _patrolPoints.Count)
            {
                _currentPatrolIndex = 0;
            }
            */

            _currentPatrolIndex = (_currentPatrolIndex + 1) % _patrolPoints.Count;
        }
        else
        {
            /**
            _currentPatrolIndex--;

            if(_currentPatrolIndex < 0)
            {
                _currentPatrolIndex = _patrolpoints.Count - 1;
            }
            */
            if (--_currentPatrolIndex < 0)
            {
                _currentPatrolIndex = _patrolPoints.Count - 1;
            }
        }
    }
}
```

UNDERWATER EFFECT SCRIPT IN C#

```
using UnityEngine;
using System.Collections;

public class underwaterEffect : MonoBehaviour
{
    public float waterHeight;

    private bool isUnderwater;
    private Color normalColor;
    private Color underwaterColor;

    // Use this for initialization
    void Start()
    {
        normalColor = new Color(0.5f, 0.5f, 0.5f, 0.5f);
        underwaterColor = new Color(0.22f, 0.65f, 0.77f, 0.5f);
    }

    // Update is called once per frame
    void Update(){
        if ((transform.position.y < waterHeight) != isUnderwater)
```

```
        {
            print(transform.position.y);
            print(waterHeight);
            isUnderwater = transform.position.y < waterHeight;
            if (isUnderwater) SetUnderwater();
            if (!isUnderwater) SetNormal();
        }
    }

    void SetNormal()
    {
        RenderSettings.fogColor = normalColor;
        RenderSettings.fogDensity = 0.01f;

    }

    void SetUnderwater()
    {
        RenderSettings.fogColor = underwaterColor;
        RenderSettings.fogDensity = 0.02f;

    }
}
```

NIPES Conference Proceedings
The 1st International Conference of the Nigerian Institution of Professional Engineers and Scientists 7th-8th Oct. 2021: 397-408
www.nipesjournals.org.ng

Cyber-Crime in Nigeria: Sociotechnical Implications, Preventive and Counter Measures

I.A. Edeoghon [a], H.E Mobote [b*]*

[a] Dept. of Computer Engineering, University of Benin, Edo State, Nigeria PMB 1154, isi.edeoghon@uniben.edu
[b] Dept. of Computer Engineering, University of Benin, Edo State, Nigeria PMB 1154, hakeem.mobote@eng.uniben.edu

Abstract
The internet platform has created unlimited opportunities for a vast array of human activities, more so in the areas of commerce and social interactions. However, correspondingly there has been an upward increase in security threats to such activities. Internet crimes are committed daily all over the world and in Nigeria as well. According to (Ibrahim, 2019) cybercrime was responsible for 43% of monetary loss in the country in the year 2016. Some reports show that Fraud-related crimes cost Nigerian banks N3.5billion in losses from July to September 2020. This work focuses its analysis on crucial cybercrimes committed per sector the world over and compares with that of Nigeria including an investigation of key cybercrimes committed in Universities in Nigeria with a focus on Edo State. At the end of this paper reasons for as well as detection, prevention and counter techniques are presented in order to combat cybercrime for not just the crime fighting bodies and the government but all related stakeholders in the country.

1. Introduction

Nowadays man's activities relying on the global information infrastructure has greatly increased. This has created a broad range of opportunities for businesses, social interactions and others. However, along with all these positive benefits this same infrastructure has become a target for increasing number of attacks by nefarious persons, with the rate and technicalities, sophistication of these attacks increasing at a very alarming rate. Such crimes against the global internet infrastructure are known as cybercrimes. A cyber-crime can be defined as any criminal activity executed on a computer or a computer network. The term broadly refers to any such crimes taking place on the world wide web or Internet. Such crimes include: forgery, fraud, embezzlement, blackmail [1].

The level and sophistication of these crimes pose constant challenges for legal systems set up to cope with this trend [2].

The seriousness of the adverse effects of cybercrime cannot be over emphasized as cybercrime can lead to damage to the reputation of a nation. For a country such as Nigeria, whose hope for economic boost relies on direct foreign investment, this can and has acted as a discouragement. This applies not only to investment from abroad but to domestic small scale and medium businesses who are also affected. As far as these businesses rely on the Internet infrastructure, they are targets. The effect of cybercrime is realized in the loss of personal confidential information, finances, intellectual copyrights and so on. Often times the older generation or what may be referred to as "Senior citizens" are prime targets. It is estimated that in the US, over 62,000 people over the age of 60 had losses as a result of cybercrime to the tune of $649 million [3].

1.2 Types of Cybercrime
According to the Council of Europe Convention on Cybercrime in 2001, cybercrime can be classed into four major categories:
1. Crimes against confidentiality, integrity, availability of personal data stored on a computer. This would include things such as illegal access to and illegal interception of such data.
2. Computer related forgery and fraud
3. Computer content related offences, e.g., child pornography

4. Computer related infringement on intellectual property and copyrights.
[1] classed cybercrime according to the area of application thus resulting in three major sectors of the society: 1. Banking 2. E-commerce 3. Educational sector

1.3 Societal Sectors Most Affected by Cybercrime in Nigeria

In this work we were able to section the crimes committed on cyberspace in terms of societal sectors in the country into five major groups, namely:
1. E-commerce
2. Banking
3. Social
4. Education
5. Telecommunications
These divisions are based on the target industry of the crime being perpetrated, whether they be people or institutions.

1.4 Cybercrime Categories vis a vis Class and Societal Sectors

The various crimes themselves include:

1. Phishing

The stealing of personal information of unsuspecting persons. It involves the theft of an identity. It can be classed as fraud against authentic businesses and institutions. The mechanism mainly lies in the use of email messages sent from mimicked authorized businesses to deceive and retrieve confidential information from the victims. As per Nigeria, it has become one of the fastest growing and is mostly used on bank customers [1]. Often times some measure of trust is built and gained in order to make the client give out personal information. For example, phishing sites can be setup to obtain a user's BVN or ATM card pin or numbers.

Class: Falls under crime against confidentiality and integrity as well computer related forgery and fraud

Sector(s) of society: E-commerce, Banking

2. Cyber-theft Banking Fraud

The security weaknesses in banks can be exploited by hackers to transfer moneys from numerous accounts to theirs in a seemingly innocuous way. This is done by transferring very small amounts from victim accounts for things such as SMS deductions, withdrawal charges such that they go almost unnoticeable in many cases resulting in millions of naira when accumulated in the accounts of these fraudsters.

Class: Falls under crime against confidentiality and integrity as well computer related forgery and fraud

Sector(s) of society: E-commerce, Banking

3. Software Piracy and distribution crime

Illegal sales of intellectual property belonging to others and protected by copyright is what constitutes this type of cybercrime. Examples include persons making money from sale of pirated software/games/music etc.

Class: Falls under computer related infringement on intellectual property and copyrights

Sector(s) of society: Social

4. Sale of non-existing or fraudulent products

This involves the sale of non-existing products or replicas which constitute this type of cybercrime especially when "pay before delivery" is mandatory.

Class: Falls under computer related forgery and fraud crimes

Sector(s) of society: E-commerce

5. Cheat code and Data Airtime Theft (DAT) theft

The unlawful use of "cheat codes" to gain illegal benefits from telecommunication service providers such as unlimited airtime and mobile data without any payments being made.

Class: Falls under crime against confidentiality and integrity

Sector(s) of society: Telecommunications

6. Cyber plagiarism

The unlawful copying and pasting of someone else ideas/words into a word processor or any other electronic document without acknowledgement of the author(s)/contributor(s) constitutes this kind of crime. Mostly committed by students in higher institutions of learning.

Class: Falls under crime against computer related intellectual property and copyrights.

Sector(s) of society: Education

7. Child pornography

The distribution, sale of pornographic material involving the participation of minors or underage children, especially involving sexual activities with older persons constitutes this kind of crime.

Class: Falls under computer related content crime.

Sector(s) of society: Social

8. Social Engineering cyber crimes

The emergence of social media platforms such as Facebook, Twitter, WhatsApp and others have served as a good ground for fraudsters to carry out their activities. Varius 'scams' have been carried out such as the following:

- Fake Charities

Seeking and soliciting for help for fake or non-existent causes.

- Fake Beneficiary (Nigerian Prince scams)

Deceiving victims that they have been left to inherit a large estate from a so called 'wealthy and deceased relative or descendant'.

Cyberbullying/Cyberstalking

Harassing an individual on the cyber space through threats, stalking and intimidation. Often times the bullies or criminals have their true profile/identity hidden or masked.

- Social identity hi-jacking

Theft of an individual's social media account(s) with the intent to impersonate in order to solicit for monies or demand for ransom.

Class: Computer related forgery and fraud crimes

Sector(s) of society: Social

9. Business Email Compromise (BEC)

This involves a fraudster(s) compromising legitimate business email accounts through social engineering means or hacking in order to mislead the victim(s) into transferring unauthorized funds to suspicious accounts by sending fraudulent emails.

Class: Computer related forgery and fraud crimes

Sector(s) of society: Social

It would be impossible to list all different types of cybercrimes as the type and the list of is growing daily, but represented above are some of the most common categories of.

1.5 Worldwide Statistics on Cyber Crime

According to [4], a large number of complaints were received in 2020, higher than any previous year from the American public. The stats are as follows:

791,790 complaints with reported losses of over $4.1 billion, a 69% jump from reported cases in 2019

Most losses came from BEC schemes ($1.8 billion), Phishing ($54 million), ransomware came in at a close third with ($29.1million).

Below is a list of victim countries with reported cases. It can be seen that Nigeria ranks 16th. But however, it is a known fact that more than 90% of cases are not reported [5].

2020 - TOP 20 INTERNATIONAL VICTIM COUNTRIES [4]
Excluding the United States
1. United Kingdom 216,633
2. Canada 5,399
3 India 2,930
4 Greece 2,314
5 Australia 1,807
6 South Africa 1,754

8 Germany 1,578
9 Mexico 1,164
10 Belgium 1,023
11 Brazil 951
12 Philippines 898
13 Italy 728
14 Spain 618
15 Netherlands 420
16 Nigeria 443
17 Pakistan 443
18 China 442
19 Colombia 418
20 Hong Kong 407

Table I: 2020 Cyber Crime by type [4]

By Victim Loss			
Crime Type	**Loss**	**Crime Type**	**Loss**
BEC/EAC	$1,866,642,107	Overpayment	$51,039,922
Confidence Fraud/Romance	$600,249,821	Ransomware	**$29,157,405
Investment	$336,469,000	Health Care Related	$29,042,515
Non-Payment/Non-Delivery	$265,011,249	Civil Matter	$24,915,958
Identity Theft	$219,484,699	Misrepresentation	$19,707,242
Spoofing	$216,513,728	Malware/Scareware/Virus	$6,904,054
Real Estate/Rental	$213,196,082	Harassment/Threats Violence	$6,547,449
Personal Data Breach	$194,473,055	IPR/Copyright/Counterfeit	$5,910,617
Tech Support	$146,477,709	Charity	$4,428,766
Credit Card Fraud	$129,820,792	Gambling	$3,961,508
Corporate Data Breach	$128,916,648	Re-shipping	$3,095,265
Government Impersonation	$109,938,030	Crimes Against Children	$660,044
Other	$101,523,082	Denial of Service/TDos	$512,127
Advanced Fee	$83,215,405	Hacktivist	$50
Extortion	$70,935,939	Terrorism	$0
Employment	$62,314,015		
Lottery/Sweepstakes/Inheritance	$61,111,319		
Phishing/Vishing/Smishing/Pharming	$54,241,075		

Table 1 shows world-wide losses in dollars as a result of various types of cybercrime. It shows that BEC or Email Account Compromise (EAC) resulting in the highest financial losses and Social Engineering specifically Romance schemes coming in at second place.

Figure 1 2020 Cyber Crime by Victim report [4]

Figure 1 shows the type of cybercrimes committed for five (5) consecutive years to 2020 in terms of number of victims count and it shows that in general the number of victims targeted from various types of cybercrimes to be on the increase with Phishing being the most widespread.

Figure 2 shows sectors of the economy most targeted by cyber-criminals worldwide [6]. It shows the Financial Institutions/Banking Industries to be the most targeted, followed by cloud-based companies and payment systems. Social Media and E-commerce come in at 4th and 5th respectively.

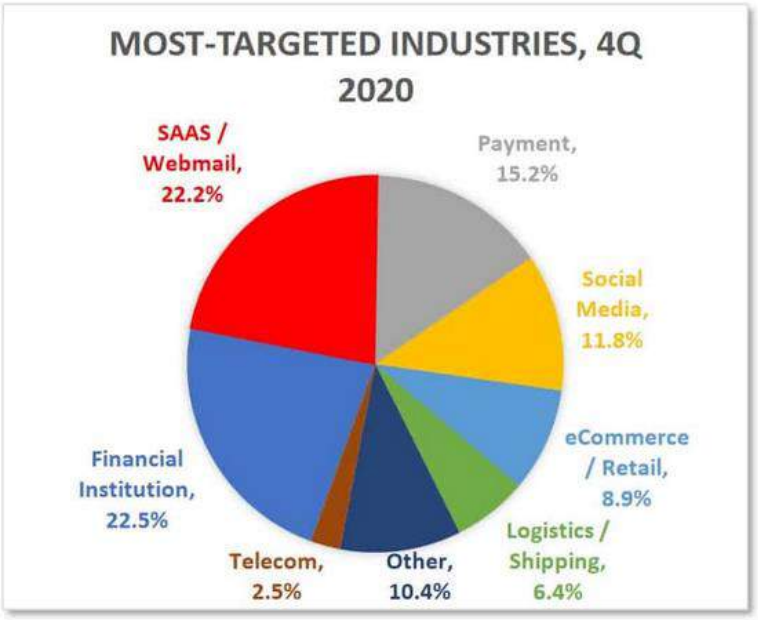

Figure 2 2020 Most Targeted Industries for Cybercrime [6]

1.6 Cybercrime on Mobile devices

1.6.1 Mobile Ad Fraud

Cybercrime is not only restricted to traditional cyberspace (the world wide web) but has spread to mobile devices. It is estimated that more than half of all online transactions are carried out on one type of mobile device or the other and with little more than 14 billion devices online [7] it has indeed become a serious problem especially during the pandemic when a lot of online transactions were made by users on their mobile phones. Majority of these cybercrimes were carried out through what has been termed as mobile ad fraud.

Mobile ad fraud is fraud committed on mobile device users by fraudsters taking advantage of inherent weaknesses in mobile advertising technology through Direct Carrier Billing (DCB) resulting in financial and other type of losses [7]. The mechanism involves tricking victims into making unauthorized purchases through 'social engineering' or 'invisible' button clicks.

DCB allows mobile users pay for goods and services through the use of their mobile phones and cyber criminals exploit this functionality.

Figure 3 presents the most targeted apps by fraudsters in their respective categories. It is observed that a vast majority of the techniques for mobile cyber-crime are trojan in nature (pretending to offer a service only to have malicious intent behind) by tricking victims into making unwanted purchases through ads on these apps with game apps and phone utility apps emerging as the most prominent vehicles for this type of crime.

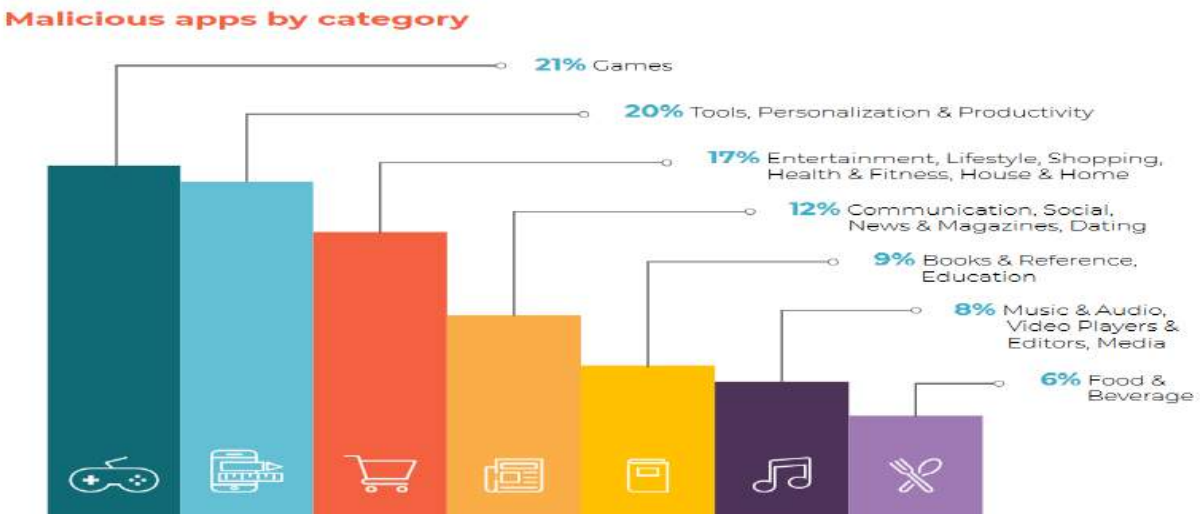

Figure 3 2020 Most Malicious mobile apps by category [7]

1.6.2 Cybercrime in Nigeria

Table 2 shows a report from [8] providing information about cybercrimes committed in Nigeria for 9 years under review running from 2010 – 2019. It shows the number of petitions which can be considered as representing the number of victims/entities. The table shows a steady rise in number of victims of cybercrime as the years progress. Although it should be noted that a lot of cases largely go unreported. The exact type of cybercrimes per case is not stated. According to [1] the major cybercrimes committed in Nigeria range from Phishing, DAT theft and BVN scams as the three most common cybercrimes carried out in Nigeria.

Table 2 Nigerian statistics for number of cybercrime cases handled for 9 years [8]

EFCC OPERATIONAL STATISTICS (2010 – 2019)

YEAR	NO OF PETITIONS RECEIVED	NO INVESTIGATED	NO OF CASES FILED IN COURT	CONVICTIONS SECURED
2010	6782	2399	206	68
2011	7,737	2,606	417	67
2012	4,914	2,062	502	87
2013	6,089	2,883	485	117
2014	4,941	2,512	388	126
2015	5,979	2,662	462	103
2016	7,045	4,660	390	195
2017	8,251	5,662	501	189
2018	9,566	5,795	515	312
2019	12,644	8,729	1,901	1,280
TOTAL	**73,948**	**39,970**	**5,767**	**2,544**

Table 3 Financial Losses in the Banking sector due to cybercrime [9]

Year	Cybercrime losses(ATM & INTERNET) (₦ billion)	Growth rate of cybercrime losses (%) year-on- year	Total Fraud Loss (₦ billion)	Contribution Of Cyber Crimes To Total Fraud (%)
2011	0.115	-	4.071	2.82
2012	0.794	590.4	4.516	17.58
2013	2.268	185.6	5.757	39.40
2014	4.438	95.6	6.193	71.66
2015	1.361	-69.3	3.173	42.89
2016	1.058	-22.2	2.4459	43.26

Table 3 shows the losses in the Banking sector due to cybercrime. It can be seen that the total fraud due to losses dropped from an all-time high in 2014 to a much lower rate in the corresponding years 2015 and 2016. This can be attributed to the concerted efforts of the Economic and Financial Crimes Commission (EFCC) in tackling cybercrime in this sector.

2. Methodology

The research design adopted is given below as:

- Research Design

In order to carry out this research the descriptive and survey research method was adopted because of its usefulness in investigating existing conditions at a set point in time.

- Sample Population

Students of the University of Benin

- Sampling Technique

Purposeful sampling technique was adopted due to the interest of the researchers in a specific set of stakeholders under the subject of interest. This was done through the distribution of online questionnaires using Google Forms © shared through links on social media accounts.

- Sample Size

The following sample sizes were chosen:

- Articles, Books, Reports, Reviews from relevant bodies.

- University of Benin: The university represents an excellent example for other universities in Nigeria both Federal and State because they share virtually the same dynamics and structure. Also, it was easier for the researchers to conduct the study here because they are domiciled within. Respondents were largely students of the institution.

-

3. Results and Discussion

Presented are the results of the online survey conducted on mostly Students of the Faculty of Engineering, University of Benin. In all 77 responses were received.

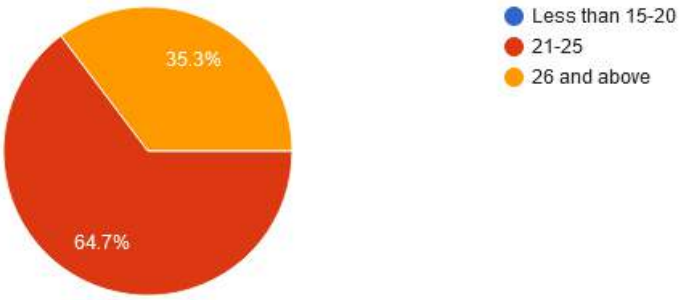

Figure 4 Age of respondents under study

The ages of the participants in the study range from 21-25 (64.7%) to 26 and over (35,3%). This is a good representation of the average age of students on the university campus, see Figure 4.

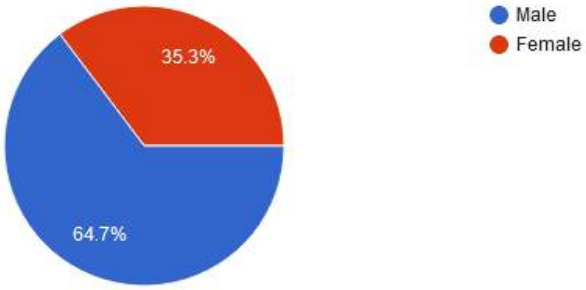

Figure 5 Sex of respondents

Most of the respondents 64.7% were male and 35.3% female as shown in Figure 5.

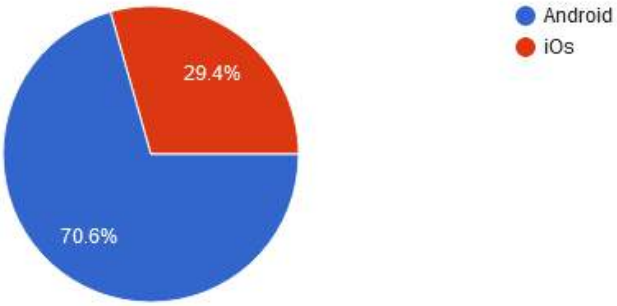

Figure 6 Mobile phone system share of the market on campus

Android represents a great share of the mobile phone market on the University campus at 70.6% and iOS or the 'i-phone' not doing badly at 29.4%, see Figure 6.

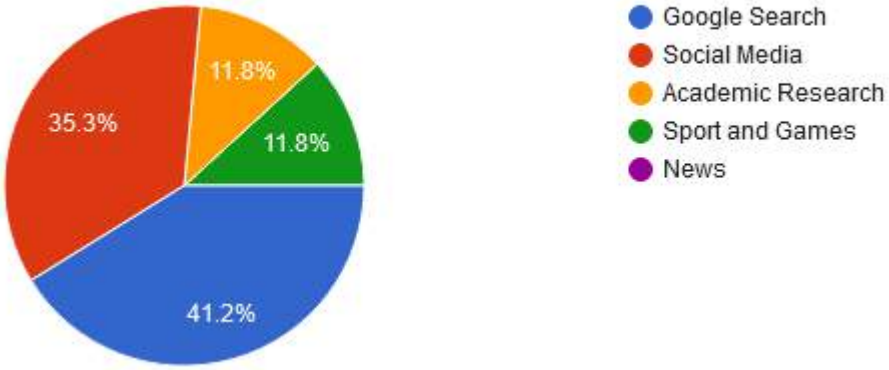

Figure 7 User activities on the Internet

Google search ranked highest among activities undertaken by students on cyber-space 41.2% followed by social media at 35.3%. Surprisingly academic research tied closely with sports in third position contrary to what would have been expected to be obtainable in the University campus both being at 11.8%! See Figure 7.

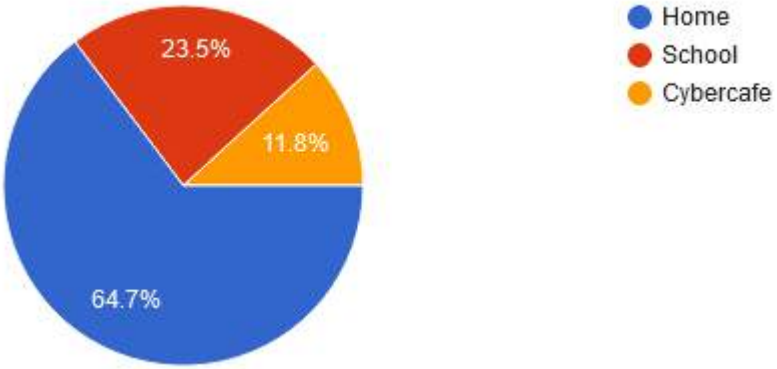

Figure 8 Locations where cybercrime is mostly carried out

Majority of the respondents believe cybercrime to be mostly carried out at home 64.7%, followed by the school premises at 23.5%. The cybercafe is ranked least 11.8%, see Figure 8.

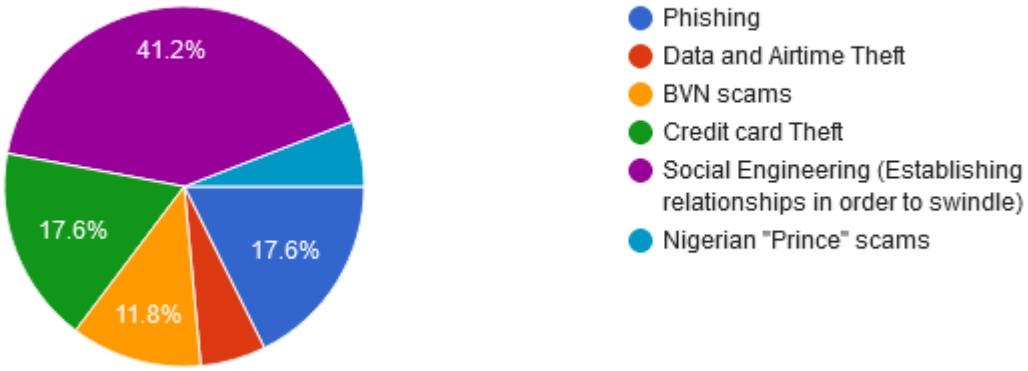

Figure 9 Most prominent cybercrimes

The most prominent of all cybercrimes committed is presented as Social Engineering at 41.2%, followed by Phishing and Credit card theft both tied at 17.06%.BVN scams follow at 11.8%. Data and Airtime theft rank least at 5.9% each. See Figure 9

3.1 Reasons Adduced for Cybercrime

Some of the reasons given by the respondents are listed below:

- Poverty
- Greed
- Unemployment
- Bad Economy
- Lack of Good jobs
- Social Influence

With poverty having the overall highest tally (11.8%) of all the probable reasons for cybercrime.

3.2 Preventive Measures Suggested

Some of the major preventive measures suggested by respondents are given below:

- Government providing basic things needed
- Creating lots of employment opportunities.
- Better security in systems.
- There should be greater attention paid to cybersecurity in Nigeria and more severe punishments should be given to those who partake in it
- By sensitizing victims
- Job creation
- Improve education, provide employment opportunities,
- Provide more resources to support developing countries
- Government should set laws against it as well as providing Employment for the youth and also making them understand that cybercrime has no Future.
- Being more security conscious when engaging in online activities.
- Government regulation, More jobs for the youth
- Job creation

- Being cautions not to disclose any information linking to your online security details, ignoring messages that enquire of your security details both through emails or text messages
- Creating awareness/sensitization of the public about the effect and punishment of cybercrime, and creation of more employment opportunities
- Provision of jobs and social amenities
- Creating a decent economy
- Create more avenues to make legitimate money in the country

4. Conclusion

There is no gainsaying that cybercrime has to be eradicated or reduced in order for the nation not to be overcome by the financial losses and loss of sense of business security. No meaningful progress can take place where crime is rampant. It has been shown that majority of cybercrime in Nigeria is carried out by youth in the society. A great majority of the respondents who are also in the age range of the participants in this crime (21-26 years) have contributed largely to this research work. The major type of cybercrime according to the students of this institution is Social Engineering (establishing relationships in order to swindle) followed by phishing and credit card theft.

Places where cybercrimes are likely to be carried out are identified as campus premises much more than the home, this is obviously for students of tertiary institutions. Poverty was identified as the major cause of cybercrime while Government policy toward providing basic amenities, job opportunities and better cyber security technologies emerged as the major solutions provided by the respondents.

The researchers agree with some of the recommendations of the respondents especially in the preventive measures proffered. If we fix the society by doing the needful (job creation, better standard of living etc.) the tendency of the youth to go into crime would be greatly reduced and for those who wish to the government agencies should be more vigilant and up to date in their strategies to deal with perpetrators.

References

[1] B. A. Omodunbi, P. O. Odiase, O. M. Olaniyan and A. O. Esan, "Cybercrimes in Nigeria: Analysis, Detection and Prevention," *FUOYE Journal of Engineering and Technology, Volume 1, Issue 1,* pp. 37 -42, 2016.

[2] S. Brenner, Law in an Era of Smart Technology, Oxford: Oxford University Press, 2007.

[3] Proshare, "Cybercrime in Nigeria: Causes and Effects," 1 9 2021. [Online]. Available: https://www.proshareng.com/news/Security---Support/Cybercrime-in-Nigeria--Causes-and-Effect/49035#.

[4] FBI, "Internet Crime report 2020," Federal Bureau of Investigation, 2021.

[5] U. Ibrahim, "The Impact of Cybercrime on the Nigerian Economy AND Banking System," *NDIC,* 2019.

[6] APWG, "APWG Phishing report for Fourth Quarter of 2020," APWG, 2020.

[7] Secure-D, "A Pandemic on Mobile," Secure-D, 2021.

[8] EFCC, "Economic and Financial Crimes Commission," 29 9 2021. [Online]. Available: https://www.efccnigeria.org.

[9] NDIC, "Annual Report," NDIC, Nigeria, 2019.

[10] NIBSS, "Business Daily," 22 2 2021. [Online]. Available: https://businessday.ng/editorial/article/rising-cyber-fraud-in-nigeria-and-banks-losses/.

NIPES Conference Proceedings
The 1st International Conference of the Nigerian Institution of Professional Engineers and Scientists 7th-8th Oct. 2021: 409-416
www.nipesjournals.org.ng

The Design and Development of A 3D Orientation Map System

Okosun. O[1] and Raifu B. T[2]
[1]Department of Computer Engineering, University Of Benin, Benin City, Nigeria
Corresponding Author: Email: Tunderaifu@gmail.com
+2348065771616, 08138026223

Abstract
Map systems has been a form of finding different locations embraced by a larger percentage of the world population and with good content can be used to convey enough information faster than most means. This project was carried out to develop a 3D map system that is used to share some insight on the different locations of departments and classes in the faculty of engineering, University of Benin to the rest of the world through the map system. The project achieved this by employing scenery local to the faculty of engineering, University of Benin a Nigerian university in Benin City and an interactive play that revolves around the environment.

1. Introduction

A map is a symbolic depiction emphasizing relationships between elements of some space, such as objects, regions, or themes. Many maps are static, fixed to paper or some other durable medium, while others are dynamic or interactive [1]. Though most commonly used to depict geography, maps may represent any space, real or fictional, without regard to context or scale, such as in brain mapping or computer network topology mapping. The space being mapped may be two dimensional, such as the surface of the earth, three dimensional, such as the interior of the earth, or even more abstract spaces of any dimension, such as arise in modeling phenomena having many independent variables. A web mapping system of the world was developed by [2]. The approach of Satellite imagery, aerial photography, street maps was adopted but the dependency on internet service, lack of interactions and detailed walkthroughs is a disadvantage to the mapping system. Maps can be more useful than globes in many situations: they are more compact and easier to store; they readily accommodate an enormous range of scales; they are viewed easily on computer displays; they can facilitate measuring properties of the region being mapped; they can show larger portions of the Earth's surface at once; and they are cheaper to produce and transport. These useful traits of maps motivate the development of map projections.

In 3D computer graphics, 3D modeling is the process of developing a mathematical representation of any surface of an object (either inanimate or living) in three dimensions via specialized software [3]. The 3D modelling of Rome scale model was carried out by [4], Models of complex buildings using Maya, procedural and parametric modelling techniques was carried out but there was Lack of interaction with model system. The modelling of Rome scale model was carried out by [5] and the use of stereo image pairs of the object was adopted to improve the quality of edges of the scanned model. The 3D modelling if a town scale model was developed by [6]. The approach of photogrammetry and Lasergrammetry was implemented and detailed models were created but these models lacked street views and walkthroughs. A 3D modelling of Beijing City scale model was developed by [7]. The use of stereo image pairs of the object improved the quality of edges of the scanned model, but these models Lacked interaction with model system. A 3D interactive maps was designed by [8] using Theory and practice3D cartography and 3d map viewer approach. No specific landscape was covered or developed.

2. Methodology

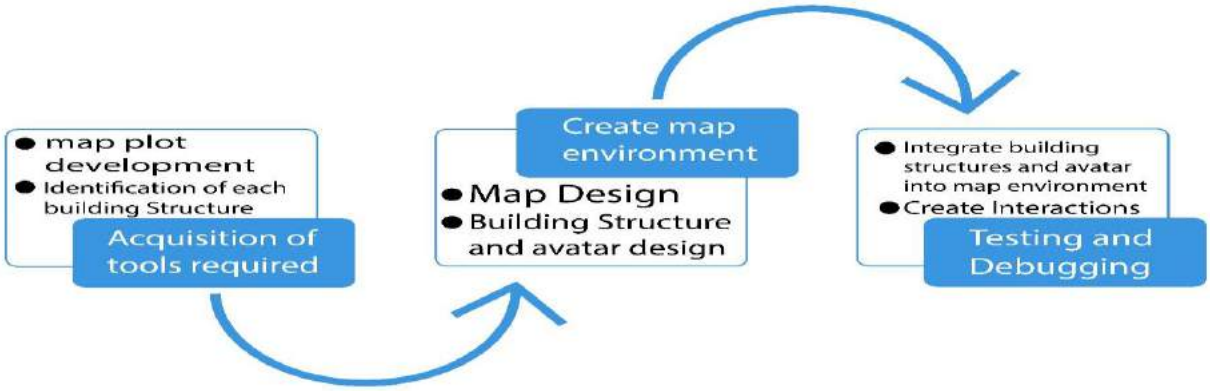

Fig 1: design System

This work employs a traditional waterfall model, infused with component reuse model shown in Fig. 1. This takes the fundamental process activities of software specification, development, validation, and evolution and represents them as separate process phases such as requirements specification, software design, implementation and testing [4]. The design is to develop full three dimensional models of each building in the Faculty of Engineering, to create a map system of Faculty of Engineering using a drawn-out plot of the Faculty and to develop interactions within the system to allow movements around map system using a modelled avatar.

2.1 Design Phase

Map models were determined and sketched using real life photos of the various buildings and environs to guide in the implementation for design for the scenery (i.e. the faculty of engineering). Necessary pictures of the part of the faculty environment and the structures to be incorporated was also carried out using the waterfall model of a software development. Waterfall Model takes the fundamental process activities of software specification, development, validation, and evolution and represents them as separate process phases such as requirements specification, software design, implementation, testing [5]. The map system was designed using the components identified as shown in the Fig 2. and the Unity game engine focus was placed on integrating the character models created using modelling tools into the overall map play.

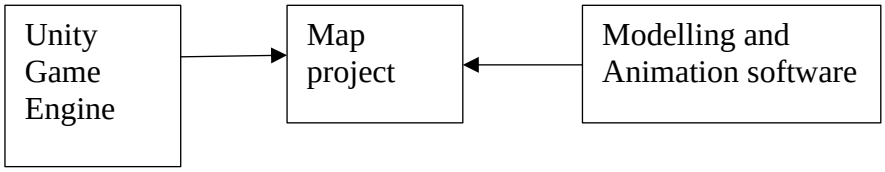

Fig 2: design System

2.2 Implementation Phase

The map objects shown in Fig 3 to Fig12 (the buildings, avatar etc.) are modelled and joined using Blender and Revit modelling tools.

A. Buildings

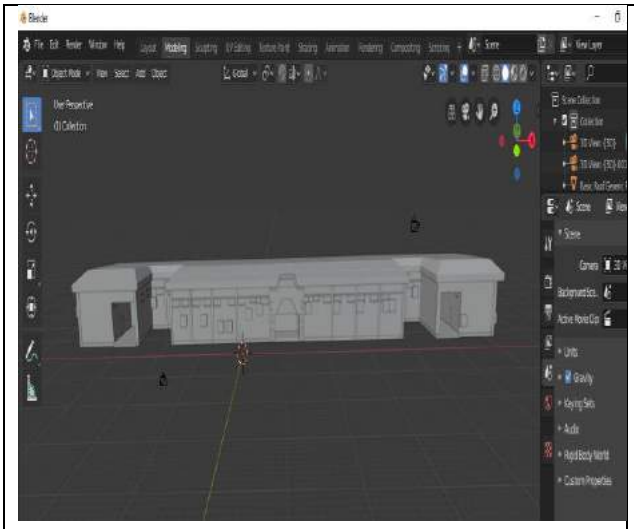

Fig 3: Petroleum Engineering Building

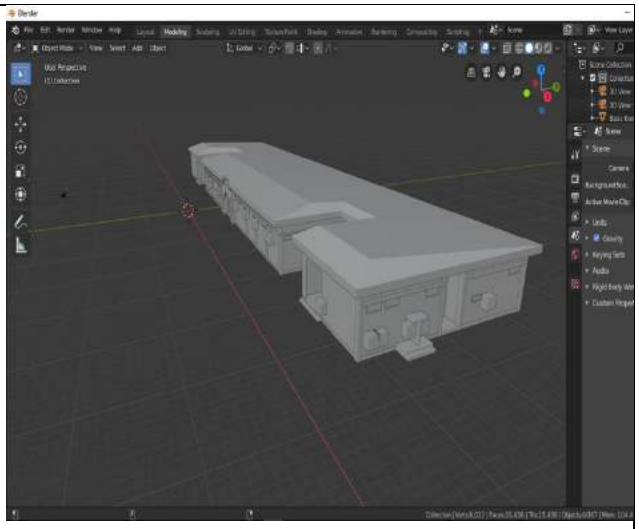

Fig 4: Petroleum Engineering Side view

Fig 5: Old 1000LT

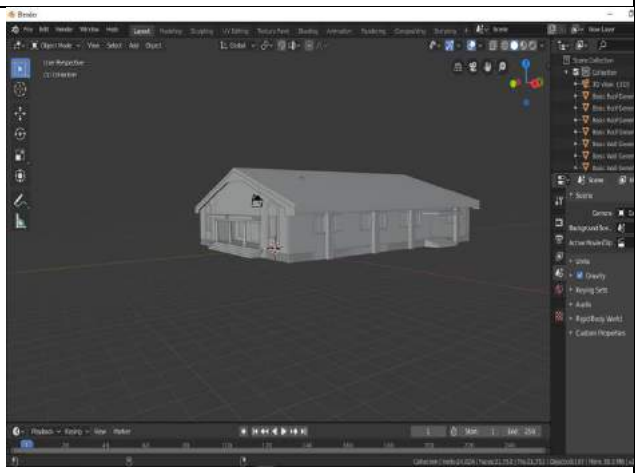

Fig 6: Old 1000LT side view

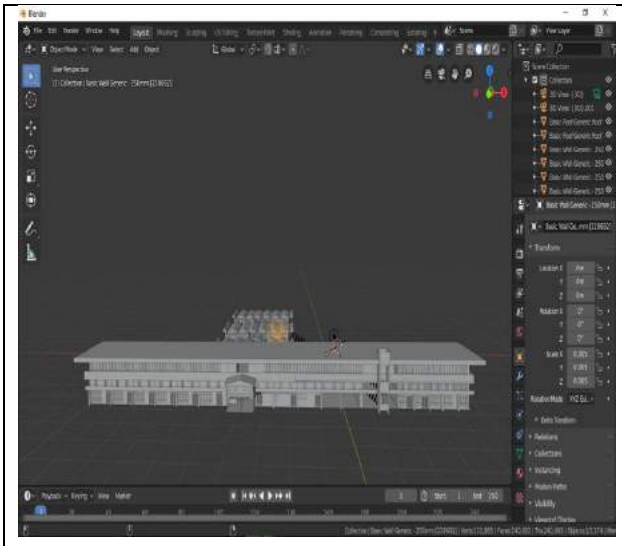

Fig 7: Main Faculty Building

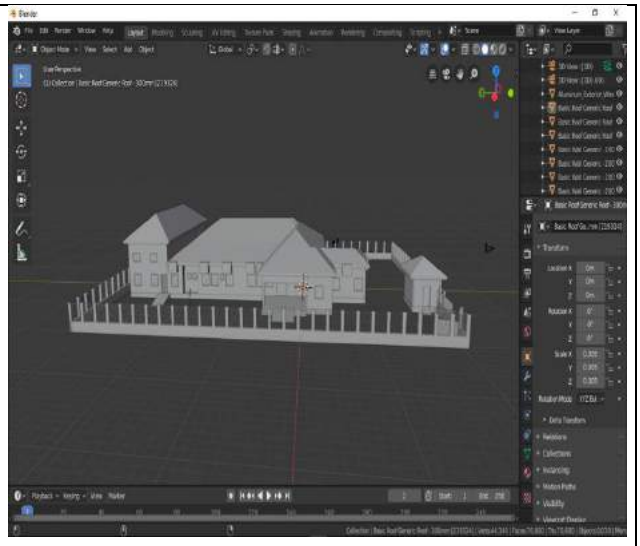

Fig 8: Chemical Engineering Building

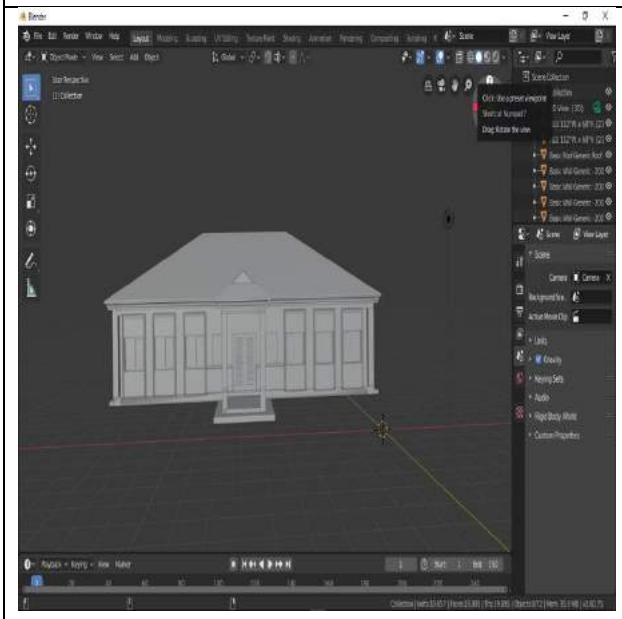

Fig 9: ADEC Building

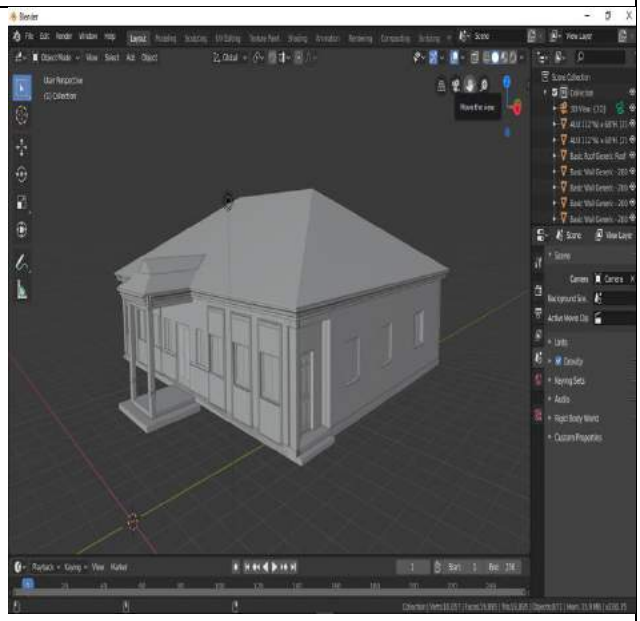

Fig 10: ADEC Building side view

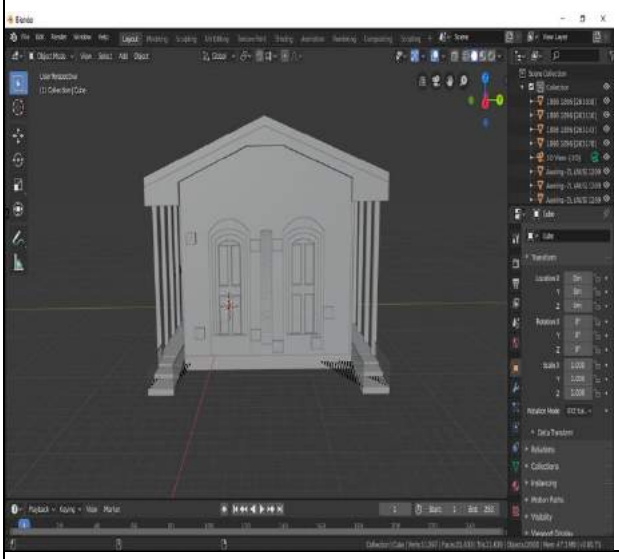

Fig 11: New 1000LT

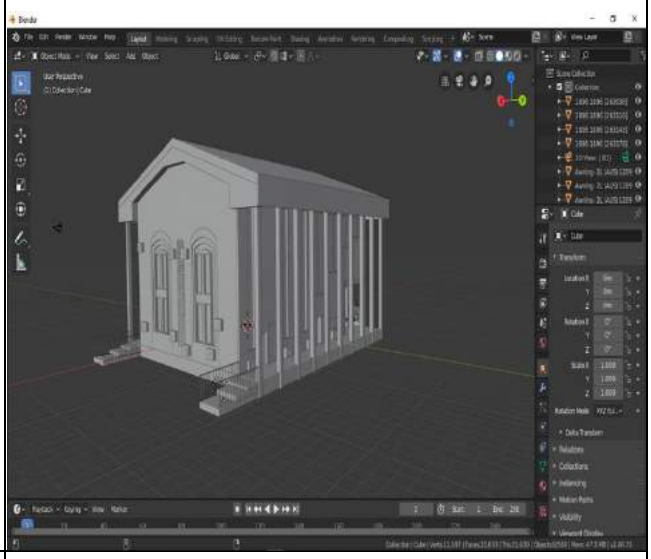

Fig 12: New 1000LT side view

Also, the scenery and environment implementation of the map logic was designed using Unity game engine. The Unity3D game engine is a cross-platform game engine with a built-in integrated development environment (IDE) developed by Unity Technologies. The Graphic rendering subsystem of the game engine manages all code that renders graphics in the map, including initialization and releasing of system resources acquired by the graphics device. The faculty buildings were designed by rendering 3D geometric primitives such as point, line, point list, line list/strip and mesh.

B. Avatar

Shown in Figure 13 is the main player (Avatar) which is similar to the Graphics Rendering Subsystem, this subsystem includes initialization and releasing of system resources acquired by the input device.

Fig. 13: Avatar

-The Input Handling subsystem of the game engine provides services for easy registration of responses to corresponding Avatar's input.

-The Collision Detection subsystem's function simulates the Avatars behavior of colliding objects and also triggers the activation of scripts due to the presence of predetermined game objects.

-Codes were used to handle responsibility (rules) of engagement in the map and how the various elements of the map interact with each other. The programming language employed in creating the code is C#.

-Adobe Photoshop graphics design software was used in this map to create the textures applied to the map character, the terrain, the level designs and other visual objects required in the map.

The designed map objects (buildings and avatar) are able to load an external 3D model, which can be encoded in .x file format, blend file format, .fbx file format into the map. In addition, 2D objects such as color-keyed bitmaps and fonts are also rendered through this subsystem. Other graphics objects that are not render-able, such as camera, light and materials, are also managed by this subsystem

C. Map Interaction Scripts

These are various code snippets used to implement the interaction of the map components and objects together in the map's scene. They are Behavioural_script, Updatehelper, Movement, Player_control, Movement_cam, Camera turn, Mouse orbit, SmoothFollow, SmoothLookAt and Gravity, each adding different functionality to the map.

3. Results and Discussion

A Windows or Android based third-person (Avatar) role playing map which has several individual components acting as one unit for the purpose of the map system. The main player (Avatar) is the actor controlled by the player. Table 1 shows the test carried out on the map which is a roleplaying simulation and observations of the actor which moves around the environment and find different locations for an ease of access during a visitation.

Table 1: Results from character contact and movement with environment

S/N	Test	Observation	Results
1	Character contact with ground around the faculty of Engineering, UNIBEN	Satisfactory	Working
2	Character movement along X axis using Unity 3d game engine Cartesian	Satisfactory	Working
3	Character movement along Y axis using Unity 3d game engine Cartesian	Satisfactory	Working
4	Character idle state	Satisfactory	Working
5	Character walking state	Satisfactory	Working
6	Character running state	Satisfactory	Working
7	Visibility of static objects; buildings, cars, mast, generators and barricades around the faculty of Engineering, UNIBEN	Satisfactory	Working
8	Collision between character and static objects that is buildings and barricades (between LT 2 and LT 4, LT 1 and LT 3) around the faculty of Engineering, UNIBEN	Satisfactory	Working
9	Input response delay ('W,A,S,D' for up, left, down and right movements respectively)	Satisfactory	Working
10	Camera to character motion	Satisfactory	Working
11	Camera view rendering	Satisfactory	Working

4. Conclusion

The Android / Computer based map system with the local content is available for the faculty of engineering, University of Benin. The map features were achieved as a Third-Person role playing system with all of the scene elements rendered over a plane. The scene was created using the faculty of engineering in the University of Benin as the focus of the system which could be added to the google map.

However as with all software projects, there is still room for improvements. Since the buildings do not contain interior scenes of both departments and classes, it could be upgraded with time, making the model a highly sophisticated map with interiors and also interactions.

References

[1] Chevrie, C. (2017). The 3D modelling of a town scale model. EuroMed 2010, XIV. Cyprus.

[2] Chiu-Shiu , C., Anrong, D., & Ziyu, T. (2005). A 3D model of the Inner City of Beijing. In B. A. Martens B (Ed.), Computer Aided Architectural Design Futures. Sydney, Austria: Springer, Dordrecht.

[3] Guidi, G., Frischer, B., & Spinetti, A. (2005). 3-D Digital Imaging and Modeling. 2005 3DIM 2005. Fifth International Conference, (p. DOI: 10.1109/3DIM.2005.2).

[4] Ian, S. (2010). Software Engineering (Vol. 9th Edition). Scotland: Pearson.

[5] James, J. (2017). 3D modelling. Retrieved September 2018, from https://en.wikipedia.org/wiki/3D_modeling

[6] Map-Google Arts & Culture. (2017, July 30). (G. A. Culture, Producer, & Google Arts & Culture) Retrieved October 2019, from artsandculture.google.com: https://arts and culture.google.com/entity/map/m04_tb?hl=en

[7] Rafal, G. (2009). 3D Interactive maps: Theory and Practice. Southwales.

[8] Russo, M., Guidi, G., Micoli, L. L., Frischer, B., Simone, M. D., Spinetti, A., & Carosso, L. (2005). 3D Digitization of a Large model of Imperial Rome. 3-D Digital Imaging and Modeling. 5th International Conference. DOI: 10.1109/3DIM.2005.2.

NIPES Conference Proceedings
The 1st International Conference of the Nigerian Institution of Professional Engineers and Scientists 7th-8th Oct. 2021: 417-433
www.nipesjournals.org.ng

Design of a Remote Controlled Pneumatic Palm Climber and Harvester (PCAH)

Iberedem Akpan, Mohammed Ndaliman

Department of Mechanical Engineering; Federal University of Technology, Minna, Nigeria
Corresponding email: iberedem.akpan@st.futminna.edu.ng

Abstract

This project is on the design of a remote controlled palm climber and harvester to fill in the technological gap in palm harvesting. It is a synergy of engineering principles and relevant technologies like pneumatics and mechatronics to solve societal problem in the area of palm production. In this project, a Palm Climber and Harvester (PCAH) was designed. The movements of individual linkages in its mechanisms were determined, the pneumatic system which produces the motion and the electronic circuit which controls the pneumatic circuits were also designed. The dimensions of the individual linkages which will withstand the working stress were calculated. These dimensions, after being simulated under working condition using SolidWorks engineering application software were found to be within safety limits. PCAH as a machine can be readily manufactured for use in the palm oil industry.

1.0 Introduction

Palm oil remains the most widely produced and consumed vegetable oil or fat on earth with over 35 million barrels produced yearly. It is eaten by more than 3 billion people worldwide, in over 150 countries of the world. It supplies 8% of energy intake for Africa and contributes 33% of the total fats and oil consumed worldwide [1]. The cultivation of palm plantations increases steadily at the rate of 5% yearly. Conversely palm climbers reduce yearly, harvesting becomes more difficult and costly due to technological gap in harvesting techniques.

There is need for a new technology to drive the sector in palm production. This technology must meet the needs for harvesting of palm fruits at a low cost, less risk; be environmentally friendly, durable and also compliant with the socio-cultural inclinations the new Nigeria. This also implies that the machine must be, time saving, less polluting, while also exploring other power source, possibly renewable energy, to power it.

The aim of this project is to design a machine which uses the motion of pneumatic actuators to climb and harvest fresh fruit bunches of the oil palm while it is being operated from the ground with a remote controller. This involves: designing the climbing and harvesting mechanism of the PCAH, designing for the motion of major linkages in the mechanisms using pneumatic actuators, calibrating the individual motion of the linkages, designing a radio wave remote controller to operate the PCAH from a distance, and evaluating the performance of PCAH. To eliminate the risk of loss of human life involved in the crude harvesting methods of palm fruits, PCAH is automated and controlled by humans using remotes. This calls for the use of Programmable logic circuit or micro controllers as an interface for controlling mechanical movements via electronic systems

Several machines have been designed to harvest coconut including the Advanced Remote-Controlled Coconut Harvesting Robot (A.R.H.H-1) [2]. However, the harvesting of Oil Palm is quite different. The tapping mechanism for Fresh Fruit Bunches (FFBs) therefore must include a protective mechanism to defend the machine against the weight of the FFB. A means of cutting the fronds and also pushing it away and the mechanism must

be designed in such a way that the weight of the FFB does not lean on the blade during tapping as it may cause failure. PCAH is therefore the first automated machine designed for the climbing and harvesting of oil palm fruits.

2.0 Functionality Design

The palm climber and harvester are designed to serve two basic functions: to climb up to the top of the tree and to cut down the palm bunch from the tree. Other functions includes: cutting down of palm bunches; clearing of the palm top, carrying a load (its weight) up and swinging its cutting arm about. Aside the functions, simplicity of design, ease of manufacture, ease of maintenance and available technology are considered paramount in the design and thus serve as constraints in the design

In order to achieve this, the following technologies are employed in the building of this machine: pneumatics, tree climbing technology, electronics and microcontrollers and electro-pneumatic technology

2.1 Climbing Mechanism Functionality Design

PCAH is made to mimic the climbing action of mammals. For a gripping action, a simple mechanism consisting of two jaws representing the legs of a mammal is considered as in Figure.1..

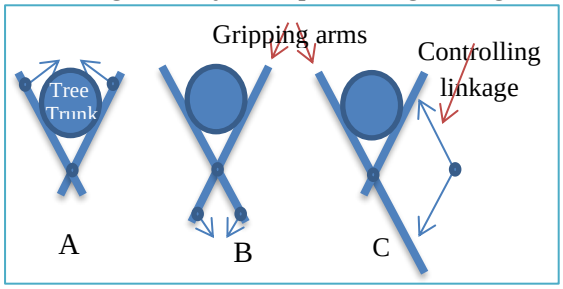

Figure 1 Different classes of lever that can be applied for the gripping arm

Also it can be found that a component of the force applied in gripping tends to cause a slipping of the contact point along its length. The geometry of the gripping arms is modified to combine the advantages arrangements A and B. The resulting mechanism as shown in Figure 2 (a), however, has a little range of tree diameter that it can accommodate. Length C and C' is then introduced as a solution as illustrated in Figure 2 (b).

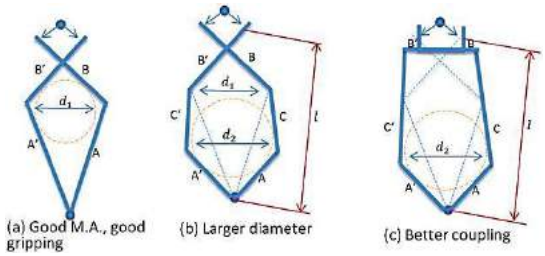

Figure 2 Different stages of modification of lnkages for greater utility

On a closer observation, it can be found that length B and B' will not completely fit together at all angles. It crosses each other as it rotates about the fulcrum as illustrated in Figure 3.

For neatness and a good assembly, the geometry of the gripping arm is again modified. It is transformed in such a way that neither the mechanical advantage nor maximum diameter is altered as illustrated in Figure 2 (c).

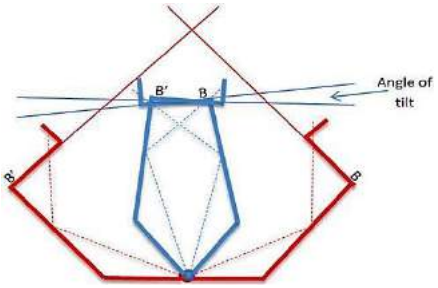

Figure 3 Illustrating the incompatibility of length B and B' at various opening angles

Length B is therefore arched along the path of the circumference such that the two arms maintain a fit coupling as opens or closes. This is as illustrated in Figure 4.

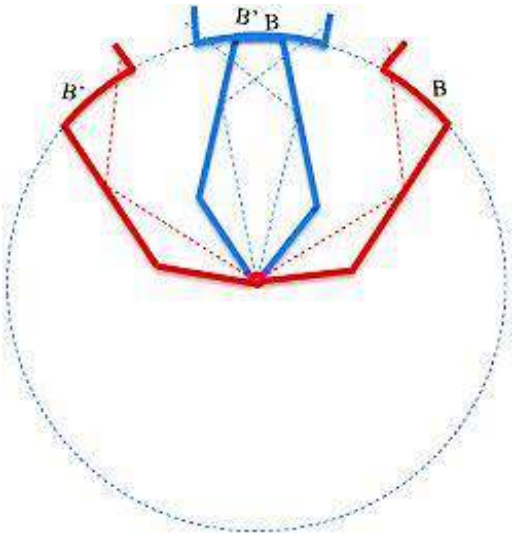

Figure 4 Illustrating the compatibility of arched length B and B' at various opening angles

The minimum and maximum diameter that can be accommodated by the mechanism can be calculated applying the laws of geometry. The arms are also designed to better to be symmetrically the same for easy replacement during maintenance.

A sliding lever is required to lower or increase the height of the arms during climbing. The lever adjusts its height by sliding across its length while pulling or pushing the arms down or up to carry out a climbing action. The continuous displacement of heights after several pulling and pushing of gripping arms as illustrated in Figure 5 climbs the tree.

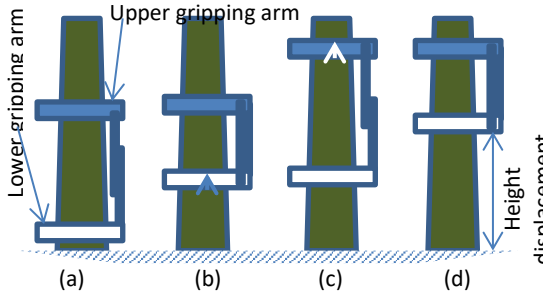

Figure 5 Climbing process of PCAH

In this case, pneumatic cylinders serve the purpose of gipping or loosening the arm and pushing or pulling the arm upwards or downwards for the climbing mechanism

2.2 Functionality Design for Harvesting Mechanism

Harvesting of palm fruit involves clearing the tree top of masquerading palm fronds and cutting down the palm fruit at its stalk. The cutting can be carried out by thrusting a wedge like machete into the stalk or by use of a rotating toothed cutter as illustrated in Figure 6. A provision is also made to allow the arm to swing about for effective work output.

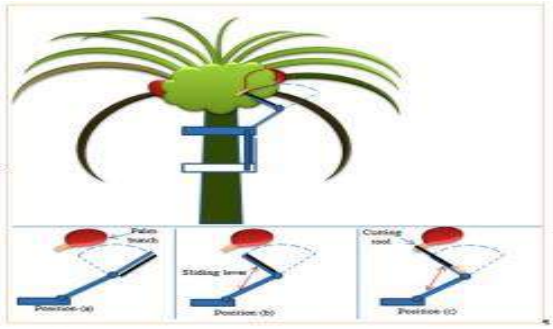

Figure 6 Mechanism for harvesting process of PCAH

2.3 Design for the Revolving Mechanism

On reaching the top, PCAH will have to revolve round the tree trunk to be able to harvest the palm fruit which palm usually bears in all directions round. The path traced by the movement of the gripping arm about the tree trunk is almost concentric to the tree trunk. A mechanical rail-like guide can therefore be provided to guide the grippers about as it rotates as in Figure 7.

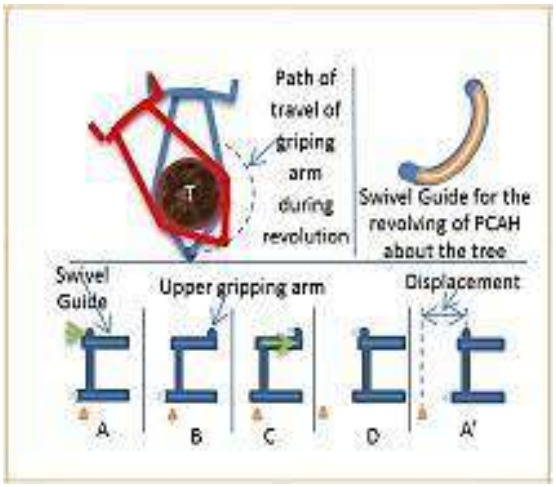

Figure 7 Revolving mechanism

The machine is displaced along the path of revolution about the tree trunk. A number of this cycles allows the machine to go round the tree trunk for all round inspection and harvest. The pushing and pulling of the arms can be done with the aid of a powered sliding lever, in this case, a pneumatic cylinder.

2.4 Pneumatic Circuit Functionality Design

Pneumatics refers to the use of compressed air to produce mechanical motion. The force produced is a product of the air pressure acting against the area of the piston. The flow of compressed air is normally

controlled by flow control valves. The flow control valve could be switched on, switched off or port changed manually, by mechanical actions or by electric switches. In this case, electric switch controlled by electronic signals is used. Most of the components are designed to be powered by pneumatic system. The pneumatic circuit diagram is as given in Appendix A1

The detailed description for each pneumatic cylinder is as shown in Table 1.

Table 1 description of pneumatic cylinders

S/No	Point of application	Piston length (mm)	Cylinder bore	Other description
1	Lower gripping arm	256	80	Double acting cylinder, magnetic piston, trunion mounting
2	Upper gripping arm	256	80	Double acting cylinder, magnetic piston, trunion mounting
3	Column	180	40-50	Double acting cylinder, magnetic piston, direct rear mounting
4	Swivel guide	260	30	Double acting cylinder, magnetic piston, front flange mounting
5	Cutting arm angle tilt	120	25	Double acting cylinder, magnetic piston, rear pivot mounting
6	Cutting blade thrust	120	25	Double acting cylinder, magnetic piston, front flange mounting

2.5 Electrical Circuit

In order to control the machine from the ground while the machine climbs up, the machine is employs the use of remote control. The remote control is designed to fourteen have keys: twelve control buttons and two power buttons. The TX-2B and RX-2B however can only transmit five channels primarily. The other channels are gotten by a combination of several primary channels.

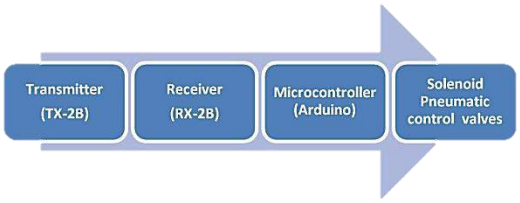

Figure 8 Command transfer sequence

The Arduino microcontroller is introduced for the logical control of the individual cylinders.

The command transfer sequence is as given in Figure 8while Table 2 shows how the electric signals are exchanged and converted to mechanical power output. All electrical circuits design is given in Appendix A2.

Table 2 Signal transfer logic and coding

S/No	Transmitter Pin No.	Channel Transmitted	Receiver Pin No.	Microcontroller Output	Command output
1	1	1	6	F	Grip lower arm
2	14	2	7	E	Loose lower arm
3	4	3	10	D	Increase column height
4	5	4	11	C	Decrease column height
5	6	5	12	B	Increase swivel angle
6		1,2		A	Decrease swivel angle
7		2,3		G	grip upper arms
8		3,4		H	Loose upper arms
9		4,5		I	Push cutting blade
10		1,2,5		J	Pull cutting blade
11		3,4,5		K	Raise cutting arm
12		1,5		L	Lower cutting arm

3.0 Design Analysis, Calculations and Synthesis

The machine comprises of two major assemblies classified based on the individual functions of the sub-systems

1. The climber: this comprises of all the parts for the climbing mechanism of the machine
2. The cutting arm, which includes all the components for the harvesting mechanism

Part1. Gripping Arm

The gripping arm sustains the weight of the machine against the tree trunk by friction. The required friction to sustain the weight of the machine is generated by increasing the gripping force pushing it against the weight of the tree trunk.

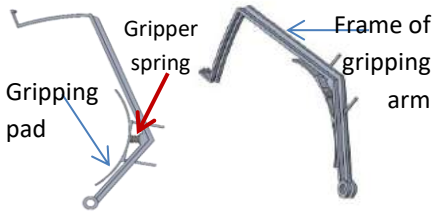

Figure 9 Gripping arms

It consists of three major mechanical components: the frame, the pad and the spring as illustrated in Figure 9.

a. Forces acting on gripping arm

When the machine is at restive position, the two pads grip the tree trunk as a means of sustaining the weight of the machine against the tree trunk. For the pads to grip the walls of the tree trunk without slipping, the friction force induced by the gripping force must be enough to overcome the weight of the machine

Given that:

1. Friction coefficient of rubber on wood is a minimum of 0.5

2. Estimated weight of machine = 50kg
3. Gravitational acceleration = 9.81m/s^2

Static friction coefficient:

$$= \frac{force\ required\ to\ slide\ the\ two\ surfaces}{forces\ pushing\ the\ surfaces\ together}$$

$$\mu_{rubber\ on\ wood} = \frac{W}{F} \qquad \ldots (equation\ 1)$$

$$\mathrm{F} = \frac{50 \times 9.81}{0.5} = 981\ \mathrm{N}$$

For proper grip, the machine is expected to produce at least 1.5 times the minimum required gripping force. A force of 1500N is taken as gripping force.

a. Stresses acting on gripper frames

The gripping force acts on the two pedals of the right and left grippers such that the force on each pedal is just half of the total, that is, 750N as in Figure 10.

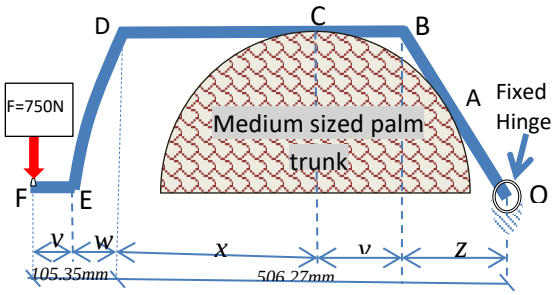

Figure 10: Schematic diagram of the gripping frames

Moment of force F acting on the frame $\|BCDEF\|$ depends on the point C. The moment increases as $\|BC\|$ reduces. This implies the smaller radius of some trees. In the limit, when $\|BC\| = 0$; maximum moment, M_{max}, due to force exerted on point F is given by

$$M_{max} = F \times (v + w + x + y + z) \qquad \ldots (equation\ 2)$$

By functionality design, $v + w = 105.35mm$ and x + y= $506.27mm$

$$\therefore\ M_{max} = 750N \times (105.35 + 506.27)mm = 458{,}715Nmm$$

In calculating the stress due to bending, the cross-section of frame $\|BCD\|$ as shown in Figure 11 is put to consideration

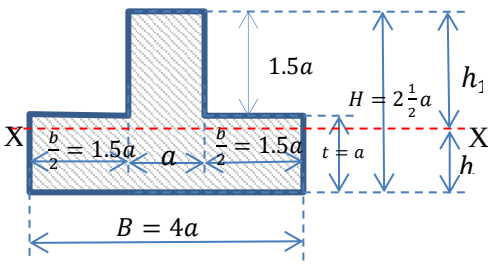

Figure 11 Cross section of frames $\|OABCD\|$

Distance from extreme fibre to neutral axis, $y\ or\ h$

$$h = \frac{(aH^2 + bt^2)}{2(aH + bt)} = \frac{37}{44}a$$

$$Moment\ of\ inertia, \quad I_{xx} = \frac{Bh^3 - b(h-t)^3 + ah_i{}^3}{3} \quad \ldots (equation\ 3)$$

$$where\ h = \frac{37}{44}a;\ \ h_1 = H - h = \frac{73}{44}a$$

$$I_{xx} = \frac{4a\left(\frac{37}{44}a\right)^3 - 3a\left(\frac{37}{44}a - a\right)^3 + a\left(\frac{73}{44}a\right)^3}{3} = 1.349897477a^4$$

$$Section\ modulus, Z = \frac{I}{y} = \frac{\left(\frac{344{,}969}{85{,}184 \times 3}\right)a^4}{\left(\frac{37}{44}\right)a} = 1.605283486a^3$$

Based on standard specification for structural support, maximum allowable tensile stress at extreme fibre for aluminium 5456-H111, $F_{t_y} = 179Mpa\ or\ 179N/mm^2$; and Factor of safety, $n_y = 1.65$ (Reddy, 2014)

$$Stress\ due\ to\ bending\ moment, \sigma_{b_t}$$

$$\sigma_{b_t} = \frac{F_{t_y}}{n_y} = \frac{M}{Z} \quad \ldots (equation\ 3.4)$$

$$\sigma_{b_t} = \frac{179\ N/mm^2}{1.65} = \frac{458{,}715Nmm}{1.605283486a^3mm^3}$$

$$a = 13.81043545mm\ \ or \cong 15mm\ to\ the\ nearest\ half - ten$$

Shear stress acting on the cross-section of beam $||OB||$ will then be

$$\frac{W}{A} = \frac{50 \times 9.81}{(60 \times 37.5) - 2 \times (22.5 \times 22.5)} = 0.3964N/mm^2$$

This is far less than the maximum allowable shear stress being over $100N/mm^2$

a. Bending stress acting on the curved part of the frame

To calculate the bending stress on the curved part of the beam, it is assumed that the point D in Figure 12 where the curve begins is fixed considering that the deflection at maximum moments of force is minimal and can be ignored.

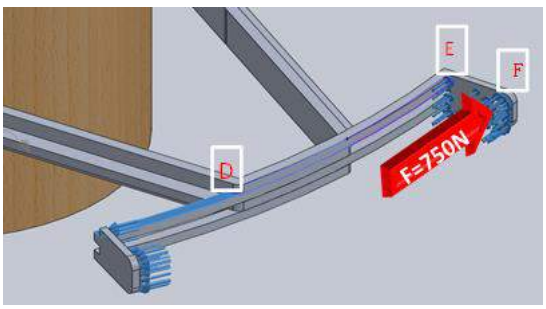

Figure 12: Showing pictorial diagram of length $||DEF||$ of gripping frames

Moment about point D $(M) =$

$$F \times (|v + w|) \quad = 79{,}012.5\ Nmm$$

b. Stress due to bending moment on the curved part of the beam

From established theories, maximum bending moment stress occurs at the outer or inner surface of the curved beam with radius R_o and R_i as represented in Figure 12 [3].

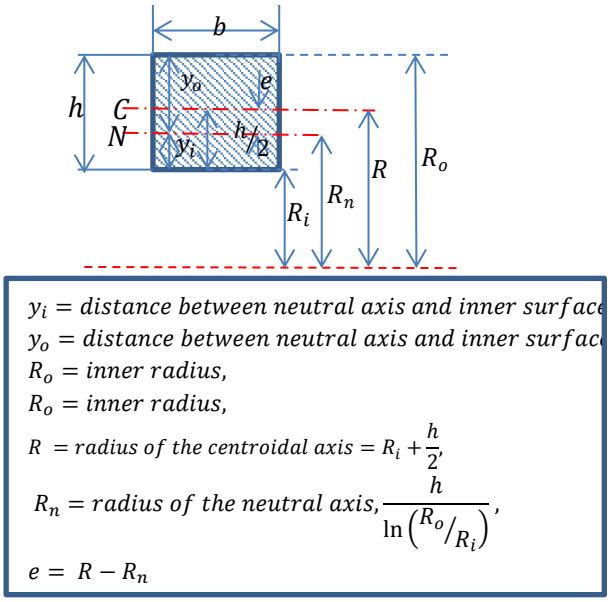

Figure 13: Cross section of curved frame ||DEF||

Maximum bending stress (compressive) at inner surface, $\sigma_{b_i} = \frac{My_i}{AeR_i}$ ... (equation 5)

Maximum bending stress (tensile) at outer surface, $= \frac{My_o}{AeR_o}$ ... (equation 6)

where M = Bending moment at any given section about centroidal axis

Maximum allowable compressive stress for aluminium 545-H111 at the extreme fibre,

$$\sigma_{b_i} = \frac{F_{cy}}{k_c.n_y} \quad \text{... (equation 7)}$$

Where F_{cy} = compressive yield strength = $152N/mm^2$; k_c = Compression co-efficient = 1.10; n_y = Factor of safety = 1.65. Relating equation 3.5 with equation 3.7

$$\sigma_{bi} = \frac{F_{cy}}{Kc.n_y} = \frac{My_i}{Ae.R_i}$$

$$\text{But } e = R - R_n = \left(R + {}^{h}/_{2}\right) - \frac{h}{Ln\left(\frac{R_o}{R_i}\right)},$$

$$A = bh = 30h \text{ since } b \text{ is already designed to be } 15mm$$

$$and\ y_i = R_n - R_i = \left({}^{h}/_{ln\left(\frac{R_i+h}{R_i}\right)}\right) - R_i$$

$$\frac{152}{1.10\times1.65} = \frac{79{,}012.5Nmm\times\left(\left({}^{h}/_{ln\left(\frac{R_i+h}{R_i}\right)}\right)-R_i\right)mm}{30hmm^2\times\left(R_i+\frac{h}{2}-\left(\frac{h}{ln\left(\frac{R_i+h}{R_i}\right)}\right)\right)mm\times R_imm}$$

Given, from functionality designs, that $R_i = 704.13$, by iterations, h can be found to be $13.7812mm$

Maximum allowable tensile stress for Aluminium at the extreme fibre

$$\sigma_{b_{outer}} = \frac{F_{ty}}{n_y} \quad \ldots (equation\ \ 8)$$

Where F_{ty} = tensile yield strength = $179N/mm^2$; n_y = Factor of safety = 1.65

Comparing equation 8 with equation 6

$$\sigma_{b_{outer}} = \frac{F_{ty}}{n_y} = \frac{My_o}{AeR_o} \ and\ R_o = R_i + h$$

$$y_o = R_o - R_n = (R_i + h) - R_n$$

$$= R_i + h - \left(\frac{h}{ln\left(\frac{R_i+h}{R_i}\right)}\right);$$

$$\frac{179}{1.65} = \frac{79{,}012.5Nmm \times \left(R_i + h - \left(\frac{h}{ln\left(\frac{R_i+h}{R_i}\right)}\right)\right)mm}{30hmm^2 \times \left(R_i + \frac{h}{2} - \left(\frac{h}{ln\left(\frac{R_i+h}{R_i}\right)}\right)\right)mm \times (R_i + h)mm}$$

By functionality design, $R_i = 704.13$; thus by iterations, h can be found to be $12.03599mm$. Since this is less than the size obtained as requirement to sustain the compressive stress at extreme fibres, the larger value, $13.7812mm$ is considered. A safe value of 15mm is assumed to give tolerance to the possibility of error during manufacturing or overloading during usage

Part 3. Spring

The spring serves two purposes: to absorb the shock on the gripper frames due to the action of pneumatic cylinders and also to sensor the excess force applied in the gripping action

a. As a shock absorber

The equivalent spring system and the forces acting on the spring are as shown in Figure 14.

F represents the force required to grip the frames together, calculated from equation 4.1 to be 1500N

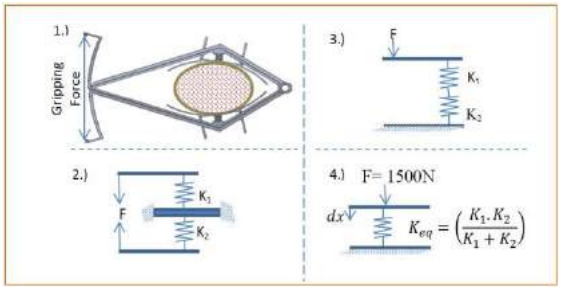

Figure 14: Schematic diagram of forces acting on springs

$$From\ Hooke's\ law, F = -K_{eq}.e = -K_{eq}dx \quad \ldots (equation\ \ 9)$$

By geometric constrain of functionality design, $x_{max} = 25mm$

$$substituting\ values\ into\ \ equation\ \ 3.9$$

$$1500N = \frac{K}{2}.25mm$$

$$K = 120N/mm$$

Part 4. Pneumatic cylinder for gripping arm

The pneumatic cylinder as represented in Figure 15 produces a push or a pull which determines the motion of the gripping arm. It is a double acting pneumatic cylinder controlled by electrical pulse signals. It is subjected to tension, compression and buckling stress depending on the length of the piston.

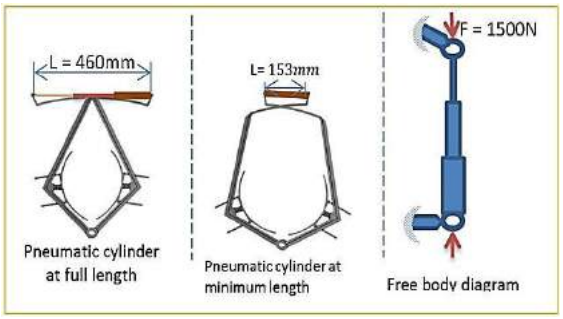

Figure 15: Pneumatic cylinder

a. Cylinder bore

The force require for the gripping action is be produced by the action of the pneumatic cylinders, the cylinder bore must be large enough to produce gripping force at working pressure. The machine is designed to function at a pressure of four bars to avoid the high energy losses, high maintenance cost and risk of accident that are usually associated with very high pressures[4, 5, 6, 7]. Also, to conserve space, and reduce weight, a telescopic piston cylinder is considered.

Required force $= \ total\ area \ \times \ woking\ pressure \times efficiency$

$$1500N = \left(\frac{\pi D^2{}_{bore}}{4}\right) \times \frac{0.4N}{mm^2} \times 0.8$$

$$D = 77.25484mm\ or\ 3inches$$

b. Stresses acting on pneumatic piston

Since the pneumatic cylinder is designed to function with hinged ends as shown in figure 3.7, the effective length $L = l = 153mm$ each ; Young's modulus (E) for aluminium $= \ 70000N/mm^2$

Moment of inertia for circular cross section $I = \frac{\pi d^4}{64}$

Based on Euler's formula,

$Buckling\ load, N_{cr} = Load \times Factor\ of\ safety \ = \frac{\pi^2 EI}{L^2}$ (Höglund, 2009)

$$= 981N \times 1.65 = \frac{\pi^2 \times 7000N/mm^2 \times \frac{\pi d^4}{64}}{(153mm)^2}$$

$$d = \left(\frac{981N \times 1.65 \times 64 \times (153mm)^2}{\pi^3 \times 7000N/mm^2}\right)^{\frac{1}{4}} \ = 10.28115797mm \ \cong \frac{1}{2} inch$$

Part 5. Column

The column is a pneumatic cylinder. Its piston moves up or down to initiate a climbing height. It connects the upper gripping arm to the lower gripping arm through the swivel guide. It is subjected to both compressive and bending stress as illustrated in Figure 16.

For columns subjected to both bending moment and compression,

$$maximum\ stress\ \sigma_{max} = \frac{load(W)}{Cross\ sectional\ Area\ (A)} + \frac{Moment\ of\ Force\ (M)}{Section\ Modulus\ (Z)} \quad \ldots (equation\ \ 10)$$

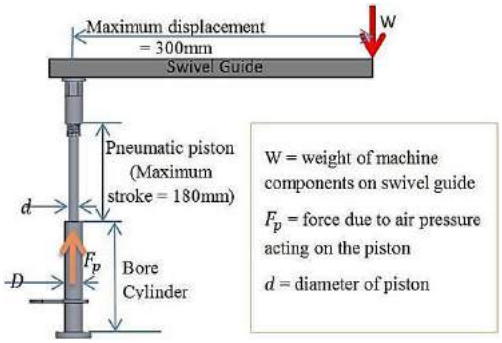

Figure 16: pneumatic cylinder column

For columns subjected to both bending moment and compression,

$$maximum\ stress\ \sigma_{max} = \frac{load(W)}{Cross\ sectional\ Area\ (A)} + \frac{Moment\ of\ Force\ (M)}{Section\ Modulus\ (Z)} \quad \dots (equation\ \ 10)$$

W= (weight of palm bunch) + (weight of cutting arm) + (weight of upper gripping arm)

$$W_{estimate} = 20kg + 10kg + 10kg = 40kg$$

$$W_{load} = (40kg \times 9.81m/s^2)N$$

Moment of Force, $M = W_{load} \times displacemet\ (s) = (40kg \times 9.81m/s^2)N \times 300mm$

Cross sectional area (A) $= \frac{\pi d^2}{4}$;

Section Modulus (Z) = $\frac{\pi d^3}{32}$

Considering aluminium for piston material, maximum allowable stress on piston

$$\sigma_{max} = \frac{F_{cy}}{k_c . n_y} \qquad \dots (from\ equation\ \ 7)$$

Where F_{cy} = compressive yield strength = $152N/mm^2$; k_c = Compression co-efficient = 1.10; n_y = Factor of safety = 1.65

Substituting values into equation 3.10, $\sigma_{max} = \frac{F_{cy}}{Kc.n_y} = \frac{W}{A} + \frac{M}{Z}$

$$\frac{152}{1.10 \times 1.65} = \frac{\left(40kg \times \frac{9.81m}{s^2}\right)N}{\frac{\pi d^2}{4}} + \frac{\left(40kg \times \frac{9.81m}{s^2}\right)N \times 300mm}{\frac{\pi d^3}{32}}$$

$$d = 24.36445007mm \cong 31.75mm\left(1\,{}^1/_4\,inch\right)$$

to common market specification

The bore diameter must be such that can produce enough force at a given pressure.

Required Force = $W_{load} = (40kg \times 9.81m/s^2)N$; Working pressure = 4.0 $bar\ or\ 0.4N/mm^2$

Estimated minimum efficiency = 80% $Required\ Force = Pressure \times Area \times Efficiency$

$$W_{load} = \left(40kg \times \frac{9.81m}{s^2}\right)N = \frac{0.4N}{mm^2} \times \frac{\pi D^2{}_{bore}}{4} mm^2 \times 0.8$$

$D_{bore} = 39.5134mm \cong 44.45mm\left(1\,{}^3/_4\,inch\right)$ to the closest market specification

Part 6. Swivel Guide

The swivel guide guides the upper gripping arm and the upper gripping arm as it rotates about the tree trunk. It is subjected to shear forces and bending moment as the components slides along its length. It functions as a cantilever thus maximum bending moment occurs when the components are at the extreme length. Its design parameters are as shown in Figure 17.

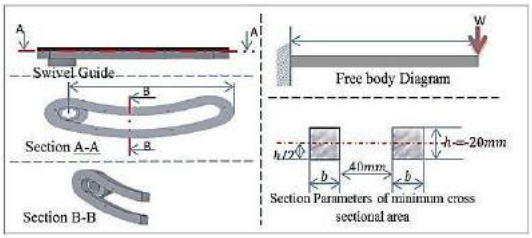

Figure 17: Swivel Guide

Minimum cross sectional area =

$$[(2b + 40\ )h - 40h]mm^2\ = (2bh)mm^2$$
$$= (40b\ )mm^2\ (substituting\ h = 20mm)$$

Moment of Inertia $(I) =$

$$\frac{(2b+40)\times h^3}{12} - \frac{40h^3}{12} = \frac{2bh^3}{12}$$

Section Modulus $(Z) = \frac{I}{y}$

$$= \left(\frac{2bh^3}{12}\right) \Big/ \left(\frac{h}{2}\right) = \frac{400b}{3}$$

Bending moment (M)

$$= \left(40kg \times \frac{9.81m}{s^2}\right)N\ \times\ 303.75mm\ = 119191.5Nmm$$

When the swivel guide is loaded, it is subjected to a tensile stress at the extreme top fibre and a compressive stress at the extreme lower fibre due to bending

a. Bending stress due to tension at upper extreme fibre

Maximum allowable tensile stress at extreme fibre due to bending

$$\sigma_{b_t} = \frac{F_{ty}}{n_y} = \frac{M}{Z}$$
$$\frac{179}{1.65} = \frac{119191.5Nmm}{\left(\frac{400b}{3}\right)}$$
$$b = 8.24019448mm$$

b. Bending stress due to tension at upper extreme fibre

Maximum allowable compressive stress at extreme lower fibre $\sigma_{b_c} = \frac{F_{cy}}{k_c.n_y}$

Where $F_{cy} = 152N/mm^2$; $k_c =\ 1.10$; $n_y =\ 1.65$

$$\frac{152}{1.10 \times 1.65} = \frac{M}{Z}$$
$$b = \left(\frac{1.65 \times 1.10 \times 3 \times 119191.5}{152 \times 400}\right)\ = 10.674304564mm$$

c. Shear stress acting on cross sectional area

The weight of the machine then rests on the swivel guide as it slides across it causing a shearing stress along its cross section. The minimum cross sectional area then must be able to overcome the stress acting on it

$$Maximum\ stress = \frac{Load}{Minimum\ cross\ sectional\ area}$$

Maximum allowable shear stress for aluminium = $= \frac{shear\ ultimate\ strength}{factor\ of\ safety}$

$$= \left(\frac{172}{1.65}\right)\frac{N}{mm^2} = \frac{(40 \times 9.81)N}{(40b)mm^2}$$

$$b = 0.0941mm$$

Maximum thickness of b which is $10.674304564mm$ is used for design

Cutting Arm

The cutting arm consists of two major assemblies: the cutting arm support lever and the cutter arm

Part 7. Cutting arm support lever

The cutting arm supports lever carries the upper gripping arm, serves as a means for sustaining the weight of the cutter arm against gravity and also to project it towards the palm bunch as illustrated in Figure 18. It is subjected to loading at an angle whose components separate into shear forces and bending moment.

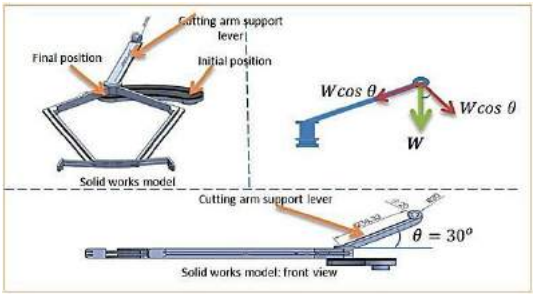

Figure 18 Cutting arm support lever

Load (W) acting on cutting arm support lever = weight of the cutting arm (estimated at 10kg)

The cross section of the arm is that of an inverted Tee with a web thickness of a and geometric ratios similar to that of Figure 19.

Shearing force along perpendicular cross section of the lever $= Wsin\,\theta$

Bending moment force along the length of the lever $= Wcos\,\theta$

Shear force component $= Wcos\,\theta$

Area of cross section $= BH - 2bh = 5.5a^2$

Moment of inertia = $2.319128787a^4$

Distance from centroid to extreme fibre $= \frac{73}{44}a$

Section modulus $=$

$\frac{2.319128787a^4}{\frac{73}{44}a} = 1.397831a^3$

Bending moment $= Wcos\,\theta \times l = 20{,}247.823762875Nmm$

$Bending\ stress =$

$$\frac{Maximum\ yield\ stress}{factor\ of\ satety} = \frac{Bending\ moment}{section\ modulus}$$

$$\frac{179\,N/mm^2}{1.65} = \frac{20{,}247.823762875Nmm}{1.397831a^3}$$

$$a = 5.1111449695mm\ or\ 10mm$$

$$to\ the\ nearest\ ten$$

10mm is considered also for ease of casting since casting of thin sections is more difficult. 6mm can also be used where readily available by extrusion.

Part 8. Cutter arm

The cutter arm does the cutting of the palm bunch. It is held in place by the cutting arm support lever in such a way that allows it to swing at an angle when pushed or pulled by the pneumatic cylinder. It is an assembly of seven components: the cutter arm casing, sliding lever, electric motor, motor pin, rotor pin, belt and the cutting blade.

4.0 Results

4.1 Graphical Modelling

Graphical modelling in this case refers to the use of imagery to represent a prototype of the machine being produced so as to aid imagination and better comprehension of the design. A model of PCAH is as shown in Figure 20. This model is based on the combination of the functionality design of the machine with its mathematical model based on the calculations carried out.

Figure 20 Solid works model of PCAH Mechanical assembly

A detailed design of the individual parts, dimensions and mechanism is as given in the appendix.

4.2 Evaluation of The Performance of The Strength of Pcah Under Working Stress

The evaluation of the performance of PCAH was carried out using an engineering design software, SolidWorks. This software analyses the stress acting on a part machine using the concept of Finite Element Analysis (FEA) where a mechanical part is treated as a mesh of very tiny, finite elements. The resultant stress acting on a load can then be found by calculating the vector sum of all the stress acting on the individual elements. The result of the simulations of the parts of PCAH under working condition is as given in Table 3,4 and 5.

Table 3 stresses acting on gripping pad under working condition

Name	Type	Min	Max
Stress1	VON: von Mises Stress	3998.61 N/m^2 Node: 230	2.19276e+008 N/m^2 Node: 17727

gripper sketch_project-Study 3-Stress-Stress1

Table 4 stresses acting on swivel guide under working conditions

Name	Type	Min	Max
Stress1	VON: von Mises Stress	7141.95 N/m^2 Node: 12078	1.83546e+006 N/m^2 Node: 14951

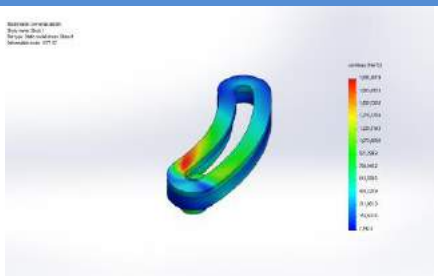

swivel assembly -Study 1-Stress-Stress1

Table 5 stresses acting on cutting arm support lever under working condition

Name	Type	Min	Max
Stress1	VON: von Mises Stress	83.9987 N/m^2 Node: 13157	1.47888e+007 N/m^2 Node: 12578

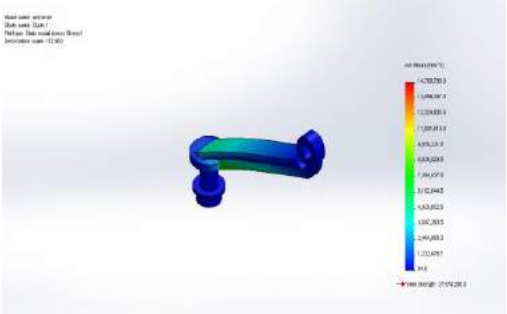

arm lever-Study 1-Stress-Stress1

Given that the maximum allowable stress for aluminium is180 GPa, it can be found that the stresses acting on the machine parts while it is working are within safe limits

5.0 Conclusion

To improve on PCAH, further research needs be made on the use of lighter materials, including plastics; a cutting arm with higher degree of freedom; vision aids; portable liquefied air; and on making PCAH more intelligent and a self-controlled machine.

References

[1] Abraham, A., Vysakh, A. S., Philip, J., Skaria, R., Praven, M. P., & Harisha, S. K. (2014). Fabricatiof of Advanced Remote-Controlled Coconut Harvesting Robot (A.R.H.H-1) Incorporating Rapid Prototyping Technology. East Point College of Engineering & Technology and R. V. College of Engineering, Mechanical Engineering, Bangalore, India.

[2] African Centre for Economic Transformation. (2013). The Oil Palm Value Capture Opportunity in Africa. Retrieved March 3, 2015, from ACET: Pathways To Transformation: http://www.acetforafrica.org/acet/pathways/agroprocessing/oil palm

[3] Croser, P., & Frank, E. (2002). Pneumatics Basic Level. Festco Didactic GmBH & Co. 73770, Denkedorf.

[4] Höglund, T. (2009). Training in Aluminium Application Technology, Lecture 2301. (E. –E. Association, Ed.) Stockholm: Royal Institute of Technology.

[5] Khurmi, R. S., & Gupta, J. K. (2005). A Textbook of Machine Design (First Multicolour ed.). (S. Chand, Ed.) Ram Nagar, New Delhi, India: Eurasia Publishing House.

[6] Reddy, C. R. (2014). Standard Specifications For Structural Supports For Highway Signs, Luminaires, And Traffic Signals. Washington, D. C., USA: American Association of State Highways and Transportation.

[7] SILAN Semiconductors. (2002). TX-2B/RX-2B: Remote controller with five channels.

AppendixA:
https://drive.google.com/file/d/1a4GaolxlPWp0MiuREbSiHtBBTDIbJwV3/view?usp=sharing